



CIGR 2018

XIX. World Congress of CIGR (International Commission of Agricultural and Biosystems Engineering)

"Sustainable Life for Children"

22 - 25 April 2018

Antalya, Turkey

PROCEEDINGS



www.cigr.org

CIGR 2018

PROCEEDINGS OF XIX. WORLD CONGRESS OF CIGR (International Commission of Agricultural and Biosystems Engineering)

EDITORS

Prof. Dr. Can Ertekin

Res. Assist. Hasan Yilmaz

ISBN: 978-605-4483-52-5

December, 2018, Antalya-TURKEY

This book contains original papers submitted to the Editor and possible errors in the texts belong to the author(s).



www.cigr.org

PREFACE

It is a great appreciation for us that the XIX CIGR World Congress hosted by The Union of Chambers of Turkish Engineers and Architects, the Chamber of Agricultural Engineers, the Departments of Agricultural Machinery and Technologies Engineering of the Faculty of Agriculture of Akdeniz and Ege University held in Antalya, Turkey with the theme of “Sustainable Life For Children” between 22-26 April, 2018.

There were 325 participants from 38 different countries. Participants were from Turkey, China, Japan, South Korea, United States, Spain, Denmark, Iran, Italy, Hungary, Poland, South Africa, Belgium, Brazil, Czech Republic, Netherlands, Portugal, Turkish Republic of Northern Cyprus, Austria, Colombia, Morocco, Oman, Romania, Russia, Taiwan, Uruguay, Australia, Canada, Estonia, Finland, Germany, Ireland, Kenya, Malaysia, Mexico, New Zealand, Nigeria and Pakistan.

Main scope of this Congress is to provide a big platform for experts from different countries working on Agricultural and Biosystems Engineering who believe in the advantages of cooperation. Main subjects of the Congress were; Land and Water, Structures and Environment, Plant Production, Energy in Agriculture, System Management, Bioprocesses, Information Technology. There was a Workshop on Image Analysis and Spectroscopy in Agriculture.

There were totally 142 oral and 91 poster presentations in the congress and workshop. The keynote speakers were Prof. Dr. Istvan Szabo (Hungary) “Agriculture in the Age of Information Technology”, Prof. Dr. Umezurike Linus OPARA (South Africa) “Engineering a new agriculture for the 21st Century to build a sustainable life for children”, Prof. Dr. Mikio Umeda (Japan) “Development of Mechanized and Smart Farming in Asia” and Prof. Dr. Margarita Ruiz Altisent (Spain) “Innovative Technologies in Postharvest”.

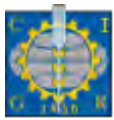
A total number of 239 abstracts were published in Abstracts Book and 44 full papers were published in Proceedings.

Special thanks are devoted to our keynote speakers, session chairs, and also to all the authors making their valuable contributions. We are thankful to those institutions and Companies for their kind support enabled us to realize this congress.

Finally we would like to express our best wishes to all members of Scientific Committee for their intensive cooperation.

Organizing Committee

2018



CIGR 2018

XIX. World Congress of CIGR



SCIENTIFIC COMMITTEE

Scientific Committee members are listed in alphabetical order according to their first names

- | | | |
|---|--|---|
| Prof. Abdullah Sessiz, Turkey | Prof. Giacomo Scarascia, Italy | Assist. Prof. Osman Gökdoğan, Turkey |
| Prof. Adnan Değirmencioğlu, Turkey | Dr. Gilles Rabatel, France | Prof. Osman Yıldız, Turkey |
| Dr. Ahmad Banakar, Iran | Assoc. Prof. Guangnan Chen, Australia | Prof. Patrizia Busato, Italy |
| Prof. Ahmet Çelik, Turkey | Dr. Guido D'Urso, Italy | Prof. Pierluigi Febbo, Italy |
| Prof. Ahmet Çolak, Turkey | Dr. Gülsüm Evrenbilek, Turkey | Prof. Pilar Barreiro Elorza, Spain |
| Prof. Ahmet Kürklü, Turkey | Prof. Halil Kurnak, Turkey | Assoc. Prof. Piotr Solowiej, Poland |
| Prof. Alaa El-din Bekhit, New Zealand | Prof. Heinz Bernhardt, Denmark | Prof. Qin Zhang, United States |
| Prof. Ali Bayat, Turkey | Prof. Hiroshi Shimizu, Japan | Prof. R. Cengiz Akdeniz, Turkey |
| Prof. Ali İhsan Acar, Turkey | Dr. Hongbin Pu, China | Prof. Ramazan Sağlam, Turkey |
| Assoc. Prof. Ali Ünlükara, Turkey | Dr. Hubert Latala, Poland | Prof. Recep Külcü, Turkey |
| Assoc. Prof. Álvaro Ramírez Gómez, Spain | Assoc. Prof. Hüseyin Güler, Turkey | Prof. Remigio Berruto, Italy |
| Prof. Amauri Rosenthal, Brazil | Prof. İbrahim Akinci, Turkey | Dr. Renfu Lu, United States |
| Dr. Ana Garrido-Varo, Spain | Prof. Irenilza de Alencar Nääs, Brazil | Prof. Sakine Özpınar, Turkey |
| Dr. Andre Aarnink, Netherlands | Prof. Istvan Szabó, Hungary | Prof. Sarp K. Sümer, Turkey |
| Prof. Antonio Brasa Ramos, Spain | Prof. Janusz Piechocki, Poland | Prof. Sedat Çalıřır, Turkey |
| Dr. Aoife Gowen, Ireland | Prof. Jiannong Xin, United States | Prof. Sedat Karaman, Turkey |
| Prof. Axel Munack, Germany | Prof. John K. Schueller, United States | Prof. Seishi Ninomiya, Japan |
| Prof. Bahattin Akdemir, Turkey | Prof. Joop Lensink, France | Assist. Prof. Selçuk Özmen, Turkey |
| Prof. Baoming Li, China | Dr. Jose Blasco, Spain | Dr. Sergio Cubero, Spain |
| Prof. Bart Sonck, Belgium | Prof. José Francisco Aguilar Pereira, Costa Rica | Prof. Servet Gulum Sumnu, Turkey |
| Prof. Berkant Ödemiş, Turkey | Dr. José M. Gonçalves, Portugal | Dr. Se-Woon Hong |
| Dr. Bosoon Park, United States | Prof. Jose M. Tarjuelo, Spain | Assoc. Prof. Shafiqur Rahman, United States |
| Assist. Prof. Burak Şen, Turkey | Dr. Jose Manuel Amigo, Denmark | Dr. Sílvia Carlos Ribeiro Vieira Lima, Brazil |
| Prof. Bülent Çakmak, Turkey | Prof. Kamil Alibaş, Turkey | Prof. Slawomir Kurpaska, Poland |
| Assoc. Prof. Chaoyuan Wang, China | Prof. Kamil Ekinci, Turkey | Dr. Stanley C. Best Sepulveda, Chile |
| Dr. Claudio Garcia, Uruguay | Prof. Karl Wild, Germany | Prof. Stefan Böttinger, Germany |
| Dr. Claus Aage Grøn Sørensen, Denmark | Prof. Kazunori Iwabuchi, Japan | Dr. Stefan Mihina, Slovakia |
| Prof. Daniel Berckmans, Belgium | Prof. Kemal Sulhi Gündoğdu, Turkey | Assoc. Prof. Sultan Kıymaz, Turkey |
| Prof. Daniel Marçal de Queiroz, Brazil | Prof. Ladislav Nozdrovicky, Slovak Republic | Prof. Şefik Tüfenkçi, Turkey |
| Assoc. Prof. Dariush Zare, Iran | Dr. Laszlo Banranvai, Hungary | Prof. Tadeusz Juliszewski, Poland |
| Prof. Da-Wen Sun, Ireland | Prof. Linus Opara, South Africa | Prof. Tami Brown-Brandl, United States |
| Dimitris K. Papanastasiou, Greece | Assist. Prof. M. Fırat Baran, Turkey | Dr. Ta-Te Lin, Taiwan |
| Prof. Eberhard Hartung, Germany | Prof. Makoto Hoki, Japan | Prof. Thiago Libório-Romanelli, Brazil |
| Dr. Dongxiao Sun-Waterhouse | Dr. Manuela Zude, Germany | Dr. Thomas Banhazi, Australia |
| Dr. Elisabeth Quendler, Austria | Assoc. Prof. Marcella Guarino, Italy | Prof. Thomas Jungbluth, Germany |
| Prof. Engin Özgöz, Turkey | Prof. Martin Libra, Czech Republic | Prof. Tolga Erdem, Turkey |
| Prof. Enrique Molto, Spain | Prof. Meral Kılıç Akyılmaz, Turkey | Dr. Tugay Ayaşan, Turkey |
| Prof. Erdem Aykas, Turkey | Prof. Miguel Castro Neto, Portugal | Prof. Vedat Demir, Turkey |
| Prof. Fátima Baptista, Portugal | Prof. Miklós Herdon, Hungary | Dr. Wilson Castro, Peru |
| Prof. Fedro Zazueta, United States | Prof. Mohamed Hatem, Egypt | Won Suk Daniel Lee, China |
| Assoc. Prof. Fernando Estellés Barber, Spain | Assoc. Prof. Mohammad Reza Alizadeh, Iran | Prof. Yeşim Benal Öztekin, |
| Assoc. Prof. Francisco Rovira-Mas, Spain | Prof. Morten Dam Rasmussen, Denmark | Turkey Prof. Yoshiyuki Shinogi, Japan |
| František Kumhála, Czech Republic | Dr. Naoshi Kondo, Japan | Assoc. Prof. Yukiharu Ogawa, Japan |
| Dr. Gamal Elmasry, Egypt | Prof. Nicola Lamaddalena, Italy | Prof. Yurtsever Soysal, Turkey |
| Assoc. Prof. Gerrit Jan Carsjens, Netherlands | Prof. Nuria Aleixos Borrás, Spain | Prof. Zeliha Bereket Barut, Turkey |
| Dr. Gerrit Polder, Netherlands | Dr. Oliver K. Shlueter, Denmark | |



CIGR 2018

XIX. World Congress of CIGR



CONTENTS

DIMSUB: A Decision Support Tool For Design And Pipe Sizing Microirrigation Systems.....	7
Multioutlet Hydrants Typology for Collective Irrigation Networks	17
The Effect of Different Boron Levels on the Yield and Some Physiological Properties of Cotton Plant under Deficit Irrigation Conditions	27
Different Tillage under Semi-Arid Mediterranean Conditions: Some Physical Soil Quality Indicators and Their Relations.....	36
The Effect of Heat Stress on Milk Yield in a Ipad Supported Dairy Cattle Enterprise	48
Landscape Fragmentation In Europe: A Comparative Analysis	59
The Power Transmission Characteristics of Overload Shafts with Different Friction Clutches and Spring Loading Conditions.....	66
Environmental Importance of Olive Groves in Cultural Landscape,	75
Urban Agriculture as a Tool for Environmental Protection	83
Determination of Threshing Performance of New Design Threshing Unit for Lavandin (Lavandula x intermedia emeric ex loisel.)	93
Determination of Separating Performance of New Design Separating Unit for Lavandin (Lavandula x intermedia emeric ex loisel.)	101
Rice Harvesting Operation by Two Combine Robots.....	108
Time Response Study of Electromagnetic Driven VRT Valves for Variable Rate Spraying System Improvement	116
Mixed Seeding Performance of a Seed Drill at Different Mixture Ratios_Under the Laboratory and Field Conditions.....	125
Prototype Twin Vacuum Disk Metering Unit for Improved Seed Spacing Uniformity Performance at High Seeding Speeds	136
Detection Of Foreign Bodies In Processed Food And Drinking By Means Of Ultrasound.....	149
Integration of photovoltaic arrays into the historic city	160
Investigation of Moisture Content, Particle Size and Pellet Die_Geometry Effects on Sawdust Pelletizing By Means of New Type Pelletizing Test Device.....	166
Natural Ventilation's Ability to Prevent High Indoor Temperatures	183
Development of an Innovative Farm Management System with Parallel Off-line and On-line Capabilities.....	192



CIGR 2018

XIX. World Congress of CIGR



Effect of Moisture Content on Physical Properties of Pumpkin (<i>telfairia occidentalis</i>) Seeds.....	202
Friction Coefficients For Gundelia Tournefortii Seed on Various Surfaces	211
Determination of Leaf Breaking Strength of Variety Candidates of Common Vetch	226
Impact of Tillage Practices on Selected Soil Physico-Chemical and Biological Conditions, and Maize Yield in Latosolic Red Soil of southern China	232
FT-IR Imaging Spectroscopy for Measurement of Times-Series Physical Parameters of Potato and Sweet Potato Tubers During Microwave Drying	247
Cutting Resistance and Energy of Rice Stem.....	257
Automated Compensation and Diagnostic System for Electrical Conductivity and pH Probes in Recirculating Hydroponics.....	264
Development and Application of Functional Food for Older People.....	272
Prediction of Soluble Solids Content of Jackfruit Using Shortwave Near Infrared	280
Assessment of Calibration and Validation of CropSyst model in winter wheat productivity in Mediterranean Environments.....	289
A ROS-Enabled Out-Door Robotic Perception System.....	298
Proximate Sensing and Application for Variable Rate Nitrogen Application on Corn Field.....	309
The Accuracy in Seed Spacing of a Seeder with Variable Ratio	317
Precise Point Positioning for a Robot Tractor using LEX Signal Transmission from Quasi-Zenith Satellite System	329
Aerial Machine Vision, Geographical Information System and Hue for Pattern Classification in Agriculture	337
Optimization of Drying Process of Coconut Meat (Cocos Nucifera L.) with Aid of Image Analysis.....	349
A New Approach to Calculation of Parcel Index for Abdurrahmanlar District	355
Changes in Low-flow Frequency under Global Warming in Tanada Catchments.....	364
A Deep Neural Network Model for Runoff Analysis	373
Physical Requirements for Vineyard Monitoring Robots	383
Database of Traction Indicators of Domestic and Foreign Tractors for OECD and ISO Systems.....	388
Effect of Top Cutting Height of Cotton Stalk On Cotton Yield	399
Foreign Body Detection Approaches In Food And Beverage Products.....	408
New trends in numerical modeling and control of photovoltaic pumping systems.....	416



DIMSUB: A Decision Support Tool For Design And Pipe Sizing Microirrigation Systems

Palau C.V., Arviza J., Balbastre I, Manzano J.

Dept. of Rural and Agrifood Engineering. Valencian Center for Irrigation Studies.
Camino de Vera s/n, 46022. Universitat Politècnica de València, Valencia, Spain
virpaes@afg.upv.es

ABSTRACT

DIMSUB is a computer program for efficiently design microirrigation systems. It was developed in Visual Basic for Applications for Excel environments and allows specific step-by-step functions for the design of irrigation subunits. Different alternatives can be considered, such as types of emitter, lateral and submain pipe sizes, irregular subunit shapes and terrain slopes. Moreover, lengths of run of lateral and submain pipes, position of the hydrant connection, head pressure and pipe head losses or pressure-compensating emitters can be assigned to evaluate the results and choose the best design alternative.

Examples of practical cases under specific crop conditions for the design of drip irrigation subunits in citrus and almond orchards in Valencia (Spain) are given using DIMSUB. Specific uniformity criteria need to be considered to achieve efficient water applications.

This user-friendly tool for the study of hydraulic variables is expected to be a valuable aid for decision making in irrigation system design.

Keywords: Microirrigation Design, Subunit, Emission Uniformity, Dripper.

INTRODUCTION

The change to pressure irrigation systems, efficiently controlled and supplied, requires the systems to be appropriately designed. Development of tools for the optimal design of hydraulic systems makes it possible for technicians and engineers to give answers and solutions to individual cases.

In microirrigation, the subunit is the set of lateral pipes connected to a manifold and controlled by a manual or automatic pressure-regulating valve. The correct design of the subunit is essential to give the correct quantity of water and fertilizer to the crops and distributed equally throughout the entire area. If water and nutrients are not uniformly applied, parts of the orchard may give reduced yields, while the yields in others will not be any higher and energy costs and water losses through filtration will rise (Holzapfel et al., 2009, Carrión et al., 2014).



The design of irrigation subunits involves the correct selection and sizing of all the components in the system, especially the type of emitter, lateral and manifold pipes, considering their technical characteristics. The uniformity of the supply will be affected by a combination of a number of design parameters that influence the pressure and flow rate at the dripper, and also the pressure variation permitted in the system (Wu I.P. 1997; Pereira et al. 2002). The relationship between the emitter flow rate and pressure is established by emitter hydraulic characteristic:

$$q = k_e \cdot H^x \quad (\text{Eq.1})$$

where q = emitter flow rate (l h^{-1}); H = pressure head (mwc); k_e = emitter discharge coefficient; x = exponent of discharge, close to 0 in pressure-compensating (PC) emitters and around 0.5 in non-pressure compensating (NPC) emitters.

The hydraulic principles involved in designing subunits are based on the fundamental conservation of energy and on the continuity equation. The evolution of the pressure in manifolds and laterals is mainly due to the slope and head losses in pipelines.

Friction head losses are estimated by the Darcy-Weisbach Equation, which for turbulent flows and smooth pipes is introduced with the modified Blasius empirical formula with $f = 0.302/\text{Re}^{0.25}$ (Re = Reynolds number). For the specific case of a head losses in a discrete flow distribution throughout a multioutlet lateral or manifold, the reduction coefficient F or Christiansen's factor is considered.

Correct and precise design requires complex calculation procedures (Lamm et al.2006; Hoffman et al.2007; Ravindra et al., 2008). Given the complexity of the design of the microirrigation subunit, in many cases sizing has been over-simplified at the expense of precision and oversizing subunits. In many cases, even at the present time, many engineers use the tables supplied by the manufacturers to determine the maximum lateral lengths and neglect to calculate the size of the manifold or the required initial pressure of the subunit.

This paper describes DIMSUB computer tool by means of actual case studies that include all the necessary variables required for the design of irrigation subunits in different types of terrain. The application treats the information introduced, extracts the hydraulic parameters of the subunits by step-by-step calculation functions for the design of the subunits to achieve uniform irrigation and helps in deciding the best design solution.

MICROIRRIGATION OPTIMUM DESIGN USING DIMSUB

DIMSUB (Arviza, 2016) is a computer program for the design of microirrigation subunits on Microsoft Excel, universally commercial software, by developing a series of user forms on Visual Basic for Applications.



Information obtained from the field and from irrigation manufacturers such as slope, terrain geometry, type of irrigation emitter (nominal flow rate and pressure regulation), lateral diameter and spacing used is required. Optimal micro-irrigation system design can be obtained by situating different feeding points and determining the length and diameter of laterals and manifolds. It can also be used to estimate the initial pressure and flow rate of a subunit to keep the energy requirements as low as possible.

In order to demonstrate the DIMSUB program's versatility and ease of use, two case studies are described and carried out in a citrus and an almond orchard in Valencia (Spain) (Figure 1).

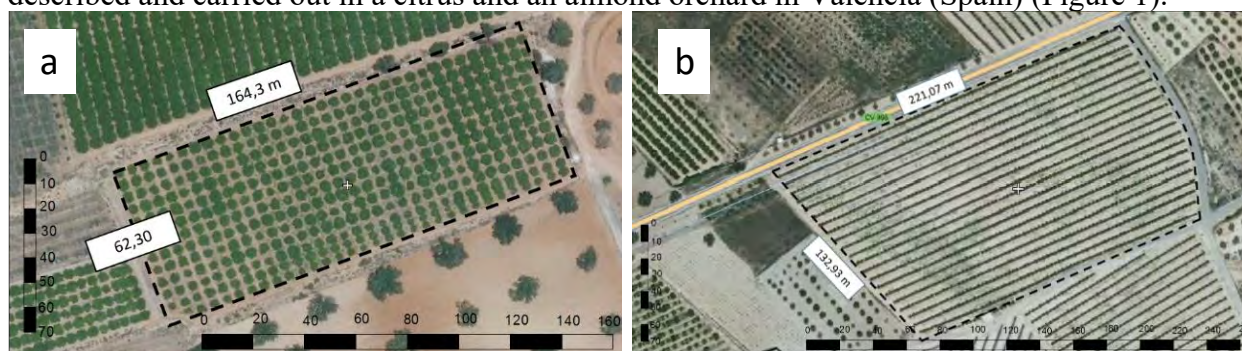


Figure 1. Real case studies. a) Regular citrus orchard in Picassent; b) Irregular geometry of almond orchard in Chulilla (Valencia, Spain).

Citrus case study

This citrus orchard in Picassent (Lat. 39° 22' 30.3''N, Long. 0° 30' 02.52''W, altitude 82.3 m), Valencia (Spain) covers an area of approximately 1.4 hectares with a rectangular geometry of 164.3 x 62.3 m, with laterals of similar length, as seen in Figure 1a.

For this design example, a commercial dripperline with outside diameter (OD) of 16 mm (Internal diameter, ID = 14.2 mm) and 3.5 l h⁻¹ emitters are used (coefficient of variation, CV <7%). Emitter spacing is 1m with double lateral per row. The laterals are on a downhill slope of -1% and the manifold is on the level (0% slope). The insertion of each dripper adds an equivalent length of 0.25 m to consider minor head losses.

Some alternatives were considered for the analysis with different emitter types and feeding points to analyze the operating mode of the DIMSUB application, as seen in Table 1.



CIGR 2018

XIX. World Congress of CIGR



Table 1. Study of various alternatives for the design of subunits.

Case studies	IRRIGATION EMITTER TYPE	Laterals Layout	Manifold Layout	Manifold pipeline size
PC 1	Pressure-compensating emitter	Extrem feeding point	Extrem feeding point	Single-pipe
PC 2	Pressure-compensating emitter	Extrem feeding point	Extrem feeding point	Two-diameters pipe
PC 3	Pressure-compensating emitter	Extrem feeding point	Paired Manifold in flat	Single-pipe size
PC 4	Pressure-compensating emitter	Extrem feeding point	Paired Manifold in flat	Two-diameters pipe
NPC 1	Non-pressure compensating emitter ($x=0,46$)	Extrem feeding point	Extrem feeding point	Single-pipe size
NPC 2	Non-pressure compensating emitter ($x=0,46$)	Extrem feeding point	Extrem feeding point	Two-diameters pipe
NPC 3	Non-pressure compensating emitter ($x=0,46$)	Extrem feeding point	Paired Manifold in flat	Single-pipe size
NPC 4	Non-pressure compensating emitter ($x=0,46$)	Paired Manifold with slope	Paired Manifold in flat	Two-diameters pipe

The first four alternatives use a pressure-compensating (PC) emitters to achieve wider pressure variations (from 5 to 40 mwc), since the emitter flow rate is always close to the nominal flow rate. For this reason, engineers can determine the subunit's permissible head pressure variation by considering the plot characteristics.

The last four alternatives include non-pressure compensating (NPC) emitters, whose flow rate and uniformity depends on the operating pressure taking into account emitter hydraulic characteristic (Eq.1).

The program allows hydraulic variables to be selected and calculated from different feeding points in either the manifold or lateral pipes, as shown in Figure 2. It can be seen that the manifold and laterals can be fed from the extreme point, from a mid-point in flat terrains with no slope, or from an intermediate point in pipes with certain slope. In this latter case, DIMSUB calculates the required uphill and downhill pipe lengths to balance the pressures in all the emitters.

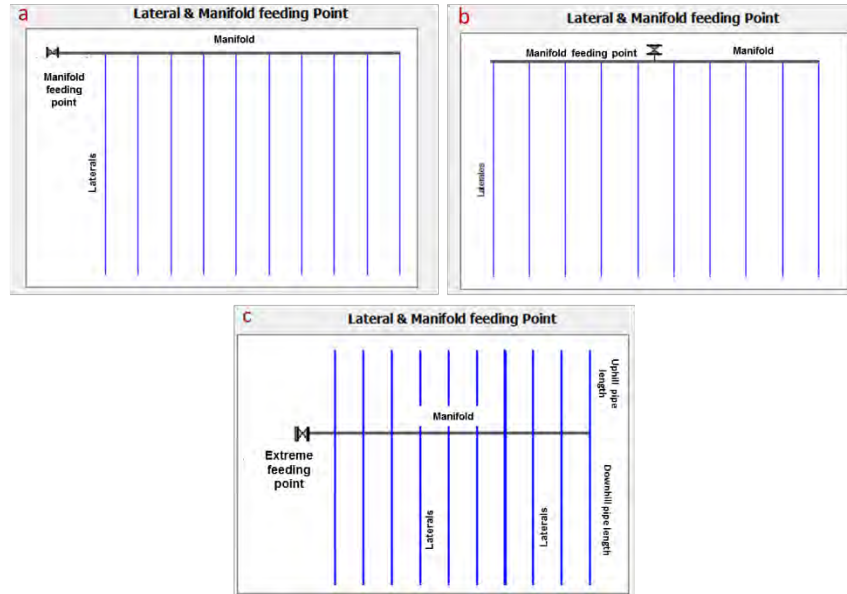


Figure 2. Subunit feeding points: a) Laterals and manifold fed from an extreme point; b) Laterals fed from extreme point and manifold fed from mid-point; c) Laterals fed from intermediate point and manifold fed from extreme point.

To begin the study of alternatives with pressure-compensating emitters, a tentative 5 mwc pressure variation is selected as the technical criteria, considering the plot characteristics in the Picassent orchard, with negligible slope and short laterals and manifolds. As shown in Figure 3, section Regulated Emitter, the minimum operating pressure is 10 mwc and maximum 15 mwc.

Figure 3 shows the data entered for the first alternative, for which the program provides the hydraulic results for the irrigation lateral in box 1, including initial flow rate, head losses, required initial pressure and pressure variation. Box 2 provides the lateral's main variables such as number of emitters, lateral slope and minor loss coefficient of the emitters.

The next step is to enter the parameters required for the design and sizing of the manifold. The size of the manifold pipe depends on the remaining maximum head losses after designing the laterals, as can be seen in the following equations (Keller and Bliesner, 1990):

$$\Delta H_{subunit} = \Delta H_{lateral} + \Delta H_{manifold} = h_{lateral} + \Delta z_{lateral} + h_{manifold} + \Delta z_{manifold} \quad (\text{Eq. 2})$$

$$h_{max\ manifold} = \Delta H_{subunit} - \Delta H_{lateral} - \Delta z_{manifold} \quad (\text{Eq. 3})$$

where ΔH =maximum pressure head variation in subunit, lateral or manifold, respectively (mwc); $h_{max\ manifold}$ =maximum pressure head loss in manifold (mwc); Δz = elevation difference (m).

The maximum head pressure variation established for subunit ($\Delta H_{subunit}$) is then shared between the lateral and manifold head losses and slopes (Eq. 2).



CIGR 2018

XIX. World Congress of CIGR



The screenshot displays the DIMSUB software interface, titled "Designing and Sizing of Drip Irrigation Subunits". It is divided into several sections for data entry and results:

- Lateral Data:** Includes Subunit (1), Sector (1), and Elevation (82.3). It features dropdowns for Lateral Layout (Extreme feeding point, Flat Paired laterals), Emitter Regulation (Non Regulated, Auto Regulated), and Manifold Material (PVC, Polyethylene LD, Polyethylene HD).
- Regulated Emitter:** Fields for Minimum Pressure (10 m), Maximum Pressure (15 m), and Emitter & lateral cost (0.55 €/m).
- Lateral calculation Variables:** A table with values for Maximum Pressure Variation (5 m), Number of Emitters (62), Lateral Slope (-1.8 m), Maximum Head losses (6.8 m), Minor Losses coefficient (1.25), Blasius C coefficient (0.466), and Blasius M coefficient (1.567E-06).
- Manifold Sizing Parameters:** A table with values for Maximum Pressure Variation (6.24 mca), Flow Rate per Lateral (217 l/h), Manifold length (164.4 m), Christensen Coefficient (0.365), Manifold Slope (0 m), Maximum Head losses (6.24 m), Manifold Flow Rate (12152 l/h), and Minimum Inside Diameter (44.7 mm).
- Manifold Data:** Includes Manifold Layout (Extreme Feeding point, Flat Paired Manifold), Lateral Layout per plant (Single Lateral per row, Double Lateral per row), Manifold type (Double Diameter Pipe), and Manifold Data (Minor Losses coefficient: 1.1, Rows of plants in Manifold: 28, Initial Distance (L0): 1.4 m, Same Row Lateral Spacing (L1): 1 m, Next Row Lateral Spacing (L2): 5 m, Manifold Slope: 0 %).
- Manifold Results:** A table with values for Inside Diameter (46.8 mm), Nominal Diameter (50 mm), Beta Coefficient (1), Manifold Head Losses (5.04 m), Initial Required Pressure (16.3 m), Final Extreme Pressure (11.2 m), and Pressure Variation in Manifold (5.21 m).
- Lateral Results:** A table with values for Initial Flow Rate (217 l/h), Christensen coefficient (0.372), Lateral Head losses (0.55 mca), Pressure Variation (-1.24 mca), Beta coefficient (1), Alpha coefficient (1), Required Initial Pressure (11.24 mca), Final Extreme Pressure (12.49 mca), Minimum Pressure (10 mca), and Uniformity coefficient (96.9 %).

On the right side, there are buttons for "Copy Results in Sheet", "Subunit Picture", "Summary Results", "Print Sheet", "Export Results", "Load Data", "Save Data", and "Quit Form".

Figure 3. DIMSUB display to introduce hydraulic data.

Following step is to enter the manifold data (box 3 in Fig.3), including: slope of the terrain, number of plant rows, distance between laterals in the rows and laterals of adjacent rows, to estimate the length of the manifold.

From the admissible head pressure variation in the subunit and lateral, DIMSUB calculates the parameters required to design the manifold piping (box 4): maximum pressure variation and maximum head loss remained for the manifold (Eq. 3), flow rate per lateral, total length and slope. Minimum pipe diameter required to stay within maximum admissible head loss is calculated. Finally, box 5 in Figure 3 shows the results obtained for the manifold pipe: nominal pipe diameter, internal diameter, real head losses, required initial pressure, final pressure and pressure variation in the manifold.

The procedure is able to efficiently analyze different solutions for a given irrigation system and makes it easy to choose the best pricewise and technical alternative. It can be clearly seen that with these subunit conditions, NPC emitters offer better hydraulic and economic conditions. Lower initial subunit pressure is required (between 10.9 and 12.1 mwc), while the cost of laterals and emitters is considerably lower Table 2 and Table 3.



CIGR 2018

XIX. World Congress of CIGR



Table 2. Results of hydraulic analysis of alternatives.

Case studies	Maximum $\Delta H_{\text{subunit}}$ (mwc)	Flow rate (l/h)	Required pressure head (mwc)	Total laterals length L (m)	Manifold D1/D2 (mm)	Manifold L1/L2 (m)
PC 1	5	14322	13,46	4216	63	162.4
PC 2	5	14322	17,4	4216	63 / 50	6.4 / 156
PC 3	5	14322	14,5	4216	40	162.4
PC 4	5	14322	17,5	4216	40/32	2 x (31.4/51)
NPC 1	2.17	14322	11.1	4216	63	162.4
NPC 2	2.17	14322	10.9	4216	63/50	66.4/96
NPC 3	2.17	14322	11.9	4216	40	162.4
NPC 4	2.17	14322	12.1	4216	40/32	2 x (66.4/16)

Table 3. Costs of alternatives studied.

Case studies	Emitters & Laterals cost ¹ (€)	Manifold pipe cost ² (€)	Subunit cost (€)
PC1	2250.60	318.30	2568.90
PC2	2250.60	220.02	2470.62
PC3	2318.80	133.49	2452.29
PC4	2318.80	199.92	2448.72
NPC1	900.24	318.30	1218.54
NPC2	900.24	257.82	1158.06
NPC3	900.24	133.49	1033.73
NPC4	900.24	132.37	1332.61

¹Cost of pipe with non-pressure-compensating emitter is €0.22/m and €0.55/m for pressure-compensating emitter.

²Cost of PVC manifold before installation: OD40 €1.62/m (PN 1.0 MPa), OD50 €1.33/m (PN 0.6 MPa), OD63 €1.96/m (PN 0.6 MPa) and OD75 €2.67/m (PN 0.6 MPa).

Almond orchard case study

This orchard is in Chulilla, Valencia (Spain) (Lat. 39° 40' 02.81''N, Long. 0° 50' 18.69''W, altitude 383.6.8 m) and covers an irregular area of approximately 2.57 hectares (Figure 1b).

Designing irregular subunit requires a special treatment, which can be carried out by outlining the terrain geometry from an image or orthophoto in DIMSUB. The manifold network is graphically defined in this way as water inlet points to the laterals and the final points of laterals of different lengths (Fig.4).

The study considered a commercial dripperline with outside diameter (OD) of 16 mm with an integral PC emitter discharging 3.5 l/h and considering an equivalent length of 0.25m. Row



CIGR 2018

XIX. World Congress of CIGR



distance is 6 m and distance between trees is 1 m. Emitter spacing is 1 m and with a double lateral per plant row. Uphill slope of 1.4% along the line of almond trees and 2% crosswise from the hydrant. The feeding point was from the extreme in manifold and from an intermediate fed point in laterals (Fig.2c). Permissible head pressure variation was 5 mwc in all the alternatives considered.

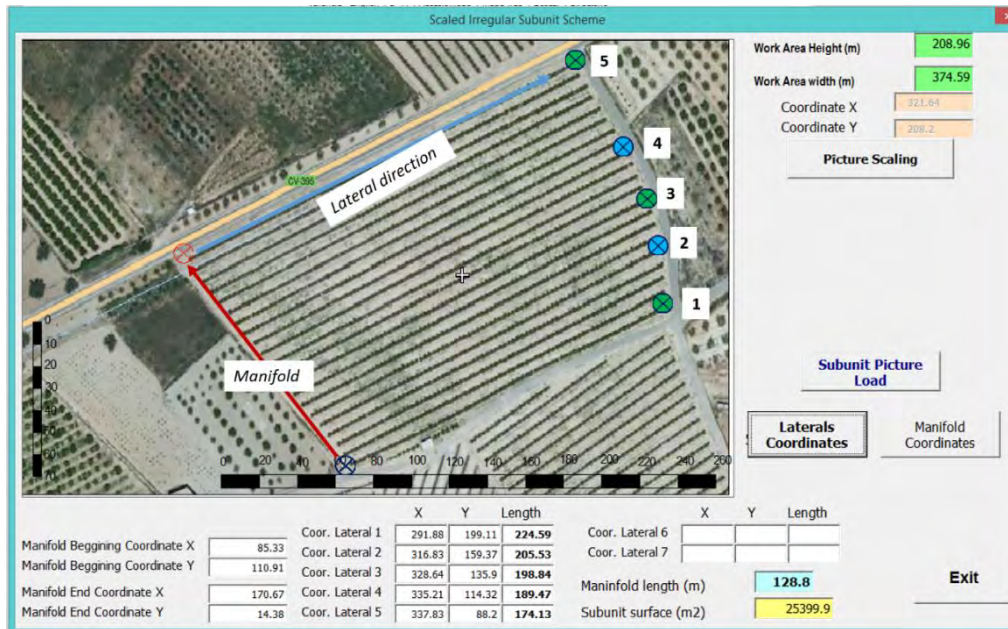


Figure 4. Scaled irregular subunit scheme.

This case of study evaluates the design results adjusting to the real irregular shape (IS) of the subunit and those obtained with a simplified regular plot shape (RS). Additionally, cases IS-2 and RS-2, show the results obtained from DIMSUB tool, adjusting the diameters with a two-diameter tapered manifold.

Table 4. Technical and economical results.

Case studies	Flow rate (l/h)	Required pressure (mwc)	Total laterals length (m)	Manifold D1/D2 (mm)	Manifold L1/L2 (m)	Emitters & Laterals cost (€)	Manifold cost (€)	Subunit cost (€)
Irregular subunit 1 (IS-1)	30631	15.42	8731	75	129.4	4802.05	345.58	5147.63
Irregular subunit 2 (IS-2)	30631	14.95	8731	75 / 63	62.4 / 67	4802.05	298.01	5100,06
Regular subunit 1 (RS-1)	30646	14.85	8734	75	129.4	4803.6	345.58	5149.28
Regular subunit 2 (RS-2)	30646	14.97	8734	75 / 63	44.4 / 85.0	4803.6	285.23	5088.93

¹Cost of pipe with self-compensating emitter is €0.55/m.



CIGR 2018

XIX. World Congress of CIGR



²Cost of PVC manifolds before installation: OD40 €1.62/m (PN 1.0 MPa), OD50 €1.33/m (PN 0.6 MPa) and OD63 €1.96/m (PN 0.6 MPa).

This study shows that adjusting the design to the geometry of the terrain does not improve the design of the subunit, technical parameters and costs are similar in all alternatives.

CONCLUSIONS

DIMSUB is a computer application that can aid in the design and sizing of individual irrigation subunits precisely and rapidly. The lateral and manifold pipes in a subunit can be graphically shown for any type of geometry.

Results obtained with this application have been validated by numerical calculation methods and by real case studies. DIMSUB designs were seen to provide a high degree of accuracy and flow uniformity. In cases with irregular geometries and slopes in either laterals or manifolds or when the optimal feeding point does not coincide with its extreme, this freeware can achieve accurate results to support decision-making.

DIMSUB Spanish version is now being used with satisfactory results by hundreds of engineers involved in microirrigation in Spain and in South America.

REFERENCES

- Arviza, J; Balbastre, I; Palau, C.V. 2016. DimSub, aplicación para el diseño y dimensionado de subunidades de riego localizado. XXXIV Congreso Nacional de Riegos, Sevilla (Spain). (in Spanish)
- Carrión, F; Montero, J; Tarjuelo, J.M; Moreno, M. 2014. Design of Sprinkler Irrigation Subunit of Minimum Cost with Proper Operation. Application at Corn Crop in Spain. Water Resources Management 28 (14): 5073-5089.
- Holzapfel, E.; Pannunzio, A.; Lorite, I.; Oliveira, A.; Farkas, I. 2009. Design and management of irrigation systems. Chilean Journal of Agricultural Research 69:17-25.
- Hoffman G.J; Evans R.G; Marvin E.J; Derrel L.M; Elliott R.L. (eds). (2007) Design and Operation of Farm Irrigation Systems (2nd edition). American Society of Agricultural and Biological Engineers (ASABE).
- Keller, J; Bliesner, R. D. 1990. Sprinkle and trickle irrigation, Van Nostrand Reinhold, New York, USA.
- Lamm F.R; Ayars J.E and Nakayama F.S. (2006). Microirrigation for Crop Production: Design, Operation, and Management. Ed Elsevier.



CIGR 2018

XIX. World Congress of CIGR



Pedras C.M.G; Pereira L.S; Gonçalves J.M. (2009). MIRRIG: a decision support system for design and evaluation of microirrigation systems. *Agricultural Water Management*, vol. 96, pp. 691-701

Pereira L.S; Oweis T; Zairi A. (2002). Irrigation management under water scarcity. *Agricultural Water Management*, vol. 57, pp. 175-206

Ravindra, V.K; Singh, R.P; Mahar, P.S. 2008. Optimal design of pressurized irrigation subunit. *Journal of Irrigation and Drainage Engineering* 134 (2):137-146.

Wu I.P. (1997). An assessment of hydraulic design of micro-irrigation systems. *Agricultural Water Management*. vol 32 (3), pp. 275-284



Multioutlet Hydrants Typology for Collective Irrigation Networks

Balbastre Peralta I., Arviza Valverde J., Manzano Juarez J., Palau Estevan C.V.
Dept. of Rural and Agrifood Engineering. Universitat Politècnica de València
Edificio 3C. Camino de Vera s/n. 46022. Valencia, Spain.
ibbalpe@agf.upv.es

ABSTRACT

Collective irrigation networks use multioutlet hydrants to deliver water to each farmer or plot. This type of hydrants allow to group elements in order to improve the management, automation and control of hydraulic variables. Although the standard EN 14267:2004 establish general definitions, the multioutlet hydrants are not deeply considered and does not exist specific methods of design and configuration. This study proposes a classification that allows to organize these devices according to their configuration and the position of the water meter. This recommended classification is a first step to improve design and management of this type of hydrants.

Keywords: Pressurized irrigation networks, multioutlet hydrant, water meter.

INTRODUCTION AND OBJECTIVES

A rational and correct usage of water resources in pressurized irrigation systems demands certain infrastructures to supply the required volumes of water from the upstream reservoirs to the plant. The pressurized irrigation systems, whether at collective or smallholding level, permit a high degree of control over the water applied, and guarantee a high rate of application efficiency.

In the Mediterranean region, the production model is based on intensive farming of small and medium-sized plots of land (medium surface less than 0.5 ha). Commonly, collective irrigation networks use multioutlet hydrants to join the net to the field. Each singular outlet serve a farmer or plot. This irrigation facility permit to group elements together for water measuring, cutting off, automation, and pressure regulation of each user. Consequently, improves the management and control of hydraulic variables.

These multioutlet hydrants are critical points of the irrigation system. The correct operation of these hydraulic facilities guarantees appropriate pressure and flow to microirrigation systems. Thus, they are essential to the management and control of the network. Actually, multioutlet hydrants permit automatically organise collective irrigation systems and register farmer's water consumptions. Consequently, this hydraulic assembly needs to be properly design, characterise and model.

The standard EN 14267:2004. Irrigation techniques-Irrigation hydrants defines a hydrant as an integrated valve system designed to ensure the supply of irrigation water to a community network from a pressurized water distribution system, that is usually located underground. A main pipe that composes the hydrant where one or more output connections are assembled, it is characterized by the diameter of the main pipe and the diameters of the output connections and



includes at least the functions of supply, cut and measurement of flow rate, and can also incorporate the functions of flow and pressure regulation.

Therefore, a multioutlet irrigation hydrant is the result of a grouping of outlets connected to the network at a point. They are usually locked in a prefabricated concrete construction, where both the control, automation and measurement elements are settled.

Even though, the location and opening sequence of the multioutlet hydrant has been well analysed, under energy and hydraulic criteria (Villa and Garcia, 2012, Jimenez Bello et al., 2015), the specific design and the hydrant configuration is not properly defined. Although the standard EN 14267 establish that the hydrants can have several outlets, it does not clarify the specifications and dispositions of pipes and complementary elements. Moreover, it has been verified that a bad configuration can cause serious problems of operation.

The aim of this study is to establish a classification that allow to organize these devices according to their configuration and the position of the water meter. Moreover, it is possible to identify the advantages and disadvantage of each defined typology. Once this classification is defined, it will be the starting point to:

- Analysing operation current state: compiling the problems that are currently under each configuration.
- Analysing technical standards that characterise this type of hydrants (EN 14267) in order to decide its adaptation to multioutlet ones
- Proposing hydraulic characterization tests for evaluating correct configurations and operations.
- Developing technical design specifications and management procedures.
- Establishing the methodology for variable analysis of multioutlet hydrants to validate hydraulic performance before installation.

MATERIALS AND METHODS

Definitions set.

Previously it is needed to introduce a series of definitions that allow to unify the nomenclature for defining the type and characteristics of the hydrant.

NDB or ND (Nominal Diameter or Nominal hydrant size): Nominal hydrant size, equal to the inlet pipe Nominal Diameter and general elements settled in this pipe.

NDP (Nominal output): Nominal diameter of the output pipe. In a multioutlet hydrant, it may be several NDP, depending on each output pipe.

OHN (Outputs hydrant number): Total number of outputs installed in the hydrant.

ON_{NDP} (Outputs number for each NDP): Total number of outputs installed for each NDP.

NFRB: Nominal flow rate of the inlet pipe and the general elements, choosing the most restrictive of all this elements.

NFRP: Nominal flow rate of outputs pipes, setting a numerical index according to the particular output considered (NFRP1: Nominal flow rate for output 1).

$$NFRB = \sum_{i=0}^{OHN} NFRP_i$$

Δh (head loss): Energy losses, for each flow rate.

Δh_N (Nominal head loss): Energy losses for the nominal flow rate.



WUA: Water use association.

Hydrant classification (Based on EN 14267 standard)

Output number

According to the number of outputs installed, it is establish the general classification:

Individual: Those that are only able to supply a plot or have a single outlet.

Multiuser: Those that have capacity to supply several plots or have more than one outlet.

By function

Four typologies can be defined:

Type 1: Closure and measurement. $\Delta h = 5$ mca

Type 2: Closure, measurement and flow rate limiter. $\Delta h = 8$ mca

Type 3: Closure, measurement and pressure regulator. $\Delta h = 8$ mca

Type 4: Closure, measuring, pressure regulator and flow rate limiter. $\Delta h = 11$ mca

Where Δh is the total head loss, measured between the upstream connection whit the distribution network and the farmer's network connection (downstream of the hydrant). The value establish for each type is the maximum that the hydrant must not exceed, working at nominal flow rates (NFRB and NFRBs).

By dimensions

The classification of the hydrants by dimensions is based on the NDB, NDP and ON_{NDP} for each type of output. The following table recommend the outputs pipes size (DNB) compatible with each NDB, the number and output pipe sizes for each NDB must be related to the maximum supply capacity of the hydrant (NFRB).

Table 1: Compatibility of the type of outputs (NDP) depending on the type of input (NDB).

Output connection nominal diameter (NDP)	Input connection nominal diameter (DNB)				
	65	80	100	150	200
20 (3/4")	X	X	X	X	X
25 (1")	X	X	X	X	X
40 (1" 1/2)	X	X	X	X	X
50 (2")	X	X	X	X	X
65 (2" 1/2)	X	X	X	X	X
80 (3")		X	X	X	X
100 (4")			X	X	X
150 (6")				X	X
200 (8")					X

By nominal pressure

The element that holds the lowest pressure is chosen as the one that its nominal pressure is extended to the hydrant; the standardized values are PN6, PN10, PN16 and PN25.



Data collection from installed hydrants

Through surveys and visits to more than 25 WUA of the Valencian Community (Spain), the morphological classification of multioutlet hydrants is established; also, these surveys are used to collect the operational problems of the different configurations. Therefore, this task is focused to identify next items: irrigation management (from on-demand to rigid scheme), main function issues, improvement proposal, hydrant automation system, maintenance operations, outlets per hydrant and supplied surface, medium plot surface, stolen components, etc.

RESULTS. TYPOLOGY AND MOST COMMON MORPHOLOGY IN MULTIOUTLET HYDRANTS.

The hydrants are classified according to the position of the water meter. Thus is it possible to distinguish two large HORIZONTAL and VERTICAL types. Within these categories, the most used configurations at present can be grouped. Then, advantages and disadvantages of their use can be identified. On other hand, the main issues detected are related with insufficient pressure, malfunction of flowmeters, filter clogging, failures of electrovalve opening, deficient material quality, leaks, poor maintenance, inadequate hydrant emplacement, incorrect selection of dimension and pipe sizes, and finally, theft and vandalism.

Table 2: Typology and morphology vertical type V1.

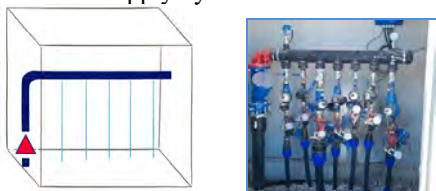
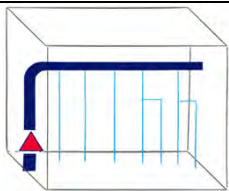
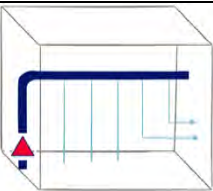
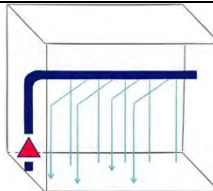
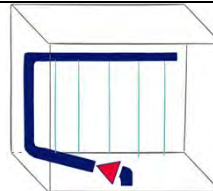
VERTICALS				
Type	V1 Vertical water meter Supply by the extreme 		<u>Advantages:</u> Simple configuration It occupies little surface Direct reading of the water meters <u>Disadvantages:</u> Vertical water meter Little space for maintenance Strainer filter in wrong position.	
Subtype	V1-1	V1-2	V1-3	V1-4
Differential characteristics	Common elements for several outlet	Unburied outlets	Excessive outlets. Addition of horizontal outlets	Horizontal common elements
Scheme				



Photo			
-------	--	--	--

Table 3: Typology and morphology vertical type V2.

VERTICALS				
Type	<p style="text-align: center;">V2 Vertical water meter Supply by the midpoint</p> <div style="display: flex; align-items: center;"> </div>		<p><u>Advantages:</u> Simple configuration It occupies little surface. Direct reading of the water meters The centred water feeding facilitates the distribution of pressures and flows. smaller diameter of the collector pipe</p> <p><u>Disadvantages:</u> Vertical water meter Little space for maintenance Strainer filter in wrong position.</p>	
Subtype	V2-1	V2-2	V2-3	V2-4
Differential characteristics	Common elements for several outlet	Common elements for several outlet. Addition of horizontal outlets	Excessive outlets. Addition of horizontal outlets	Horizontal common elements
Scheme				
Photo				



Table 4: Typology and morphology horizontal type H1.

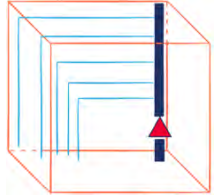
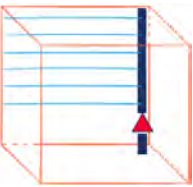
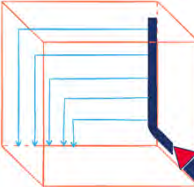
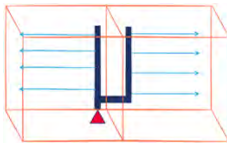
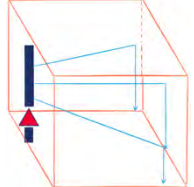



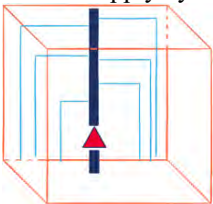

HORIZONTALS				
Type	H1 Horizontal water meter Supply by the extreme 		<u>Advantages:</u> Water meter horizontal. More space for maintenance. Easy anchoring of wall outlets. <u>Disadvantages:</u> Strainer filter in wrong position. More surface occupied Indirect reading of the water meters. Lower number of outlets per hydrant.	
Subtype	H1-1	H1-2	H1-3	H1-4
Differential characteristics	Unburied outlets	Horizontal common elements	Unburied outlets, con doble colector	Outlets in angle
Scheme				
Photo				

Table 5: Typology and morphology horizontal type H2.

HORIZONTALS				
Type	H2 Horizontal water meter Supply by the midpoint  		<u>Advantages:</u> Water meter horizontal. More space for maintenance. Easy anchoring of wall outlets. The centered water feeding facilitates the distribution of pressures and flows. Smaller diameter of the collector pipe. <u>Disadvantages:</u> More surface occupied	
Subtype	H2-1	H2-2	H2-3	H2-4
Differential characteristics	Unburied outlets	Horizontal common elements	Horizontal common elements. Unburied outlets	Horizontal common elements. 90° elbow needed. Water



Subtype	H2-1	H2-2	H2-3	H2-4
				meter on horizontal pipes.
Scheme				
Photo				

Table 6: Typology and morphology horizontal type H3.

HORIZONTALS				
Type	H3 Horizontal water meter		<i>Advantages:</i> Horizontal water meter All elements in horizontal position Less enclosure height <i>Disadvantages:</i> Less number of outlets per hydrant. Access and maintenance problems.	
Subtype	H3-1	H3-2	H3-3	H3-4
Differential characteristics	Access from the top, little occupation space, little surface occupied	Common elements in lateral position. On valve-box	Common elements in lateral position. On valve- house	Several outlet levels.
Scheme				
Photo				



Example of classification, designation and marking of hydrants.

In order to unify and propose the hydrant identification, unifying the main characteristics of it, both dimensional and functional, is showed an example of classification. It is proposed that the following characteristics appear in the marking and designation.

Morphological code of the configuration according to the arrangement of the general elements and water meters. (Previous sections)

Function.

Number of Outputs. ONH.

Nominal diameter in mm of the general elements NDB.

Nominal flow of the hydrant in m³/h. NFRB

Nominal diameter in mm of the outputs. Referring to the ND of the water measuring element installed in the intake or outlet. NDP.

Number of outputs of each ND. ONNDP.

Nominal pressure in bars. Chosen from the element with lower pressure of the set of hydrant elements. NP.

The following table shows all the parameters indicated in the previous list applied in an example.

Table 7: Example data nomenclature for the hydrant of the figure 3.

V1					
Function		Type 3			
OHN		7			
Dimensions					
NDB		100			
NFRB		112			
Output	NDP	25	40	50	80
	ONNDP	2	3	1	1
Presure (bar)		6		Pressure gauge	

The designation of the hydrant according to the classification described above will be:

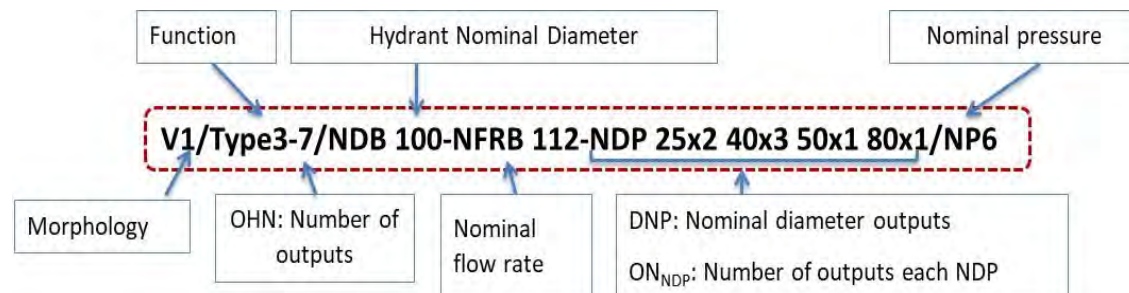


Figure 2: Designation of the hydrant example



Figure 3: Detail of the hydrant example

DISCUSSION AND CONCLUSION

In view of the proposed classification, it is checked that many of the configurations installed do not meet the minimum dimensional or operational requirements for hydrants, or at least the objectives set out in their installation. Therefore, it is essential to know which configurations are valid and which are deficient. The classification it is only a first step, in order clarify the goodness of each typology.

The current standard is designed mainly to individual hydrants so it is needed adapt the standard EN 14267:2004 to these configurations. Also is needed to settle valid configurations in hydraulic characterization tests that allow engineers and technicians select the proper type.

In parallel, a method of hydraulic analysis that allows to verify and design configurations of this type of hydrants should be proposed. This method will be used to validate hydrant operation before its installation in the network.

Finally, a design protocol or technical specifications for multioutlet hydrants must be developed that fill this gap in the design of irrigation facilities.

REFERENCES

- AEN/CTN68, 2005. UNE-EN 14267 Irrigation techniques - Irrigation hydrants. 2005. Madrid: AENOR.
- CR Alhama de Murcia 2015. C.R. Alhama de Murcia. [resource on line] <http://www.cralhama.org>.
- Miranda Ivars, M. and Arviza Valverde, J. 2011. Análisis de la problemática actual en el funcionamiento de hidrantes en redes colectivas de riego a presión. Diseño de un hidrante tipo y elaboración de las prescripciones técnicas que deben cumplir los elementos que lo componen.



CD-RO. Valencia: Universidad Politécnica de Valencia.
Jimenez-Bello M.A., Royuela A., Manzano J., Garcia Prats A., Martinez-Alzamora F. 2015. Methodology to improve water and energy use by proper irrigation scheduling in pressurised networks Agricultural Water Management, 149, pp. 91-101.
Villa F.G., Garcia Prats A. 2012. *Using Location-Allocation Algorithms to Distribute Multioutlet Hydrants in Irrigation Networks Design*. Journal of Irrigation and Drainage Engineering Volume 138 Issue 4 - April 2012
MUNASA 2015. Munasa. [resource on line] www.munasa.es.



The Effect of Different Boron Levels on the Yield and Some Physiological Properties of Cotton Plant under Deficit Irrigation Conditions

Berkant ODEMIS¹, Hatice DELICE²

¹Mustafa Kemal University, Faculty of Agriculture, Biosystem Engineering, Hatay, Turkey

²Uludağ University, Faculty of Agriculture, Biosystem Engineering, Bursa, Turkey
bodemisenator@gmail.com

ABSTRACT

The research was carried out in the Amik Plain in 2016 to determine the extent to which the boron fertilizer enhances the floral behavior of the cotton plant. The experiment was planned that each treatment is composed six rows which is 15 m long and designed according to the split-plot design. Carisma variety was used as a plant material.

The crop was exposed to four water regimes, I₀; rainfed (control), I₁₀₀; full irrigation where the soil moisture brought to the field capacity, I₆₆; 66% of full irrigation treatment, I₃₃; %33 of full irrigation treatment.

In the experiment, boron fertilizer was applied by spraying three different doses at intervals of about ten days only during the flowering period. Fertilizer doses were regulated as 75 ppm for B₁, 300 ppm for B₂ and 750 ppm for B₃. Etidot 67 (28% B) (Disodium Octaborate Tetrahydrate) (Na₂B₈O₁₃.4H₂O) was used as the boron fertilizer.

According to the results of the research, 306.5 mm, 612.9 mm and 928.7 mm irrigation water was applied to I₃₃, I₆₆ and I₁₀₀, respectively, during the trial season. Evapotranspiration values range from 1015.1 mm (I₁₀₀B₁) to 216.6 mm (I₀B₀). Stoma conductance values were measured as 574.54, 422.66, 342.54 and 245.06 mm² m² sec⁻¹ for I₁₀₀, I₆₆, I₃₃ and I₀, respectively. Leaf chlorophyll content values were measured as 39.97, 47.52, 51.03, 52.11 µmol m⁻² at irrigation levels (I₁₀₀, I₆₆, I₃₃ and I₀, respectively). The highest yield was obtained from I₆₆B₁ treatment (622.7 kg da⁻¹) while the lowest yield from I₀B₀ treatment. (182.4 kg da⁻¹).

Keywords: Water stress, cotton, chlorophyll content, stomatal conductance, yield, Turkey

INTRODUCTION

In arid and semi-arid areas, agricultural production is largely water dependent. Climatic changes in the last century have led to changes in many climate parameters, especially rainfall. The reduction in rainfall has caused drought in many countries. The long-term average amount of rainfall in our country, which is around 646 mm, declined to 506.6 mm in 2017. Decreased by 15.2% compared to the previous year (2016) (Anonymous, 2018).

Berkant ODEMIS Hatice DELICE>.<'' The Effect of Different Boron Levels on the Yield and Some Physiological Properties of Cotton Plant in Deficit Irrigation Water Conditions''



CIGR 2018

XIX. World Congress of CIGR



In many regions, irrigation possibilities during the growing season are gradually diminishing due to decreased rainfall and storage. This situation increases the importance of cultural practices that will provide resistance to arid conditions in agricultural production.

Generally, studies for drought mitigation, on genetic modification of plants have an important place, but cultural practices such as irrigation and fertilization are also vital.

However, in cases where soil water is limited, the effects of different fertilizers on the drought tolerance of plants; it is important to determine the effects of increasing or decreasing the tolerance.

As it is known, fertilizer management in drought conditions is very complicated. Numerous researches have been done to determine the relationship of fertilization and drought tolerance in recent years (Ma et al., 2004; Garg et al., 2004; Hu et al., 2008).

Boron has been known for a long time as one of the most basic micro elements required for the growth and development of cotton (Oosterhuis, 2001). Physiologically, Boron deficiency adversely affects the rate of stomatal conductance and net photosynthesis, plant growth and dry matter accumulation, and the number of flowers in the flowers.

The aims of this study are to determine the effects of applying different water stress and boron doses on stomatal conductance and chlorophyll content in cotton.

2. MATERIAL and METHOD

The study was carried out in the silty clay loamy soil in the Amik plain which is the most intensive region of cotton cultivation (Table 1) in Hatay Province in 2016. The widely grown variety in the region, *Carisma type cotton plant* was used for the experiment. The split-plot design was used with four irrigation levels, three fertilizers doses and three replications for each treatment.

In the research, irrigation treatments were conducted as I_0 , non-irrigation (control) treatment; I_{100} , full irrigation (to replenish the soil water until field capacity); I_{66} , the treatment of 66% of full irrigation; I_{33} , the treatment of 33% of full irrigation. The drip irrigation system was used in treatment. The first irrigation was applied when 50% of the available capacity was consumed.

Boron was applied by spraying in 3 different doses at intervals of about ten days only during the flowering period. Etidot 67 Disodium Octaborate Tetrahydrate ($\text{Na}_2\text{B}_8\text{O}_{13} \cdot 4\text{H}_2\text{O}$) was used as fertilizer with a content of 20.8%. Boron doses were formed as B_0 , Reference (without boron); B_1 , 75 ppm; B_2 , 300 ppm; B_3 , 750 ppm.

In this study, stomatal conductivity and chlorophyll content were measured in the plant to determine the effects of boron application on plant physiology.

Stomatal conductivity and chlorophyll content were measured one day before irrigation, from 10:00 to 15:00, where the air was not cloudy. The stomatal conductivity was measured by 'DECAGON SC-1 Parameter. Chlorophyll content was measured by SPAD instrument. Measurements were made on 3 plants and 3 leaves in all applications, up to 2 times per leaf. To determine the water consumption of the irrigation levels, soil samples were taken by gravimetric



CIGR 2018

XIX. World Congress of CIGR



methods from all the irrigation levels before each irrigation. The evapotranspiration and water use efficiency (WUE) values of the treatments were determined according to the "Soil Water Budget" method (Eq. 1 and 2).

$$Et=I+R-Dp-R_0\pm\Delta S \quad (1)$$

$$WUE= Y/Et \quad (2)$$

Et: Evapotranspiration (mm), I: Amount of irrigation water (mm), R: Precipitation (mm), Dp: Soil percolation (mm), Ro: Runoff (mm), Y: Yield (kg da⁻¹), Et: Evapotranspiration (mm), $\pm\Delta S$: Difference in soil moisture between the beginning of the season and the end of the season (mm), WUE: Water-use efficiency (kg da mm⁻¹) (Garrity et al., 1982).

Table 1. Soil properties of the trial area

Depth (cm)	Sand (%)	Silt (%)	Clay (%)	Texture	pH	ECe(μmhos cm ⁻¹)
0-30	59.5	15.2	25.2	SiCL	7.5	824
30-60	57.5	19.2	23.2	SiCL	7.6	560
60-90	53.5	17.2	29.2	SiCL	7.8	429
90-120	61.5	15.2	23.2	SiCL	7.6	400

FC: Field capacity, WP: Wilting point, OM: Organic matter, N: Nitrogen

(Continued) Table 1. Soil properties of the trial area

Depth (cm)	CaCO ₃ (%)	N (%)	OM (%)	FC (%)	WP (%)	As (g cm ⁻³)
0-30	2.265	1.42	0.33	21.3	13.4	1.660
30-60	0.680	1.65	0.34	24.1	14.2	1.676
60-90	0.905	2.01	0.38	25	14.5	1.540
90-120	0.300	2.12	0.37	25.2	14.7	1.489

FC: Field capacity, WP: Wilting point, OM: Organic matter, N: Nitrogen

The harvesting area was 13.04 m² for each replication. Statistical analyzes were performed using the Duncan test in the SPSS 18 software.

3.RESULTS

Irrigation Water, Evapotranspiration, Yield and Water Use Efficiency

The amount of precipitation during the experiment was 149.2 mm. A total of 7 irrigation water application was made during the study. In the experiment, 149 mm, 306 mm, 622 mm, 929 mm irrigation water (excluding rainfall) was applied in I₃₃, I₆₆ and I₁₀₀ irrigation treatments, respectively. Evapotranspiration (ET) was increased as the irrigation water amount increased. ET

Berkant ODEMIS Hatice DELICE>.<'' The Effect of Different Boron Levels on the Yield and Some Physiological Properties of Cotton Plant in Deficit Irrigation Water Conditions''



CIGR 2018

XIX. World Congress of CIGR



was determined for I_0 , I_{33} , I_{66} , I_{100} treatments as much as 274 mm, 604 mm, 855 mm, 1045 mm, respectively (Table 2).

Table 2. Irrigation water (I), Evapotranspiration (ET), Yield (Y) and Water use efficiency (WUE) mean values

Boron levels	Irrigation levels	Irrigation water(mm)	ET (mm)	Yield (kg da ⁻¹)	WUE (kg da mm ⁻¹)
B_0	I_0	149	282	182	0.65
	I_{33}	306	533	290	0.54
	I_{66}	622	774	543	0.70
	I_{100}	929	1017	507	0.50
B_1	I_0	149	272	190	0.70
	I_{33}	306	647	370	0.57
	I_{66}	622	882	623	0.71
	I_{100}	929	1115	530	0.47
B_2	I_0	149	264	174	0.66
	I_{33}	306	604	333	0.55
	I_{66}	622	870	506	0.58
	I_{100}	929	1028	517	0.50
B_3	I_0	149	276	197	0.71
	I_{33}	306	633	343	0.54
	I_{66}	622	895	490	0.55
	I_{100}	929	1019	534	0.52

The highest yield was obtained from $I_{66}B_1$ (623 kg da⁻¹) and the lowest yield from I_0B_2 treatment (174 kg da⁻¹). The effect of irrigation level, boron doses and interaction of these on yield was found significant ($p<0.01$), (Table 3). Using the parabolic relation between irrigation water and yield, it was calculated that the highest yield (556 kg) was obtained from irrigation water of 763 mm (Figure 1). A second-order insignificant relationship was determined between boron and yield. The relationship between boron and yield was not significant (Yield= $-9.76x^2+47.37x+350.42$, $R^2=0.27$ ns, $n=4$). The highest yield was obtained from the dose B_1 (428 kg da⁻¹). The yield values of B_0 and B_2 doses were approximately the same (381 and 383 kg da⁻¹). The highest WUE value among irrigation levels was calculated at I_0 irrigation level (0.68 kg da mm⁻¹). For the I_{33} , I_{66} and I_{100} treatments, WUE were 0.55, 0.63 ve 0.50 kg da mm⁻¹ respectively



CIGR 2018

XIX. World Congress of CIGR



(Fig. 3). The calculated WUE values for boron applications are approximately the same. The highest WUE value was calculated for B₁ (0.61 kg da mm⁻¹) and the lowest WUE was calculated for B₂ (0.57 kg da mm⁻¹).

Table 3. Yield variance analysis results

Source	Sd	SS	MS	F
Irrigation Levels	3	1016553.4	338851.1	504.88**
Boron Doses	3	17657.6	5885.8	8.77**
Irrigation L.*Boron Doses	9	25874.7	2874.9	4.28**
Error	47	1081562.3		

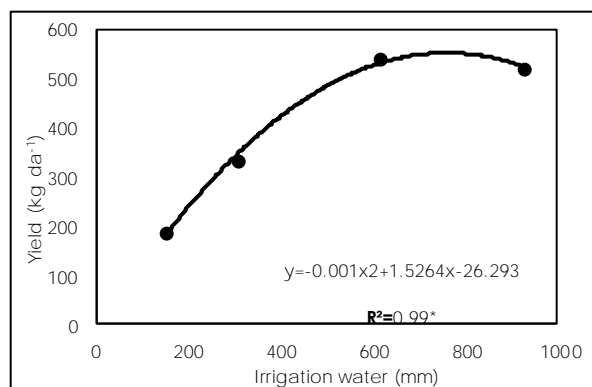


Figure 1. Irrigation water-yield relationship

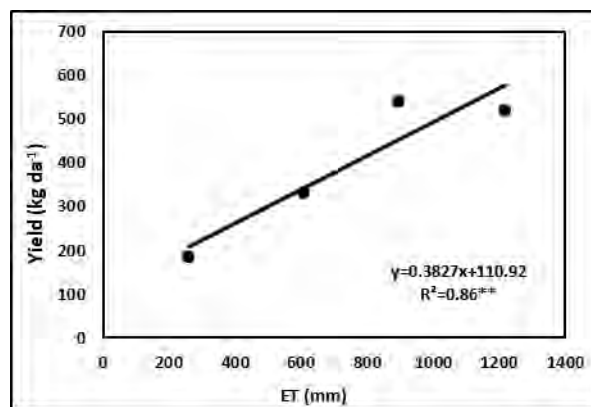


Figure 2. Evapotranspiration - yield relationship

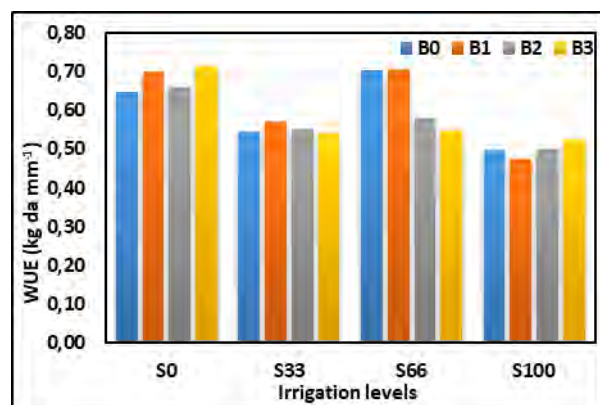


Figure 3. Water use efficiency between irrigation levels

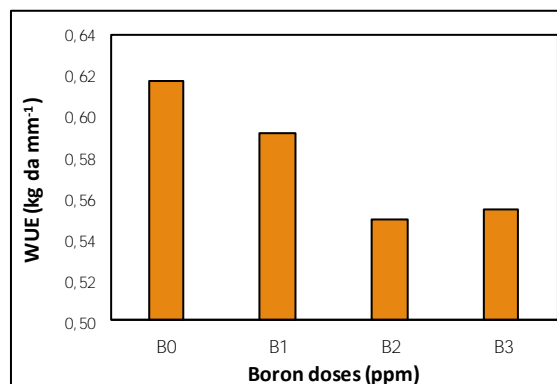


Figure 4. Water use efficiency between boron doses

3.2 Stomatal Conductance

Berkant ODEMIS Hatice DELICE>.<'' The Effect of Different Boron Levels on the Yield and Some Physiological Properties of Cotton Plant in Deficit Irrigation Water Conditions''



CIGR 2018

XIX. World Congress of CIGR



The degree of openness of the stoma is an important criterion of plant water requirement because it is associated with the rate of transpiration. As is known, stomas are sensitive to water stress. High stomatal conductivity indicates that the stomas are open and transpiration is fast. According to the results statistical analysis, the effect of irrigation levels and boron doses on stomatal conductivity was found to be significant ($p < 0.01$). However, the irrigation level and boron doses interaction has not effect on stomatal conductivity. Stomatal conductance mean values were measured as 574.54, 422.66, 342.54 and 245.06 $\text{mmol m}^{-2} \text{sec}^{-1}$ in I_{100} , I_{66} , I_{33} and I_0 , respectively. Stomatal conductivity values of boron doses were determined as 470.45, 364.19, 374.46 and 375.67 $\text{mmol m}^{-2} \text{sec}^{-1}$ in B_0 , B_1 , B_2 and B_3 doses, respectively. Generally, as the amount of irrigation water increased, the stomatal conductivity increased. The highest stomatal conductivity among the boron doses was obtained from the treatment of B_0 . Increasing boron doses (B_1 , B_2 , B_3) were found to cause stress in the plant and reduce stomatal conductivity. The highest stoma conductance among the boron doses was obtained from the B_0I_{100} treatment ($673.77 \mu\text{mol m}^{-2}$). According to the results of the Duncan analysis, B_1 , B_2 and B_3 treatments were in the same statistical group, B_0 treatment was in a different group. Stoma conductivity, yield and evapotranspiration values were performed significant correlations and was found polynomial relationship. Regression analysis showed that stoma conductance increased by 99% in evapotranspiration and by 94% an increase in production.

Table 3. Stomatal conductance variance analysis results

Source	Stomatal Conductance ($\text{mmol m}^{-2} \text{sn}^{-1}$)			
	Sd	SS	MS	F
Irrigation Level	3	2795446.02	931815.34	51.56**
Boron Doses	3	356834.47	118944.82	6.58**
Irrigation L.*Boron Doses	9	60003.91	6667.10	0.360ns
Error	176	3180239.97	18069.54	

Generally, as the amount of irrigation water increases, the stoma conductance increases. Among the boron doses, the highest stomatal conductance was obtained from the reference treatment. It was observed that the applied boron doses reduce the stoma conductance as a cause of stress in the plants. The highest stoma conductance was obtained from the $I_{100}B_0$ ($673.77 \text{ mmol m}^{-2} \text{sn}^{-1}$).

Table 4. Mean values of stomatal conductivity of irrigation levels

Irrigation Levels / Boron Doses	Stomatal Conductivity ($\text{mmol m}^{-2} \text{sn}^{-1}$)	Min.	Max.
I_0	245.02	206.73	283.31
I_{33}	342.54	304.25	380.83

Berkant ODEMIS Hatice DELICE>.<'' The Effect of Different Boron Levels on the Yield and Some Physiological Properties of Cotton Plant in Deficit Irrigation Water Conditions''



CIGR 2018

XIX. World Congress of CIGR



I_{66}	422.66	384.37	460.95
I_{100}	574.54	536.25	612.83
B_0	470.46	432.17	508.76
B_1	364.19	325.90	402.48
B_2	374.46	336.17	412.75
B_3	375.67	337.37	413.96

3.3 Chlorophyll Content

The chlorophyll content of the leaf is one of the physiological parameters that best respond to stress conditions. In the measurements, leaf chlorophyll content was statistically different between irrigation levels ($p < 0.01$). However, boron doses and irrigation level and boron doses interaction were not significant on the leaf chlorophyll content (Table 5). The leaf chlorophyll content values were 39.97, 47.52, 51.03, 52.11 $\mu\text{mol m}^{-2}$ (I_{100} , I_{66} , I_{33} , I_0 , respectively). Leaf chlorophyll content values of boron doses were 47.83, 47.54, 48.54 and 46.69 $\mu\text{mol m}^{-2}$ for B_0 , B_1 , B_2 and B_3 , respectively. In general, chlorophyll content decreased as the amounts of irrigation water increased. According to the results of Duncan analysis, the I_{33} and I_0 were in the same group, while the I_{100} and I_{66} were in different groups. Boron doses were formed in 3 groups (B_1 and B_0 in the same group). The highest chlorophyll content (52.11 $\mu\text{mol m}^{-2}$) was obtained from the I_0 treatment in irrigation treatment (Table 6).

Table 5. Chlorophyll content variance analysis results

Source	Chlorophyll Content ($\mu\text{mol m}^{-2}$)			
	Sd	SS	MS	F
Irrigation Levels	3	5403.869	1801.290	183.68**
Boron Doses	3	104.515	34.838	3.55*
Irrigation L.*Boron Doses	9	136.523	15.169	1.547ns
Error	224	2196.601	9.806	

Table 6. Mean values of chlorophyll contents of irrigation levels and chlorophyll contents

Irrigation Levels/Boron Doses	Chlorophyll Content ($\mu\text{mol m}^{-2}$)	Min.	Max.
I_0	52.11	51.32	52.91
I_{33}	51.00	50.21	51.80
I_{66}	47.52	46.72	48.32
I_{100}	39.98	39.18	40.77
B_0	47.83	47.04	48.63
B_1	47.54	46.75	48.34
B_2	48.54	47.74	49.34

Berkant ODEMIS Hatice DELICE>.<'' The Effect of Different Boron Levels on the Yield and Some Physiological Properties of Cotton Plant in Deficit Irrigation Water Conditions''



CIGR 2018

XIX. World Congress of CIGR



B ₃	46.70	45.90	47.50
----------------	-------	-------	-------

When the time-dependent changes in chlorophyll content were examined, it was determined that the highest values were at different stress levels at different dates. The highest value in I₀ was measured in 3 Ağustos, I₃₃ and I₆₆ on 11 August and I₁₀₀ on 18 August. August 3 was closer to the beginning of flowering; August 11 is a date closer to the middle of flowering. The highest value of water for I₁₀₀ was measured on 21 July (beginning of flowering). For treatment I₁₀₀, the chlorophyll values decreased most rapidly in time. Although it showed a low tendency to increase during the trial period, it was mostly followed by a constant course. Other irrigation levels changed in this range. It was not expected that the chlorophyll values of I₁₀₀ decreased rapidly. This was attributed to the fact that boron is affecting especially the young leaves. The reason that chlorophyll content decreased as evapotranspiration increased is that applied boron caused a stress by dissuasion because stomata were always open in I₁₀₀ treatment. The high levels of boron doses were determinant in evapotranspiration and yield. The effect of chlorophyll content on water consumption and yield was found insignificant. The results showed that spad values couldn't be used to predict the yield.

CONCLUSIONS

Boron, an important micro element as plant nutrient element, increases the flower attitude in plants in conditions where there is no water stress (Anonymous, 2016). In our study, it was observed that boron fertilizer applied at the dose of B₁ caused an increase in yield. The highest yield was obtained from I₆₆B₁ (622.7 kg da⁻¹). According to this, it is possible to save 35% of the irrigation water compared to the full irrigation treatment. However, water use efficiency and evapotranspiration amount decreased due to an increase in boron doses.

In general, as the amount of irrigation water increases, stomatal conductivity increased. Numerous studies showed that the stoma conductance increases at different levels due to different amounts of moisture content in the root zone (Karakaya and Ödemiş, 2015, Delice and Ödemiş, 2017). Decreasing soil moisture, salinity and fertilizer applications causes a decrease in stomatal conductance as soil moisture could not be used effectively (Demirel and Ödemiş, 2016, Fidalgo et al., 2004). Also, stomatal conductance could change significantly depending on cultural application on leaf surface condition. The highest stomatal conductivity in boron doses was obtained from the B₀ treatment. Boron doses (B₁, B₂, B₃) have been shown to cause stress in plants and reduce stomatal conductivity. Kazgöz and Ödemiş (2017) stated that stoma conductivity in the applied sulfur parcels is significantly lower than the control parcel. Ödemiş et al., (2017), stated that irrigation water increased stomatal conductance ($p < 0.01$) but foliar applied sulfur did not. The same results with respect to stomatal conductance were observed also in chlorophyll content. The dose of boron fertilizer applied by spraying caused partial stress in the plant. Generally, as the irrigation level increases, chlorophyll content decreased. As a result, changes in leaf surface conditions cause changes in leaf hydraulic



CIGR 2018

XIX. World Congress of CIGR



properties. In conditions where soil moisture is sufficient, the stomatal conductivity or transpiration rate in the usual course has been subject to stress depending on the dose of the fertilizer applied to the leaf surface. The efficiency increase seen in B1 dose shows that boron manure has an effect on yield, but physiological stresses due to leaf surface closure weaken the availability of physiological parameters in predicting yield.

REFERENCES

- Anonim, 2016. Ulusal Bor Araştırma Enstitüsü El Kitabı, Ankara, 2016.
- Bayrak, H., Önder, M., Gezgin, S., 2005. "Bor Uygulamalarının Nohut (*Cicer arietinum* L.) Çeşitlerinde Verim ve Bazı Verim Unsurlarına Etkileri". S.Ü. Ziraat Fakültesi Dergisi 19 (35): 66-74.
- Bowen, J.E. and Gauch, H.G., 1965. "Essentiality of Boron for *Dryopteris Dentata* and *Selaginella Apoda*" American Fern Journal 55: 67-73.
- Blevins, D.G. and Lukaszewski, K., 1998. Boron in Structure and Function Annual Rev. Plant Physiology Plant Molecular Biology, 49: 481-500.
- Delice, H., Ödemiş, B., 2017. Determination of Effects of Divided Fertilizer in Different Growth Stage on Some Yield Characteristics of Soybean Cultivated Under Water Deficit. ICAFOF, 626-627. Nevşehir/Türkiye.
- Demirel, E., Ödemiş, B., 2016. Determination of vegetative and generative characteristics of different cotton varieties under drought stress. Journal of Infrastructure and Ecology of Rural Areas. 1169-1177.
- Demirtaş, A., 2006. "Bor Bileşikleri ve Tarımda Kullanımı" Atatürk Üniv. Ziraat Fak. Derg.37 (1), 111-115, ISSN: 1300-9036.
- Fidalgo, R., Times, V.C., Silva, J. 2004. Providing multi dimensional and geographical integration based on gdwand meta models. In proceedings of the Brazilian Symposium on Databases. Brasilia, Brazil, pp. 148-162.
- Garrity, P. D., Watts D. G., Sullivan C. Y. and Gilley J. R., 1982. Moisture deficits and grain sorghum performance. Evapotranspiration yield relationships. Agron. J., 74: 815-820.
- Hamurcu, M., Harmankaya, M., Soylu, S., Gökmen, F., Gezgin, S., 2006. Makarnalık Buğdayın (*Triticum durum* L.) Bazı Besin Elementleri Kapsamına Farklı Dozlarda Bor ve Demir Uygulamalarının Etkisi. Süleyman Demirel Üniversitesi Ziraat Fakültesi Dergisi 20(38): 1-8.
- Karakaya, Z., Ödemiş, B., 2015. Doğu Akdeniz İklim Koşullarında Yetiştirilen Bakteri Aşılı ve Aşısız Soyanın Su Verim İlişkilerinin Belirlenmesi. I. Ulusal Biyosistem Mühendisliği Kongresi, Bursa.
- Ödemiş, B., Akışcan, Y., Akgöl, B., Can, D., 2017. Kısıtlı su koşullarında yapraktan uygulanan kükürt dozlarının pamuk bitkisinin kuraklık toleransına etkileri. 214O254 numaralı Tübitak Projesi.
- Punchana, S., Jamjod, S. and Rerkasem, B., 2004. Response to Boron Toxicity in Boron Efficient and Inefficient Wheat Genotypes 4. Int. Crop Sci. Cong., Sept., Brisbane, Australia.



Different Tillage under Semi-Arid Mediterranean Conditions: Some Physical Soil Quality Indicators and Their Relations

Zeliha B. BARUT ^{1,*}, M.Murat Turgut ² . Ismail ÇELİK ³

¹ Çukurova Un., Fac. of Agriculture, Dept. of Agr. Mach. and Tech.Eng., Turkey

² Dicle Un., Fac. of Agriculture, Dept. of Agr. Mach. and Tech.Eng., Turkey

³ Çukurova Un., Fac. of Agriculture, Department of Soil Science, Turkey

* Corresponding author. Email: zbbarut@cu.edu.tr

ABSTRACT

Saturated hydraulic conductivity (HC), soil bulk density (BD), aggregation index (AI) and penetration resistance (PR), and relationship between them based on six tillage practices were evaluated under semi-arid Mediterranean conditions. The experiment was conducted on a randomized complete block design with three replicates. The tillage methods were: conventional tillage with residue incorporated (CTS), conventional tillage with residue burned (CTB), reduced tillage with heavy tandem disc harrow (RTD), reduced tillage with rotary tiller (RTR), reduced tillage with heavy tandem disc harrow for the first crop + no-tillage for the second crop (RNT), and no tillage (NT). The study was conducted in wheat-corn-wheat-soybean crop rotations for two years. At the end of the study, the effect of tillage systems on BD, HC, AS and PR was statistically different ($P < 0.05$) while it was no significant at the beginning of the experiment for 0-30 cm soil depth. The hydraulic conductivity was higher ($9.79 \times 10^{-6} \text{ m sn}^{-1}$) in CTS, and followed by CTB, RTR, RTD, RNT and NT practices, respectively. However, the AI, BD and PR values were higher (0.46 mm, 1.41 gr cm^{-3} and 2.15 MPa , respectively) in NT than the other plots. The relationship between HC with PR is better than the other soil properties with the highest coefficient of determination of 0.98 and inverse linear. But, there are a linear relationship between BD and AI with PR.

Keywords: Soil bulk density, hydraulic conductivity, penetration resistance; aggregation index, tillage, Turkey.

INTRODUCTION

Soil quality indicators can be used to evaluate sustainability of land use and soil management practices in agro ecosystems. Soil quality indicators can be defined as the soil processes and properties that are sensitive to changes in soil functions (Doran and Jones 1996). Karlen (2004) also expresses that soil quality assessment is simply a tool focused on dynamic soil properties and processes that are useful for assessing the



CIGR 2018

XIX. World Congress of CIGR



sustainability of soil management practices. Etchevers et al. (2000) also recommended that the indicators such as soil organic matter, penetration resistance, infiltration capacity, soil aggregation, pH, bulk density and soil salinity can be used in evaluating soil quality. Tillage systems have been compared in terms of soil quality and environment in a great deal of research.

Penetrometer resistance and bulk density are used as critical indicators of soil compaction. Plant roots are affected negatively by soil layer with high mechanic resistance. Increment in soil mechanic resistance decreases rate of root elongation and penetration of the roots into the soil. Besides, higher penetrometer resistance values also reflect a higher compaction level, which can produce adverse effects like a decrease in crop growth (Barut and Akbolat, 2005). Soil compaction is an increase in the density of soil and reduction in porosity, associated with an increase in strength and a reduction in hydraulic conductivity. Soil compaction causes problems including poor aeration, drainage, excessive runoff and erosion. Heavy field traffic in conventional tillage system is one of the great effects of soil compaction. Soil bulk density is usually included in minimum data sets used to evaluate tillage effects on soil quality (Logsdon and Karlen, 2004). Higher bulk density values are a sign of higher compaction level. The soil bulk density decreased with the degree of soil manipulation during tillage practices. Significantly lower soil bulk density in conventional tillage system could be due to the incorporation of crop residues by tillage to the surface soil depth (Bhattacharyya et al. 2006). However, Roscoe and Burman (2003) detected that conventional tillage system caused significant increase in bulk density and soil compaction comparing no-tillage system. Conservation tillage also leads to positive changes in soil physical properties, such as aggregate stability (Dalal, 1992).

Aggregates not only physically protect soil organic matter (Tisdall and Oades, 1982), but also influence microbial community structure (Hattori, 1988), limit oxygen diffusion (Sexstone et al., 1985), regulate water flow (Prove et al., 1990) and reduce run-off and erosion (Barthes and Roose, 2002). Soils with low aggregate index tend to form surface crusts and compacted surface soils, which can reduce air exchange and seed germination, increase plant stress and reduce water infiltration and thus storage of water received as rainfall. This leads to runoff, erosion and flooding risk downstream during heavy rainfall. Soil management, specifically the use of different tillage systems, affects soil aggregation directly by physical disruption of the macroaggregates, and indirectly through alteration biological and chemical factors (Barto et al., 2010). The decrease in soil aggregate stability will result in soil nutrient depletion and erosion (Borie et al., 2006).



CIGR 2018

XIX. World Congress of CIGR



The effects of tillage on soil hydraulic properties have been reported by several authors, as shown by the results of McGarry et al., (2000). Seventy percent of a field is passed by vehicle traffic in a conventional tillage system (Raper and Kirby 2005). Soil bulk density and penetration resistance increased with increase in the number of traffic passes while air permeability was decreased with increase traffic intensity (Mamman and Ohu, 1998).

Bhattacharyya et al. (2006) compared the effects of no-tillage and conventional tillage practices in a four-year study, and reported that the hydraulic conductivity values were higher in no-tillage than tilled soils. The effects of tillage practices on soil physical properties such as aggregation, bulk density, porosity, hydraulic properties, soil compaction, and water retention are variable. Information on changes in soil hydraulic conductivity and soil strength properties, especially in heavy clayey soil, due to tillage practices is limited. Therefore, this study was performed to determine the effects of conventional and conservation tillage practices on saturated hydraulic conductivity, soil bulk density and penetration resistance in wheat-corn-wheat-soybean rotations in a clay soil under semi-arid climatic conditions. Besides, the relationship between soil quality indicators (BD, HC and AI) also was evaluated based on soil penetration resistance for the long-term sustainability of agricultural ecosystems.

2. MATERIALS AND METHODS

2.1. Experimental site

This study was carried out at the Agricultural Research Area of Çukurova University located near Adana, Turkey (37°00'54'' latitude N, 35°21'27'' longitude E, 32 m above sea level) in 2009 and 2011. The area is affected by Mediterranean climate. The Mediterranean region has hot and arid summers and mild, rainy winters. From 1979 to 2008, annual rainfall average was 768 mm. Annual temperature average is 19.3°C, though monthly averages range from 29,6 °C in August to 9.9 °C in January according to the long-term average. The soil structures of the study area were 18% sand, 32% silt, 50% clay, pH 7.8 and organic carbon content 0.9%. The soil with a slope of about 1% had a pH of 7.82, bulk density of 1.31 Mg m⁻³, total organic carbon of 8.76 g kg⁻¹, CaCO₃ of 244 g kg⁻¹, and electrical conductivity of 0.15 dS m⁻¹ (Celik et al. 2009).

The rotations of winter wheat (*Triticum aestivum* L.)-corn (*Zea Mays* L.), wheat-soybean (*Glycine max.* L.) and wheat were applied in all treatments from 2006 to 2009. The treatments were conventional tillage with residue incorporated in soil (CTS), conventional tillage with residue burned (CTB), reduced tillage with heavy tandem disc-harrow (RTD), reduced tillage with rotary tiller (RTR), reduced tillage with heavy



CIGR 2018

XIX. World Congress of CIGR



tandem disc harrow for the first crop + no-tillage for the second crop (**RNT**), and no tillage (**NT**). The plots were of 12-m width and 40-m length. The details of the six different tillage and sowing methods used in the study are given in Table 1. The experiment field was prepared as a randomized complete block design with three replications.

The crop rotation was wheat-corn in the 2006-2007, wheat-soybean in the 2007-2008 and wheat in the 2008-2009 growing seasons, respectively. The growing period of winter wheat was from November to the first week of June and for corn or soybean was from the second week of June to the first week of October.

The total herbicide (500 g ha⁻¹ Glyphosate) was used to control weeds in the NT and RNT treatments two weeks prior to sowing. Composed NP-fertilizers were applied in the seedbed at rates of 172 kg N ha⁻¹ and 55 kg P₂O₅ ha⁻¹ for wheat, 250 kg N ha⁻¹ and 60 kg P₂O₅ ha⁻¹ for corn, and 120 kg N ha⁻¹ and 40 kg P₂O₅ ha⁻¹ for soybean. Winter wheat was sown in the first weeks of November 2006, 2007, and 2008 at seeding rate of 240 kg ha⁻¹ and harvested in the first weeks of June 2007, 2008, and 2009. Corn and soybean were sown in the third weeks of June and harvested in the second weeks of October 2007 and 2008. Corn and soybean were sown at seeding rates of 8.4 and 23.6 plants per m², respectively. Corn and soybean were sprinkler-irrigated once in every 13-day and nine times totally during the growing period. The amount of water was identical for all treatments, and no irrigation water was applied to the wheat.

Table 1. Tillage methods, depth of tillage, and type of the equipments used in the study

Tillage Methods	Winter wheat (2006, 2007, 2008)	Second crop maize or soybean (2007, 2008)
Conventional tillage with residue incorporated in the soil (CTS)	Stover chopping of second crop Mouldboard plough (30-33 cm) ^{a)} Disc harrow (2 passes, 13-15 cm) Float (2 passes) Drill (4 cm)	Stubble chopping of wheat Heavy tandem disc harrow (18-20 cm) Disc harrow (2 passes, 13-15 cm) Float (2 passes) Planter (8 cm)
Conventional tillage with residue burned (CTB)	Stover burning of second crop Mouldboard plough (30-33 cm) Disc harrow (2 passes, 13-15 cm) Float (2 passes) Drill (4 cm)	Stubble burning of wheat Chisel plow (35-38 cm) Disc harrow (2 passes, 13-15 cm) Float (2 passes) Planter (8 cm)
Reduced tillage with heavy tandem disc harrow (RTD)	Stover chopping of second crop Heavy offset disc harrow (2 passes, 18-20 cm) Float (2 passes) Drill (4 cm)	Stubble chopping of wheat Rotary tiller (13-15 cm) Float (2 passes) Planter (8 cm)
Reduced tillage with rotary tiller (RTR)	Stover chopping of second crop Rotary tiller (13-15 cm) Float (2 passes)	Stubble chopping of wheat Rotary tiller (13-15 cm) Float (2 passes)



CIGR 2018

XIX. World Congress of CIGR



	Drill (4 cm)	Planter (8 cm)
Reduced tillage with heavy tandem disc harrow + no-tillage (RNT)	Stover chopping of second crop Heavy offset disc harrow (18-20 cm) Float (2 passes) Drill (4 cm)	Stubble chopping of wheat Herbicide treatment No-till planter (8 cm)
No-tillage (NT)	Stover chopping of second crop Herbicide treatment No-till drill (4 cm)	Stubble chopping of wheat Herbicide treatment No-till planter (8 cm)

^{a)} Figures in parenthesis are average working depth of the equipments

2.2. Soil sampling

In order to determine the effects of tillage practices on soil properties, disturbed and undisturbed samples were collected three times throughout the research period from 0-10 cm, 10-20 cm and 20-30 cm depths. The first samples were taken in June 2006 following the establishment of the plots. The second samples were taken immediately after the wheat harvest on June 2008.

The twenty four undisturbed samples per tillage treatment were collected by using a steel cylinder of 100 cm³ volume (5 cm in diameter, and 5.1 cm in height). Bulk density and saturated hydraulic conductivity were determined from undisturbed soil samples. The bulk density was measured by the core method (Blake & Hartge 1986), and saturated hydraulic conductivity was determined by the falling-head method (Klute and Dirksen, 1986). A wet sieving method was used to determine the indices of soil aggregation. The wet sieving method of Kemper and Rosenau (1986) was used with a set of sieves, which have openings of 4, 2, 1, and 0.5 mm diameters.

Soil penetration resistance was determined by a hand-pushing electronic cone penetrometer following ASAE standard procedures (ASAE, 1994), using a cone with 1 cm² base area, 60° included angle and 80 cm driving shaft; readings were recorded at 10 mm intervals. The measurements were performed at 6 points in each plot, following wheat harvest. Soil moisture content and penetration resistance were measured at the same time. In order to determine the soil moisture content, soil samples were taken from each parcel and depths of 0-15, 15-30 and 30-45 cm.

The texture of the research area was homogeneous throughout the parcels, and no significant differences were determined at the three depths. The mean bulk density, hydraulic conductivity and penetration resistance values of tillage treatments were ranged between 1.20 and 1.44 Mg m⁻³, 7.33 and 9.05 m s⁻¹ × 10⁻⁶, and 0.601 and 0.984 MPa for 10-20 cm and 20-30 cm depths, respectively.



2.3. Statistical analysis

One-way analysis of variance (ANOVA) was applied to assess the effects of tillage treatments on saturated hydraulic conductivity, aggregate stability and soil bulk density for the three soil depths of 0-10, 10-20, and 20-30 cm separately. Penetration resistance values were compared for 0-10, 11-20 and 21-30 cm soil depths separately. Following the ANOVA test, the Tukey test was performed to compare differences in means of the parameters at significance level of 0.05. In addition this, regression analysis was performed to reveal the relationship between the variables.

3. RESULTS AND DISCUSSIONS

3.1. Effects of tillage on the soil

The effects of tillage systems on bulk density, penetration resistance, hydraulic conductivity and aggregation index were significantly different ($P < 0.05$). The lowest bulk density, penetration resistance values were obtained with conventional tillage with residue incorporation (CTS), as 1.28 Mg m^{-3} and 1.27 MPa , respectively. However, the highest bulk density and penetration resistance values were in NT (1.41 Mg m^{-3} and 2.06 MPa), respectively (Table 2). Soil bulk density and penetration resistance were increased in reduced tillage and NT systems, while decreased in conventional tillage (CTS and CTB) systems. Kanwar (1989) reported that tillage systems have altered bulk density and porosity of soils. The increases in bulk density of the soil with no-tillage treatments have previously been reported by Xu and Mermoud (2001). But, greater bulk density values under conventional tillage systems were also reported when compared to no-tillage (Roscoe and Burman, 2003). Similarly, the penetration resistance values were the highest under no-tillage and reduced tillage, while the lowest values were obtained in CTS and CTB (Table 2). Penetration resistance value under NT was 62-38% higher than those under CTS and CTB respectively. Reduced and especially no-tillage treatments caused to increase penetration resistance compared with conventional tillage methods. Similar results of greater penetration resistance in NT than



CIGR 2018

XIX. World Congress of CIGR



CT were reported by Alvarez et al. (2009). The increase in bulk density and penetration resistance under reduced tillage and no-tillage indicated probable soil compactions (Table 2). Lower bulk density and penetration resistance obtained in conventional tillage (CTS and CTB) might be attributed to short term loosening effect of tillage, and incorporation of crop residue to soil surface layers. The use of chisel that tills about 35 to 38 cm probably lowered the penetration resistance and bulk density in CTB than in CTS especially at 21-45 cm depth.

Table 2. Effect of different tillage methods on hydraulic conductivity, aggregation index bulk density and penetration resistance for each depth in 2008

Tillage	Depth (cm)	Hydraulic Conductivity ($\text{m sn}^{-1} \times 10^{-6}$)	Aggregation Index (mm)	Bulk Density (g cm^{-3})	Penetration Resistance (MPa)
CTS	0-10	9,79 [#] ±0,03 [†] a ^{&}	0,26 [#] ±0,02 [†] cd ^{&}	1,27 [#] ±0,03 c ^{&}	0,946±0,361
	10-20	8,80±0,04 a	0,29±0,02 bc	1,27±0,05 c	1,331±0,040
	20-30	7,28±0,07 a	0,31±0,07 b	1,30±0,02 b	1,541±0,126
CTB	0-10	9,47±0,05 a	0,21±0,02 d	1,33±0,05 abc	1,23±0,511
	10-20	8,64±0,06 a	0,26±0,01 c	1,30±0,05 bc	1,653±0,032
	20-30	6,00±0,04 b	0,31±0,04 b	1,33±0,02 b	1,604±0,049
RTD	0-10	7,95±0,10 bc	0,35±0,01 b	1,32±0,02 abc	1,393±0,636
	10-20	6,80±0,04 bc	0,38±0,07 ab	1,34±0,04 abc	2,203±0,051
	20-30	6,34±0,06 ab	0,41±0,07 ab	1,36±0,03 ab	2,135±0,036
RTR	0-10	8,53±0,03 ab	0,31±0,01 bc	1,29±0,04 bc	1,383±0,631
	10-20	7,99±0,09 ab	0,35±0,02 abc	1,31±0,04 abc	1,916±0,082
	20-30	5,93±0,03 b	0,41±0,04 ab	1,35±0,05 ab	1,806±0,049
RNT	0-10	7,23±0,03 bc	0,34±0,04 b	1,37±0,01 ab	1,789±0,566
	10-20	6,22±0,08 c	0,37±0,03 ab	1,39±0,01 ab	2,121±0,032
	20-30	5,86±0,02 b	0,42±0,01 ab	1,41±0,02 a	2,203±0,077
NT	0-10	6,66±0,02 c	0,41±0,01 a	1,40±0,01 a	1,919±0,735
	10-20	6,15±0,02 c	0,43±0,02 a	1,41±0,01 a	2,105±0,109
	20-30	5,72±0,03 b	0,46±0,02 a	1,41±0,02 a	2,152±0,121

Different tillage practices have significant impacts on aggregation index (AI) of soils. The mean AI values of tillage practices were significantly differed from each other (Table 2). The highest AI value was in NT with 0.43 mm and the lowest AI was under CTB with 0.26 mm. The crop residue on soil surface of NT may have stabilized aggregates by protecting organic matter from microbial degradation. The reduced rate of



organic matter mineralization led to improve soil structure. Thus, more stable aggregates in the surface soil were associated with NT treatment compared to CT and RT treatments. The effects of tillage systems on HC was also significantly different ($P < 0.05$). Saturated hydraulic conductivity of 0-10 cm soil depth was greater as compared to that of 10-20 cm and 20-30 cm depths. The increase in bulk density and penetration resistance with depth induced a decrease ($P < 0.05$) in HC of subsurface soils (Table 2). The highest HC values were obtained from conventional tillage with residue incorporated in CTS with $9.79 \times 10^{-6} \text{ m sn}^{-1}$ and conventional tillage with residue burned in CTB with $9.47 \times 10^{-6} \text{ m sn}^{-1}$. NT systems have the lowest HC values (Table 2).

Saturated hydraulic conductivity was increased with increasing the intensity and depth of the tillage operation to prepare the seed bed for the first and the second crops. Reduced and no-tillage applications induced to decrease hydraulic conductivity compared with conventional tillage methods (Table 2). Similarly, Heard et al. (1988) attributed the greater hydraulic conductivity in conventionally tilled soils to greater number of voids and cracks caused by tillage implement. However, Chan and Mead (1989) noted that no-tilled soils had greater hydraulic conductivity than tilled soils. On the other hand, no differences in hydraulic conductivity between conventional tillage, minimum tillage and no-tillage soils were reported by Horne et al., 1992. High bulk density values obtained under no-tillage and reduced tillage systems are the indications of soil compaction (Abu-Hamdeh 2003), and might be the cause of low hydraulic conductivity obtained in no-tillage and reduced tillage systems (Table 2).

3.2. Relations of Soil Quality Indicators

The relationship between BD, HC and AI with PR are essential (Figure 1). There is a linear relationship between BD and PR with the coefficient of determination of 0.85 (Table 2a). Soil bulk density is fundamental to soil compaction. It is clear that mechanical compaction increase bulk density in most soils. So, the effect of tillage methods has been similar on BD and PR. The conventional tillage treatments produce lower bulk density and penetration resistance than under conservation tillage treatment.

There is an inverse linear relationship between HC and PR with the coefficient of determination of 0.98 (Table 2b). This relationship is better than other soil indicators. The increasing of soil compaction causes to decrease saturated hydraulic conductivity. Celik et al. (2009) reported the soil compaction causes to decrease saturated hydraulic conductivity in soils. The relationship between AI with PR is crucial with the coefficient of determination of 0.80 (Figure 1c).



CIGR 2018

XIX. World Congress of CIGR



There is a linear relationship between them. The increase of the penetration resistance had a positive effect on aggregation index of the soil. Poor soil aggregation makes the soil more difficult to manage, as it reduces its ability to drain excess.

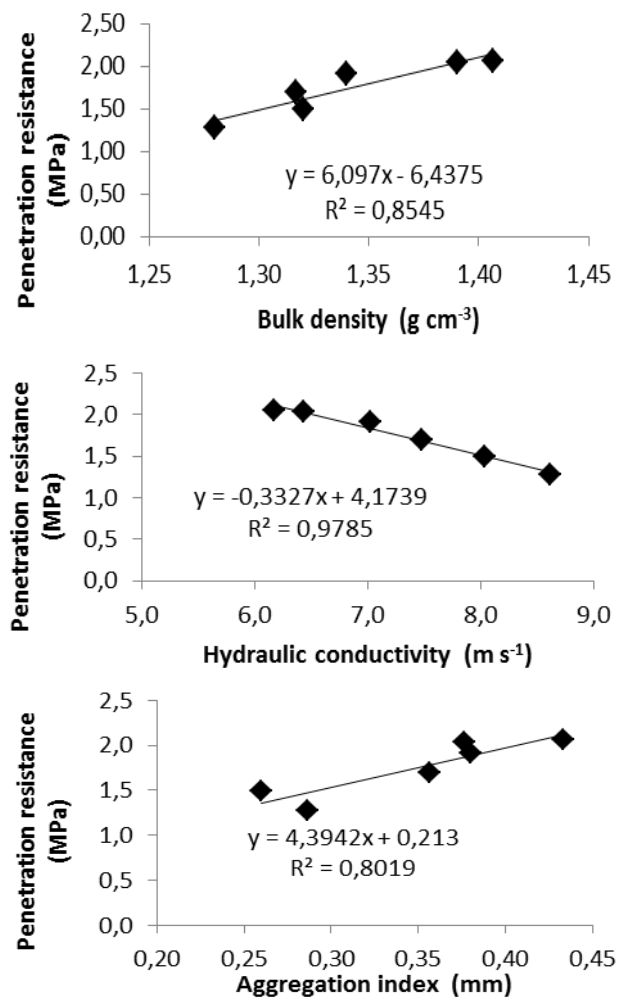


Figure 1. Relationship between hydraulic conductivity, aggregation index and bulk density based on penetration resistance

4. CONCLUSIONS

Conventional tillage methods were resulted in higher saturated hydraulic conductivity but lower bulk density and penetration resistance than no-tillage and reduced tillage. The hydraulic conductivity values under NT in 2008 were lower 30% at 0-30 cm depth than that in CTS.



CIGR 2018

XIX. World Congress of CIGR



The hydraulic conductivity was improved in tilled soils due to decreased soil compaction and soil loosening. The bulk density and penetration resistance were significantly greater under no-tillage and reduced tillage.

Despite no-tillage and the reduced tillage treatments had the higher bulk density and penetration resistance values, aggregation index values of these treatments were better than conventional tillage. The relationship between saturated hydraulic conductivity, bulk density and aggregation index with penetration resistance are very important. There are linear relationships between soil bulk density and aggregation index with penetration resistance, but opposite relationship with saturated hydraulic conductivity.

ACKNOWLEDGEMENT

The authors would like to express their sincere thanks to TUBITAK (The Scientific and Technological Research Council of Turkey) for financially supporting the research project with TOVAG-114O021 code.

REFERENCES

- Abu-Hamdeh, N.H. 2003. Soil compaction and root distribution for okra as affected by tillage and vehicle parameters. *Soil and Tillage Research* 74(1): 25-35
- Alvarez, C.R., M.A. Taboada, F.H. Gutierrez Boem, A. Bono, P.L Fernandez and P. Prystupa. 2009. Topsoil properties as affected by tillage systems in the Rolling Pampa Region of Argentina. *Soil Science Society of America Journal* 73(4): 1242-1250
- ASAE, 1994. Soil cone penetrometers. S313.2 in *Standards Engineering Practices Data*, ASAE Standards, St. Joseph, MI.
- Barto, E.K., F. Alt, Y. Oelmann, W. Wilcke and M.C. Rillig. 2010. Contributions of biotic and abiotic factors to soil aggregation across a land use gradient. *Soil Biology and Biochemistry*, 42: 2316-2324.
- Barthes, B., E. Roose. 2002. Aggregate stability as an indicator of soil susceptibility to runoff and erosion validation at several levels. *Catena*, 47, 133–149
- Barut, Z.B. and D.Akbolat. 2005. Evaluation of Conventional and Conservation Tillage Systems for Maize. *Journal of Agronomy*, 4:122-126.
- Bhattacharyya, R, V. Prakash, S. Kundu and H.S. Gupta. 2006. Effect of tillage and crop rotations on pore size distribution and soil hydraulic conductivity in sandy clay loam soil of the Indian Himalayas. *Soil and Tillage Research* 86(2): 129-140
- Blake, G.R. and K.H. Hartge. 1986. Bulk density. In: Klute, A. (Ed.), *Methods of Soil Analysis. Part 1. Physical and Mineralogical Methods*, 2nd ed. Agron. Monogr. 9. ASA-SSA, Madison, WI, pp: 363-375



CIGR 2018

XIX. World Congress of CIGR



Celik, I, I. Ortas, Z.B. Barut, M. Gok, A. Sariyev, A. Demirbas, C. Akpinar and Y. Tulun. 2009. Effects of different soil tillage systems on soil quality parameters and crop yields. Final report of the TUBITAK project (The Scientific and Technological Research Council of Turkey, Grant No: 106O023) pp:163 (in Turkish).

Dalal, R.C. 1992. Long-term trends in total nitrogen of a Vertisol subjected in zero tillage, nitrogen application and stubble retention. *Australian Journal of Soil Research* 30(2): 223-231

Doran, J.W. and A.J. Jones. 1996. *Methods for Assessing Soil Quality*. Soil Science Society of America Special Publication Number 49, 410 pp.

Etchevers, J.D., R.A. Fischer, I. Vidal, K.D. Sayre, M.A. Sandoval, K. Oleschko and S. Roman. 2000. Labranza de conservacion, indices de calidad del suelo y captura de Carbono. In: *Memorias Simposio Internacional de Labranza de Conservacion*, Ins. Nacional de Investigaciones Forestales y Agro Pecuarias-Produce, Mazatlan, Sinaloa, Mexico.

Hattori, T. 1988. Soil aggregates in microhabitats of microorganisms. *Rep. Inst. Agric. Res. Tohoku Univ.* 37, 23–36.

Horne D.J., C.W. Ross and K.A. Hughes. 1992. 10 years of a maize oats rotation under three tillage systems on a silt loam in New Zealand. 1. A comparison of some soil properties. *Soil and Tillage Research* 22(1–2): 131-143

Kanwar, R.S. 1989. Effect of tillage system on the variability of soil water tensions and water content. *Trans. ASAE* 32(2): 605-610

Karlen, D.L. 2004. Soil quality as an indicator of sustainable tillage practices. *Soil & Tillage Research* 78:129-130

Kemper W.D. and R.C. Rosenau. 1986. Aggregate stability and size distribution. In: Klute, A. (Ed.), *Methods of Soil Analysis. Part 1. Physical and Mineralogical Methods*, 2nd ed. Agron. Monogr. 9. ASA-SSA, Madison, WI, pp. 425-442.

Mamman, E. and J.O. Ohu. 1998. The effect of tractor traffic on air permeability and millet production in a sandy loam soil in Nigeria. *Ife J. Technol.* 8(1): 1-7

McGarry, D., B.J. Bridge and B.J. Radford. 2000. Contrasting soil physical properties after zero and traditional tillage of an alluvial soil in the semi-arid subtropics. *Soil and Tillage Research* 53(2): 105-115

Prove, B.G., R.J. Loch, J.L. Foley, V.J. Anderson and D.R. Younger. 1990. Improvements in aggregation and infiltration characteristics of a krasnozem under maize with direct drill and stubble retention. *Aust. J. Soil Res.* 28, 577–590.

Raper, R.L. and J.M. Kirby. 2005. *Soil Compaction: How to do it, Undo it, or Avoid doing it*. ASABE Distinguished Lecture Series No. 30, pp:1-14



CIGR 2018

XIX. World Congress of CIGR



Sexstone, A.J., N.P. Revsbech, T.B. Parkin and J.M. Tiedje. 1985. Direct measurement of oxygen profiles and denitrification rates in soil aggregates. Soil Sci. Soc. Am. J. 49, 645–651.

Tisdall, J.M. and J.M., Oades, 1982. Organic matter and water-stable aggregates in soils. J. Soil Sci. 62, 141–163.

Xu, D. and A. Mermoud. 2001. Topsoil properties as affected by tillage practices in North China. Soil and Tillage Research 60(1): 11-19



CIGR 2018

XIX. World Congress of CIGR



The Effect of Heat Stress on Milk Yield in a Ipard Supported Dairy Cattle Enterprise

Erdal TRKMEN¹, Erkan YASLIOĐLU

¹Bursa Provincial Directorate of Agriculture and Rural Development Support
erdal.turkmen@tkdk.gov.tr

ABSTRACT

In this study, the effect of heat stress on the milk yield in an operation supported by the IPARD fund by the Agricultural and Rural Development Support Institution (ARDSI) was evaluated by means of temperature-humidity index. It is aimed to determine the effect of barn design on temperature-humidity index, and to find out relationship between milk yield and temperature-humidity index.

Between 18.12.2016 and 22.10.2017 in the řahinky district of Karacabey, Bursa province, the temperature-humidity index values were calculated based on the temperature and relative humidity values continuously measured with 1 hour intervals at 7 different points of milk production operation.

It was determined that milk yield decreased at higher THI values that exceed 72. Additionally, the production of milk per animal is decreased by 0.15 kg in case of one-unit increase in the average THI. Similarly, Ravagnolo et al. (2000) emphasized that when THI exceeds 72, milk yield decreased by 0.2 kg for one-unit increase in THI.

Statistical analysis was performed to determine the time period in which the effect of THI values on milk yield was higher. West et al. (2003) reported that the THI two days prior to hot weather conditions had the greatest effect on milk yield, whereas an increasing effect for up to 5 days and the decreased effect after 5 days was observed according to our results. It has been concluded that ventilation systems should be improved in order to control the high THI values that cause economic losses.

Keywords: ARDSI, Dairy Farm, IPARD, Milk Yield, THI, Turkey.

INTRODUCTION

Erdal TRKMEN and Erkan YASLIOĐLU. "The effect of heat stress on milk yield in an IPARD supported dairy cattle enterprise".



CIGR 2018

XIX. World Congress of CIGR



IPARD is the support of agriculture and rural development, adopted by the European Commission for Rural Development, the fifth component of the IPA. These supports, which include different measures and implemented as IPARD-I with a grant amount of 1 052 000 000 Euros between 2007 and 2014, are applied as IPARD-II with an amount of 1 045 000 000 Euros between 2014 and 2020.

In Turkey, 42 provinces, which applied for grant support for enterprises engaged in livestock production up to 70%, are also supported under this program. In this process, the minimum criteria published together with the call guides are compulsory and the investors are directed accordingly. It is aimed to obtain a certain system of agricultural structures which is one of the most important elements for successful operation.

In this study, the effect of heat stress on milk yield was evaluated through the indoor temperature humidity index in an operation in the Şahinköy village of Karacabey, Bursa, supported by the IPARD Funds of the European Union through the Agricultural and Rural Development Support Institution (ARDSI). It is also aimed to determine the effect of the barn design on the temperature humidity index and thus how the milk yield is affected from temperature humidity index variations.

LITERATURE

Dikmen and Hansen (2009), defined the heat stress as the sum of external forces acting on an animal that causes an increase in body temperature and evokes a physiological response (Polsky and Keyserlingk 2017). Heat stress results in total annual economic losses to the US livestock production industry ranging from \$1.69 to 2.36 billion, of which \$900 million is specific to the US dairy industry, stemming from decreased milk production, compromised reproduction, and increased culling (St-Pierre et al., 2003). Escalating global temperatures (Schär et al., 2004) combined with global increases in the number of production animals and the intensification of agriculture (Renaudeau et al., 2012), including (but not limited to) emerging economies (von Keyserlingk and Hötzel, 2015), has caused that heat stress is becoming an important challenge of the global dairy industry.

Armstrong (1994) described stress categories as follows:

THI <71 thermal comfort zone (assuming the THI does not drop below the thermoneutral conditions of dairy cows, which induces cold stress),

THI = 72 to 79 mild heat stress, THI = 80 to 90 moderate heat stress, THI >90 severe heat stress.

De Rensis et al. (2015) defined THI <68 to be outside the thermal danger zone for cows. Mild signs of heat stress are observed at THI of 68 to 74, and a THI ≥ 75 will cause drastic decreases



CIGR 2018

XIX. World Congress of CIGR



in production performance. According to Johnson (1985) and Du Preez et al. (1990), Milk production is not affected by heat stress when mean THI values are between 35 and 72. However, milk production and feed intake begin to decline when THI reaches 72 and continue to decline sharply at a THI value of 76 or greater (Bouraoui et al., 2002)

Two experiments were conducted to measure the effects of heat stress, using THI, on milk production, milk composition and dry matter intake (DMI) of lactating Friesian-Holstein cows under the Mediterranean climate. Daily THI was negatively correlated to milk yield ($r = -0.76$) and feed intake ($r = -0.24$). When the THI value increased from 68 to 78, milk production and DMI were decreased by 21% and 9.6%, respectively. Milk yield decreased by 0.41 kg per cow per day for each unit increase at the THI values above 69. Milk fat (3.24 vs. 3.58%) and milk protein (2.88 vs. 2.96%) were lower for the summer group. Summer heat stress reduced milk yield and DMI, altered milk composition and affected the physiological functions of confined lactating Holstein cows managed under Mediterranean climatic conditions (Bouraoui et al., 2002).

Yazgan (2017), stated that one day earlier from daily milking was yielded best decisive factor. In contrast to this study, West et al. (2003) and Freitas et al. (2006) reported that THI two day earlier had the greatest influence on heat stress. Bohmanova et al., (2008), concluded that weather data 3 day before the test date explained more of the variability of milk yield than weather data 1 or 2 day before the test date or on the test date itself. The threshold of heat stress was set to a mean THI of 72 for all herds. Ravagnolo and Misztal (2000) report milk production decrease of 0.2 kg per THI unit, which is similar to the results obtained in this study. West et al. (2003) reported the loss of 0.88 kg milk per THI unit.

According to the Bouraoui et al. (2002), milk production (kg per cow per day) = $47.722 - 0.4129 \times \text{THI}$ ($R^2 = 0.76$). This regression indicates that, in general, for each point increase in the THI value above 69, there was a decrease in milk yield of 0.41 kg per cow per day. The value of this relationship for predictive purposes is relatively high, as depicted by an R^2 value of 0.76. A large part of the variation in daily milk yield could therefore be attributed to heat stress. The drop in daily milk production in this study was higher than the 0.32 and 0.26 kg per cow respectively reported by Ingraham et al. (1979) and Johnson (1980) for each point increase of the THI values above 70.



MATERIALS AND METHODS

3.1. Material

3.1.1. Research area location and characteristics

The Karacabey district of Bursa province has an important place in terms of dairy cattle farm, and also includes important milk production, processing and training facilities. This study was carried out in a dairy cattle farm, established by the support of the Agriculture and Rural Development Support Institution, in Şahinköy, Karacabey district of Bursa province, Turkey. The selected farm is located on 40°14'25.04"N latitude, 28°18'19.65"E longitude.



Figure 3.1. The location of studied dairy cattle farm in Turkey

Investigated barn is a head to head free-stall barn with 120 milking cow capacity. The barn was constructed as a single block structure including milking cow room, young stock room, maternity room, treatment room, and the milking parlor. The manure management system consists of the manure scraper system and the manure storage. When viewed from the perspective of Google Earth data and barn buildings directions, the operation is oriented exactly (at a 0-degree angle) in the north-south direction. The average altitude of the operator is 18 meters.

3.1.2. Research area climate data

Long-term (1926-2016) climate data of Bursa province are given in Table 3.1.



CIGR 2018

XIX. World Congress of CIGR



Table 3.1. Long-term (1926-2016) Climate data of Bursa Province (Anonymous 2017)

	Jan.	Feb.	Mar.	April	May	June	July	Aug.	Sept.	Oct.	Nov.	Dec.	Ann.
Ave. Temp. (°C)	5,30	6,10	8,30	12,90	17,60	22,00	24,50	24,20	20,10	15,40	10,90	7,30	14,60
Ave. Max. Temp. (°C)	9,40	10,70	13,70	18,90	23,80	28,30	30,80	31,00	27,20	22,00	16,60	11,50	20,30
Ave. Low. Temp. (°C)	1,70	2,10	3,50	7,20	11,30	14,80	17,10	17,10	13,60	10,10	6,40	3,50	9,00
Ave. Sunrise Time (hours)	2,50	3,30	4,20	5,50	7,50	10,60	10,50	10,10	8,60	5,40	4,10	2,60	74,90
Ave. Number of Days with Precipitation	14,50	13,30	12,20	11,20	8,70	5,80	2,90	2,80	5,00	9,00	11,10	14,20	110,70
Monthly Total Rainfall Ave. (mm)	89,10	76,70	70,10	63,00	49,20	33,30	21,60	16,60	42,00	66,80	78,40	100,7	707,50
Highest Temp. (°C)	23,80	26,90	32,50	36,20	38,20	41,30	43,80	42,60	40,10	37,30	34,00	27,30	43,80
Min. Temp. (°C)	-20,5	-25,7	-10,5	-4,2	0,8	4,0	8,3	7,6	3,3	-1,0	-8,4	-17,9	-25,7

3.2. Method

General measurement studies continued for 10 months between 18.12.2016 and 22.10.2017 at 7 different points of operation; temperature, relative humidity, dew point temperature values continued for 305 days provided that they were recorded for 24 hours, one after the other.

The measurement values between 01.05.2017 and 01.10.2017 have been taken into consideration for reflecting the summer measurement values. Milk yields were obtained on the producer's receipts showing the sales to the relevant company carried out every day due to contractual production by the operator.

For the analysis of the change in milk yield in the hottest periods of the year, the months in which the Temperature Humidity Index values were highest were subjected to a special investigation. Metrics between 01 May and 01 October 2017 were evaluated.

Two separate studies were performed, with mean THI values of the second operating points and the third point average temperature with the highest average temperature. In addition, a detailed examination of the yield regression of THI was attempted to understand the mechanism of action at different times in order to understand the duration of the beneficial effect of THI.

In the study, the temperature is specified by the moisture index value (Yousef 1985);

THI = $t_{db} + 0.36 t_{dp} + 41.2$ is used.

Here, THI: temperature-humidity index, t_{db} : dry-bulb temperature (°C), t_{dp} : dew point temperature (°C). Hourly THI values were obtained using the hourly average values of the dry-bulb temperature and the dew point temperature. These obtained THI values were analyzed.



CIGR 2018

XIX. World Congress of CIGR



RESULTS AND DISCUSSION

Table 4.1. Operating milk yield, temperature and THI values

Variable	Mean	Minimum	Maximum	SD
Milk Yield (lt)	2 779.5	2505.0	2987.0	100.2
Temperature (°C)	23.3	15.1	30.85	3.37
THI	70.4	60.24	79.01	4.28

The milk yield, temperature and THI values are given in Table 4.1. Milk production with an average of 95 milk cows was carried out. Daily averages of temperature and THI values were considered.

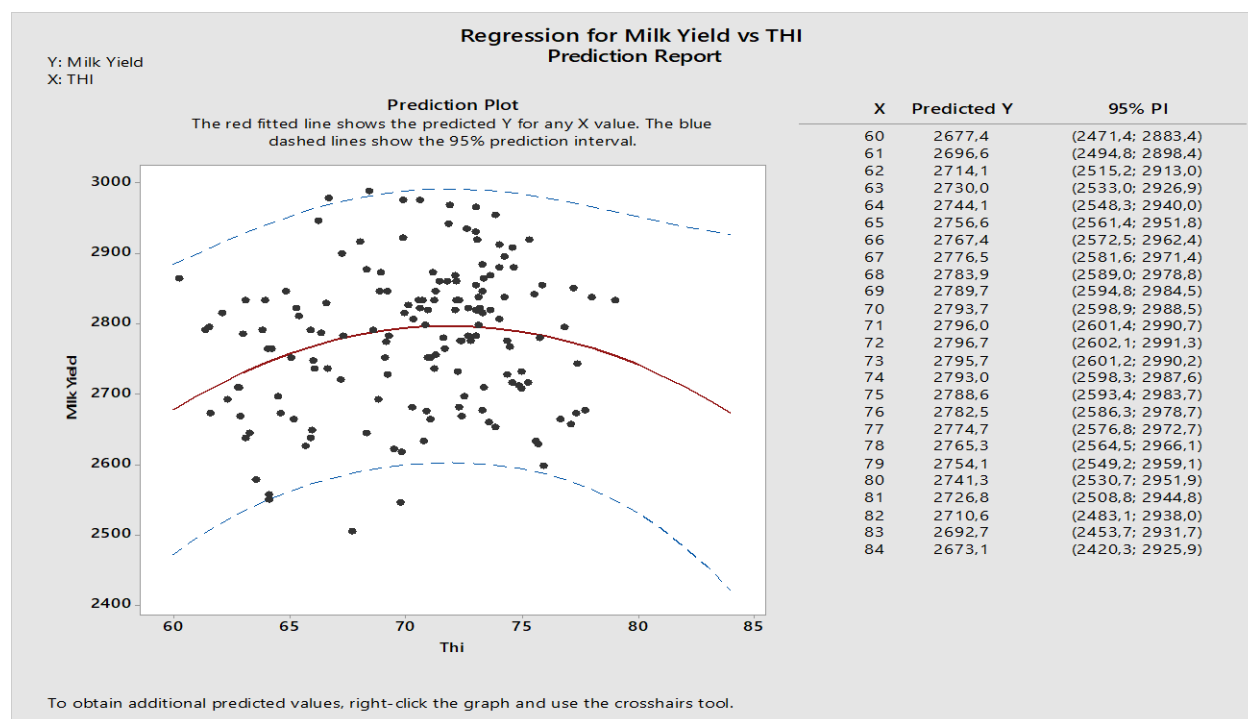


Figure 4.1. Regression for Milk Yield vs THI

The relationship between THI and milk yield was statistically significant ($P < 0.012$), as seen in the graph (Figure 4.1), a decrease in yield after 72 THI was observed. The decrease in milk yield was determined as 0.15 kg on the same day and the next day averaged per unit THI increase per



CIGR 2018

XIX. World Congress of CIGR



animal. This lower value than other studies can be attributed to effectiveness of ventilation system. Ravagnolo and Misztal (2000) found that the milk yield per kg of THI increased by 0.2 kg per THI increase; Bouraoui et al. (2002) found that for every increase in THI > 69, milk yield decreased by 0.41 kg per day.

THI values were investigated on the same day, 1, 2, 3, 4, 5, 6 and 7 days delayed impact assessment (Table 4.2.).

Table 4.2. Milk yield THI regression values according to days

Day	Coefficient of determination		Correlation coefficient	
	R ²	P	r (Spearman rho)	P
0	5,68	0,012	0,156	0,054
1	7,96	0,002	0,079	0,331
2	10,90	0,001	-0,020	0,807
3	13,71	0,001	-0,103	0,205
4	14,96	0,001	-0,148	0,066
5	16,54	0,001	-0,157	0,051
6	13,11	0,001	-0,139	0,086
7	9,30	0,001	-0,106	0,192

Single regression analysis values increased up to the fifth day. It began to decrease with the sixth day. The highest single R² value and the correlation coefficient were determined on day 5.

Simple regression analyzes and correlation coefficient (Spearman Rho) were determined for days with THI > 72 (Table 4.3.).



CIGR 2018

XIX. World Congress of CIGR



Table 4.3. Milk yield THI regression values according to days (THI>72)

Day	Coefficient of determination		Correlation coefficient	
	R ²	P	r (Spearman rho)	P
0	6,03	0,043	-0,205	0,094
1	14,88	0,001	-0,313	0,009
2	32,73	0,001	-0,459	0,000
3	41,30	0,001	-0,579	0,000
4	42,40	0,001	-0,587	0,000
5	37,15	0,001	-0,564	0,000
6	31,11	0,001	-0,567	0,000
7	25,06	0,001	-0,488	0,000

In days with THI> 72, the 4-day delayed effect has the highest correlation and regression values. Multiple regression analyzes were employed for diurnal variations (Figure 4.2.).

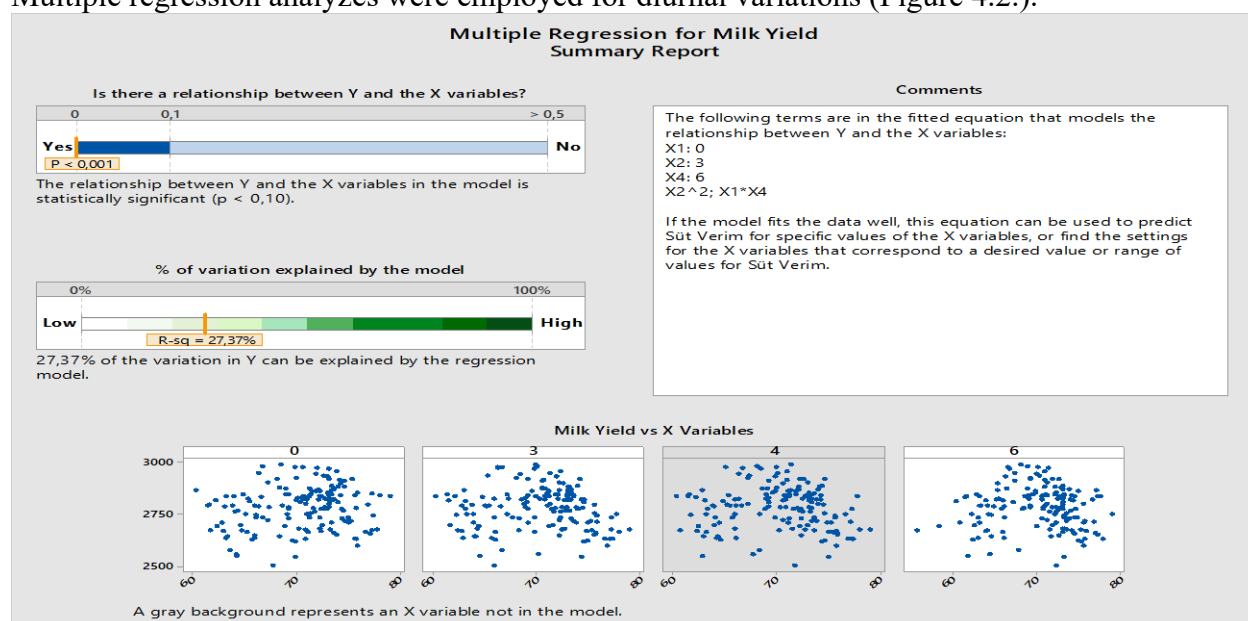


Figure 4.2. Multiple regression for Milk Yield



CIGR 2018

XIX. World Congress of CIGR



On Days 0, 3 and 6, $R^2 = 27,37\%$, $P < 0,001$ was obtained.

Multiple regression analyzes were determined for days with $\text{THI} > 72$ (Figure 4.3.).

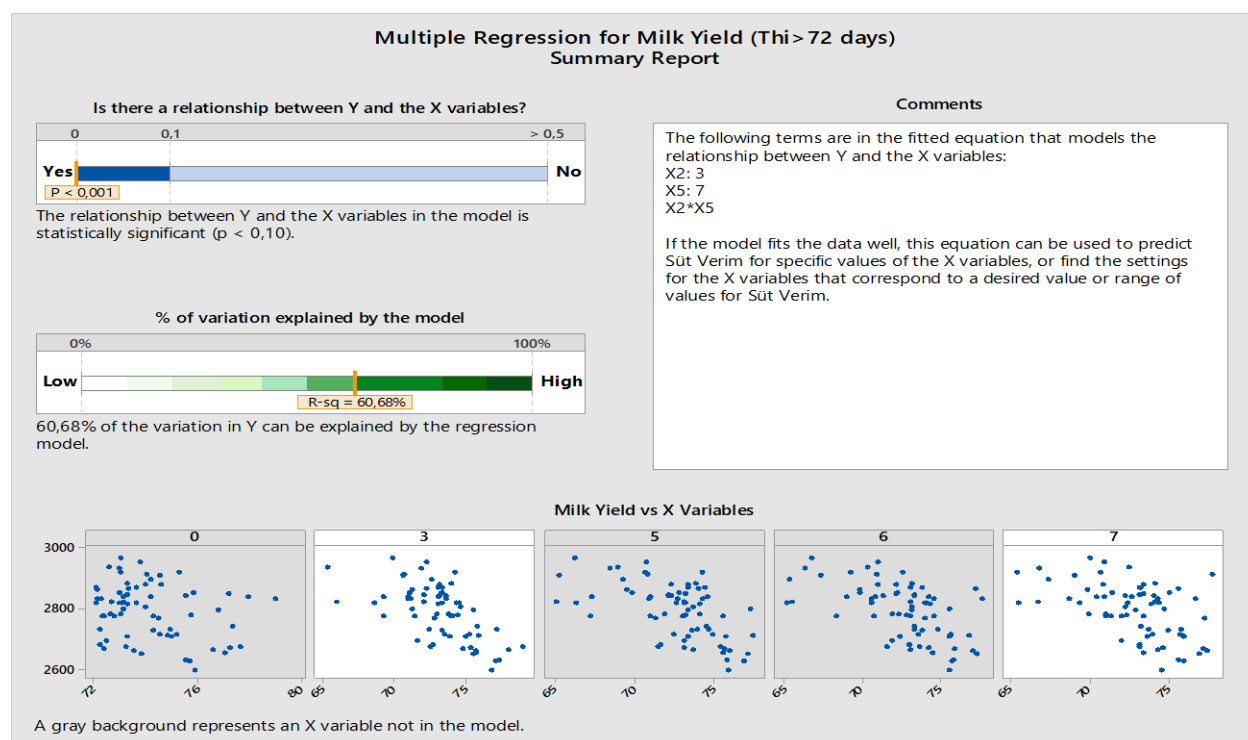


Figure 4.3. Multiple regression for Milk Yield ($\text{THI} > 72$ days)

On Days 3 and 7, $R^2 = 60.68\%$, $P < 0,001$ was obtained.

CONCLUSIONS

The relationship between THI and milk yield was statistically significant ($P < 0,012$), as seen in the graph, a decrease in yield after THI value of 72 was observed. The decrease in milk yield was determined as 0.15 kg on the same day and the next day averaged per unit THI increase per animal. Single regression analysis values increased up to the fifth day. It began to decrease with the sixth day.



CIGR 2018

XIX. World Congress of CIGR



The highest single regression value ($R^2=16.54$, $P<0.001$) and the correlation coefficient ($r=-0.157$) were determined on day 5. In days with $THI>72$, the 4-day delayed effect has the highest correlation ($r=-0.587$, $P<0.001$) and regression ($R^2=42.40$, $P<0.001$) values. The mechanism of the effect of the value of Temperature Humidity Index on milk yield and the process requires more detailed studies. Milk yield is influenced by THI values at a much longer period than the THI values at the same day.

ACKNOWLEDGEMENT

The author gives special thanks to Scientific Research Unit of Bursa Uludag University for the financial support with project of DDP(Z)-2016/3.

REFERENCES

- Anonymous, 2017. Turkish State Meteorological Service Statistical Data (in Turkish). <https://www.mgm.gov.tr/veridegerlendirme/il-ve-ilceler-istatistik.aspx?k=A&m=BURSA-> (Access: 12.11.2017).
- Bohmanova, J., Misztal, I., Cole, J. B. 2007. Temperature-Humidity Indices as Indicators of Milk Production Losses due to Heat Stress. *Journal of Dairy Science*, 90: 1947-1956.
- Bohmanova, J., Misztal, I., Tsuruta, S., Norman, H.D., Lawlor, T.J. 2008. Short communication: Genotype by environment interaction due to heat stress. *Journal of Dairy Science*, 91: 840-846.
- Bouraoui, R., Lahmar, M., Majdoub A., Djemali, M., Belyea, R. 2002. The relationship of temperature-humidity index with milk production of dairy cows in a Mediterranean climate. *Anim. Res.* 51: 479–491.
- Collier R.J., Zimbelman R.B. 2007. Heat Stress Effects on Cattle: What We Know and What We Don't Know. 22nd Annual Southwest Nutrition & Management Conference Proceedings, February 22-23, 2007, Tempe, Arizona, USA.
- Dikmen, S., Hansen, P. J. 2009. Is the temperature-humidity index the best indicator of heat stress in lactating dairy cows in a subtropical environment? *Journal of Dairy Science*, 92:109-116.
- Du Preez J.H., Giesecke W.H., Hattingh P.J. 1990. Heat stress in dairy cattle and other livestock under Southern African conditions. I. Temperature-humidity index mean values during the four main seasons, Onderstepoort *J. Vet. Res.* 57: 77–86.
- Freitas, M.S., Misztal, I., Bohmanova, J., West, J. 2006. Utility of on- and off-farm weather records for studies in genetics of heat tolerance. *Livestock Science*, 105: 223–228.



CIGR 2018

XIX. World Congress of CIGR



Gantner, V., Mijić, P., Kuterovac, K., Solić D., Gantner, R. 2011. Temperature-humidity index values and their significance on the daily production of dairy cattle. *Mljekarstvo*. 61(1): 56-63.

Ingraham R.H., Stanley R.W., Wagner W.C. 1979. Seasonal effect of the tropical climate on shaded and nonshaded cows as measured by rectal temperature, adrenal cortex hormones, thyroid hormone, and milk production, *Am. J. Vet. Res.* 40: 1792-1797.

Johnson, H.D. 1980. Depressed chemical thermogenesis and hormonal functions in heat. In: *Environmental Physiology: Aging, Heat, and Altitude*. Elsevier /North Holland, New York, pp. 3–9.

Johnson H.D. 1985. Physiological responses and productivity of cattle, in: Yousef M.K. (Ed.), *Stress physiology in livestock. Basic principles*, Vol. 1, 4–19, CRC Press, Boca Raton, Florida, pp. 4–19.

Polsky, L., Keyserlingk M.A.G. 2017. Invited review: Effects of heat stress on dairy cattle welfare. *Journal of Dairy Science*. 100: 8645–8657.

Ravagnolo, O., Misztal, I., 2000. Genetic component of heat stress in dairy cattle parameter estimation. *Journal of Dairy Science*, 83: 2126-2130.

St-Pierre, N.R., Cobanov, B., Schnitkey, G. 2003. Economic losses from heat stress by US livestock industries. *Journal of Dairy Science*, 86: 52-77.

West, J.W., Mullinix, B.G.; Bernard, J.K., 2003. Effects of hot, humid weather on milk temperature, dry matter intake, and milk yield of lactating dairy cows. *Journal of Dairy Science*, 86: 232-242.

Yazgan, K. 2017. Determining heat stress effect in Holstein dairy cattle using daily milk yield and meteorological data obtained from public weather station in Sanliurfa province of Turkey. *Indian Journal of Animal Research*, 51(6): 1002-1011.

Yousef, M. K. 1985. Stress physiology in livestock. *CRC Press*, Volume 2: 357–358. Boca Raton, FL.



CIGR 2018

XIX. World Congress of CIGR



Landscape Fragmentation In Europe: A Comparative Analysis

Andrea De Montis^{1,2}, Antonio Ledda¹, Vittorio Serra^{1,2}

¹Department of Agricultural Sciences, University of Sassari, 07100, Italy

²Department of Civil and Environmental Engineering and Architecture, University of Cagliari, 09123, Italy

E-mail: andreadm@uniss.it

ABSTRACT

Landscape fragmentation (LF) has been acknowledged as one of the main causes of biodiversity loss. The phenomenon consists of large-scale transformation of habitat patches in smaller fragments that tend to be more isolated over time. LF can be due to transport and mobility infrastructures (TMIs), and affects local climatic conditions, habitat quality, and isolation of animal and plant species. The literature supplies scholars with various indicators able to quantify the ecological impact of LF.

In this work, we assess and compare LF in four landscape units (LUs) of approximately the same surface area –two LUs in Wales (the UK) and two in Sardinia (Italy)- belonging to quite different ecological and institutional European contexts. We apply the Barrier Fragmentation Index (BFI), which takes into account the barrier effect of road infrastructures with reference to the perception of the hedgehog (*Erinaceus europaeus* L), a target species quite common in both the countries. We also measure LF through the Urban Fragmentation Index (UFI), which appreciates the effect of urbanized areas. While measuring the BFI, we consider the number of patches, the length of TMIs traits without discontinuities such as bridges and tunnels, the perimeter and area of the LUs, and the probability of barrier effect that varies according to the type of TMIs. We quantify the UFI taking into account area of the LUs and the extent and perimeter of urbanized areas.

We measured the highest values of BFI and UFI, respectively, in the ‘North East Wales’ (299733.70) and in ‘South East Wales’ (7.06). We registered the lowest values of the same indicators in the inner mountainous LU ‘Limbara’ (1441.57 for BFI, and 0.24 for UFI), in Sardinia. These results are a clear sign that coastal and more populated LUs are the most fragmented. These indications are key for planners and decision makers towards proper courses of actions toward defragmentation.

Keywords: Landscape fragmentation, Fragmentation indices, Urban Fragmentation Index, Barrier Fragmentation Index.



INTRODUCTION

In the last decades there has been a drastic reduction of habitats size and ecological connectivity. This phenomenon is related to increase of human needs, urban and rural sprawl, and transport infrastructures, which triggered landscape fragmentation processes (Harrisson et al., 2012). Landscape fragmentation (LF) can be defined as the dynamic process, where larger landscape fragments, or patches, tend to become smaller and more insulated than in their original condition (EEA, 2011). The LF phenomenon has effects on land use change and contribute to habitats and biodiversity loss (see, for example, Gibson et al., 2013, Foley et al., 2011; Foley et al., 2005). This process can be caused by linear transport and mobility infrastructures (TMIs) such as railways and roads and by urbanised surfaces, which can reduce the movement of animal species and landscape connectivity (LC) (Bissonette, Adair, 2008), i.e. a higher impedance to movement for mainly animal species, depending on the land cover pattern (Scolozzi and Geneletti, 2012). LF is measurable through indices, such as the Barrier Fragmentation Index (BFI), that measures LF caused by TMIs considering also the barrier effect, and the UFI, that quantifies LF caused by urbanized areas. This essay unfolds as follows. In the next section, we describe proposed methods and case studies. In the third and fourth section, we respectively present and discuss the results, while in the fifth section we report on the concluding remarks.

2. MATERIALS AND METHODS

Scientific literature is rich in indices able to measure LF, but few indices can be used to quantify LF caused by TMIs (Bruschi et al., 2015). In this work, we propose the Barrier Fragmentation Index, which allows us to assess LF caused by TMIs. BFI considers the barrier effect, that is, the way animal species perceive TMIs as obstacle (De Montis et al., 2017). The barrier effect is measurable by using the parameter F , which varies according to type of TMIs (Scolozzi, Geneletti, 2012). We consider as target species the European Hedgehog (*Erinaceus europaeus italicus*), whose values of $F(B)$ are reported in Table 1.

Table 8. Values of $F(B)$ according to the type of TMIs. Source: Scolozzi and Geneletti (2012).

(B) Type of infrastructure	$F(B)$
Fast-moving (two-lane) national roads and railways	0.95
Asphalted secondary (one or two-lane) roads with moderate traffic	0.50
Rural and forest paved roads	0.05

$F(B)$ is assessed by using a Delphy survey able to process the opinions of scientists, professionals, and experts with specific knowledge background about the target species.



CIGR 2018

XIX. World Congress of CIGR



The BFI obeys to the following equation:

$$BFI = \frac{\left(\sum_{i=1}^{i=n} L_i \cdot F(B)_i \right) \cdot N \cdot P}{A}$$

where L_i stands for length of TMIs traits, excluding discontinuities (bridges, viaducts, and tunnels), N for number of fragments, P and A respectively for perimeter and area of the LU.

Urbanization induces effects on ecological networks (De Montiset al., 2016) and causes fragmentation processes and soil consumption, which produce qualitative and quantitative effects on habitat, flora, and fauna (Astiaso Garcia et al., 2013). LF due to urban areas can be assessed through the UFI (Astiaso Garcia et al., 2013; Battisti and Romano, 2007; Biondi et al., 2003). According to Romano and Zullo (2013) and Battisti and Romano (2007), the UFI obeys to the following equation:

$$UFI = \frac{\sum_{i=1}^{i=n} Aurb_i}{At} \cdot \frac{\sum_{i=1}^{i=n} p_i}{2\sqrt{\pi \sum_{i=1}^{i=n} Aurb_i}}$$

where $Aurb_i$ stands for the extension in squared meters of the urban area, p_i for the perimeter in meters of the urban area, and At for the extension in squared meters of the LU area. The first term of the equation quantifies the incidence of urbanized areas on the LU surface; the second one stands for ratio between the perimeter of the urban area and the circumference of the equivalent circle (Romano and Zullo 2013). UFI ranges between zero (for absence of urban areas) and the value of the second term of the equation (Battisti et al. 2013). We apply the metrics in four Landscape Units (LUs) of approximately the same extent (about 1000 km²), in Sardinia (Italy) and Wales (the UK) (Figure 1).



CIGR 2018

XIX. World Congress of CIGR

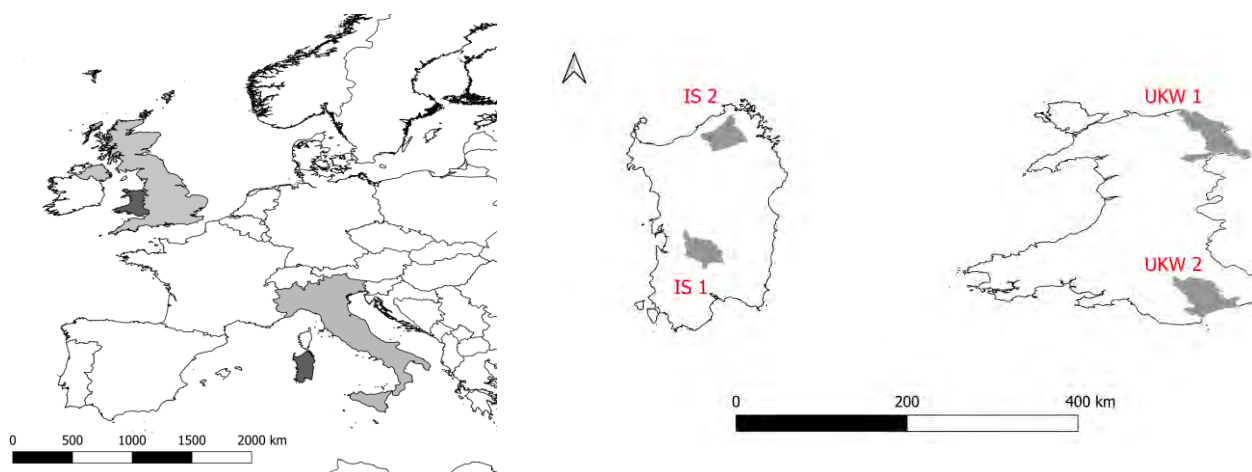


Figure 1. On the left: in dark gray, Sardinia and Wales. On the right: in gray: Regione delle Giare basaltiche (IS1), Limbara (IS2), North-East (UKW1), and South-East (UKW2). Source: our elaboration of data provided by Global Administrative Areas and Regions Sardinia and Wales.

We use the GIS to perform our study, because it has been proved useful in spatial analysis and in measuring landscape (habitat) fragmentation (De Montis et al., 2018; De Montis et al., 2017). We use data freely available online (RAS, 2008; Wales, 2017).

In order to apply the BFI, we implement a GIS and use data in shapefile format. Tunnels and bridges were excluded from TMIs traits. Then, we obtained and counted the number of landscape fragments. Finally, the values of the F(B) were associated with each type of TMIs. As for the UFI, we use data in shapefile format relating to urbanized areas, including, inter alia, urban and suburban industrial areas, rural buildings and so on. Microsoft Excel 2010 has supported the GIS analysis.

RESULTS

Table 2 shows the results of the application of the indicators:

Table 2. The assessment of LF according to BFI, UFI.				
State, region	Code	LUs	BFI	UFI
Italy, Sardinia	IS1	Regione delle Giare basaltiche	13568.89	0.43
	IS2	Limbara	1441.57	0.24
UK, Wales	UKW1	North East Wales	299733.70	3.40
	UKW2	South East Wales	296164.12	7.06



CIGR 2018

XIX. World Congress of CIGR



The results of Table 2 show that the most fragmented LUs are those from Wales. We obtained the highest values of BFI (299733.70) and UFI (7.06) in the Welsh LUs. Limbara shows the lowest values for both BFI 1441.57 and UFI 0.24.

4. DISCUSSION

Limbara appears as the least fragmented LU, with the lowest values of BFI and UFI. Limbara is a mountainous area with low density of urbanized areas and TMIs. The low values of BFI suggest a more favourable habitat for the hedgehog in the Sardinian LUs. In general, the Welsh coastal areas appear as the most fragmented according to BFI and UFI because of high urban pressure and high road density. That means the Welsh LUs are characterized by high level of human pressure consisting of infrastructures and settlements, which contribute in splitting up the landscape in several and smaller fragments than the two Sardinian LUs. On the whole, we stress three main findings. Firstly, we demonstrate that a set of indices can be applied in different geographical contexts according to a comparative approach. Secondly, the BFI, an index scarcely used in scientific literature, has proved consistent with well-known indexes that have been tested in previous international studies. Finally, through the proposed method we are able to identify critical areas where the hedgehog has its habitat. Thus, defragmentation measures could be planned at strategic level in order to reconnect habitat patches, enabling the hedgehog in crossing TMIs or urbanized areas.

5. CONCLUSION

We measured the effect of TMIs on the target species European hedgehog and the LF due to urbanized areas. We have developed a comparative approach by using two indices - BFI and UFI - that can give us information on the degree of LF. We applied the metrics in four geographical contexts, in Sardinia (Italy) and Wales (the UK). We found that the highest values of BFI and UFI characterised coastal and most populated areas (the most fragmented). In future studies, we aim at applying the metrics in other contexts and on different target species. This study provides quantitative measure of LF and could aid planners when defragmentation strategies need to be defined.



CIGR 2018

XIX. World Congress of CIGR



6. REFERENCES

- Astiaso Garcia, D., Bruschi, D., Cinquepalmi, F., Cumo, F., 2013. An estimation of urban fragmentation of natural habitats: case studies of the 24 Italian national parks. *Chem. Eng. Trans.* 32, 49–54.
- EEA (2011). *Landscape fragmentation in Europe*, Joint EEA-FOEN report. Copenhagen: European Environment Agency.
- Battisti C., 2004 “Frammentazione ambientale, connettività, reti ecologiche: un contributo teorico e metodologico con particolare riferimento alla fauna selvatica”. Provincia di Roma, Assessorato alle politiche agricole, ambientali e protezione civile, 246 pp.
- Battisti, C., Romano, B., 2007. *Frammentazione e connettività. Dall’analisi ecologica alla pianificazione ambientale*. CittàStudi, Torino.
- Bissonette, J.A., Adair, W. 2008. Restoring habitat permeability to roaded landscapes with isometrically scale wildlife crossings. *Biol. Conserv.*, 141(2): 482-488.
- De Montis, A., Caschili, S., Mulas, M., Modica, G., Ganciu, A., Bardi, A., Ledda, A., Dessena, L., Laudari, L., Fichera, C.R., 2016. Urban-rural ecological networks for landscape planning. *Land Use Policy* 50, 312–327, <http://dx.doi.org/10.1016/j.landusepol.2015.10.004>.
- De Montis, A., Martin, B., Ortega, E., Ledda, A., Serra, V. 2017. Landscape fragmentation in Mediterranean Europe: A comparative approach. *Land Use Policy*, 64: 83-94.
- De Montis, A., Ledda, A., Ortega, E., Martín, B., Serra, V., 2018. Landscape planning and defragmentation measures: an assessment of costs and critical issues. *Land Use Policy*, 72, pp. 313-324.
- Jaeger, J.A.G., 2000. Landscape division, splitting index, and effective mesh size: new measures of landscape fragmentation. *Landsc. Ecol.* 15 (2), 115–130.
- Foley, J.A., DeFries, R., Asner, G.P., Barford, C., Bonan, G., Carpenter, S.R., Chapin, F.S., Coe, M.T., Daily, G.C., Gibbs, H.K., Helkowski, J.H., Holloway, T., Howard, E.A., Kucharik, C.J., Monfreda, C., Patz, J.A., Prentice, I.C., Ramankutty, N., Snyder, P.K., 2005. Global consequences of land use. *Science* 309 (5734), 570–574.
- Foley, J.A., Ramankutty, N., Brauman, K.A., Cassidy, E.S., Gerber, J.S., Johnston, M., Mueller, N.D., O’Connell, C., Ray, D.K., West, P.C., Balzer, C., Bennett, E.M., Carpenter, S.R., Hill, J., Monfreda, C., Polasky, S., Rockström, J., Sheehan, J., Siebert, S., Tilman, D., Zaks, D.P.M., 2011. Solutions for a cultivated planet. *Nature* 478 (7369), 337–342.
- Gibson, L., Lynam, A.J., Bradshaw, C.J.A., He, F., Bickford, D.P., Woodruff, D.S., Bumrungsri, S., Laurance, W.F., 2013. Near-complete extinction of native small mammal fauna 25 years after forest fragmentation. *Science* 341 (6153), 1508–1510.



CIGR 2018

XIX. World Congress of CIGR



Gulinck, H. Wagendorp, T. (2002). References for fragmentation analysis of the rural matrix in cultural landscapes. *Landscape Urban Plann* 58:137–146

RAS, 2008. Carta dell'uso del suolo [Regional Land Cover Map –RLCM]. <http://www.sardegnageoportale.it/argomenti/cartedelsuolo.html>.

Romano, B., Zullo, F., 2013. Valutazione della pressione insediativa: indicatori e sperimentazione di soglie. In: Battisti, C., Conigliaro, M., Poeta, G., Teofili, C.(Eds.), *Biodiversità, disturbi, minacce*. Editrice Universitaria Udinese, Udine, pp. 170–177.

Scolozzi, R., Geneletti, D., 2012. Assessing habitat connectivity for land-use planning: a method integrating landscape graphs and Delphi survey. *J. Environ. Plan Manag.* 55 (6), 813–830.

Wales, 2017. Land use map. digimap.edina.ac.uk.

[https://digimap.edina.ac.uk/?utm_campaign=2118466_EDINA%20DFS:%20June%20Service%20Update%20\(Students\)&utm_medium=email&utm_source=dotmailer&dm_i=27JU,19EMA,7O4LSK,41F3R,1](https://digimap.edina.ac.uk/?utm_campaign=2118466_EDINA%20DFS:%20June%20Service%20Update%20(Students)&utm_medium=email&utm_source=dotmailer&dm_i=27JU,19EMA,7O4LSK,41F3R,1). Accessed Nov 2 2017.



CIGR 2018

XIX. World Congress of CIGR



The Power Transmission Characteristics of Overload Shafts with Different Friction Clutches and Spring Loading Conditions

Bülent Çakmak¹, İkbâl Aygün¹, Erdem Aykas¹

¹Department of Agricultural Engineering and Technology, Faculty of Agriculture,
Ege University, İzmir, Turkey
bulent.cakmak@ege.edu.tr

ABSTRACT

The power take-off (PTO) drive shafts, is one of the main ways to transfer power from the tractor to drive implements. To avoid overloads the PTO shaft must be implemented with a protective friction clutch. The friction clutch mechanisms has an important role particularly to a safety clutch for protecting machine drive lines especially useful in connecting the drive shafts of agricultural implements such as tractors or the like. A clutch particularly suitable for machine drives in agricultural implements including a clutch hub, a clutch sleeve, and spring-loaded members operative to engage and disengage for controlling torque transmission through the clutch. The friction discs within the clutch when the maximum torque is exceeded automatically disengaged the clutch. Upon achievement of a nominal torque which is spring-loaded in the clutch hub, may automatically re-engage the clutch.

In this study, load carrying characteristics of shafts with overloading clutches used in agricultural machineries were examined. Three shafts with overloading clutches which were made for different friction loaded by spring were mounted to the PTO shaft of the tractor and tested according to the TS 10990. The hydraulic dynamometer was used for breaking of shafts. Different compression strokes for spring were applied for loading friction clutch for comparison of slippage torque and transmitted power of clutches under loading.

Regression equations were obtained using slippage torques and power transmission data for different spring compressions strokes. By using these equations, one can adjust properly usable storks of spring for limiting torques of friction clutches.

Keywords: Shaft, Overloading clutch, Slippage torque, Compression spring, Turkey

INTRODUCTION

In the mechanization of agriculture works, most of the machines are commonly operated by tractors. The aging of agricultural machines, the absence or removal of safeguards, and working with worn, damaged protectors appear to be risk factors for the physical conditions of machines and used equipment (Beer et al., 2007). The use of machinery in agricultural production ensures timely production of different agricultural operations and an increase in labor productivity. However, during the operation, faults occur in machine elements due to different effects.

Bülent Çakmak, İkbâl Aygün, Erdem Aykas, “The Power Transmission Characteristics of Overload Shafts with Different Friction Clutches and Spring Loading Conditions”



CIGR 2018

XIX. World Congress of CIGR



The causes of malfunctions in agricultural machinery are presented in main groups as follows (Önal et al. 1994):

Fatigue

Wear

Overload

Using inaccurate and uninformed

In these groups, problems arising from overloading can be eliminated by using constructive solutions in motion transmission. For this purpose, drive shafts used in the transmission of motion are used in the mechanism that interrupts the movement under excessive load (Figure 1). The clutches installed on drive shaft will protect agricultural machinery against overloading and, thus, prevent machinery from failing or needing repairs. Overloading most commonly occurs when work begins and before the machine reaches its optimum speed of operation. However, machine may also overload if you drive too fast, if you process too much harvested crop at once or if your unit is blocked by foreign objects. Typical applications include: forage wagon, stable manure spreader, round baler, rotary harrow, gathering units on field choppers, snow blowers, etc.

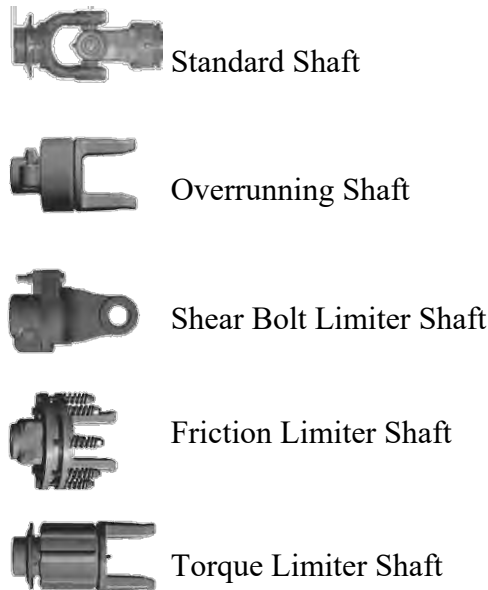


Figure 1. The standard and limiter shaft types in widely used

The Power Take-Off (PTO) shaft is an efficient means of transferring mechanical power between farm tractors and machines. The tractor's stub shaft, often called the PTO transfers power from tractor to the PTO-driven machine. Power transfer is accomplished by connecting a drive shaft



from the machinery to the tractor's PTO stub shaft. The PTO and drive shaft rotate at 540 rpm or 1000 rpm when operating at full recommended speed. At all speeds, they rotate in proportion to the speed of the tractor engine. The PTO and drive shaft is also one of the oldest and most persistent hazards associated with farm machinery. The high risk created by the PTO driveshaft has been noticed since the time they were used first. In 1957, initial legal regulations for the complete protection of shafts were developed in England. In the coming years, standards including basic requirements of shaft protections were used in agricultural machines by ASABE and ISO (ISO, 2004; ASABE, 2015).

Some types of deformation occurred when the PTO and drive shaft are overloaded. These deformations are a shaft tube twisting, shaft tube breaking, yoke breaking, inner shaft breaking, cross breaking and PTO shaft breaking. The friction limiter shaft is most commonly used one of clutch PTO drive shaft because has a very simple construction, repair and maintenance when compare the other types of drive shafts (Figure 2). The clutches installed on drive shaft will protect against overloading of shaft.

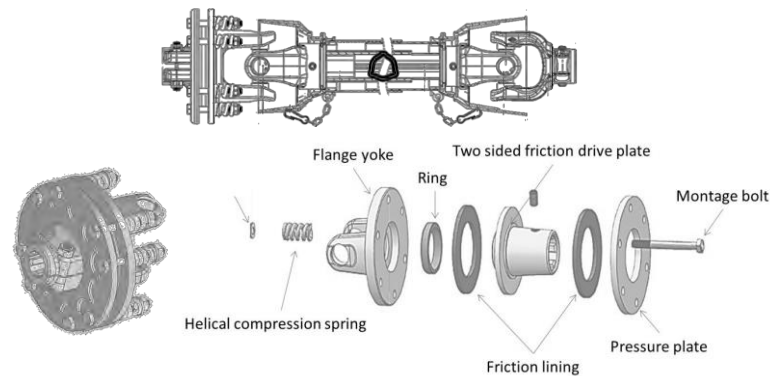


Figure 2. The friction limiter clutch of PTO Drive shaft

The friction limiter clutch of PTO Drive shaft consists of some basic parts as: helical compression springs, friction lining, pressure plate, flange yoke, ring and two sided friction drive plate. This clutch with 2 or 4 discs with free wheel. It is useful on machines with high levels of rotational inertia, which could cause breakage of transmission in case of sudden stop. For doing this be adjust spring compression load to pressure plate of clutch. In order to apply a balanced and sufficient pressure, all springs used in the clutch must have the same characteristics and the same load size.

In this study was obtained performance and accuracy of friction torques of shafts with different friction lining and spring load. The study findings were compared with the company declarations



about the performance selected PTO drive shafts. Then were examined the load carrying characteristics of shafts with overloading clutches used in agricultural machinery.

MATERIAL AND METHOD

In this study three different PTO drive shafts with friction limiter clutch were selected randomly for controlling the overload work performance (Figure 3). The PTO shaft of the tractor tested according to the TS 10990 (Anonymous 1993). All shafts have two friction lining with different size and 8 compressing springs which are different wire diameter and length (Table 9).



Figure 3. PTO drive shafts used in study

Table 9. Some specifications of friction linings used in clutch and shafts

Spring Steel Wire	Shaft A	Shaft B	Shaft C
Friction lining outer diameter, mm	122	140	160
Friction lining inner diameter, mm	81	87	97
Friction lining thickness, mm	4	4	4.8
Total weight of shaft, kg	14	21	24
Shaft length, min.- max., mm	950-1280	950-1250	950-1210

According to the DIN standard round spring steel wires has three main qualities. Little and often is static and variable loads for C class (Table 10). The difference between these steels; the combination of materials, heat treatment, and cold-molding and then the resulting strength limits and surface quality. A helical compression spring is a mechanical device used to store or release energy. It can also absorb shock or maintain a force between two surfaces. Compression springs are coil springs that resist a compressive force applied axially. Loads can be classified according to their application requirements: static (the spring is expected to operate between specified loads a few times only), cyclic (the spring is expected to cycle between specified loads many times), or dynamic (the spring is subjected to a high rate of load application, causing periods of excessive



CIGR 2018

XIX. World Congress of CIGR



stress). These springs are linear and thus have the same rate per mm throughout the entire spring.

Table 10. Some spring specifications of overloading clutch used in drive shafts

Spring Steel Wire	Shaft A	Shaft B	Shaft C
Material (EN 10270/1)	C Class		
Material code	SH		
Chemical analysis (in %) (EN 10270/1)	C: 0.35 to 1.00 / Si: 0.10 to 0.30 / Mn: 0.50 to 1.20 P: max. 0.035 / S: max. 0.035 / Cu: max. 0.20		
Tensile Strength (N mm ⁻²) (EN 10270/1)	1590-1880		
Wire diameter (mm)	4.6	6.7	6.7
Total coil number	6	4	4
Free length (mm)	38	35	35
Loaded length (factory setting, mm)	30.60 ±0.40	29.90 ±0.30	28.80 ±0.30
Spring rate, N mm ⁻¹	464	1347	1347
Inner diameter (mm)	8.6	10.9	10.9
Outer diameter (mm)	17.8	24.3	24.3

Friction lining was made by compound organic resin with copper wire. Coefficient of friction disc surface was 0.35 for organic. Friction linings are compressed by helical springs. These springs allow the linings to “slip” while engaging and disengaging.

Compression spring load: The force applied to a spring that causes deflection. It can be determined by multiplying the spring rate by deflection. It was carried out at 4 different spring compression loads according to free length of spring. For each load, the length of the spring is set in a precision of 1/100 mm. In order to apply uniform loading of clutch all adjustment nuts were tightened equally. All springs used in the clutch have the same characteristics but different size. Thus, the clutch was set at balanced and different pressure.

The study was carried out with a hydro dynamometer connected to a 4WD tractor of Fiat 80-66 brand at 80 HP (Table 11). M&W brand P-355 (USA) model hydro-dynamometer was used to load the PTO drive shaft at different load. The hydro-dynamometer was positioned and operated that the shaft axis and the tractor's PTO axis coincided during all trials (Figure 4). Torque values of the shafts are measured using the special purpose Torque meter which can measure the torque value of the tractor PTO shaft up to a maximum of 3000 Nm. Hydraulic dynamometer was used as a brake device. Both torque value and rotational speed are measured on the torque meter at the same time. The maximum torque and speed was determined for friction concept which is set at different spring loads. Four consecutive trials were carried out on the concept of friction for each loading of friction clutch. Because of the number of tests increase, the heat generated by the



friction can change the friction surface profile between the lining and the steel compression plate.

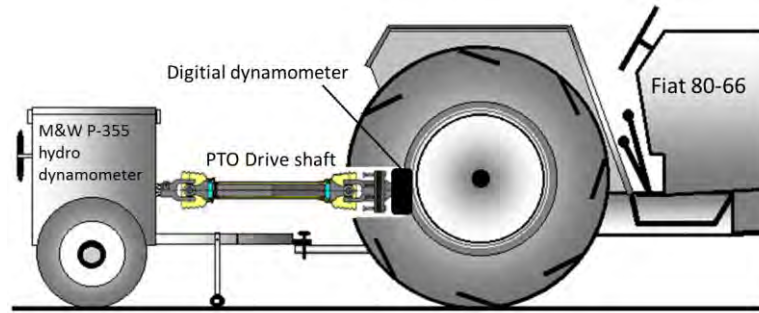


Figure 4. The operational position of hydro-dynamometer, tractor, shaft and dynamometer (Cakmak and Aykas, 2002)

Table 11. Some technical specification of TF 80-66 DT tractor (Taşbaş et al. 1999)

TF 80-66 DT	Power	Engine revolution	PTO revolution
At maximum PTO speed	52.8 kW (71.7 HP)	2500 min ⁻¹	614 min ⁻¹
At Standard PTO speed (540 min ⁻¹)*	50.3 kW (68.3 HP)	2200 min ⁻¹	540 min ⁻¹

* Trials were carried out at standard PTO speed.

RESULTS

It is important to know spring characteristics used in clutch for stable clutch performance. In order to determine spring characteristics was fully compressed and then unloaded a few times them. Thus it was obtained behavior of Compression Spring Hysteresis of helical spring. Hysteresis is mechanical energy loss occurring during loading and unloading of a spring within the elastic range. The mechanical energy loss is important for reliable clutch used on PTO drive shaft.

The hysteresis values of helical compression spring for selected shaft cultch were shown in Figure 4. The mechanical energy loss of 4.9% occurred in shaft A. The reduction of about 866 N was detected for each compression spring used in the friction limiter clutch. In this case it means that the first set mechanical load will be lost.

For Shaft B the mechanical energy loss is 4.3%. It means that the compression force loss is about 2015 N for each compression spring used in the friction. In this case it means that the first set mechanical load will be lost. For Shaft C the mechanical energy loss is 4.1 %. The



CIGR 2018

XIX. World Congress of CIGR



compression force loss is 1917 N for each compression spring used in the friction. The first set mechanical load will be lost.

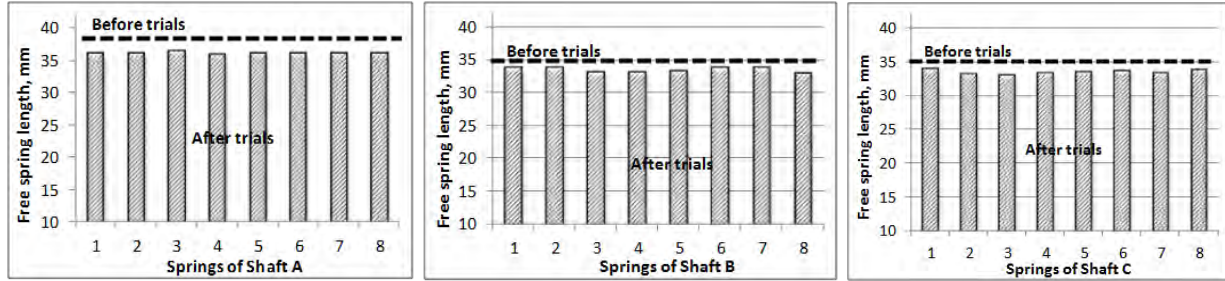


Figure 4. The mechanical energy loss as length loss of compression of helical spring

In this study also obtained the relation between helical spring compression force and transmitted force and power. Then was calculated regression equations for each PTO drive shaft. Figure 5, Figure 6 and **Hata! Başvuru kaynağı bulunamadı.** show transmitted torque and power values by the shaft A, shaft B and shaft C in different spring loads. The rhombus points are the results of the experiments. The star point represents the declaration of torque and power rating that the shaft company.

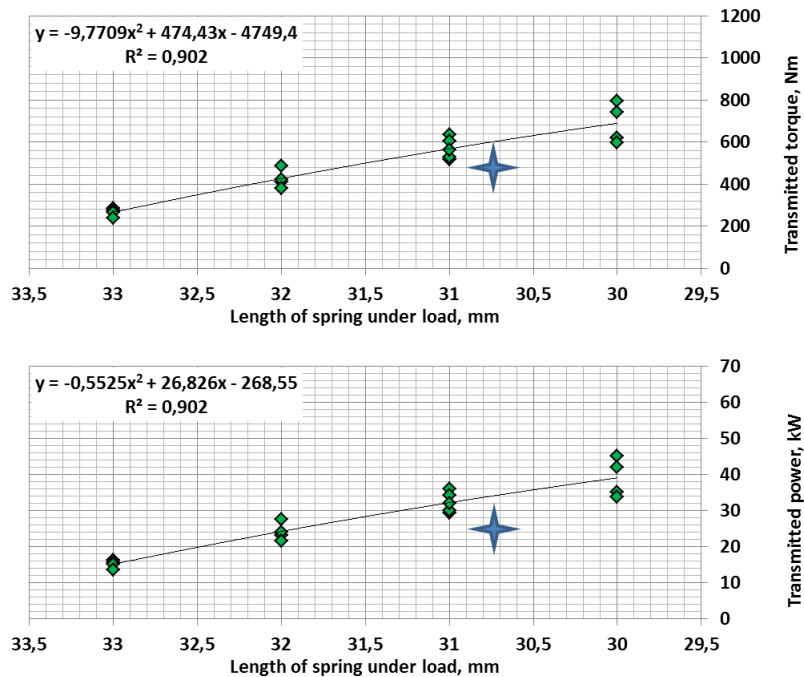


Figure 5. Maximum transmitted torque and power for Shaft A at different spring loads



CIGR 2018

XIX. World Congress of CIGR



It was obtained the model of regression from the results for each shaft. The R square value is about 0.9 for shaft A and 0.98 for shaft B. It was also found a considerable difference between study results and shaft firm declaration for specific working conditions.

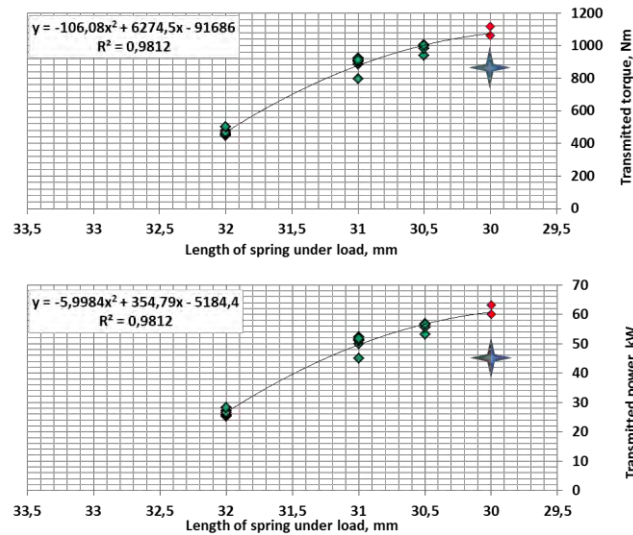


Figure 6. Maximum transmitted torque and power for Shaft B at different spring loads

These figures show transmitted torque and power values for each shaft in different spring loads. When the dimensions of lining and transmitted torque are raising the study values and firm values are getting closer each other.

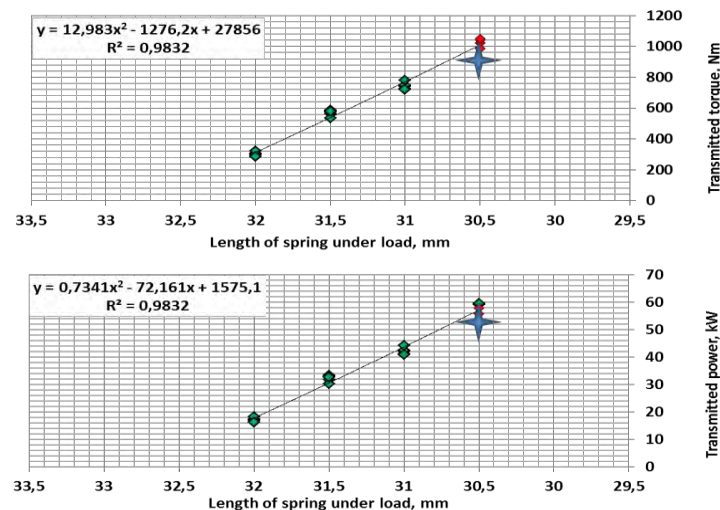


Figure 7. Maximum transmitted torque and power for Shaft C at different spring loads



CIGR 2018

XIX. World Congress of CIGR



DISCUSSION

The main outcomes of the study could be collected as follow;

When the loaded spring length increases (the pressure is increased) the transmitted values of torque and power by shaft had increase. This is an expected result.

Permanent deformation occurred in free spring length after the tests for all springs used on shaft clutches. This value is 4-5% on average. This ratio means a loss of compression force between 800 and 2000 N per spring according to the spring characteristics.

It has been determined that the values given by the producer the selected shafts are deviated from the actual results. The transmitted torque and power values of the shafts as a function higher than the company declaration. This can cause problems related to the machine and system powered by PTO.

It is important that the characteristics of the shafts are exactly known for each working conditions for safer operation.

REFERENCES

ASABE, 2015. Agricultural tractors- Rear-mounted power take-off types 1, 2, 3 and 4-Part 1: General specifications, safety requirements, dimensions for master shield and clearance zone, Standard, ANSI/ASABE AD500P1:2014 FEB2015

Çakmak B., Aykas E., 2002. Load Carrying Characteristics of Shafts With Overloading Clutches, The Journal of Agricultural Faculty of Ege University, Vol: 39, No:3, 129-136 pp., 2002 (Abstract in English)

ISO, 2014. Agricultural tractors - Rear-mounted powers take-off types 1, 2, 3 and 4-Part 1: General specifications, safety requirements, dimensions for master shield and clearance zone. ISO Standard 500-1:2014(EN). International Standard Organization, 5 p.

Önal, İ. Uçucu R., Aykas, E., 1994. T.C. Başbakanlık Güneydoğu Anadolu Projesi Bölge Kalkınma İdaresi Başkanlığı GAP Bölgesinde Tarımsal Mekanizasyon Gereksinimleri Etüdü Projesi TEMAV 34. Seminer Görev No C-1 Öngörülen Alet- Makine Setlerinde Arıza Olasılıklarının Belirlenmesi ve Arıza Gruplarının Çözümlemesi, Ankara

Taşbaş, H., Aygöl, A., Devecioğlu, Ö., Doğangüzel, D., 1999. Müdürlüğümüzce Testi Yapılan Yerli ve İthal Tarım Traktörlerinin OECD Test Koduna Göre Belirli Özellikleri. Tarım ve Köyişleri Bakanlığı Tarım Alet ve Makinaları Test Merkezi Müdürlüğü Yayın No:6, Ankara



CIGR 2018

XIX. World Congress of CIGR



Environmental Importance of Olive Groves in Cultural Landscape, The Case Study of Antalya

Reyhan Erdogan¹, Zeynep Zaimoğlu²

¹Department of Landscape Architecture, Akdeniz University, Antalya, Turkey

²Department of Environmental Engineering, Cukurova University, Adana, Turkey
reyherdogan@gmail.com

ABSTRACT

Olive (*Olea europaea*), is a tree species unique to the Mediterranean climate, which is eaten with its fruit. Olive groves which have importance in terms of the sustainability of urban ecosystems are essential for the planning of the Mediterranean cities. Urban vegetation in olive groves increase property values improve privacy and provide many environmental benefits. They reduce heating and cooling costs, reduce pollution, take up carbon dioxide, produce oxygen, provide habitat for wildlife, hold water and reduce soil erosion. Antalya is the Mediterranean city. It has been the center of culture, art, architecture and mythology throughout its history.

With its nature made up of dark blue seas, spectacular Taurus mountains, fervent waterfalls and world known holiday villages is what makes Antalya the capital of Tourism. There are too many hotels and new tourism facilities have still been built in the city. The rise of the building sector affects all the planning actions all over the city. Because of this, in urban areas hard surface density is rising and by the conclusion of this process affects the urban areas. Under these conditions, the identities of the cities are lost and decrease of the green areas like olive groves affect life quality of the public. Antalya has very important olive grove which is called “Zeytinpark” is the largest green space in a city in Turkey. There are 23 thousand olive trees in

Zeytinpark in the size of 2630 decares. This area was declared as “Grade 1 Natural Protected Area” by Antalya Cultural and Natural Heritage Protection Board on 26.10.1998. This area was separated as ‘Agricultural Qualities Protection Area’ with the decision of the protection board on 14.06.2007. Despite all this, Zeytinpark is in danger of losing its original quality. Human impact on natural landscapes through urbanization era is becoming more and more dramatic and is the cause of serious environmental problems in Antalya as well as in Turkey. In this research olive grove which is valuable for urban ecosystem was defined on urban structural plan for Antalya. It was proposed some suggestions for protecting and using Zeytinpark olive grove.

Reyhan Erdogan, Zeynep Zaimoglu. “Environmental Importance of Olive Groves in Cultural Landscape, The Case Study of Antalya”



CIGR 2018

XIX. World Congress of CIGR



The olive grove an important landscape component. However, the area that are represent of the agricultural Mediterranean vegetation are facing extinction in urban because of rapid urbanization in Antalya. Zeytinpark should be preserved as it is with the existing properties. It must be transferred to future generations with a sustainable management understanding.

Keywords: Olive groves, Mediterranean, urbanization, protection, environment, Turkey

INTRODUCTION

The olive tree in all the holy books is the symbol of the most important virtues and values for holiness, abundance, justice, health, pride, victory, prosperity, wisdom, redeem, purification and rebirth. Antalya is decorated with olive trees. Approximately a hundred olive trees were planted in the refugees and crossroads of Antalya (Figure 1).



Figure 1. Olive trees in Antalya (Original, 2018)

This sacred tree is the symbol of immortality in all mythologies. Today, the passenger who visits the Aegean coasts of Anatolia can rest under the olive trees he lived in the shadow of Homeros, and hear this old wise tree whispering to his ear:«I belong to everyone and I do not belong to anyone, I was here before you came, so I will be here later as you go» It really did. Throughout the history of the olive tree, with its shadow, its wood, its fruit and its unique oil; it was a commodity that gave life and power to societies and people.

Reyhan Erdogan, Zeynep Zaimoglu. “Environmental Importance of Olive Groves in Cultural Landscape, The Case Study of Antalya”



CIGR 2018

XIX. World Congress of CIGR



Solon's laws, which were accepted as one of seven scholars in ancient Greece, applied severe penalties to the olive tree cutters. This is the first known olive conservation law in history. But unfortunately, we are not protecting our olive grove in Turkey. Punishment is not deterrent (Figure 2).



Figure 2. Olive trees for sale in the Aegean region (Anonymous, 2018)

Olive (*Olea europaea*), is a tree species unique to the Mediterranean climate, which is eaten with its fruit. Olive groves which have importance in terms of the sustainability of urban ecosystems are essential for the planning of the Mediterranean cities. Urban vegetation in olive groves increase property values improve privacy and provide many environmental benefits. They reduce heating and cooling costs, reduce pollution, take up carbon dioxide, produce oxygen, provide habitat for wildlife, hold water and reduce soil erosion.

In Turkey, as of 2013, 826 hectares of land, which is around 2 % of the total agricultural land, is dedicated to olive production. At the beginning of 1990s, this area was around 870 hectares. Olive cultivation area has shrunk almost 40 % in 1990s, with rapid opening of olive orchards to urbanization. Starting from the beginning of 2000s, the area dedicated to olive orchards has extended to its former levels with support policies of the government. As of 2014, there are 169 million olive trees, of which 83 % is olive bearing (Gürkan, 2015).

Since 2004, the share of olive bearing trees fell from a level of 90 % because of the newly established orchards in the last decade. In 2014, around 1.8 million tons of olives are harvested, of which almost $\frac{1}{4}$ of it is used for table olive production and $\frac{3}{4}$ for olive oil production. When



CIGR 2018

XIX. World Congress of CIGR



we look at the trend of olive production, we can easily see the high periodicity, which is one of the main problems in Turkey (Gürkan, 2015).

40,000 acres of olive trees were planted in the Cumhuriyet District of Şarköy in 1995 with the support of the state. With the permission to build in the area, the olive grove fell to 18 thousand acres. Olive trees were cut in areas near the sea and many sites were established (Figure 3) (Anonymous, 2017).



Figure 3. Olive trees were cut in Şarköy (Anonymous, 2017).



CIGR 2018

XIX. World Congress of CIGR



OLIVE TREES IN ANTALYA AS A CULTURAL LANDSCAPE

Cultural landscapes are landscapes that have been affected, influenced, or shaped by human involvement. A cultural landscape can be associated with a person or event. It can be thousands of acres or a tiny homestead. It can be a grand estate, industrial site, park, garden, cemetery, campus, and more. Collectively, cultural landscapes are works of art, narratives of culture, and expressions of regional identity. There are primarily four types of cultural landscapes, although any given landscape may fall under more than one typology. Cultural landscapes are a legacy for everyone. These special sites reveal aspects of our country's origins and development as well as our evolving relationships with the natural world. They provide scenic, economic, ecological, social, recreational, and educational opportunities helping communities to better understand themselves. Neglect and inappropriate development put our irreplaceable landscape legacy increasingly at risk. Too often today's short-sighted decisions threaten the survival and continuity of our shared heritage. It is everyone's responsibility to safeguard our nation's cultural landscapes. The ongoing care and interpretation of these sites improves our quality of life and deepens a sense of place and identity for future generations (The Cultural Landscape Foundation, 2018).

Antalya is the Mediterranean city. It has been the center of culture, art, architecture and mythology throughout its history. With its nature made up of dark blue seas, spectacular Taurus mountains, fervent waterfalls and world known holiday villages is what makes Antalya the capital of Tourism. There are too many hotels and new tourism facilities have still been built in the city. The rise of the building sector affects all the planning actions all over the city. Because of this, in urban areas hard surface density is rising and by the conclusion of this process affects the urban areas. Under these conditions, the identities of the cities are lost and decrease of the green areas like olive groves affect life quality of the public.

Antalya has a very important olive grove which is called “**Zeytinpark**” is the largest green space in a city (Figure 4). Zeytinpark was 22.000 decares in 1935. It was not easy at that time to create this olive grove. It has historically important. Now, there are 23 thousand olive trees in Zeytinpark in the size of 2.630 decares. This area was declared as "Grade 1 Natural Protected Area" by Antalya Cultural and Natural Heritage Protection Board on 26.10.1998. This area was separated as 'Agricultural Qualities Protection Area' with the decision of the protection board on 14.06.2007. Despite all this, Zeytinpark is in danger of losing its original quality (Figure 5).

Reyhan Erdogan, Zeynep Zaimoglu. “Environmental Importance of Olive Groves in Cultural Landscape, The Case Study of Antalya”



CIGR 2018

XIX. World Congress of CIGR



Figure 4. Zeytinpark is the biggest green area in Antalya (Google map, 2018)

The olive grove an important landscape component. However, the area that are represent of the agricultural Mediterranean vegetation are facing extinction in urban because of rapid urbanization in Antalya. Zeytinpark should be preserved as it is with the existing properties. It must be transferred to future generations with a sustainable management understanding.



Figure 5: Some views from Zeytinpark (Original, 2018)

Reyhan Erdogan, Zeynep Zaimoglu. “Environmental Importance of Olive Groves in Cultural Landscape, The Case Study of Antalya”



CIGR 2018

XIX. World Congress of CIGR



Today, there are excellent training programs carried out in Zeytinpark. One of them is “The Nature Academy The Nature Academy is an educational program that includes children of using all their senses for learning of nature and culture of Antalya. At the same time children try to nature. In this training program, the principles of learning which develop critical thinking skills, questioning, doing and experiencing are adopted. This study was conducted by T.C. Antalya Governorship, Antalya Provincial Directorate of National Education and Antalya Zeytinpark A.Ş. in the 11 th January 2016. The program aims to educate preschool and elementary school children with games.

There are some different kinds of projects for Zeytinpark. First project which is designed on 400 decares of which no olive trees are located, is calculated as 15 million Turkish Liras in 2014. The project has bird tunnel, watchtower, olive museum, youth center, country coffeeshouse, horse farm, olive market, urban values exhibition area, plant species education center, exhibition area, unobstructed life center in nature, learning center in nature, multi-purpose sports field, grass dunes, children playground, fragrance hills, cruise terrace, Zeytinpark square, artificial pond, area of ornamental plants in Mediterranean Region, area of medicinal aromatic plants, area of endemic species in Mediterranean Region, area of Mediterranean Region fruits and their production areas. There is another project about Zeytinpark is really different. Ottoman and Seljuk style theme park wanted to design in Zeytinpark (Anonymous, 2014b).

CONCLUSION

Zeytinpark cleans the air in Antalya city by absorbing 2.600 tons of dust and 610.000.000 m³ of carbon dioxide every year (Anonymous, 2016). It should not be spent for rent. It should not be converted to an ordinary park. It enjoys agricultural tradition from the past, introducing the olives of the region to the visitors. Zeytinpark is the cultural heritage of the city with its open green area and nature. All plants and natural objects found in the field must be protected. All new objects and equipment to be applied to the area should be designed so as not to disturb the area.

Activity areas should be designed to be hidden in natural tissue. Visitors should be offered the opportunity to experience activities together with nature. Zeytinpark should serve children, young people and all people with its whole prosperity for education (Figure 6).

Reyhan Erdogan, Zeynep Zaimoglu. “Environmental Importance of Olive Groves in Cultural Landscape, The Case Study of Antalya”



CIGR 2018

XIX. World Congress of CIGR



Figure 6. Meeting with nature in Antalya (Original, 2018)

The new projects for Zeytinpark should be abandoned. In this study different kinds of recommended field uses are dangers for sustainable of park. The project can be damaging the existing structure of olive fields. There should not be an Ottoman and Seljuk style theme park to be built in the area of cultural heritage.

REFERENCES

- Anonymous, 2018. <http://www.hurriyet.com.tr/ekonomi/300-yillik-agac-5-bin-lira-2947774>
Erişim tarihi: 10 Ocak 2018
- Anonymous, 2017. <https://www.sozcu.com.tr/2017/gundem/sarkoyde-kesilen-zeytin-agaclarinin-yerine-siteler-yukseliyor-2028433/> Erişim tarihi: 5 Ocak 2018
- Anonymous, 2016. Antalya Zeytinpark, Doğa Çağırıyor, <http://www.zeytinpark.com.tr/>, Erişim tarihi: 5 Ocak 2018
- Anonymous, 2014a. <https://emlakkulisi.com/antalya-zeytinpark-projesinde-sona-yaklasildi/221930>, Erişim tarihi: 8 Ocak 2018
- Anonymous, 2014b. <https://emlakkulisi.com/hakan-tutuncu-vakif-ciftligini-halka-kazandiracagiz/289284>, Erişim tarihi: 10 Ocak 2018
- Google map, 2018.
- Gürkan, N.P. 2015. Turkish Olive and Olive Oil Sectoral Innovation System: A Functional - Structural Analysis, The Graduate School Of Social Sciences Of Middle East Technical University PhD Thesis, 411 p.
- The Cultural Landscape Foundation, 2018. About Cultural Landscapes
<https://tclf.org/places/about-cultural-landscapes>, Erişim tarihi: 15 Ocak 2018

Reyhan Erdogan, Zeynep Zaimoglu. "Environmental Importance of Olive Groves in Cultural Landscape, The Case Study of Antalya"



CIGR 2018

XIX. World Congress of CIGR



Urban Agriculture as a Tool for Environmental Protection

Reyhan Erdogan¹ Zeynep Zaimoğlu²

¹Department of Landscape Architecture, Akdeniz University, Antalya, Turkey

²Department of Environmental Engineering, Cukurova University, Adana, Turkey
reyerdogan@gmail.com

ABSTRACT

Urban agriculture is an activity which is using plantation, animal rearing along with input production and distribution, processing and marketing of produced goods for the purpose of income generation and providing the required fresh food. It is an integral part of the city's ecological and economic system which uses typical possibilities unique to the city itself. It has the potential to change food safety, the benefits of conservation of nature, and even the form of the city. As a sustainable environmental tool, it can improve the heat islands and effects in cities, creates green areas, reduce flood floods and improve air quality. Since food production takes place locally, there is also the potential to reduce energy, quality, crop loss and pollution from transport.

Urban agriculture is being thought to as an alternative model in Turkey and especially Antalya. Agricultural activities continue in Antalya city in small scale. It is important to have access to clean food, for the children to be involved in the growth processes of the plants and to experience being a producer and a self-sufficient society. Urban must have a discernment of agriculture that is renewable, sustainable, ethical, supports recycling, protects limited water resources, gives priority to ecological balance, gives maximum benefit to areas, chooses nature compatible material, refuses to use chemical drugs and supports causal relationship.

The new understanding of agricultural design, in which urbanites share this process with landscape architects, should actually aim to be a part of our lives. For this reason, agricultural activities should be widespread on small scales as well as on large scales. Roofs, terraces, and even balconies, must be made out of idle spaces. These areas can give new life spots to urban areas where all these headings are applied and not only drowned by aesthetic concerns. Urban agriculture areas should be protected in Antalya and urban agriculture should be supported.

Keywords: Urban agriculture, Environmental protection, Antalya, Turkey



CIGR 2018

XIX. World Congress of CIGR



INTRODUCTION

Human when he lives in the city needs to relationship with the nature, soil, plant and animal. Urban agriculture is an activity which is using plantation, animal rearing along with input production and distribution, processing and marketing of produced goods for the purpose of income generation and providing the required fresh food. It is an integral part of the city's ecological and economic system which uses typical possibilities unique to the city itself. It has the potential to change food safety, the benefits of conservation of nature, and even the form of the city. As a sustainable environmental tool, it can improve the heat islands and effects in cities, creates green areas, reduce flood floods and improve air quality. Since food production takes place locally, there is also the potential to reduce energy, quality, crop loss and pollution from transport.

Urban agriculture has the ability to supply and feed an urban population. While this argument refers to the ability of providing actual food for people and establishing a food secure community, it can also be extended to encompass a variety of functions that complement lives of urbanites. In addition to giving urban residents the chance to grow their own food, urban agricultural activities can also help generating income through the selling of food products, it can provide a sustainable urban environment through maintenance of urban ecosystems, and finally it can enhance cultural and social ties within a community and create food aware communities and also residents who can claim right to participate in the development of urban spaces (Çağlayık Eloğlu, 2012).

There are different kinds of urban agriculture concept. These are allotment gardens, community gardens and city farms. The urban agriculture concepts share common characteristics within but these can change according to their location, and region (Akyol, 2011). Table 1 gives the characteristics of urban agriculture concepts.



CIGR 2018

XIX. World Congress of CIGR



Table 1. Criteria for urban agriculture concepts (Akyol, 2011).

	Allotment gardens	Community gardens	City farms
Aim	To supply food for family or individual, Hobby.	To supply food for community, Hobby, Social gathering.	To supply food for city, Trade, Education, Social gathering, Sports and Recreation.
Location	Inner urban area	Urban-urban fringe (vacant lots, unexploited area within educational or health facilities)	Urban fringe
Size	Up to 1000 m ² each allotment appr: 250 m ²	1000-5000 m ²	More than 10.000 m ²
Ownership	State owned or private (rented to management)	Stateowned, Association owned, Charity owned	Individual, Association owned, Land trusts, and Local authorities
Management	Lease holders (individuals, families).	An organizing group of individuals who volunteer for working.	Voluntary workers, Paid employees
Consumer	Individuals, families who manage the land.	Volunteer workers and individuals in neighborhood.	Citizens who come to buy the products.
Access to the garden/farm	Limited (The land belongs to the holder during the rent period)	Open for access. (The entrance hours depends on the organization community rules).	Semi limited. (Open for educational, sports, and community activities).
Features	Raising beds, Warehouse, Compost area, Hedges as boundaries (optional).	Open and undercover cultivation areas, Warehouses, Lawn, Community gathering squares, Compost area, Little recreation	Open and undercover cultivation areas, Accommodation, Recreational and resting areas, Compost area, Education activity places, Sport facilities. Sales area
Products	Vegetable, fruit, ornamental plants	Vegetable, fruit, ornamental plants	Any kind of plant and animal production

URBAN AGRICULTURE IN THE WORLD

According to the UNDP, there are 800 million people across the globe who are working on urban agriculture. Furthermore %15 of the world's food need is provided by urban agriculture. For example in Canada Vancouver %44 of the homeowners and in Toronto %40 of homeowners are

Reyhan Erdogan, Zeynep Zaimoglu. "Urban Agriculture as a Tool for Environmental Protection"



CIGR 2018

XIX. World Congress of CIGR



engaged in urban agriculture. After 10 years of development with the help of the urban agriculture, the food needs of the half of Havana city's is being provided and thousands of people are being employed in Cuba (Yilmaz, 2015).

Farming systems are continuously changing in European peri-urban fringes and planning strategies specifically designed for a sustainable development of the urban-rural interface have been proposed in an increasing number of cities.

Urby Staten Island that is 900-apartment complex in the New York City is an example of a self-contained community with an agricultural area of 450 square meters, communal kitchen, well water filtered for drinking and many other features (Figure 1). Between a weekly farm stand, the three restaurants they supply with vegetables, a “veggie pick-up bundle, and donations to a local food bank, they’re plowing through the more than 50 types of produce, which includes everything from mustard greens to cutting flowers to Asian broccolini (Amelinckx, 2016).



Figure 1. Empress Green, a 4,500-square foot urban farm located at Urby Staten Island, a 900-apartment complex in New York City (Amelinckx, 2016, Mazzara, 2016).

THE IMPORTANCE OF URBAN AGRICULTURE IN TURKEY

Turkey had its share from the urbanization trends as well as it has seen a rise in the urbanization process in the last decades. While the urban population accounted to 38.5% of the total population in 1970s, it reached 65% in 2005 indicating a massive change in population dynamics (Ozer, Vardar and Ozer, 2007). Today, 75 % of the total population is living in urban areas in Turkey (TUIK, 2018).

Due to urban activities and preferences of city municipalities in Turkey, it is progressively lost green areas in urban areas (Figure 2).

Reyhan Erdogan, Zeynep Zaimoglu. “Urban Agriculture as a Tool for Environmental Protection”



CIGR 2018

XIX. World Congress of CIGR



Figure 2. Cutting urban trees in the historical city centres of Konya and Sivas (Kocakurt, 2018).

We need more green area, safety food and sustainable life for our children. The number rose to 30 metropolitan cities with law No. 6360 issued in 2012 in Turkey. The municipal boundary was extended to the provincial border. Half of the 39,000 villages gained neighborhood status. Village concept is over. In the metropolitan areas, the agricultural lands are in rapid danger of concreting. Turkey's population is increasing. It is imperative to protect the agricultural land in order to provide the necessary food for the increasing population (Figure 3) (Anonymous, 2018).



CIGR 2018

XIX. World Congress of CIGR



Figure 3. Cultural heritage, İstanbul Yedikule Bostanları (Atalık, 2016).

Especially in cities such as Istanbul, most of the free space is used as a waste landfill and excavation casting area, besides visual pollution, unhealthy areas occur. Areas covered with grass and bushes turn into a crime scene. At this point, urban agriculture undertakes an important function, and the community gardens and urban farms, as well as improving the visibility of the environment they are located in, provide security.

According to Ahern (2002), landscape planning is an action to conserve unique, scarce and rare resources, to prevent it from dangers, to control the use of rare resources and to decide areas for development. Landscape architecture aims to help local authorities and municipalities about sustainable planning and management of urban agricultural areas. On the one hand, planning is a useful tool for protecting and sustainable use of these ecosystems; on the other hand, it is very productive for local inhabitants in the terms of awareness-raising about the sustainable use of these areas (Erdoğan et.al, 2015).

URBAN AGRICULTURE IN THE ANTALYA

Its practices in Turkey is quite limited availability. Regulations of laws are required for the increase of urban agriculture applications.



CIGR 2018

XIX. World Congress of CIGR



Antalya is the Mediterranean city in Turkey Figure 4. Human impact on natural landscapes through urbanization era is becoming more and more dramatic and is the cause of serious environmental problems in Antalya as well as in Turkey. Table 2. Urban agriculture is being thought to as an alternative model in Antalya. Agricultural activities continue in Antalya city in small scale. It is important to have access to clean food, for the children to be involved in the growth processes of the plants and to experience being a producer and a self-sufficient society. Urban must have a discernment of agriculture that is renewable, sustainable, ethical, supports recycling, protects limited water resources, gives priority to ecological balance, gives maximum benefit to areas, chooses nature compatible material, refuses to use chemical drugs and supports causal relationship.

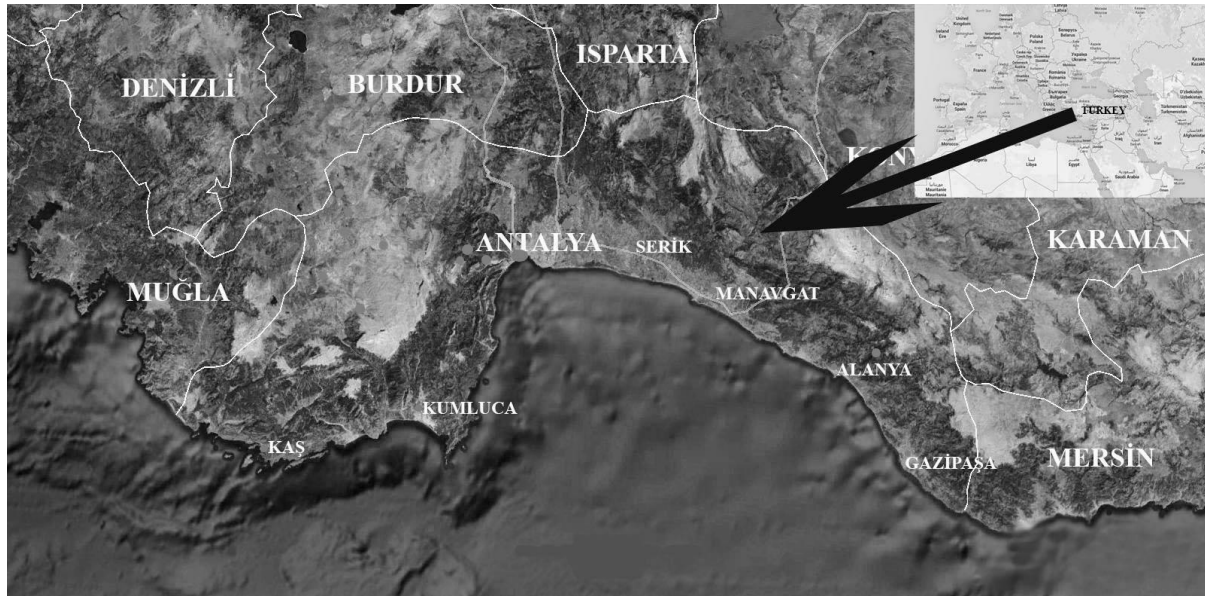


Figure 4. Topografic map of Antalya

Table 1: Plants in the orchards in Antalya

Familia	Species
Rutaceae	<i>Citrus aurantium</i>
	<i>C. deliciosa</i>
	<i>C. grandis</i>
	<i>C. limon</i>
	<i>C. medica</i>
	<i>C. nobilis</i>
	<i>C. sinensis</i>
	<i>C. unshiu</i>

Reyhan Erdogan, Zeynep Zaimoglu. “Urban Agriculture as a Tool for Environmental Protection”



CIGR 2018

XIX. World Congress of CIGR



	<i>C. paradisi</i>
Rosaceae	<i>Eriobotrya japonica</i>
Moraceae	<i>Ficus carica</i> subs. <i>carica</i>
	<i>Morus alba</i>
	<i>M. alba</i> , <i>pendula</i> ‘
	<i>M. nigra</i>
	<i>M. rubra</i>
Musaceae	<i>Musa acuminata</i>
Myrtaceae	<i>Myrtus communis</i> subsp. <i>communis</i>
Oleaceae	<i>Olea europea</i> var. <i>europea</i>
Cactaceae	<i>Opuntia ficus-indica</i>
Rosaceae	<i>Prunus cerasifera</i>
Punicaceae	<i>Punica granatum</i>
Vitaceae	<i>Vitis vinifera</i>

It is very important for a healthy and sustainable urban life that people are open to these options and that the city offers opportunities. Because the physical and spiritual health of individuals is the main element of community health. Recognizing this, local governments offer hobby gardens to urban people in order to bring people together with nature and land and to make them feel good about themselves.

The community garden that Antalya Metropolitan Municipality provides at Çakırlar will be an example of this approach. A "Hobby Garden Project" has been established in an area of 78.000 m² in Antalya's Bahtılı District. In this area, 348 parcels, each consisting of garden of 81 m² and house of 5 m², provide citizens with the opportunity to make hobby purposefully agricultural production (Figure 5). In the facility which is projected on an area of approximately 140.000 m², in order to meet the social needs of the users; running tracks, cafeterias, sports facilities, mosque, children's play areas are designed. The purpose of this declaration is to provide suggestions to ensure effective use of hobby gardens and to increase their usefulness.



CIGR 2018

XIX. World Congress of CIGR



Figure 5. Antalya Metropolitan Municipality's Hobby Garden Project (Brn.air, 2018).

CONCLUSION

Urban agriculture is an important tool for ensuring sustainable urban development. While expanding the boundaries of the city, it should not be neglected to create agricultural land in addition to protecting agricultural lands. Our historical estates should not be converted into shopping centers for the economic purpose.

The new understanding of agricultural design, in which urbanites share this process with landscape architects, should actually aim to be a part of our lives. For this reason, agricultural activities should be widespread on small scales as well as on large scales. Roofs, terraces, and even balconies, must be made out of idle spaces. These areas can give new life spots to urban areas where all these headings are applied and not only drowned by aesthetic concerns. Urban agriculture areas should be protected in Antalya and urban agriculture should be supported. New developments integrated urban agriculture into Antalya's development plan, and production permeated every surface.

An urban farming community must be support with local governments.

Turkey Community Garden Association should be created to improves people's quality of life by providing a catalyst for neighborhood and community development, stimulating social interaction, encouraging self-reliance, beautifying neighborhoods, producing nutritious food, reducing family food budgets, conserving resources and creating opportunities for recreation, exercise, therapy and education.



CIGR 2018

XIX. World Congress of CIGR



The Association should support community gardening by facilitating the formation and expansion of state and regional community gardening networks; developing resources in support of community gardening; and, encouraging research and conducting educational programs.

6. REFERENCES

- Akyol, M., 2011. Evolution Of Urban Agriculture Concept And Determination Of Design Criteria, Istanbul Technical University, Institute Of Science And Technology, M.Sc. Thesis, page, 99.
- Amelinckx, A., 2016. Meet the Woman Who Runs NYC's First Commercial Farm in a Residential Development, <http://modernfarmer.com/mtmf/empress-green-urby-staten-island/>
- Anonymous, 2018. <http://www.arkitera.com/haber/27463/kent-ve-tarim--birbirine-muhtac-iki-arkadas>
- Atalık, A., 2016. Kent ve tarım birbirine muhtaç iki arkadaş, <https://www.birgun.net/haber-detay/kent-ve-tarim-birbirine-muhtac-iki-arkadas-125110.html>
- Çağlayık Eoğlu, S., 2012. Urban Agriculture in Istanbul: The Road to Food Security and Sustainability, Master Thesis, Norwegian University of Life Sciences, Department of Agroecology, page 53.
- Erdoğan R., Dirik H., Oktay H.E., 2015. "Protecting and Sustainable use of Meadows which is Under Pressure of Urbanization And Tourism in the Case Study of Antalya", Ciosta 2015, St. Petersburg, RUSYA, 26-28 Mayıs 2015, pp.272-281
- Kocakurt, H., 2018. <http://www.arkaguverte.com/gundem/agacla-bir-sorunlari-olmali-sivasin-oncesi-ve-sonrasi-karar-sizin-47946/>
- Mazzara, B., 2016. Staten Island's Hottest Amenity: A Commercial Farm? <https://www.bisnow.com/new-york/news/sustainability/meet-the-farmer-in-residence-of-staten-islands-rooftop-commercial-farm-66863>
- Ozer, G., Vardar, E., and N. Ozer, 2007. Unplanned Settlements within the context of Urbanization Process of Turkey. FIG Commission 3 Workshop, Athens, Greece.
- TUIK, 2018. Turkey Statistics Institution Datas
- Yılmaz, Ç., 2015. Kentsel Tarımın Avrupa Birliği ve Türkiye'deki Geleceği, T.C. Gıda Tarım ve Hayvancılık Bakanlığı, AB Uzmanlık Tezi, s.87



CIGR 2018

XIX. World Congress of CIGR



Determination of Threshing Performance of New Design Threshing Unit for Lavandin (*Lavandula x intermedia emeric ex loisel.*)

Deniz YILMAZ¹, Mehmet Emin GOKDUMAN¹

¹ Department of Agricultural Machinery and Technologies Engineering, Faculty of Agriculture, University of Suleyman Demirel, Isparta, Turkey

denizyilmaz@sdu.edu.tr

ABSTRACT

In this study, the threshing system performances required for Lavandin (*Lavandula x Intermedia Emeric Ex Loisel.*) have been determined. Physico-mechanical properties used in the design of the threshing system were determined in three different moisture range for lavandin plant and the system design has been made according to the harvest moisture values.

In this study, threshing efficiency, work efficiency, power requirement and specific energy consumption values of the threshing unit developed were determined. In order to determine the threshing performance of the prototype, experiments were made at 3 different moisture ranges, 3 different drum speed, 3 different drum-concave open and 3 different feeding rates. Each experiment was performed in 3 replicates. As a result, a total of 243 experiments were carried out for a plant in the threshing experiments.

According to the study results, threshing efficiency for Lavandin (*Lavandula x Intermedia Emeric Ex Loisel.*) in the study has been changed between 45.69% and 95.56%. Work efficiency of threshing units has been changed between 0.67 kg/h and 12.27 kg/h. Power requirements and specific energy consumption of threshing units have been determined as 0.200- 1.081 kW and 0.027-0.592 kWh/kg respectively.

This study is contained some of the TUBITAK-3501-National Young Researchers Career Development Program (CAREER) Project named “Determination of Some Threshing and Separation Parameters of Medical and Aromatic Plants and Development of Prototype (111O179).

Keywords: Lavandin (*Lavandula X Intermedia Emeric Ex Loisel.*), Threshing, Design, Aromatic plant, Turkey

INTRODUCTION



Lavandin is one of the most important medical aromatic plant used in the perfumery industry. Lavandin species are hybrid between the Lavender and spike lavender varieties. Lavender, from Lamiaceae family in the form of shrubby, is a perennial, valuable and essential oil plant and is grown primarily in Mediterranean and Balkan countries and in many countries around the world (Fig. 1).



Figure 1. The lavandin plant

Turkey has a great potential about medical aromatic plants thanks to its climate and plant diversity. However, most of the medicinal and aromatic plants are wildy harvested from nature and harvesting and post harvesting processes are carried out by conventional methods or semi-mechanical systems. Therefore, some problems are emerged in harvesting, transporting, threshing and cleaning of medical aromatic plants. In order to the help overcome disadvantages in the mechanization of lavandin cultivation threshing parameters of lavandin plant should be known for new design threshing systems.

In this study, the threshing parameters and system performances required for Lavandin (*Lavandula x Intermedia Emeric Ex. loisel.*) have been determined. The system performance of machine is indicate with the threshing efficiency, the work efficiency, the power requirement and specific energy consumption for lavandin threshing machine. In order to determine the threshing performance of the prototype, experiments were made at 3 different moisture ranges, 3 different drum speed, 3 different drum-concave open and 3 different feeding rates. Each experiment was performed in 3 replicates.



2. MATERIALS AND METHODS

The specific threshing unit designed for lavandin plant has been used during the performance experiments. The threshing unit consists of 2 rasp bar type threshing cylinders, 2 gear motors, torque meter for power measurement, cylinders distance mechanism (Fig. 2). The system also has product observation window on the main frame. For this study, the lavandin plants (*Lavandula x Intermedia Emeric Ex Loisel.*) were harvested by hand from the experimental field in The University of Isparta Applied Science, Turkey.

In order to calculate the torque and the power consumed by the threshing unit a torque meter connected between the reducer electric motor and the drum shaft.

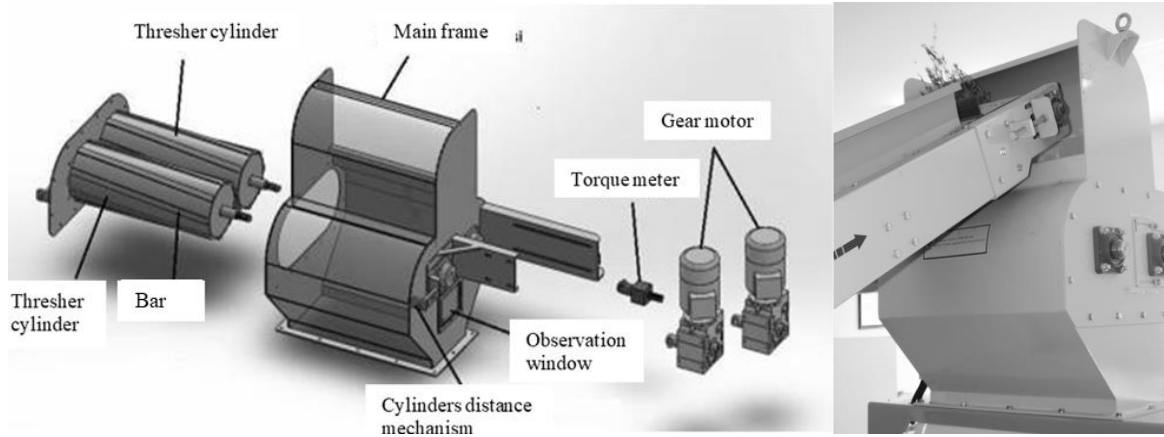


Figure 2. The threshing unit used in the experiments

The lavandin plants have been dried in the rooms at 35 ° C after harvesting. In order to determine the threshing performance of system the experiments have been conducted at 3 different moisture contents as 8.4%, 11.8% and 14.3% d.b. The threshing cylinders (drum) speeds of the unit have been determined as 100, 250 and 400 rpm. 3 different drum-concave open for the threshing unit have been adjusted as 14, 15 and 16 mm. The product feeding rates have been determined as 190, 380, 570 kg/h. Conveyor belt speed of feeding unit is determined as 0.26 m/s. Each experiment has been performed in 3 replicates. The operating parameters of the threshing system for lavandin plant carried out at 3 different moisture contents have been given in Table 1.



CIGR 2018

XIX. World Congress of CIGR



Table 1. The operating parameters of the threshing unit for lavandin plant

Drum Speed (rpm)			Drum-Concave Opening (mm)			
Cylinder 1			Cylinder 2	1	2	3
1	2	3				
100	250	400	35	14	15	16

3. RESULTS AND DISCUSSIONS

Because of the experiments conducted depending on the moisture content of the lavandin, drum-concave opening, feeding rate and drum speed of the threshing system, the threshing efficiency values have been range from 45.69% to 95.56%. The threshing unit efficiency for lavandin plant depending on the 3 different moisture contents are given in Fig. 3.

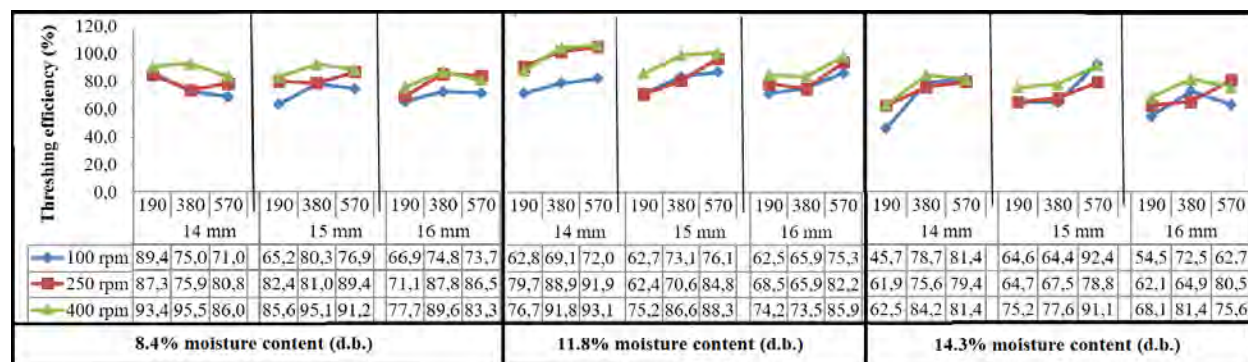


Figure 3. The effect of drum-concave opening × feeding rate × drum speed on the threshing efficiency at different moisture contents

As a result of the threshing experiments depending on the moisture content of the lavandin plant, the threshing efficiency have been decreased as the moisture content have been increased. The triple interaction of drum-concave opening × feeding rate × drum speed on the threshing efficiency at 8.4%, 11.8 and 14.3% d.b. moisture contents has have been found statistically significant ($p < 0.05$). The highest threshing efficiency value has been found at 8.4% d.b. moisture content, 14 mm drum-concave opening, 400 rpm drum speed and 380 kg/h feeding rate. On the other hand, the lowest efficiency value has been found as. 45.69% d.b at the same moisture content, 14 mm drum-concave opening, 100 rpm drum speed and 190 kg/h feed rate.



According to the result of the study conducted depending on the moisture content of the lavandin plant, drum-concave opening, feeding rate and drum speed of the threshing system, the work efficiency values of the system was given in Fig. 4.

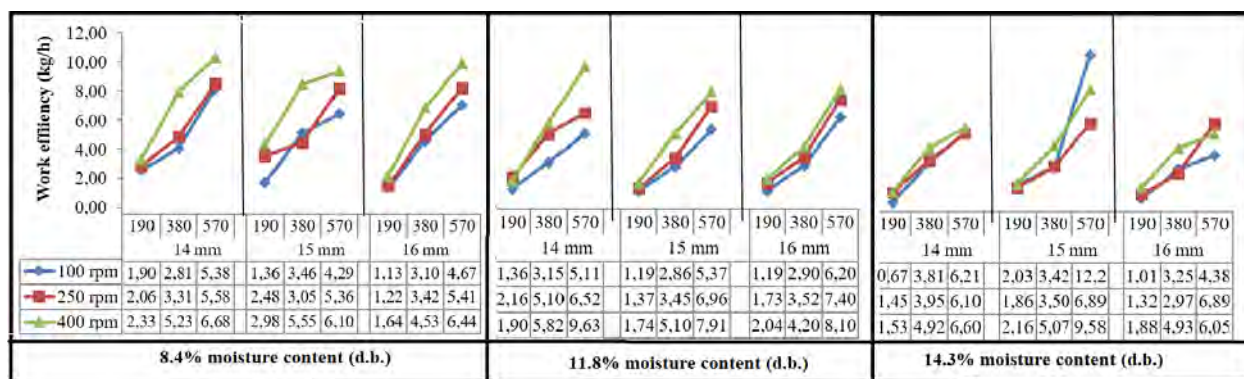


Figure 4. The effect of drum-concave opening × feeding rate × drum speed on the work efficiency at different moisture content

According to the result of the study depending on the moisture content of the lavandin plant, the work efficiency has increased with increasing moisture content. The triple interaction of drum-concave opening × feeding rate × drum speed on the work efficiency at 8.4%, 11.8% and 14.3% d.b. moisture contents has been found statistically significant ($p < 0.05$). The work efficiency values changed between 0.67 kg/h to 12.27 kg/h. The highest and lowest work efficiency values have been found as 14.3% d.b. at same moisture content. Whereas the lowest work efficiency value has been determined at 14 mm drum-concave opening, 100 rpm drum speed and 190 kg/h feed rate, the highest values have been observed at 100 rpm drum speed and 570 kg/h feed rate.

Power requirement of the threshing unit should be known for system performance. The power requirement values of the threshing units carried out at 3 different moisture contents are presented in Figure 5.



CIGR 2018

XIX. World Congress of CIGR

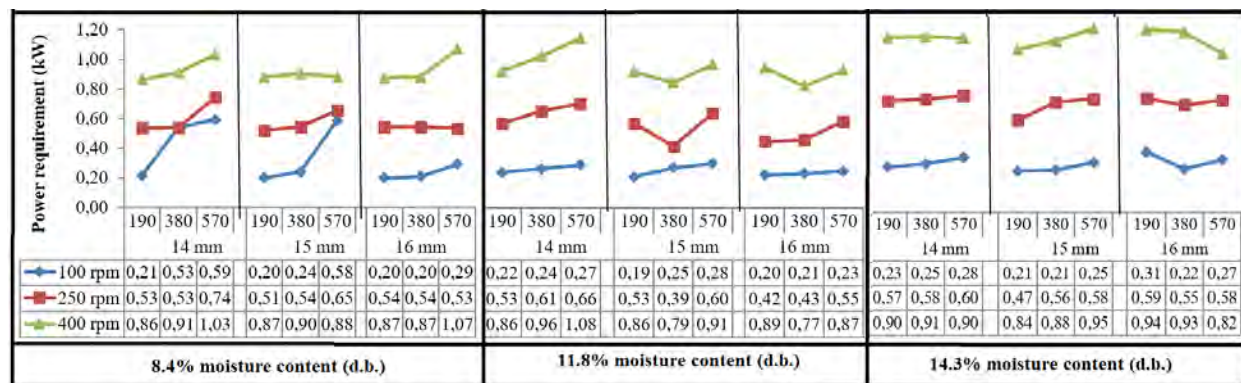


Figure 5. The effect of drum-concave opening × feeding rate × drum speed on the power requirement at different moisture contents

The power requirement values of the system according to the measured values depending on the moisture content of the lavandin, drum- concave opening, feeding rate and drum speed of the threshing unit, varied between 0.200 kW to 1.081 kW. The triple interaction of drum-concave opening×feeding rate×drum speed on the power requirement at 8.4% 11.8% and 14.3% d.b. moisture contents have been found statistically significant ($p < 0.05$). Power requirement decreased up to 11.8% of moisture content. At the 14.3% of moisture content the power requirement values increased again with the increasing of the moisture content of the lavandin plant. While the lowest and highest power requirement of the threshing unit for lavandin plant at same moisture content of 11.8 % d.b. the lowest and highest values have been obtained at 100 and 400 rpm drum speed, respectively. The drum-concave opening and feed rate values for minimum power requirement for threshing of lavandin plant is determined as 15 mm and 190 kg/h.

Specific energy consumption of machine must be known for the proper system performance of threshing unit. The specific energy consumption values of the threshing unit carried out at 3 different moisture contents were varied from 0.027 to 0.592 kWh/kg and presented in Figure 6.

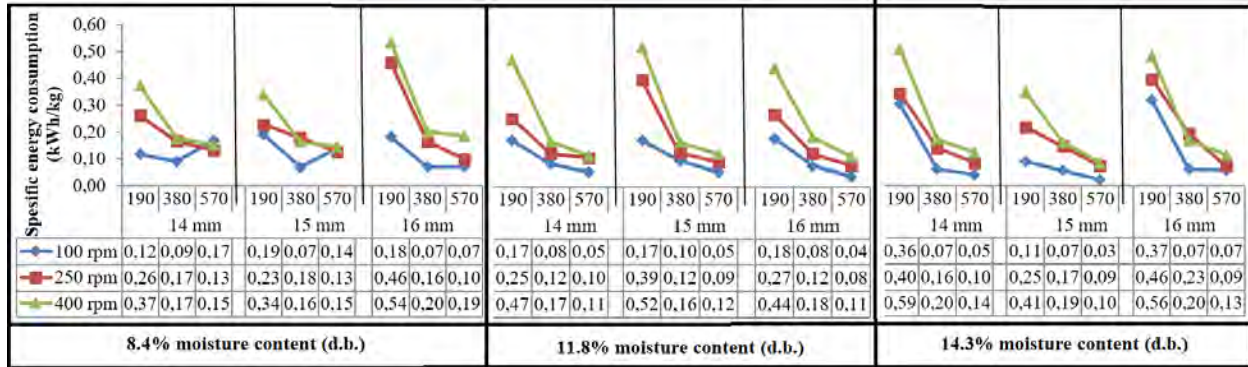


Figure 6. The effect of drum-concave opening × feeding rate × drum speed on the specific energy consumption at different moisture contents

The triple interaction of drum-concave opening × feeding rate × drum speed on the specific energy consumption at 8.4%, 11.8% and 14.3% d.b. moisture contents have been found statistically significant ($p < 0.05$). The lowest and highest specific energy consumption values of threshing unit for lavandin plant has been determined at %14.3 of moisture content. While specific energy consumption of threshing unit for lavandin plant has been lowest at 15 mm drum-concave opening, 570 kg/h feeding rate and 100 rpm drum speed, it has been highest at 14 mm drum-concave opening, 190 kg/h feeding rate and 400 rpm drum speed.

4. CONCLUSIONS

In this study, threshing unit performance values and working parameters have been determined for the lavandin plant. The threshing efficiency, work efficiency and specific energy consumption values of new design threshing unit have been determined.

When the new design threshing unit for lavandin plant is examined in terms of threshing efficiency, it is recommended to operate the threshing unit with 8.4% d.b. moisture content at 14 mm drum-concave opening, 380 kg/h feeding rate and 400 rpm. On the other hand, it is suggested that for the high work efficiency, threshing unit can be performed with 14.3% d.b. moisture content, 15 mm drum-concave opening, 570 kg/h feeding rate and 400 rpm drum speed for the lavandin plants. The working parameters should be selected as 11.8% moisture content, 15 mm drum-concave opening, 190 kg/h feeding rate and 100 rpm drum speed for the minimum power requirement. The working parameters of the threshing unit for the minimum specific energy consumption should be selected as 14.3% d.b. moisture content, 15 mm drum-concave opening, 570 kg/h feeding rate and 100 rpm.



CIGR 2018

XIX. World Congress of CIGR



According to the results, it can be said that the most suitable working parameters for the threshing of lavandin plants are 14.3% of moisture content, 15 mm of drum-concave opening, and drum speed values is recommended as 100 or 400 rpm.

5. ACKNOWLEDGEMENTS

This study is included a part of the project TUBITAK-3501-National Young Researchers Career Development Program (CAREER) "Determination of Threshing and Separation System Parameters of Some Medicinal Aromatic Plants and Development of Prototype (111O179)" We would like to thank the TUBITAK for its contributions to the project conducted by Deniz YILMAZ.

6. REFERENCES

- Anonymous, 2005. "European Community Biodiversity Clearing-House Mechanism". Glossary of Biodiversity Related Terms.
- Anonymous, 2012. Tıbbi ve Aromatik Bitki İşletmelerinin Yapısal Analizi, Batı Akdeniz Tarımsal Araştırma Enstitüsü Müdürlüğü, Antalya.
- Arın, S., Akdemir, B., Kayışoğlu, B. 1988. Trakya Bölgesinde Bitkisel Üretimde Enerji Bilançosunun Oluşturulması. Tarımsal Mekanizasyon 11. Ulusal Kong. Bildiri Kitabı, Sayfa: 124–135, Erzurum.
- Baydar, H. 2009." Tıbbi ve Aromatik Bitkiler Bilimi ve Teknolojisi (Genişletilmiş 3. Baskı)", Isparta: Süleyman Demirel Üniversitesi Yayınları, 51.
- Çelik, H. K., Akıncı, İ. 2012.Tarım Makineleri Tasarımı ve Geliştirilmesinde Bilgisayar Destekli Tasarım ve Mühendislik Uygulamaları. 27. Tarımsal Mekanizasyon Ulusal Kongresi, 5-7 Eylül, Samsun.
- Faydaoğlu, E., Sürücüoğlu, M. S. 2011. Geçmişten günümüze tıbbi ve aromatik bitkilerin kullanılması ve ekonomik önemi. Kastamonu Üniversitesi Orman Fakültesi Dergisi, 11(1), 52-67.
- Kutzbach, H.D. 2003. "Approaches for Mathematical Modelling of Grain Separation. International Conference on Crop Harvesting and Processing". CD version, 2, Kentucky USA.
- Sonmete, M. H., Demir, F. 2006. Yerli Tip Harman Makinasında Aspiratör Kanat Tiplerinin Ayırma Performansına Etkisinin Belirlenmesi. Selçuk Tarım ve Gıda Bilimleri Dergisi, 20(38), 88-97.



CIGR 2018

XIX. World Congress of CIGR



Determination of Separating Performance of New Design Separating Unit for Lavandin (*Lavandula x intermedia emeric ex loisel.*)

Deniz YILMAZ ¹, Mehmet Emin GOKDUMAN ¹

¹ Department of Agricultural Machinery and Technologies Engineering, Faculty of Agriculture, University of Suleyman Demirel, Isparta, Turkey

*Corresponding author email: denizyilmaz@sdu.edu.tr

ABSTRACT

Lavender, from Lamiaceae family in the form of shrubby, is a perennial, valuable and essential oil plant and is grown primarily in Mediterranean and Balkan countries and in many countries around the world.

For many years, mechanization of harvesting and threshing has been successfully implemented for various crops and has been developed depending on technological progress. However, the processes of threshing, separating and cleaning of medicinal aromatic plants are carried out by conventional methods (by hand) after the products are dried. This case leads to damage in the product, loss of labor and yield. In order to help to overcome these disadvantages and separate the dried products from the foreign materials such as stalk, spall and dust special separating systems designed depending on the plant are needed.

In this study, the separation-cleaning performances required for Lavandin (*Lavandula X Intermedia Emeric Ex Loisel.*), for our country and the Mediterranean Region, have been determined. Performance values and working limits of the prototype designed have been determined. The separation system consists of two sieves which have adjustable vibrating, velocity and inclination features.

According to the study results, separating efficiency for Lavandin (*Lavandula X Intermedia Emeric Ex Loisel.*) used in the study has been changed between 48.86% and 99.65%. Work efficiency of separation units has been changed between 0.39 kg/h and 3.81 kg/h. In different operations, specific power consumption of separation unit has been changed between 3.48 kW/kg and 39.65 kW/kg.

*This study is contained some of the TUBITAK-3501-National Young Researchers Career Development Program (CAREER) Project named “Determination of Some Threshing and Separation Parameters of Medical and Aromatic Plants and Development of Prototype (111O179).

Keywords: Lavandin (*Lavandula X Intermedia Emeric Ex Loisel.*), separating, design, aromatic plants, Turkey



CIGR 2018

XIX. World Congress of CIGR



INTRODUCTION

Harvesting, threshing, separating and cleaning medical aromatic plants is very important. For many years, mechanization of harvesting and threshing has been successfully implemented for various crops and has been developed depending on technological progress. It has been taken considerable steps about the medicinal-aromatic plant mechanization and different types of separating systems with the increasing demand for medicinal and aromatic plants used in harvesting and threshing machines. However, the processes of threshing, separating and cleaning of medicinal aromatic plants especially lavandin plants are carried out by conventional methods (by hand) after the products are dried. These traditional methods cause damage to the product, loss of labor and yield for the lavandin plants. Therefore, in order to overcome these disadvantages and separate the dried products from the foreign materials such as stalk, spall and dust special separating systems designed depending on the lavandin plant are needed.

It is known that it is necessary to use modern technology in agricultural production in order to use full agricultural potential in Turkey. For this purpose, it is should be known the performance of industrial plants such as lavandin for new designed machines.

In this study, the separation-cleaning performances required for Lavandin plant (*Lavandula x intermedia emeric ex loisel.*) have been determined. The system performance of machine is indicate with the separating efficiency, the work efficiency and specific power consumption values. In order to determine the separation performances of the separating system, 3 different sieve type experiments were performed depending on the amount of 3 different feedings. Experiments were carried out at 3 different sieve speeds and 3 different sieve slopes for lavandin. Each trial was performed in 3 replicates.

2. MATERIALS AND METHODS

The specific separating unit designed for lavandin has been used during the performance experiments. The separating unit consists of chassis, mainframe, two sieves, which have adjustable vibrating, velocity and inclination features, sieve housings, inclination adjusting mechanism and material outlet unit. (Fig. 1). In the separating system, there is a vibrating mechanism allowing the material to remain on the sieve longer. The system also has product observation window on the main frame.



CIGR 2018

XIX. World Congress of CIGR

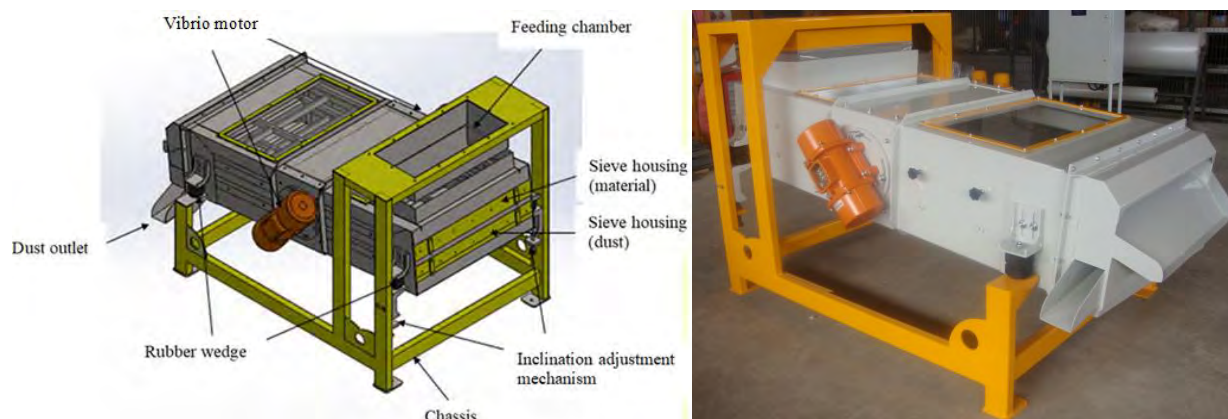


Figure 1. The separating unit used in the experiments

For this study, the lavandin plants (*Lavandula x Intermedia Emeric Ex Loisel.*) were harvested by hand from the experimental field in The University of Isparta Applied Science, Turkey. Performance tests of the separating unit have been carried out in Harvesting Machinery Laboratory.

The lavandin plants have been dried in the rooms at 35 ° C after harvesting. When medicinal plant materials are prepared for use in dry form, the moisture content of the material should be kept as low as possible in order to reduce mould damage and other microbial infestation (Máthé, 2015). Therefore, the moisture content value of lavandin plant has been selected as 11.8 %d.b. between 10-12%. In order to determine the separating performance of system for lavandin plant the experiments have been conducted at 3 different sieves type as 4 and 6 mm round hole sieves, 4-20 oblong sieve. The sieve velocity of the unit has been determined as 35, 40 and 45 Hz. 3 different sieves inclination of separating unit have been adjusted as 14, 15.8 and 17.6%. The product feeding rates have been determined as 190, 380, 570 kg/h. Each experiment has been performed in 3 replicates. The operating parameters of the separating unit for sage plant carried out at 3 different sieve types have been given in Table 1.

Table 1. The operating parameters of the separating unit for lavandin plant

Sieve velocity (Hz)			Sieve inclination (%)		
1	2	3	1	2	3
35	40	45	14 (8°)	15.8 (9°)	17.6 (10°)



CIGR 2018

XIX. World Congress of CIGR



The flowers and dusts were fell from the holes in the sieve to the bottom sieve during the separating process. The materials taken from product outlet chambers were weighed. The power requirement is measured by the ammeter connected to the vibro-motor depending on the current change and the specific power requirement of the separating unit were calculated.

3. RESULTS AND DISCUSSIONS

According to results of the experiments conducted with different sieves for sage plant, depending on sieve velocity, feeding rate and sieve inclination of the separating unit, the separating efficiency values have been range from 48.86% to 99.65%. The separating unit efficiency values for lavandin plant depending on the 3 different sieve types have been given in Figure 2.

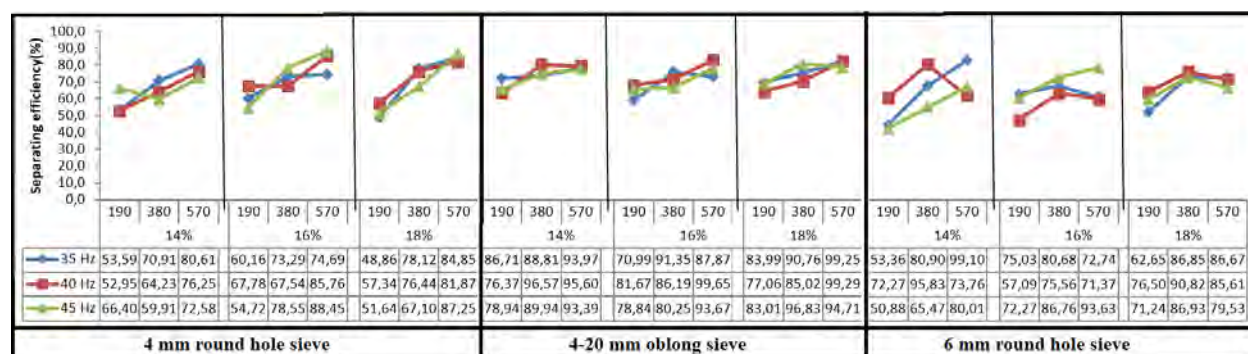


Figure 2. The effect of sieve velocity, feeding rate and sieve inclination on the separating efficiency with different sieve types

As a result of the separating experiments for lavandin plant depending on the sieve types, the highest separating efficiency value has been found at 15.8 % sieve inclination, 570 kg/h feeding rate and 40 Hz of sieve velocity with 4 -20 oblong sieve type. The lowest separating efficiency has been observed experiments conducted with 4 mm round hole sieve at 17.6% sieve inclination, 190 kg/h feeding rate and 35 Hz of sieve velocity. The separating efficiency value of the system were found low in the experiments carried out with 4 mm round hole sieve. The triple interaction of sieve velocity, feeding rate and sieve inclination on the separating efficiency with 3 different sieve types have been found statistically significant ($p < 0.05$).

According the result of the study conducted depending on the sieve types for sage plants, sieve velocity, feeding rate and sieve inclination of the separating unit, the work efficiency values have been given in Figure 3.



CIGR 2018

XIX. World Congress of CIGR

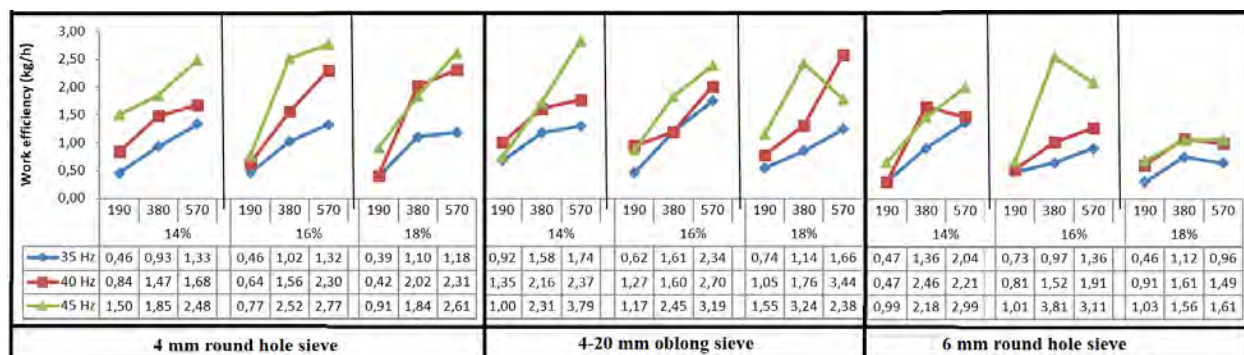
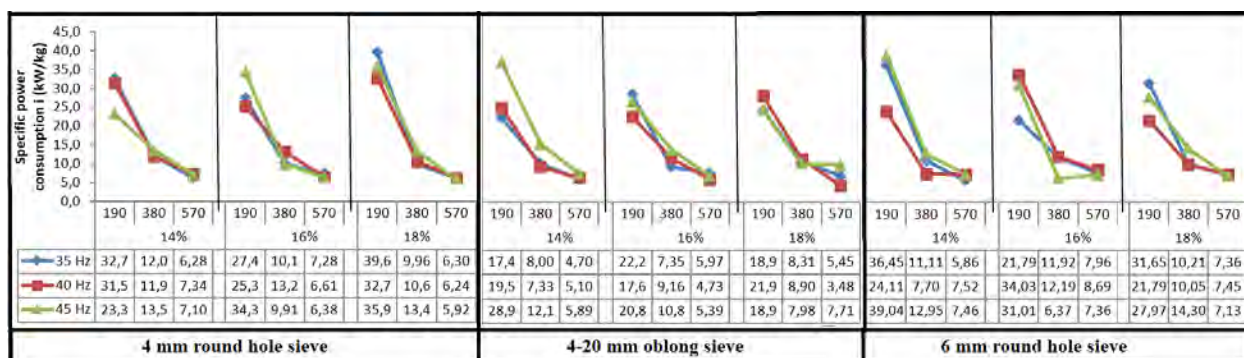


Figure 3. The effect of sieve velocity, feeding rate and sieve inclination on the work efficiency with different sieve types

The triple interaction of sieve velocity, feeding rate and sieve inclination on the separating efficiency with 3 different sieve types have been found statistically significant ($p < 0.05$).

According to the result of the study depending on the sieve types for the lavandin plant, the work efficiency values has been found to be low at 4 mm round hole sieve type. The lowest value observed at 35 Hz sieve velocity, 190 kg/h feeding rate and 17.6% sieve inclination as 0.39 kg/h. The work efficiency values changed between 0.39 kg/h and 3.81 kg/h. The highest work efficiency value has been determined at 15.8% of sieve inclination, 45 Hz sieve velocity and 380 kg/h feeding rate in the experiment conducted with 6 mm round hole sieve.

Specific power consumption is one of the most important parameters for designing systems and must be known in order for the proper system performance of separating unit for lavandin plant. The specific power consumption values of separating system carried out with 3 different sieve types have been presented in Figure 4.





CIGR 2018

XIX. World Congress of CIGR



Figure 4. The effect of sieve velocity, feeding rate and sieve inclination on the specific power consumption with different sieve types

The specific power consumption values of the system according to the measured values depending on the sieve types for the lavandin plant, sieve velocity, feeding rate and sieve inclination of the separating unit, varied between 3.48 kW/kg and 39.65 kW/kg. The triple interaction of velocity, feeding rate and sieve inclination on the specific power consumption with 4 mm, 6 mm round hole sieves and 4-20 mm oblong sieve have been found statistically significant ($p < 0.05$). While the specific power consumption of separating unit for lavandin plant has been lowest at 15.8 % sieve inclination, 570 kg/h feeding rate and 40 Hz of sieve velocity with 6 -20 oblong sieve type, it has been highest at 17.6% sieve inclination, 570 kg/h feeding rate and 40 Hz sieve velocity with 4-20 oblong sieve type.

4. CONCLUSIONS

In this study, separating unit performance values and working parameters have been determined for the lavandin plant. The separating efficiency, work efficiency and specific power consumption values of new design separating unit have been determined. This study has been included important parameters for lavandin cultivation.

When the new design separation unit for lavandin plant is examined in terms of separating efficiency, it has been suggested to operate with 4-20 oblong sieve at 570 kg/h feed rate, 40 Hz sieve velocity and 15.8% sieve inclination. On the other hand, it is suggested that for the high work efficiency, separating unit can be performed with 4-20 mm oblong sieve, at 570 kg/h feed rate, 40 Hz sieve velocity and 17.6% sieve inclination. In order to reduce specific power consumption of the unit the parameters must be selected as 15.8 sieve inclination, 570 kg/h feeding rate and 45 Hz sieve velocity with 4-20 oblong sieve. According to the results, it can be said that the most suitable sieve type for lavandin plant is 4-20 oblong sieve.

5. ACKNOWLEDGEMENTS

This study is included a part of the project TUBITAK-3501-National Young Researchers Career Development Program (CAREER) "Determination of Threshing and Separation System Parameters of Some Medicinal Aromatic Plants and Development of Prototype (111O179)" We would like to thank the TUBITAK for its contributions to the project conducted by Deniz YILMAZ.



CIGR 2018

XIX. World Congress of CIGR



6. REFERENCES

- Anonymous, 2005. “European Community Biodiversity Clearing-House Mechanism”. Glossary of Biodiversity Related Terms.
- Anonymous, 2012. Tıbbi ve Aromatik Bitki İşletmelerinin Yapısal Analizi, Batı Akdeniz Tarımsal Araştırma Enstitüsü Müdürlüğü, Antalya.
- Arın, S., Akdemir, B., Kayışoğlu, B. 1988. Trakya Bölgesinde Bitkisel Üretimde Enerji Bilânçosunun Oluşturulması. Tarımsal Mekanizasyon 11. Ulusal Kong. Bildiri Kitabı, Sayfa: 124–135, Erzurum.
- Baydar, H. 2009.” Tıbbi ve Aromatik Bitkiler Bilimi ve Teknolojisi (Genişletilmiş 3. Baskı)”, Isparta: Süleyman Demirel Üniversitesi Yayınları, 51.
- Çelik, H. K., Akıncı, İ. 2012. Tarım Makineleri Tasarımı ve Geliştirilmesinde Bilgisayar Destekli Tasarım ve Mühendislik Uygulamaları. 27. Tarımsal Mekanizasyon Ulusal Kongresi, 5-7 Eylül, Samsun.
- Faydaoğlu, E., Sürücüoğlu, M. S. 2011. Geçmişten günümüze tıbbi ve aromatik bitkilerin kullanılması ve ekonomik önemi. Kastamonu Üniversitesi Orman Fakültesi Dergisi, 11(1), 52-67.
- Kutzbach, H.D. 2003. “Approaches for Mathematical Modelling of Grain Separation. International Conference on Crop Harvesting and Processing”. CD version, 2, Kentucky USA.
- Máthé, Á. ed., 2015. Medicinal and aromatic plants of the world: scientific, production, commercial and utilization aspects (Vol. 1). Springer.
- Sonmete, M. H., Demir, F. 2006. Yerli Tip Harman Makinasında Aspiratör Kanat Tiplerinin Ayırma Performansına Etkisinin Belirlenmesi. Selçuk Tarım ve Gıda Bilimleri Dergisi, 20(38), 88-97.



CIGR 2018

XIX. World Congress of CIGR



Rice Harvesting Operation by Two Combine Robots

Michihisa Iida¹, Ryo Asada¹, Masahiko Suguri¹, Ryohei Masuda¹

¹Graduate School of Agriculture, Kyoto University
Sakyo-ku, Kyoto, Kyoto 606-8502, Japan
iida@elam.kais.kyoto-u.ac.jp

ABSTRACT

In order to solve shortage and aging of working force in Japanese agriculture, automation and robotization of agricultural vehicles are promoted and are merged with information and communication technology (ICT) currently. To improve the efficiency of farming operation much more, cooperative harvesting system by combination of multi robots is proposed in this study. Two robots, that are 4-row head-feeding combines, have been developed to automate rice harvesting operation in Kyoto University. They have installed a multi-GNSS receiver, a GPS compass, and an IMU as navigation sensors. To avoid collision each robot, wireless modems are equipped to communicate position, attitude, and working status of each combine. In order to evaluate performance of cooperative harvesting operations by two combine robots, field test by block harvesting method was conducted in a rice paddy field. Field test results showed that the combine robots could harvest rice crop cooperatively without leaving rice and any collision and the block harvesting method improved the working efficiency to 24 % against the side-by-side harvesting method.

Keywords: Autonomous vehicle, collision avoidance, head-feeding combine, wireless communication.

INTRODUCTION

Global population is growing up rapidly and increases up to 9 billions near in the future. Agriculture plays an important role to produce food and energy. Under this situation, rural and agricultural areas that are taking charge of food production in Japan have serious problem of the workforce shortage, that is, decrease of the farmer population and aging of the farmer. In addition, it is required that efficient farming operation should reduce cost for producing foods. For the purpose, small agricultural fields will be consolidated into a large and rectangular field, and large agricultural machinery such as tractors and combine harvesters are developed and used year by year. Furthermore, automation and robotization of agricultural machinery are considered to be one of the effective ways for improving the productivity and quality of field works. Therefore, researchers and engineers have been studying and developing agricultural robots for automation of farm works in Japan.



CIGR 2018

XIX. World Congress of CIGR



Iida et al. (2013) developed a head-feeding combine robot to harvest rice automatically in a paddy field. This robot could harvest rice while following a target path according to the guidance by a RTK-GNSS and a GPS compass. Kurita et al. (2012 and 2017) reported on an operation framework for autonomous rice harvesting. They developed an integrated algorithm for robotic operation and cooperation with farm workers to automate each subsection of harvesting and unloading process by a combine robot. Furthermore, in order to improve the operational efficiency of harvesting process, Iida et al. (2016) reported on manned and unmanned combines to harvest rice effectively in the same field. In that study, the human operator who drives the manned combine kept the unmanned combine watch for the safety. However, it was difficult the operator drove the combine while watching another combine. Thus, Iida et al. (2017) reported that two combine robots could harvest rice side-by-side cooperatively. Nevertheless, the working efficiency in the side-by-side harvesting method was still not enough. In this paper, the block harvesting method by two combine robots will be proposed to improve the working efficiency of rice harvesting operation.

The objective of this study is to develop a multi-machine system that enables two combine robots to harvest rice crops cooperatively. In this system, both combines can communicate each position and working status by using the wireless communication. Field test was conducted to measure the working efficiency in the block harvesting method by two combines in the same field.

MATERIALS AND METHODS

Test Vehicles

Figure 1 shows two prototypes of robots developed in this study. The robots were remodeled 4-row head-feeding combines (Kubota Corp., ER467 and ER470). These combines can harvest 4 rows of rice plants at the same time. In Japanese rice paddy field, rice plants are planted in row spaced 0.3 m apart. Thus, the swath width of the header is 1.2 m ($0.3\text{m} \times 4$ rows). Though both combines can harvest rice crop at the maximal speed 1.65 m/s. they normally harvest in a range of 0.8 – 1.2 m/s. As the combine has a grain tank of the capacity 1400 L, it can store the harvested grain there.



CIGR 2018

XIX. World Congress of CIGR



Combine robot 1 (model: ER470)



b) Combine robot 2 (model: ER467)

Figure 1. Prototypes of head-feeding combine robots.

Figure 2 illustrates a controller network for the combine robot. The robot required the precise position and direction to harvest rice along crop rows. So, it has a multi-GNSS receiver (Topcon Corp., AGI-3) and GPS compass (Hemisphere Inc., ssV-102) to detect the position and heading at a rate of 10 Hz. The GNSS receiver can catch signals from the GPS and GLONASS satellites. Wireless receivers are used to obtain the correction data signal from the GNSS base station. Additionally, the IMU, Xsens Technologies B.V., MTi-30AHRS, is used to detect yaw angle of robots at the higher rate than 50 Hz.

The combine originally has more than ten electronic control units (ECUs) for the controls of engine, traveling and steering units, header, thresher and so on. These ECUs communicate together via a controller area network (CAN) bus. The operating and driving systems of the combine are drive-by-wire (DBW). Therefore, to control those units of the combine, the software of ECUs is reprogrammed for automatic drive.

A wireless controller can send the start/stop signal to the combine robot remotely. A four-colored lamp indicates the status of the robot and the navigation system.



In order to improve the efficiency of harvesting operation, two combines should work cooperatively in the same field. However, two combines may collide with each other. Therefore, the wireless modems are used to communicate the position, attitude and working status of the other at the rate of 10 Hz (Figure 3). This wireless modem is a 760 MHz-band transceiver for the Intelligent Transport Systems (ITS) developed by Panasonic Corporation. It uses the protocol in accordance with ITS FORUM RC-013 V1.0. The communication contents include the common data area (62 bytes) of the time, position, status and etc. of vehicle, and the free data area (100 bytes) that the user can define. In this study, the working status of the combine robot is implemented in the free data area. The working status means the laps and direction of the current harvest, the status that the robot is harvesting or turning. The robot can determine the relative distance and angle between vehicles from the common data area. In addition, the robot can detect that the other is coming near or going away from the free data area.



Figure 3. A communication system between combine robots by wireless modems.

Cooperative harvesting operation in block harvesting method

In this study, cooperative harvesting operation means that two combines harvest rice crop in the same field at the same time as shown in Figure 4. However, it is difficult to start harvesting from the beginning because of the narrow entrance into the field. Before harvesting rice by two combines, a combine that human operator drives harvests 3-4 laps of rice crops from outside in order to make turning spaces at the corner. After that, each combine starts harvesting each block of rice autonomously according to the independent target paths as shown in Figure 4. These paths can be planned from the locus of the combine when the human operator drove. The target paths are counter-clockwise spiral shape. The robots follow these target paths to harvest rice. The GNSS data of both robots were recorded as the logs while the robots are harvesting rice.

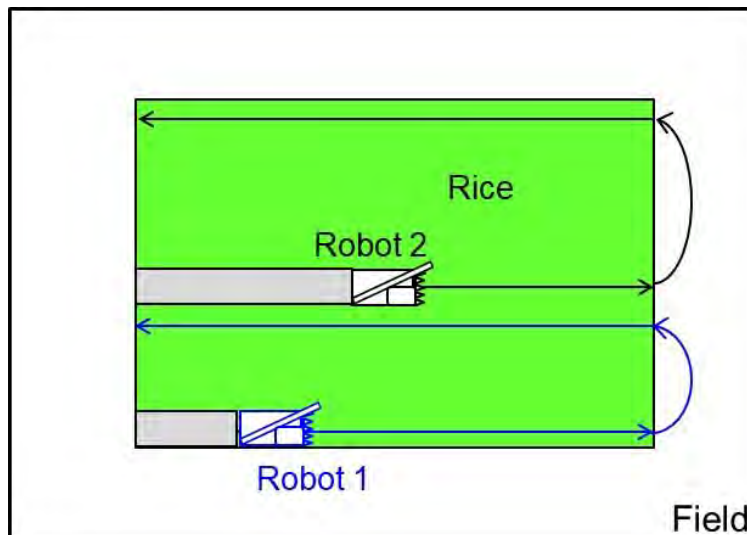


Figure 4. Harvesting method by two combines.



CIGR 2018

XIX. World Congress of CIGR



Collision avoidance

In order to avoid collision between robots, the robot 2 decreases speed or stops to avoid collision with the robot 1, depending on the relative distance and angle between vehicles. For the purpose, we apply three patterns of the following action.

Each robot has an allowance range not to collide with the other. This allowance range is 3 m in the forth and back direction, and 1m in the left and right direction. When this allowance range overlap that of the other, the robot stops at once.

While two robots are harvesting rice in the same direction and the relative distance between robots becomes less than 20 m, the robot 2 decreases the speed to avoid collision. In addition, when the relative distance becomes less than 5m, the robot 2 stops at once.

While the robot 1 is turning at the headland and the robot 2 is coming nearer than 7.5 m, the robot 2 stops until the robot 1 goes away at the distance 7 m.

Experimental method

The field experiment was conducted to evaluate the performance of cooperative harvesting operation by two combine robots. The test field was a paddy field of the private farmer in Tobishima Town, Aichi Prefecture, Japan. The variety of rice is Koshihikari (*Oryza sativa* L). The soil condition of the field was dry and hard because it was good weather before the test.

RESULTS AND DISSCUSSION

Figure 5 is the test scene of harvesting operation by two combines. The robot 2 harvested rice while keeping the relative distance between robots.





Figure 5. Harvesting scene by two combine robots.

Figure 6 shows the traveling loci of two combine robots measured by GNSS receivers. In this field test, the pattern 1 for avoidance collision did not occur. The field test demonstrated the cooperative harvesting operation by two combine robots successfully without collision and any troubles.

Table shows the working efficiencies of rice harvesting operation in side-by-side method and block harvesting method. The working efficiency in the side-by-side harvesting method refers to the paper reported by Iida et al (2017). The block harvesting method improved the working efficiency to 24 % against the side-by-side harvesting method.

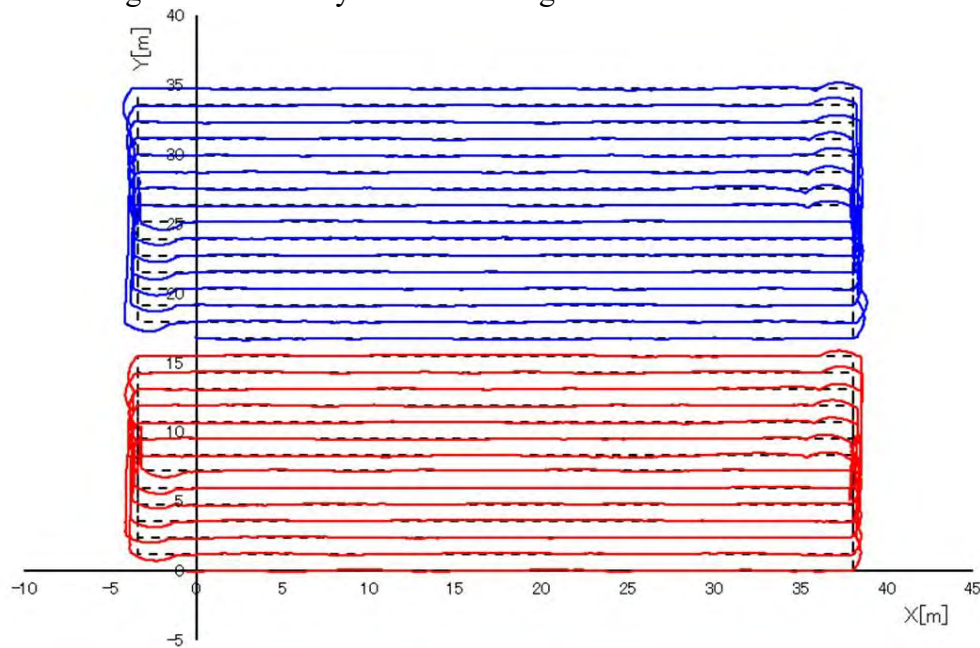


Figure 6. Traveling loci of two combine robots in block harvesting method.

Table Comparison of working efficiency in side-by-side and block harvesting methods.

Classification	Side-by-side harvesting	Block harvesting
Robot 1 (a/h)	21.2	22.3
Robot 2 (a/h)	16.8	24.8
Two robots (a/h)	32.5	40.2

CONCLUSIONS



CIGR 2018

XIX. World Congress of CIGR



In this study, cooperative harvesting method by two head-feeding combine robots was developed by using the wireless communication. Field test was conducted to measure the working efficiency in block harvesting method by two robots.

In this test, the robots could harvest rice crop cooperatively without collision and troubles. The result indicates the wireless communication is useful and effective for cooperative operation of multi-robot system. The block harvesting method improved the working efficiency to 24 % against the side-by-side harvesting method.

ACKNOWLEDGEMENTS

This study was financially supported by grants from the Cross-ministerial Strategic Innovation Promotion Program (The Next Generation Creative Technology in Agriculture, Forestry and Fisheries).

REFERENCES

- Iida, M., Uchida, R., Zhu, H., Suguri, M., Kurita, H., Masuda, R., Path-Following Control of a Head-Feeding Combine Robot, *Engineering in Agriculture, Environment and Food*, 6(2), 61-67, 2013.
- Iida, M., Watanabe, T., Seki, H., Suguri, M., Onoyama, H., Sasaki, R., Harada, S., masuda, R., Coordination of Two Combine Robots for Rice harvesting Operation, *Proceedings ISMAB 2016*, 507-512, 2016.
- Iida, M., Harada, S., Sasaki, R., Zhang, Y., Asada, R., Suguri, M., Masuda, R., Multi-combine robot system for rice harvesting operation, *ASABE paper No.1700321*, 2017.
- Kurita, H., Iida, M., Suguri, M., Masuda, R., 2012. Application of Image Processing Technology for Unloading Automation of Robotic Head-Feeding Combine Harvester, *Engineering in Agriculture, Environment and Food*, 5(4), 146-151.
- Kurita, H., Iida, M., Cho, W., SUGuri, M., 2017. Rice Autonomous Harvesting: Operation Framework, *Journal of Field Robotics*, 1-16.



Time Response Study of Electromagnetic Driven VRT Valves for Variable Rate Spraying System Improvement

Arezou Lak^{1*}, Hosein Behfar²

Department of Biosystem Engineering, Faculty of Agriculture, University of Tabriz, Tabriz, Iran

*Correspondence: arezoolak71@gmail.com

ABSTRACT

The invariant distribution of herbicides makes it possible to treat weed free areas, areas with low weed density and high weed density areas the same. One of the main defects of overusing herbicides is the transfer of these chemicals to food through the soil, causing dangerous diseases such as cancer in humans. By developing a system for application of herbicides, chemicals can be used only at required locations, and the weed rate can be changed due to the rate of weed density. Consequently using of these chemicals would be reduced. Variable rate spraying systems which are currently used in the world do not have satisfactory efficiency in Duty cycles of less than 20% due to pressure variations and therefore variations in particle diameter. As a result, the range of spraying changes gets limited. For investigating the mentioned points, a variable rate spraying system was firstly created by using the PWM method and then diagrams of response time of valve is obtained via an oscilloscope. By studying the output circuit response, it was determined that the voltage did not immediately reach a specified value and the valve did not immediately open and this occurred with a delay time. So before the valve is completely opened, the time set for the valve to be opened by the duty cycle is over and it is closed, thus it results in the pressure changes in the lower duty cycles. It is indicated that the reason is decreasing of the average voltage level and the response time of the valve circuit. In the current study, in order to increase the range of spraying, instead of a voltage of 12 volts, high voltages were used. If the voltage rises, the time to reach the specified working voltage will decrease, so the valve will open earlier. By exploring the response timing of the valve, it was found that if



CIGR 2018

XIX. World Congress of CIGR



high frequencies are used, the time between successive openings will decrease. As a result, the pressure changes of the lower duty cycles will reduce, consequently the number of winding coil per unit of length decreased. Unfortunately, this has a reverse effect on electromagnetic power. For fulfilling the both effects, the length of the winding core increased, and simultaneously the number of rounds was kept constant, the ratio of the round per unit of length was reduced. Because of the low thickness of the wire, the possibility of burning the winding increases. Therefore, only 20% of the diameter of the wire was reduced to increase the resistance value. The experiments showed that simultaneous changing the frequency (15 Hz) and raising the voltage in lower duty cycles can reduce the duty cycle to 5% without effective decreasing in pressure.

Keywords: Herbicides, variable rate spraying system, response time, PWM, duty cycle

INTRODUCTION

Weeds are a significant restriction and cost to agricultural production worldwide. Estimates indicate that yield losses could range from 29% in wheat to 47% in rice crops without weed control (Oerke, 2005). Weeds are managed in soya bean mainly by herbicides (Niekamp and Johnson, 2001; Datta et al., 2017). Although pesticide facilitates controlling the main crop pest (including weeds), it contains irreparable effects for human health. Unwarranted use of herbicide also contains negative effects for soil biota and the ecosystem services they provide. By developing a system for application of herbicides, chemicals can be used only at required locations, and the weed rate can be changed due to the rate of weed density. Site-specific weed management (SSWM) makes use of spatial information for locating and removing weeds, and consequently areas of field that do not require weed control are not treated. Targeted weed patch herbicide application caused 69.5% saving in comparison to the conventional application (Loghavi and Mackvandi, 2008).



CIGR 2018

XIX. World Congress of CIGR



Herbicide rates, in the flow rate control systems are regulated by changing the flow rates of nozzles. Variable Rate Technology (VRT) is a management tactic for coping with the spatial variability in the field. Flow management can be set through pulse width modulation (PWM) (Liu et al., 2014; Giles and Comino, 1990). The modulation rate (or duty cycle) of the PWM solenoid valve determines the variable flow rate function while the spray pattern remains unchanged (Giles and Comino, 1990) for instance, when a modulation rate is 80%, the nozzle discharges spray during 80% of its duty cycle and then closes during the rest of the duty cycle.

Droplet size is one of the most salient factors that influence spray quality on target areas. It is essential to maintain a constant droplet size distribution to achieve a consistent spray quality (Gu et al, 2011). Droplet sizes did not vary significantly with modulation rates of 20–100%. Droplet size variations were minimized when the variable-rate nozzle was operated at a constant liquid pressure and when a 10% or lower modulation rate was not used (Gu et al, 2011). The Volume Median Diameter (VMD) at a duty cycle of 10% was significantly different from the rest (Gopalapillai et al., 1999).

The objective of developing the modified valve was increasing the variation range of variable rate spraying. Given that the systems currently used in the world do not have appropriate function in duty cycles of less than 20%. This is due to pressure variations and hence droplet size Variations that results in reducing the performance of the device. In areas where the weed density is very low, using of duty cycles of more than 20% causes excessive using of the chemicals and therefore spraying is not proportional to the weed density. As a result, a modified valve for operating in the duty cycle of less than 20% at the constant pressure is required. To achieve this goal the valve response time was investigated.



2. MATERIAL AND METHODS

2.1 Design of the New PWM Control System

The flow rate control module for this system consists of microcontroller based PWM signal generator (MCU), PWM- controlled solenoid valve driver unit (L298p, Motor shield, Arduino) and solenoid valve (Transl Co). Flow rates discharged from the solenoid valve are commensurate with the open time. A computer was used to execute the variable-rate control. Field weed map was on the PC and it could establish the relations between the flow rate and the weed density. MCU (ATMEGA328, Arduino) could generate the PWM signal easily. It was employed for adjusting product application rates on -the -go, based on user directions or digital application rate maps, the PWM signals are amplified by the solenoid valve driver unit to adapt to the power of the solenoid valve. Driver unit provides square-wave signals for the solenoid valve (Figure 1).

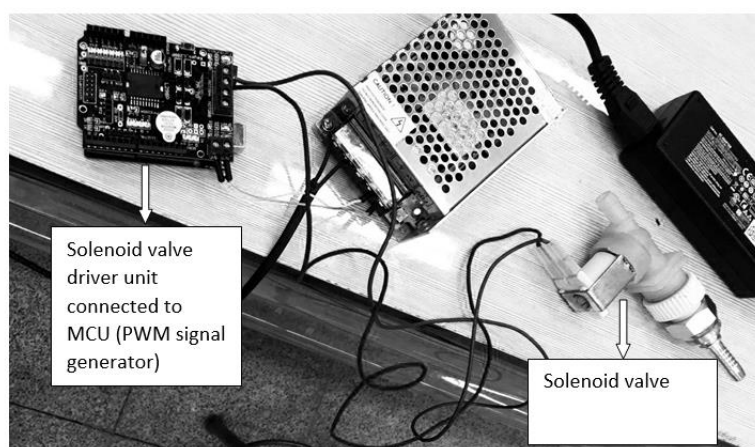


Figure1. Flow rate control system

After designing and testing the existing electrical system, modified valve was designed and manufactured with the intention of increasing the variable rate spraying efficiency.



2.2 Investigation of Valve Response Time

An equivalent electrical circuit of valve is a resistor of (R) series with an inductor (L) (Figure 2).

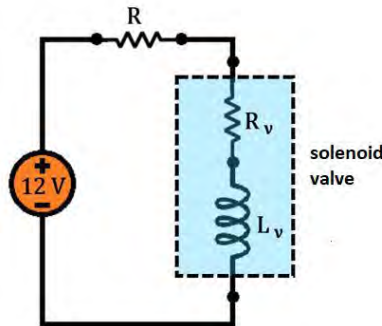


Figure2. An electrical circuit of valve

The RL circuit in each step input (part of the pulse circuit used in the PWM circuit to change the flow rate) is an exponential function:

$$V = V_0(1 + e^{-t/\tau}) \quad (\text{Eq.1})$$

Where V is the voltage (volt), V_0 is the initial voltage (volt), t is the time (seconds), and τ is the time constant of the circuit (1/seconds).

Hence, it can be seen from equation (1) that the voltage does not reach a specified value instantly and the valve opens with a delay time. Due to the valve response time, when the duty cycle reaches below 20%, there is not enough time for valve to open because of two reasons:

1. Before the valve is fully opened, the time set for the valve to be opened by the duty cycle is over and the valve is closed.
2. As we know, one of the consequences of electric voltage pulse is decreasing the average voltage level. Although the valves are designed for specific operating voltages (for example, 12 volts), the cause of valves damage is not instantaneous voltages (Average power and therefore



CIGR 2018

XIX. World Congress of CIGR



average voltage of $P = VI$ causes the burning of the valve). Thus, by considering these two problems, instead of 12 volts, high voltages were used. The more the decreasing in the duty cycle the higher the voltage level we would have.

If the voltage rises, the V_0 coefficient increases in the above relationship and the time to reach the specified working voltage decreases, so the valve will be opened earlier. The valves used in variable rate spraying systems operate at a frequency of 10 Hz. When the timing response is fast, high frequencies can be used. If high frequencies are used, the time between successive openings will be lower thus pressure- change in lower duty cycles will decrease. In doing so, some changes were made in the valve to speed up the response time. t is a time constant and its value is proportional to the time of reaching the stability and opening the valve. Through declining t value, the response time of the valve will be faster. Accordingly, the value of τ should be reduced. According to the equal of $\tau = L / R$, the value of L must be reduced and the R value must be increased. For decreasing the value of L the ratio of the number of windings coil per unit length should be reduced. Unfortunately, this has a reverse effect on electromagnetic power. For fulfilling the both effects, the length of the winding core increased, and simultaneously the number of rounds was kept constant, the ratio of the round per unit of length was reduced. Because of the low thickness of the wire, the possibility of burning the winding increases. Therefore, only 20% of the diameter of the wire was reduced to increase the resistance value.

DISCUSSION AND RESULTS

The graphs of valve timing response obtained via oscilloscope for various frequencies are shown in Figure 3.

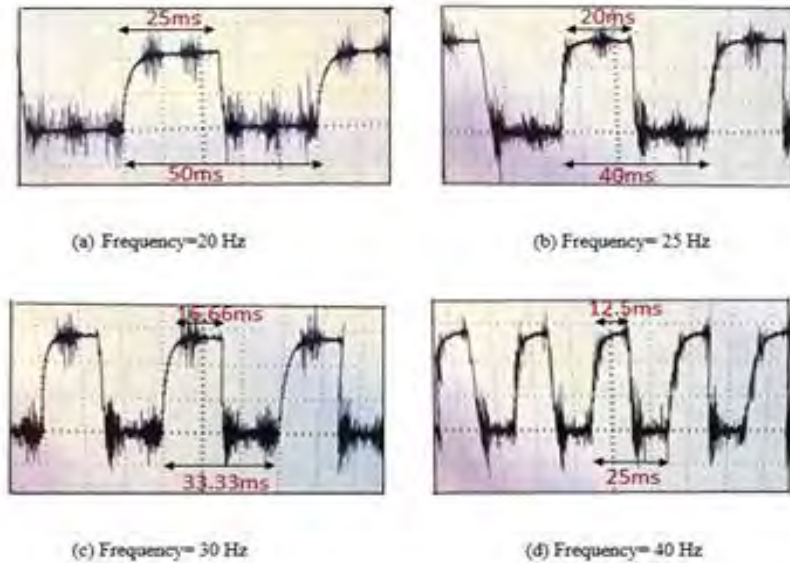


Figure3. PWM waveforms generated by MCU chips with different frequencies .Time resolution = 10 ms per division on the abscissa, and voltage resolution = 5 V per division on the ordinate.

The diagrams of valve response time were plotted in Excel and the corresponding equations were obtained. By using one of the response time parameter (settling time), function constants were obtained (equation 3). As it is evident, the response time of the valve is an exponential function (equation 4).

$$V = 12(1 - e^{-at}) \quad (\text{Eq.2})$$

$$T_s = \frac{4}{a} = 0.01 \rightarrow a = 400 \left(\frac{1}{s} \right) \quad (\text{Eq.3})$$

Through combining equations 2 and 3:

$$V = 12(1 - e^{-400t}) \quad (\text{Eq.4})$$



After making mentioned modifications, the electrical system of variable rate spraying was tested all over again by using the new valve. In order to investigate the accuracy of this system, laboratory tests were conducted at the frequency of 15 Hz ,5 levels of duty cycle (5%, 10%,30%, 50%, 70%) and 3 operating pressure levels (2, 3, 4 bar). Linear relationships between the mean flow rate of three replications and Duty cycle for the Teejet nozzle at operating pressures from 2 to 4 bar for frequency 15 Hz are shown in Figure 4.

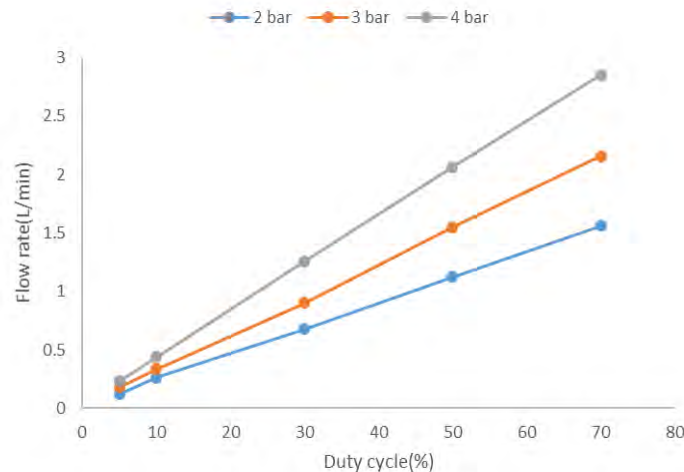


Figure 4. Mean flow rate at operating pressure of 2, 3 and 4 bar for duty cycles (5-70%)

Flow rate and PWM duty cycle's relationship was linear for the new solenoid valve:

$$Q = aD + b \quad (\text{Eq.5})$$

Where Q is the nozzle flow rate (L/Min),” a “and” b “are the calibration constants and DC is the PWM-controlled duty cycle.

Consistent with this equation, it is apparent that flow rate increases by increasing the duty cycle.

Through using this equation - which was obtained by testing modified valve- the appropriate flow rate can be applied even in areas where weed density is low and the unnecessary use of chemicals can be avoided.



CIGR 2018

XIX. World Congress of CIGR



CONCLUSION

- By modifying the solenoid valve, the duty cycle can be reduced down to 5% through concurrently varying the frequency (15 Hz) and increasing the voltage in lower duty cycles.
- In places where the amount of herbicides required is low owing to the low weed density, the agricultural spraying consumption can be reduced as much as possible and it would be possible to prevent its negative effects on humans and the environment.
- By using the duty cycle in the range of 5-100%, the variation range of the variable rate spraying can be increased with no effective pressure drop.

5. REFERENCES

- Datta, A., Ullah, H., Tursun, N., Pornprom, T., Knezevic, S.Z., & Chauhan, B.S. 2017. Managing weeds using crop competition in soybean [*Glycine max* (L.) Merr.]. *Crop Prot.* 95, 60–68.
- Giles, D. K., & Comino, J. A. 1990. Droplet size and spray pattern characteristics of an electronic flow controller for spray nozzles. *J. Agric. Eng. Res.*, 47(4), 249-267.
- GopalaPillai, S., Tian, L., & Zheng, T. 1999. Evaluation of a flow control system for site-specific herbicide applications. *Transactions of the ASAE* 42:863-870.
- Gu, J., Zhu, H., Ding, W., & Jeon, H. 2011. Droplet size distributions of adjuvant-amended sprays from an air-assisted five-port PWM nozzle. *Atomization and Sprays*, 21(3), 263-274.
- Liu, H., Zhu, H., Shen, Y., Chen, Y., & Ozkan, H. E. 2014. Development of digital flow control system for multi-channel variable-rate sprayers. *Transactions of the ASAE* 57(1): 273-281.
- Loghavi, M. & Mackvandi, BB. 2008. Development of a target oriented weed controlsystem. *Computers and electronics in agriculture* 63(2):112-118.
- Niekamp, J.W., & Johnson, W.G. 2001. Weed management with sulfentrazone and flumioxazin in no-tillage soyabean (*Glycine max*). *Crop Prot.* 20, 215–220.
- Oerke, E.-C. 2005. Crop losses to pests. *J. Agric. Sci.* 144, 31.



CIGR 2018

XIX. World Congress of CIGR



Mixed Seeding Performance of a Seed Drill at Different Mixture Ratios Under the Laboratory and Field Conditions

Arzu YAZGI¹, Erdem AYKAS¹, Tuncay GUNHAN¹, Behcet KIR²,
Gulcan DEMIROGLU TOPCU²

¹Ege University, Faculty of Agriculture, Department of Agricultural Engineering and
Technology, 35100, Bornova, Izmir/Turkey

²Ege University, Faculty of Agriculture, Department of Field Crops 35100, Bornova,
Izmir/Turkey

arzu.yazgi@ege.edu.tr

ABSTRACT

The objective of this study was to evaluate the applicability of a seed drill for mixed seeding under the laboratory and field conditions. The performance of the seeder was determined using pure barley (*Hordeum vulgare* L.), pure common vetch (*Vicia sativa* L.), and mixtures of both seeds at different seed mixture ratios. The indicators of seeding quality, flow uniformity, and seed distribution uniformity across the rows were determined by the measurement of seed weights. The other indicator, in-row seed spacing uniformity, was investigated by sticky belt tests under the laboratory conditions while in-row plant spacing uniformity was determined after emerging of the plants in the field. Five different mixture rates of barley:vetch (100:0, 75:25, 50:50, 25:75, and 0:100) were used in the laboratory and field experiments. Experiments in the laboratory were conducted at three forward speeds (1.0, 1.5, and 2.0 m s⁻¹) while the field experiments were achieved at 1.5 ms⁻¹. Flow evenness and seed distribution uniformity across the rows were evaluated based on the coefficient of variation (CV). In-row seed/plant spacing uniformity was determined using the variation factor (V_f) and goodness criterion (λ). In laboratory conditions, the CV values of flow evenness were found to range from 1.0% to 5.5% for barley and from 0.3% to 2.1% for vetch. Seed distribution uniformity values of each row unit were found to range from 4.2% to 10.7% and from 0.4% to 1.4% for barley and vetch, respectively. The λ values were between 66.4% and 86.0% for laboratory conditions, while these values were 78% and 86% for field conditions. The V_f values ranged from 0.43 to 1.28 and from 0.36 to 0.77 for laboratory and field conditions, respectively. Based on the experimental results and calculations, it was found that the combined seed drill could be used effectively for seeding of barley and vetch mixtures at different seed mixture ratios in laboratory and field conditions.

Keywords: Barley, common vetch, mixture ratio, seed distribution uniformity, Turkey.

Arzu YAZGI, Erdem AYKAS, Tuncay GUNHAN, Behcet KIR, Gulcan DEMIROGLU TOPCU.
“Mixed Seeding Performance of a Seed Drill at Different Mixture Ratios Under the Laboratory
and Field Conditions”



CIGR 2018

XIX. World Congress of CIGR



INTRODUCTION

In Turkey, forage crops production gained more importance after the declaration of new subsidies to improve the animal production. Besides agro-ecological studies and breeding efforts for suitable crop varieties, agro-technical solutions have to be adapted. The production and yield of alternative forage crops depend more or less on performance of appropriate seeding and other necessary operations such as irrigation, plant protection and fertilizing. The successfully applications of all these inputs are important, but the major bottle neck is the placement of seeds at right depth and evenness into the soil. Because of the weak stem structure, vetch grows horizontally on the soil surface and cannot stand perpendicular. This property causes not only a low yield of grass and seed, but also decreases the feed quality of vetch. For that reason it is preferred to grow vetch mixed with cereals such as barley (Bakoglu, 2004).

The studies conducted by agronomists on mixture of vetch and barley mostly concentrate on plant efficiency, feed quality and land equivalent ratio (LER) at different mixture ratios in small experimental fields. Acikgoz and Cakmakci (1986) investigated different seed mixtures of common vetch-barley, common vetch-oat and common vetch-rye under Bursa conditions. They reported that the highest yield efficiency of herbage and hay was obtained using mixture of barley and vetch however the ratio of barley must be below 50%. Soya et al. (1996) reached also the conclusion that less vetch in the vetch-barley mixtures increases the yield.

There are many researches on mechanical and pneumatic seed drills were conducted by agricultural engineers. Within these studies were generally investigated the seed flow evenness of various seeds and the effect of operative parameters on machine performance. Kumar and Durairaj (2000) examined the seed distribution evenness of different seeds under different air velocity and feed ratios and found out that distributor geometry had significant importance on seed distribution uniformity. Uygan and Guler (2005), studied on barley, oat and rye in order to determine the effect of air velocity and seeding rate on flow evenness for different types of distributors of pneumatic seed drill and found out ideal distributor head type was T type and air velocity was 26 m s^{-1} . Bayhan et al. (2009) examined seeding rate and variation of seed distribution evenness based on the different PTO values and found that the best value was 300 min^{-1} . Yazgi et al. (2012), determined that the seed flow evenness was at medium quality level ($CV=1.9-2.7\%$), the seed distribution uniformity of furrow openers was at good/very good quality level ($CV=2.9-4.6\%$) and in row seed distribution uniformity was at medium quality ($\lambda=60\%-63.33\%$) in barley seeding using pneumatic seed drill. Yazgi et al. (2013) tested both seed and fertilizer units of combine direct seed drill with wheat and fertilizer respectively in their study. They determined the machine was sufficient to use for both fertilizing and seeding in means of the flow characteristics of seed and fertilizing units. Yazgi et al. (2017) conducted a study on mixed seeding performance of a combine seed drill using pure, pure common vetch and

Arzu YAZGI, Erdem AYKAS, Tuncay GUNHAN, Behcet KIR, Gulcan DEMIROGLU TOPCU.
“Mixed Seeding Performance of a Seed Drill at Different Mixture Ratios Under the Laboratory and Field Conditions”



mixture of both seeds at different ratios in laboratory conditions. They found that machine was sufficient to use for mixed seeding conditions at different mixture ratios.

It's not known if any study was conducted for comparing of mixed seeding performance of a combine seed drill under laboratory and field conditions. For this reason the study was planned and the performance of the seeder was determined using pure barley (*Hordeum vulgare* L.), pure common vetch (*Vicia sativa* L.), and mixtures of both seeds at different seed mixture ratios in laboratory and also field conditions. The results were evaluated for the applicability of the combined seed drill for mixed seeding under the laboratory and field conditions.

2. MATERIALS AND METHODS

An 18-row combined seed drill with separate seed and fertilizer metering systems was used in the laboratory and field conditions (Figure 1). While the seed metering unit of the drill had a studded roller, the fertilizer metering unit had a fluted roller. Seed and fertilizer come from different hoppers to different rollers and then pass through the different tubes separately. The seed and fertilizer then combine with one another near the double disc furrow opener and fall together to the soil in a mixed form. The mixed seeding condition was met using the barley in the seeding unit and the common vetch in the fertilizer unit (Figure 1). The seeding and fertilizing rates can be independently adjusted by a tri-cam mechanism. Barley (*Hordeum vulgare* L.) with a thousand seed mass of 45.4 g and common vetch (*Vicia sativa* L.) with a thousand seed mass of 44.2 g were used in this study.



Figure 1. Combined seed drill and mixed seeding condition

The seed drill was tested to determine seeding rate, flowing characteristics of seed mixture as flow uniformity and seed distribution uniformity across the rows by weighing seed collected for 30 s with three replications. The experiments for the flow uniformity and seed distribution

Arzu YAZGI, Erdem AYKAS, Tuncay GUNHAN, Behcet KIR, Gulcan DEMIROGLU TOPCU.
“Mixed Seeding Performance of a Seed Drill at Different Mixture Ratios Under the Laboratory and Field Conditions”



CIGR 2018

XIX. World Congress of CIGR



uniformity across the rows were conducted at three different forward speeds (1.0, 1.5, and 2.0 m s⁻¹) and three different seeding rates (metering unit scale positions of 20, 60, and 100). Seed weights obtained from each row unit were measured by a digital scale with the precision of 0.01 g and recorded to Microsoft Excel. The data were evaluated as CV (%) values based on Onal (2011) and are shown in table 1. The drill seed and fertilizer meters were driven by an electronically controlled gear motor which provided synchronization between the forward speed of the drill and the meter rotational speeds.

Table 1. Qualitative evaluation adjectives corresponding to values of seed flow evenness and seed distribution uniformity across the rows

Seed flow evenness, CV (%)	Seed distribution uniformity across the rows, CV (%)	Evaluation
<1	<4	Very good
1 - 2	4 - 6.3	Good
2 - 3	6.3 - 8.9	Moderate
3 - 4	8.9 - 12.5	Sufficient
>4	>12.5	Insufficient

The seed drill was tested to determine the in-row seed spacing uniformity using barley in the seeding unit and vetch in the fertilizing unit on a greased belt stand. The greased belt experiments were conducted using pure barley (100%), pure common vetch (100%) as well as different mixtures of barley:common vetch (75:25, 50:50, 25:75) for seeding rates of 100 kg ha⁻¹ and 200 kg ha⁻¹ in order to evaluate the seeding quality. Seeding quality was evaluated based on the criteria given by Onal (2011) for the seed drills. In the experiments the forward speeds of 1.0, 1.5, and 2.0 m s⁻¹ were applied and the numbers of seeds on 300 segments were determined and evaluated for each test.

The seed drill was also tested to determine the in-row plant spacing uniformity using barley in the seeding unit and vetch in the fertilizing unit in the field conditions. The field experiments were conducted at the forward speed of 1.5 m s⁻¹ using pure barley (100%), pure common vetch (100%) as well as different mixtures of barley:common vetch (75:25, 50:50, 25:75) for seeding rates of 200 kg ha⁻¹ and 100 kg ha⁻¹ for barley and vetch, respectively. The experiments were planned based on the principles of randomized block design.

The in-row seed and plant spacing uniformity obtained by computer-aided classification was defined by the values of variation factor (V_f) (eq. 1) and the goodness criterion (λ) which describes how well the data fit a Poisson distribution. The V_f and variance (S^2) of the seed and plant distribution were calculated using equations 1 and 2 (Griepentrog, 1991). In these equations x_i is the expected number of seeds/plants in the segment, f_i is segment ratio which is the percentage of the segments with different number of seeds/plants, and n is total sample number.

Arzu YAZGI, Erdem AYKAS, Tuncay GUNHAN, Behcet KIR, Gulcan DEMIROGLU TOPCU.
“Mixed Seeding Performance of a Seed Drill at Different Mixture Ratios Under the Laboratory and Field Conditions”



CIGR 2018

XIX. World Congress of CIGR



$$V_f = \frac{S^2}{\mu} \quad (1)$$

$$S^2 = \frac{\sum_{i=1}^n x_i^2 f_i - (x_i f_i)^2 / n}{n-1} \quad (2)$$

Based on “ V_f ” values obtained from the experiments, the character of in-row seed/plant spacing was determined. If $V_f > 1.1$, it indicates there are undesired misses and multiples within the in-row seed/plant spacing. If $0.9 < V_f < 1.1$, this indicates the in-row seed/plant spacing matches a Poisson distribution. If $V_f < 0.9$, this indicates the in-row seed/plant spacing may be characterized as precision seeding. Additionally, the evenness quality of the in-row seed/plant spacing was determined by a goodness criterion which defines the percentage of segments with 1, 2, and 3 seeds/plants and is interpreted using Table 2.

Table 2. In-row seed spacing uniformity	
Goodness criterion, λ (%)	Evaluation
≥ 72	Very good
72 - 65	Good
65 - 55	Moderate
< 55	Insufficient

In the goodness criteria evaluation, the average of number of seeds/plants per segment, μ , was chosen to be $\mu=2$, and the segment length, a , was calculated according to equation 3 (Onal, 2011).

$$a = \frac{100 \cdot \mu \cdot \sigma}{b \cdot N} \quad (3)$$

where, σ is thousand seed mass (g/1000 seeds), b is row spacing (cm), and N is seeding rate (kg ha⁻¹). The segment length in sticky belt experiments conducted with mixed seed was calculated as $\mu=2$ based on the seed which has the higher ratio in the seed mixture and the numbers of barley and common vetch seeds in the same segment were determined separately.

3. RESULTS

3.1 Results of the flow experiments

The results of the weighing experiments to determine seeding rate, flowing characteristics of seed mixture as flow uniformity and seed distribution uniformity across the rows are given figure 2, table 2 and table 3. The seeding rate values were determined varying between 0 and 520 kg ha⁻¹ for barley in seeding unit, while these values were between 0 and 710 kg ha⁻¹ for vetch in fertilizing unit.



CIGR 2018

XIX. World Congress of CIGR



Based on the results of the flow experiments with barley in the seeding unit, the performance of the seeder was found sufficient for flow evenness and seed distribution uniformity across the rows using barley (Table 3). The seeder had a very good quality in vetch seeding at different forward speeds and seed rates (Table 4) for flow evenness and seed distribution uniformity across the rows. As a result, the seed drill had a satisfactory quality under the laboratory conditions in terms of flow evenness and in-row seed spacing uniformity of row units for both barley and vetch seeds.

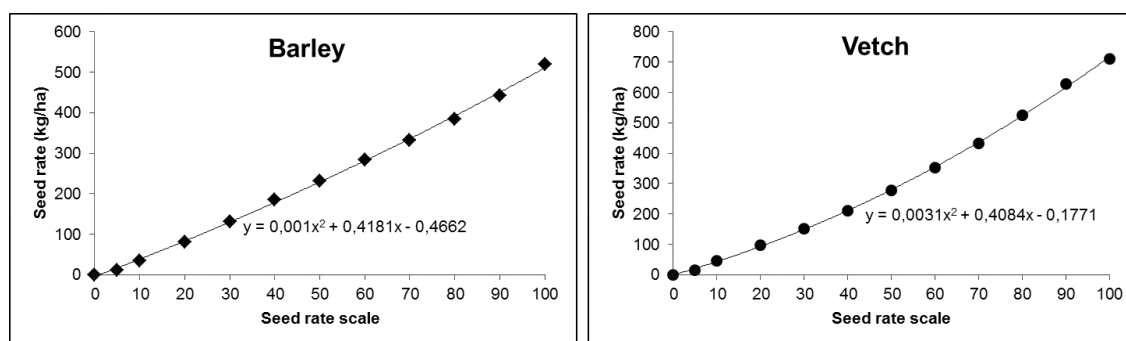


Figure 2. Seed rate results of barley and vetch at different seed rate scale positions

Table 3. Weighing measurements for barley in the seeding unit

Forward Speed (m s ⁻¹)	Scale Position ^[a]	Seeding rate (kg ha ⁻¹)	Seed flow evenness		Seed distribution uniformity across the rows	
			CV (%)	Evaluation	CV (%)	Evaluation
1.0	20	84	3.2	Sufficient	8.8	Moderate
	60	319	2.3	Moderate	7.0	Moderate
	100	626	5.5	Insufficient	4.2	Good
1.5	20	90	2.9	Moderate	6.9	Moderate
	60	349	1.0	Good	9.8	Sufficient
	100	642	2.4	Moderate	10.7	Sufficient
2.0	20	92	2.4	Moderate	7.2	Moderate
	60	341	2.5	Moderate	7.8	Moderate
	100	655	1.4	Good	8.6	Moderate

Arzu YAZGI, Erdem AYKAS, Tuncay GUNHAN, Behcet KIR, Gulcan DEMIROGLU TOPCU.
“Mixed Seeding Performance of a Seed Drill at Different Mixture Ratios Under the Laboratory
and Field Conditions”



CIGR 2018

XIX. World Congress of CIGR



Table 4. Weighing measurements for vetch in the fertilizing unit

Forward Speed (m s ⁻¹)	Scale Position ^[a]	Seeding rate (kg ha ⁻¹)	Seed flow evenness		Seed distribution uniformity across the rows	
			CV (%)	Evaluation	CV (%)	Evaluation
1.0	20	92	2.1	Moderate	1.4	Very good
	60	326	0.3	Very good	0.5	Very good
	100	650	0.5	Very good	0.7	Very good
1.5	20	90	1.2	Good	0.5	Very good
	60	320	0.3	Very good	0.4	Very good
	100	631	1.2	Good	0.6	Very good
2.0	20	90	1.2	Good	0.9	Very good
	60	317	0.9	Very good	0.8	Very good
	100	624	0.9	Very good	0.7	Very good

^[a] Scale position is the metering unit setting on the drill which determines the seeding rate

3.2 Results of the sticky belt experiments

The results obtained from mixed seeding experiments with five different barley:vetch mixture ratios (100:0, 75:25, 50:50, 25:75, and 0:100) and three different forward speeds (1.0, 1.5, and 2.0 m s⁻¹) are given in Table 5 related to seeding characterization and quality.

Based on the results, the combined seed drill had the ability to sow a barley and common vetch mixture in certain ratios with the in-row seed spacing uniformity characterized as random or precision seeding, generally (Table 5). The V_f values decreased with increasing of forward speed except pure vetch (0:100) and the seeding character got better.

Based on the results, it was found that seed distribution quality of seed mixture was in “very good” quality, generally. Most of goodness criteria values were found higher than 72%. It means that the combined seed drill was capable of sowing barley and common vetch seeds and their mixtures, with ratios of satisfactory quality.

Table 5. Seed distribution uniformity results at different mixture ratios

Mixture ratio (Barley:Vetch)	Forward speed (m/s)	V_f	Seeding characterization	λ , %	Seeding quality
100:0	1.0	0.98	Random seeding	71.9	Good
	1.5	0.97	Random seeding	75.2	Very good
	2.0	0.87	Precision seeding	75.2	Very good
75:25	1.0	0.78	Precision seeding	79.3	Very good
	1.5	0.82	Precision seeding	78.8	Very good
	2.0	0.70	Precision seeding	83.6	Very good
50:50	1.0	1.20	Undesirable seeding	69.2	Good
	1.5	0.98	Random seeding	73.2	Very good

Arzu YAZGI, Erdem AYKAS, Tuncay GUNHAN, Behcet KIR, Gulcan DEMIROGLU TOPCU.
“Mixed Seeding Performance of a Seed Drill at Different Mixture Ratios Under the Laboratory and Field Conditions”



CIGR 2018

XIX. World Congress of CIGR



25:75	2.0	0.85	Precision seeding	79.2	Very good
	1.0	0.49	Precision seeding	83.2	Very good
	1.5	0.46	Precision seeding	86.0	Very good
	2.0	0.43	Precision seeding	83.6	Very good
0:100	1.0	1.05	Random seeding	72.8	Very good
	1.5	1.10	Random seeding	70.4	Good
	2.0	1.28	Undesirable seeding	66.4	Good

3.3 Results of the field experiments

The results obtained from mixed seeding experiments with five different barley:vetch mixture ratios (100:0, 75:25, 50:50, 25:75, and 0:100) at forward speed of 1.5 m s⁻¹ are given in Table 6 related to seeding characterization and quality in the field conditions.

Based on the results, plant distribution quality of mixture was found in “very good quality” and all of goodness criteria values were found higher than 72%. That means the seeding characterization was found as “precision seeding”.

Table 6. Plant distribution uniformity results at different mixture ratios

Mixture ratio (Barley:Vetch)	V _f	Seeding characterization	λ, %	Seeding quality
100:0	0.45	Precision seeding	80.8	Very good
75:25	0.54	Precision seeding	82.8	Very good
50:50	0.60	Precision seeding	78.4	Very good
25:75	0.36	Precision seeding	78.0	Very good
0:100	0.77	Precision seeding	86.0	Very good

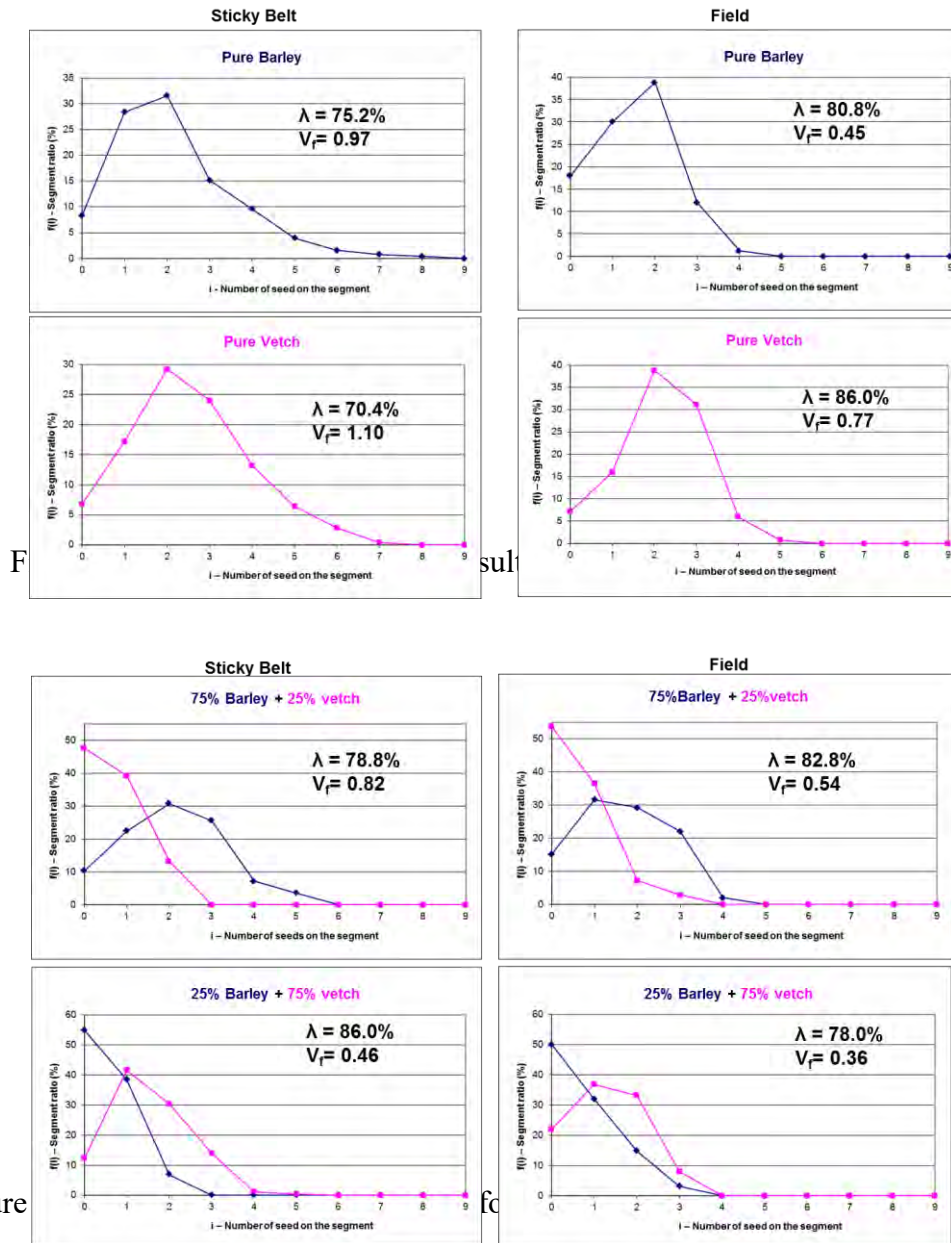
3.4 Comparison of sticky belt and field tests results

The results obtained from mixed seeding experiments in the laboratory and the field conditions with five different barley:vetch mixture ratios (100:0, 75:25, 50:50, 25:75, and 0:100) at forward speed of 1.5 m s⁻¹ are given in figure 3 and figure 4. The results showed that the sticky belt results and field results are in harmonious each other. Additionally, performance of the seeder in the field was found higher than in the laboratory for pure barley and pure vetch in goodness criterion and variation factor (Figure 3). The mixture of 75:25 had a better plant distribution in the field than the seed distribution in the laboratory, while the seed distribution was found higher quality than the plant distribution for the mixture of 25:75 (Figure 4).



CIGR 2018

XIX. World Congress of CIGR



4. CONCLUSION

Based on the experimental results and calculations, it was found that the combined seed drill could be used effectively for seeding of barley and vetch mixtures at different seed mixture ratios in laboratory and field conditions.

Arzu YAZGI, Erdem AYKAS, Tuncay GUNHAN, Behcet KIR, Gulcan DEMIROGLU TOPCU.
“Mixed Seeding Performance of a Seed Drill at Different Mixture Ratios Under the Laboratory and Field Conditions”



CIGR 2018

XIX. World Congress of CIGR



5. REFERENCES

- Acikgoz, E., & Cakmakci, S. (1986). Hay Yield and Its Quality of Common Vetch+Cereal Mixtures in Bursa Conditions. *Journal of Agricultural Faculty of Uludag University*, (1986) 5: 65-73.
- Bakoglu, A. (2004). Determination of Biological Yield and Land Equevalent Ratio in Common Vetch (*Vicia sativa* L.) and Barley (*Hordeum vulgare* l.) Mixtures at Different Rates Cropping. *Dogu Anadolu Arastirmalari*.
- Bayhan, Y., Kayisoglu, B., Ulger, P., & Akdemir, B. (2009). A Research on the Determination of Sowing Performance of Pneumatic Precision Drill for Cereals Sowing. *Journal of Tekirdag Agricultural Faculty*, 2009 6 (2).
- Griepentrog, H.W. (1994). Saatgutzuteilung von Raps. *Forschungsbericht Agrartechnik der Max-Eyth-Gesellschaft (MEG) 247*, Dissertation, Kiel.
- Kumar, V. J. F., & Durairaj, C. D. (2000). Influence of head geometry on the distributive performance of air-assisted seed drills. *J.Agric. Engng Res.* 75 (1), Article No: Jaer. 1999.0490, 81-95, Silsoe.
- Onal, I. (2011). Seeding, Planting and Fertilizing Machines. *Publications of Ege University Faculty of Agriculture*, No: 490, İzmir.
- Soya, H., Avcioglu, R., & Geren, H. (1996). Effect of Barley (*Hordeum vulgare* L.) as Nurse Crop and Rate of Mixtures and Row Spacing on the Seed Yield and Yield Characteristics of Common Vetch (*Vicia sativa* L.). *Proceeding of 3rd National Congress on Pasture and Forage* 17-19 June 1996, Erzurum, p:328-333.
- Uygan, F., & Guler, I. E. (2005). The Effects of Distributor Head Type, Air Velocity and Seeding Rate on Flow Evenness in Pneumatic Seed Drills. *Atatürk University, Journal of the Faculty of Agriculture*.36 (1), 59-67, 2005. ISSN 1300-9036.



CIGR 2018

XIX. World Congress of CIGR



Yazgi, A., Dumanoglu, Z., Kuldemir, N., Aygun, I. D., & Masoumi, A. (2012). Determination of the Machine Performance for Wheat Seeding by Pneumatic Seed Drill. *Journal of Agricultural Machinery Science*, 2012, 8 (1), 35-40.

Yazgi, A., Aykas, E., & Altınoz, Z. (2013). Determination of the Flowing Characteristics of Seed and Fertilizer for a Domestic Combined Direct Drill. *Journal of Agricultural Machinery Science*, 2013, 9 (3).

Yazgi, A., Aykas, E., Dumanoglu, Z., & Topcu, G. D. (2017). Seed Mixture Flowing Characteristics of a Seed Drill for Mixed Seeding. *Applied Engineering in Agriculture*, 33(1):63-71.



Prototype Twin Vacuum Disk Metering Unit for Improved Seed Spacing Uniformity Performance at High Seeding Speeds

Adnan Degirmencioglu, Bulent Cakmak, Arzu Yazgi

Ege University, Faculty of Agriculture, Department of Agricultural Engineering and Technology, 35100-Bornova-Izmir/Turkey

adnan.degirmencioglu@ege.edu.tr

ABSTRACT

The objective of this study was to design and develop a prototype precision metering unit with twin vacuum disks so that seeding can be achieved at higher forward speeds while reducing the peripheral speed of the vacuum disk for improved seed spacing uniformity and increased field work capacity. In order to meet this objective, a new precision seeding unit with twin vacuum disks, each mirrored view of the other and geometrically the same, was designed in an animated drafting software and then was manufactured and used for the laboratory experiments. Three crop seeds were used to determine the performance of the new metering unit in the lab on sticky belt test stand. Two alternative measures were used to quantify the seed spacing accuracy and polynomial functions using the principles of Response Surface Methodology were developed to calculate the optimum level of the variables. The tests performed in the laboratory at 2, 3 and 4 ms^{-1} forward speeds resulted in improved seed spacing accuracy values while the quality of feed index measure went down once the forward speed increased from 2 to 4 ms^{-1} . The quality of feed index with new metering unit was obtained to be 100% at 2 ms^{-1} while it was almost 98% for all crop seeds at 3 ms^{-1} . The forward speed of 4 ms^{-1} resulted in quality of feed index values of 92, 96 and 96% for cotton, sunflower and corn seeds, respectively.

Keywords: Accuracy, mathematical modeling, planter, polynomial functions, precision seeding, response surface methodology, Turkey.

INTRODUCTION

Agricultural machinery related operations are required to be achieved at the highest field work capacity while the performance is at desired level. The field work capacity for any operation can be maximized if the operation is achieved at high forward speeds for a machine with a specific operating width. Precision seeding, such as many field operations should be conducted in such a way that the seed spacing accuracy should fall into the accepted level.



CIGR 2018

XIX. World Congress of CIGR



As a result of accurately incorporated seeds into the soil, competition among plants in order to receive moisture and nutrient should be avoided.

Previous studies have demonstrated that three factors mainly contribute to the performance of a vacuum type metering unit. One of the factors is the peripheral speed of the vacuum disk as it is associated with the forward speed of the planter while the other two factors are the vacuum applied on vacuum disk and the hole diameter (Yazgi and Degirmencioglu, 2007). Staggenborg et al. (1999) studied the effect of planter speed and seed firmers on corn stand establishment and for this purpose a randomized complete block experiment was conducted. The performance of the planter was evaluated based on the mean plant spacing, standard deviation in spacing, and four indices (miss, multiple, quality of feed, and precision). The main conclusion from their study was that increased corn seeding speed adversely affected plant spacing uniformity performance.

Studies on the performance of a precision seeder mostly focused on vacuum pressure applied to the vacuum plate, the most common metering system in precision seeders. In a study, Singh et al. (2005) studied the effect of operational speed of the vacuum plate, vacuum pressure and shape of the entry of seed hole on performance related measures. These measures were miss index, multiple index and quality of feed index. However, they used a vacuum plate with holes at 2.5 mm diameter for cotton seeds and found that the metering system with a speed of 0.42 m s^{-1} and a vacuum pressure of 2 kPa produced superior results with a quality of feed index of 94.7% and a coefficient of variation of 8.6% in seed spacing. In another study, Panning et al. (2000) focused on five seeders that are different in terms of configuration for seed spacing uniformity and they carried out experiments at three field speeds using a seed location method in the field and a laboratory method involving an opto-electronic sensor system.

Moody et al. (2003) tested the performance of a row crop seeder in the field at three seed meter rotational speed of 0.16, 0.23 and 0.31 rev s^{-1} with corresponding forward speeds of 4.8, 7.2 and 9.7 km h^{-1} using cotton seeds. They concluded that the seed spacing variability increased with increased peripheral speed while the quality of feed indices ranged between 76.2 and 91.4%.

In order to overcome the reduced seed spacing accuracy at high seeding speeds as it corresponds with peripheral speed of the vacuum disk and achieve desired seed spacing, the peripheral speed of the vacuum disk should be reduced and this can be achieved by either increasing the seed spacing or increasing the number of holes on vacuum disk. Seed spacing for different row crops varies based on the crop in order to obtain an optimal plant population per unit area. Hence, the most obvious solution to increase seeding rate and decrease the peripheral speed of the vacuum disk is to increase the number of holes on vacuum disk. However, the number of holes on a vacuum plate can only be increased to a certain limit before this may result in vacuum band around the holes which causes a significant reduction in seeding performance due to increased multiple seeds held by single holes (Onal et al, 2012). Another option to reduce the peripheral speed of the vacuum disk is to use twin vacuum that oppose each other so that the seeds released by one disk is placed in between the ones released by the other one. The edition of a second seed

Adnan Degirmencioglu, Bulent Cakmak, Arzu Yazgi. "Prototype Twin Vacuum Disk Metering Unit for Improved Seed Spacing Uniformity Performance at High Seeding Speeds"



plate reduces rotational speed of a single seed plate while increasing the overall per row seeding rate when compared to a single vacuum disk. Therefore, a study was conducted and the objective of this study was to design and develop a prototype precision metering unit with twin vacuum disks so that seeding could be achieved at higher forward speeds to improve seed spacing uniformity performance and to increase field work capacity.

2. DESIGN OF A PROTOTYPE PRECISION METERING UNIT WITH TWIN VACUUM DISKS

Vacuum type precision seeder performance in terms of seed incorporation into the soil could be viewed in two parts. The first one is the metering unit performance and the second one is the rolling and bouncing of seeds on soil surface due to forward speed and impact angle of the seed. Metering unit performances are usually determined in the laboratory while obtaining the overall performance of a seeder requires field tests.

The study conducted in the laboratory by Yazgi and Degirmencioglu (2016) indicated that an average forward speed of 1 ms^{-1} is the speed that seed spacing accuracy for corn, cotton and sunflower can reach to a maximum level. Based on this finding, a new approach was realized to reduce the peripheral speed of the vacuum disk while achieving the desired seed spacing. This new approach was assumed to be the solution to the problem since using twin disks in order to obtain the same theoretical seed spacing would reduce the peripheral meter speed to half as compared to a single vacuum disk with the same number of holes on the disk. Since each disk releases seeds at two times greater than the theoretical seed spacing. This means that seeds by one vacuum disk are placed in between the seeds released by the other vacuum disk. This approach is depicted in figure 1.

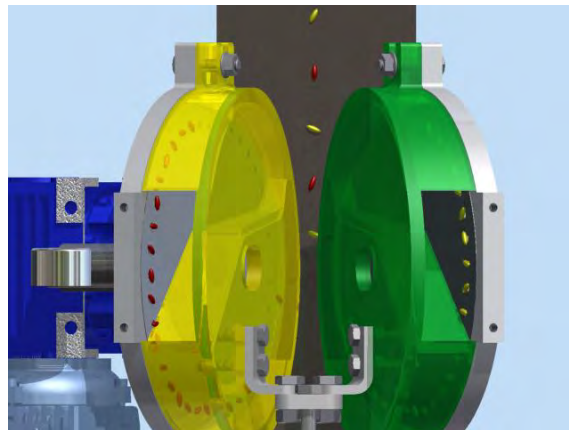


Figure 1. Conceptual view of twin disks metering unit.



In order to create a twin vacuum disk metering system, a new vacuum type metering system was designed in computer animated drafting software and then was manufactured. The technical dimensions (in mm) and the view of the left metering unit only (in the direction of travel) are depicted in figure 2 thru 5 since the left and right metering units are mirrored versions of each other and geometrically the same. The metering units were made of aluminum and manufactured on a CNC lathe by a private company.

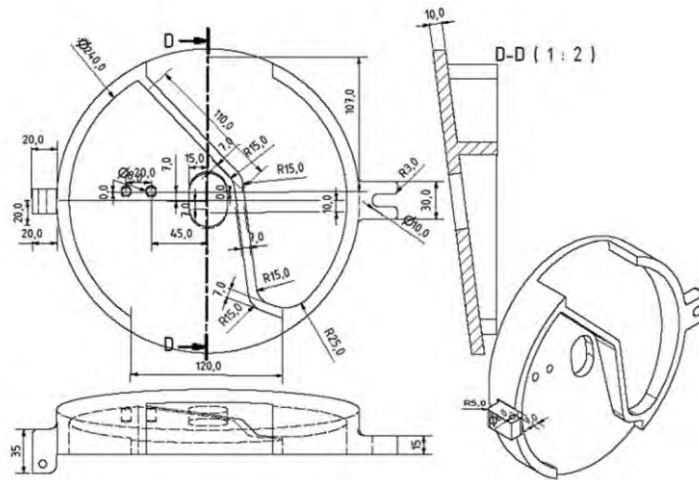


Figure 2. Technical dimensions and view of the left side metering unit in the direction of travel (dimensions are in mm).

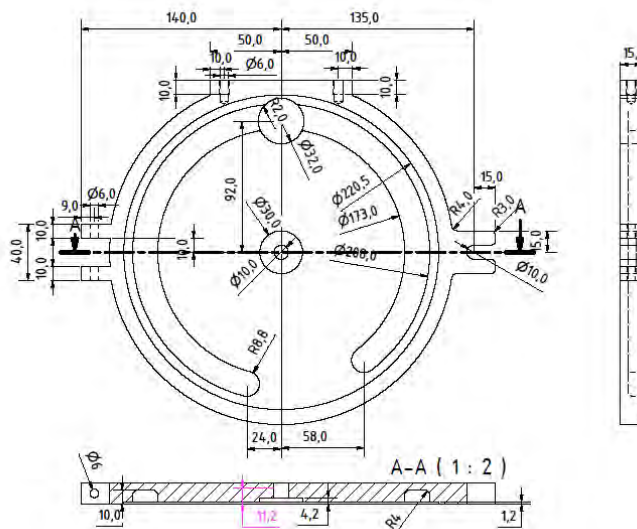


Figure 3. Technical dimensions and view of the lid for left side metering unit in the direction of travel (dimensions are in mm)



CIGR 2018

XIX. World Congress of CIGR



Figure 4. Manufactured view of the left side metering unit.



Figure 5. Manufactured view of the lid for left side metering unit.



CIGR 2018

XIX. World Congress of CIGR



3. MATERIAL AND METHODS

Three different crop seeds (corn, cotton and sunflower) were used for the laboratory experiments in order to test the performance of the new metering system. The physical properties of the seeds are given in table 1.

Table 1. Physical properties of the seeds used in the study

Seed	Length (a; mm)	Width (b; mm)	Thickness (c; mm)	Sphericity [£] (%)	Thousand seed mass (g)	Bulk density (kg m ⁻³)
Corn	11.3 (0.46)	6.9 (0.43)	3.8 (0.32)	59.0 (2.00)	251.3 (2.55)	805.9 (4.7)
Cotton	8.7 (0.52)	4.8 (0.32)	4.24 (0.28)	65.0 (3.00)	91.9 (0.25)	593.6 (5.6)
Sunflower	11.9 (0.48)	5.9 (0.27)	6.2 (0.44)	54.0 (2.00)	83.2 (1.01)	424.1 (1.3)

Numbers in paranthesis are the standard deviations. Sphericity was calculated as $\xi = (a.b.c)^{1/3}/a$

A sticky belt stand to evaluate the performance of the seeder was used for the tests performed in the laboratory. The belt was 15 m long and 14 cm wide. The measurement of seed distances was carried out at a distance of 10 m approximately. The vacuum type metering unit with twin disks was mounted on a special test stand. Each vacuum disk with 36 holes was rotated about 50° from the vertical direction so that the seeds could be placed in the same line and driven by an electric motor. The disks were coupled by a stiff coupling made of polyurethane in such a way that the holes of one of the vacuum disks were off set of the other disk so that the seeds released from one disk can be placed in between the seeds released by the other one. The necessary vacuum at different levels was provided by the fan of a separate unit driven by the power take off (PTO) of the tractor. The grease belt was driven separately and special care was given to provide synchronization of the forward speed associated with the peripheral speed of the vacuum plate and belt speed.

Each vacuum disk was set to provide a seed spacing of 23.6 cm so that the desired theoretical seed spacing (Z_t) of 11.8 cm could be achieved for all of the seeds used in the study. In order to facilitate this study, seed spacing measurements and evaluations were performed using a computerized measurement system (CMS) on a sticky belt test stand (Onal and Onal 2009). In order to determine how the prototype metering unit was performed under different seeding conditions in the laboratory. Three different performance criterion defined by Kachman and Smith (1995), quality of feed index (I_{qf}), multiple index (I_{mult}) and miss index (I_{miss}) indicates were evaluated.

Other performance measure was the one called root-mean-square deviation (E_{rms}) from the theoretical seed spacing as proposed by Yazgi and Degirmencioglu (2007). The functions to be developed based on this criterion are considered to be penalty functions since any deviation from the theoretical seed spacing is penalized. This definition is given below.

Adnan Degirmencioglu, Bulent Cakmak, Arzu Yazgi. "Prototype Twin Vacuum Disk Metering Unit for Improved Seed Spacing Uniformity Performance at High Seeding Speeds"



CIGR 2018

XIX. World Congress of CIGR



$$E_{rms} = \sqrt{\frac{\sum_{i=1}^N (Z - Z_t)^2}{N}} \quad (1)$$

where: Z_t is theoretical seed spacing; Z is the measured seed spacing and N is the number of measurements.

As a statistical and mathematical technique, Response Surface Methodology (RSM) was employed in this study as it was used by Yazgi and Degirmencioglu (2007) in order to develop performance functions and to optimize the constructional-related variable (hole diameter) and the operating related variables (peripheral speed of the seed plate and vacuum pressure) for each seed separately. Central Composite Design, one of the designs in RSM was selected to study the above mentioned variables and based on this design five levels for each independent variable were considered. These levels were coded as -1.682, -1, 0 (center point), +1 and +1.682, respectively (Box and Draper, 1987). The coded and uncoded levels of the variables are given in Tables from 2 to 4 for corn, cotton and sunflower seeds. A total of 20 experiments for each seed were carried out in three replications and each replication included a total of approximately 60 seed spacings.

Table 2. Coded and uncoded levels of the peripheral speed (X_1) of the vacuum disk for all seeds

Seed	Step value (ms^{-1})	Coded level of the peripheral speed (X_1)				
		-1.682	-1	0	1	1.682
For all seeds	0.028	0.036 (0.52)	0.056 (0.8)	0.084 (1.2)	0.112 (1.6)	0.131 (1.87)

Numbers in parantehesis are the ground speeds corresponded to peripheral speed of the vacuum disk.

Table 3. Coded and uncoded levels of the hole diameter (X_2) used in the study

Seed	Step value (mm)	Coded level of hole diameter (X_2)				
		-1.682	-1	0	1	1.682
Corn	1.0	2.318	3.0	4.0	5.0	5.682
Cotton	0.5	1.660	2.0	2.5	3.0	3.340
Sunflower	0.5	1.159	1.5	2.0	2.5	2.841

Table 4. Coded and uncoded levels of the vacuum (X_3) for all seeds used in the study

Seed	Step value (kPa)	Coded level of vacuum (X_3)				
		-1.682	-1	0	1	1.682
For all seeds	2.0	2.64	4.0	6.0	8.0	9.36



CIGR 2018

XIX. World Congress of CIGR



4. RESULTS AND DISCUSSION

The results obtained from experiments are given in Tables 5, 6 and 7, for corn, cotton and sunflower seeds, respectively.

In order to build performance functions in coded form of the three dependent (performance related) variables, the following transformation (Rawlings, 1988) was made for all performance indices except E_{rms} so that the predictions from the developed functions should not exceed 100%.

$$y = \arcsin\left(\sqrt{\frac{I_{qf}}{100}}\right) \quad (2)$$

No significant model for any of performance indices was developed for corn seeds. Hence the verification tests for corn seeds were achieved based on the results obtained from the experiments.

Table 5. Performance results obtained from the RSM based experiments for corn seeds

Run number	Coded independent variables			Performance indices			
	Peripheral speed (X_1)	Hole diameter (X_2)	Vacuum (X_3)	I_{qf} (%)	I_{mult} (%)	I_{miss} (%)	E_{rms}
1	-1	-1	-1	100	0	0	3.9
2	-1	1	-1	96.7	3.3	0	4.1
3	1	-1	-1	88.9	3.7	7.4	8.4
4	1	1	-1	100	0	0	2.6
5	-1	-1	1	92.6	3.7	3.7	4.8
6	-1	1	1	96.7	3.3	0	3.5
7	1	-1	1	89.7	6.9	3.5	6.5
8	1	1	1	92.9	3.6	3.6	8.6
9	-1.682	0	0	100	0	0	2.1
10	1.682	0	0	100	0	0	2.9
11	0	-1.682	0	96	0	4	5.5
12	0	1.682	0	100	0	0	2.5
13	0	0	-1.682	96.2	0	3.9	10.0
14	0	0	1.682	100	0	0	1.5
15	0	0	0	100	0	0	1.5
16	0	0	0	100	0	0	2.6
17	0	0	0	100	0	0	1.5
18	0	0	0	100	0	0	2.6
19	0	0	0	100	0	0	1.5
20	0	0	0	100	0	0	2.6



CIGR 2018

XIX. World Congress of CIGR



Table 6. Performance results obtained from the RSM based experiments for cotton seeds

Run number	Coded independent variables			Performance indices			
	Peripheral speed (X ₁)	Hole diameter (X ₂)	Vacuum (X ₃)	I _{qf} (%)	I _{mult} (%)	I _{miss} (%)	E _{rms}
1	-1	-1	-1	83.3	0	16.7	10.2
2	-1	1	-1	96.9	3.1	0	2.4
3	1	-1	-1	75.8	8.2	16	14.1
4	1	1	-1	100	0	0	2.5
5	-1	-1	1	92.3	0	7.7	10.0
6	-1	1	1	97.4	2.6	0	4.8
7	1	-1	1	79.3	0	21.7	10.0
8	1	1	1	96.2	0	3.8	5.9
9	-1.682	0	0	100	0	0	2.3
10	1.682	0	0	100	0	0	2.7
11	0	-1.682	0	92.3	0	7.7	5.9
12	0	1.682	0	93.4	3.3	3.3	5.3
13	0	0	-1.682	92.6	0	7.4	6.3
14	0	0	1.682	96.3	3.7	0	1.8
15	0	0	0	96.3	0	3.7	4.7
16	0	0	0	100	0	0	1.5
17	0	0	0	100	0	0	1.8
18	0	0	0	100	0	0	1.7
19	0	0	0	96.3	0	3.7	1.7
20	0	0	0	100	0	0	1.7

Table 7. Performance results obtained from the RSM based experiments for sunflower seeds

Run number	Coded independent variables			Performance indices			
	Peripheral speed (X ₁)	Hole diameter (X ₂)	Vacuum (X ₃)	I _{qf} (%)	I _{mult} (%)	I _{miss} (%)	E _{rms}
1	-1	-1	-1	78.3	4.4	17.4	11.1
2	-1	1	-1	100	0	0	4.8
3	1	-1	-1	71.4	7.1	21.4	37.0
4	1	1	-1	96.4	3.6	0	5.6
5	-1	-1	1	100	0	0	2.4
6	-1	1	1	96.3	3.7	0	4.2
7	1	-1	1	87.5	4.2	8.3	6.4
8	1	1	1	93.1	6.9	0	5.7
9	-1.682	0	0	100	0	0	2.6
10	1.682	0	0	100	0	0	2.9
11	0	-1.682	0	91.3	0	8.7	11.3
12	0	1.682	0	100	0	0	3.2
13	0	0	-1.682	70	0	30	11.5
14	0	0	1.682	100	0	0	3.4

Adnan Degirmencioglu, Bulent Cakmak, Arzu Yazgi. "Prototype Twin Vacuum Disk Metering Unit for Improved Seed Spacing Uniformity Performance at High Seeding Speeds"



CIGR 2018

XIX. World Congress of CIGR



15	0	0	0	100	0	0	2.6
16	0	0	0	100	0	0	2.9
17	0	0	0	100	0	0	2.8
18	0	0	0	100	0	0	2.9
19	0	0	0	100	0	0	2.8
20	0	0	0	100	0	0	2.6

The performance model with an R^2 of 60.4 % was the only model developed for cotton seeds. The quality of feed index model given below for cotton seeds (YCI_{qf}) resulted from the stepwise regression analysis at a probability level of 95% even though all three variables were defined in quadratic form.

$$YCI_{qf} = 1.51 - 0.095 X_2^2 + 0.087 X_2 - 0.082 X_3^2 \quad (R^2 = 60.36\%) \quad (3)$$

This model may be considered to have a low coefficient of determination but once the raw data are examined, it is seen that the I_{qf} performance varies in a narrow range and this may be the consequence of the model with low R^2 . The optimum level of the variables in the model given above was found in a software to be 0.457 and 0 for the variable X_2 and X_3 , respectively. The original level of the variables on the other hand can be calculated as follows;

$$\frac{X_2 - 2.5}{0.5} = 0.457 \Rightarrow X_2 = 2.72 \text{ mm} \quad (4)$$

$$\frac{X_3 - 6}{2} = 0 \Rightarrow X_3 = 6.0 \text{ kPa} \quad (5)$$

For sunflower seeds, only quality of feed index (YSI_{qf}) and miss index (YS_{miss}) models were developed. The quality of feed index model and the optimum level of the variables as found to be 0.504 and 0.17 for hole diameter and vacuum in coded form, respectively and their levels in original unit of these variables are given below.

$$YSI_{qf} = 1.556 - 0.122 X_3^2 + 0.102 X_3 + 0.093 X_2 - 0.12 X_2 X_3 - 0.072 X_2^2 \quad (R^2 = 78.47\%) \quad (6)$$

$$\frac{X_2 - 2}{0.5} = 0.504 \Rightarrow X_2 = 2.25 \text{ mm} \quad (7)$$

$$\frac{X_3 - 60}{2} = 0.17 \Rightarrow X_3 = 6.34 \text{ kPa} \quad (8)$$

The miss index model for sunflower seeds was in the following form while the optimum level of the variables in coded form was found to be 1.07 and 0.17 for hole diameter and vacuum, respectively.

$$YS_{miss} = 7.9 \times 10^{-5} - 0.125 X_2 - 0.117 X_3 + 0.102 X_3^2 + 0.077 X_2 X_3 + 0.052 X_2^2 \quad (R^2 = 87.81\%) \quad (9)$$

The level of the variables in original units as calculated below was found to be 2.54 mm for the hole diameter and 6.34 kPa for the vacuum level.

$$\frac{X_2 - 2}{0.5} = 1.07 \Rightarrow X_2 = 2.54 \text{ mm} \quad (10)$$



CIGR 2018

XIX. World Congress of CIGR



$$\frac{X_3 - 60}{2} = 0.17 \Rightarrow X_3 = 6.34 \text{ kPa} \quad (11)$$

The optimum level of the variables as calculated from the models given above for sunflower seeds are similar and verifies each other, especially the vacuum level from both models are the same.

The common point of the developed models given above and raw data is that the performance functions are free of peripheral speed of the vacuum disk. This finding proves the hypothesis that the use of twin disks can reduce the peripheral speed so that seed capture and holding characteristics are improved within a certain range between 0.036 and 0.131 ms^{-1} . Hence, precision seeding can be achieved at higher seeding speeds once the optimum level for hole diameter and vacuum are set to the correct level for each seed.

Some verification tests were conducted in the laboratory on a sticky belt test stand in order to test if the precision seeding performance can be maximized at high seeding speeds. In these tests, the planter forward speed was set to 2 , 3 and 4 ms^{-1} . But the tests at 3 and 4 ms^{-1} were achieved with twin vacuum disks, each with 72 holes while the tests at 2 ms^{-1} was conducted by the use of 36 hole vacuum disks. The peripheral speed of the vacuum disk remained unchanged by the use of 36 hole vacuum disk at 2 ms^{-1} and 72 hole vacuum disks at 3 and 4 ms^{-1} to obtain the theoretical seed spacing of 11.8 cm .

The results from the verification tests conducted in the laboratory on the sticky belt test stand are given in table 8. As seen from the table, the quality of feed index was 100% while very low E_{rms} values were obtained at the tests conducted at 2 ms^{-1} for all crops while the same index declined as the speed increases. On the other hand, the miss index increase with the increase in forward speed and no multiples was occurred in any of the tests. The increase in miss index with the increase in forward speed could be attributed to the fact that the vacuum need may change at higher forward speeds. Centrifugal forces at forward speed of 3 and 4 ms^{-1} may overcome the forces such that the seeds are sucked into the hole by vacuum as determined at a forward speed ranging between 0.52 and 1.87 ms^{-1} .

The E_{rms} values increased with the increase in forward speed but all of the E_{rms} values were considerably low as compared to an ideal E_{rms} value of zero that represents perfect seed spacing accuracy.



CIGR 2018

XIX. World Congress of CIGR



Table 8. Results from the verification tests achieved at different planter speeds

Seed	Hole diameter (mm)	Vacuum (kPa)	Planter speed (ms ⁻¹)	Performance indices		
				I _{qf} (%)	I _{miss} (%)	E _{rms}
Corn	4	6	2.0	100	-	1.6
			3.0	97.9	2.1	2.4
			4.0	95.6	4.4	2.7
Cotton	2.5	6	2.0	100	-	1.8
			3.0	97.7	2.3	2.0
			4.0	92.2	7.8	3.1
Sunflower	2.5	6	2.0	100	-	2.1
			3.0	97.8	2.2	2.3
			4.0	96.4	3.6	2.6

5. CONCLUSIONS

The followings were concluded from the study conducted:

- The twin disk metering unit as developed in this study eliminated the effects of peripheral speed that deteriorate the seed spacing accuracy at a certain range
- A new design of a metering unit with twin vacuum disks was able to provide acceptable levels of seed spacing accuracy for three different crop seeds
- The quality of feed index with new metering unit was obtained to be 100% at 2 ms⁻¹ while it was almost 98% for all crop seeds at 3 ms⁻¹. The forward speed of 4 ms⁻¹ resulted in quality of feed index values of 92, 96 and 96% for cotton, sunflower and corn seeds, respectively.
- The new metering unit is applicable to use for conventional row crop seeders as well as direct seeders.
- The performance in direct seeders equipped with seed tubes may increase by the use of this new design since seeds are dropped into the seed tube at a lower speed as compared to conventional precision seeders with single vacuum disk.
- The polynomial models developed in this study can be used to determine the performance measures for different plant densities that require different theoretical seed spacings.

5. ACKNOWLEDGMENT

The authors acknowledge the financial support of Ege University to carry out this study as a research project.



CIGR 2018

XIX. World Congress of CIGR



6. REFERENCES

- Box, G.E.P., & Draper, N. (1987). Empirical Model-Building and Response Surfaces. New York, John Wiley & Sons, 669 p.
- Kachman, S.D., & Smith, J.A. (1995). Alternative Measures of Accuracy in Plant Spacing Planter Using Single Seed Metering. Transactions of the ASAE 38(2): 379-387.
- Moody, F.H., Hancock, J.H., & Wilkerson, J.B. (2003). Evaluating planter performance-cotton seed placement accuracy. ASAE Paper No. 03 1146, St Joseph, Michigan, USA.
- Onal, O., & Onal I. (2009). Development of a computerized measurement system for in-row seed spacing accuracy, Turk J Agric For, 33 (2009) 99–109.
- Onal, I., Degirmencioglu, A., & Yazgi, A. (2012). An evaluation of seed spacing accuracy of a vacuum type precision metering unit based on theoretical considerations and experiments. Turk J Agric For, 36 (2012): 133-144.
- Panning, J.W., Kocher, M.F., Smith, J.A., & Kachman, S.D. (2000). Laboratory and field testing of seed spacing uniformity for sugar-beet planters. Applied Engineering in Agriculture, 16(1): 7–13
- Rawlings J.O. (1988). Applied Regression Analysis, Wadsworth & Brooks/Cole Advanced Books & Software
- Singh, R.C., Singh, G.D., & Saraswat, C. (2005). Optimisation of design and operational parameters of a pneumatic seed metering device for seeding cotton seeds. Biosystems Engineering, 92(4): 429–438
- Staggenborg, S.A., Fjell, D.L., Devlin, D.L., Gordon, W.B., Maddux, L.D., & Marsh, B.H. (1999). Selecting optimum seeding dates and plant populations for dryland corn in Kansas. J. Prod. Agric. 12:85-90.
- Yazgi, A., & Degirmencioglu, A. (2007). Optimisation of the seed spacing uniformity performance of a vacuum-type precision seeder using response surface methodology. Biosystems Engineering. 97 (3) 347– 356.
- Yazgi, A., & Degirmencioglu, A. (2016).Development of Prediction Functions for a Maximized Precision Seeding Performance Based on Optimized Variables. Journal of Agriculture Faculty of Ege University, 53 (2):179-187.



Detection Of Foreign Bodies In Processed Food And Drinking By Means Of Ultrasound

Mohammadreza Zarezadeh*, Mohammad Aboonajmi

Department of Agro-technology, Abouraihan Campus, University of Tehran, Tehran, Iran

Email address: mr.zarezadeh@ut.ac.ir

ABSTRACT

Detection of foreign bodies in food and drinking products play an important role in quality assurance and customers satisfaction. There are many approaches to detect and identification of foreign bodies (FBs) which each one has advantages and disadvantages. However ultrasound-based measurement ways have showed potential in various food processing applications, such as concentration gauging, flow measurement, level detection, food shelf life monitoring, food properties assessment and FBs detection. The basis of ultrasound diagnosis and FBs detection is transmitting ultrasound waves to tested canned food and drink with specific frequency and power, then returned signals processing and analyzing. Ultrasound is non-destructive and does not spoil foods physically or hygienically. Ultrasound approach can be very useful when other approaches such optical approach is not possible.

Keywords: foreign body detection, food safety, FB, Non-destructive, ultrasound, Iran

INTRODUCTION

The quality control is an important aspect in food production. The major purpose of this control is to verify the acceptability of food in term of safety. The development of new techniques for the quality control continues to increase according to the requirements imposed by the consumers and the authentication of food security. There are several non-destructive methods for food quality control including image processing (Jafari et al.(2014)), metal detection (Zhao et al (2003)), X-ray detection (Nielsen et al. (2013)), visible/infrared (IR)/ hyper-spectral imaging systems (camera/laser-based), mechanical detection, electrical impedance tomography, ultrasonic approach etc. The potential of ultrasound as a tool for non-destructive quality control of food products is currently under investigation. The ultrasonic waves have a valuable feature that consists in its ability to characterize opaque materials such as packed UHT (R.R.B. Singh et al., 2014) and packed fruit juice (Luis Elvira et al., 2014).



Figure 1. Detection of beverage Cans for Leak by ultrasound

One of foods quality parameters is absence of foreign bodies (FBs). A foreign body is defined as a piece of undesirable solid matter present in a product. Some of the most frequency observed foreign bodies (FBs) in food and beverages are include: pests, glass, metals (Djekic et al., 2017), plastic particles, wood, rock, bone, etc. The food manufacturer's objective is to supply products completely free from foreign bodies, in order to meet the consumers' expectations (Wallin and Haycock, 1998). It has been considered a serious offense for food manufacturers to carelessly fail to detect the presence of the foreign body inside their food products. Ultrasound-based systems with low intensity, are non-hazardous with relatively low costs. They are widely used in medical diagnosis and in industrial defect detection, and as such they are considered to be a highly promising candidate for foreign body detection in foods. A noted characteristics of ultrasonic imaging is that a slightly specification of materials is realizable as the result of the complicated manner in which the ultrasound signal interacts with the material. Shung et al. (1992) showed that some of ultrasound propagation characteristics can be used to define a medium such as food. These characteristics include attenuation & absorption, backscatter, velocity and nonlinearity. Another advantage of ultrasonic-based systems is that they are more adaptable to various test environments and conditions than systems based on other techniques. Ultrasound sensors can be made as small as a catheter tip of 1.2mm diameter, on which a circumferential array of 64 elements can be formed and placed in the coronary arteries or veins of the heart to image blood flow. (Crowe et al, 2000)

2. THEORY

The most frequency used wave modes in FBs detection in processed food are compressive and shear waves. First type can be used to foreign body detection in liquids, semi-fluid or solids foods. A compressive waves are effective only for inspection applications where strict transducer orientation conditions can be readily realized to avoid refraction issues. Shear waves can be used to inspect solid and semi-fluid foods. An advantage of shear wave is that it has larger tolerance for sensor alignment than compressive wave owing to its lower propagation velocity. However, shear waves cannot be used to inspect liquid foods such as beverages since the shear modulus of a liquid is zero and no shear wave can propagate as a consequence. Decreases in waves energy in materials takes place in propagation course as do



other forms of energy. The rate at which the wave energy decreases differs for different materials. It is quantitatively described by the attenuation coefficient in units of nepers per meter [Np/m]. The attenuation coefficient is frequency dependent: a high frequency acoustic wave attenuates faster than a low frequency acoustic wave (Basir and Zhao 2004). During wave transmitting from one material to another, part of the energy is reflected at the interface and part of it, transmitted through the second material.

The (Reflected ultrasound wave amplitude / incident ultrasound wave amplitude) ratio is known as the reflection coefficient (R). The ratio between the transmitted part and the incident ultrasound wave is referred to as the transmission coefficient (T). They are calculated using the following equations:

$$\text{Eq. 1} \quad R = (Z_2 - Z_1) / (Z_1 + Z_2)$$

$$\text{Eq. 2} \quad T = 2Z_2 / (Z_1 + Z_2)$$

Where Z_1 and Z_2 are the acoustic impedances of the first material and the second material respectively (Basir and Zhao 2004).

2.1. Types Of Ultrasonic Transducer

2.1.1 Piezoelectric Transducers

Materials are named Piezoelectric, are used to make ultrasonic transducers. As the name indicates, when pressure is applied to them, they generate electricity.

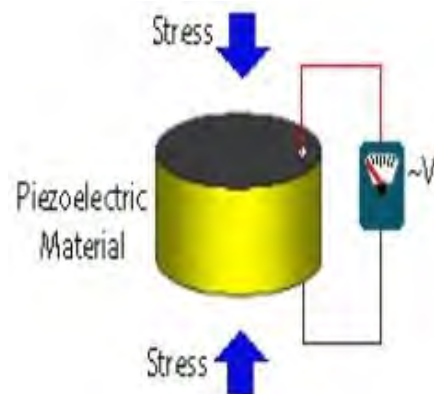


Figure 2. Piezoelectric effect

Conversely, they change their shape with electric excitement (fig. 2). Generally, an ultrasonic piezoelectric transducer was designed to generate and/or receive compressive wave: change in thickness of a piezoelectric disc or film is related to electric signal change. An ultrasound beam produced by a disc or film is unfocused and can be focused in a manner analogous to focusing light, since geometric acoustic analysis applies when the wavelength is less than the object dimension. An acoustic lens can be made of a solid or a liquid (Birks and Green, 1991). They are normally integrated in the transducer. The main weaknesses of common piezoelectric transducers is that they need contacts to transmit acoustic energy to the object to be inspected. The contact mode limits the scope of application and the detection speed of



such transducers. Transducers are easily worn due to transducer-to-object contact. When allowed, water can be used as a coupling medium to overcome this problem. However, high speed movement between the transducer and the objects can induce serious water turbulence in scanning. This turbulence deteriorates the signal-to-noise ratio. Some non-contact ultrasound transducers have been developed. These non-contact transducers include air coupled transducers, electromagnetic acoustic transducers (EMAT) and laser-ultrasound systems.

2.1.2 Air Coupled Transducers

Some authors works on air coupled transducers (Fathizadeh and Aboonajmi (2017) and Bhardwaj (2002)). However there are two types of air coupled ultrasonic transducers depending on the specific mechanism they employ. One type uses a piezoelectric mechanism, and the other type uses an electrostatic (capacitance) mechanism. In piezoelectric designs, the key problem is to eliminate the acoustic impedance mismatch between the piezoelectric ceramic and air. Equation 2 depicts how the transmitted energy is very small when an ultrasound wave is transmitted from a piezoelectric transducer to the air due to small impedance and high attenuation of the air. Researchers and transducer experts have been designing piezoelectric devices by manipulating the acoustic impedance transitional layers in front of the piezoelectric element. Typically, these layers have low impedance (less than $1 \times 10^6 \text{ Kg/m}^2\text{s}$). Using compressed fibers as the final matching layer, a piezoelectric air coupled transducer can propagate up to 5MHz ultrasound through nearly all materials in non-contact mode. (Bhardwaj, 2002).

2.2 Principle Of FB Detection In Food Containers

In comparison to A-Scan in non-destructive testing (NDT) for mechanical parts inspection and B-Scan in medical diagnosis, foreign body detection in food containers has some peculiarities. A-Scan uses the echo signal information in a certain time zone (time gating) to detect flaws in a mechanical part (Fig. 3): (i) when an ultrasound is transmitted to a clear portion, an echo signal from the back surface of the part can be received; (ii) When a small flaw is on the path of the ultrasound beam, echo signals will appear ahead of the back surface echo in the time domain; and (iii) the back surface echo will disappear if the flaw is large enough to intercept most of the beam from the transducer. In both cases, A-Scan uses the back surface echoes of a mechanical part as a reference signal (Basir and Zhao 2004).

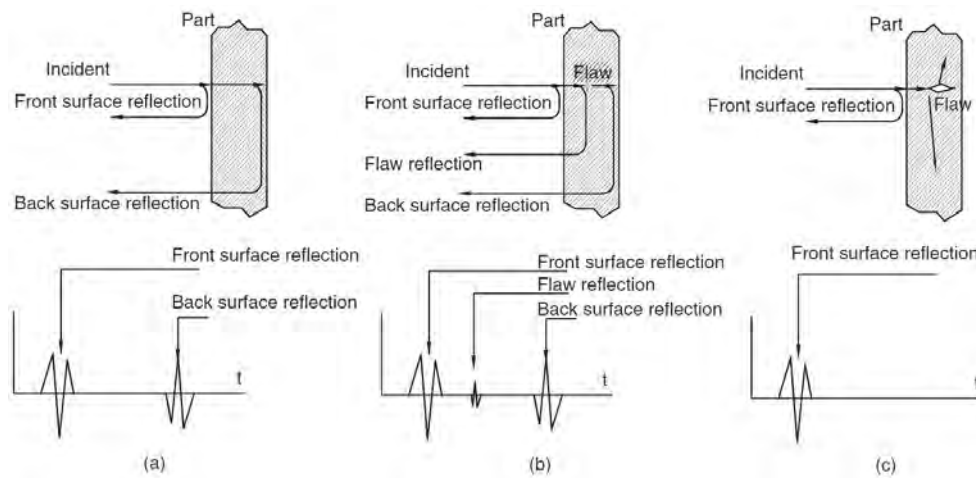


Figure 3. Illustration of the principle of flaw detection in a mechanical part using an ultrasound signal (Basir and Zhao 2004): (a) good part and echo signals, (b) small flaw in the part and echo signals, and (c) big flaw in the part and echo signals.

Figure 4 is an illustration of this problem in the cross-section plane perpendicular to the bottle's axis. In this plane, the ultrasound incident is at point A of the bottle, but the outlet is at point E. It is out of the reach of the transducer (the thickness is exaggerated in the figure for the sake of refraction angle drawing). For a glass bottle of inner diameter 50mm, thickness 2mm, filled with water, the maximum tolerant incident angle is 1° for a transducer of diameter 6.25mm. This tolerance will not be readily reached without adjusting the transducer orientation, especially for containers with complicated convex or concave surfaces. However, if on-line orientation adjustment is performed, the inspection speed will decrease, complicating equipment control. The transducer orientation is a 3-D issue.

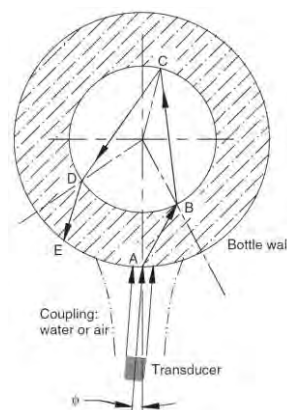


Figure. 4 Illustration of the effect of large difference in ultrasound velocities between the coupling/package/food materials on ultrasonic transmission path.



3. Some Studies On Ultrasonic Detection Application

Ouacha et al. (2015) showed that air traces in the UHT milk packet is detectable Non-destructively by ultrasound. They have demonstrated this by following the evolution of ultrasonic parameters: the peak to peak amplitude and the flight-time. We noticed that the flight-time is the most informative parameter because it shows the difference between sterilized package and unsterilized one at an early stage. In the temperature 35 °C, we noticed that both parameters show simultaneously the difference between the both studied cases. This important result shows that 35 °C is suitable for the characterization of UHT milk package because it is the ideal one for bacterial growth in comparison with the others temperatures Zhao et al. (2003), Detected metal, glass and plastic pieces in bottled beverages by using ultrasound waves. Foreign bodies were detected by scanning the flat bottom of the beverage container. Based on acoustic modeling, they developed and tested a method for detection and identification of foreign bodies. (Fig 5) A signal processing algorithm for time–frequency analysis is used to discriminate between beverage and contaminants from ultrasound echoes. Effective detection ability for materials such as glass, metals, and plastic, with sizes from 10 to 2.5 mm² is demonstrated.

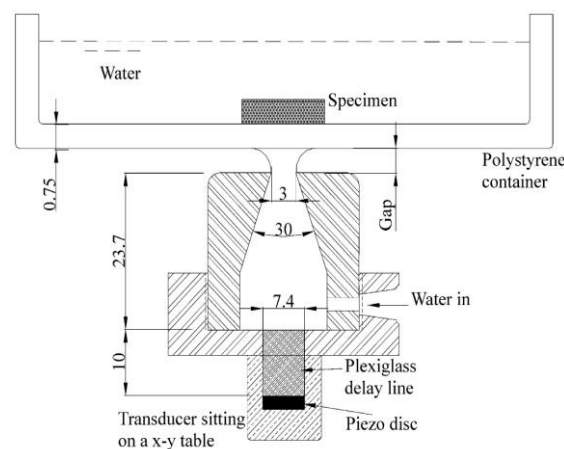


Figure 5. A prototype of a foreign body detector using an ultrasonic technique
Zhao et al. (2003)

Meftah and Mohd Azimin (2012), like the above authors, Detected foreign bodies in canned foods by means of ultrasonic approach. The transducer and the setup can detect foreign bodies inside a canned food container. However, a foreign body of 1 mm thickness cannot be detected according to the above setup. Performance of the FB detection system strongly depends on the very specific acoustic impedance of the foreign body and the alimentary product we are working with. In case of beverages, detection up to 4 millimeter foreign body size has been done for rock and metal FB. Mohd Khairi (et al. 2016) used two dimensional (2D) of finite element method in order to detect the foreign body in food container using an ultrasonic measurement system. They applied Comsol acoustic module to foreign object detection in the dairy product where various conditions such as frequency, foreign body



material and thickness of container wall were simulated. They used high frequency (300 kHz) due to detecting much smaller foreign bodies (they used steel and glass pieces as foreign object). They reported that the total acoustic pressure is reduced significantly from 0.420 Pa to 0.350 Pa when the size of steel was increased from 5 mm to 10 mm. A similar correlation was also obtained for glass material where 0.354 Pa was reduced to 0.278 when the size of glass was increased to 10 mm. They also used low frequency. For the 45 kHz frequency, the difference in total acoustic pressure between 5 mm and 10 mm foreign body is only 0.020 Pa but for 300 kHz frequency, the difference is 0.076 Pa. results showed that a higher frequency presents a more significant difference in total acoustic pressure compared to lower frequency. Also demonstrated that the finite element method can assist the designing and development of an ultrasonic measurement system in the food industry field.

4. CONCLUSIONS

FBs are found in many food containers of various shape and material. Ultrasound properties are diverse for foods and packaging materials. An effective, reliable, fast and low cost FB detection system, including the method and equipment, should be designed based on product and packaging specifications.

REFERENCES

- Abdolabbas Jafari, Atefeh Fazayeli, Mohammad Reza Zarezadeh. (2014). Estimation of orange skin thickness based on visual texture coarseness. *Biosystems engineering*. 117. pp 73-82.
- Bosen Zhao, Otman A. Basira, Gauri S. Mittal (2003). Detection of metal, glass and plastic pieces in bottled beverages using ultrasound. *Food Research International* 36 pp. 513–521
- E. Ouacha, B. Faiz, A. Moudden, I. Aboudaoud, H. Banouni, M. Boutaib (2015). Non-destructive detection of air traces in the UHT milk packet by using ultrasonic waves. *Physics Procedia* 70 pp. 406–410.
- Fathizadeh, Zahed and Aboonajmi, Mohammad (2017). Nondestructive air-coupled ultrasound measurement in the food industries. *Proceedings of the 4th Iranian International NDT Conference* Feb 26-27.
- Ilija Djekic, Danijela Jankovic, Andreja Rajkovic, (2017). Analysis of foreign bodies present in European food using data from Rapid Alert System for Food and Feed (RASFF). *Food Control*.
- Luis Elvira, Carmen M. Durán, José Urréjola, Francisco R. Montero de Espinosa. (2014). Detection of microbial contamination in fruit juices using noninvasive ultrasound. *Food Control* 40, pp 145-150.
- Meftah, H. and Mohd Azimin, E. (2012). Detection of foreign bodies in canned foods using ultrasonic testing. *International Food Research Journal* 19(2) pp. 543-546



CIGR 2018

XIX. World Congress of CIGR



Mikkel Schou Nielsen, Torsten Lauridsen, Lars Bager Christensen, Robert Feidenhans. (2013). X-ray dark-field imaging for detection of foreign bodies in food. Food Control 30. pp 531-535

Mohd Taufiq Mohd Khairi, Sallehuddin Ibrahim, Mohd Amri Md Yunus, Mahdi Faramarzi, Muhammad Abdul Illah Abd Rahman, Muhammad Sani Gaya. (2016). Finite element simulation for detecting the foreign body based on ultrasonic sensor. Journal of Food Process Engineering.

O. A. Basir and B. Zhao (2004). Detecting foreign bodies in food. Chapter 12 Ultrasound. pp 204-223

R.R.B. Singh, A.P. Ruhil, D.K. Jain, A.A. Patel, G.R. Patil. (2009). Prediction of sensory quality of UHT milk – A comparison of kinetic and neural network approaches. Journal of Food Engineering 92 pp.146–151.

Shung k k, smith m b and tsui b m w (1992) Principles of Medical Imaging, San Diego, Academic Press, 85–91.

Wallin, P. and Haycock, P. 1998. Foreign Body Prevention, Detection and Control. Glasgow, U.K.: Blackie.



Integration of photovoltaic arrays into the historic city

T. Olšan¹, M.Q. Dang¹, M. Libra¹, V. Poulek¹, J. Sedláček¹, V. Avramov², V. Beránek³

¹ Czech University of Life Sciences Prague, Czech Republic

² ENESA, joint-stock company, Prague, Czech Republic

³ Solarmonitoring, Ltd., Prague, Czech Republic
libra@tf.czu.cz

ABSTRACT

Facades of roofs and building are considered as a suitable place to install small photovoltaic arrays. In historic cities, however, the installation of photovoltaic panels must not compromise the concept of architecture. We have designed a number of photovoltaic systems with photovoltaic panels installed on fixed and movable stands and inclined to the south. Prague, however, is a historic city, and in its center such an arrangement of the power plant was not possible. This article presents two photovoltaic arrays with a very similar design, which are located in Prague. Due to location in the city's historical center. Flexible photovoltaic strips based on amorphous silicon thin films were used. The strips are arranged horizontally over the roof and are not normally seen from street. The article describes the design of both photovoltaic arrays and presents the results of the 7-year monitoring of data by the monitoring system developed by the authors.

Keywords: Photovoltaics, Solar System, Photovoltaic Panel, Energy.

INTRODUCTION

Recently investigation of the energy efficient building is more and more important especially because of the increasing availability of the renewable energy sources. A review about the photovoltaic self-consumption in buildings and household power consumption was written for example in (Luthander et al., 2015; Munkhammar et al., 2015), data about building energy consumption and renewable energy consumption were presented in (Mathew et al., 2015; Depoorter et al., 2015). The especially flat roofs of the large buildings were deemed by the authors of this article suitable for such utilisation. We have also summarized more detailed theoretical and practical experiences in the photovoltaics, for example in the work mentioned below (Poulek and Libra, 2010).

There was a photovoltaic's boom in the Czech Republic due to subsidiary policy and a number of larger or smaller solar PV arrays have been built. This boom culminated in the year 2010 and then a strict change of legislation has been adopted. Approximately 2000 MW_p (in total) of PV arrays and PV systems were installed in the Czech Republic before the year 2011 and this value was increased only to 2100 MW_p till the present time.

The photovoltaic (PV) array on the National Theatre roof in central part of Prague was designed and installed during the years 2008 and 2009. The PV array on the roof of the



football stadium “Slavia Praha” in the district Prague-Vršovice was installed in the year 2010. With respect to its location in Prague historical area and national heritage protection it was inapt to use a classical construction with southward inclined PV panels based on crystalline silicon. It was very imperative to decide for a construction that would fully rest on the roof with its entire surface and would thus not interfere with the roof’s contour in this precious locality. The flexible photovoltaic foils based on thin semiconductor layers have been therefore used that in maximum measure conform to the modern outlook of the buildings mentioned above.

The similar PV arrays were installed like building integrated (BIPV) or field installation. They were constructed like on-grid or off-grid. The reference (Dursun and Zden, 2014) shows for example the off-grid PV array used for irrigation. The construction of flexible PV foils on other bases is dealt with in detail elsewhere (Larsen-Olsen et al., 2012). The other various types of electrical interconnection for photovoltaic arrays are discussed in the reference (La Manna et al., 2014). Another building integrated PV (BIPV) systems are investigated also in (Mandalaki et al., 2014; Shan et al., 2014).

MATERIALS AND METHODS

The PV array on the Prague National Theatre - New Scene Building roof (see Fig. 1) was designed so that it comprises two identical parts on the southern and northern halves of the roof. The only difference is given by the fact that the southern part was inclined by about 3° southward and the northern part by about 3° northward. Flexible PV foils of the nominal output power 0.406 kW_p have been used. PV cells based on thin semiconductor layers are encapsulated in the plastic material, they are mutually interconnected and they are directly integrated into the common roof PVC foils. Waterproof connectors are located on their back side. In both parts of this PV array, four PV foils were connected in series, eight of these series were connected in parallel and via a three-phase inverter Fronius IG 150 Plus, the generated electric power was supplied to the main power network. Fig. 2 shows the wiring diagram as an example. On the National Theatre New Scene’s roof are altogether 64 foils with an overall rated output of 26 kW_p (in two independent branches per 13 kW_p). A certain difference in the generated electric power can be expected, because one branch is slightly inclined southward and the other northward.



Figure 1. PV array on the Prague National Theatre - New Scene Building roof.

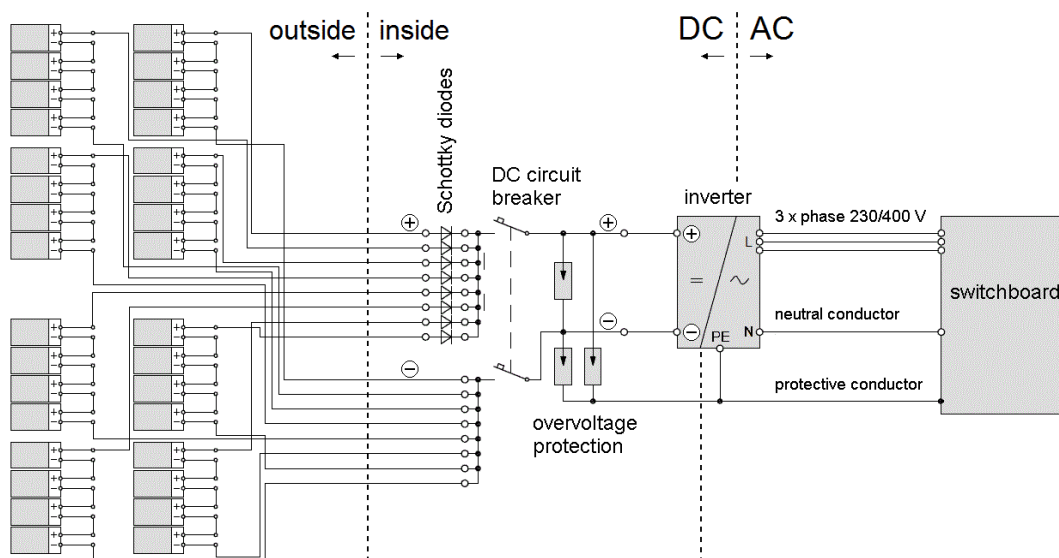


Figure 2. Wiring diagram of the PV array on the National Theatre - New Scene Building roof.

The PV array on the roof of the football stadium was constructed using flexible water-resistant PV foils VAEPLAN V Solar 432 with nominal output power 432 W_p. 1040 foils in total (in nearly horizontal position) are connected into eight independent sections and these sections are connected into eight merge switchboards. 26 strings are connected into each switchboard and each string consists of 5 PV foils. Switchboards are equipped with fuse disconnecters and with DC disconnecters ABB OT160E4 with protection against overvoltage. The DC power is then led out to the inputs of electronic inverters. The nominal

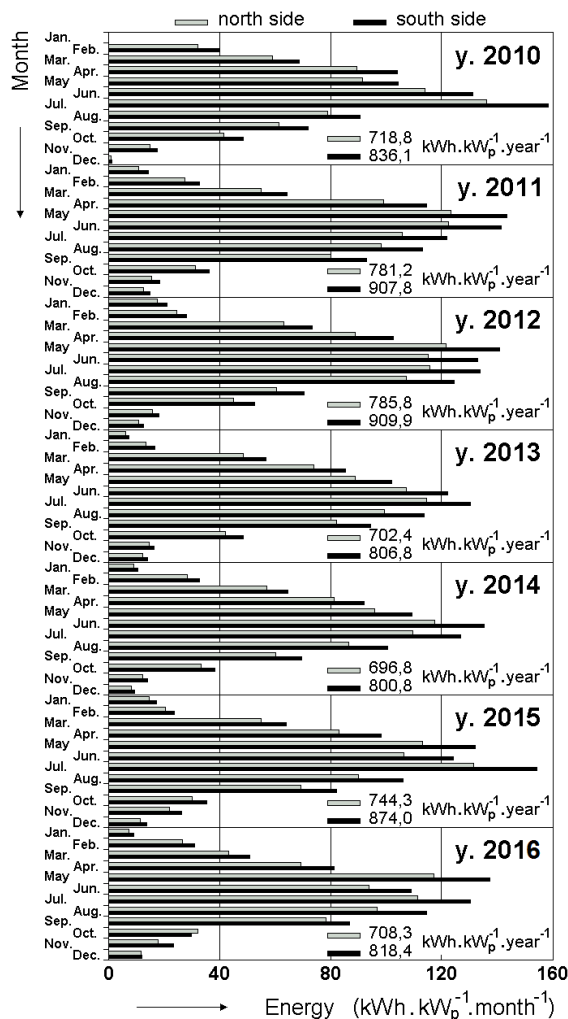


Figure 4. Electric energy produced in the PV array on the National Theatre - New Scene Building roof during the years 2010-2016.

power of the PV array is therefore 449 kW_p in total. Fig. 3 shows a more detailed view of the PV foils and surrounding architecture.

Two inverters produced by Power-One Aurora (type PVI-CENTRAL-220.0-CZ) with a three-phase AC output are used to connect the PV array to the three phase AC power grid. Each inverter consists of four sections and each section has maximum power of 55 kW. Each section has output to the central busbar. The power is then carried out to the transformer. The eight sections are thus connected to the two inverters and the maximum power on the side of AC power grid is 440 kW_p.



Figure 3. PV array on the football stadium roof.

RESULTS AND DISCUSSION

The results of seven-years (respective six-years) monitoring of the electric energy production by the PV arrays described above are presented in the following diagrams. Fig. 4 shows results from the PV system on the Prague National Theatre - New Scene Building roof, Fig. 5 shows results from the PV array installed on the football stadium roof. The values are recalculated per 1 kW_p of installed peak output power to make the results comparable. It is evident that the year-round values correspond with the values expectable in Prague (50° north

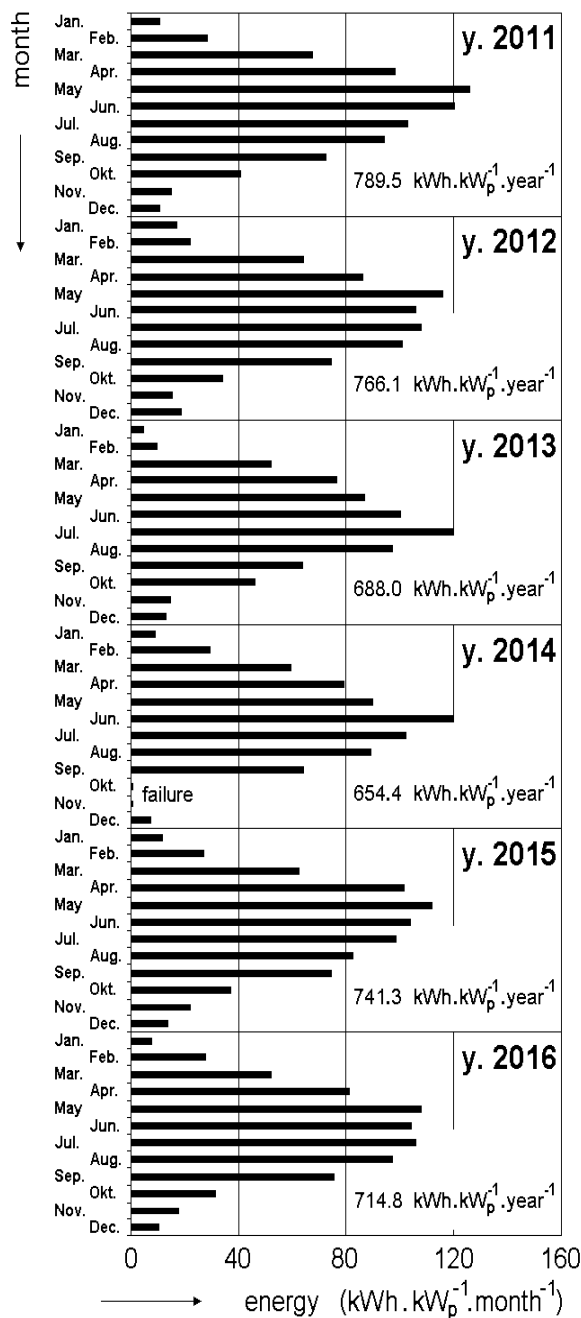


Figure 5. Electric energy produced in the PV array on the football stadium roof during the years 2011-2016.

latitude, 15° east) according to the internationally used programme for forecast of the produced electric energy amount “Photovoltaic Geographical Information System”

(<http://re.jrc.ec.europa.eu/pvgis/apps4/pvest.php#>). In winter months, the amount of produced electric power is affected by the snow deposits on the roofs. Provided that snow would be regularly removed the amount of produced electric energy would be somewhat higher, but this could not be proved. This is evident from the zero amount of produced electric energy in January 2010 and from the minimum amount in December 2010. During last years, there was nearly no snow in Prague.

We can also see from the Fig. 4 that on the New Scene Building there is always the amount of produced electric energy higher in parts inclined southward in comparison with parts inclined northward. We compared the theoretic calculation with the experimental data and the results were presented in (Libra et al., 2016). There was a good correspondence between the theory and experiment.

We also monitored the temperature of the photovoltaic foils because the efficiency of the photovoltaic energy conversion decreases with the increasing temperature (Libra et al., 2017). The manufacturer determines the 0,21 %/°C power decrease in the case of the used photovoltaic foils. Photovoltaic foils are glued directly on the water-resistant surface of the roof which makes the cooling from the bottom side limited. Therefore, the temperature reached up to 60 °C during the hottest summer days. Fig. 6 describes dependence of the temperature of the photovoltaic foils relative to time during selected March days at the

turn of winter to spring of the year 2015 (PV array on the roof of the football stadium).



Dependence of the air temperature relative to time is presented as well in the figure. We can clearly see the alternation of morning minimum temperatures and afternoon maximum temperatures. The differences between temperatures is much higher during sunny days. At night, the temperature of PV foils is usually lower than the air temperature due to heat radiation. On the contrary, the temperature of PV foils is higher than the air temperature during the day as a result of absorption of solar radiation. Fig. 7 shows an example of the time serie of the instantaneous power during a selected sunny day (PV array on the roof of the football stadium) and the value of the electric energy produced during this day.

CONCLUSIONS

We consider the reconstruction above mentioned roofs with the incorporated PV array a suitable solution. Regardless of the fact that the PV arrays described above can cover only a small part of the power consumption, the roofs are purposefully used. The PV array construction on the basis of flexible PV foils was the only acceptable alternative with respect to the Prague historical centre conservation requirements. The arrays are not visible and the view on the Neo-Renaissance building of the National Theatre is not distracted as well as the view on the New Scene Building (see fig 8).

The energy production within the 6÷7 years period is better than expected. The energy production degradation is ranging from 3÷4%. It is low value for a-Si thin film panels laminated in polymer foils. The typical degradation value is about 5% (Radue & Dyk, 2010). Additionally, the panels are installed with very low tilt angle 3 degrees only. The polluted air in the center of big city is contributing to substantial soiling of the panels. So the soiling loss alone can contribute to 2-3% of the degradation. These results indicate that a-Si PV panels laminated in plastic film can have low degradation of the energy production even if it is installed horizontally in polluted urban environment.

We intend to continue in the collection of data and it will be certainly interesting to observe how the measured values will change in connection with the whole construction ageing. The expected lifetime is approximately 12 years in the case of PV foils based on a-Si thin films encapsulated in polymer foils.

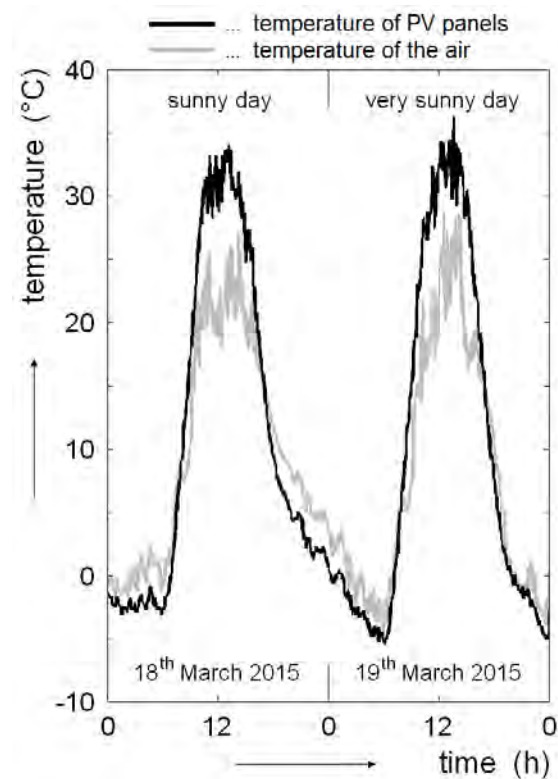


Figure 6. Time series of the photovoltaic foils temperature and air temperature during selected days (PV power plant on the roof of the football stadium).

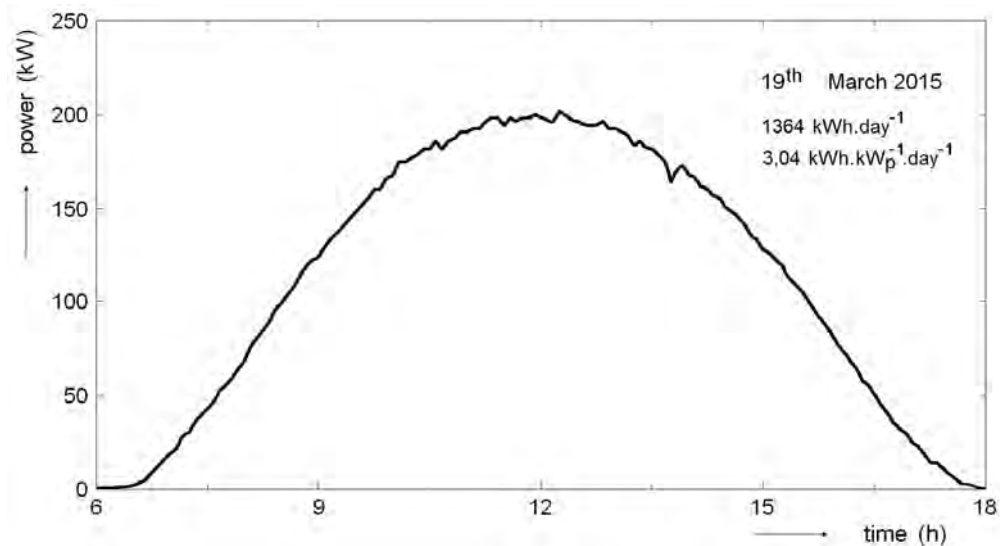


Figure 7. Time serie of the instantaneous power during a selected very sunny day (PV array on the roof of the football stadium).



Figure 8. PV arrays on the roofs are not seen from the street, the view is not distracted.

REFERENCES

- Depoorter, V., Oró, E. & Salom, J., 2015. The location as an energy efficiency and renewable energy supply measure for data centres in Europe. *Applied Energy*, **140**, 338–349.
- Dursun, M. & Zden, S., 2014. An efficient improved photovoltaic irrigation system with artificial neural network based modeling of soil moisture distribution - A case study in Turkey. *Computers and Electronics in Agriculture*, **102**, 120-126.
- La Manna, D., Vigni, V.L., Sanseverino, E.R., Di Dio, V. & Romano, P., 2014. Reconfigurable electrical interconnection strategy for photovoltaic arrays: A review. *Renewable and Sustainable Energy Reviews*, **33**, 412–426.
- Larsen-Olsen, T.T., Andersen, T., R., Andreasen, B., Bottiger, A.P.L., Bundgaard, E., Norrman, K., Andreasen, J.W., Jorgensen, M. & Krebs, F.C., 2012. Roll-to-roll processed polymer tandem solar cells partially processed from water. *Solar Energy Materials & Solar Cells*, **97**, 43–49.



- Libra, M., Olšan, T., Avramov, V., Poulek, V. 2016. Low degradation of a-Si solar panels of the building integrated PV power plant in Prague historical area. *Agronomy Research*, **14**, 4, p. 1386-1394,
- Libra, M., Poulek, V., Kouřim, P. 2017 Temperature changes of I - V characteristics of photovoltaic cells as a consequence of the Fermi energy level shift. *Research in Agricultural Engineering*, **63**, 1, p. 10-15.
- Luthander, R., Widén, J., Nilsson, D. & Palm, J., 2015. Photovoltaic self-consumption in buildings: A review. *Applied Energy*, **142**, 80–94.
- Mandalaki, M., Tsoutsos, T. & Papamanolis, N., 2014. Integrated PV in shading systems for Mediterranean countries: Balance between energy production and visual comfort. *Energy and Buildings*, **77**, 445–456.
- Mathew, P.A., Dunn, L.N., Sohn, M.D., Mercado, A., Custudio, C. & Walter, T., 2015. Big-data for building energy performance: Lessons from assembling a very large national database of building energy use. *Applied Energy*, **140**, 85–93.
- Munkhammar, J., Widén, J. & Rydén, J., 2015. On a probability distribution model combining household power consumption, electric vehicle home-charging and photovoltaic power production. *Applied Energy*, **142**, 135–143.
- Poulek V. & Libra M., 2010. Photovoltaics, theory and practice of solar energy utilization. ILSA, Prague, 169 pp. ISBN 978-80-904311-2-6.
- Radue, C. & Dyk, E.E., 2010. A comparison of degradation in three amorphous silicon PV module technologies. *Solar Energy Materials & Solar Cells*, **94**, 617–622.
- Shan, F., Tang, F., Cao, L. & Fang, G., 2014. Dynamic characteristics modeling of a hybrid photovoltaic–thermal solar collector with active cooling in buildings. *Energy and Buildings*, **78**, 215–221.



Investigation of Moisture Content, Particle Size and Pellet Die Geometry Effects on Sawdust Pelletizing By Means of New Type Pelletizing Test Device

Sina Haghighat¹ and R. Cengiz Akdeniz¹

¹Ege University, Department of Agricultural Machinery and Technologies Engineering,
35100, Bornova/Izmir – TURKEY
haghighatsina@yahoo.com

ABSTRACT

As the bulk density of sawdust is low, storage, transport and usage problems are encountered during applying it as fuel. So, to overcome these problems, densification process is necessary. The volumetric heating value of sawdust is increased by densification process. One of the major methods for biomass densification is pelletizing. As it is known, there are a lot of independent parameters which affect the pelletizing process. Among these parameters the material moisture content, particle size and pellet die diameter to length ratio have a great role on pelletizing process. Therefore, in this study the effects of material moisture content at three levels (8%, 15% and 20%), particle size at three levels ($\phi < 2$ mm, $\phi < 1.6$ mm and $\phi < 1$ mm) and pellet die diameter to length ratio at three levels (6, 8 and 10) are studied on mechanical durability of pellets, density of pellets and energy consumption of pelletizing process by the new type pelletizing test device. The effects of independent variables on dependent variables are evaluated by means of ANOVA Variance Analysis at the confidence level of %95. Also, in this study the mathematical models related to pelletizing process are created among the independent and dependent variables. In laboratory scale, biomass pelletizing tests are done by means of simplified pelletizing apparatus. Unfortunately these apparatus, can not completely illustrate pelletizing process. So, in this study in order to clarify pelletizing process much more effectively the new type pelletizing device which is developed by authors was used.

Keywords: Moisture Content, Particule Size, Pellet Die Geometry, Pelletizing Process, Sawdust, New Type Pelletizing Test Device.

INTRODUCTION

Biomass is the third-largest energy resource in the world, after coal and oil. Biomass provides about 1,250 million tons of oil equivalents (Mtoe) and supplies about 14% of the world's annual energy consumption (Purohit et al., 2006; Werther et al., 2000; and Zeng et al., 2007).

The most important advantages of biomass consumption are that they are renewable and sustainable, and can significantly reduce net carbon emissions when compared with fossil fuels.



Many of the developed and industrialized nations carry out research and development activities, in order to use biomass energy resource more efficiently. Because of these research and development activities, in the USA and most of Europe biomass is already a competitive resource for energy production. USA and Sweden obtain about 4% and 13% of their energy, respectively, from biomass (Hall et al., 1992).

One of the major limitations of biomass as energy source is its low density, typically ranging from 60–80 kg/m³ for agricultural straws and grasses and 200–400 kg/m³ for woody biomass like wood chips (Sokhansanj and Fenton., 2006; Mitchell et al., 2007). These low densities often make biomass material difficult to store, transport, and utilize.

In order to use biomass energy source effectively, the density of biomass must be increased. Commercially, increasing the density of biomass by about tenfold and help overcome feeding, storing, handling, and transporting problems, is done by using pellet mills (Haghighat and Akdeniz, 2014).

Pelletisation of biomass is a mass and energy densification for materials that possess low bulk densities such as sawdust, straw and other herbaceous energy crops. The process reduces transportation costs, provides better handling and feeding of the biomass and efficient storage with less dust formation (Haghighat and Akdeniz, 2014). The commercial pellet mills are shown in Figure1.



Figure 1. Typical pelletizing machine (Kocamaz Makina)

In pelletizing equipment, the incoming feed from the feeder is delivered to the conditioner for addition of steam or binders such as molasses to improve the efficiency of pelletizing process. The feed from the conditioner is discharged into the pelletizing die. Biomass pellets are formed in pelletizing chamber by compacting and forcing through die openings by rollers in a mechanical process (Haghighat and Akdeniz, 2014). In the pelletizing die, the feed material is pressed through open-ended cylindrical holes (dies) made in the periphery of a ring. One to three small rotating rolls push the feed material into the die holes from inside of the ring towards the outside of the ring. One or two adjustable knives placed outside the ring cut the pellets into desired lengths (Tumuluru et al. 2010).

The densified biomass quality directly depended on process variables of pelletizing such as: die diameter, die temperature, die geometry, pressure, binder usage, and biomass pre-heating, retention time, rolls die ring gap, feed rate (Wetzel, 1985, MacMahon, 1984, Shaw, 2008). In



order to achieve biomass pellets with best quality, low energy consumption and high capacity and determining the basic mechanism of the pelletizing process, it is necessary to evaluate all effective parameters on pelletizing process of pelletizing machine (Akdeniz and Haghighat, 2014).

Nowadays, during the experiments which are conducted in a laboratory about densification and pelletizing of biomass materials generally simplified pelletizing apparatus are used as it is shown in Figure 2 (Mani et al. 2006).



Figure 2. Simplified pelletizing test apparatus

Unfortunately, pelletizing tests which are done by simplified pelletizing apparatus take place in a static condition, the studies carried out with this method can not present and simulate the real pelletizing process and this simulation method is not sufficient for this purpose.

So, in order to obtain realistic data about pelletizing process of biomass material, it is needed to use a new type biomass pelletizing test device which is developed to overcome the problems given above.

In this study, to carry out the pelletizing test it is used the new type pelletizing test device which is designed and constructed by Akdeniz and Haghighat.

According to, Akdeniz and Haghighat, 2014, commercial pelletizing machine is consisting of; feed hopper, conditioner and feeding unit, pelletizing chamber and it's equipments (such as pelletizing cylindrical die, pelletizing rollers, pellet roller shaft and bearings, pellet die shaft and bearings and drive mechanism), pelleted material hopper and chassis (Fig 3).

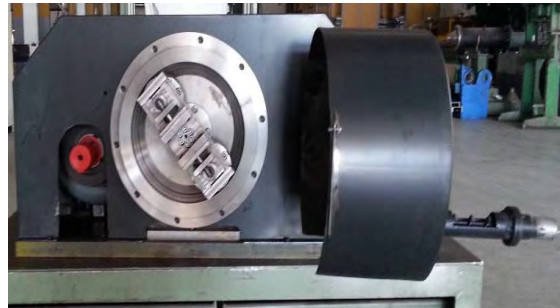


Figure 3. The new type biomass pelletizing test device

In this study, the pelletizing characteristics of sawdust material are investigated by simplified and new type pelletizing test device. The effects of material moisture content at three levels (8%, 15% and 20%), particle size at three levels ($\phi < 1.6$ mm, $\phi < 1$ mm and $\phi < 0.5$ mm) and pellet die diameter to length ratio at three levels (4, 6 and 8) are studied on enhanced pellet's mechanical durability and density. The effects of independent variables on dependent variables are evaluated by means of ANOVA Variance Analysis at the confidence level of %95. Also, the mathematical models related to pelletizing process are created. In this study, the differences between results which are obtained by simplified and new type pelletizing test device are proved by t-test method.

2. MATERIAL

Sawdust which was used in the experiments was bought from a furniture producing company and was stored in laboratory for one month before experiments. Before the realizing the pelletizing tests in this study, it is necessary to determine moisture content, particle size and bulk density of sawdust material. The moisture content of sawdust was measured at wet basis as to ASABE Standard S358.2 for forages (ASABE Standards, 2006a) by oven drying the samples at 103 ± 2 °C for 24 h (Fig.4). In this study, the moisture content of sawdust was about %8.7.



Figure 4. Sawdust samples and drying oven

Bulk density of sawdust was measured using the grain bulk density apparatus. The sample was placed on the funnel and dropped at the center of a 0.5 (L) steel cup continuously. Since the sample was fluffy and did not flow down readily through the funnel, it was stirred using a



thin rod in order to maintain a continuous flow of the material. The cup was leveled gently by a rubber-coated steel rod and weighed (Fig. 5). Mass per unit volume gave the bulk density of the biomass in kg/m^3 . In this study, the bulk density of sawdust was about 453 kg/m^3 .



Figure 5. Sawdust samples bulk density measurement device

In order to determine and adjust the particule size of the sawdust for pelletizing test in this study, the Retsch Test Sieve sets were used (Fig.6). Sieve sets was selected as (2; 1,6; 1,0 mm).



Figure 6. Sieve set

In order to determine mechanical durability of sawdust pellets, the increasing radial force is applied on a pellet pieces. The force which the pellet crushing is occurred is the pellet's mechanical durability limit. The pellet durability test device is shown in Figure 7.



Figure 7. Pellet mechanical durability test



During sawdust pelletizing tests, for determining the obtained pellets density, in the first step, the volume of the pellets after cutting both ends of the pellets in smooth pattern is determined by measurement of pellets dimensions. In the second step, the weight of the pellet is measured by weighting device. The obtained pellets density is calculated by dividing the pellet's mass to volume (Fig. 8). The accuracy of dimension and weight measurement device is respectively, 0.01mm and 0.001 gram.



Figure 8. Pellet density tests

3. METHOD

The aim of this study is to investigate the pelletizing characteristics of sawdust material by simplified and new type pelletizing test device. The effect of material moisture content at three levels (8%, 15% and 20%), particule size at three levels ($\varnothing < 1.6$ mm, $\varnothing < 1$ mm and $\varnothing < 0.5$ mm) and pellet die diameter to length ratio at three levels (4, 6 and 8) are studied on pellet's mechanical durability and density of pellets (Fig 9).



Figure 9. Pelletizing tests

The effects of independent variables on dependent variables are evaluated by means of ANOVA variance analysis at the confidence level of %95. Also, the mathematical models related to pelletizing process are developed. In this study, the differences between results which are obtained by simplified and new type pelletizing test device are proved by t-test method. T- Test method is applied in this study to prove the existence of difference between the results which are obtained by new type and simplified pelletizing test devices statistically.



The results of t- test will be verified the efficiency of new pelletizing test device compare to simplified pelletizing test apparatus. The statistical analyses and mathematical models related to results which are obtained through this study are done by means of SPSS Software.

4. RESULTS

4.1. Sawdust Pellet's Mechanical Durability

According to obtained results, mechanical durability for sawdust pellet by new type pelletizing test device, during this study is illustrated in Fig (10, 11 and 12).

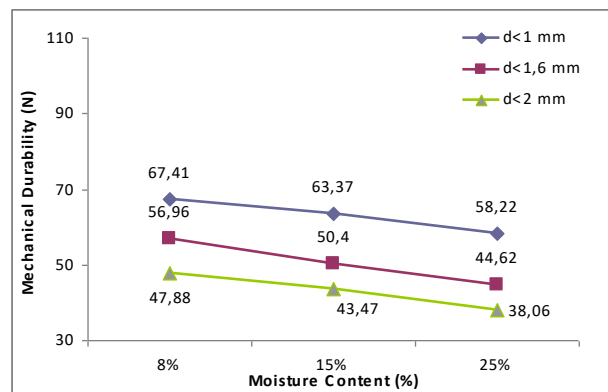


Figure 10. Mechanical durability of sawdust pellets by new type pelletizing test device at L/D= 6

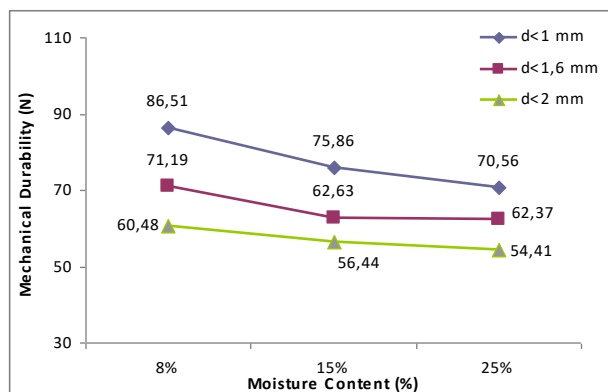


Figure 11. Mechanical durability of sawdust pellets by new type pelletizing test device at L/D= 8

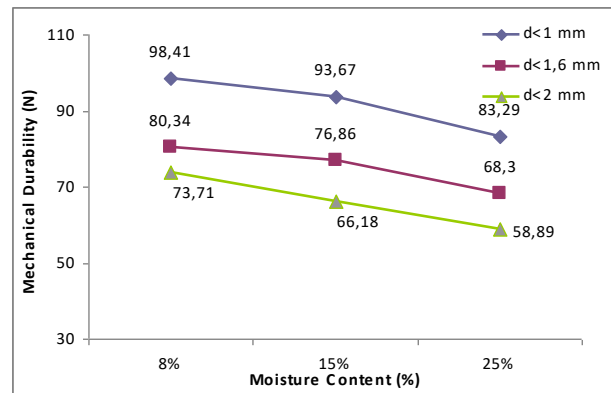


Figure 12. Mechanical durability of sawdust pellets by new type pelletizing test device at L/D= 10

The minimum and maximum values related to mechanical durability of sawdust pellets by new type pelletizing test device are obtained as 38.05 (N) and 98.41 (N) at the condition of (d<2mm, moisture content of %25, L/D=6) and (d<1mm, moisture content of %8, L/D=10) respectively.

According to ANOVA statistical analysis in this research, the effect of moisture content, particle size and pellet die (L/D) on enhanced mechanical durability of pellets were significant at %95 confidence levels.

The linear mathematical model related to pellets mechanical durability of sawdust pellets and material moisture content, particle size and pellet die diameter to length ratio (L/D) is obtained as below.

$$M.D. = 59,05 + 6,362\left(\frac{L}{D}\right) - 22,077d - 0,669Wb$$

$$R^2 = 0.977$$

As it is mentioned before, in laboratory scale generally the simplest pelletizing test apparatus are used but these device are not able to simulate the real pelletizing processes. So, in this study in order to compare the results obtained from simplest pelletizing test device by the results obtained by new type pelletizing test device, the pelletizing test was done by simplest pelletizing test device too. The results related to mechanical durability of sawdust pellets by simplified pelletizing device is shown in Fig 13, 14, 15.

The minimum and maximum values related to mechanical durability of sawdust pellets by new type pelletizing test device are obtained as 24 (N) and 93 (N) at the condition of (d<2mm, moisture content of %25, L/D=6) and (d<1mm, moisture content of %8, L/D=10) respectively.

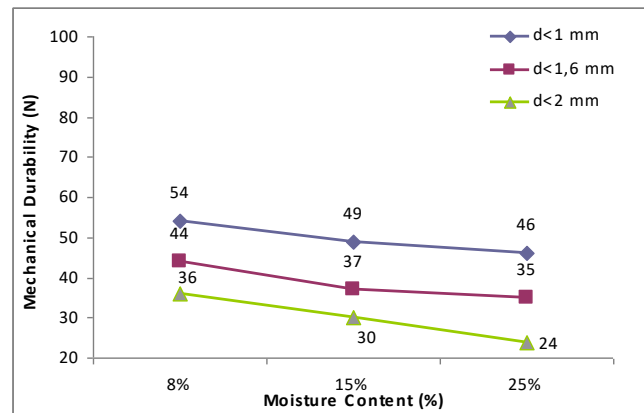


Figure 13. Mechanical durability of sawdust pellets by simplified pelletizing test device at $L/D=6$

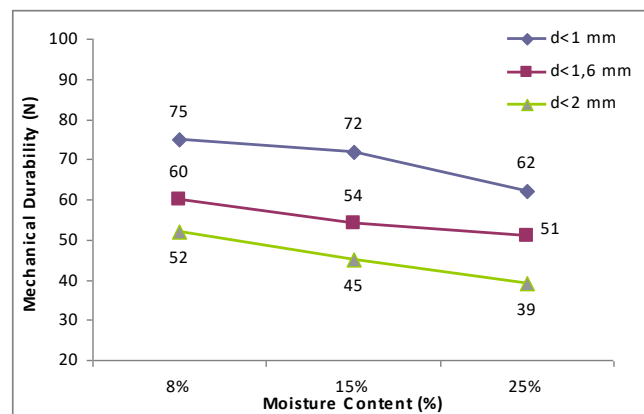


Figure 14. Mechanical durability of sawdust pellets by simplified pelletizing test device at $L/D=8$

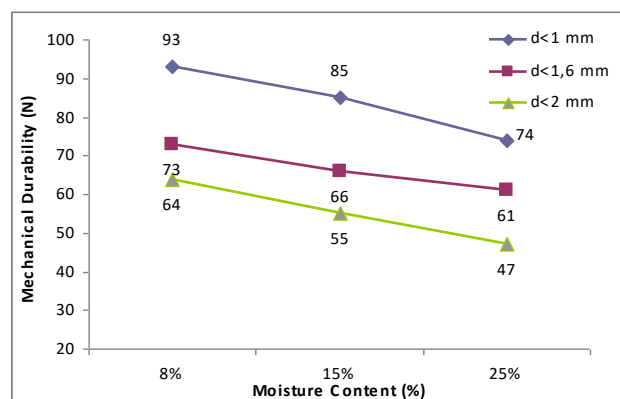


Figure 15. Mechanical durability of sawdust pellets by simplified pelletizing



test device at $L/D = 10$

In order to compare the mean difference between the results of mechanical durability of sawdust pellets by simplest and new type pelletizing tests, the t- student test is done in this study.

During the t-test analysis the data related to maximum mechanical durability of pellets are used. These values are measured at the pellets having at 8% moisture content, $d < 1\text{mm}$ particule size and $L/D=10$.

Table 1. T- Test Results for mechanical durability of pellets

	Leven's Test for Equality of Variances		t-test for Equality of Means						
	F	Sig.	t	df	Sig. (2-tailed)	Mean Difference s	Std. Error Differences	95% Confidence Interval of the Differences	
								Lower	Upper
Equal variances assumed	0,072	0,79	-13,38	58	0	-5,433	0,406	-6,25	-4,62
Equal variances not assumed			-13,38	57,34	0	-5,433	0,406	-6,25	-4,62

The t-test analysis results is shown that, there is a significant difference between the results obtained by simplest and new pelletizing test devices for sawdust mechanical durability of pellets at %95 confidence levels (Table.1).

4.2. Density of Sawdust Pellets

Results related to density of sawdust pellets during pelletizing process by new type pelletizing machine are illustrated in Fig 16, 17, 18.

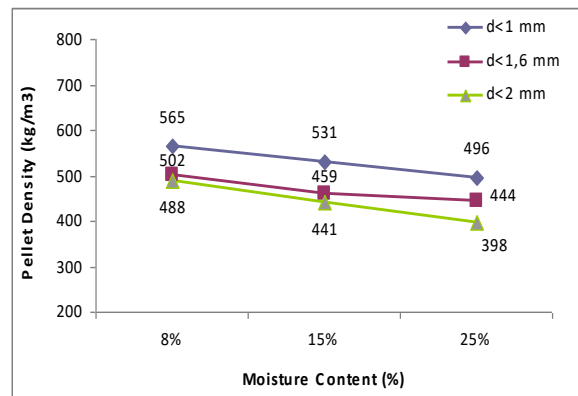


Figure 16. Density of sawdust pellets by new type pelletizing test device at $L/D = 6$

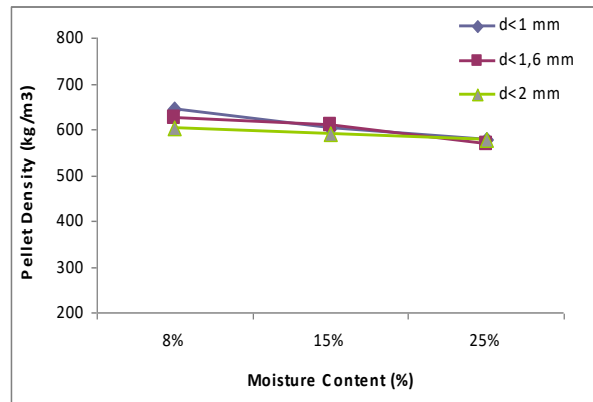


Figure 17. Density of sawdust pellets by new type pelletizing test device at L/D= 8

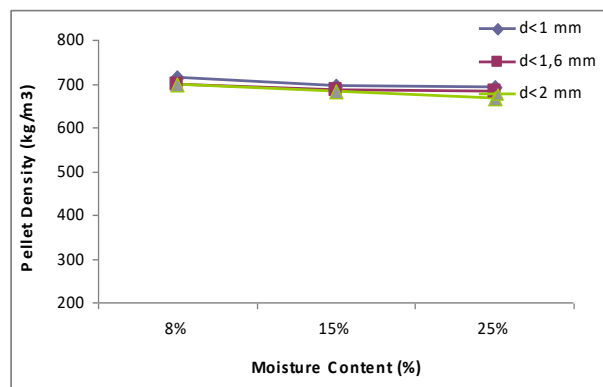


Figure 18. Density of sawdust pellets by new type pelletizing test device at L/D= 10

The minimum and maximum values related to density of sawdust pellets by new type pelletizing test device are obtained as 398 (kg/m³) and 715 (kg/m³) at the condition of (d<2mm, moisture content of %25, L/D=6) and (d<1mm, moisture content of %8, L/D=10) respectively.

According to ANOVA statistical analysis, the effect of moisture content, particle size and pellet die diameter to length ratio (L/D) on pellet capacity were significant at %95 confidence levels. The linear mathematical model related to density of sawdust pellets and material moisture content, particuletical size and pellet die diameter to length ratio (L/D) is obtained as below.

$$\rho = 287,008 + 53,093\left(\frac{L}{D}\right) - 48,752d - 2,895Wb$$

$$R^2 = 0.96$$

The results related, to density of sawdust pellets by simplified pelletizing test device is shown in Fig 19, 20 and 21. The minimum and maximum values related to sawdust pellets density



by new type pelletizing test device are obtained as 243 (kg/m³) and 665 (kg/m³) at the condition of ($d < 2$ mm, moisture content of %25, $L/D=6$) and ($d < 1$ mm, moisture content of %8, $L/D=10$) respectively.

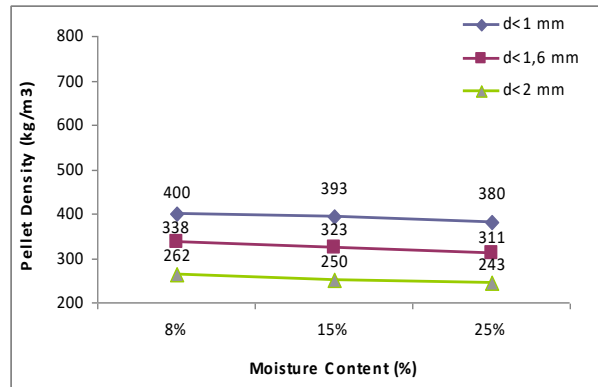


Figure 19. Density of sawdust pellets by simplified pelletizing test device at $L/D=6$

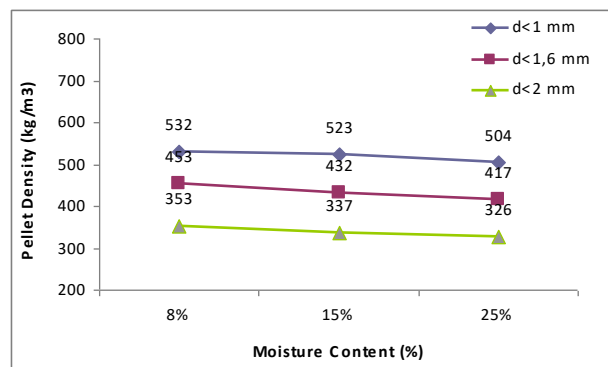


Figure 20. Density of sawdust pellets by simplified pelletizing test device at $L/D=8$

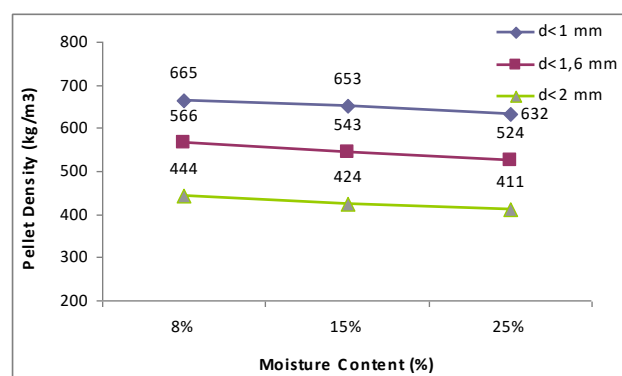


Figure 21. Density of sawdust pellets by simplified pelletizing test device at $L/D=10$



During the t-test analysis for determining the difference between simplified and new type pelletizing test device, data having the maximum density of pellets values for sawdust pelletizing are used. The maximum density of pellets data is determined with the pellets at 8% moisture content, $d < 1\text{mm}$ particle size and $L/D=10$.

Table 2 T- Test Results for density of Pellet's

	Leven's Test for Equality of Variances		t-test for Equality of Means						
	F	Sig.	t	df	Sig. (2-tailed)	Mean Differences	Std. Error Differences	95% Confidence Interval of the Differences	
								Lower	Upper
Equal variances assumed	2,132	0,15	-247,189	58	0	-155,833	0,63	-157,095	154,571
Equal variances not assumed			-247,189	58,341	0	-155,833	0,63	-157,095	154,571

The t-test analysis results is shown that, there is a significant difference between the results obtained by simplified and new pelletizing test devices for density of sawdust pellets at %95 confidence levels.

4.3. Energy Consumption for Sawdust Pelletizing

Results related to energy consumption data related to sawdust pelletizing process by new type pelletizing test device are illustrated in Fig 22, 23 and 24.

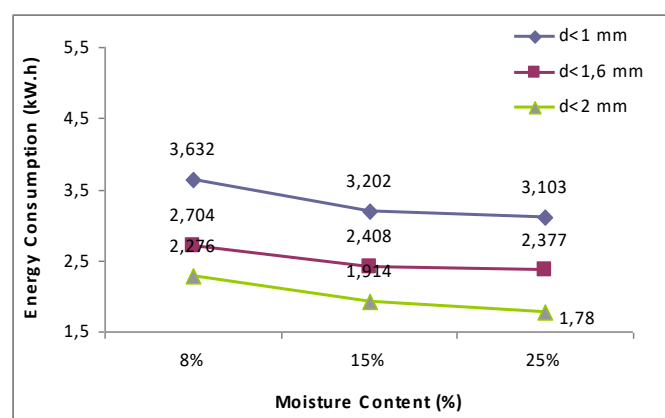


Figure 22. Energy consumption for sawdust pelletizing process by new type pelletizing test device at $L/D=6$

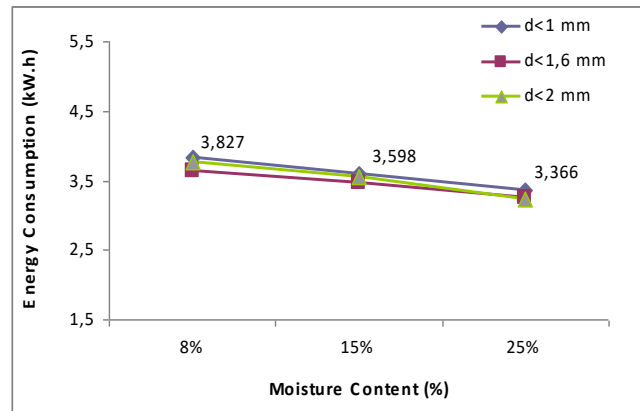


Figure 23. Energy consumption for sawdust pelletizing process by new type pelletizing test device at L/D= 8

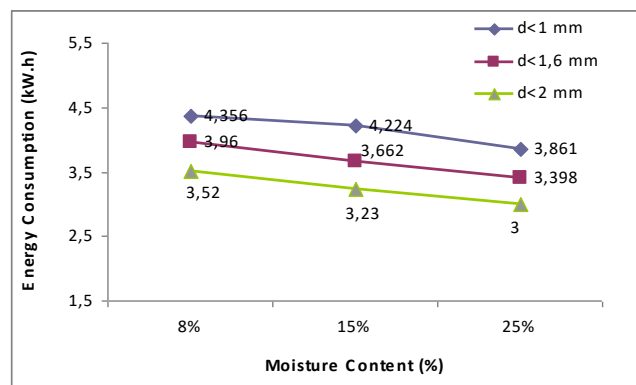


Figure 24. Energy consumption for sawdust pelletizing process by new type pelletizing test device at L/D= 10

The minimum and maximum values related to energy consumption of sawdust during pelletizing process are obtained as 1.78 (kWh) and 4.35 (kWh) with the pellets having the properties of d<2mm, moisture content of %25, L/D=6) and (d<1mm, moisture content of %8, L/D=10), respectively.

According to ANOVA statistical analysis in this research, the effect of moisture content, particle size and pellet die (L/D) on pellet capacity were significant at %95 confidence levels.

The linear mathematical model related to energy consumption of sawdust pellets and material moisture content, particle size and pellet die (L/D) is obtained as below.

$$E = 2,808 + 0.27\left(\frac{L}{D}\right) - 0.855d - 0.28Wb$$

$$R^2 = 0.885$$



5. DISCUSSION

In this study, according to the results of ANOVA Analysis the effect of sawdust particle size, sawdust moisture content and pellet die (L/D) ratio were significant on pellet's mechanical durability, density and energy consumption for sawdust pelletizing process at % 95 probability levels.

By considering the results of this study, it is understood that decreasing the particle size of sawdust result, increasing the density, mechanical durability and energy consumption of enhanced pellets because of the increasing the specific surface area of sawdust particles. Hence, the internal and external force between sawdust particles and die circumference are raised. Therefore, because of the much more pelletizing force the pellets have much more mechanical durability, density and needs more energy consumption for pelletizing.

As it is obtained from this study, it is shown that increasing the moisture content of sawdust during pelletizing tests result in decreasing the density, mechanical durability and energy consumption of enhanced pellets because of the decreasing the internal and external friction ratio between sawdust particles and die circumference. Therefore, less pelletizing forces are occurred during pelletizing process. So, the pellet's durability, density and energy requirement for pelletizing process is decreased.

By increasing the (L/D) ratio of pelletizing die, due to the increasing the contact area between the sawdust particles and die too, much more pelletizing force are applied to material. Therefore by increasing the (L/D) ratio the mechanical durability, density and needs more energy consumption for pelletizing are increased.

The minimum and maximum values related to mechanical durability of sawdust pellets produced by new type pelletizing test device are obtained as 38.05 (N) and 98.41 (N) at the condition of ($d < 2\text{mm}$, moisture content of %25, $L/D=6$) and ($d < 1\text{mm}$, moisture content of %8, $L/D=10$) respectively. The minimum and maximum values related to mechanical durability of sawdust pellets produced by simplified type pelletizing test device are obtained as 24 (N) and 93 (N) at the condition of ($d < 2\text{mm}$, moisture content of %25, $L/D=6$) and ($d < 1\text{mm}$, moisture content of %8, $L/D=10$) respectively.

The minimum and maximum values related to density of sawdust pellets by new type pelletizing test device are obtained as 398 (kg/m^3) and 715 (kg/m^3) at the condition of ($d < 2\text{mm}$, moisture content of %25, $L/D=6$) and ($d < 1\text{mm}$, moisture content of %8, $L/D=10$) respectively. The minimum and maximum values related to density of sawdust pellets by new type pelletizing test device are obtained as 243 (kg/m^3) and 665 (kg/m^3) at the condition of ($d < 2\text{mm}$, moisture content of %25, $L/D=6$) and ($d < 1\text{mm}$, moisture content of %8, $L/D=10$) respectively.



The minimum and maximum values related to energy consumption of sawdust during pelletizing process are obtained as 1.78 (kWh) and 4.35 (kWh) at the condition of ($d < 2\text{mm}$, moisture content of %25, $L/D=6$) and ($d < 1\text{mm}$, moisture content of %8, $L/D=10$), respectively.

As it is determined in this study, the results related to density and mechanical durability of pellets which are obtained from simplified pelletizing test device are statistically different from the results achieves from new type pelletizing test device at %95 probability level. So, it is suggested to use new type pelletizing test device instead of simplified pelletizing test device in laboratory scale.

6. REFERENCES

ASAE S269.4 DEC1991 (R2007): Cubes, Pellets, and Crumbles - Definitions and Methods for Determining Density, Durability, and Moisture Content. American Society of Agricultural and Biological Engineers, St. Joseph, MI, USA, 2006, p. 624 - 626.

ASABE Standards, Moisture measurement - forages ASABE S358.2, ASABE Standards 2006, American Society of Agricultural and Biological Engineers, St. Joseph, MI, USA, 2006, p. 608.

ASABE Standards. (2006b). S424.1 Method of Determining and Expressing Particuletical Size of Chopped Forage Materials by Screening. ASABE, St. Joseph, MI. pp. 619–621.

Akdeniz, R.C.; Haghighat Shishvan, S. (2014). *The requirement for new biomass pelletizing test device*. First international conference “renewable energy sources- engineering, technology, innovation”. Krynica, Poland.

Haghighat Shishvan, S.; Akdeniz, R.C. (2014). *Development of a method for mechanical strength analysis of pelletizing machine*. 12th International Congress on Mechanization and Energy in Agriculture. Cappadocia - Nevsehir –TURKIYE.

Hall, D., O., F. Rosillo-Calle, and P. de Groot. 1992. Biomass energy: lessons from case studies in developing countries. *Energy Policy* 20: 62–73.

Mani, S.; Tabil, L. G.; Sokhansanj, S. (2006). *Effects of compressive force, particuletical size and moisture content on mechanical properties of biomass pellets from grasses*. Biomass and Bioenergy, 97: 1420–1426.

Mitchell, P., J. Kiel, B. Livingston, and G. Dupont-Roc. 2007. Torrefied Biomass: A Foresighting Study into the Business Case for Pellets from Torrefied Biomass as a New Solid Fuel. *All Energy*.

Purohit P., A. K. Tripathi, T. C. Kandpal, 2006. Energetics of Coal Substitution by Briquettes of Agricultural Residues. *Energy*, 31: 1321–1331.



CIGR 2018

XIX. World Congress of CIGR



Sokhansanj, S. and Fenton, J. 2006. Cost benefit of biomass supply and pre-processing enterprises in Canada. Biocap, Canada.

Tumuluru, J. S.; Wright, C. T.; Kenney, K. L.; Hess, J. R. (2010). *A technical review on biomass processing: densification, preprocessing, modeling, and optimization*. 2010 ASABE Annual International Meeting. Paper Number: 1009401.

Werther J., M. Saenger, E. U. Hartge, T. Ogada, and Z. Siagi, 2000. Combustion of Agricultural Residues. *Progress in Engineering and Combustion Science*, 26: 1–27.

Zeng X. Y., Y. T. Ma., L. R. Ma, 2007. Utilization of Straw in Biomass Energy in China. *Renewable and Sustainable Energy Revisions*, 11: 976–987.



CIGR 2018

XIX. World Congress of CIGR



Natural Ventilation's Ability to Prevent High Indoor Temperatures

Rikke Koch Hansen^{1*}, Bjarne Bjerg¹

¹University of Copenhagen, Department of Veterinary and Animal Sciences, Groennegaardsvej 2, DK1870 Frederiksberg C,
rkh@sund.ku.dk

ABSTRACT

A desire to reduce energy consumption associated with mechanical ventilation in conventional pig housing has led to the development of a new hybrid ventilated building design. Here large adjustable openings for natural ventilation are combined with a mechanical ventilation system for under floor removal and subsequent cleaning of a limited amount of air. To ensure competitive construction costs the building was designed with large building width (>50 m) which potentially is a challenge in relation to obtain sufficient ventilation in the entire animal occupied zone. Therefore, the aim of this study was to investigate to which extend it was possible to ensure satisfactory low ambient temperature for the animals in a wide hybrid ventilated building for finisher pigs when Danish summer conditions were considered.

Measurements were conducted in one 22 m long and 51 m wide section of the first hybrid ventilated building for finisher pigs, designed by the Danish company Agrifarm. Measured temperatures in six different pens were compared with outdoor temperature, room air temperature, and with estimated values for achievable pen temperatures by maximised utilization of the openings. The applied threshold for exceeding pen temperature was 24°C.

The data covered a warm summer period with small finisher pigs (336 hours), and a relative chilly summer period with large finisher pigs (850 hours). The average pen temperature was above 24°C in 60% of the time for the two periods together and for that percentage of time, the average pen temperature was 26.5°C and 26.7°C, which was 3.2°C and 5.4°C higher than the outdoor temperature for the two periods, respectively. In addition, there was a statistical significant difference of 2°C and 1.7°C between highest and lowest average measured pen temperature, for small and large pigs, respectively. The potential opening area for natural ventilation was fully utilised in 348 of the 535 hours where the average pen temperature was above 24°C. Calculated in relation to all 535 hours with pen temperature above 24°C the maximum achievable decrease was only 0.2°C.

In conclusion, the hybrid ventilated building was unable to keep the animals' ambient temperature down at a sufficient level for more than half the time, during summer, and full utilisation of the natural ventilation had a negligible influence on reducing this temperature. To meet this challenge, it is suggested to investigate supplementary cooling methods.

Keywords: Natural Ventilation, Finisher Pigs, Thermal Comfort Zone, Exceeding Ambient Temperature, Denmark



CIGR 2018

XIX. World Congress of CIGR



Table 12. Nomenclature

Abbreviation	Definition with unit
a	Opening area of section (m^2)
A	Area of the building's surface (m^2)
h	Height of window (m)
l	Length of window (m)
Max opening area	Maximum available opening area of building (m^2)
S	Specific heat of air ($Jm^{-3}C^{-1}$)
T	Temperature ($^{\circ}C$)
ΔT	Temperature difference between outdoor and indoor ($^{\circ}C$)
U	Building's average U-value ($Wm^{-2}C$)
v	Velocity in the openings (m/s)
Q	Ventilation airflow (m^3/s)
Φ_h	Heat supply from heaters (W)
Φ_s	Animals' sensible heat production (W)
θ	Angle of the maximum opening for a given window ($^{\circ}$)
<i>Subscripts</i>	
Modified	At maximised opening area (calculated)
Old	At actual opening area (measured)
Out	Outdoor
Pen	At pen level
Window	At given window

INTRODUCTION

Finisher pigs housed under undesirable high temperatures risk to develop heat stress. Heat stress is known for several negative physiological effects such as reduced growth, due to reduced feed intake and compromised gastrointestinal health (Ross *et al.* 2017). According to ASAE (1986), the highest feed efficiency for finisher pigs is found at ambient temperatures between 20 and 24°C. This complies with a comparison of published research results, showing the highest feed efficiency on average was found at an ambient temperature of 22.5°C (Hansen & Bjerg 2018). To consider uncertainties in the compared studies, the upper threshold temperature was set to 24°C in this work. Even in relative chilly summer periods, it can be challenging to keep the temperature below this threshold in the animal occupied zone. The ventilation system plays an essential role in cooling the pigs by fresh air supply. Most housing facilities for pigs in Denmark are equipped with a mechanical ventilation system for this purpose. This is energy consuming and is therefore associated with monetary costs (Andonov *et al.* 2003) and larger greenhouse gas emission. Natural ventilation is known to have considerable lower energy consumption than a mechanical system (Bjerg *et al.* 2013; Chiumenti *et al.* 1989). Aiming an environment friendly livestock facility with low energy consumption, a new building concept recently arose in



CIGR 2018

XIX. World Congress of CIGR



Denmark. This system has hybrid ventilation with partly natural ventilation and partly mechanical pit ventilation. The first of these finisher pig facilities was put into production in summer 2015 and consequently, the knowledge of its ability to keep the temperature within the pigs' thermal comfort zone, during summer, is scarce. The aim of this work is to investigate hybrid ventilation's ability to keep the temperature below the upper threshold temperature in the animal occupied zone, during summer.

MATERIALS AND METHODS

2.1 Facility and Ventilation System

Measurements took place in a 22.40 m · 50.99 m sized section, consisting of two equally sized subsections with four rows of 10 pens each. All pens measured 5.20 m · 2.55 m with 1.60 m solid floor, 0.80 m drained floor (slatted floor with longer distance between the slots) and 2.70 m slatted floor and housed, in most cases, 17 pigs. The natural ventilation consisted of two openings above each other in the sidewall (h: 0.6m, l: 20.4m and h: 1.0m, l: 22.4m) one in the middle of the roof face (h:1.0m, l:22.4m) and one in ridge (h:1.0m, l:22.4m), on each side of the building. The upper sidewall, roof and ridge openings had a maximum opening angle of 90°, where the bottom sidewall opening was limited to 54°. Adjustment of the window openings was based on a room temperature set point of 19°C, but the opening area was corrected as the wind speed increased. With the applied correction, the maximum possible opening area for each of the building's openings appears from table 2, calculated based on Equation 1.

$$Max\ opening\ area_{window} = \sin(\theta) * h * l \quad (1)$$

Table 2. Maximum opening area at different wind speeds

Wind speed	Bottom sidewall	Top sidewall	Roof	Ridge	Total
m/s	m ²	m ²	m ²	m ²	m ²
0	33.0	26.9	44.8	44.8	149.5
2	33.0	26.9	44.8	38.1	142.8
4	28.9	20.2	38.1	38.1	125.2
6	24.8	21.5	40.3	38.1	124.7
8	24.8	22.2	39.2	37.0	123.1
10	24.8	23.5	39.2	35.8	123.3
12	21.5	26.9	42.6	24.6	115.5
14	19.0	22.2	37.0	13.4	91.6
16	16.5	20.2	33.6	9.0	79.2
18	16.5	13.4	22.4	6.7	59.1
20	16.5	13.4	22.4	4.5	56.8

The mechanical pit ventilation worked at a constant effect of 14.1 m³/hr/pig, which was automatically controlled based on data from integrated measurement wings.



CIGR 2018

XIX. World Congress of CIGR



In addition to the ventilation system, the building was equipped with high-pressure cooling sprinklers activated at outdoor temperatures above 23°C.

2.2. Data collection

The data collection was carried out in two periods to cover a situation with spring (mild weather) and large finisher pigs and a situation with summer (warmer weather) and small finisher pigs. Details of the data collection period are seen from table 3 and 4.

Table 3. Size and number of pigs in the two periods (Hansen 2016)

Pig size	Subsection	Period start	Period end	Weight start	Weight end	Pigs, start	Pigs, end
		Date	Date	kg	kg	No.	No.
Large pigs	1A	04-05-2016	07-06-2016	84.9	118.8	665	661
Large pigs	1B	04-05-2016	07-06-2016	77.9	111.8	659	654
Small pigs	1A	11-07-2016	24-07-2016	40.3	73.6	679	677
Small pigs	1B	11-07-2016	24-07-2016	47.4	80.8	683	681

Table 4. Outdoor conditions during the two periods (Hansen 2016)

Period	Average outdoor temperature	Minimum outdoor temperature	Maximum outdoor temperature	Average wind speed	Minimum wind speed	Maximum wind speed
	°C	°C	°C	m/s	m/s	m/s
Small pigs	20.21	11.48	31.38	1.82	<0.10	6.50
Large pigs	16.88	3.33	30.03	2.13	<0.10	9.47

Once every minute, VE10 temperature sensors (VengSystem A/S, Denmark) measured the pen temperature (height 0.7 m above floor) in pens located towards the middle in both subsection as number 2, 5 and 8 from the central aisle, and the value was logged. The room temperature was measured in the middle of each subsection (two sensors at each location), 1.5 m above floor (PT100 temperature sensors, Bitlink Interface Aps, Denmark). Information about wind speed, wind direction, outdoor temperature and rain was gathered by a weather station, placed on top of a neighbouring building. For detailed information about the building and management of the pigs, see Hansen (2016).



2.3. Data treatment

Aiming to investigate situations with too high pen temperatures, the applied dataset was restricted to hours with an average pen temperature above 24°C. SAS 9.4 and Microsoft Excel was used for data treatment. Data from the period with small and large finisher pigs, respectively, were treated individually.

First step was to identify hours with a potential for increased ventilation. This was done by restricting the dataset for hours where the opening area had been above 95 % of the possible (defined in table 2). Next step was to identify the hours where the pen temperature could have been lowered to 24 °C or below by maximised opening area. A modified average pen temperature was then calculated, as the achievable pen temperature. The modified pen temperature, $T_{pen\ modified}$, was calculated both for a situation with limitation of the maximum opening area, due to increased wind speed (table 2), and a situation without these limitations, meaning that a maximum opening area of 149.5 m² could be reached independent of wind speed. Equation 2 was used for the calculation, under the assumption of Equation 3:

$$T_{pen\ modified} = T_{out} + \Delta T_{modified} \quad (2)$$

$$\Delta T_{modified} = \Delta T_{old} * \frac{1}{k} \quad (3)$$

The value of k depended on the expected primary driving force of the natural ventilation. If the natural ventilation was wind driven, which was assumed at wind speeds above 1 m/s, k was calculated from Equation 4. This calculation assumed that the air exchange roughly could be assumed proportional to the buildings opening area.

$$k = \frac{Max.opening\ area}{Actual\ opening\ area} \quad (4)$$

The background for the assumption of proportionality was a rewrite of the building's heat balance, given by Equation 5.

$$\Phi_s + \Phi_h = Q * S * \Delta T_{old} + U * A * \Delta T_{old} \quad (5)$$

During summer, the only heat production in the building was the animals' sensible heat production, as heaters were turned off. Further, a large opening area was expected and the primary heat loss was expected through ventilation openings. In comparison, only a negligible amount of heat was lost as transmission heat loss and consequently this term was removed from the equation. The equation was then reduced to:

$$\Phi_s = Q * S * \Delta T_{old} \quad (6)$$

From Equation 6 it is seen that if the heat production was kept fixed and the air exchange would increase with a factor k then the temperature difference was reduced with a factor 1/k.

If the air exchange was driven by thermal buoyancy, which was expected at wind speeds below 1 m/s, then k was calculated from Equation 7.

$$k = \left(\frac{Max.opening\ area}{Actual\ opening\ area} \right)^{\frac{2}{3}} \quad (7)$$



CIGR 2018

XIX. World Congress of CIGR



Equation 7 is based on the assumption that the velocity in the openings, v , is proportional with the square root of ΔT_{old} , written in Equation 8.

$$v = k_1 * \sqrt{\Delta T_{old}} \quad (8)$$

Where the assumptions that ΔT_{old} is inversely proportional with L (Equation 9) and that v is equal to L divided by the opening area, a (Equation 10), are inserted, resulting in Equation 11. k_1 and k_2 being constants.

$$\Delta T_{old} = k_2 * \frac{1}{L} \quad (9)$$

$$v = \frac{L}{a} \quad (10)$$

$$L = a^{\frac{2}{3}} * (k_1 * \sqrt{k_2})^{\frac{2}{3}} \quad (11)$$

Finally, boxplots were generated to compare room temperature with measured and modified pen temperatures. The boxplots showed the mean values, the 95 % confidence intervals, and the minimum and maximum values.

A CFD simulation of airflow in and around a corresponding pig section was used as aid to explain how the airflow could cause the observed temperature difference between pens. The conditions used for the simulation were that the wind direction was perpendicular to the building with a wind speed of 1 m/s. The opening areas in the used CFD model were a bit smaller than during the conducted measurement, and the design of the ridge openings were not completely comparable, whereas the remaining dimensions were. The CFD simulation was performed as describe in Bjerg *et al.* (2013), except that ventilations flaps were treated as interior and the outdoor temperature was set to 20 °C.

RESULTS

In the period with small finishers, the average pen temperature exceeded 24°C in 125 out of 336 hours. In 15 out of the 125 hours with exceeding pen temperature, it would have been possible to increase the building's opening area. These observations had an average pen temperature of 26.8°C. In the period with large finisher pigs, the average pen temperature exceeded 24°C in 410 out of 850 hours. In 172 of these hours, there was a potential to increase the opening area. The average pen temperature for the 172 hours was 26.6°C.

The CFD simulation result shown in figure 1 illustrates how the openings in the windward side of the building worked as inlets, and the openings in the leeward side of the ridge and the roof worked as outlets. Consequently, the lowest temperatures were found in the windward side, close to the central aisle. According to the simulation, only a few pens could provide a temperature below 24°C when the outdoor temperature was 20°C.



CIGR 2018

XIX. World Congress of CIGR

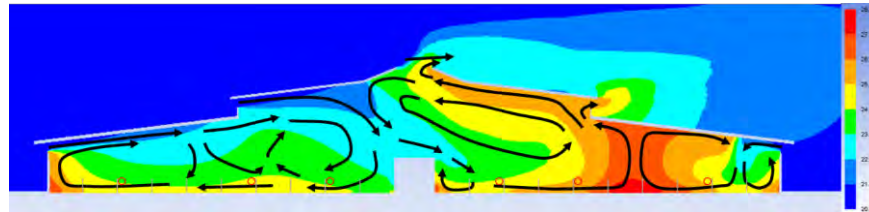


Figure 1. CFD simulation of airflow inside the building at 20 °C outdoor temperature and a wind speed of 1 m/s. The grey lines illustrates the pen partitions and the red circles the measurement points (pen 1-6 from windward side)

The temperature in pens across the unit was varying and for hours with an average pen temperature above 24°C. Some pens provided an average temperature of approximately 25.5°C whereas other provided an average temperature of approximately 27.5°C, as illustrated in figure 2. Increasing the opening area to the maximum available, either with (w.l.) or without (wo.l.) limitations due to corresponding wind speed, did not affect the average pen temperature in the period with small finishers. With large finishers the average pen temperature showed a significant, but small reduction when the opening area was fully maximized without limitations to wind speed. With limitations, there was not seen a temperature reduction by increased opening area.

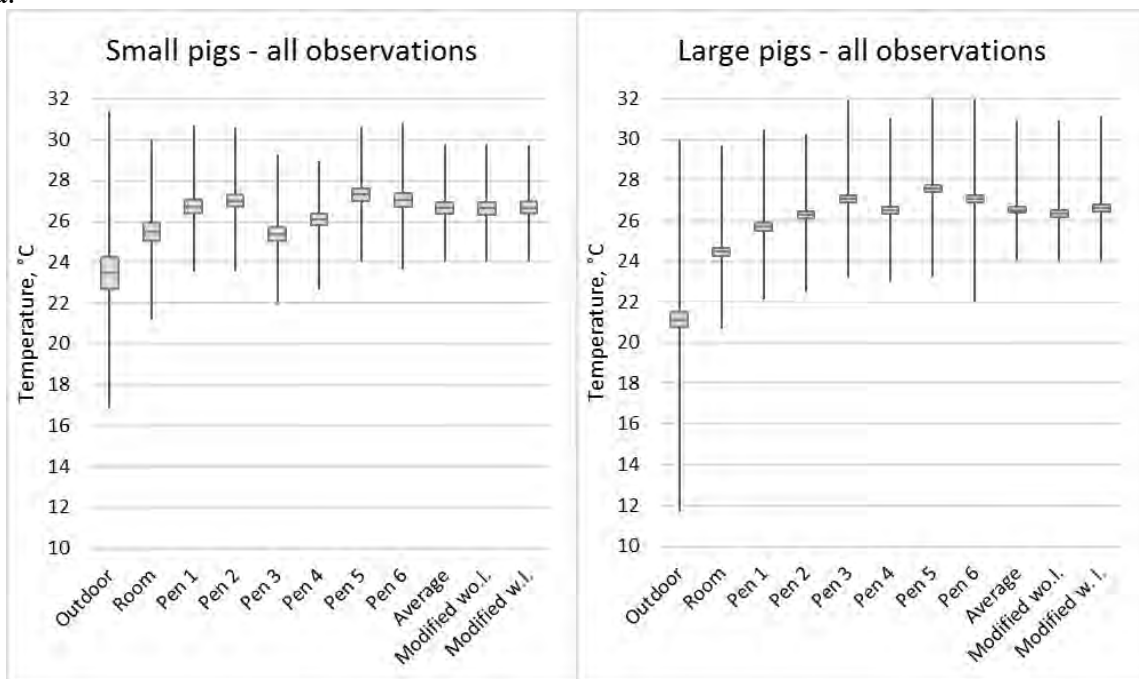


Figure 2. Boxplot showing mean value, 95% confidence intervals, and minimum and maximum values of measured outdoor, room and pen temperatures and modified pen temperature when small (left hand graph) and large (right hand graph) finisher pigs were housed



CIGR 2018

XIX. World Congress of CIGR



DISCUSSION

Investigation of the temperature level in the animal occupied zone showed several hours with temperatures above 24 °C, in both periods. It was suggested that maximised utilisation of the openings of the natural ventilation system could prevent these exceeding temperatures to some degree. Calculation of the modified temperatures showed differently. When small pigs were housed under summer conditions, results showed no effect of increased opening area, in the hours where increased opening area would have been possible. This is explainable, as it only would have been possible to increase the opening area for a small amount of the hours with exceeding pen temperatures (15 out of 125 hours). At the same time, the outdoor temperature was higher in this period, compared to the period with large finishers, which further reduces the ability to cool by ventilation with outdoor air.

With large pigs, the opportunity to reduce the temperature by increased opening area was expected higher. This was because exceeding temperatures mainly originated from a larger heat production inside the unit, due to larger animals and lower outdoor temperatures. This expectation was supported by data showing a large number of hours with exceeding temperatures and a possibility to increase the opening area (172 out of 410 hours). Despite expectations, results showed no effect of increasing the opening area, when the maximum available area was limited to wind speed. Without these limitations, a small improvement in the pen temperature could be achieved, by increased natural ventilation. For the period with large finishers, the average pen temperature was 26.6°C for the hours with potential for increased opening and with a corresponding outdoor temperature of 21°C. The small influence of maximised opening area indicates that the total opening area was not big enough to provide sufficient air exchange in situations with large animals and moderate-warm weather. In investigated situations, results showed that the hybrid ventilation with a pit ventilation of 14.1 m³/pig/hour and a natural ventilation system with 149.5 m² available opening area per section (1360 pen places) was not able to keep the temperature below 24°C for a considerable part of the time. However, this work only considered temperature. It is known that both humidity and velocity would affect the pigs' experience of the ambient temperature. Increasing velocity induces a chill effect and consequently, the experienced temperature will be lower than the measured (Bjerg *et al.* 2017). If the velocity induced by the natural ventilation had been included in the measurements, it would have been possible to give a more reliable picture of whether the temperatures above 24°C were critical for the pigs' wellbeing.

CONCLUSION AND PERSPECTIVES

Results showed a considerable number of hours where pen temperatures exceeded the threshold of where the production performance was expected to begin deteriorate. This also applied for hours, where the ventilation openings were not fully utilised, which often occurred in the period when large finisher pigs were housed. However, subsequent calculations indicated a very limited potential to reduce pen temperatures in these periods by maximisation of existing openings.



CIGR 2018

XIX. World Congress of CIGR



This potential was eliminated when considering the installed algorithmic for adjustment of the opening area in relation to wind speed.

Aiming to provide lower pen temperatures during summer, the next step would be to investigate supplementary cooling methods, for instance floor cooling in the existing floor heating pipes.

REFERENCES

American Society of Agricultural and Biological Engineers (ASABE). 1986, Revised 2017. Design of Ventilation Systems for Poultry and Livestock Shelters. ASAE EP 270.5 DEC1986 (R2017)

Andonov, K., Daskalov, P. & Martev, K. 2003. A New Approach to Controlled Natural Ventilation of Livestock Buildings. Biosystems Engineering, 84(1):91-100

Bjerg, B., Hansen, P. and Pedersen, E.F. 2013. CFD Analyses of Temperature Distribution in a Hybrid Ventilated Pig Unit. Acta Hort. (ISHS) 1008:135-141

Bjerg, B., Pedersen, P., Morsing, S., Zhang, G. 2017. Modeling Skin Temperature to Assess the Effect of Air Velocity to Mitigate Heat Stress among Growing Pigs. ASABE 2017 Annual International Meeting.

Chiumenti, R., Donantoni, L. & Guercini, S. 1989. Natural versus Mechanical Ventilation: A Comparison Study between Two Fattening Piggeries Carried Out in Summer. Land and Water Use 1321-1329

Hansen, R. K. 2016. Influence of changes in outdoor conditions on air quality and thermal comfort at pen level in a hybrid ventilated finisher unit. Master thesis. University of Copenhagen.

Hansen, R. K., Bjerg, B. 2018. Optimal ambient Temperature with regard to Feed Efficiency and Daily Gain of finisher pigs. EurAgEng 2018 conference from 8 – 12 July 2018. In https://ageng2018.com/sites/default/files/ageng2018_book_of_abstracts_-_draft_version.pdf assessed September 2 2018.



CIGR 2018

XIX. World Congress of CIGR



Development of an Innovative Farm Management System with Parallel Off-line and On-line Capabilities

G. Vasileiadis¹, D. Katikaridis¹, G. Banias¹, D. Bochtis¹

¹ Centre for Research and Technology – Hellas (CERTH), Institute for Bio-economy and Agri-technology (iBO), 57001 Thessaloniki, Thessaloniki, Greece

D. Bochtis, Institute for Bio-economy and Agri-technology, Centre for Research and Technology – Hellas, 57001 Thessaloniki, Thessaloniki, Greece,
d.bochtis@certh.gr

ABSTRACT

Recent advances in farm machinery telematics, wireless broadband, cloud computing and mobile devices provide a significant opportunity to automate and streamline much of the complexity surrounding Knowledge based Agriculture. In this light, software, tools and practices must be adapted to the overwhelming flow of information. Therefore, farm management information systems (FMIS) need to be able to comply with various standards and formats of datasets and inputs as well as provide targeted output to human and non-human clients. The groundwork for such a system was laid to provide a stable and at the same time expandable system that will facilitate the receiving of information, the processing of data and finally the distribution of information to the stakeholders that will benefit from accurate and, wherever applicable, upstream information.

Besides the human stakeholders documenting information to the system, the proposed architecture involves an extended array of information sources that cover the agricultural activities in a multi spectrum set. Unmanned ground and aerial vehicles (UGV & UAV) will execute extensive and repetitive measuring work and provide an interactive real-time application platform for further integration of automatization in the agricultural industry. The data refreshment and the repeated measurements constitute a dynamic and real-time monitoring system, capable of short response times to systemic events and when possible for pre-emptive actions also. Data collected is processed by algorithms that extract information formatted for application by human or non-human actors of the system. Combining real-time data, scientific interpretation and human generated information results to an integrated Decision Support System (DSS) that is capable of outlining actions utilising multi criteria systems, thus increasing reliability besides efficiency and automatization.

Additionally, more practical aspects of the production system are integrated to provide a central reference point for the actors of the system (i.e. financial data regarding equipment and its use is pre-calculated in relation to common field work). In this light, financial data regarding equipment and its use is pre-calculated in relation to common field work.



CIGR 2018

XIX. World Congress of CIGR



This paper addresses both technical and functional structure of the developed FMIS. Furthermore, the applicability of the developed FMIS is demonstrated by use of the tools that were developed to enhance management practices.

Keywords: Farm Management System, Decision Support Systems, Off-Line Planning, On-Line Monitoring, Greece

INTRODUCTION

Recent advances in farm machinery telematics, wireless broadband, cloud computing and mobile devices provide a significant opportunity to automate and streamline much of the complexity surrounding Knowledge based Agriculture. Simultaneously, the agri-food sector is being pressured to achieve a paradox balance between higher yield demands and lower resource usage for sustainability reasons affecting economic, societal and environmental aspects of the bio-economy industry (von Wirén-Lehr, 2001). Population growth exacerbates pressure on quantity of production while hindering factors as climate change (Mueller et al., 2012), soil compaction (Hamza et al., 2005) and numerous other factors work counterproductive to the demands. The effect is intensified by the increase of calorific demands per capita as the Food and Agriculture Organization (FAO) of the United Nations (UN) indicates in its database (Figure 7), by 10.25% in a 20 years period with an annual average increase rate of 0,489% (FAOSTAT, 2018).

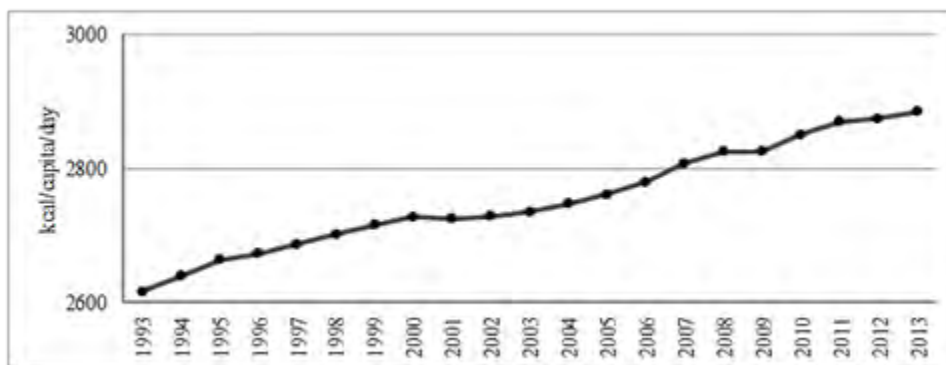


Figure 7 World food supply in 1993-2013 (FAOSTAT, 2018)

In response to this demand the agri-food sector has enhanced extensively the cultivars of numerous profitable and in-demand crops and this resulted to increasing the complexity of the already multifaceted system of bio-economy. The industrialisation of agriculture has contributed to the complexity significantly (Falguera et al., 2012). On the contrary, traditional empirical knowledge driven agriculture had little need for documentation. The model was based on knowledge transfer from one generation to the next and the contribution of each to the pool of information was limited. The latter has been reflected even until recently in surveys (Kuhlmann et al., 2001) with the farmers devaluing the latent value of data in detailed records. However, the rise of information systems software development in agriculture has recently raised awareness of



CIGR 2018

XIX. World Congress of CIGR



the data management aspect (DLG, 2018). Since technological leaps come at a cost, it can be forbidding for small sized farms to adopt them due to limited investment resources (Gilles, 2017). This hindering factor is ameliorated partly by the egalitarian effects of maturing technology and even open source proposals (Mesas-Carrascosa et al., 2015) decreasing partly the capital investment in Precision Agriculture. It is a necessary condition to have access to data generated by operational activities for the farm manager to be able to harness effectively the potential of this evolution. Transforming raw data to applicable and therefore valuable information is a post-processing step that is strongly dependent on the structure supporting data manipulation (Guastaferro et al., 2010).

2. TECHNICAL PLATFORM

Development of iBO's Farm Management Information System (FMIS) is based on a mix of functional product design and soft systems methodology to benefit from the multidimensional approach.

Within this context, soft systems methodology (SSM) was chosen for its flexibility and action research orientation. The approach facilitates the exploration of the problem from a bottom up perspective, producing even the definition of the problem within the process. It includes formal checking processes of development stages and their respective outputs. Aiming to produce a highly functional product that despite being an intangible offering has considerable influence on the tangible world, SSM caters to all these needs and at the same time is open structured to foster innovative approaches.

Functional product design guidelines were followed from the conceptualisation phase to ensure that the informational platform will serve needs identified by experts. Since the resulting product is intangible, service design aspects were also considered. Functional features also serve to increase adoptability and development speed by attracting active beta testers that will fuel the development process even further.

The information platform was built using the postGIS database communicating through a Django REST framework. Django supports Python and enables development of custom solutions and introduction of specialised tools to the needs of farm operations. Moreover, since it is a complete framework, development time is significantly lower than designing and implementing an inhouse developed architecture (Plekhanova, 2009). Front-end system development is based on a combination of ReactStrap, Bootstrap and the classic schema of HTML/CSS. Using Bootstrap eases transferring the interface to a portable device such as a smartphone or tablet.

Google Maps is a ubiquitous GIS system, used daily for navigation and not only purposes. In this light, Google Maps has been integrated into the FMIS as a favourably working factor for adoptability. Moreover, Google provides an API used to integrate their service in third-party projects. The extensive functionality covers mapping to navigating and overlaying polygon drawing inputs to custom overlays.

```

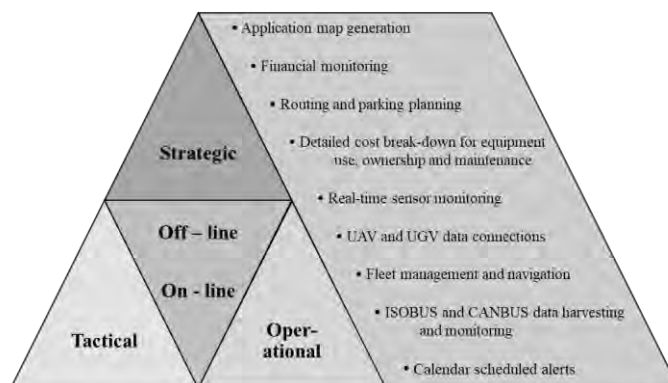
graph LR
    subgraph ClientSide [Client side]
        LoginForm[Login Form]
        InterfaceClient[Interface]
        CookiesJS[CookiesJS]
    end
    subgraph ServerSide [Server side]
        PostGIS[PostGIS PostgreSQL]
        DjangoREST[Django REST framework]
    end
    subgraph Actions
        Request[Request and save personal data and stats]
        PythonScript[A python script calculates the total costs]
    end
    subgraph InterfaceBox [Interface]
        Home[Home]
        Fields[Fields]
        Machinery[Machinery]
        RealTime[Real-time sensor monitoring]
        UAV[UAV and UGV connectivity]
        Costs[Costs]
    end
    GoogleMaps[Google Maps API Calls]

    InterfaceClient --> LoginForm
    LoginForm --> CookiesJS
    CookiesJS -- authentication --> PostGIS
    PostGIS --> DjangoREST
    DjangoREST --> PythonScript
    PythonScript --> Request
    Request <--> PythonScript
    PythonScript --> Costs
    Costs --> UAV
    UAV --> RealTime
    RealTime --> Machinery
    Machinery --> Fields
    Fields --> Home
    Home --> GoogleMaps
    GoogleMaps --> Fields

```

The architecture and technological framework of iBO's FMIS (Figure 8) is based on an open source and access tools with positive effects on security, adaptability and scalability. Furthermore, the FMIS was strategically developed on a web-based framework to ensure that it is platform independent. Accessibility requirements include personal, mobile computing devices and non-human actors such as UAVs and UGVs or Internet of Things devices, ranging from weather stations to future enhanced sensor networks and other information systems clients.

The role assignment of iBO's FMIS lead to functional specifications with a core focus to management processes. More specifically, Figure 9 illustrates the underlying framework of DSS systems at three levels of decision processes. Integrating this core construct to the system, functions aim to off-line or on-line support of the end-user. Features' supportive role in this scheme depends on the application context for the information provided.



G. Vasileiadis, D. Katikaridis, G. Baniyas, D. Bochtis “Development of an Innovative Farm Management System with Parallel Off-line and On-line Capabilities”



CIGR 2018

XIX. World Congress of CIGR



3.1. On-line Functional Specifications

On-line information retrieval and logging through the platform serves multiple purposes and needs. The value of prompt and real-time information is especially high in agricultural systems that are by definition dependent on multiple and unpredictable factors. Combining temporal and spatial data (Blackmore, 2000) is the cornerstone of precision agriculture and iBo's FMIS was developed in full alignment with this core construct of precision agriculture.

Data from installed sensor networks in test fields is not only logged and retrievable, it can also be monitored in real-time through the web interface. Further enhancing value and applicability of data, the system allows for introduction of manually defined rules along with precompiled sets combining parameters that imply conditions signalling important events. These are not restricted to negative meteorological events, e.g. frost, but can also be associated with crop specific infestations. For example, humidity and temperature within certain ranges favour mold growth in greenhouses or covered crops. Their value can be further extended by integrating multiple sources of measurements and processing them to extract important information such as optimal harvesting times.

iBo's FMIS functionality can be realised primarily with the use of advanced sensor carrying platforms, e.g. multi- and/or hyperspectral imaging executed by UAVs and UGVs. Both are used within the context of this project to collect input data. Processed multispectral images provide an array of measurements regarding plant stress, biomass or even weed pressure (Lamb, 2000).

Fleet management module is an integral part of the FMIS. A holistic approach to the management needs of agricultural systems cannot omit the management of investment-intensive equipment. Vehicles in typical use case scenarios are expected to be set-up and move from storage facilities to fields and execute work as planned. These operations related activities are monitored and assisted by using the FMIS interface. Based on Google Maps API, the platform provides information on equipment locations and dynamically adapts routes to conditions in effect during the execution. Fleet information can be enhanced and enriched by ISOBUS and CANBUS compliant equipment (Darr, 2012). Modern machinery providing communicative protocols is capable of bidirectional information flow. Interactivity is a feature exploited by real-time data collection in the platform and also allows for mid-operation corrective actions by farm managers.

Data collected and translated in structured and targeted information packages can generate secondary data and produce meta-products and reports. For example, the existence of GNSS units on equipment used is a source of geo-reference coordinates that can be assigned to any operation, measurement or entity that could benefit from it. The FMIS system is intended to efficiently manage, i.e. collect and post-process, data to aid multi-criteria decision support systems. Indicatively, yield mapping, agrochemicals applications, fertilizer applications, irrigation needs, and labour use are some of the operational data that geo-referencing data can be appended to. Finally, it should be noted that calendar entries are also generated dynamically as defined by operation related events. The dynamic calendar is a feature that can be updated with scientific knowledge and in-practice techniques constantly.



CIGR 2018

XIX. World Congress of CIGR



3.2. Off-line Functional Specifications

FMISs were traditionally intended to manage agricultural holdings from a back office and this has a negative effect on their scope of use. The goal of most products offered is to manage operations already executed and offer limited future planning options. In this context, conventional functionalities such as financial data overview and warehouse logistics are available to the users. Crops, farm supplies and equipment stored are monitored and reported to end-users requesting information. Direct ordering to equipment manufacturers for consumables or to agricultural supplies providers is considered as conventional functionality of the FMIS. The end-user creates an account by registering the desired user id and a password that serves to protect against unauthorized access to the data entered or generated. Farming data security is an important aspect that will be part of a heated discussion in the following years (DLG, 2018).

Based on the detailed data collected, the FMIS offers optimisation of routing and storing for vehicles and implements. The benefit from an optimised approach of horizontal (Crujssen et al., 2007) or interorganisational logistics is already proven in practice to be beneficially for participating organisations. The end-user accesses the familiar interface of Google Maps via the FMIS and plots routes to evaluate the operational plan in terms of travel distance and time spent in non-value adding operations.

Depreciation is a factor heavily affecting book-value of equipment, although it is often omitted from typical farm operational budgeting. However, the invested capitals need to be recovered through effective and profitable operation to be able to sustain competitive advantage. This multifaceted system can be assessed at various levels of detail ranging from basic break-even analysis to applying structured Multi Criteria Decision Methods (MCDM), e.g. Analytic Hierarchy Process. In the proposed FMIS elements that can provide input to a Cost Benefit Analysis are calculated in detail. More specific, a Python program has been created to complement the documentation provided by ASABE (ASABE, 2015) for the ownership, use and maintenance of machinery and implements. User-input is needed for some fields and wherever applicable, default values are already filled in the forms to increase user-friendliness of an innately input-intensive system.

Application maps in-service for Variable Rate fertilizer applications, known as prescription maps use a relatively scarce sampling grid (Fleming et al., 2000). The advent of lower-cost sensors and unmanned automated vehicles, combined with the development of algorithms processing these data, have changed the quality, use and resolution of these maps radically. The extent of this evolution in agricultural data is such, that besides modern equipment adopting these standards, various retro-fit solutions are available to upgrade older machinery. Consequently, the FMIS has been designed to cater to these needs and be able to produce application maps compliant with modern machinery. Primary sources of data are the readouts of CANBUS and ISOBUS data from machinery used in fields and or, measurements executed by unmanned vehicles.



CIGR 2018

XIX. World Congress of CIGR



Scheduling of field work is an essential improvement in streamlining farm management processes. Therefore, the FMIS features a scheduling module for management to be able to predict costs, generate payroll reports and be able to ensure the required labour-force before time. The calendar functions are to include also predefined work-packages covering basic field work. This feature aids in the standardisation of work, planning and consistency of practices. Therefore, it can also be used to enhance training of new personnel, since user-customisation is bound to be limited due to the default effect (Della Vigna, 2009).

Overall, off-line activities' main direction is the evaluation of data in depth and be able to incorporate information extracted from the system to strategic and tactical planning. Whereas, on-line activities primary target to support operational planning while at the same time utilise the technological capacity of multi-source data harvesting.

4. APPLICABILITY OF IBO'S FMIS

The platform's holistic approach on farm resources, both tangible and intangible, allows for insightful assessment of strategic decisions and goals as well as handling dynamic events on an operational level.

4.1 Dashboard Welcome Screen

The graphical user interface (GUI) of the welcome screen offers a synoptic view of key performance and operational data. A brief list of upcoming events is present, along with yield data when available. Environmental impact is also displayed introducing Life Cycle Assessment (LCA) elements that will eventually become part of the reporting scheme in agriculture. A positive effect of deploying an FMIS is the automatization of reporting procedures and the ability to retrieve reportable data and format them to required formal schemes.

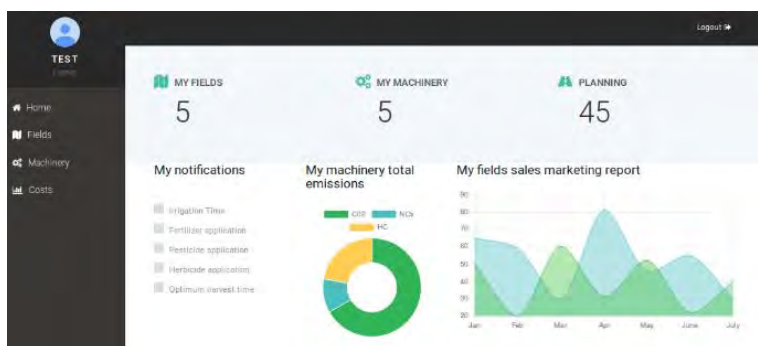


Figure 10 IBO's FMIS dashboard overview

4.2. Field Registration

The registration process of fields is designed to be intuitive. Using Google Maps' familiar interface, the end-user can point and click on the external boundaries of the field regardless of



outline complexity (Figure 11). The resulting polygon is enhanced with information regarding description and the entry is automatically saved to the users' database.



Figure 11. Field registration process

4.3 Field Management

The field management module displays information in graphical and textual comprehensive formats. Visual communication elements and selected textual data convey effectively the information needed to navigate through the list to the field of interest (Figure 12).

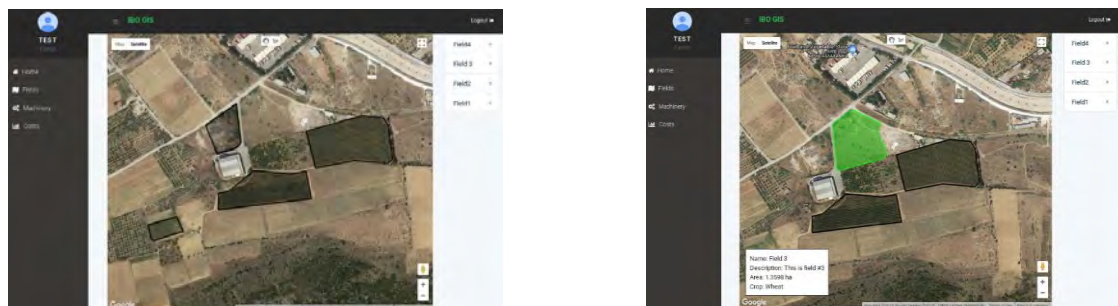


Figure 12. (a) Fields overview, (b) field extended information display

5. CONCLUSIONS

IBO's FMIS is designed to act as a framework supporting informed decisions for managers of agricultural holdings. Based on principles of precision agriculture, expected outcomes are, in general, reduction of inputs and higher resource utilisation efficiency. The application developed is compliant with these guidelines. Innovative however, is the shift of focus on off-line and on-line decision support functions.

Direct benefits also include improved cashflows, since a more detailed financial plan can be plotted. This in turn alleviates risk and uncertainty by real-time monitoring of financial outcomes and comparing expected to planned outcomes. The positive influence extends to a broad array of stakeholders. Wholesalers of agricultural production will benefit from scheduled harvesting and



CIGR 2018

XIX. World Congress of CIGR



timely deliveries, whilst producers operating within business accepted norms, upgrade their position in the value chain of the industry.

Furthermore, the reduction of inputs is expected to have a significant positive impact at the environment. Besides direct reduction of emissions and use of potentially harmful supplies, monitoring and reporting environmental performance introduces corporate responsibility elements to agricultural management practices. The end-users of FMIS will eventually embrace the new techniques and way of thinking, enabling further professional evolvement and adoption of eminent changes in technology and practices.

Higher control over production parameters can lead to harvesting multiple variations of products within the same field. Consequently, resulting to lower rates of rejected products and enabling the farmer to diversify the production, increasing financial stability. Furthermore, records of inputs and outputs constitute a database, upon which accurate budgeting and cost benefit analysis can be evaluated. Post-processing can transform data to applicable information and feed downstream self-improving algorithms, ultimately introducing artificial intelligence elements.

6. ACKNOWLEDGMENTS

The work was supported by the project "Research Synergy to address major challenges in the nexus: energy-environment-agricultural production (Food, Water, Materials)" - NEXUS, funded by the Greek Secretariat for Research and Technology (GSRT) – Pr. No. MIS 5002496.

7. REFERENCES

- ASABE (2015) 'D497.5: Agricultural Machinery Management Data', *ASABE Standards*.
- Blackmore, S. (2000) 'Developing The Principles of Precision farming', in *International Conference on Precision Agriculture*, p. 5.
- Cruijssen, F., Dullaert, W. and Fleuren, H. (2007) 'Horizontal Cooperation in Transport and Logistics: A Literature Review', *Transportation Journal*, 46(3), pp. 22–39.
- Darr, M. (2012) 'CAN Bus technology enables advanced machinery management', *Resource: Engineering and Technology for Sustainable World*, 19(5), pp. 10–11.
- DellaVigna, S. (2009) 'Psychology and Economics: Evidence from the Field', *Journal of Economic Literature*, 47(2), pp. 315–372.
- DLG (2018) *Digital Agriculture A DLG position paper*. Frankfurt am Main.
- Falguera, V., Aliguer, N. and Falguera, M. (2012) 'An integrated approach to current trends in food consumption: Moving toward functional and organic products?', *Food Control*. Elsevier,
- G. Vasileiadis, D. Katikaridis, G. Banias, D. Bochtis "Development of an Innovative Farm Management System with Parallel Off-line and On-line Capabilities"



CIGR 2018

XIX. World Congress of CIGR



26(2), pp. 274–281.

Fleming, K. L. et al. (2000) ‘Evaluating Farmer Defined Management Zone Maps for Variable Rate Fertilizer Application’, *Precision Agriculture*. Kluwer Academic Publishers, 2(2), pp. 201–215.

Gilles, D. (2017) *Smart Agriculture for All Farms*. Brussels, Belgium.

Guastaferro, F. et al. (2010) ‘A comparison of different algorithms for the delineation of management zones’, *Precision Agriculture*. Springer US, 11(6), pp. 600–620.

Hamza, M. A. and Anderson, W. K. (2005) ‘Soil compaction in cropping systems: A review of the nature, causes and possible solutions’, *Soil and Tillage Research*. Elsevier, 82(2), pp. 121–145.

Kuhlmann, F. and Brodersen, C. (2001) ‘Information technology and farm management: Developments and perspectives’, *Computers and Electronics in Agriculture*, 30(1–3), pp. 71–83.

Lamb, D. W. (2000) ‘The use of qualitative airborne multispectral imaging for managing agricultural crops - A case study in south-eastern Australia’, *Australian Journal of Experimental Agriculture*. CSIRO PUBLISHING, 40(5), pp. 725–738.

Mesas-Carrascosa, F. J. et al. (2015) ‘Open source hardware to monitor environmental parameters in precision agriculture’, *Biosystems Engineering*. Academic Press, 137, pp. 73–83.

Mueller, N. D. et al. (2012) ‘Closing yield gaps through nutrient and water management’, *Nature*. Nature Publishing Group, 490(7419), pp. 254–257.

Plekhanova, J. (2009) *Evaluating web development frameworks: Django, Ruby on Rails and CakePHP, The IBIT Report*. Philadelphia.

von Wirén-Lehr, S. (2001) ‘Sustainability in agriculture — an evaluation of principal goal-oriented concepts to close the gap between theory and practice’, *Agriculture, Ecosystems & Environment*. Elsevier, 84(2), pp. 115–129.



CIGR 2018

XIX. World Congress of CIGR



Effect of Moisture Content on Physical Properties of Pumpkin (*telfairia occedentalis*) Seeds

Akindele F. ALONGE¹, Edidiong D. UBAK and Elijah G. IKRANG

¹Department of Agricultural and Food Engineering, Faculty of Engineering,
University of Uyo, Uyo, Akwa Ibom State, Nigeria
Email address: akindelealonge@uniuyo.edu.ng

ABSTRACT

Fluted pumpkin is a creeping vegetable shrub that spread low across the ground with large lobed leaves and long twisting tendrils harvesting of fluted pumpkin takes place 120-150days, after sowing. The seed contains 13% oil and is used for cooking, manufacturing and cookie formulation. One Hundred samples of fluted pumpkin (*telfairia occedentalis*) seeds used in this study were obtained from the University of Uyo farm, Akwa Ibom State, Nigeria. The samples use manually cleaned and screened in the Food Engineering Laboratory (where the practical was carried out), to remove foreign matter dust, dirt immature and broken seeds. The screened samples were used in the determination of physical properties at four (4) different moisture levels. In this research work, the size, dimensions, volume, bulk and porosity, were evaluated for fluted Pumpkin seed as a function of moisture content in the range of 8.20 to 4.14 (d.b%). Few physical properties of the pumpkin seed was significantly affected by moisture content variation. The length, width, thickness and unit mass of Fluted pumpkin seed decreased from 3.169 to 2.756 mm, 1.137 to 0.837 mm, 3.106 to 2.760 mm and 8.15 to 4.23 g, respectively, as the moisture content decreased. While the sphericity, geometric mean diameter, bulk density and porosity decreased from 71.7 to 69.7%; 2.23 to 1.92 mm; 2.68 to 2.24 g mm⁻³; 39 to 35%, respectively. The results indicated that the modifications of moisture content of Fluted Pumpkin seeds caused a variation with linear regression in its dimensions, volume, unit mass, sphericity, for filling and emptying for the variety.

Keywords: physical, properties, pumpkin, moisture content

INTRODUCTION

Fluted pumpkin is one of the most popular vegetables in Nigeria, it is locally known by the name “ugu” in Igbo language in Nigeria. The reason for the popularity and acceptance of the vegetable is that its seed, shoot and stems are sought after items of diet and highly nutritious (Giami et al., 2005). Pumpkin (*telfairia occedentalis*) is extensively used as vegetable processed food and feed stock in different parts of the world. Although very little information is available about the production statistics of pumpkin. The average yield of fruit is reported to be 25 tons/ha (Choudhary, 2001). The pumpkin fruit contains significant amount of seed which is normally



discarded. The seed contain more than 45% oil, 30% protein and yield ranging between 450 and 1.57 tons/ha (Lazos, 2004). Pumpkin can indeed be considered to be a potential source of edible oil and protein next to groundnut (Choudhary, 2011). Figures 1 and 2 show the pumpkin fruit and seeds

Anon (2018) highlighted the benefits of fluted pumpkin in treatment of anaemia because of the high levels of protein and iron in the plant and as a result of haematinic properties of the fluted pumpkin leaves. The root of the plant possesses anti plasmodial and schizonticidal properties making it capable of treating parasitic malarial infections. The plant contains high amounts of phosphorus making it useful for keeping off onset of kidney diseases like kidney stone. He also noted that fluted pumpkin seed oil contain high amounts of anti-oxidative properties such as oleic acid, vitamin A, alkaloids, tannins and linoleic acid which makes it capable of treating infertility in males by boosting the functionality of the testicles for an increased sperm count.

He further noted that the seed has been highly recommended for nursing mothers due to its lactating properties. The large dark-red seed is rich in protein and fat which can be eaten whole, ground into a powdery form to be used for certain kind of soup or made into a fermented porridge as the case may be. The fluted pumpkin is also considered as oilseed due to its high oil content of about 30%. The shoots contain high levels of potassium and iron while the seeds are made up of 27% crude proteins and 53% fat. In Akwa Ibom State and other parts of South Eastern Nigeria, the seed is thoroughly boiled and eaten as snacks.

Since the physical properties of pumpkin seed and kernel are the pre-requisites for the design of equipment for handling, dehulling and other processes. It is essential to determine these properties (Makanjuola, 1972). Ramakrishna (1986) measured the size and the shape of the seeds of two pumpkin varieties and correlated the dimension of the seed and kernel with various physical properties of pumpkin seed including densities, velocity and surface roughness. Teotia *et.al.*, (1989) also determined different form of density of seeds, kernels and hull using three commercial varieties of pumpkin seeds. Some engineering properties of pumpkin seeds, such as hull breaking load, surface roughness, transport velocity and densities were reported. The design of storage, handling and processing systems for bulk materials such as pumpkin requires data on bulk and handling properties namely, size dimensions, sphericity, bulk and particle densities on most commonly used structural surface materials.





CIGR 2018

XIX. World Congress of CIGR



Figure 1: Fluted Pumpkin

Figure 2: Fluted Pumpkin seeds

Theories used to predict the pressures and loads on storage structures require geometrical mean, sphericity and bulk density. Also the design of hoppers for processing machinery requires data on bulk density and angle of repose. Bulk density is used in the design of drying and aeration systems because it affects the resistance to airflow of a stored bulk. Therefore the determination and consideration of these properties has an important role in the pumpkin industry. Bulk and handling properties have been studied for various crops such as pigeon pea, caper seed, fenugreek seed, green soya beans, rice and barley grains.

However, detailed measurement of all principle dimensions of pumpkin seed and kernel as well as their correlation and variations in physical properties at various levels of moisture content has not been investigated. (Teotia *et al.*, 1989). This paper presents the result on determination of various physical properties namely size, shape, densities, and coefficient of static friction against different material surface and angle of response of pumpkin seed and kernel different moisture contents

MATERIALS AND METHOD

Sample preparation

One Hundred samples of fluted pumpkin (*telfairia occedentalis*) seeds used in this study were obtained from the University of Uyo Farm, Akwa Ibom State, Nigeria. The samples were manually cleaned and screened in the Food Engineering Laboratory to remove foreign matter dust, dirt immature and broken seeds. The screened samples were then used in the determination of physical properties at four (4) different moisture levels.

The seeds were divided into batches of twenty seeds each. Oven drying method was employed with a drying time of 3hours at a drying temperature of 105⁰C and four moisture content levels. Physical properties were determined at each of the moisture levels and result presented for statistical analysis. Moisture content at which each of the physical properties were measured were 8.2%, 7.71%, 5.81% and 4.14% (d.b) with four (4) replicates at each level.

The following materials and equipment were used for the work. One Hundred samples of fluted pumpkin seeds, Electronic weight balance, Laboratory drying oven, Laboratory desiccator, graduated cylinder, Venier calliper, Tracing paper, Graph sheets.

Weight Determination

Each of the seeds were labeled and weighed on the weighing balance and the total weight determined. The average of nut weighed is shown in equation 1 (Oje et al., 1993).

Mathematically,

$$W_{avg} = (W_1 + W_2 + ..W_n) / n \quad 1$$

where w₁, w₂...w_n = weight of individual seeds

n= Total number of seeds

Moisture Content Determination

Akindele F. ALONGE, Edidiong D. UBAK and Elijah G. IKRANG “Effect of Moisture Content on Physical Properties of Pumpkin (*telfairia occedentalis*) Seeds”



CIGR 2018

XIX. World Congress of CIGR



The moisture content dry basis will be determined by using the method by Mohsenin (1986) which involved oven drying. In this method, the initial weight of each sample is obtained (W_1) and final weight (W_2) is also obtained after drying at 105^0 c. mathematically:

$$MC_{db} = [(W_1 - W_2) / W_2 * 100] \quad 2$$

Seed Size

Dimensions (major, intermediate and minor diameters): the dimensions were obtained by using venier caliper. The Arithmetic mean diameter, Geometric mean diameter (D_e) and the sphericity (ϕ) were obtained by the expression:

$$AMD = [(L + W + T) / 3] \quad 3$$

where L = major diameter of the seed

W= intermediate diameter

T= minor diameter of seed

AMD= Arithmetic mean Diameter.

This method was proposed by (Mohsenin, 1986) and had been used by Adejumo *et al.*, (2009) for okra seed and (Hsu *et. al.*, 1991) for pistachios.

The Geometrical Mean Diameter (G.M.D) was determined using the expression

$$GMD = (LWT)^{1/3} \quad 4$$

$$Sphericity(\phi) = [(LWT)^{1/3} / L] \quad 5$$

Seed Surface Area

The surface area of the seeds was measured by the following relationship given by McCabe et al. (1986).

$$S = \pi D_e^2 \quad 6$$

$S = \pi D_e^2$ where D_e is the Geometric mean diameter of the product.

π = a constant

Seed Volume

The volume of the seed was determined experimentally using the expression given by Alonge and Adigun (1999).

$$Volume(V) = (\pi D^3 / 6) = [\pi(LWT) / 6] \quad 7$$

where L = major diameter of the seed (mm)

W= intermediate diameter (mm)

T= minor diameter of seed (mm)

Seed Density

(a) The true density of the seed was computed by taking the ratio of seed weight (g) to seed volume mm^3



CIGR 2018

XIX. World Congress of CIGR



Mathematically

$$\rho_t = (\text{seed weight}) / (\text{seed volume}) \quad 8$$

(b) The bulk density (ρ_b) was evaluated by taking the weight of the seeds in bulk and dividing it with the bulk volume (Owolarafe et al; 2007).

Mathematically ρ_b

$$\text{Weight of seed } (W) / \text{Bulk Volume } (V) \quad 9$$

where W = weight of seed (g) V = Volume of seed (cm³)

Porosity (P)

The porosity was determined using the equation

$$P = [1 - (\rho_b / \rho_t) * 100] \quad 10$$

Where ρ_b = the bulk density (gmm⁻³)

ρ_t = The True density (gmm⁻³)

P = Porosity

RESULTS AND DISCUSSION

Dimensions and Unit Mass

The mean values for the length, width and thickness measured at different moisture contents in the range of 8.2% - 4.13% (d.b) for fluted pumpkin seed are given in Table 1. As the moisture content reduced, the three linear dimensions reduced due to drying. This reduction in linear dimensions was also observed for millet in which the length decreased from 4.163 mm -3.522, width 3.211 mm to 2.735 mm and thickness reduced from 2.788 mm to 2.18 mm for a moisture content reduction from 22.5% to 5% d.b (Baryeh, 2002). This could also be reversed in terms of swelling of the seed and the moisture content and other dimensions will certainly increase.

Table 1: The Axial dimension of Fluted Pumpkin Seed at different moisture contents

Properties of flute pumpkin	Moisture content levels			
	First level Fourth level	Second level	Third level	
Moisture content (db)	8.20 (2.95)	7.710 (0.96)	5.82(2.15)	4.13(0.44)
Major dia. (L) mm	3.169 (0.369)	2.940(0.333)	2.895(0.3194)	2.756(0.2967)
Minor dia. (T) mm	3.106 (0.558)	2.971(0.381)	2.966 (0.603)	2.760(0.309)
Intermediate dia. (W) mm	1.137 (0.607)	0.837(0.244)	1.042 (0.388)	0.934(0.357)
Geometric mean dia.(GMD) mm ³	2.232 (0.0715)	1.941(0.062)	2.076 (0.042)	1.922(0.038)
Sphericity(%)	0.704 (0.025)	0.660 (0.023)	0.7170 (0.013)	0.697 (0.012)
Surface Area mm ²	17.00 (1.004)	11.84 (0.699)	13.540 (0.691)	11.61 (0.593)
Volume mm ³	1.865 (0.057)	1.218 (0.038)	1.4914 (0.059)	1.184(0.04)

Akindele F. ALONGE, Edidiong D. UBAK and Elijah G. IKRANG “Effect of Moisture Content on Physical Properties of Pumpkin (*telfairia occedentalis*) Seeds”



CIGR 2018

XIX. World Congress of CIGR



Ave. Mass (g) 8.15 (1.504) 4.230 (4.163) 5.8900 (2.116) 5.36(1.826)

Values in brackets are standard deviation

The length and thickness of the seed have no significant difference (Table 2.0), while there is significant difference ($P < 0.01$) in the width (Table 2.0) and this implies that little reduction in the moisture level of the seed was more pronounced in the width axis as compared to the length and thickness of the seed. The linear dimensions however were not significantly different at the various level of moisture content except at Level (3). This implies that the values can be used as a representation of the linear dimensions at any moisture level without any significant effect on the seed (Table 1).

Volume

Table 2 shows pumpkin seed volume changes at different moisture contents. The seed volume was observed to decrease linearly from 1.865 to 1.14 when the moisture content decreased from 8.2% to 4.13% (d.b.).

Table 2: Mean of the physical properties of the Fluted Pumpkin seed

Length(L) (mm)	Width(W) (mm)	Thickness(T) (mm)	True density (ρ_t g/mm ³)	Bulk density (ρ_b g/mm ³)	Porosity P (percentage %)
2.94 ^a	0.99 ^b	2.95 ^a	4.10 ^a	2.53 ^b	0.38 ^a

Mean followed by the same letter are not significantly different from each other

Geometric Mean Diameter, Surface Area and Sphericity

In Tables 1 and 2, it is seen that the geometric mean diameter (GMD) and surface area (S) reduced from level (1) to level (2) but increased in level (3) and then reduced in level (4). Hence, it is dependent on the three linear dimensions which were observed to suffer some form of reduction. There is no significant difference in the sphericity of the seed despite moisture variation. However, the behavior of sphericity (Φ), which reduces and then tends to increase, is dependant mainly on the width of the seed, which exhibits a similar behaviour behavior. Sphericity of the pumpkin seed ranged from 0.71-0.66%. It was observed that there is little effect of moisture content on the sphericity of the fluted pumpkin seed. Geometric mean diameter of the fluted Pumpkin was higher than those reported for the sorghum seed (Mwithiga and Sifuna, 2006), Caper Seed (Dursun and Dursun, 2005).

Table 3: Mean of the physical properties of Fluted Pumpkin at different moisture content

Moisture content(d b)	Length(L) (mm)	Width(W) (mm)	Thickness(T) (mm)	True density (ρ_t g/mm ³)	Bulk density (ρ_b g/mm ³)	Porosity P (%)
8.2	3.17 ± 0.37	1.14 ± 0.61	3.11 ± 0.56	4.37 ± 0.09	2.68 ± 0.05	0.39 ± 0.01
7.7	2.94 ± 0.33	0.84 ± 0.24	2.97 ± 0.38	3.47 ± 0.16	2.24 ± 0.10	0.35 ± 0.01

Akindele F. ALONGE, Edidiong D. UBAK and Elijah G. IKRANG “Effect of Moisture Content on Physical Properties of Pumpkin (*telfairia occedentalis*) Seeds”



CIGR 2018

XIX. World Congress of CIGR



5.8	2.90 ± 0.32	1.04 ± 0.38	2.97 ± 0.60	3.95 ± 0.13	2.55 ± 0.08	0.35 ± 0.02
4.1	2.76 ± 0.30	0.93 ± 0.36	2.76 ± 0.31	4.53 ± 0.09	2.92 ± 0.06	0.35 ± 0.02

Bulk Density

The experimental results of the bulk density for pumpkin seed at different moisture levels are presented in Table 3. The bulk density (ρ_b) of the seed reduced from 2.68 g/mm^3 - 2.24 g/mm^3 from moisture content of 8.2 to 7.7 % (d.b) and then increased from 2.5 - 2.9 g/mm^3 from moisture content of 5.8 to 4.1 % (d.b). This shows that the bulk density is a function of the weight and volume of the seed as the average weight of the seed at a moisture content of 5.8 increased and also the volume as compared to that at a moisture content of 8.2% (d.b).

Porosity

In Table 3, since porosity depends on the bulk as well as true densities, the magnitude of variation in porosity depends on these factors only. The values of porosity were calculated using the data on bulk and particle densities of the fluted pumpkin seed. For pumpkin seed, porosity varied from 39% to 35% as the moisture content changed from 8.2 to 4.13 (d.b. %).

Conclusion

Several physical properties of Pumpkin seed were investigated in moisture contents ranging from 8.2 to 4.13 (d.b.%). The results showed that this differential moisture content of Fluted Pumpkin seeds caused a variation in its dimensions, volume, unit mass and sphericity. The porosity for Fluted Pumpkin seed decreased with moisture content. The bulk density decreased with decreased in moisture content and then increases uniformly with a further decrease in the moisture content. This study reveals that there is clear effect of moisture content in most of the physical properties of pumpkin seed. These properties are very useful in the design of equipment used for processing, transportation and storage.

REFERENCES

- Adejumo, A. O, Ajav, E. A. and Igbeka, J.C (2009). Effect of Moisture Content on some Frictional and Aerodynamic Properties of Okra (*Abelmoschus Esculentus* (L) (Moench) Varieties. Proceedings of 3rd International Conference of WASAE and 9th International Conference of NJAE. Ife –Ife, Nigeria: (249-255)pp
- Alonge, A. F. and Adigun, Y. J (1999): Some Physical and Aerodynamic Properties of Sorghum as related to threshing and cleaning. Nigerian Journal of Pure and Applied Sciences (NJPAS). Volume 13, page 992-998
- Anonymous (2018). Benefits of Fluted pumpkin. <https://agriculturenigeria.com/farming-production/horticulture/fluted-pumpkin>. Accessed April 2, 2018
- ASABE (2006). American Society of Agricultural and Biological Engineers (ASABE) Standards.

Akindele F. ALONGE, Edidiong D. UBAK and Elijah G. IKRANG “Effect of Moisture Content on Physical Properties of Pumpkin (*telfairia occedentalis*) Seeds”



CIGR 2018

XIX. World Congress of CIGR



Baryeh E. A (2002). Physical Properties of millet. Journal of Food Engineering, Volume 51, Issue 1, January 2002, Pages 39-46

Bradbury, J.H., Collins and N. A. pylotis, 1984. Digestibility of protein of the Histological components of cooked and Raw Rice. Br. Nutrition; 52:507-513.

Choudhary, B (2001): Vegetable crops. In: Handbook of Agricultural Indian Council of Agricultural Research, New Delhi. 401-102.

Deshpande, S. D., S. Bal and T. P Ojha (1993): Physical properties of soybean. Journal of Agricultural Engineering Research 56(2), 89-98.

Dursun, E. and I. Dursun, 2005. Some physical properties of caper seed. Biosystems Engineering, 92: 237-245.

Giami, S. Y and Wachku, O. C (1997): Composition and Functional Properties of Unprocessed and locally processed seed from three under Utilized Food Sources in Nigeria. Journal Plant Food Human Nutrition. 50:27-36.

Giami, S.Y; S.C, Achinewhu and C. Ibakee (2005): The quality and Sensory Attributes of Cookies supplemented with fluted pumpkin (*Telfairia Occidentals Hook*) Seed Flour in J. Food Science Technology, 40:613-620.

Hsu, M.H, Mannapperuma, J.D. and Singh, R. P. (1991): Physical and Thermal Properties of Pistachios'' Journal of Agricultural Engineering Research 49(4):311-321.

Lazos, E.S. (2004): Nutritional Fatty Acid and Oil Characteristics of pumpkin and melon seeds. Journal of Food Science. 51(9):1382-1383.

Makanjuola G. A (1972): A study of some of the physical properties of melon seeds. Journal of Agricultural Engineering Research 12:128-137.

McCabe, W.L., J.C. Smith and P. Harriot (1986). Unit operations of chemical engineering. New York: McGraw-Hill, http://en.wikipedia.org/wiki/Unit_Operations_of_Chemical_Engineering

Mohsenin, N.N. 1986. Physical Properties of Plant and Animal Materials. 3rd Ed. Gordon and Breach Science Publishers. NewYork.

Mwithiga G and Sifuna M. M (2006). Effect of moisture content on the physical properties of three varieties of sorghum seeds. Journal of Food Engineering, Volume 75, Issue 4, August 2006, Pages 480-486

Oje, K, Alonge, A. F and Adigun, Y.J. (2003): Variation of physical properties of Melon Seeds at their different moisture levels'' Journal of Food Science Technology, 36(4): 42-45pp.

Oje, K.(1991): Some Physical Properties of Oil Bean Seed Journal of Agricultural Engineering Research, 50.305-313.

Akindele F. ALONGE, Edidiong D. UBAK and Elijah G. IKRANG "Effect of Moisture Content on Physical Properties of Pumpkin (*telfairia occedentalis*) Seeds"



CIGR 2018

XIX. World Congress of CIGR



Owolarafe , O.K; Olabige, T.M. and Faborode, M. O.(2007): “Macro Structural Characterization of Palm Fruit at Different Processing Conditions” Journal of Food Engineering. 78:1228-1232.

Ramakrishna, P. (1986). Melon Seeds - Evaluation of Physical Characteristics. Journal Food Science and Technology 23 (3), 158–160

Teotia, M.S.; Ramakrishna, P.; Berry, S.K.; Kaur, S. (1989). Some Engineering Properties of Pumpkin (*Cucurbita moschata*) Seeds. Journal Food Engineering. 9, 153–162



CIGR 2018

XIX. World Congress of CIGR



Friction Coefficients For Gundelia Tournefortii Seed on Various Surfaces

Reşat Esgici ¹, F. Göksel Pekitkan ², Emin Güzel ³, Abdullah Sessiz ^{2*}

¹ Dicle University, Faculty of Agriculture, Department of Agricultural Machinery and Technologies Engineering, Diyarbakir, Turkey

² Dicle University, Bismil Vocational High School, Diyarbakir, Turkey

³ Cukurova University, Faculty of Agriculture, Department of Agricultural Machinery and Technologies Engineering, Adana, Turkey

asessiz@dicle.edu.tr

ABSTRACT

Gundelia tournefortii, as known kenger, is a thorny plant that grows naturally. The main objective of this study was to determine the static coefficient of friction (μ_s) and kinetic coefficient of friction (μ_k) for gundelia tournefortii seeds at 9.60%, 16.20%, 31.30 % and 42.30% moisture content (wet basis) on four contact surfaces namely, galvanized steel, chromium, PVC and rubber, six different sliding velocities (5, 10, 15, 20, 25, 50 mm/s) and three level of loading force (15, 20 and 25 N pressure). The Gundelia Tournefortii seeds used in this study were collected from nature, Diyarbakir province, Turkey, 2017. Friction force was measured by Lloyd instrument test machine.

In general, for all tested contact surfaces, μ_s and μ_k increased with increasing moisture content and applied load. The maximum static and kinetic coefficients of friction were observed on rubber surface, followed by PVC, galvanized steel and chromium. While the values of static coefficients of friction ranged from 0.4709 to 0.6471, kinetic coefficients of friction values ranged from 0.4310 to 0.6069 depend on surface materials. Both static and kinetic coefficient of friction much slightly decreased with increase added load during the sliding on different surface materials. No significant differences in the average values of the coefficient of kinetic friction were observed between sliding velocity on all surface materials.

Keywords: Friction coefficient, Sliding velocity, Contact surface, Design, Gundelia Tournefortii

INTRODUCTION

Gundelia tournefortii is a thorny plant (Figure 1) that grows naturally in different regions of Turkey, especially the Southeastern and Eastern Anatolia, Mediterranean and Aegean regions. The green part, root and seed part of this plant are utilized. The both green parts and roots are consumed by people as vegetables and also, it is argued by farmer that the gundelia tournefortii seeds's increases milk production and quality, both green parts and seeds has consumed as animal feed. It is also used as a medicinal plant and gum in addition to its use as food and feed.



CIGR 2018

XIX. World Congress of CIGR



Fig.1. The green part of *gundelia tournefortii* plant and roots.

So, this plant has important for human foods and animal feed. The demand for this plant is increasing rapidly. Therefore it will be important industrial plant in future. So, when we consider this plant as an industrial product, it is necessary to know exactly the some engineering properties of the *gundelia tournefortii* plant and seeds. One of the import properties is the friction force. Because, the knowledge of frictional properties of plant material is essential for design of mechanical units in agricultural machinery and equipment of related harvest and post-harvest industries (Kashaninejad et al., 2008). So, this information is valuable not only to engineers but also to the food scientists and processor and breeders (Nesvadba et al., 2004; Sessiz et al., 2007; Lorestani et al., 2012; Kaliniewicz, 2013; Kaliniewicz et al., 2015; Ghodki and Goswami, 2016). Therefore, there is a need to reduce the energy requirements of agricultural machinery and reduce farm production costs. One factor that affects the performance and energy efficiency of crop handling and harvesting equipment is the friction coefficients between seeds and machine surfaces (Shinners et al., 1991). Friction forces perform between two contact surface, the material generally moves or slides in direct contact with trough, casing, and other components of the machine. Friction is defined by the empirical law: $F = \mu \square \square N$, where F is the horizontal force required to move a material in contact with a surface, μ is the coefficient of friction, and N is the applied normal force (Mohsenin, 1986; Kostaropoulos et al., 1997; Blau, 2001; Boac et al., 2009; Nyendu et al., 2014). There are two types of friction: static and kinetic. The resistive force (friction) when a stationary object begins motion is called the static coefficient of friction (μ_s) and when the object is already in motion is called kinetic coefficient of friction (μ_k). Usually, the kinetic frictional force is less than the maximum value of the static frictional force. Authors suggest reducing μ_s by 25% to obtain μ_k (Blau, 2001).

The friction coefficient of agricultural products depend on moisture content, normal pressure, surface condition, and additionally, in case of kinetic friction coefficients, the sliding velocity is also an important factor (Mohsenin, 1986; Shinners et al., 1991; Öztürk and Sabahoğlu., 1994; Beyhan at al., 1994; Ibrahim, 2008; Kalkan and Kara., 2011; Bakhtiari et al. 2011; Sologubik et al 2013; Shafaei and Kamgar, 2017). To reduce frictional losses and increase efficiency, it is desirable to select materials with low friction coefficients to be in contact with surface during handling and storing operations (Nyendu et al., 2014; Obi and Offorha., 2015). Therefore, exact determination of friction coefficients of the crop on different contact surfaces can be useful in performance optimization of mechanical equipment such as



CIGR 2018

XIX. World Congress of CIGR



conveyors, separation, cleaning, drying and storing structure (Mohsenin, 1986; Baryeh, 2002, Amin et al., 2005; Mir et al., 2013; Shafaei and Kamgar, 2017).

A comprehensive investigation of friction coefficients for *Gundelia tournefortii* seeds taking several experimental conditions into considerations will be useful for optimization of storage, transporting and processing structures, especially bins. Until now many study related to frictional properties have been conducted by many researchers and several friction coefficients have developed for different agricultural products on various surfaces (Beyhan et al., 1994; Kostaropoulos et al., 1997; Baryeh, 2002; Çolak and Saçılık, 2002; Konak et al., 2002; Saçılık et al., 2003; Subramanian and Viswanathan, 2007; Nwakonobi and Onwualu, 2009; Pradhan et al., 2009; Lorestani et al., 2012; Aremu et al., 2014; Kaliniewicz et al., 2015; Özlü and Güner, M., 2016). But, there is no data relating to moisture-dependent friction properties of the *Gundelia tournefortii* seeds. In recent years, the need to determine of plant properties in datasets has greatly increased. Therefore, it is very important to know some of the frictional properties of the *Gundelia tournefortii* seeds in future for optimization of related industry structures and agricultural equipment.

In light of the above mentioned information, the objectives of this study was to determination of static and kinetic friction coefficients of *Gundelia tournefortii* seed at different moisture content, contact surface, loading pressure and sliding velocity and comparing statistical significance of the effect of different treatment levels on static and kinetic friction coefficients for each moisture content level and contact surface.

MATERIALS AND METHODS

Seed Collection and Moisture Content

The naturally grown the *Gundelia Tournefortii* seeds (Figure 2) used in this study were collected from nature, location of Silvan, Diyarbakır province, Turkey, 2017. To obtained seeds, the whole plants were threshed by a threshing machine. Before the tests, the seeds were cleaned manually to remove any foreign material. Then, seeds were divided into four parts in order to obtain different moisture level and transported to laboratory of Dicle University, Faculty of Agriculture Department of Agricultural Machinery and Technologies Engineering.



Fig. 2. The seed of *Gundelia tournefortii*

Initial moisture content of seeds of *Gundelia tournefortii* was determined by using ASAE standard method 352.2 (ASABE Standards, 2008). Four samples each weighing 25 g were weighed and placed in an oven set at 103 °C for 24 h. Then, samples were again weighed and moisture content of the seed calculated according to w.b. To achieve higher moisture contents, the water was sprayed into seeds before tests. To distribute uniformly throughout the seeds, the seeds were mixed by manually during the wetting. Then the samples were sealed in separate plastic bags and kept in a refrigerator at 5 °C for one week. Before starting each test, the required quantities of the conditioned seeds were taken out of the refrigerator and was allowed to warm up to room temperature (Deshpande et al., 1993; Masoumi and Tabil, 2003; Dursun and Dursun, 2005; Sessiz et al., 2007; Fathollahzadeh et al., 2008; Figueiredo et al., 2011; Ndukwe and Ejirika, 2016; Esgici et al., 2017). The moisture content levels were obtained in the range of 9.60 to 42.30 % w.b. with five replications at each level.

Coefficients of Friction

The static and kinetic friction coefficients of *Gundelia tournefortii* seeds were measured on four various contact surfaces (chromium, galvanized steel, PVC and rubber) at four different levels of moisture content (9.60 %, 16.20 %, 31.30 % and 42.3 %) and six sliding velocities (5, 10, 15, 20, 25 and 50 mm/s) and three different loading weight (1.5, 2.0 and 2.5 kg), (also the experiment was conducted with preload for comparison). Before starting each experiment, the contact surfaces were cleaned and eliminate any remaining matter from previous experiments. Each experiment was accomplished in five replications.

An apparatus was constructed that allowed the seed to slide across the contact surfaces. The experimental equipment consisted of a frictionless pulley fitted on a frame, topless and bottomless plywood box of inside dimensions 250 x 250 x 90 mm³, loading pan, and test surfaces. The friction testing box was connected to Instron testing machine by means of a steel cable, parallel to the surface of the material and passed over a frictionless pulley with a pan hanging from it. The box placed on the test surface was filled with a known quantity of the seeds and weights were added to the loading pan until the box began to slide. The box was raised with pulley slightly so as not to touch the surface (Usrey et al., 1992; Amin et al.,

Reşat Esgici, F. Göksel Pekitkan, Emin Güzel, Abdullah Sessiz “Friction Coefficients For *Gundelia Tournefortii* Seed on Various Surfaces”



2004; Sessiz et al., 2007; Nyendu et al., 2014). A schematic of the instrument and apparatus is shown in Figure 3.

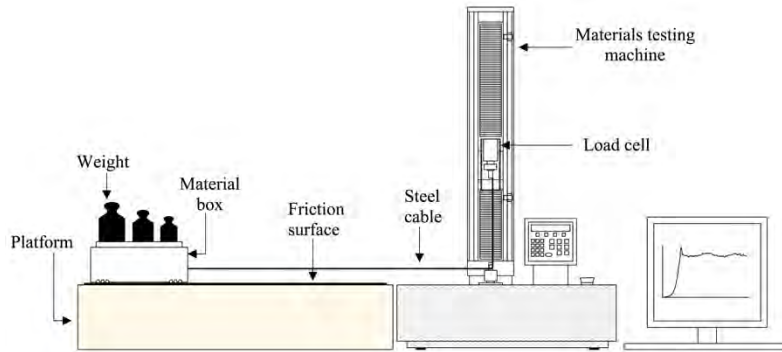


Fig. 3. The friction test apparatus and Instrument test machine.

The friction force as a function of time (displacement) was measured by Instron universal testing machine. A computer data acquisition system recorded all the friction force during test run, the digitized friction force data were used to compute the friction coefficients. A typical friction force- time curve is shown in Figure 4. The upper yield point corresponds to maximum frictional force. In this study, once the test was started, force increased with time as the surface resisted movement until it started to move at which time the force declined slightly. This first peak force was considered as the maximum static frictional force. After force slightly declined, measured values of during the movie were considered as kinetic frictional force.

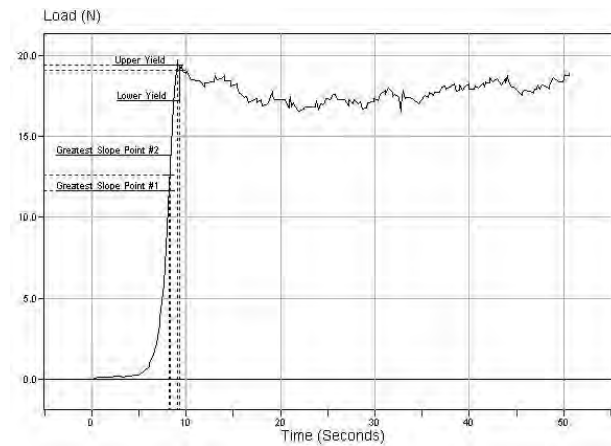


Fig. 4. Typical frictional force-time curve.

The coefficient of friction (μ) is defined as the ratio of the friction force (F) to the normal force (W) on contact surface:

$$\mu = \frac{F}{W}$$



CIGR 2018

XIX. World Congress of CIGR



According to this formula and friction force, the static coefficient of friction (μ_s) and kinetic coefficient of friction (μ_k) were determined using the following formulas (Chandrasekar and Viswanathan, 1999; Blau, 2001; Balasubramanian, 2001; Amin et al., 2004; Kaleemullah and Gunasekar, 2002; Sessiz, 2005; Aviara et al, 2014).

$$\mu_s = \frac{F_s}{W}$$
$$\mu_k = \frac{F_k}{W}$$

Where: F_s is the force required just to move the box with seeds, F_k is the force required to move the box with a slight push and W is the weight of box plus seeds plus added weight.

Statistical Analysis

An analysis of variance (ANOVA) of the three factor randomized complete block design with five replications were performed to detect significant differences in the observations due to the effect of moisture content, surface material, applied load and sliding velocity of each factor using the MSTATC software. The regression analysis was performed using Microsoft Excel 2010 software. Means were compared at the 1 % level of significance using Duncan's multiple range tests to identify the specific differences among treatments means.

RESULTS AND DISCUSSION

Effect of Moisture Content on Friction Coefficient

The static and kinetic coefficient friction of *Gundelia tournefortii* seeds against moisture content in the range of 9.6% - 42.30 % w.b. are presented in Table 1 and Figure 5. As shown in Table 1 and Figure 5, the effect of moisture content on coefficients of friction were found significant ($p < 0.01$) and the differences between moisture content level were also observed significant. The both static and kinetic coefficient of friction significant increased ($p < 0.01$) linearly with the increase of moisture content for all contact surface (Table 1 and Figure 5). While the moisture content of seeds increased from 9.60 % to 42.30 % w.b., the static coefficient of friction increased from 0.402 to 0.742, kinetic coefficient of friction increased from 0.372 to 0.709. According to Table 1, minimum and maximum friction coefficients were obtained in the lowest and highest level of moisture content on chromium and rubber, respectively. The interactions were also significant influence on the coefficients of friction at 1% level.

The reason of this situation may be due to the increased adhesion between the seeds and the contact surfaces at higher moisture contents (Seifi and Alimardani, 2010; Sologubik et al., 2013; Ghodki and Goswami, 2016). It is also observed that the static coefficients of friction were found to be greater than kinetic coefficients of friction in all moisture contents. The results are consistent with the report available for different seeds such as for alfalfa (Shinners



at al., 1991), for inshell and husky hazelnuts (Beyhan et al., 1994), olive (Çolak and Saçılık, 2002), for caper fruit (Sessiz et al., 2007), for watermelon seed (Koocheki et al., 2007), millet (Baryeh, 2002), hazelnuts (Aydin, 2002), caper fruit (Sessiz et al., 2007), wheat grain (Mahasneh and Rababah, 2007), and wheat grain (Zaalouk and Zabady, 2009). Amin et al. (2005) also determined that the coefficient of friction of pulse grains on various surfaces at different moisture content. They reported that coefficient of friction increased with increase moisture content for all grains and surface materials. Nyendu et al. (2014) determined that coefficient of friction increased with increase moisture content for eight structural surfaces.

The derived regression equations as a function of moisture content are given on Figure 5. As seen from Figure, R values were found high and the linear relationship were observed between moisture content (Mc) and friction (μ).

Table 1. The average static and kinetic coefficients of friction of *gundelia tournefortii* seeds at different moisture contents.

Moisture content, %	Friction Coefficients	
	Static (μ_s)	Kinetic (μ_k)
9.60	0.402 ^{d*}	0.3722 ^d
16.20	0.428 ^c	0.3918 ^c
31.30	0.635 ^b	0.5942 ^b
42.30	0.742 ^a	0.7096 ^a
LSD	0.007864	0.007864

* Different letters show significant differences at probability level of 1%.

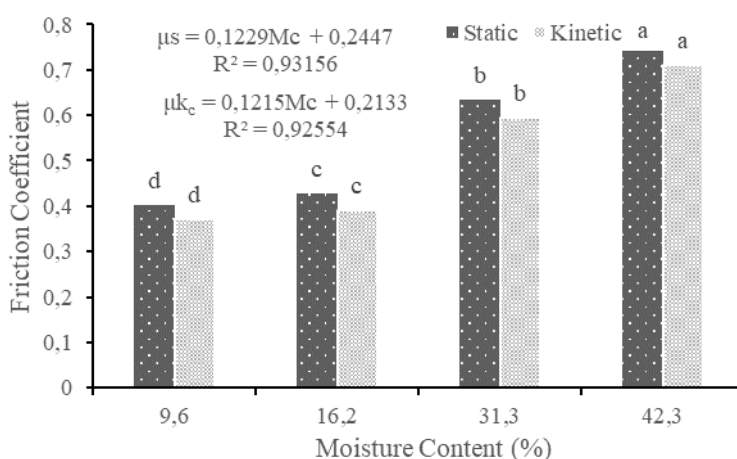


Fig. 5. The static and kinetic coefficient of friction as a function of moisture content.

Effect of Surface Material on Friction Coefficient

The mean values of the static and kinetic friction coefficients on various contact surfaces are reported in Table 2 and Figure 6. As seen in Table 2 and Figure 6, there were found significant ($p < 0.01$) differences in the coefficients of friction between surface materials. The



CIGR 2018

XIX. World Congress of CIGR



maximum static and kinetic coefficients of friction were observed on rubber surface, followed by PVC, galvanized steel and chromium. The lowest static and kinetic friction coefficients were determined on the chromium contact surface. This is may be due to chromium surface materials more smooth surface than the other surfaces. Also, it can be stated that the effect of surface materials and their interactions on static and kinetic coefficients of friction were found significant at 1% probability level. It was also observed that both the static and kinetic coefficient of friction increased with increase moisture content on all contact surfaces. While the values of static coefficients of friction ranged from 0.4709 to 0.6471, kinetic coefficients of friction values ranged from 0.4310 to 0.6069 depend on surface materials. Static coefficients of friction values were observed higher than kinetic coefficients of friction for all surface materials (Table 2 and Figure 6). Both static and kinetic coefficients friction on rubber surface are found to be much significantly higher than those of other surfaces. This situation can be explained that the surface of rubber more rough than the chromium and other used test surfaces. Smoother surface resulted in lower adhesion force between the seeds and the surface and thereby, the lower static and kinetic coefficients of friction were obtained on chromium surface (Visvanathan et al., 1996; Shafaei and Kamgar, 2017). Similar results were reported by Kaliniewicz (2013). According to Kashaninejad et al. (2008), the higher moisture content make surface of material more sticky than the others. So, as moisture content increased, the static coefficient of friction also increased. We can argue that friction depends on the material surface of roughness and friction forces. This situation is causes the increase of energy consumption. Similar results were reported by Çolak and Saçılık (2002) for olive, Amin et al., (2004) for lentil seed, Sessiz (2005) for olive, Kashaninejad et al. (2008) for soybean, Tavakoli et al., (2009) for soybean, Sologubik et al. (2013) for barley, Shafaei and Kamgar (2017) for wheat grain, Kaliniewicz (2013) for some cereal seeds such as wheat, rye, barley, oats and triticale. These effects on static and kinetic coefficient of friction are necessary engineering considerations that should be taken in designing crop handling equipment and storage structures to reach the best operation conditions (Shafaei and Kamgar, 2017). Also, the regression equations between friction coefficients and surface materials are given on the Figure 6.

Table 2. The mean static and kinetic coefficient of friction on various surfaces.

Surface material	Friction Coefficients	
	Static(μ_s)	Kinetic(μ_k)
Chromium	0.4709 ^d *	0.4310 ^d
Galvanized steel	0.5240 ^c	0.4954 ^c
PVC	0.5658 ^b	0.5344 ^b
Rubber	0.6471 ^a	0.6069 ^a
LSD	0.007864	0.006811

* Different letters show significant differences at probability level of 1%.

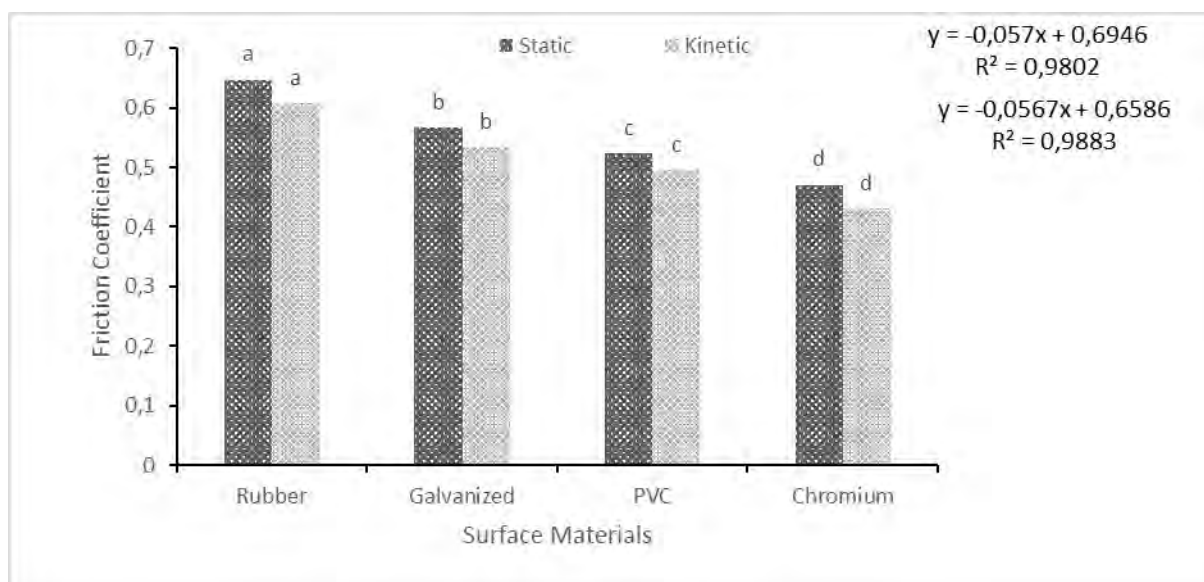


Fig. 6. The static and kinetic coefficient of friction as a function of surface materials.

Effect of Applied Weight on Friction Coefficient

The mean values recorded for the frictional properties at different applied weight levels are shown in Tables 3 and Figure 7. According to Table 3 and Figure 7, the effect of added load on seed box was found significant on frictional coefficient. Both static and kinetic coefficient of friction much slightly decreased with increase added load during the sliding on different surface materials. However, it was expected that the added weight on the seed box more increase friction coefficients on all contact surface, but the results did not verify this expectation. However, there were also found significant differences between no applied load on the box and other applied weight. This finding is supported by the Sabahoğlu and Öztürk (1996) for some wheat varieties. They reported that friction coefficients slightly decreased with increase added load on seed box.

Table 3. The static and kinetic coefficient of friction depends on added weight.

Added weight,g	Friction Coefficients	
	Static(μ_s)	Kinetic(μ_k)
The box plus seed weight (1.895+ 1000 = 2.895), no extra load	0.00828	0.0678
4.395	0.5559 ^a	0.5200 ^a
4.895	0.5557 ^a	0.5191 ^a
5.395	0.5544 ^b	0.5117 ^b
LSD	0.006811	0.006811

* Different letters show significant differences at probability level of 1%.

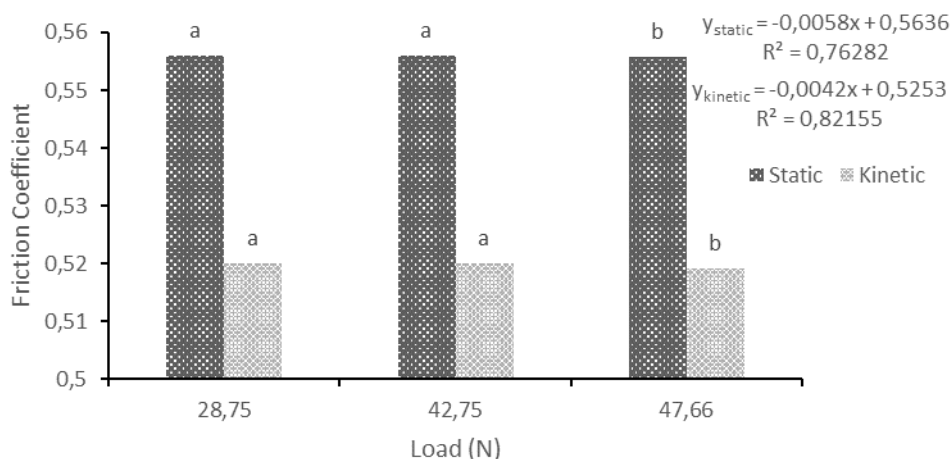


Fig. 7. The static and kinetic coefficient of friction as a function of added weight.

Effect of Sliding Velocity on Friction Coefficient

The static and kinetic friction coefficients are presented in Table 4 depend on sliding velocity. ANOVA showed that both coefficients of friction were not affected significantly ($p>0.05$) by sliding velocity. As seen in Table 4 and Figure 8, no significant differences in the average values of the coefficient of kinetic friction were observed between sliding velocity on all surface materials. Similar results were reported by Puchalski et al., (2003) for apple, Çalışkan and Vursavuş (2009) for Washington orange. Shinnars et al. (1991) reported that the coefficients of friction not affected the velocity of travel but there were affected by moisture content and normal pressure. Also, the effects of interactions were not found significant for friction coefficients. The main values of the static and kinetic coefficients ranged from 0.551 to 0.554, 0.5160 to 0.5209 depend on sliding velocities, respectively. These results showed that sliding velocity insignificantly affected static and kinetic friction coefficients of gundelia tournefortii seeds. However, the analysis of variance and Duncan's test results showed that a significant effect of preload velocity on the static and sliding velocity on kinetic coefficient of friction (Table 4).

Table 4. The static and kinetic coefficient of friction depends on sliding velocity.

Sliding velocity, mm/s	Friction Coefficients	
	Static(μs)	Static(μs)
Preload (mean values)	0.0828	0.0678
5	0.551 ^{ns*}	0.5160 ^{ns}
10	0.552 ^{ns}	0.5165 ^{ns}
15	0.552 ^{ns}	0.5175 ^{ns}
20	0.553 ^{ns}	0.5185 ^{ns}
25	0.554 ^{ns}	0.5186 ^{ns}
50	0.554 ^{ns}	0.5209 ^{ns}
LSD	0.007320	0.007320



* Different letters show significant differences at probability level of 1%.

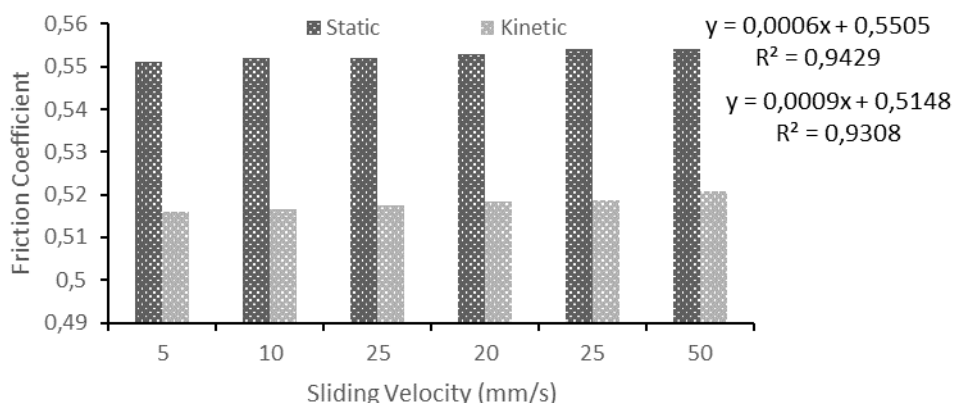


Fig. 8. The static and kinetic coefficient of friction as a function of sliding velocity.

CONCLUSIONS

For all tested contact surfaces the static and kinetic coefficients of friction increased linearly with the increase of moisture content. While the moisture content of seeds increased from 9.60 % to 42.30 % w.b., the static coefficient of friction increased from 0.402 to 0.742, kinetic coefficient of friction increased from 0.372 to 0.709. While moisture content increased from 9.6 % to 42.30 %, the rate of static and kinetic coefficient of friction is increased 84.5 % and 90 %, respectively. The maximum static and kinetic coefficients of friction were observed on rubber surface, followed by galvanized steel, PVC and chromium. While the values of static coefficients of friction ranged from 0.4709 to 0.6471, kinetic coefficients of friction values ranged from 0.4310 to 0.6069 depend on surface materials. The values were static coefficient of friction higher than kinetic coefficient of friction for all moisture content and surface materials. Both static and kinetic coefficient of friction much slightly decreased with increase added load during the sliding on different surface materials. No significant differences in the average values of the coefficient of kinetic friction were observed between sliding velocity on all surface materials.

REFERENCES

- Al-Mahasneh, M. A. and Rababah, T. M. 2007. Effect of moisture content on some physical properties of green wheat. *J. Food Eng.* 79, 1467–1473.
- Amin, M. N, Ahammed, S., Roy, K. C. and Hossain, M. A. 2005. Coefficient of friction of pulse grains on various surfaces at different moisture content. *International Journal of Food Properties*. ISSN: 1094-2912 (Print) 1532-2386 (Online) Journal homepage: <http://www.tandfonline.com/loi/ljfp20>
- Amin. M. N, Hossain, M. A. and Roy, K. C. 2004. Effects of moisture content on some physical properties of lentil seeds. *Journal of Food Engineering* 65, 83-87.

Reşat Esgici, F. Göksel Pekitkan, Emin Güzel, Abdullah Sessiz “Friction Coefficients For Gundelia Tournefortii Seed on Various Surfaces”



CIGR 2018

XIX. World Congress of CIGR



Aremu, D. O, Babahide, N. A. and Ogunlade, C. A. 2014. Comparison of Some Engineering Properties of Common Cereal Grains In Nigeria International Journal of Engineering Science Invention ISSN (Online): 2319 – 6734, ISSN (Print): 2319 – 6726 www.ijesi.org Volume 3 Issue 4 April 2014 PP.10-14.

ASABE Standards 2008. Moisture measurement – unground grain and seeds. St. Joseph, Mich.: ASABE.

Aviara, N. A., Lawal, A. A., Mshelia, H. M. and Musa, D. 2014. Effect of moisture content on some engineering properties of mahogany (*Khaya senegalensis*) seed and kernel. Vol. 60, 2014, No. 1: 30–36 Res. Agr.

Aydin, C. 2002. Physical properties of hazelnuts. Biosyst ng. 65: 297–303.

Bakhtiari, M. R., Ahmad, D., Othman, J. and Ismail, N. 2011. Physical and mechanical properties of kenaf seed. Appl. Eng. Agric. 27 (2), 263–268.

Balasubramanian, D. 2001. Physical properties of raw cashew nut. Journal of Agricultural Engineering Research, 78, 291–297.

Baryeh, E. A. 2002. Physical properties of millet. Journal of Food Engineering. 2002. 51(1), P. 39-46

Beyhan, M. A., Nalbant, M. and Tekgüler, A. 1994. Determination of coefficient of friction in the grain and husk hazelnuts for different surfaces. Proc. XV. National Congree on Agricultural Mechanization' September 20-22, Antalya, Turkey, 343-352.

Blau, P. J. 2001. The significance and use of the friction coefficient_ Tribology. International 34 (2001) 585–591

Boac, J. M. and Maghirang, D. P. 2009. Material and interaction properties of selected grains and oilseeds for modeling discrete particles. An ASABE Meeting Presentation, Paper Number: 09-7166

Chandrasekar, V. and Viswanathan, R. 1999. Physical and thermal properties of coffee. Journal of Agricultural Engineering Research, Volume 73, Issue 3, July 1999, Pages 227-234

Çalışkan, N. and Vursavuş, K. 2009. Washington Navel Portakalın Hasat Sonrası İşlemlere Yönelik Fiziksel ve Sürtünme Özelliklerinin Nelirlenemsi. Tarım makinaları Bilimi Dergisi. 5(1),83-92.

Çolak, A. and Saçılık, K. 2002. Zeytinin (*Olea europaea* L.cv. Memecik) Sürtünme Katsayılarının Belirlenmesi. Tarım Bilimleri Dergisi, 8(2), 11-118.

Deshpande, S. D, Bal, S. and Ojha, T. P. 1993. Physical properties of soybean. Journal of Agricultural Engineering Research, 56, 89-98

Dursun, E. and Dursun, I. 2005. Some physical properties of caper seed. Biosyst. Eng. 92 (2), 237–245.

Esgici, R., Özdemir, G., Pekitkan, F. G., Elicin, A. K., Öztürk, F. and Sessiz, A. 2017. Some engineering properties of the Şire grape (*Vitis Vinifera* L.). Scientific Papers. Series B,



CIGR 2018

XIX. World Congress of CIGR



Horticulture. Vol. LXI, 2017. Print ISSN 2285-5653, CD-ROM ISSN 2285-5661, Online ISSN 2286-1580, ISSN-L 2285-5653. June 8-10, Bucharest, Romania.

Fathollahzadeh, H., Mobli, H., Jafari, A., Rajabipour, A., Ahmadi, H. and Borghei, A. M. 2008. Effect of Moisture Content on Some Physical Properties of Barberry. *American-Eurasian J. Agric. & Environ. Sci.*, 3 (5): 789-794, ISSN 1818-6769

Figueiredo, A. K., Baümler, E., Riccobene, I. C. and Nolasco, S. M. 2011. Moisture-dependent engineering properties of sunflower seeds with different structural characteristics. *Journal of Food Engineering* 102 (2011) 58–65

Ghodki, B. M. and Goswami, T. K. 2016. Effect of moisture on physical and mechanical properties of cassia. *Cogent Food & Agriculture* (2016), 2: 1192975

Ibrahim M. M. 2008. Determination of dynamic coefficient of friction for some materials for feed pellet under different values of pressure and temperature. *Misr J Ag Eng* 2008;25(4):1389–409.

Kaleemullah, S. and Gunasekar, J. J. 2002. Moisture-dependent physical properties of arecanut kernels. *Biosystems Engineering*, 82(3), 331–338.

Kaliniewicz, Z. 2013. Analysis of frictional properties of cereal seeds *African Journal of Agricultural Research* Vol. 8(45), pp. 5611-5621, DOI: 10.5897/AJAR2013.7361 ISSN 1991-637X

Kaliniewicz, Z., Markowski, P., Anders, A. and Jadwisieńczyk, K. 2015. Frictional Properties of Selected Seeds *Technical Sciences* 18(2), 2015, 85–101.

Kalkan, F. and Kara, M. 2011. Handling, frictional and technological properties of wheat as affected by moisture content and cultivar. *Powder Technology* 213 (2011) 116–122

Kashaninejad, M., Ahmadi, M., Daraei, A. and Chabra, D. 2008. Handling and frictional characteristics of soybean as a function of moisture content and variety. *Powder Technology* 188 (2008) 1–8

Konak, K., Carman, K. and Aydin, C. 2002. Physical properties of chick pea seeds. *Biosystems Engineering*, 82 (1): 73-78.

Koocheki, A., Razavi, S. M. A., Milani, E., Moghadam, T. M., Abedini, M., Alamatian, S. and Izadkhah, S. 2007. Physical properties of watermelon seed as a function of moisture content and variety. *Int. Agrophysics*, 2007, 21, 349-359

Kostaropoulos, A. E., Mandala, J., Spiess, W. E. and Saravacos, G. D. 1997. Factors influencing the friction of raisins during processing and handling. *J. Food Eng.*, 33(3-4), 385-393. doi:[http://dx.doi.org/10.1016/S0260-8774\(97\)00037-X](http://dx.doi.org/10.1016/S0260-8774(97)00037-X)

Lorestani A. N., Rabani R. H. and Khazaei Y. 2012. Design and construction of an automatic coefficient of friction measuring device. *Agric Eng Int: CIGR J* 2012;14 (1):120–4.

Masoumi, A. A. and Tabil, L. G. 2003. Physical properties of chickpea (*C. arietinum*) cultivars. An ASAE Meeting presentation, Las Vegas, Nevada, 27–30 July, 2003, USA. Paper No: 036058.

Reşat Esgici, F. Göksel Pekitkan, Emin Güzel, Abdullah Sessiz “Friction Coefficients For Gundelia Tournefortii Seed on Various Surfaces”



CIGR 2018

XIX. World Congress of CIGR



- Mir, S. A., Bosco, S. J. D. and Sunooj, K. V. 2013. Evaluation of physical properties of rice cultivars grown in the temperate region of India International Food Research Journal 20(4): 1521-1527
- Mohsenin, N. N. 1986. Physical properties of plant and animals materials (2nd ed.). New York, NY: Gordon and Breach Science Publishers.
- Ndukwu, C. and Ejirika, C. 2016. Physical properties of wild Persian walnut (*Juglans regia* L.) from Nigeria Cogent Food & Agriculture (2016), 2: 1232849
- Nesvadba, N., Houska, M., Wolf, W., Gekas, V., Jarvis, D. and Sadd, P. A. 2004. Database of physical properties of agro-food materials. Journal of Food Engineering, 61, 497–503.
- Nwakonobi, T. U. and Onwualu, A. P. 2009. Effect of moisture content and types of structural surfaces on coefficient of friction of two Nigerian food grains: sorghum (*Sorghum bicolor*) and millet (*Pennisetum glaucum*)". XI(Manuscript 1152).
- Nyendu, G. C., Pflum, S., Schumacher, P., Bern, C. J. and Brumm, T. J. 2014. Friction Coefficients For Dried Distillers Grains On Eight Structural Surfaces. Applied Engineering in Agriculture 30 (2014): 673–678, doi:10.13031/aea.30.10453.
- Obi, O. F. and Offorha, L. C. 2015. Moisture-dependent physical properties of melon (*Citrullus colocynthis* L.) seed and kernel relevant in bulk handling, Cogent Food & Agriculture (2015), 1: 1020743
- Özlü, R. R. and Güner, M. 2016. Determination of the Physical Properties of the Canola Seeds in Different Moisture Content Levels. JAFAG, ISSN: 1300-291, E-ISSN: 2147-8848,10-24
- Öztürk, R. and Sabahoğlu, Y. 1994. Biyolojik malzemelerin sürtünme katsayılarının belirlenmesine ilişkin yöntemlerin değerlendirilmesi. Tarımsal Mekanizasyon 15. Ulusal Kongresi Bildiri Kitabı, S.353-362. Antalya.
- Pradhan, R. C., Naik, S. N., Bhatnagar, N. and Vijay, V. K. 2009. Moisture-dependent physical properties of jatropha fruit. Ind. Crops and Products, 29(2-3), 341-347. doi:http://dx.doi.org/10.1016/j.indcrop.2008.07.002
- Puchalski, C., Brusewitz, G. H. and Ślipek, Z. 2003. Coefficients of friction for apple on various surfaces as affected by velocity. Agricultural Engineering International: the CIGR Journal of Scientific Research and Development". Manuscript FP 03 002. Vol. V. December 2003.
- Sabahoğlu, Y. and Öztürk, R. 1996. Bazı Buğday Çeşitlerinin Sürtünme Katsayılarının Belirlenmesi. 6th. International congress on Agricultural Mechanization and Energy.
- Sacilik, K., Öztürk, R. and Keskin, R. 2003. Some physical properties of hemp seed. Biosyst. Eng., 86(2), 191-198. doi:http://dx.doi.org/10.1016/S1537-5110(03)00130-2
- Seifi, M. R. and Alimardani, R. 2010. The Moisture Content Effect on Some Physical and Mechanical Properties of Corn (Sc 704). www.ccsenet.org/jas Journal of Agricultural Science Vol. 2, No. 4; December 2010



CIGR 2018

XIX. World Congress of CIGR



Sessiz, A. 2005. Physical properties of some green olive cultivars. Proceedings of the International Congress on Mechanization and Energy in Agriculture & 27th International Conference of CIGR Section IV: The Efficient Use of Electricity and Renewable Energy Sources in Agriculture, Sep.27-29,2005, İzmir-TURKEY

Sessiz, A., Esgici, R. and Kızıl, S. 2007. Moisture-dependent physical properties of caper (Capparis Ssp) Fruit. Journal of Food Engineering, 79,1426-1431. Elsevier, London.

Shafaei, S. M. and Kamgar, S. 2017. A comprehensive investigation on static and dynamic friction coefficients of wheat grain with the adoption of statistical analysis. Journal of Advanced Research 8 (2017) 351–361

Shinners, K. J., Koegel, R. G. and Lehman, L. L. 1991. Friction Coefficient of Alfalfa. ASAE. Vol.34(1), 33-37.

Sologubik, C. A., Campanonec, L. A., Paganob, A. M. and Gely, M. C. 2013. Effect of moisture content on some physical properties of barley. Industrial Crops and Products 43 (2013) 762– 767

Subramanian, S. and Viswanathan, R. 2007. Bulk density and friction coefficients of selected minor millet grains and flours. J.Food Eng., 81(1), 118-126.

Tavakoli, H., Rajabipour, A. and Mohtasebi, S. S. 2009. Moisture-dependent some engineering properties of soybean grains. Agric. Eng. Int. CIGRE J. XI

Usrey, L. J., Walker, J. T. and Loewer, O. J. 1992. Physical characteristics of rice straw for harvesting simulation. Transactions of the ASAE, 1992.

Visvanathan, R., Palanisamy, P. T., Gothandapani, L. and Sreenarayanan, V. V. 1996. Physical properties of neem nut. J. Agric. Eng. Res. 63 (1), 19–25.

Zaalouk K. and Zabady, F. I. 2009. Effect of moisture content on angle of repose and friction coefficient of wheat grain. 77th J. Ag. Eng., 26(1): 418-427 Process Engineering.



CIGR 2018

XIX. World Congress of CIGR



Determination of Leaf Breaking Strength of Variety Candidates of Common Vetch

Mehmet OTEN^{1*} Onder KABAS²

¹Batı Akdeniz Agricultural Research Institute, 07100, Antalya, Turkey

²Akdeniz University, Vocational School of Technical Sciences, 07070, Antalya, Turkey
moten07@hotmail.com

ABSTRACT

The study was conducted to determine whether there is a difference in leaf breaking strength between candidates variety of common vetch in order to minimize leaf breaks which causes over large loss in common vetch forage production. The experiment was carried out at the Bati Akdeniz Agricultural Research Institute, at Department of Field Crop during 2017-2018 season. The experiment was established by randomized complete block design. Breaking strength of the leaves and leaflet were measured using a universal testing machine. Measurements were made of with 10 plants for each replication, on 3 leaflet on the fourth leaf on the main stem belongs to 4 different from variety candidates of common vetch. In addition, the thickness of the leaf stalk diameter, stalk cross-sectional areas, stalk of rupture energy, rupture stress is calculated. As a result of the experiment, wide variation among candidates of common vetch was determined. Batem3 and Batem4 candidates varieties had the least yield lose during the harvest. It can be said that the determination of the rupture strength between variety candidates is important for decrease yield loss.

Key Words: Common vetch; Breaking strength; Mechanical properties; Turkey

INTRODUCTION

Common vetch (*Vicia sativa* L.) is cultivated under rainfed conditions in the semi-arid regions of Turkey and other Mediterranean regions (Icarda, 1998). Vetches (*Vicia* spp.) are legumes and they well adapted to winter growth in the Mediterranean environments (Abd El Moneim et al., 1988; Acikgoz, 2001). Turkey's West Mediterranean region has very suitable ecological conditions in winter for annual forage production in crop rotation. Common vetch is used as a cover crop, green manure, pasture, silage, and hay. Its high dry matter and nitrogen accumulation, make it an excellent winter leguminous cover crop. When planted alone, it can provide substantial amounts of N to the following crop. It can reach 60-150 cm height when planted alone. It can be taller when planted with a tall companion crop that provides structural support for climbing to the vetch. However, it's stems are thin, branched, and usually smooth. Leaves are composed of 4 to 10 paired leaflets, terminate with a tendril, and usually their surface smooth. Because of having weak and thin stem, the vetches can spread on the ground. This lead to the difficulties on the harvest losses on the yield and decreases on the forage quality (Anlarsal and Yucel, 1995). In their study, Oten et al.(2018), reported that there were wide variation among genotypes in terms of rupture resistans and the

M. Oten, O. Kabas "Determination of Leaf Breaking Strength of Variety Candidates of Common Vetch"



CIGR 2018

XIX. World Congress of CIGR



rupture strength can be used as a selection criteria in alfalfa which another feed crop. The objective of this study was to determine some physical-mechanical properties for breaking strength of four candidates variety.

MATERIALS AND METHODS

Location, Climate Data and The Soil of The Experimental Sites

This study conducted in Batı Akdeniz Agricultural Research Institute (BATEM) in Aksu Antalya. Some properties of the trial area soil were given in Table 1. According to test results; the soil is saltless, high calcareous, clayey, strong alcali and low organic matter content.

Table 1. Some physical and chemical characteristics of the soils of the experimental sites

pH	8.3	Strong alkaline
Lime (%)	24.7	Very hight
EC (mikromhos)	190.0	Saltless
Silica (%)	14.0	
Clay (%)	45.0	
Alluvion (%)	44.0	
Organic matter (%)	1.7	Low

* BATEM, 2018

Monthly average, minimum and maximum temperatures, monthly total rainfall and monthly relative humidity for each year were given in Table 2. Lower precipitation has occurred than the average long period. The maximum temperature value is high while the minimum temperature values are low.

Table 2. Climate Data (Long Period-2012-2015)

Year	Climate element	2017				Month				2018			
		IX	X	XI	XII	I	II	III	IV				
2017-2018	Precipitation (mm)	234.0	122.0	56.0	41.0	74.0	4.0	0.0	0.0				
	Relative humidity (%)	67.0	62.6	58.6	72.2	71.0	66.6	60.3	52.4				
	Average temperature (°C)	8.9	9.2	12.5	16.7	20.5	26.0	29.4	29.1				
	Maximum temperature (°C)	17.9	20.3	25.7	33.0	34.9	43.2	43.4	41.2				
	Minimum temperature (°C)	1.1	0.3	0.9	6.7	13.1	14.0	17.7	16.7				
Long Period	Precipitation (mm)	224.9	156.30	96.20	58.30	31.80	7.90	3.00	2.40				
	Relative humidity (%)	9.80	10.40	12.70	16.10	20.50	25.40	28.40	28.20				
	Average temperature (°C)	15.00	15.50	18.00	21.30	25.60	30.90	34.10	34.20				
	Maximum temperature (°C)	5.90	6.20	8.00	11.10	15.00	19.60	22.60	22.60				

Material and The Experimental Design

Four candidate variety of common vetch (*Vicia sativa* L.) were used as plant materials in this study. Measurements were made with 10 plants for each replication, on 3 leaflets on the fourth leaf on the main stem belongs to 4 different variety candidates of common vetch. In

M. Oten, O. Kabas “Determination of Leaf Breaking Strength of Variety Candidates of Common Vetch”



CIGR 2018

XIX. World Congress of CIGR



addition, the thickness of the leaf stalk, stalk cross-sectional areas, rupture energy and rupture stress of leaf and leaflet were calculated. Leaf break strength was calculated in ten plants randomly selected from each replications in the trial area. Leaf and leaflet breaking strength were investigated at 12.8% moisture content. Determination of strength of leaves from stem was used texture analyzer that it has rates of 10 Hz data sampling and has a load cell with a capacity of 1000 N (Figure 1). The device was calibrated in accordance with the calibration template before analysis. The sensitivity and solubility of the used texture analyzer is 0.1 mm. The leaves were fixed to the device in a simple manner. When the leaf was ruptured, the value was detected as a breaking strength and saved to computer. Force-deformation graphs were created with the help of the obtained data (Figure 2). The area under the force deformation graph gives the rupture energy. Measurements of leaf breaking strength in each candidate varieties were made separately on plant samples. For determining of leaf breaking strength was used 8 mm min⁻¹ drawing speed (ASAE, 2009). Data were analyzed by using the SAS packet program. The differences between means were separated by multiple range test of Duncan (Duzgunes et al., 1987).

3.RESULTS AND DISCUSSION

Variance analysis of observational values in candidate varieties of common vetch given were Table 3. Leaf breaking strength, leaflet breaking strength, stalk diameter, stalk cross-sectional areas, rupture stress of leaf, rupture stress of leaflet, rupture energy leaf and rupture energy leaflet of common vetch candidates varieties given were Table 4.

Table 1. Variance analysis of observational values

Variations Source	DF	Sum of Squares							
		Leaf Breaking Strength (N)	Leaflet Breaking Strength (N)	Stalk Diameter (mm)	Stalk cross- sectional Areas (mm ²)	Rupture Stress of Leaf (Nmm ⁻²)	Rupture Stress of Leaflet (Nmm ⁻²)	Rupture Energy of Leaf (Nmm)	Rupture Energy of Leaflet (Nmm)
Variety	3	11.16**	1.27**	9.31**	426.97**	0.11**	0.01**	32.25**	3.67**
Time	1	1.59**	2.53**	2.66**	126.89**	0.02*	0.03**	4.62**	7.32**
Variety*Time	3	22.34**	0.68**	0.67 ^{ns}	45.75*	0.18**	0.007**	64.57**	1.96**
Error	16	0.65	0.1	1.46	64.45	0.05	0.002	1.89	0.3

*, $P \leq 0.05$; **, $P \leq 0.01$; ns, nonsignificant

According to variance analysis, there were statistically significant ($P < 0.01$) differences among varieties and time. Also all interaction (varieties*time) were found statistically significant ($P < 0.01$) except stalk diameter character. The significance of the interactions remarks that according to the vegetation stage, the rupture strength values showed differences between varieties. It is an expected result to have higher rupture strength values with vegetation stage. The highest leaf breaking strength were measured at Batem3 and Batem4, 4.84 N and 4.50 N respectively in 50% flowering time. The lowest leaf breaking strength were measured at Batem1 in 50% flowering time and Batem3-Batem4 in 10% flowering time. It was detected higher breaking strength at the time of flowering 50% than 10% flowering time. Leaflet breaking strength ranged from 0.39 to 1.66 N, depending on the candidates varieties of common vetch. The highest leaflet breaking strength was obtained from Batem3 in 10% flowering time, while the lowest leaflet breaking strength was obtained from candidates variety of Batem4 in 50% flowering time. There was no significant difference in varieties*time interaction with regard to the stalk diameter trait, however the variation in



CIGR 2018

XIX. World Congress of CIGR



candidates varieties were statistically significant ($P < 0.01$). While Batem2, Batem3 in the same group, Batem1 and Batem4 were in the other group. It is also in terms of stalk diameter among the years showed great differences. The candidates varieties with the highest stalk cross-sectional areas were determined in Batem3 in 50% flowering time. Because of vegetative development, the stalk cross-sectional area was higher at the second observation time. The highest rupture stress of leaf were determined in 10% flowering time in Batem1 and 50% flowering time in Batem4, both of them were same statistical group. The highest rupture stress of leaflet were determined in Batem1, Batem3 and Batem4 in 10% flowering time, it is possible to conclude that 10% flowering time was higher than the 50% flowering time for rupture stress. While the lowest rupture energy of leaf were determined in Batem1 in 50% flowering time and in Batem4 in 10% flowering time, the highest rupture energy of leaf were determined in 50% flowering time in Batem3 and Batem4, in 10% flowering time in Batem1. The rupture energy of leaflet ranged from 0.67 to 2.82 Nmm, depending on the candidates varieties of common vetch. The highest rupture energy of leaflet was obtained from Batem3 in 10% flowering time, while the lowest rupture energy of leaflet was obtained from candidates variety of Batem4 in 50% flowering time.

Table 4. Breaking strength, stalk diameter, stalk cross-sectional area, rupture stress and energy in leaf and leaflet of candidates common vetch.

Time	Varieties	Investigated traits							
		Leaf Breaking Strength (N)	Leaflet Breaking Strength (N)	Stalk Diameter (mm)	Stalk cross-sectional areas (mm ²)	Rupture Stress of Leaf (Nmm ⁻²)	Rupture Stress of Leaflet (Nmm ⁻²)	Rupture Energy of Leaf (Nmm)	Rupture Energy of Leaflet (Nmm)
Time to 10 % flowering	Batem1	4.16 bc	1.32 b	3.37	8.99 d	0.48 a	0.151 a	7.08 ab	2.25 b
	Batem2	1.95 e	0.58 cd	4.74	17.46 bc	0.11 c	0.034 bc	3.31 d	0.99 cd
	Batem3	3.71 c	1.66 a	4.25	14.21 cd	0.26 bc	0.117 a	6.31 c	2.82 a
	Batem4	1.91 e	1.13 b	3.44	9.36 d	0.20 bc	0.123 a	3.25 e	1.92 b
Time to 50 % flowering	Batem1	1.95 e	0.63 cd	3.69	10.75 d	0.14 c	0.058 b	2.57 e	1.07 c
	Batem2	2.94 d	0.46 cd	5.15	20.91 ab	0.14 c	0.026 c	5.00 d	0.79 cd
	Batem3	4.84 a	0.61 cd	5.45	23.36 a	0.20 bc	0.026 bc	8.23 a	1.03 cd
	Batem4	4.50 ab	0.39 d	4.12	13.38 cd	0.33 ab	0.029 bc	7.65 ab	0.67 d
CV (%)		6.32	9.49	7.07	13.55	24.02	16.96	6.32	9.51

Means with different letters in the same column are significantly different ($P < 0.01$)



Figure 1. Teksture analyzer

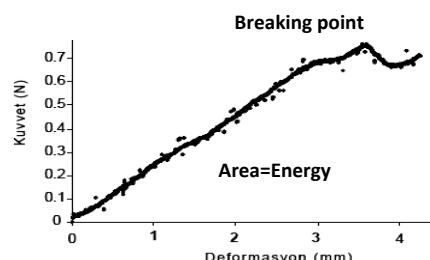


Figure 2. Force deformation graph

Some physical-mechanical properties as breaking strength, stalk diameter, stalk cross-sectional area, rupture stress and rupture energy in leaf and leaflet on different plant have been carried out by some researchers that Ince et al., (2005) (in sunflower),

M. Oten, O. Kabas “Determination of Leaf Breaking Strength of Variety Candidates of Common Vetch”



CIGR 2018

XIX. World Congress of CIGR



Yılmaz and Gokduman, (2014a) (in thymus), Yılmaz and Gokduman, (2014b) (in lavender), Yılmaz and Gokduman, (2015) (in *Salvia officinalis*) and Oten et al. (2018) (in alfalfa). Because of studies were carried out on different plant species, results have been found in different from our results.

CONCLUSION

Due to the weak nature of common vetch, leave losses during harvest lead to yield losses therefore it is important to develop varieties with high breaking strength. In the experiment which aimed to reveal the differences in breaking strength among the newly developed four varieties and also some physical-mechanical properties were determined. According to the data obtained from this research, it was found that differences among four candidates varieties statistically significant. Batem3 and Batem4 candidates common vetch varieties had the least yield loss during the harvest. It can be said that Batem3 and Batem4 candidates varieties which will be presented to the registry will suffer less efficiency loss during harvest.

REFERENCES

- Abd El Moneim, A.M., Cocks P.S. & Swedan, Y. (1988). Yield stability of selected forage vetches (*Vicia* spp.) under rain fed conditions in West Asia. *Journal of Agriculture Science*, 111: 295-301.
- Acikgoz, E., (2001). Feed Crops. U.U. Empowerment Foundation Publications No: 182, 584 pp., Bursa.
- Anlarsal, A. E. & Yucel, C. (1995). Determining the most suitable seeding rates and cutting times of fieldpea-triticale mixtures under lowland conditions. *Agr. Med.*, 124: 207-212.
- ASAE, (2009). Compression test of food materials of convex shape. ASAE S368.4 DEC 2000 (R2008). American Society of Agricultural and Biological Engineers, St. Joseph, Michigan, USA, pp. 678- 686.
- Duzgunes, O., Kesici, T., Kavuncu, O. & Gurbuz, F. (1987). Research and Trial Methods. Ankara University Publication of Faculty of Agriculture 1021. P. No:295, Ankara
- Icarda, 1998. Annual Report. International center for agricultural research in the dry areas, Aleppo, Syria.
- Ince, A., Ugurluay, S., Guzel, E., & Ozcan. M.T. (2005). Bending and shearing characteristic of sunflower stalk residue. *Biosystems Engineering*, 92(2):175-181.
- Oten, M., Kabas, O. & Kiremitci, S. (2018). Determination of leaf breaking strength in some clover genotypes collected from Antalya natural flora. *Derim*, 2018/35(1) doi:10.16882/derim.2018.339204.
- SAS, (1998). INC SAS/STAT users' guide release 7.0, Cary, NC, USA.



CIGR 2018

XIX. World Congress of CIGR



Yılmaz, D. & Gokduman, M.E. (2014a). Physicalmechanical properties of Origanum onites at different moisture contents. *Journal of Essential Oil Bearing Plants*, 17(5):1023-1033.

Yılmaz, D. & Gokduman, M.E. (2014b). Effect of moisture contents on physical-mechanical properties of lavender (Lavandula X Intermedia Emeric Ex Loisel.). *Journal of Essential Oil Bearing Plants*, 17(6):1224-1232.

Yılmaz, D. & Gokduman, M.E. (2015). Determination of physicalmechanical properties of (*Salvia officinalis* L.)at different moisture contents. *Suleyman Demirel University Journal of Faculty of Agriculture*, 10(1):73-82.



CIGR 2018

XIX. World Congress of CIGR



Impact of Tillage Practices on Selected Soil Physico-Chemical and Biological Conditions, and Maize Yield in Latosolic Red Soil of southern China

Evans Asenso¹, Lian Hu², Fuseini Issaka³, Kai Tian¹, Lina Zhang¹, Luyong Zhang¹, Jiefeng Zeng¹, Yan-Fei Zhu¹, Jiuhao Li^{1*}

¹College of Water Conservancy and Civil Engineering, South China Agricultural University, Guangdong 510642, China.

²College of Engineering, South China Agricultural University, Guangdong 510642, China.

³College of Natural Resource and Environment, South China Agricultural University, Guangdong 510642, China.

* Corresponding author: Li Jiuhao, E-mail: jhli@scau.edu.cn, Tel: +86-13602879798

ABSTRACT

Tillage practices influence physical, chemical and biological properties of the soil and have a major impact on soil productivity and sustainability. This study was conducted to determine the effects of different tillage practices on soil physico-chemical and biological conditions, and the impact of such tillage practices on maize yield on a middle term (7 years) consistent tillage practice typical latosolic red soil of southern China. Subsoiling (SS), two passes of rotary tillage (2RT), subsoiling + two passes of rotary tillage (SS+2RT) and zero tillage (ZT) were studied in a randomized complete block design with three replications. After two years field experiment in 2016 and 2017, tillage practices showed positive effects on soil properties and maize yield. The highest soil physical properties, soil organic matter (SOM) and nutrient levels in their available form N and P as well as exchangeable K were recorded in the ZT. Subsequently, analysis of soil microbial levels showed that ZT recorded the highest levels of bacterial and actinomycetes at the soil depth of 0-40 cm, whilst SS increased fungal levels in the soil depth of 0-40 cm. The mean highest grain yield (7.37 ton ha⁻¹) was recorded under SS, while the lowest (6.73 ton ha⁻¹) under ZT. The results suggest that SS was more suitable for achieving higher yield in latosolic red soil resulting in a sustainable agricultural system.

Keywords: Tillage, Bulk Density, SOM, Microbial Count, Maize Yield, Southern China

INTRODUCTION

Holistic management of arable soil is the key to dealing with the most intricate, dynamic and interrelated soil properties, thereby upholding sustainable agricultural production systems.

E Asenso, L Hu, F Issaka, K Tian, L Zhang, L Zhang, J Zeng, Y-F Zhu, J Li*. "Impact of tillage practices on selected soil physico-chemical and biological conditions and maize yield in latosolic red soil of Southern China".



CIGR 2018

XIX. World Congress of CIGR



Any soil management practice that changes the heterogeneous body may result in detrimental upshots (Derpsch et al., 2010; Wolfarth et al., 2011). Inappropriate management practices cause depletion of organic matter and other nutrients as well as deterioration in crop output (Ramos et al., 2011). Tumbling uproar of soil by reduced tillage influences several physical properties (López-Garrido et al., 2012), chemical properties (Page et al., 1989), and biological properties (Bronick and Lal, 2005; Muñoz et al., 2007) of the natural soil body.

Soil tillage is among the significant factors affecting soil properties and crop yield. Among the crop production factors, tillage contributes up to 20% (Khurshi et al., 2006) and affects the sustainable use of soil resources through its influence on soil properties (Lal and Stewart, 2013).

The proper use of tillage practices can improve soil related constraints, while improper tillage may cause a range of undesirable processes, e.g. soil structure destruction, accelerated erosion, loss of organic matter and fertility, and disruption in cycles of water, organic carbon, and plant nutrients (Lal, 1993). Use of excessive and unnecessary tillage operations is often harmful to soil. Therefore, currently there is significant interest and emphasis on the shift to the conservation tillage and no-tillage method for the purpose of controlling erosion process (Iqbal et al., 2005). Conventional tillage practices modify soil structure by changing its physical properties such bulk density (Wander et al., 1998; Grant and Lafond, 1993), soil penetration resistance (Grant and Lafond, 1993), soil moisture content (Rashidi, 2008) and water holding capacity (Trojan and Linden, 1998). Annual disturbance and pulverization caused by conventional tillage gives birth to a finer and loose soil structure compared to conservation and no-tillage method which leave the soil intact (Rashidi, 2008). The change of number, shape, continuity and size distribution of pore network controls the ability of soil to store and transmit air, water and agricultural chemicals and, thus, in turn, regulates erosion, runoff, and crop performance (Khan et al., 2001). Soil physico-chemical and biological characteristics are influenced by tillage practice, which in turn alter plant growth and yield (Wasaya et al., 2011). Reducing tillage positively influences several aspects of the soil whereas excessive tillage practices give rise to other phenomena that are harmful to soil.

Thus, the objectives of this study were to determine the impact of subsoiling (SS), two passes of rotary tillage (2RT), two passes of rotary tillage + subsoiling (2RTSS) and zero tillage (ZT) on (a) soil physical properties and the distribution of chemical and biological conditions in 0-40 cm soil depth and (b) maize yield in a typical latosolic red soil of southern China.

2. MATERIALS AND METHOD

2.1.1. Study Site description

A field experiment was conducted for 2 consecutive years (2016-2017) on a middle term (7 years) consistence tillage practice farm of Wufengtai Agricultural Investment Co. Ltd., which was located in Heyuan City (24⁰09'N, 114⁰23'E and 121m above sea level) Lianping County,

E Asenso, L Hu, F Issaka, K Tian, L Zhang, L Zhang, J Zeng, Y-F Zhu, J Li*. "Impact of tillage practices on selected soil physico-chemical and biological conditions and maize yield in latosolic red soil of Southern China".



CIGR 2018

XIX. World Congress of CIGR



Guangdong Province, China. The research station was characterized by a central sub-tropical monsoon climate with an annual mean temperature and precipitation of 1779.7 mm and 19.5 °C respectively. The site also had an annual humidity of 79% which occurred in May, June and July. The field experiment was conducted on a level terrain with red latosolic soil which is a typical soil type in the Province, and it is classified as a sandy-loam soil based on the FAO/UNESCO soil classification systems (FAO, 1993). This acidic soil had a particle size distribution of sand 57.9%, silt 18.7%, Clay 23.4% with an average profile acidity of pH 4.73. The soil had a bulk density of 1.38 g cm⁻³, soil penetration resistance 2.12 MPa and porosity of 46.15 %. The soil conditions at the soil depth of 0-40 cm before the start of the experiment are shown in Table 1. The weather data were recorded from a standard weather station at the experimental site.

2.1.2. Experimental design and treatments

In this study, a randomized complete block design with three replications in 1.5 m wide by 100 m long plot were used. The four soil tillage practices (treatments); two passes of rotary tillage (2RT), subsoiling (SS), two passes of rotary tillage + subsoiling (2RTSS) and zero tillage (ZT) were applied to the experimental plots in 2016 and 2017. The hybrid maize (Yue Tian 26) was sown at a spacing of 0.3 m within rows and 0.5 m between rows of 44,400 plant ha⁻¹ population density by a 2BMQE-2A seeder. All in-crop fertilizer of NPK was applied at planting (N: 220 kg ha⁻¹, P: 80 kg ha⁻¹ and K: 150 kg ha⁻¹).

2.2 Measured parameters

2.2.1. Bulk density

Soil bulk density was used as a significant indicator of changes in soil structure and water retention capacity (Arshad et al., 1999) and was progressively determined from 50 mm diameter sampler cores to a depth of 40 cm (Blake, 1965). The soil was measured from undisturbed soil cores collected from four depths (0-10 cm, 10-20 cm, 20-30 cm, 30-40 cm). Soil cores were weighed wet, dried in an oven at 105 °C for 48 h, and weighed again to determine the soil water content and bulk density (Ferraro and Ghersa, 2007). Gravimetric water content was multiplied by soil bulk density to obtain the volumetric water content. Soil porosity was then calculated from the bulk density as

$$\text{Total porosity} = \left(1 - \frac{\rho_b}{\rho_s}\right)$$

where ρ_b is the bulk density and ρ_s is the average particle density (2.65 g cm⁻³).

A FIELDSCOUT, SC 900 Soil Compaction Meter (Spectrum Technologies, Inc) was used in measuring the soil penetration resistance.

E Asenso, L Hu, F Issaka, K Tian, L Zhang, L Zhang, J Zeng, Y-F Zhu, J Li*. "Impact of tillage practices on selected soil physico-chemical and biological conditions and maize yield in latosolic red soil of Southern China".



Table 1. Basic soil condition of the experimental site

Soil characteristics	Values
pH	4.73
SOM (g kg ⁻¹)	21.13
Available N (mg kg ⁻¹)	105.75
Available P (mg kg ⁻¹)	68.05
Exchangeable K (mg kg ⁻¹)	185.26
Bacterial (×10 ⁵ cfu g ⁻¹ dry soil)	1.13
Actinomycetes (×10 ⁴ cfu g ⁻¹ dry soil)	1.65
Fungi (×10 ³ cfu g ⁻¹ dry soil)	1.06

2.2.2 Soil pH, SOM, available N and P and exchangeable K determination

Soil pH was determined by the potentiometric method, SOM was determined by the volumetric method of oil bath-heated potassium dichromate oxidation, soil available N was determined by the decomposition diffusion method, soil available P was determined by the hydrochloric acid-ammonium or fluoride extraction-molybdenum anti-colorimetric method and soil exchangeable K was determined by the ammonium acetate extraction-flame atomic absorption spectrophotometer method as all described (Bao, 2000).

2.2.3. Bacteria, fungi and actinomycetes determination

The soil samples were soaked into 90 ml deionized water at the rate of 10 g, later this mixture was shaken for 10 minutes and kept for 5 minutes. Thereafter, 1 ml of the supernatant was diluted twice and inoculated in a diluted water at the constant temperature of 30 °C. All samples were performed in triplicate, and were used for enumeration of bacteria, actinomycete and fungal count. The viable microbial counts were analyzed by the standard technique of serial dilution and pour plating. Enumeration of bacteria and fungi was carried out in soil extract agar medium (Parkinson et al., 1971). The Kenknight's Agar medium was used for the enumeration of actinomycetes (Wellington and Toth, 1963). After allowing for the development of discrete microbial colonies during incubation under suitable conditions, the colonies were counted and the number of viable bacteria, fungi and actinomycetes [expressed as colony forming units (cfu)] per gram dry weight soil was estimated by taking into account the soil dilutions.

2.3. Maize yield determination

Maize yield was determined from ten randomly selected from each of the replicated treatments by manual harvesting, threshing and air-drying of the grain to 13.5% moisture content.

2.4. Statistical analysis

Analysis of variance for the measured parameters were performed using IBM SPSS 23.0 and treatments means were compared using Duncan's multiple range test (DMRT) at 5% probability level.

E Asenso, L Hu, F Issaka, K Tian, L Zhang, L Zhang, J Zeng, Y-F Zhu, J Li*. "Impact of tillage practices on selected soil physico-chemical and biological conditions and maize yield in latosolic red soil of Southern China".



CIGR 2018

XIX. World Congress of CIGR



3. RESULTS

3.1. Soil bulk density and soil porosity

The soil bulk density of different tillage practices increased significantly when compared to the initial data (Table 2). Before the start of the experiment, the mean bulk density in the tilth (0-40cm) was 1.38 g cm^{-3} . After the two-year experiment, the soil bulk density at the soil depth of 0-40 cm under 2RT, SS, 2RTSS and ZT increased by 5.07%, 2.17%, 4.35% and 7.79% respectively. The bulk density of 2RT, SS and 2RTSS significantly decreased at the soil depth of 0-20 cm compared to the ZT, while at 20-40 cm there was a high significant difference when compared to SS ($P < 0.05$).

The soil porosity of different tillage practices increased significantly under SS and 2RTSS and also decreased significantly under 2RT and ZT compared to the initial data (Table 2). Before the experiment, the mean soil porosity in the tilth (0-40 cm) was 46.15%. After the two-year experiment, soil porosity under SS and 2RTSS increased by 2.62% and 0.87% respectively, however, 2RT and ZT decreased significantly by 0.38% and 3.38% respectively at the soil depth of 0-40 cm. The soil porosity of SS, 2RTSS and 2RT significantly increased compared to ZT at the soil depth of 0-20 cm, while at 20-40 cm there was a high significant reduction under ZT, 2RT and 2RTSS compared to SS ($P < 0.05$).

Table 2. Mean soil bulk density and porosity at the soil depth of 0-40 cm

Soil depth (cm)	Soil bulk density (g cm^{-3})				Soil porosity (%)			
	2RT	SS	2RTSS	ZT	2RT	SS	2RTSS	ZT
0-10	1.26b	1.23d	1.25c	1.30a	52.99c	54.29a	53.36b	51.86d
10-20	1.39b	1.34d	1.37c	1.50a	48.14c	49.88a	48.88b	44.22d
20-30	1.57a	1.54b	1.57a	1.57a	41.61c	42.73a	41.98b	41.42c
30-40	1.57b	1.54d	1.56c	1.58a	41.61c	42.54a	41.98b	41.05d

2RT: two passes of rotary tillage, 2RTSS: two passes of rotary tillage + subsoil, SS: subsoiling, ZT: zero tillage.
Means followed by different letters within the same column are significantly different at $P < 0.05$.

3.2. Soil chemical condition

The soil pH of SS, 2RTSS and 2RT increased by a small, but statistically significant margin (1.06%, 0.85% and 0.63%) respectively at the soil depth of 0-40 cm in comparison to that of 0.21% under ZT (Table 3) compared to the initial data. The soil pH of SS, 2RT and ZT significantly increased compared to 2RTSS at the soil depth of 0-20 cm, while at 20-40 cm there was a high significant reduction under ZT compared to 2RT, SS and 2RTSS ($P < 0.05$).

Tillage practices on ZT resulted in significantly higher ($P < 0.05$) increase in SOM in the measured soil profile (0-40 cm) as shown in Table 3, compared to the initial data. There was a

E Asenso, L Hu, F Issaka, K Tian, L Zhang, L Zhang, J Zeng, Y-F Zhu, J Li*. "Impact of tillage practices on selected soil physico-chemical and biological conditions and maize yield in latosolic red soil of Southern China".



CIGR 2018

XIX. World Congress of CIGR



significant increase of 4.45% SOM in the 0-40 cm soil depth under the ZT compared to a significant reduction of 14.71%, 6.77% and 4.04% under 2RTSS, 2RT and SS respectively. The SOM of ZT, 2RT and SS had higher significant increase (24.14%, 13.58% and 13.58% respectively) compared to 7.52% under 2RTSS at the soil depth of 0-20 cm, while there was a higher significant reduction (49.54%, 35.71% and 27.21%) under 2RTSS, 2RT and SS as compared to 17.92% under ZT at the 20-40 cm soil depth.

ZT resulted in significantly higher ($P < 0.05$) increase in soil available N in the measured soil profile (0-40 cm) as shown in Table 3, compared to the initial data. There was a significant increase of 11.83%, 2.43% and 1.37% soil available N in the 0-40 cm soil depth under the ZT, 2RT and SS compared to a significant reduction of 3.63% under 2RSST respectively. The soil available N of ZT had higher significant increase compared to 2RT, 2RTSS and SS at the soil depth of 0-20 cm, while there was a higher significant reduction (46.65%, 30.93%, 30.51% and 14.08%) under 2RTSS, 2RT, SS and ZT at the 20-40 cm soil depth respectively.

Tillage practice on ZT resulted in significantly higher ($P < 0.05$) increase in soil available P in the measured soil profile (0-40 cm) as shown in Table 3, compared to the initial data. There was a significant increase of 18.15%, 5.82% and 4.26% soil available P in the 0-40 cm soil depth under the ZT, SS and 2RT respectively compared to higher significant reduction of 22.75% under 2RTSS. The soil available P of ZT had higher significant increase compared to SS, 2RT and 2RTSS at the soil depth of 0-20 cm, while there was a higher significant reduction of SAP at the 20-40 cm soil depth in the order of ZT>2RT>SS>2RTSS.

ZT resulted in significantly higher ($P < 0.05$) increase in soil exchangeable K in the measured soil profile (0-40 cm) as shown in Table 3, compared to the initial data. There was a significant increase of 13.04% and 1.90% soil exchangeable K in the 0-40 cm soil depth under the ZT and 2RT compared to a significant reduction of 6.17% and 5.05% under 2RSST and SS respectively. The soil exchangeable K of ZT had higher significant increase compared to 2RTSS, 2RT and SS at the soil depth of 0-20 cm, while there was a higher significant reduction (62.81%, 46.35%, 29.74% and 16.88%) under 2RTSS, SS, 2RT and ZT at the 20-40 cm soil depth respectively.

E Asenso, L Hu, F Issaka, K Tian, L Zhang, L Zhang, J Zeng, Y-F Zhu, J Li*. "Impact of tillage practices on selected soil physico-chemical and biological conditions and maize yield in latosolic red soil of Southern China".



CIGR 2018

XIX. World Congress of CIGR



Table 3. Mean soil chemical condition for 2RT, 2RTSS, SS and ZT treatment

Soil depth (cm)	pH				SOM (g kg ⁻¹)				Available N (mg kg ⁻¹)				Available P (mg kg ⁻¹)				Exchangeable K (mg kg ⁻¹)			
	2RT	SS	2RTSS	ZT	2RT	SS	2RTSS	ZT	2RT	SS	2RTSS	ZT	2RT	SS	2RTSS	ZT	2RT	SS	2RTSS	ZT
0-10	4.81ab	4.82a	4.80 ab	4.79b	26.43b	26.76ab	24.83c	29.13a	154.04b	150.07c	148.76d	161.48a	183.95b	176.83c	139.45d	202.69a	275.81c	283.62b	276.43c	295.31a
10-20	4.80b	4.81a	4.79b	4.78c	21.58a	21.24a	20.60a	23.32a	117.72b	116.74b	115.22b	126.22a	60.58c	74.11c	45.79d	77.62a	193.73b	169.86c	194.01b	222.34a
20-30	4.76a	4.78a	4.78a	4.74a	16.27a	17.67a	15.76a	19.54a	90.92b	90.97b	85.71c	113.02a	26.06b	24.40c	23.48c	27.44a	141.44b	127.05d	131.88c	172.82a
30-40	4.67ab	4.69a	4.69a	4.65b	14.86a	15.55a	12.49b	16.29a	70.61b	71.00b	58.50c	72.38a	13.21b	12.71c	12.66c	13.85a	143.91b	126.13b	95.69c	144.17a

2RT: two passes of rotary tillage, 2RTSS: two passes of rotary tillage + subsoil, SS: subsoiling, ZT: zero tillage. Means followed by different letters within the same column are significantly different at $P < 0.05$.

E Asenso, L Hu, F Issaka, K Tian, L Zhang, L Zhang, J Zeng, Y-F Zhu, J Li*. "Impact of tillage practices on selected soil physico-chemical and biological conditions and maize yield in latosolic red soil of Southern China".

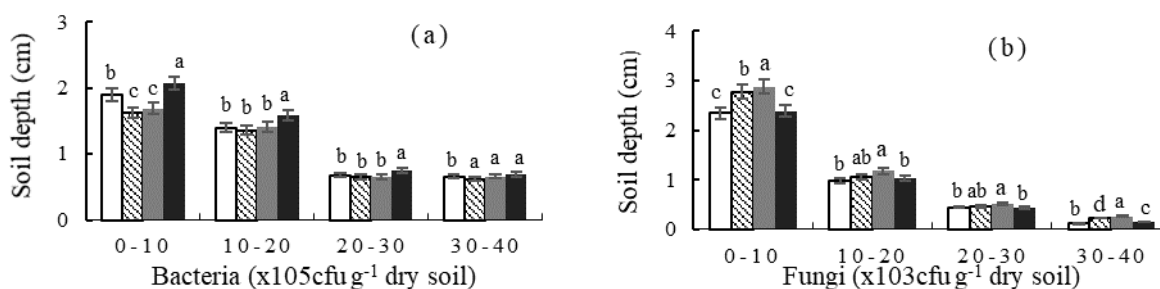


3.3. Soil biological conditions

Tillage practice under ZT resulted in significantly higher ($P < 0.05$) levels of soil bacteria in the measured soil profile (0-40 cm) as shown in Figure 1a, compared to the initial data. There was a significant increase of 12.39% and 2.65% soil bacteria in the 0-40 cm soil depth under the ZT and 2RT respectively compared to a significant reduction of 6.60% and 42.73% under 2RTSS and SS respectively. The soil bacteria of ZT and 2RT had higher significant increase (61.95% and 46.02% respectively) compared to 37.17% and 31.36% under 2RTSS and SS respectively at the soil depth of 0-20 cm, while there was a higher significant reduction of SBT at the 20-40 cm soil depth in the order of ZT>2RT>SS>2RTSS.

SS and 2RTSS resulted in significantly higher ($P < 0.05$) levels of soil fungi level in the measured soil profile (0-40 cm) as shown in Figure 1b, compared to the initial data. There was a significant increase of 14.15% and 6.6% soil fungi level in the 0-40 cm soil depth under the SS and 2RTSS respectively compared to a significant reduction of 8.16% and 6.00% under 2RT and ZT respectively. The soil fungi level of 2RTSS, SS and ZT had higher significant increase compared to 2RT at the soil depth of 0-20 cm, while at 20-40 cm soil depth there was a higher significant reduction under ZT and 2RT compared to SS and 2RTSS.

ZT resulted in significantly higher ($P < 0.05$) levels of soil actinomycetes in the measured soil profile (0-40 cm) as shown in Figure 1c, compared to the initial data. There was a significant increase of 18.18% and 3.64% soil actinomycetes in the 0-40 cm soil depth under the ZT and 2RT compared to a significant reduction of 12.24% and 3.13% under 2RSST and SS respectively. The soil actinomycetes of ZT and 2RT had higher significant increase compared to SS and 2RTSS at the soil depth of 0-20 cm, while there was a higher significant reduction under SS, 2RTSS and 2RT compared to ZT at the 20-40 cm soil depth.



E Asenso, L Hu, F Issaka, K Tian, L Zhang, L Zhang, J Zeng, Y-F Zhu, J Li*. "Impact of tillage practices on selected soil physico-chemical and biological conditions and maize yield in latosolic red soil of Southern China".



CIGR 2018

XIX. World Congress of CIGR

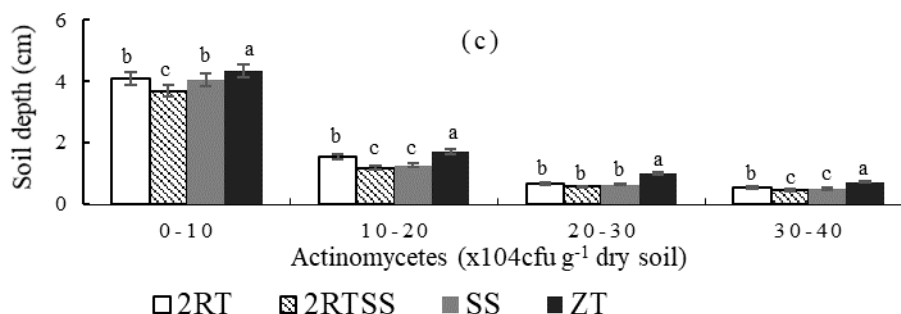


Figure 1. Mean changes in soil biological condition at the soil depth of 0-40 cm. (a) bacterial levels (b) fungal levels (c) Actinomycetes levels. 2RT: two passes of rotary tillage, 2RTSS: two passes of rotary tillage + subsoil, SS: subsoiling, ZT: zero tillage. Bars with different letters are significantly different at $P < 0.05$.

3.4. Maize yield

Treatments effects on maize yield were significantly different ($P < 0.05$) after the two years study Table 4. Mean maize yield under SS was 9.81% higher than under ZT compared to 5.60% and 3.08% under 2RTSS and 2RT respectively.

Table 4. Mean maize yield as affected by tillage practices

Tillage practice	Grain yield (ton ha ⁻¹)
2RT	7.14b
SS	7.36a
2RTSS	6.97c
ZT	6.73d

2RT: two passes of rotary tillage, 2RTSS: two passes of rotary tillage + subsoil, SS: subsoiling, ZT: zero tillage. Means are significantly different at $P < 0.05$.

4. DISCUSSION

The improvement of maize yield under SS may be due to favorable soil physical properties. First, the use of SS caused a slight increase in soil bulk density and soil porosity alleviating soil compaction to improve root penetration in the soil (Batey, 2009; Hamza and Anderson, 2005). With two years of experiment, beneficial impacts of SS were evident in reducing bulk density compared to the ZT in the 0-40 cm soil depth indicating fracture of the plow in the sub soil layer. In addition to the slight increase in soil bulk density, SS also increased slightly in soil porosity compared to ZT in the 0-40 cm soil depth. The consistent improvement in soil porosity under SS was most probably related to increase aggregate stability and residue cover (Oliveira and Merwin, 2001).

E Asenso, L Hu, F Issaka, K Tian, L Zhang, L Zhang, J Zeng, Y-F Zhu, J Li*. "Impact of tillage practices on selected soil physico-chemical and biological conditions and maize yield in latosolic red soil of Southern China".



CIGR 2018

XIX. World Congress of CIGR



The changes in soil pH might be enhanced by SS, but it was due to the protection of the soil surface from hard setting, improved pore size, aggregated stability and the resultant improvement in infiltration capacity under the SS.

High SOM in the ZT especially in the 0-20 cm soil depth, was attributed to increase input from crop residues and considerable reduction in soil disturbances. The intensive tillage and residue removal of 2RT and 2RTSS treatments continued to contribute to significant SOM losses. Similarly, Zibilske et al. (2002) also reported that ZT concentrated SOM in the top soil layer, whereas in a comparison with conventional tillage, ZT significantly increased SOM.

There was a lower uptake of soil available N by SS than under ZT, which may be attributed to an exacerbated leaching into deeper soil layers to contaminate the groundwater. However, higher soil available N was observed under ZT than under SS. Similarly, a study on Mollisols in Nebraska, available N was significantly greater under zero tillage than conventional tillage (Six et al., 1998). In another study, soil available N content was also significantly increased under ZT (Martin-Rueda et al., 2007). Higher available N in ZT treatment may be attributed to less loss through immobilization, volatilization, denitrification, and leaching (Malhi et al., 2001).

Available P and exchangeable K were higher under ZT treatment probably due to higher SOC as a result of high SOM levels and surface applied K and P fertilizers. Franzluebbers and Hons, (1996) and Zibilske et al. (2002) reported that improvement of soil available P was due to redistribution or mining of available P at lower soil depths. Also, work done (Redel et al., 2007; Rheinheimer and Anghinoni, 2003) showed a high amount of available P under ZT treatment compared to the conventional tillage (2RT, 2RTSS and SS) and have attributed it to an increase in contact time between P and soil particles (Phiri et al., 2001). In the present findings, the exchangeable K concentrations were higher in ZT treatment. Yin and Vyn (2002) also observed more soil exchangeable K in case of ZT treatment as compared to SS treatment.

Different tillage practices appreciably influenced soil microorganism. The bacteria level was significantly higher under ZT which might be due to the presences of residue causing more accumulation of SOM on the soil surface and as a consequence increased the abundance of microbial levels particularly bacteria (Matthew, 2012). Bacteria levels under the other treatments (2RTSS, 2RT and SS) were significantly lower as crop residues left over after harvesting of the preceding maize crop, was incorporated into the soil during tillage practice and later decomposed by organism. Thereafter, the bacteria level was less under 2RTSS, 2RT and SS (Younesabadi et al., 2014).

Similar trend was observed in the case of actinomycetes levels. Higher actinomycetes levels under ZT might also be due to the presences of residues of preceding maize crop causing accumulation of SOM, which increased the soil aeration and SOC as a result of high SOM under ZT. Fungal level was significantly higher under SS compared to the ZT and the other tillage practices. This might be due to the loosen up of the soil by breaking the hard pan which

E Asenso, L Hu, F Issaka, K Tian, L Zhang, L Zhang, J Zeng, Y-F Zhu, J Li*. "Impact of tillage practices on selected soil physico-chemical and biological conditions and maize yield in latosolic red soil of Southern China".



CIGR 2018

XIX. World Congress of CIGR



improved the soil structure resulting in improved infiltration and aeration leading to high fungal levels.

Highest yield of maize was achieved under SS, and this might be due to lower bulk density aiding root penetration and distribution of plant available nutrient coupled with elongation of root system in the subsoil to increased uptake of nutrients by maize (Cai et al., 2014). There was a lower yield under the ZT treatment hence, some greater significant differences compared to SS. Yields are often compared through different tillage systems, and authors often report that a higher yield can be achieved with a conventional tillage in comparison with ZT. According to Sartori and Peruzzi (1994), corn cultivated with minimum tillage methods produced around 20–25% less than those based on ploughing, while the yield reduction is even more obvious with ZT. Among tillage practices, conventional tillage and ZT in corn production, the highest yield had been obtained with the conventional tillage (Borin and Sartori, 1995).

5. CONCLUSION

After two years field experiment in 2016 and 2017, tillage practices showed positive effects on soil properties and maize yield. The highest soil physical properties, soil organic matter (SOM) and nutrient levels in their available form of N and P and as well as exchangeable K were recorded in the ZT. Subsequently, analysis of soil microbial levels showed that ZT recorded the highest levels of bacterial and actinomycetes at the soil depth of 0–40 cm, whilst SS increased the fungal levels in the soil depth of 0–40 cm. The mean highest grain yield (7.37 ton ha⁻¹) was recorded under SS, while the lowest (6.73 ton ha⁻¹) under ZT. The results suggest that SS was more suitable for achieving higher yield in latosolic red soil resulting in a sustainable agricultural system.

ACKNOWLEDGMENT

This research was supported by the National Key Research and Development Program of China (2016YFD0700301) and the National Natural Science Foundation of China (31601225).

E Asenso, L Hu, F Issaka, K Tian, L Zhang, L Zhang, J Zeng, Y-F Zhu, J Li*. “Impact of tillage practices on selected soil physico-chemical and biological conditions and maize yield in latosolic red soil of Southern China”.



CIGR 2018

XIX. World Congress of CIGR



REFERENCES

- Arshad, M.A., A.J. Franzluebbers, and R.H. Azooz. 1999. Components of surface soil structure under conventional and no-tillage in northwestern Canada. *Soil and Tillage Research* 53(1):41-47.
- BAO, S.D. 2000 Soil and Agricultural Chemistry Analysis [M]. 3rd ed. Beijing: China Agriculture Press. pp. 1-329.
- Batey, T. 2009. Soil compaction and soil management-a review. *Soil Use Management*. 25(4):335-345.
- Blake, G.R. 1965. Bulk density. In: Black, C.A. (Ed.). Methods of Soil Analysis. Part 1. Physical and Mineralogical Properties, SSSA Inc., Madison. WI, USA. pp. 374-390.
- Borin, M., and L. Sartori. 1995. Barley, soybean and maize production using ridge tillage, no-tillage and conventional tillage in north-east Italy. *Journal of Agricultural Engineering Research* 62(4):229-236.
- Bronick, C.J., and R. Lal. 2005. Soil structure and management: a review. *Geoderma* 124:3-22.
- Cai, H., W. Ma, X. Zhang, J. Ping, X. Yan, J. Liu, J. Yuan, L. Wang, and J. Ren. 2014. Effects of subsoil tillage depth on nutrient accumulation, root distribution, and grain yield in spring maize. *The Crop Journal* 2:297-307.
- Derpsch, R., T. Fredrich, A. Kassam, and L. Hongwen. 2010. Current status of adoption of no-till farming in the world and some of its main benefits. *International Journal of Agricultural and Biological Engineering* 3(1):1-25.
- FAO. 1993. World Soil Resources: An Explanatory Note on the FAO World Soil Resources map at 1:25,000,000 Scale. In: Report, W.S.R. (Ed.). Food and Agriculture Organization of the United Nation, Rome, pp. 61.
- Ferraro, D.O., and G.M. Ghera. 2007. Quantifying the crop management influences on arable soil condition in the Inland Pampa (Argentina). *Geoderma* 141:43-52.
- Franzluebbers, A.J., and F.M. Hons. 1996. Soil profile distribution of primary and secondary plant available nutrients under conventional and no tillage. *Soil and Tillage Research* 39(3-4):229-239.
- Grant, C.A., and G.P. Lafond. 1993. The effects of tillage systems and crop sequences on soil bulk density and penetration resistance on clay in southern Saskatchewan. *Canadian Journal of Soil Science* 73(2):223-232.

E Asenso, L Hu, F Issaka, K Tian, L Zhang, L Zhang, J Zeng, Y-F Zhu, J Li*. "Impact of tillage practices on selected soil physico-chemical and biological conditions and maize yield in latosolic red soil of Southern China".



CIGR 2018

XIX. World Congress of CIGR



Hamza, M.A., and W.K. Anderson. 2005. Soil compaction in cropping systems: A review of the nature, causes and possible solutions. *Soil and Tillage Research*. 82(2):121-145.

Iqbal, M., A.U. Hassan, A. Ali, and M. Rizwanullah. 2005. Residual effect of tillage and farm manure on some soil physical properties and growth of wheat (*Triticum aestivum* L.). *International Journal of Agriculture and Biology* 1:54-57.

Khan, F.U.H, A.R. Tahir, and I.J. Yule. 2001. Intrinsic implication of different tillage practices on soil penetration resistance and crop growth. *International Journal of Agriculture and Biology* 1:23-26.

Khurshid, K., M. Iqbal, M.S. Arif and A. Nawaz. 2006. Effect of tillage and mulch on soil physical properties and growth of maize. *International Journal of Agriculture and Biology* 8(5):593-596.

Lal, R. 1993. Tillage effects on soil degradation, soil resilience, soil quality and sustainability. *Soil and Tillage Research* 27(1-4):1-8.

Lal, R., and B.A. Stewart. 2013. (Eds.). Principles of Sustainable Soil Management in Agroecosystems, vol. 20, CRC Press.

López-Garrido, R., M. Deurer, E. Madejón, J.M. Murillo, F. Moreno. 2012. Tillage influence on biophysical soil properties: the example of a long-term tillage experiment under Mediterranean rainfed conditions in South Spain. *Soil and Tillage Research* 118:52-60.

Malhi, S.S., C.A. Grant, A.M. Johnston, and K.S. Gill. 2001. Nitrogen fertilization management for no-till cereal production in the Canadian Great Plains: a review. *Soil and Tillage Research* 60(3-4):101-122.

Martin-Rueda, I., L.M. Munoz-Guerra, F. Yunta, E. Esteban, J.L. Tenorio, and J.J. Lucena. 2007. Tillage and crop rotation effects on barley yield and soil nutrients on a Calciortidic haploxeralf. *Soil and Tillage Research* 92(1-2):1-9.

Mathew, R.P., Y. Feng, L. Githinji, R. Ankumah, and K.S. Balkcom. 2012. Impact of no-tillage and conventional tillage systems on soil microbial communities. Hindawi Publishing Corporation. *Applied Environment Soil Science* 2012 (548620)10, <http://dx.doi.org/10.1155/2012/548620>.

Muñoz, A., A. López-Piñeiro, and M. Ramírez. 2007. Soil quality attributes of conservation management regimes in a semi-arid region of south western Spain. *Soil and Tillage Research* 95(1-2):255-265.

E Asenso, L Hu, F Issaka, K Tian, L Zhang, L Zhang, J Zeng, Y-F Zhu, J Li*. "Impact of tillage practices on selected soil physico-chemical and biological conditions and maize yield in latosolic red soil of Southern China".



CIGR 2018

XIX. World Congress of CIGR



Oliveira, M.T., and I.A. Merwin. 2001. Soil physical conditions in a New York Orchard after eight years under different groundcover management systems. *Plant and Soil* 243(2):233-237.

Page, A.L., R.H. Miller, and D.R. Keeney. 1982. Methods of Soil Analysis. Part 2. Chemical and Microbiological Properties. 2nd Edition. American Society of Agronomy, Soil Science Society of America, Madison, Wisconsin, USA.

Parkinson, D., T.R.G. Gray, and S.T. Williams. 1971. Methods for studying ecology of soil microorganisms. IBP Hand Book 19, Blackwells Science Publication Limited, Oxford.

Phiri, S., E. Barrios, I.M. Rao, and B.R. Singh. 2001. Changes in soil organic matter and phosphorus fractions under planted fallows and a crop rotation system on a Colombian volcanic-ash soil. *Plant and Soil* 231(2):211-223.

Ramos, M.E., A.B. Robles, A. Sánchez-Navarro, and González-Rebollar. 2011. Soil response to different management practice in rainfed orchards in semiarid environments. *Soil and Tillage Research* 112(1):85-91.

Rashidi, M., and F. Keshavarzpour. 2008. Effects of different tillage methods on soil physical properties and crop yield of melon (*Cucumis melo*). *American-Eurasian Journal of Agriculture and Environmental Sciences* 3:31-36.

Redel, Y.D., R. Rubio, J.L. Rouanet, and F. Borie. 2007. Phosphorus bioavailability affected by tillage and crop rotation on a Chilean volcanic derived Ultisol. *Geoderma* 139(3-4):388-396.

Rheinheimer, D.D., and I. Anghinoni. 2003. Accumulation of soil organic phosphorus by soil tillage and cropping systems under subtropical conditions. *Communication in Soil Science and Plant Analysis* 34(15-16):2339-2354.

Sartori, L., and A. Peruzzi. 1994. The evolution of no-tillage in Italy: a review of the scientific literature. Experience with the Applicability of No-tillage Crop Production in the West-European Countries, Proceedings of 1st EC Workshop, pp. 119-130, Wissenschaftlicher Fachverlag, Giessen, Germany, June.

Six, J., E.T. Elliot, K. Paustian, and J.W. Doran. 1998. Aggregation and soil organic matter accumulation in cultivated and native grassland soils. *Soil Science Society of America Journal* 62(5):1367-1377.

Trojan, M.D., and D.R. Linden. 1998. Macro porosity and hydraulic properties of earthworm-affected soils as influenced by tillage and residue management. *Soil Science Society of American Journal* 62(6):1687-1692.

Wander, M.M., M.G. Bidart, and S. Aref. 1998. Tillage impacts on depth distribution of total and particulate organic matter in three Illionis soils. *Soil Science Society of American Journal* 62(6):1704-1711.

E Asenso, L Hu, F Issaka, K Tian, L Zhang, L Zhang, J Zeng, Y-F Zhu, J Li*. "Impact of tillage practices on selected soil physico-chemical and biological conditions and maize yield in latosolic red soil of Southern China".



CIGR 2018

XIX. World Congress of CIGR



Wasaya, A., M. Tahir, A. Manaf, M. Ahmed, S. Kaleem, and I. Ahmad. 2011. Improving maize productivity through tillage and nitrogen management. *African Journal of Biotechnology* 10(81):19025-19034.

Wellingtonn, E.M.H., and I.K. Toth. 1963. Microbiological and Biochemical properties. University of Warwick.

Wolfarth, F., S. Schrader, E. Oldenburg, J. Weinert, and J. Brunotte. 2011. Earthworms promote the reduction of Fusarium biomass and deoxynivalenol content in wheat straw under field conditions. *Soil Biology and Biochemistry* 43(9):1858-1865.

Yin, X., and T.J. Vyn. 2002. Residual effects of potassium placement and tillage systems for corn on subsequent no-till soybean. *Agronomy Journal* 94(5):1112–1119.

Younesabadi, M., T.K. Das, and S. Paul 2014. Tillage and weed management effect on weed, non- target toxicity in soil and yield of soybean. *International Journal of Farming and Allied sciences* 3(9): 962-969.

Zibilske, L.M., J.M. Bradford, and J.R. Smart. 2002. Conservation tillage induced changes in organic carbon, total nitrogen and available phosphorus in a semi-arid alkaline subtropical soil. *Soil and Tillage Research* 66(2):153–163.

E Asenso, L Hu, F Issaka, K Tian, L Zhang, L Zhang, J Zeng, Y-F Zhu, J Li*. “Impact of tillage practices on selected soil physico-chemical and biological conditions and maize yield in latosolic red soil of Southern China”.



CIGR 2018

XIX. World Congress of CIGR



FT-IR Imaging Spectroscopy for Measurement of Times-Series Physical Parameters of Potato and Sweet Potato Tubers During Microwave Drying

Wen-Hao Su¹, Da-Wen Sun^{*1}, Serafim Bakalis²

¹ School of Biosystems and Food Engineering, University College Dublin (UCD), National University of Ireland, Belfield, Dublin 4, Ireland

² Department of Chemical and Environmental Engineering, University of Nottingham

dawen.sun@ucd.ie

ABSTRACT

Time series spectroscopic and physical parameters (such as hardness, resilience, springiness, cohesiveness, gumminess and chewiness) were obtained from potato and sweet potato tuber samples during microwave baking. These data were analyzed using partial least square regression (PLSR) and locally weighted partial least squares regression (LWPLSR). The predictability of spectra in full wavenumber region ($4000\text{--}600\text{ cm}^{-1}$) were calculated and compared based on PLSR and LWPLSR. The results of this research reveal that FT-IR imaging spectroscopy has potential to be used for non-invasive determinations of physical parameters of both potato and sweet potato tubers during microwave dehydration.

Keywords: MIR spectroscopy; Textural property; Potato; Microwave; Multivariate analysis;

INTRODUCTION

Potato and sweet potato are primary staple foods in many parts of the world (Su et al., 2015; Su and Sun, 2016c, d, e, 2017c). During heat treatment, tuber physical parameters related to sensory attributes would be changed a lot based on the interactions of starch molecular with non-starch polysaccharides and sugars (Su and Sun, 2017a). Because of the starch gelatinization and retrogradation behaviour in the thermal processing, the tuber textural property (TTP) could have many changes (Kim et al., 1997). The food texture is normally defined as an integration of mechanical attributes of a food product perceptible relying on tactile, mechanical, visual and auditory receptors. As a critical sensory attribute, the texture of tuber product is mainly depended on its chemical compositions such as starch contents, non-starch polysaccharides, lignin and protein (Kita, 2002). The textural parameters of tuber products mainly involve hardness, resilience, springiness, cohesiveness, gumminess and chewiness (Su et al., 2018b). However, the



CIGR 2018

XIX. World Congress of CIGR



conventional detection methods for evaluation of tuber texture are based on appearance and taste, which is not only inaccurate but also time-consuming (Davies and Dixon, 1976). To eliminate the influence from human factors, the mechanical measurement methods such as texture profile analysis and the 3-point bending test have been proposed to detect the food texture (Fagan et al., 2007a). Nevertheless, the texture analyser with strong destructiveness and low efficiency is not the ideal solution. More importantly, both the sensory and instrumental evaluation approaches are suitable for sampling inspection, which means that only a small number of samples can be detected. However, the tuber industry requires a non-destructive and cost-effective technique for rapid and effective inspection of tuber texture.

Near and mid-infrared (NIR/MIR) spectroscopic techniques are proved to provide information for qualitative and quantitative analyses of food and food products (Alexandrakis et al., 2012; Klaypradit et al., 2011; Su et al., 2018a; Su et al., 2017a; Su and Sun, 2016a, b, 2017b; Su et al., 2017b). Specifically, the MIR spectroscopy monitors the vibrational and rotational motions of molecules in which very small differences in sample composition can be measured (Su and Sun, 2018a, b). As MIR spectra are rich in information on both physical states and molecular structures of food components, it allows for not only chemical determination of organic constituents but also physical identification of food texture property. MIR spectroscopy with attenuated total reflectance (ATR) has been identified as having considerable potential for real-time application in food industry. Many studies have investigated the potential of the IR spectroscopy to determine food sensory texture attributes including hardness, shear force, adhesiveness, chewiness, cohesiveness and springiness (Cai et al., 2011; Fagan et al., 2007a; Fagan et al., 2007b; Wu et al., 2014). However, there are few researches on measurement of textural property of tuber products using MIR spectroscopy. Our study sought to investigate the Fourier transform mid-infrared attenuated total reflectance (FTMIR-ATR) spectroscopic technique in quantitative prediction of the textural property of microwave baked tuber products. Spectral analysis potato tuber samples at 5 time points was conducted. On the basis of the results, 6 different textural parameters including hardness, resilience, springiness, cohesiveness, gumminess and chewiness were evaluated by developing multivariate analytical methods.

2. MATERIALS AND METHODS

2.1. Samples preparation

To develop a robust calibration model, fresh potato and sweet potato samples from five types (25 samples for each type) in terms of Rooster red potato (origin: UK), Desiree red potato (origin: UK), Evangeline sweet potato (origin: Egypt), Abees sweet potato (origin: Egypt), organic Abees sweet potato (origin: Egypt) were purchased and then transported to the freshness keeping compartment (about 4 °C, relative humidity 85%) to reduce moisture loss and enzyme activity of tubers. After being peeled and sliced to the thickness of 10 mm (the axial length of 15 mm), 25



samples of each tuber variety were divided into five equal parts (5 samples for each part) and then respectively baked in a lab-scale microwave oven (800 W) for 0, 10, 20, 30, 35s, resulting in 125 samples (25×5) in total for five tuber varieties, eventually. Each sample was first scanned by a FT-IR spectral imaging system before the reference values of textural parameter being collected.

2.2 Data collection of FT-IR microspectral imaging system

The samples were analyzed using a LUMOS FT-IR microscope (Bruker Optics, Germany) in ATR mode (Cao et al., 2016; Woess et al., 2017). This system was equipped with a liquid nitrogen cooled narrow-band photoconductive mercury cadmium telluride (MCT) detector, a deuterated triglycine sulfate (DTGS) detector, a highly resolving digital CCD camera, a germanium (Ge) ATR crystal, a solid state laser, a IR beam splitter, and a permanently aligned RockSolid™ interferometer which was extremely insensitive against mirror tilts, vibrations and thermal effects. All components were motorized and electronically coded. The images of regions of interest were captured by the CCD camera. The aperture was $20 \mu\text{m} \times 20 \mu\text{m}$ to obtain a high S/N ratio as well as a high spatial resolution, which allowed high quality MIR spectra to be acquired in the wavelength range of 2500–16680 nm (4000 to 600 cm^{-1}) at 4 cm^{-1} spectral resolution. Before each sample scan, a background scan was acquired with an empty sample plate. To remove any interference from the previous sample, the ATR crystal was cleaned using 70% ethanol and dried with a pure cotton fabric after each sample scan. Then, a total of 32 successive scans for each point of a sample were co-added and converted to absorbance based on the OPUS 7.2 software. More detailed information about the schema of the equipment as well as detector theory and technology can be found in the study of Bhargava and Levin (2008). The spectra of 4 typical points from each sample (Figure 1) were collected and averaged to represent that sample.

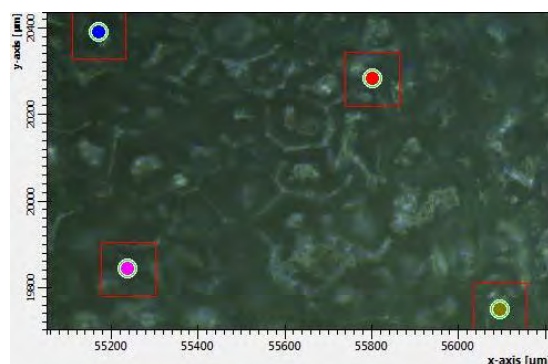


Figure. 1. The microscopic image of a tuber sample collected by the FT-MIR imaging system.



CIGR 2018

XIX. World Congress of CIGR



2.3 Textural property measurement

The textural property of a tuber sample was assessed by performing double compression test using a TA.XT.plus texture analyser (Stable Micro Systems Ltd., Godalming, Surrey, England) fitted with a 30 kg load cell. The force and height calibrations were executed prior to tests as these calibrations ensured that the measurements made by the Texture Analyser were accurate. In order to calculate the textural parameters accurately, the tests should be conducted with the same test and post-test speeds.

Moreover, to replicate the biting action well, the diameter of compression plate used was larger than the diameter of tuber samples (15 mm) so that the tested samples can not only barrel out but also be fully contacted and properly compressed. In addition, different compression distances from the strain of 20% to 80% were tested to emulate the chewing action. It was found that the 40% strain was more appropriate to evaluate tuber samples after observing their behaviours. Therefore, each sample in this study was axially compressed twice to 40% deformation with a 40-mm diameter cylindrical aluminium plate at the pre-test speed of 2.0 mm/s, and the test and post-test speed of 1.0 mm/s, respectively.

After the first compression, the plate returned to the trigger position. The trigger type was auto and the trigger force was 5.0 g. The interval between two compressions was 10 s. The acquisition of time data was 500 points per second. In this study, one tuber sample was first analysed by the FTMIR-ATR spectroscopic system and its textural property was then inspected using the texture analyser. After, the force–time deformation curve of the tuber sample could be displayed based on the fully integrated Texture Exponent 32-bit software in the computer. The textural parameters including hardness, resilience, springiness, cohesiveness, gumminess and chewiness could be acquired from the force–time deformation curve for analysis. According to such an operation process, both spectral data and textural parameters of all the five categories of tuber samples from 0s to 35s were collected. The specific definition and calculation of relevant mechanical parameters of texture can be found in the study of Trinh and Glasgow (2012). Other textural parameters such as adhesiveness, stringiness and fracturability were not calculated in this test because of their intrinsic attributes.

2.4 Spectral pre-treatment

The obtained spectra mainly contained the tuber sample information but might involve systemic noises due to instrumental drift and light scattering. To develop an accurate spectroscopic model, the raw spectra should be corrected by applying mathematical pre-processing methods to reduce the undesirable information. In this study, spectral data were treated with four pre-processing methods: first derivative (1st Der) (7 points window, 2 order polynomial), second derivative (2nd Der) (7 points window, 2 order polynomial), orthogonal signal correction (OSC), and mean centering (MC). Specifically, 2nd Der and OSC were first individually used to the data. Meanwhile, the methods of MC combined with both 1st Der and OSC were respectively applied.



CIGR 2018

XIX. World Congress of CIGR



The optimal pre-processing technique would be survived when the lowest root mean square error of cross validation (RMSECV) and highest correlation coefficient (R) were acquired.

2.5 Regression model development

Locally weighted partial least squares regression (LWPLSR) can be seen as a suitable strategy to estimate the nonlinear dependence relation between **X**-block (i.e., spectra) and **Y**-block (i.e., analyte concentrations), and to facilitate the selection of proper calibration sets. For each unknown sample to be predicted, local regression models are carried out using specific calibration equations to improve prediction accuracy by selecting a reduced set of calibration spectra providing similar features. The closest samples characterized by a minimum distance between the query and the calibration samples can be employed for local model calculation. This is on basis of using partial least squares regression (PLSR) algorithm to extract a set of latent variables (LVs) explaining the sources of variation of spectral signals correlated to sample composition. The sample size of the LWPLSR models varied between 10 and 300 in steps of 10. The optimal combination of the aforementioned parameters was selected from results obtained by a multi-parametric approach using the RMSECV as response function.

2.6 Assessment of model accuracy

The performance of PLS models was assessed using R and RMSE in calibration (R_C , RMSEC), cross-validation (R_{CV} , RMSECV), and prediction (R_P , RMSEP). The time-series variation of tuber texture property during microwave baking was analyzed using the software of IBM SPSS Statistics 24.0 version.

3. RESULT AND DISCUSSION

3.1 Detection of TTP using PLSR in the full-wavenumber region

FTMIR-ATR technique allowed the development of calibration models for quantification of TTP. The cross-validated PLSR models were developed to determine the textural properties in various tuber products based on the chemical information from their spectra. To evaluate the applicability of the proposed PLSR for the measurement of TTP, an independent set of samples was then assessed using a predicted PLSR model.

All kinds of spectral pre-treatment algorithms were adopted to remove both additive and multiplicative noise effects in the spectra and improve the accuracy of the developed models. The effects of spectral pre-processing algorithms on performances of PLSR models were inspected. It was found that the generated models using the OSC plus MC-corrected spectral data with MC in **Y**-block presented the best performance for prediction of hardness, resilience, springiness and gumminess, with R_P of 0.846, 0.893, 0.563 and 0.798, respectively. Although the spectra processed only by the OSC plus MC without **Y**-block MC provided similar R statistics in PLSR, the RMSEC, RMSECV and RMSEP were almost doubled.



CIGR 2018

XIX. World Congress of CIGR



The PLSR with 2nd Der provided the best prediction model to determine the tuber cohesiveness. However, it was realized that the 2nd Der of the MIR spectra lowered the accuracy of PLSR model for the detection of resilience, probably because the spectra contained the interfering variance which was increased using this data pre-processing. In addition, the highest accuracy ($R_P = 0.797$, RMSEP=34.598) for measuring chewiness was existed in the PLSR model developed using the OSC, followed by the spectral pre-processing method of OSC plus MC (in X-block) with another MC in Y-block. Overall, the model performance can be fully improved based on optimal pre-treatment algorithms. Moreover, the most optimal pre-processing methods were acquired by the OSC plus MC-corrected spectra with MC in Y-block, providing more precise predictions when compared to other pre-processing approaches.

3.2 Improving the measuring accuracy of TTP using LWPLSR

Although a good correlation between the IR spectral features and the TTP reference values has been presented in the PLSR, the detection accuracy still needs to be improved to meet the requirement of the advanced food processing. Based on the optimal pre-processing method, the LWPLSR model was then constructed to study the correlation between the FTMIR-ATR spectra and textural property reference values acquired at five different time points. For determination of tuber springiness using LWPLSR model, the better performance ($R_P = 0.520$, RMSEP = 0.114) was obtained based on the spectral data without pre-processing, which was lower than the capacity of PLSR model using the OSC plus MC-corrected spectra with MC in Y-block.

Nevertheless, it was found that the best calibration models for prediction of other five textural properties were acquired by employing the pre-processing method, and the R_P values were 0.878 for hardness, 0.911 for resilience, 0.666 for cohesiveness, 0.815 for gumminess and 0.817 for chewiness, respectively. Based on the LWPLSR model, these five coefficients being used to predict tuber textural properties were comparatively higher than the R_P values collected from PLSR models with the exception of the R_P for cohesiveness. This indicated that the PLSR model could obtain higher efficiency for evaluating tuber cohesiveness and springiness, although better detection accuracy of other four textural parameters were acquired in the LWPLSR model. Therefore, the accuracy of quantitative detection of TTP can be further optimized by combining the full-wavenumber PLSR with LWPLSR model (Figure 2).

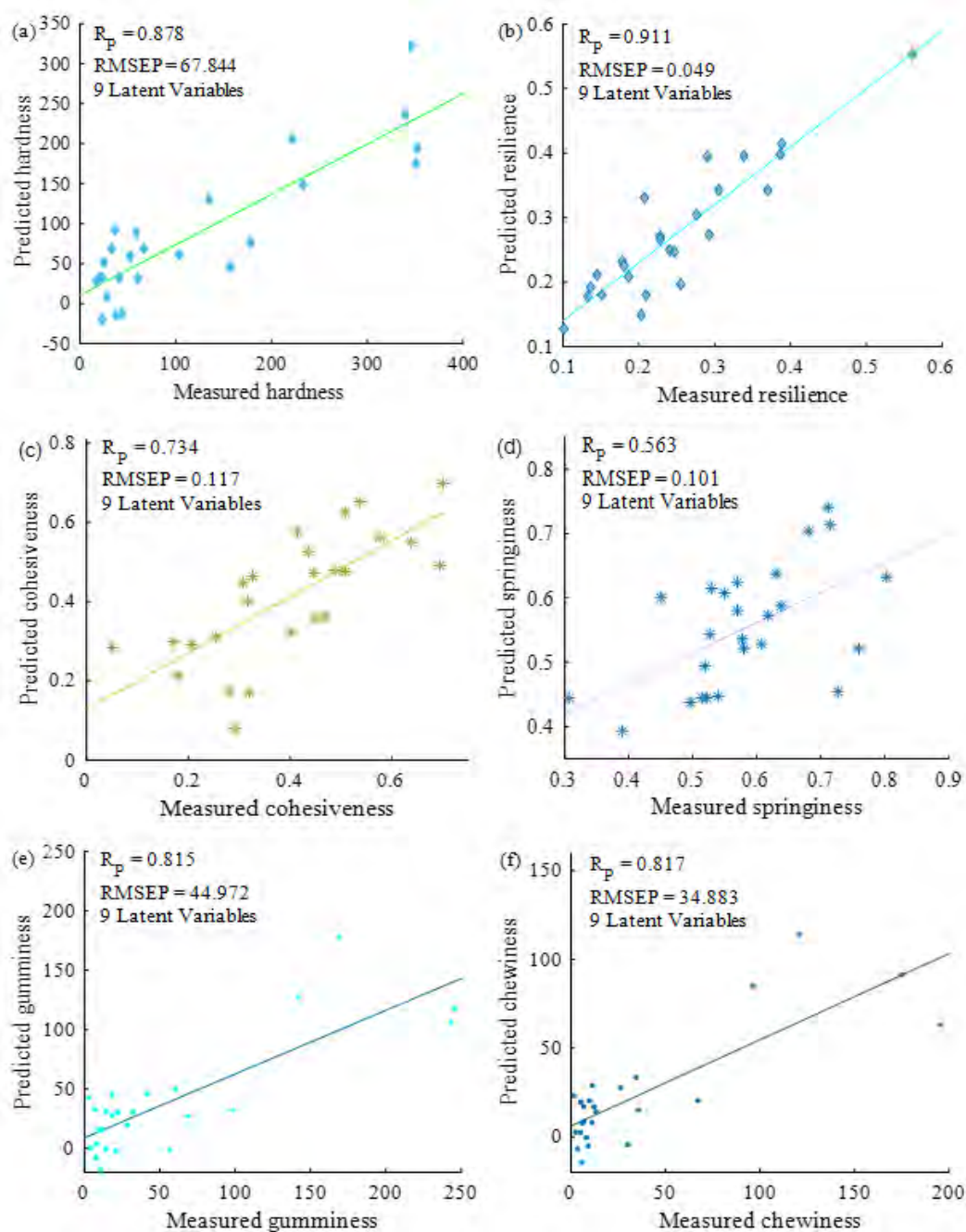


Figure 2. The performance of the optimal PLSR model (c and d) and LWPLSR model (a, b, e and f) for prediction of TTP.



CIGR 2018

XIX. World Congress of CIGR



4. CONCLUSIONS

In this study, the feasibility of MIR spectroscopy for the evaluation of tuber physical parameters including hardness, resilience, springiness, cohesiveness, gumminess and chewiness was investigated. The result of this study revealed that FT-MIR spectroscopy can be considered as an effective technique for non-invasive and rapid measurement of textural property of tuber products. In the future research, more tuber samples from different varieties and origins will be investigated based on various spectroscopic techniques to verify the effectiveness of developed new chemometric algorithms.

5. REFERENCES

- Alexandrakis, D., Downey, G. & Scannell, A.G., 2012. Rapid non-destructive detection of spoilage of intact chicken breast muscle using near-infrared and Fourier transform mid-infrared spectroscopy and multivariate statistics. *Food and Bioprocess Technology* 5(1), 338-347.
- Bhargava, R. & Levin, I.W., 2008. *Spectrochemical analysis using infrared multichannel detectors*. John Wiley & Sons.
- Cai, J., Chen, Q., Wan, X. & Zhao, J., 2011. Determination of total volatile basic nitrogen (TVB-N) content and Warner–Bratzler shear force (WBSF) in pork using Fourier transform near infrared (FT-NIR) spectroscopy. *Food Chemistry* 126(3), 1354-1360.
- Cao, X., Loussaert, J.A. & Wen, Z.-q., 2016. Microspectroscopic investigation of the membrane clogging during the sterile filtration of the growth media for mammalian cell culture. *Journal of Pharmaceutical and Biomedical Analysis* 119, 10-15.
- Davies, H. & Dixon, N., 1976. Evaluation of potato texture by taste and by appearance. *American Journal of Potato Research* 53(6), 205-210.
- Fagan, C.C., Everard, C., O'Donnell, C., Downey, G., Sheehan, E., Delahunty, C., O'Callaghan, & D., 2007a. Evaluating mid-infrared spectroscopy as a new technique for predicting sensory texture attributes of processed cheese. *Journal of Dairy Science* 90(3), 1122-1132.
- Fagan, C.C., Everard, C., O'Donnell, C., Downey, G., Sheehan, E., Delahunty, C., O'Callaghan, & D., Howard, V., 2007b. Prediction of processed cheese instrumental texture and meltability by mid-infrared spectroscopy coupled with chemometric tools. *Journal of Food Engineering* 80(4), 1068-1077.
- Kim, Y.S., Wiesenborn, D.P. & Grant, L.A., 1997. Pasting and thermal properties of potato and bean starches. *Starch - St rke* 49(3), 97-102.
- Kita, A., 2002. The influence of potato chemical composition on crisp texture. *Food Chemistry* 76(2), 173-179.



CIGR 2018

XIX. World Congress of CIGR



Klaypradit, W., Kerdpi boon, S. & Singh, R.K., 2011. Application of artificial neural networks to predict the oxidation of menhaden fish oil obtained from Fourier transform infrared spectroscopy method. *Food and Bioprocess Technology* 4(3), 475-480.

Su, W.-H., Arvanitoyannis, I.S. & Sun, D.-W., 2018a. Trends in Food Authentication, *Modern Techniques for Food Authentication*. Elsevier, pp. 731-758.

Su, W.-H., Bakalis, S. & Sun, D.-W., 2018b. Fourier transform mid-infrared-attenuated total reflectance (FTMIR-ATR) microspectroscopy for determining textural property of microwave baked tuber. *Journal of Food Engineering* 218, 1-13.

Su, W.-H., He, H.-J. & Sun, D.-W., 2015. Application of hyperspectral imaging technique for measurement of external defects of potatoes. *Biosystems Engineering and Research Review* 20, 9.

Su, W.-H., He, H.-J. & Sun, D.-W., 2017a. Non-destructive and rapid evaluation of staple foods quality by using spectroscopic techniques: a review. *Critical Reviews in Food Science and Nutrition* 57(5), 1039-1051.

Su, W.-H. & Sun, D.-W., 2016a. Comparative assessment of feature-wavelength eligibility for measurement of water binding capacity and specific gravity of tuber using diverse spectral indices stemmed from hyperspectral images. *Computers and Electronics in Agriculture* 130, 69-82.

Su, W.-H. & Sun, D.-W., 2016b. Facilitated wavelength selection and model development for rapid determination of the purity of organic spelt (*Triticum spelta* L.) flour using spectral imaging. *Talanta* 155, 347-357.

Su, W.-H. & Sun, D.-W., 2016c. Multivariate analysis of hyper/multi-spectra for determining volatile compounds and visualizing cooking degree during low-temperature baking of tubers. *Computers and Electronics in Agriculture* 127, 561-571.

Su, W.-H. & Sun, D.-W., 2016d. Potential of hyperspectral imaging for visual authentication of sliced organic potatoes from potato and sweet potato tubers and rapid grading of the tubers according to moisture proportion. *Computers and Electronics in Agriculture* 125, 113-124.

Su, W.-H. & Sun, D.-W., 2016e. Rapid visualization of moisture migration in tuber during dehydration using hyperspectral imaging. *CIGR-AgEng conference*(Jun. 26–29, 2016), Aarhus, Denmark.

Su, W.-H. & Sun, D.-W., 2017a. Chemical imaging for measuring the time series variations of tuber dry matter and starch concentration. *Computers and Electronics in Agriculture* 140, 361-373.



CIGR 2018

XIX. World Congress of CIGR



Su, W.-H. & Sun, D.-W., 2017b. Evaluation of spectral imaging for inspection of adulterants in terms of common wheat flour, cassava flour and corn flour in organic Avatar wheat (*Triticum spp.*) flour. *Journal of Food Engineering* 200, 59-69.

Su, W.-H. & Sun, D.-W., 2017c. Hyperspectral imaging as non-destructive assessment tool for the recognition of sweet potato cultivars. *Biosystems Engineering and Research Review* 22, 21.

Su, W.-H., Sun, D.-W., He, J.-G. & Zhang, L.-B., 2017b. Variation analysis in spectral indices of volatile chlorpyrifos and non-volatile imidacloprid in jujube (*Ziziphus jujuba* Mill.) using near-infrared hyperspectral imaging (NIR-HSI) and gas chromatograph-mass spectrometry (GC-MS). *Computers and Electronics in Agriculture* 139, 41-55.

Su, W.H. & Sun, D.W., 2018a. Fourier Transform Infrared and Raman and Hyperspectral Imaging Techniques for Quality Determinations of Powdery Foods: A Review. *Comprehensive Reviews in Food Science and Food Safety* 17(1), 104-122.

Su, W.H. & Sun, D.W., 2018b. Multispectral Imaging for Plant Food Quality Analysis and Visualization. *Comprehensive Reviews in Food Science and Food Safety* 17(1), 220-239.

Trinh, K.T. & Glasgow, S., 2012. On the texture profile analysis test. *Chemeca 2012: Quality of life through chemical engineering: 23-26 September 2012, Wellington, New Zealand*, 749.

Woess, C., Unterberger, S.H., Roeder, C., Ritsch-Marte, M., Pemberger, N., Cemper-Kiesslich, J., Hatzer-Grubwieser, P., Parson, W. & Pallua, J.D., 2017. Assessing various Infrared (IR) microscopic imaging techniques for post-mortem interval evaluation of human skeletal remains. *PloS one* 12(3), e0174552.

Wu, D., Sun, D.-W. & He, Y., 2014. Novel non-invasive distribution measurement of texture profile analysis (TPA) in salmon fillet by using visible and near infrared hyperspectral imaging. *Food Chemistry* 145, 417-426.



CIGR 2018

XIX. World Congress of CIGR



Cutting Resistance and Energy of Rice Stem

Reşat ESGİCİ¹, F. Göksel PEKİTKAN², Abdullah SESSİZ²

¹Bismil Vocational High School, Dicle University, Diyarbakır, TURKEY

²Faculty of Agriculture, Department of Agricultural Machinery and Technologies Engineering,
Dicle University, Diyarbakır, TURKEY
resgici@dicle.edu.tr

ABSTRACT

The aim of this study was to compare the rice stem cutting properties for two local rice varieties, Karacadağ Karakılçık and Karacadağ Beyaz.

In this study, the cutting energy of rice stem was examined at different internode positions. The experiments were conducted at stem moisture contents of 70.81 %, 41.60 % and 7.5 % w.b. and three internode positions lower (N1), medium (N2) and higher (N3) mm down from the panicles. The stem cutting force and energy was measured with an Universal Testing Machine.

The test results show that the cutting force increased linearly with the increase moisture content. The obtained cutting force values varied from 72.19 N to 17.74 N and 55.35 N to 15.43 N, for Karakılçık and Beyaz varieties, respectively. However, there were found significant differences among the varieties. The maximum values were observed from Karakılçık variety. The cutting energy decreased with decrease moisture content. While the maximum cutting energy was obtained at 70.81 % moisture content as 10.85 Ncm and 8.70 Ncm for Karakılçık and Beyaz varieties, respectively. The lowest values were obtained at 7.50 % moisture content for both varieties.

Keywords: Rice stem, Shearing resistance, Force, Energy.

INTRODUCTION

One of important rice grower region is Southeastern part in Turkey. In this region, two important rice varieties, Karacadağ Karakılçık and Karacadağ Beyaz, are grown and 95 % of rice cultivation area and production was performed in Şanlıurfa, Diyarbakır and Mardin provinces (especially, Karacadağ region) and harvesting is performed heavily by manually and combine harvesters. These varieties are different each other features according to stem and kernel. However, the both varieties are harvested with the same combine harvester and operating parameters during the harvesting period. Therefore, the grain losses are excessive. The main problem of rice production is the high rate of loss broken rice kernel during the harvesting, threshing and post harvesting processing stage. So, it is necessary to reduce these losses.



CIGR 2018

XIX. World Congress of CIGR



For this, we know that physical and mechanical properties for selecting design and operational parameters of equipment relating to harvesting and threshing (Wozniak, 2001; Correa et al., 2007; Esgici et al., 2016).

The objective of this study was to assess the maximum rice stem cutting force and cutting energy along the length of rice stem for two local varieties under different moisture and internode conditions.

MATERIALS AND METHODS

Experimental Materials and Moisture Content

Two rice varieties, Karacadağ Karakılçık and Karacadağ Beyaz, were obtained in 2016 from a commercial farm of Diyarbakır province, Southeastern part of Turkey, with panicles at during harvesting season (Fig. 1). The harvested rice samples were transported to laboratory of Department of Agricultural Machinery and Technologies Engineering, Dicle University, Agriculture Faculty, Turkey and storage at temperature of 4 °C for 4 weeks until uniform moisture content was obtained for all samples. The measured of some average rice physical properties are given in Table 1.



Fig. 1. Rice panicles (left: Beyaz (white), right: Karakılçık (Dark).

Table 1. Some rice physical properties both variety.

Physical properties	Rice variety	
	Karakılçık (dark)	Beyaz (white)
Plant height, mm	1062	1140
Panicle length, mm	41.70	39.47
Panicle weight, g	2.18	2.03
Stem diameter, mm	3.33	3.05

In order to determine the average moisture content of rice stem, four samples of 25 g stem for each variety were weighed and dried in an oven of 103°C for 24 h and then reweighed (ASABE



2006) for m.c. measurements. The average moisture contents were obtained as 70.81 %, 41.60 % and 7.5 % w.b., respectively.

Stem Cutting Properties

Before cutting tests, the rice stems were cutted manually at ground-level at three internodes, namely; first, second and third internode and the internodes were labeled as N1, N2, and N3, respectively (Fig. 2). The fourth and the other lower stem internodes from the ear were not considered because these internodes are usually left on the field (Tavakoli et al., 2009a; Zareiforush et al., 2010). The stem internodes were separated out according to their position down from the ear (Yore et al., 2002; Chandio et al., 2013). In each internode diameters were measured using a digital caliper with the accuracy of 0.01 mm. Three diameter measurements were taken for each sample and averaged. The internode diameter of the stem (mm) was converted to cross-section area in mm².

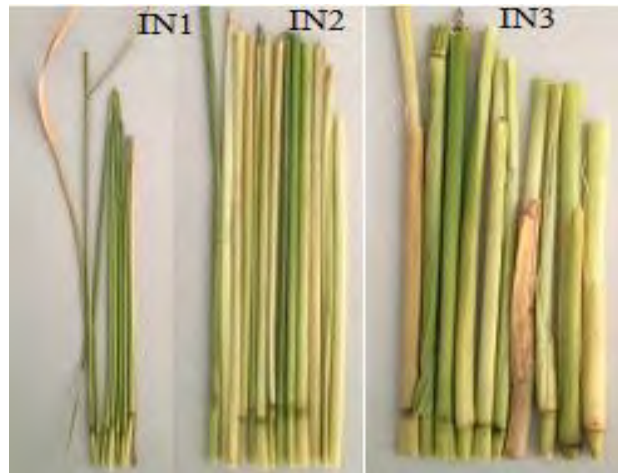


Fig. 2. Rice stem internodes: IN1, IN2, and IN3: The first, second, and third internodes, respectively

Cutting tests were conducted with an Instron Universal Materials Testing Machine, Lloyd LRX Plus, as shown in Fig. 3. The applied force was recorded as a function of displacement. The rice stem specimens for the cutting tests were obtained from whole plants randomly selected. During the tests, the samples of rice stems were placed on the table in its flat position. Loading was applied vertical direction (Lu and Siebenmorgen, 1995; Sessiz et al., 2015; Esgici et al., 2017). Cutting measurements were performed at 30 mm/min fixed cutting speed for all tests.

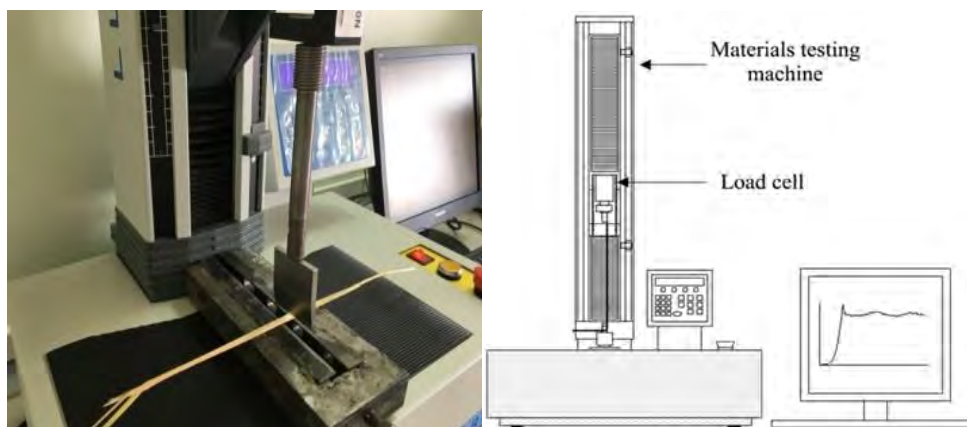


Fig. 3. The cutting test of rice stem with Llyod LRX Plus Testing Machine.

The cutting energy was calculated by measuring the surface area under the force-deformation curve (Mohsenin, 1986; Yore et al., 2002; Chen et al., 2004; Nazari et al., 2008; Wozniak, 2001; Chandio et al., 2013; Sessiz et al., 2015). The cutting energy and displacement was calculated by material testing machine. The area under cutting force-deformation curve was obtained by using a NEXYGEN computer program. A computer data acquisition system recorded all the force-displacement curves during the cutting process.

This study was planned as a completely randomized block design. Cutting force and cracking was determined with twenty-five replications in each treatment. Experimental data were analyzed using analysis of variance (ANOVA) and the means were compared at the 1 and 5 % levels of significance using the Tukey multiple range tests in JMP software, version 11.

RESULTS AND DISCUSSION

The main values for the cutting force and cutting energy of rice stems for both varieties at different moisture content are presented in Table 2. The results of variance analysis indicated that the cutting force and energy values of rice stems is closely related to stem moisture content and variety. The stem cutting force requirement increased linearly with the increase moisture content. Both cutting force and cutting energy values were significant decrease ($p < 0.01$) from the 70.81 to 7.5 % moisture content. The obtained cutting force values varied from 72.19 N to 17.74 N and 55.35 N to 15.43 N, for Karakılçık and Beyaz varieties, respectively (Table 2). However, there were found significant differences among the varieties. The maximum values were observed from Karakılçık variety. That's the results indicated that the stem resistance of Karakılçık variety is higher than Beyaz variety. This means that the energy need for cutting of Karakılçık variety is more than Beyaz variety. So, before start to a new design a harvesting or threshing machine, we must consider such as this values. Similar results were obtained for cutting energy depends on moisture content. The cutting energy decreased with decrease



CIGR 2018

XIX. World Congress of CIGR



moisture content. While the maximum cutting energy was obtained at 70.81 % moisture content as 10.85 Ncm and 8.70 Ncm for Karakılçık and Beyaz varieties, respectively. The lowest values were obtained at 7.50 % moisture content for both variety (Table 2). The similar results were found by Yore et al. (2002) for rice straw.

Table 2. The change of mean cutting force and energy depend on moisture content for Karakılçık and Beyaz paddy varieties.

Moisture content, % w.b.	Variety*			
	Karakılçık**		Beyaz**	
	Cutting force, N	Cutting energy, Ncm	Cutting force, N	Cutting energy, Ncm
70.81	72,19 ^a	10.85 ^a	55,35 ^a	8.70 ^a
41.60	60,65 ^b	8.70 ^b	46,28 ^b	5.89 ^b
7.50	17,74 ^c	3.15 ^c	15,43 ^c	2.39 ^c
Mean	50.19 ^a	7.56 ^a	39.02 ^b	5.66 ^b

*All data represent the average of three replications with 15 values.

**means followed by the same letter in each column are not significantly different by Tukey's multiple range test at the 5 % level.

The average values of cutting force and energy for internodes with three stem diameter are presented in Table 3. As shown in Table 3, the cutting force and energy values were found to be decreased statistically significant ($p < 0.01$) from lower region (IN3) to upper region (IN1). There were found significant differences between internodes and varieties. Cutting forces and energies for three internodes and both varieties were found significantly different. The higher cutting force energy and values were found in the third internode (IN3) compared to the other internodes at both Karakılçık and Beyaz variety because of the accumulation of more mature fibers and higher diameter in the stem (Li et al., 2014). However, according to the Tukey's multiple range tests, both the cutting force and cutting energy of Karakılçık variety values is significantly greater ($p < 0.01$) than Beyaz rice variety. The cutting force results of internodes IN1, IN2 and IN3 varied from 33.93 N to 67.67 N and 22.94 to 53.72 N, for Karakılçık and Beyaz varieties, respectively (Table 3). Also, the values of energy varied from 4.80 Ncm to 11.46 Ncm and 3.07 to 8.65 Ncm for Karakılçık and Beyaz variety, respectively. This means that the energy requirement for shearing of Karakılçık variety is more than Beyaz variety. This effect could be related to higher stem resistance of stem wall thickness of cross-sectional area of Karakılçık compared to the Beyaz variety. It was concluded that when increasing cutting height towards from the third internode to the first internode, it can be more energy saving during the rice harvesting. The similar results were obtained by Alizadeh et al. (2011) for rice stem, Li et al., (2014) for two different rice varieties. Also, these results are in agreement with Yore et al. (2002) for rice straw, Tavakoli et al. (2009b) determined shear strength for wheat and barley straw and Zareiforush et al. (2010) for rice straw, Chandio et al. (2013) for wheat and rice straw, Alizadeh et al. (2011) for rice stem. Tavakoli et al. (2010) compared mechanical



CIGR 2018

XIX. World Congress of CIGR



properties of two varieties of rice straw. They results showed that the cutting force and energy requirement were different both varieties.

Table 3. The change of mean cutting force and energy depend on stem region internodes) for stem of Karakılçık and Beyaz paddy varieties.

Stem diameter, mm	Variety*			
	Karakılçık**		Beyaz**	
	Cutting force, N	Cutting energy, Ncm	Cutting force, N	Cutting energy, Ncm
1.5 (upper region, IN1)	33.92 ^c	4.80 ^c	22.94 ^c	3.07 ^c
3.5 (middle region, IN2)	48.98 ^b	6.44 ^b	40.42 ^b	5.26 ^b
4.5 (lower region, IN3)	67.67 ^a	11.46 ^a	53.72 ^a	8.65 ^a
Mean	50.19 ^a	7.56 ^a	39.02 ^b	5.66 ^b

*All data represent the average of three replications with 15 values.

**means followed by the same letter in each column are not significantly different by Tukey's multiple range test at the 5 % level.

CONCLUSIONS

In this study, the mechanical properties of two varieties of rice stem at three internode positions were compared at three moisture content. The higher cutting force energy and values were found in the third internode (IN3) compared to the other internodes at both Karakılçık and Beyaz variety. However, results show that the average cutting strength and cutting energy of Karakılçık rice variety were significantly higher than those of Beyaz rice variety. The cutting location and diameter of stem are significant factor in cutting force and energy.

REFERENCES

- Alizadeh, M.R., Ajdadi, F.R., Dabbaghi, A. (2011) Cutting energy of rice stem as influenced by internode position and dimensional characteristics of different varieties. *AJCS* 5(6):681-687, ISSN:1835-2707.
- ASABE Standards, 2006. S358.2: 1:1 Measurement –Forages. 52nd edn. American Society of Agricultural Engineers, St Joseph MI.
- Chandio, F.A., Changying J., Tagar, A.A., Mari, I.A., Guangzhao, T., Cuong, D.M. (2013) Comparison of mechanical properties of wheat and rice straw influenced by loading rates. *African Journal of Biotechnology* Vol. 12(10), pp. 1068-1077.
- Chen, Y., Gratton, J.L., Liu, J. (2004). Power requirements of hemp cutting and conditioning. *Biosystems Engineering* Vol. 87(4), pp. 417-424.



CIGR 2018

XIX. World Congress of CIGR



Correa, P.C., Silva, F.S., Jaren, C., Junior, P.C.A., Arana, I. (2007) Physical and mechanical properties in rice processing. *Journal of Food Engineering* Vol:79, pp: 137–142.

Esgici, R., Özdemir, G., Pekitkan, F.G., Elicin, A.K., Öztürk, F., Sessiz, A. (2017) Some engineering properties of the Şire grape (*Vitis Vinifera* L.). *Scientific Papers. Series B, Horticulture*. Vol. LXI, 2017. Print ISSN 2285-5653, ISSN 2286-1580, ISSN-L 2285-5653. June 8-10, Bucharest, Romania.

Esgici, R., Sessiz, A., Bayhan, Y. (2016) The relationship between the age of combine harvester and grain losses for paddy. *International Scientific Journal. Mechanization in Agriculture*. Issue: 1/2016, 18-21, ISSN 0861-9638, Sofia, Bulgaria.

Li, Y.N., Li, K., Ding, W.M, Chen, K.J, Ding, Q.S. (2014) Correlation between head rice yield and specific mechanical property differences between dorsal side and ventral side of rice kernels. *Journal of Food Engineering*, (123) 60–66.

Lu, R., Siebenmorgen, T.J. (1995) Correlation of HRY to selected physical and mechanical properties of rice kernels. *Transactions of the ASAE* 38 (3), 889–894.

Mohsenin, N.N. (1986) *Physical properties of plant and animal materials*. Gordon and Breach Science Publishers, New York.

Nazari, G.M., Tabatabaeifar, A., Jafari, A., Sharifi A., Rafiee S. (2008) Bending and shearing characteristics of alfalfa stems. *Agricultural Engineering International the CIGR Ejournal*. Manuscript FP 08 001. Vol. X. May.

Sessiz, A., Esgici, R., Özdemir, G., Eliçin, A.K., Pekitkan, F.G. (2015). Cutting properties of different grape varieties *Agriculture & Forestry*, Vol. 61. Issue 1: 211-216, 2015, DOI: 10.17707 /AgricultForest. 61.1.27 Podgorica.

Tavakoli, H, Mohtasebi, S.S., Jafari, A. (2009a) Physical and mechanical properties of wheat straw as influenced by moisture content. *Int. Agrophysics* 23(2):175-181.

Tavakoli, H., Mohtasebi, S.S., Rajabipour, A., Tavakoli, M. (2009b) Effects of moisture content, loading rate, and grain orientation on fracture resistance of barley grain. *Research in Agricultural Engineering*, 55(3), 85-93.

Tavakoli, M., Tavakoli, H., Azizi, M.H., Haghayegh, G.H. (2010) Comparison of mechanical properties between two varieties of rice straw. *Advance Journal of Food Science and Technology* 2(1): 50-54.

Wozniak, W. (2001) Mechanical properties of wheat grain in relation to internal cracks *Int. Agrophysics*, 15, 59-64.

Yore, M.W., Jenkins, B.M., Summers, M.D. (2002) Cutting properties of rice straw. *ASAE. Annual Int Meeting / CIGR XV the World Congress*. USA, 28-31 July:1-9.

Zareiforush, H., Mohtasebi, S.S., Tavakoli, H., Alizadeh, M.R. (2010) Effect of loading rate on mechanical properties of rice (*Oryza sativa* L.) straw. *Aust J. Crop. Sci.* 4(3):190-195.

Reşat ESGİCİ, F. Göksel PEKİTKAN, Abdullah SESSİZ. "Cutting Resistance and Energy of Rice Stem"



CIGR 2018

XIX. World Congress of CIGR



Automated Compensation and Diagnostic System for Electrical Conductivity and pH Probes in Recirculating Hydroponics

Woo-Jae Cho¹, Hak-Jin Kim^{1,2,*}, Dae-Hyun Jung¹, Seung-Hwan Yang³

¹Department of Biosystems and Biomaterials Engineering, College of Agriculture and Life Sciences, Seoul National University, Seoul, 08826, Republic of Korea

²Research Institute for Agriculture and Life Sciences, Seoul National University, Seoul, 08826, Republic of Korea

³Convergence components & agricultural machinery group, Korea Institute of Industrial Technology, Jeonju, 54853, Republic of Korea
kimhj69@snu.ac.kr

ABSTRACT

In closed hydroponics, the nutrient solutions are reused based on the measurement of pH and electrical conductivity (EC) using portable or bench top analyzers equipped with electrode probes to effectively maintain the nutrient status of the reused solution in an optimal level for crop growth. However, a main problem with this practice is that the EC and pH probes can provide inconsistent responses due to signal drifts which can be induced when the probes are immersed in the solution for a long time. In that sense, frequent calibration of pH and EC probes would allow more accurate monitoring of nutrients for crop growth in closed systems. In addition, the implementation of an automatic electrode diagnostic system with an alarm function would be useful in operating hydroponic nutrient management system due to the ability to alert the grower to detect the malfunctions or failures of the electrodes. In this study, an automated compensation and diagnostic system was developed to more accurately monitor changes in pH and EC values in hydroponic solutions. The system could check the status of the pH and EC probes based on the measurement of their drifts by automatic introduction of normalization solution with known concentrations and compensate the drifts by one-point normalization. The pH and EC measurements were conducted before supplying the nutrient solutions to the growing bed of plants. The effectiveness of the developed system was evaluated by a comparison to a standard method involving sampling and laboratory analysis while growing lettuce plants based on the ebb and flow method. From the results, RMSEs of the EC and pH probes without compensation were 68.68 $\mu\text{S}/\text{cm}$ and 0.15 pH. With compensation, RMSEs of the EC and pH probes were 38.26 $\mu\text{S}/\text{cm}$ and 0.11 pH. Application of the developed system to a closed hydroponic cultivation system proved to be feasible in precision hydroponic nutrient management by reducing the RMSEs of the EC and pH measurements.

Keywords: Electrical Conductivity, Ph, Automation, Compensation, Diagnostic System, Republic Of Korea

Woo-Jae Cho, Hak-Jin Kim, Dae-Hyun Jung, Seung-Hwan Yang. "Automated Compensation and Diagnostic System for Electrical Conductivity and pH Probes in Recirculating Hydroponics"



CIGR 2018

XIX. World Congress of CIGR



INTRODUCTION

Hydroponics has been widely used in modern horticulture due to the several advantages such as fewer diseases, less pesticides, and higher yields. In particular, recirculating hydroponic solution is considered to be a more effective method to reduce the waste of the fertilizers and minimize the environmental impact of hydroponic systems. In closed systems, the nutrient solutions are reused based on the measurement of pH and electrical conductivity (EC) using portable or bench top analyzers equipped with electrode probes to effectively maintain the nutrient status of the reused solution in an optimal level for crop growth. However, a main problem with this practice is that the EC and pH probes can provide inconsistent sensitivity responses due to signal drifts which can be induced when they are immersed in the solution for a long time (Devlin et al., 2013; Hakonen and Hulth, 2008; Ncube et al., 1991; Robinson and Lawrence, 2006). Therefore, regular calibration with pH and EC measurements would be necessary to allow more accurate monitoring and management of nutrients for crop growth in closed systems. Currently, most of the commercial hydroponic nutrient management systems are operated based on a manual calibration of pH and EC probes and provide no diagnostic information about the real-time status of the probes to indicate whether they work properly or not, which makes it hard to detect the malfunctions or failures of the electrodes. One-point normalization method can be used to compensate for the drifts of the probes that might occur over time. In addition, drifts measured from the one-point normalization can be utilized as a diagnostic factor for confirming the probes function correctly (Tian et al., 2000).

The objectives of this study were to develop an automated compensation and diagnostic system for pH and EC probes used in hydroponic fertilizer management systems with the capability to compensate for signal drifts and detect their malfunctions in real time.

CONSTRUCTION OF AUTOMATED COMPENSATION AND DIAGNOSTIC SYSTEM

One-point normalization is a simple method for detecting a drift in a probe. After a probe is used for a period of time, the probe is immersed in normalization solution with known sensing value. Then drift of the probe can be calculated by comparing the measured value and the known value. Based on the method, an automated compensation and diagnostic system was designed to conduct one-point normalization method automatically, modified from a common closed hydroponic system.

Basic hydroponic system was an ebb and flow system used in the previous study (Jung et al., 2015). The hydroponic system included a 100 L nutrient solution tank, a nutrient solution

Woo-Jae Cho, Hak-Jin Kim, Dae-Hyun Jung, Seung-Hwan Yang. "Automated Compensation and Diagnostic System for Electrical Conductivity and pH Probes in Recirculating Hydroponics"



CIGR 2018

XIX. World Congress of CIGR



supplying pump (PP50Y, Hwarang System Co., Ltd., South Korea), and a growing bed with fluorescent lamps. And for supplying the normalization solution while isolating from the nutrient solution, four electric actuated ball valves (KE006, ACE valve, Republic of Korea) and one normalization solution supplying pump (PE-350MA, WILO, Germany) were applied to an EC/pH sensor channel. Additional EC and pH probes were equipped to a bypass to verify the system performance. For the EC and pH measurements, two sets of an EC probe (HI7635, Sistemes Electrònics Progrés S. A., Spain) and a pH probe (HI1001, Hanna instruments, USA) were employed. The signals of the probes were converted by a transmitter (TRANSMITTER pH/EC, Sistemes Electrònics Progrés S. A., Spain) and the converted signals were read using a data acquisition system (NI cDAQ-9174, National Instruments, USA) with an 8-channel current input module (NI-9203, National Instruments, USA). The constructed system was shown in Figure 1.

For controlling the valves and the pumps to conduct a normalization procedure, a personal computer was used with a lab-made software based on a LabVIEW (v2015, National Instruments, USA).

One-point normalization solution was prepared following the modified Yamazaki's hydroponic formulations for lettuce (Jung et al., 2015), which had EC 1210 $\mu\text{S}/\text{cm}$ and pH 6.99.

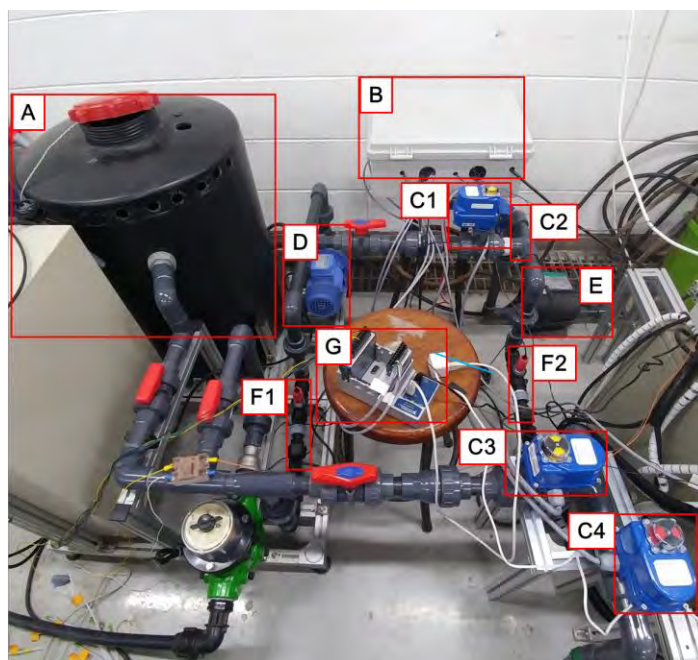


Figure 1. View of the automated compensation and diagnostic system. A: Nutrient solution tank; B: Control box with the transmitters for EC/pH probes; C1-4: Electric actuated ball valves; D: Nutrient solution supplying pump; E: Normalization solution supplying pump; F1-2: EC/pH probes as a control group (F1) and an experimental group (F2); G: Data acquisition system.

Woo-Jae Cho, Hak-Jin Kim, Dae-Hyun Jung, Seung-Hwan Yang. "Automated Compensation and Diagnostic System for Electrical Conductivity and pH Probes in Recirculating Hydroponics"



COMPENSATION AND DIAGNOSTIC PROCEDURE

To compensate the drifts of the probes and check the operation status of the probes, the system was programmed to control the valves and the normalization solution pump with six different steps. The system operation for the normalization of the probes is shown in figure 2. In the first step, the system is in idle state and the probes are used to measure the EC and pH of the nutrient solution supplied, while the valve #2 and #4 are closed. When the time is up to start the normalization, the second step is started. The valve #1 and #3 are closed and then the valve #2 is opened. After the valve #2 is opened, the pump is powered on and the remaining nutrient solution is drained. In the third step, valve #4 is opened and the sensor channel is filled with the normalization solution. In the fourth step, all valves are closed and the pump is powered off. During the fourth step, the measured values by the EC and pH probes immersed in the normalization solution are compared with the known values of the normalization solution and the differences among the probes are calculated as an index of drift (Eq. 1). The status values of the EC and pH probes are calculated using Eq. 2 to determine whether they work properly or not. When the drift index is more than 10% compared to the known concentration of the calibration solution, a LED alarm in user interface (UI) is turned on, which means the probe should be precisely calibrated or changed.

$$\text{Drift (EC,pH)} = C_o - C_k \quad (1)$$

where C_o is the concentration originally measured by the EC or pH probe and C_k is the known concentration of the normalization solution.

$$|(\text{Drift (EC,pH)})/C_k| \geq 0.1 \rightarrow \text{Probe status warning}$$

$$|(\text{Drift (EC,pH)})/C_k| < 0.1 \rightarrow \text{Probe normal status} \quad (2)$$

In the 5th step, valve #4 is closed and the pump is powered to drain the remaining normalization solution. In the 6th step, the valves and pump are then returned to the idle state returned to the first step.

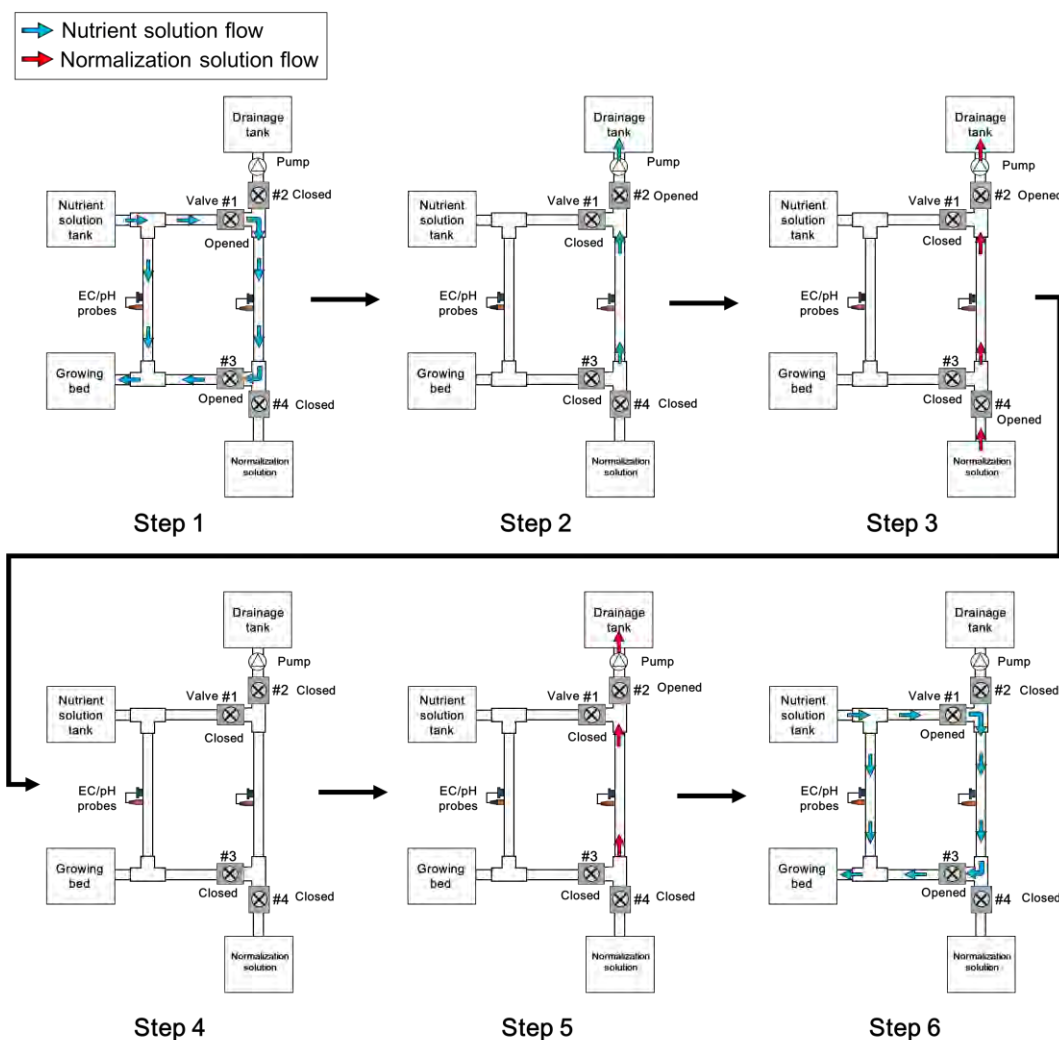


Figure 2. The diagram of the system operation for the one-point normalization.

SYSTEM EVALUATION

The developed system was applied to the recirculating test platform used in our previous studies for the evaluation (Cho et al., 2017; Jung et al., 2015). Lettuce was cultivated by a recirculating hydroponic system based on the ebb-and-flow method. The nutrient solution was supplied for 17 min and flowed back into the nutrient solution tank by gravity. The recirculation was repeated every 2 hours. Prior to the nutrient solution supply, the normalization sequence was operated. During the cultivation, the EC and pH probes were used to monitor the nutrient solution and the concentrations measured by the probes without normalization were compared with the

Woo-Jae Cho, Hak-Jin Kim, Dae-Hyun Jung, Seung-Hwan Yang. "Automated Compensation and Diagnostic System for Electrical Conductivity and pH Probes in Recirculating Hydroponics"



CIGR 2018

XIX. World Congress of CIGR



concentrations measured by the probes with normalization (figure 3). From the results, the measurements from the probes without normalization showed root mean square errors (RMSEs) of 68.68 $\mu\text{S}/\text{cm}$ and 0.15 pH. The measurements from probes with normalization showed RMSEs of 38.26 $\mu\text{S}/\text{cm}$ and 0.11 pH, which were less than those of the probes without normalization.

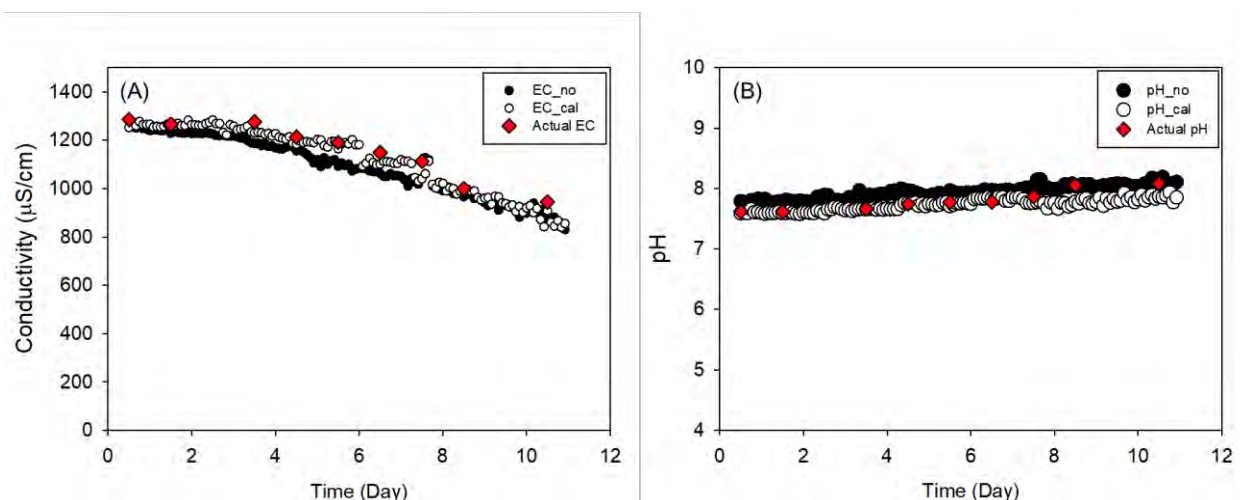


Figure 3. Changes in EC (A) and pH (B) measured with the probes with normalization (black circle) and without normalization (white circle).

Sensor drifts during the cultivation could be identified from the measurements of the concentrations of the normalization solution using the probes without normalization (figure 4). There were differences of 276.5 $\mu\text{S}/\text{cm}$ and 0.20 pH between the first day and the last day, which might be related to the sensor drifts. Also, the drift of EC probe was larger than the drift index (10%), the LED alarm in UI was turned on to inform the EC probe should be recalibrated or changed (figure 5)

During the period, the RMSEs of 143.3 $\mu\text{S}/\text{cm}$ and 0.15 pH were appeared, which supported the necessity of the drift compensation for allowing more accurate sensing and management of the nutrient solutions.



CIGR 2018

XIX. World Congress of CIGR

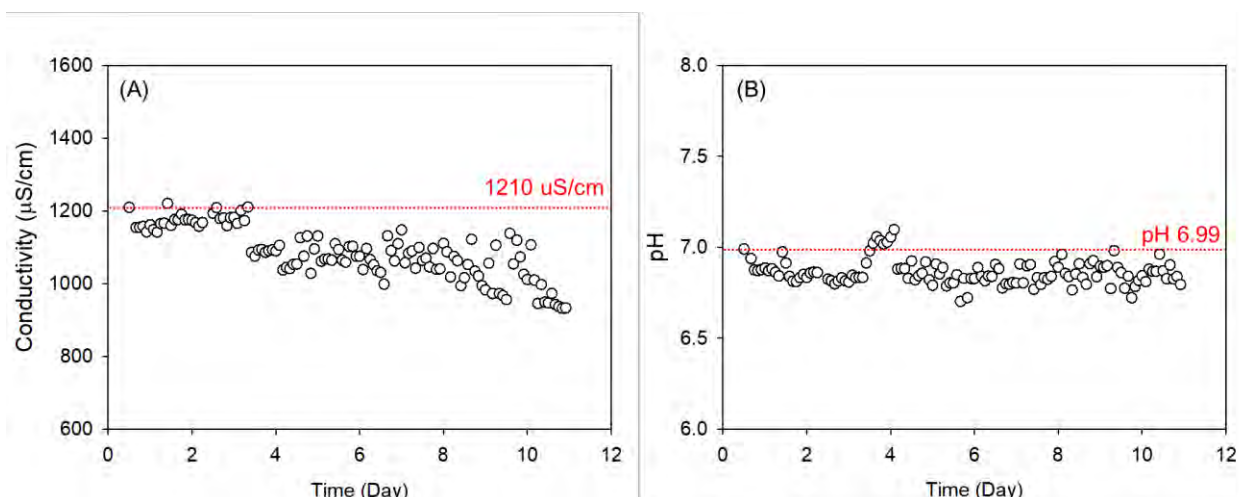


Figure 4. Changes in EC (A) and pH (B) of the normalization solution measured by the probes without normalization.

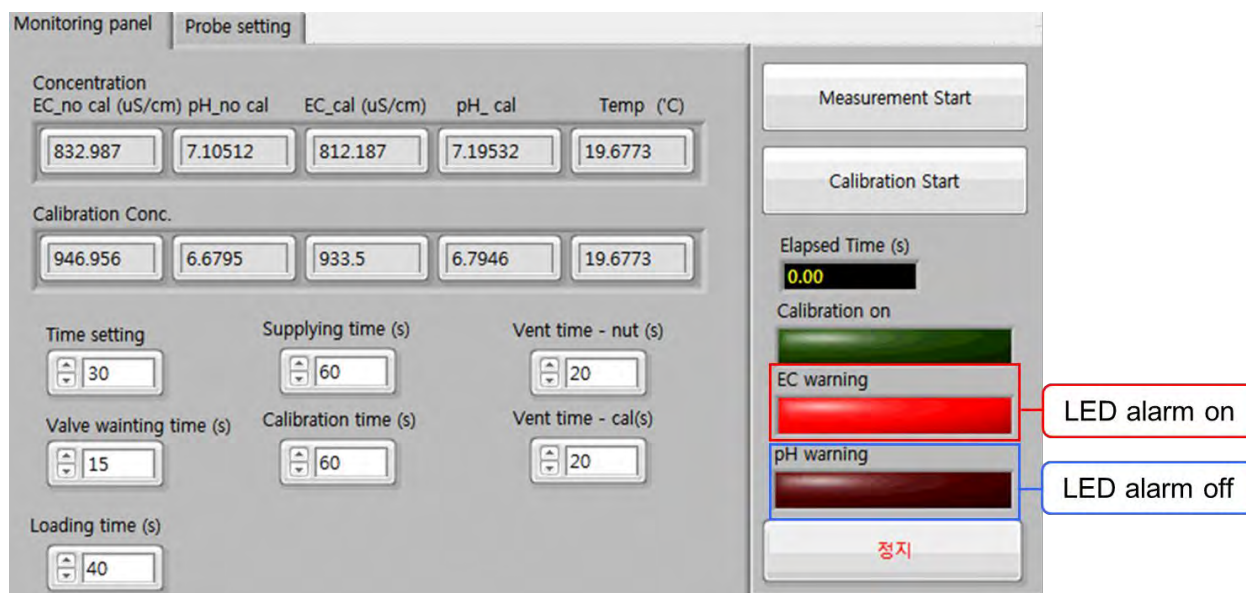


Figure 5. LED alarm in UI from the last day.

CONCLUSION

Through the test, the drifts of the EC and pH probes during the cultivation were verified and the feasibility of the automated compensation and diagnostic system was evaluated.



CIGR 2018

XIX. World Congress of CIGR



During the cultivation, the results show the trend of the EC and pH of the nutrient solution were more accurately monitored by the probes with normalization, showing the lower RMSEs. In addition, the status of the pH and EC probes were diagnosed based on the drifts by automatic one-point normalization application. The implementation of the diagnostic system with an alarm function would be useful in the hydroponic nutrient management systems due to the ability to alert the grower to detect the malfunctions or failures of the electrodes.

Overall, application of the developed system to a closed hydroponic cultivation system proved to be feasible in precision hydroponic nutrient management due to an improvement in the accuracy of the pH and EC measurements.

6. REFERENCES

- Cho, W.J., Kim, H.J., Jung, D.H., Kang, C.I., Choi, G.L., Son, J.E., 2017. An Embedded System for Automated Hydroponic Nutrient Solution Management. *Transactions of the Asabe* 60, 1083-1096.
- Devlin, L., Jamal, M., Razeeb, K.M., 2013. Novel pH sensor based on anthraquinone–ferrocene modified free standing gold nanowire array electrode. *Analytical Methods* 5, 880-884.
- Hakonen, A., Hulth, S., 2008. A high-precision ratiometric fluorosensor for pH: Implementing time-dependent non-linear calibration protocols for drift compensation. *analytica chimica acta* 606, 63-71.
- Jung, D.H., Kim, H.J., Choi, G.L., Ahn, T.I., Son, J.E., Sudduth, K.A., 2015. Automated Lettuce Nutrient Solution Management Using an Array of Ion-Selective Electrodes. *Transactions of the Asabe* 58, 1309-1319.
- Ncube, F., Kastrinakis, E., Nychas, S., Lavdakis, K., 1991. Drifting behaviour of a conductivity probe. *Journal of hydraulic research* 29, 643-654.
- Robinson, K.L., Lawrence, N.S., 2006. Sulfide sensing via differential counter ion diffusion rates through redox-modulated poly (vinylferrocene) microparticles. *Electrochemistry communications* 8, 1055-1061.
- Tian, G. Y., Z. Zhao, and R. Baines. 2000. A fieldbus-based intelligent sensor. *Mechatronics* 10(8):835-849.



CIGR 2018

XIX. World Congress of CIGR



Development and Application of Functional Food for Older People

Józef Grochowicz¹, Anna Fabisiak², Adam Ekielski³

¹Warsaw School of Tourism and Hospitality Management,

² College of Rehabilitation based in Warsaw.

³ Department of Production Management and Engineering, Warsaw University of Life Sciences, 166 Nowoursynowska St. Zip Code: 02-787 Warsaw

adam_ekielski@sggw.pl

ABSTRACT

Introduction. The paper presents the nutrition problems of the elderly persons in the international cross-section. Nutritional recommendations propagated in European countries and addressed to people are very different. The acceptance and willingness to buy functional foods by consumers has been widely studied, but no research has been carried out on the attitude of older consumers towards innovative products with health consequences. This study shows how older consumers perceive functional food and new health-improving products, how willing they are to buy these products and what factors affect their purchases. The continuous development of the functional food products market is being observed. Another factor are changes in the consumer's attitude towards functional food products and lifestyle. Consumers increasingly believe that food contributed to the health-oriented changes in their eating habits.

Objective and Methods. The first part of the study contains a review of functional products available on the market, manufactured exclusively for the elderly and their characteristics against the background of varied nutritional needs of older people. It also contains an overview of the current state in terms of legal provision and the labelling of these products on the European market. In the second part of the research, the opinion of seniors on the role and place of special food for the elderly in their diet as well as possibilities and limitations were analyzed.

Conclusions. The research shows that the market for older consumers is not homogeneous. Based on a qualitative, in-depth approach, the study distinguishes consumer groups with different understanding of health and attitudes towards health-improving products that affect the readiness of people to buy such products. These groups include consumers looking for healthy products, critical and cautious consumers and consumers of natural healthy products. Different motives and barriers of using products with health claims have also been identified and described.

Keywords: Functional food, Nutrition, Elderly adults, Poland

Józef Grochowicz, Anna Fabisiak, Adam Ekielski. "Development and Application of Functional Food for Older People"



CIGR 2018

XIX. World Congress of CIGR



INTRODUCTION

1.1. Definitions, terminology

The relationship between the type of food consumed and the state of health has been already established. The influence of bioactive components on different functions and states of the human body is a subject of continuous research in an interdisciplinary approach, comprising biochemistry, nutrition, gastroenterology and technology of producing/ modifying bioactive food. As a result, the search for dependence between different substances or ingredients and individual conditions or diseases of the organism led to the division of the studied food components and the emergence of those that show these positive effects. Natural functional food contains bioactive ingredients whose type and level of content determines its effect on various body functions. Based on many years of research, it is known that a diet based on plant products reduces the risk of many chronic diseases, and phytochemical compounds reduce the risk of cancer. The list of such products is much larger and includes many other types of vegetables such as roots (red beet) or leafy ones (kale, broccoli, spinach) as well as fruit (avocado, pomegranate, berries etc.).

Processed functional food means both products from which undesirable or harmful ingredients have been removed, such as sugar, fatty acid or excess of salt, as well as ones additional bioactive ingredients. Some of them are described as below:

Cactus pear – its protective spectrum include; anticancer, antiviral, antiinflammatory and anti-diabetic, neurological and cardiovascular actions. On functional and nutraceutical food market in form of juice and edible pulp. It is a rich source of fiber and minerals (Hasler, 2002),

Argan oil - the health properties of argan oil are known from years. It was used to treat liver diseases and to cure hypercholesterolemia and atherosclerosis (Guillaume and Charrouf, 2016),

Seaweeds – are rich of such bioactive substances like: polysaccharides, proteins, lipids, polyphenols, vitamins, minerals with antibacterial, antiviral and antifungal properties (Holdt and Kraan, 2011),

Chia seeds - rich in α -linolenic acid and dietary fibres; antidiabetic and anticancer properties also founded (Patel, 2015),

Grape seeds - The seed extract is recognized as food supplement for prevention of many diseases (Pate, 2015),

Functional foods may support not only an optimal health but also help to diminish the risk of disease. The list of their positive influence is continuously growing.

Providing health benefits from functional food is a relatively new concept both in terms of research and production technology, hence the growth and popularity in society, including producers and consumers. However, legal status and legal regulations regarding food law are not yet well documented and harmonized. Currently functional food is one of the most intensively investigated and promoted areas in the sciences of food and nutrition, but the information and promotion of new products is still insufficient (Holdt and Kraan, 2011).



CIGR 2018

XIX. World Congress of CIGR



2. SENIORS-THEIR NUTRITIONAL REQUIREMENTS AND EXPECTATIONS

One can predict that in the near future, the largest group of consumers will be seniors. By 2018, 10% of the global population will be over the age of 65, according to the research in Canada, the percentage of people over 65 in 2041 can reach up to 25% (Gyles at all, 2010).

In the EU-27 part of population aged 65 or older are set to rise from 17% in 2010 to 30% in 2060. One in eight people will be aged 80 or older in 2060 (Source: Eurostat; <http://www.optifel.eu/the-project/>).

In such situation the developing of innovative food and services designed for elderly populations is a new challenge for food industry and catering but the products offered on the market for them are very limited in terms of accessible functional ingredients that are used. Although the average life expectancy of consumers is increasing considerably, the healthy lifespan is not growing parallelly. The aim of this study is to analyze the actual development of functional food for elderly appearing on the market and their interest, acceptance and purchasing.

2.1. General principles of nutrition for the elderly

Various ailments and health problems as well as inhomogeneity of the population group to which elderly people belong and changes caused by the aging of the body are an important element affecting the way of eating. In older age, the proportions of individual components are important, whose share in energy supply should be: for carbohydrates 50-70%, fats 20-35% and proteins 10-15%. The standards for protein for the elderly are 0.73g / kg m.c. Recommendations on fat intake account for total fat intake and consumption of polyunsaturated fatty acids in an amount of about 10% of energy. The ratio of polyunsaturated fatty acids n-6 to n-3 should be 4-5:1.

Many publications discuss the potential role of antioxidant vitamin concentrations in blood plasma, the impact of the nutritional status of the body on their serum content and the intake of these nutrients with food, their bioavailability. An important element of proper nutrition in this group is also adequate fluid supply. Older people feel less thirsty. One of the reasons for low consumption of fluids is also the fear of edema and frequent excretion due to dysfunctions of the kidneys and urinary tract (Milan and Cameron-Smith, 2015; Gawęcki and Roszkowski, 2013).

Malnutrition was a significant problem among the elderly. The British Association for Parenteral and Enteral Nutrition (BAPEN) published a definition for the term "Malnutrition," which refers to a lack, excess, or imbalance in an individual requirement for energy, protein, and other nutrients in which a deficiency would alter body composition and function (Kraus, 2015; (<http://www.bapen.org.uk/>)).

Of the 190 elderly people, 43% were at risk of malnutrition. Similar results were obtained when 157 people were examined, 47% of whom were undernourished, deficiency related to vitamin D intake at the third level lower and 1.6% lower for folic acid. The reduction of consumption of the



CIGR 2018

XIX. World Congress of CIGR



above-mentioned ingredients and additionally of vitamin C, zinc and magnesium is visible in people aged 75 and over. Therefore, there is a need to develop the food industry in products with increased nutritional density, functional products whose impact will have a beneficial effect on the rationalization of nutrition of older people (Leslie and Hankey, 2015).

2.2. Characteristics of the social group and pathophysiological differentiation of older people

Currently, in developed countries, the population of people over 65 is 14%, while in developing countries around 5%. The aging of the population is a significant and lasting global trend. Global data suggests that the percentage of adults over the age of 60 will increase from 12% to 27% until 2050 ([/www.who.int/ageing/projects/age-friendly-environments/en](http://www.who.int/ageing/projects/age-friendly-environments/en), <http://esa.un.org/unpd/wpp/index.htm>; http://dx.doi.org/10.1787/health_glance-2013.en). The European population over the age of 65 will increase by an additional 20% by 2050 (European Commission 2015). According to a report by the United Nations, the proportion of people in the world aged 60 is projected to increase by 56% between 2015 and 2030 (www.un.org/en/development/desa/population/publications). Aging of an organism is a complex concept, because it is difficult to separate the natural changes of aging of an organism from the pathological changes. During common ageing, organ changes result only from the passage of time and in people whose rate of change is slower this process is called positive aging (successful aging). Unfortunately, this applies only to 10% of the population of this group. The severity of age-related changes may be related to diseases previously experienced. Pathological factors include: cardiovascular and respiratory diseases, endocrine, neurological disorders, etc. (Santeramo et al 2018).

2.3. Functional food and the elderly

An important role in accepting functional food is played by consciousness, personal motivation and the socio-demographic situation. An element in the consumer's opinion would be, above all, the inclusion of information on health claims. Older people, after the age of 65, paid particular attention to functional foods, including dairy products and low-fat products. Older people were more likely to include functional products of their diet due to the awareness of its impact on health (Santeramo et al 2018; Bimbo et al 2017).

3. METHODOLOGY AND RESULTS

As an important factor in the creation of functional products is information on the packaging its visual attractiveness and consistency of food. It is also important to consider the impact on appetite and a different sense of taste. Older people have a raised sensory test; a feeling of sweet,



CIGR 2018

XIX. World Congress of CIGR



salty and sour feeling is four times higher than in young people (www.who.int/ageing/projects/age-friendly-environments/en/)

In order to evaluate the perception of functional food by the elderly, a pilot study was conducted among participants of the University of the Third Age (n = 38, the average age of 69).

The pilot studies carried out show that when purchasing functional food the price plays an important role (26%). The most important meaning among the respondents when choosing the purchase of functional food were pro-health (43%) and the price of products (26%). The price of functional products was also a factor that limits the purchase of functional food as well as the income of older people (24%). These results are confirmed by other studies Anninou 2017; Singh and Kaur (2017); Siro et al (2008).

The research shows that the main factor limiting the purchase of functional food was the lack of information on the availability of this food (13%). The majority of respondents is satisfied from improved health after eating functional products (40%). However, there is a great difficulty in determining the classification of nutrients that occur in functional foods. The respondents included fiber and minerals (44%) and vitamins (15%) among the most frequent ingredients. Difficulties and discrepancies in responses were regained when asked about the benefits of using functional foods. According to the respondents, this food was associated with increased immunity of the organism and with the slowing down of the aging process (31%). A similar difficulty was raised by the question regarding the association of the definition of functional food. In 42% functional food was associated with the tested with health food, healthy food (16%). However, a significant part of the respondents (8%) could not answer this question. A significant proportion of the respondents (73%) does not know the exactness of functional food or have not met with it at all. The most characteristic products for the functional food of respondents were dairy products (60%), cereal products (cereal-45%).

4. NEW PRODUCTS FOR SENIORS

A large number of available bioactive ingredients and additives make it easy to compose products dedicated to older people or with specific requirements. Therefore, quite a lot of new products are created, designed by teams of technologists in larger companies or even in start-ups, because they are still niche products. In Nutrasolutions (September 2017) some new products are described, such as enriched whey protein and chia yoghurts, or finely ground oat grains (preparedfoods.com), production of probiotics in the form of tablets (www.jrspharma.com), new coffee blends containing various additives such as turmeric, cinnamon, acai berry or guarana or chamomile and lavender. Many such products have also been designed under the aforementioned EU project (www.optifel.eu). In recent years, many research centers have focused on finding food for older people, in particular on mixtures that provide the required nutrients and help in eating and feeding people with ailments such as type 2 diabetes. New products such as: pates, mashed potatoes and creams based on the addition of inulin to meat, lentils and pumpkin. The respondents showed 87% acceptance of the sensory evaluation For older people with diabetes, it



CIGR 2018

XIX. World Congress of CIGR



is recommended to mix functional foods that are rich in vegetables with a low fiber content, as well as watercress, soy, bran, tuna and pear fruit, strawberries, apricots). In contrast, commercial products (low-fat, low-sodium). Light cookies (low fat, no sugar) such as: whole grain bread, sugar-free gelatin, Light manchego cheese without lactose, light milk without lactose with the addition of calcium, vitamins A and D, light natural yogurt (no sugar, no lactose) (Coronado at all 2015).

5. SUMMARY AND CONCLUSIONS

1. The barrier of market development is also high prices of products of the functional food segment.
2. The dangers posed by the development of this food market, it can also include abuses on the part of food producers involving the forbidden determination of products with pro-health terms (because a significant part of them is accompanied by health claims). In Poland, there is a significant development of functional food, which is why it is necessary to popularize marketing research. The main argument for this is the need to conduct professional research on new products throughout the full innovation cycle, which significantly reduces the risk of a failed product.
3. Food for the elderly people should be simple based on the flavors that are known to them. On the other hand, it should be designed to change the taste sensation, take into account the consistency, information on the packaging and the availability of the packaging.
4. The diet of older people may be the same as in healthy people and a well-designed functional food may be helpful in controlling certain diseases.

There is a need for research on:

- 1/ how much of bioactive substance should be daily consumed with food to get a lasting effect and what should be the conversion factor (size of the portion, mass),
- 2/ what are the rules for checking whether the content of the active ingredient is reproducible in subsequent products,
- 3/ there are often difficulties in the form of changing the trade name and modifying the composition of the dietary supplement containing a specific bioactive substance
- 4/ there is a need for legal regulations and a better flow of information for both food producers and consumers.

Acknowledgements

The study reported here was prepared with the support of the project 217906/E-176/S/2016.



CIGR 2018

XIX. World Congress of CIGR



REFERENCES

- 2012: OECD. Available from: http://dx.doi.org/10.1787/health_glance-2013.en
- Admassu H., Wei Z., Ruijin Y., Mohammed A.A. G., Elmuez A (2015). Development Of Functional Foods: Sea Weeds (Algae) Untouched Potential And Alternative Resource - A Review. *Int. J Sci. Technol. Res.* 4, 9, 109-115.
- Bimbo et al. (2017) Consumers' acceptance and preferences for nutrition-modified and functional dairy products: A systematic review. *Appetite*, 113, 141-154.
- Coronado, H.M., Gutiérrez, T.R., Vega, L.S., Radilla, V.C., Vazquez, F.M. and Ramírez, V.M.L. (2015) Functional Foods, Old Age and Diabetes. *Food and Nutrition Sciences*, 6, 1507-1513 <http://dx.doi.org/10.4236/fns.2015.616155>
- Gawęcki J. Roszkowski W. (2013). *Żywnienie u progu i schyłku życia*. Wyd. UP, Poznań
- Guillaume D., Charrouf Z., (2016) Functional Food and Sustainable Development. Once Met in the Argan Forest: The Tale of the Argan Oil. In : Kristbergsson K., Ötles S. (eds.), *Functional Properties of Traditional Foods*, Integrating Food Science and Engineering Knowledge Into the Food Chain 12, DOI 10.1007/978-1-4899-7662-8_22: Springer Science+Business Media, New York 309
- Gyles C.L., Carlberg J.G., Gustafson J., Davlut D.A., Jones P.J. (2010) Economic valuation of the potential health benefits from foods enriched with plant sterols in Canada. *Food and Nutrition Research*. 54, 23-29.
- Hasler C. M. (2002) Functional foods: benefits, concerns and challenges – a position paper from the American Council on Science and Health. *J Nutr* 132, 3772–3781.
- Holdt S.L., Kraan S., (2011). Bioactive compounds in seaweed: functional food applications and legislation. *J. Appl. Phycol.* (2011) 23:543–597, DOI 10.1007/s10811-010-9632-5. Published online: 9 February 2011 # Springer Science+Business Media B.V.
- Kraus A., (2015) Development of functional food with the participation of the consumer. Motivators for consumption of functional products. *International Journal of Consumer Studies* 39,2–11.
- Leslie W., Hankey C., (2015) Aging, nutritional status and health. *Healthcare*. 3, 648-658.
- Milan A., Cameron-Smith D. (2015) Digestion and Postprandial Metabolism in the Elderly. *Advances in Food and Nutrition Research*. 76, 79-124.
- Pate S., (2015), Grape Seeds: Agro-Industrial Waste with Vast Functional Food Potential Springer International Publishing Switzerland *Emerging Bioresources with Nutraceutical and Pharmaceutical Prospects*, Applied Environmental Science and Engineering for a Sustainable Future



CIGR 2018

XIX. World Congress of CIGR



Santeramo F. G at all. (2018) Emerging trends in European food, diets and food industry Food Research International

Singh P. Kaur N. , (2017), Deciphering the consumer behavior facets of functional foods: A literature review. *Appetite* 112, 167-187.

Siro I, Kapolma E, Lugasi A. (2008) Functional food. Product development, marketing and consumer acceptance-A review, *Appetite*, 51, 456-467.

Source: Eurostat; <http://www.optifel.eu/the-project/>

The British Association for Parental and Enteral Nutrition (BAPEN)
<http://www.bapen.org.uk/>.(accessed 16.02.2018)

United Nations, Department of Economic and Social Affairs, Population Division. World Population Ageing 2015-Highlights. Available online:
http://www.un.org/en/development/desa/population/publications/pdf/ageing/WPA2015_Highlights.pdf

WHO, World Health Organisation. (2017). UNDESA. World population prospects: the 2017 revision. Available from: <http://esa.un.org/unpd/wpp/index.htm>. Accessed 2018 February 2.

WHO. Age-friendly environments in Europe A handbook of domains for policy action (2017). Available from: <http://www.who.int/ageing/projects/age-friendly-environments/en/>



CIGR 2018

XIX. World Congress of CIGR



Prediction of Soluble Solids Content of Jackfruit Using Shortwave Near Infrared

^{1,2}Nawi,N.M., ¹Abdullah.N., ¹Lazim.S.S.R.M.

¹Department of Biological and Agricultural Engineering, Faculty of Engineering, Universiti Putra Malaysia, 43400, UPM Serdang, Selangor, Malaysia.

²Institute of Plantation Studies, Universiti Putra Malaysia

nazmimat@upm.edu.my

ABSTRACT

Soluble solids content (SSC) is an important quality attributes for jackfruits. This attribute is mainly used to determine the maturity of the fruit. However, there is no reliable and low-cost technology available which can be used by farmers for rapid screening of their jackfruits in an orchard. This preliminary research aimed to explore the potential application of a low-cost shortwave near infrared (SWNIR) spectrometer to non-destructively predict SSC of jackfruit samples from their outer skins. A total of 120 portions were produced from four jackfruit samples. The spectral data collected from the skin surface of each portion was later correlated with its SSC. Partial least square (PLS) method was used to develop both calibration and prediction models to correlate the spectral data with SSC. For the calibration model, it was found that the coefficient of determination (R^2) and root mean square of calibration (RMSEC) was 0.77 and 2.88, respectively. For the prediction model, the R^2 and root means square error of prediction (RMSEP) were 0.74 and 2.97, respectively. These results indicated the SWNIRS has the potential to be applied for predicting SSC of jackfruits from outer skin surfaces to determine the maturity level of the fruit.

Keywords: Jackfruit, Soluble solids content (SSC), Maturity, Spectroscopy, Non-destructive, Malaysia

INTRODUCTION

Jackfruit (*Artocarpus heterophyllus*) is the largest tree-borne fruit which is typically planted throughout the tropic and subtropic regions (Baliga et al., 2011). Among the main producing countries for jackfruits were Brazil, Thailand, Indonesia, India, Philippines and Malaysia (Madruga et al., 2014). In Malaysia, approximately 5,097 ha of land were planted with jackfruit, producing about 28,042 Mt of fruit with the production values up to RM58 million (DOA, 2017).



CIGR 2018

XIX. World Congress of CIGR



The shape of a jackfruit is typically round-cylindrical with the range of mass, length and diameter were about 3.5 to 10 kg, 30 to 100 cm and 25 to 50 cm, respectively (Leong et al., 2016).

Jackfruit which composes of several berries of yellow pulp and brown seeds are rich in carbohydrates, complex B vitamins and minerals. The berries can be eaten fresh or processed into jams, compotes, frozen fruit pulps, juices and soft drinks (Madruge et al., 2014). However, about 60% of the whole fruit is non-edible, consisting of prickly rind, inner non-edible perianth and a central core, which comprise non-utilized waste (Begum et al., 2014). Jackfruit also contains free sugar (sucrose), fatty acids, ellagic acid, and amino acids like arginine and tryptophan (Swami et al., 2012).

Jackfruit is one of the important fruits in Malaysia because these fruits are not only sold for domestic market, but they are also exported to several countries including Singapore, China, Europe and Japan. In order to supply the optimum quality fruits to costumers, the fruit should be harvested at the right maturity level. Optimum level of maturity during harvest may give the best eating quality and also prolong shelf life of the produce. The maturity of the fruits can be assessed directly based on external features such as color, size and shape (Zhang et al., 2014), or indirectly based on internal attributes such as soluble solids content (SSC), acidity, moisture content and nutritional content.

Nowadays, non-destructive measurement method for determining the quality of fruit is getting popular. Near infrared spectroscopy (NIRS) has been successfully used to non-destructively determine the SSC in several fruits such as citrus fruits (Liu et al., 2010) apples (McGlone et al., 2002), guavas (Hsieh and Lee, 2005), kiwifruits (McGlone and Kawano, 1998), mandarins (Gómez et al., 2006), mangoes (Schmilovitch et al., 2000) and pears (Nicolai et al., 2008). Recently, rapid development of a portable and low-cost spectrometer with a shorter wavelength ranges from 200 to 1100 nm appeared promising to be employed for fruit maturity detection (Nawi et al., 2013). However, there is no published study regarding the application of NIRS to predict SSC from jackfruits in order to determine the maturity level of the fruits. Therefore, the goal of this research was to investigate the feasibility of using portable and low-cost spectrometer to predict SSC from jackfruit samples. The specific objective was to develop partial least square (PLS) model for predicting SSC from the jackfruit skin samples.

2. MATERIALS AND METHOD

2.1 Sample preparation

A total of 120 portions were extracted from four matured jackfruit samples. The jackfruit samples were purchased from Meadow Spring Orchard Ltd. Pty., Selangor, Malaysia. Each jackfruit was first weighed to obtain the mass of the fresh jackfruit. Each sample was divided



into five vertical portions (top, upper middle, middle, lower middle and bottom) and six horizontal portions, giving 30 portions for each fruit sample (Figure 1). Each portion was scanned on its skin surface by using a spectrometer. After the spectral reading, each portion subjected to size reduction process prior to SSC measurement.

2.2 Spectral measurements

Spectral data was captured from skin surface of each portion using visible shortwave near infrared (SWNIR) spectrometer (Ocean Optic HR4000, Ocean Optics Inc., Dunedin, Florida) with an effective wavelength ranged from 200 to 1100 nm. This high-resolution miniature fiber optic spectrometer was equipped with a charge-coupled device (CCD) detector, having an optical resolution of 0.50 nm. The spectral data of each portion was recorded three times and averaged before it was used in the development of calibration and prediction models. The spectral measurement was conducted inside a black box which was illuminated by a halogen light source (Model: HL 2000, Ocean Optics Inc., Dunedin, Florida). A scanning distance between the skin surface and the probe was fixed at 15 mm. The spectral data were collected and transformed into a computer with the application of SpectraSuite software (Ocean Optics Inc. Finland). In order to avoid a low signal-to-noise ratio, some obvious noise was removed from both ends of the wavelength, leaving only the wavelength regions between 500 nm and 950 nm were used for the analysis.

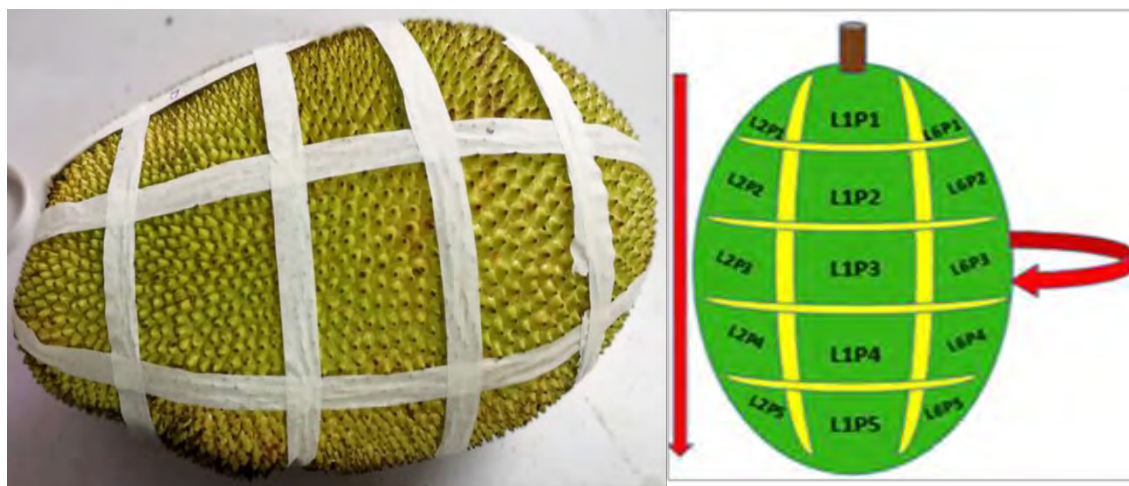


Figure 1. Marking for each portion of jackfruit sample



CIGR 2018

XIX. World Congress of CIGR



2.3 Soluble solids content (SSC) measurements

After spectral reading, each portion was sliced into cube, blended and squeezed to get juice samples for SSC measurements. Juice samples were dropped onto a handheld digital refractometer (Pal-1, Atago Co., Tokyo, Japan) in order to measured SSC ($^{\circ}$ Brix) of skin juice. Juice samples from each portion were measured in three replicates and the average SSC was taken for further analysis.

2.4 Development of calibration and validation models

Before partial least square (PLS) method was applied to build both calibration and prediction models, principal component analysis (PCA) was employed to extract useful information from the spectra, decrease the noise and determine the optimum number of latent variables (Wu et al., 2008). PCA is a well-known chemometrics method to find maximum variability in sample grouping which is used as new axes called principle components (PCs) or latent variables (LVs) (Nawi et al., 2013). PCA could also be used to identify spectral outliers which can reduce the performance of model in each data set. PCA identified outliers from the influence plot which displays the sample residual x-variances against leverages.

In this study, the development of the PLS model was achieved by full cross-validation (leave-one-out) method (Nawi et al., 2013). External validation was used in this study to assess the performance of the PLS models. The samples in the external validation set had not been used for the calibration development. Before calibration, samples were divided into two sets; 75% of the samples were used to develop calibration and 25% of the samples were used to validate the predictive equation (validation set).

The performance of the PLS models were further improved by using pre-treatment methods. The effect of several pre-treatment methods on the performance of PLS models including smoothing by moving average, multiplicative scatter correction (MSC), first and second derivatives, standard normal variate (SNV) transformation and Savitzky-Golay were investigated. After several attempts, it was found that a combination of Savitzky-Golay and SNV given the best performance for PLS models.

All statistical analysis included PCA, PLS modeling and pre-treatment methods were implemented using the Unscrambler X 10.3 (CAMO AS, Trondheim, Norway). In the end, the performance of the PLS models was evaluated by the root mean square error of calibration (RMSEC) and the coefficient of determination for calibration (R^2) for the calibration model. For the prediction model, the root mean square error of prediction (RMSEP) and the coefficient of determination for prediction (R^2) were used.



3. RESULTS AND DISCUSSION

3.1 Statistical characteristic of soluble solids content

The statistical characteristic of the SSC for jackfruit portions at different vertical levels are presented in Table 1. Each vertical level comprised 24 portions. From the table, it can be seen that the jackfruit portions from the top vertical level had the highest SSC value of 13.43 Brix. For the minimum SSC values, it was found that the portions from the middle and lower middle vertical levels had the lowest SSC values of 5.47 Brix. In terms of mean values, jackfruit portions from the upper middle and bottom vertical portions had the highest (8.01 Brix) and the lowest (7.51 Brix) values. The data indicate that the SSC of jackfruit skin varied from the top to the bottom. Since the information from the outer surface texture is an important characteristic for quality determination of fruits, the selection of the right portion is an important procedure in determining the maturity of the crop.

Table 1. Statistical characteristics of SSC for jackfruit samples at different portions

Vertical level	No. of Portion	SSC (Brix)			
		Min	Max	Mean	Std Dev.
Top	24	5.73	13.43	7.64	2.04
Upper middle	24	5.63	11.67	8.01	1.81
Middle	24	5.47	11.10	7.93	1.69
Lower middle	24	5.47	11.00	7.65	1.79
Bottom	24	5.60	10.53	7.51	1.45

3.2 Spectral overview of the jackfruit skin samples

Typical reflectance curves for spectral data measured from the skin surface at different vertical portions are shown in Figure 2. From the figure, the absorption peaks can be observed around 550 nm, 680 nm and 940 nm. All the peaks could be related to some chemical properties of the skin samples. The absorption peaks are most likely related to the presence of carotenoids (around 500 nm), anthocyanins (550 - 600 nm), chlorophyll (678 nm) and water (940 nm) (Van Beers et al., 2017). The absorption peak around 680 nm could be associated with the chlorophyll content which represents the color characteristics in the fruit (El-Masry et al., 2007). The peak around 940 nm was due to reaction of chemical characteristic and water in the skin. The 940 nm wavelength was useful for prediction fruit firmness (Moons et al., 1997) and SSC (Lu, 2004).

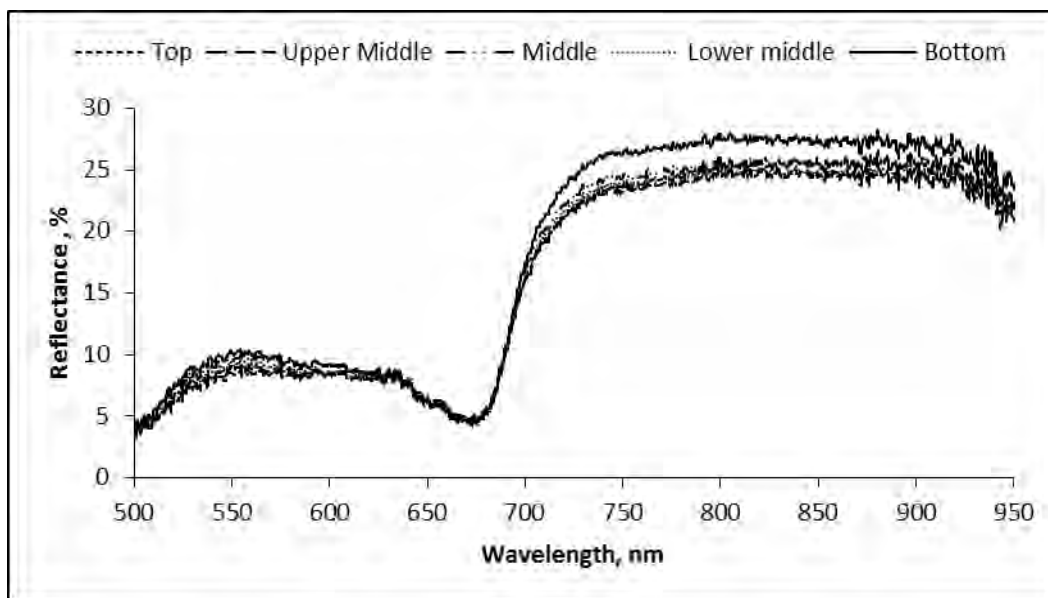


Figure 2. Reflectance spectral data for the top to bottom skin portion from 500 - 950 nm

3.3 Prediction of SSC using spectral data

The spectral data ranged from 500 - 950 nm were used to establish PLS model for predicting SSC from skin surface. The performance of PLS model in predicting SSC for both calibration and prediction models are presented by the scatter plots in Figure 3 (a) and (b), respectively. The R^2 and RMSEC values for the calibration model were 0.77 and 2.88 Brix, respectively. The prediction accuracy of this model for the whole samples was moderate with R^2 value of 0.74 and RMSEP value of 2.97 Brix, respectively. This finding is similar to the study published by Jie et al., (2014) who reported that the best prediction with a correlation coefficient (R^2) of 0.70 and RMSEP of 0.33 Brix or the prediction set for watermelon with visible and near-infrared (Vis/NIR) spectroscopic technology for a non-destructive on-line detection. This research and the study by Jie et al. (2013) had similar issue when applying spectroscopic methods on the fruits with thick skin. However, the R^2 value found from this study is slightly lower than the study conducted by Jie et al. (2013) as the jackfruit has a rough, irregular and thorny surface.



CIGR 2018

XIX. World Congress of CIGR

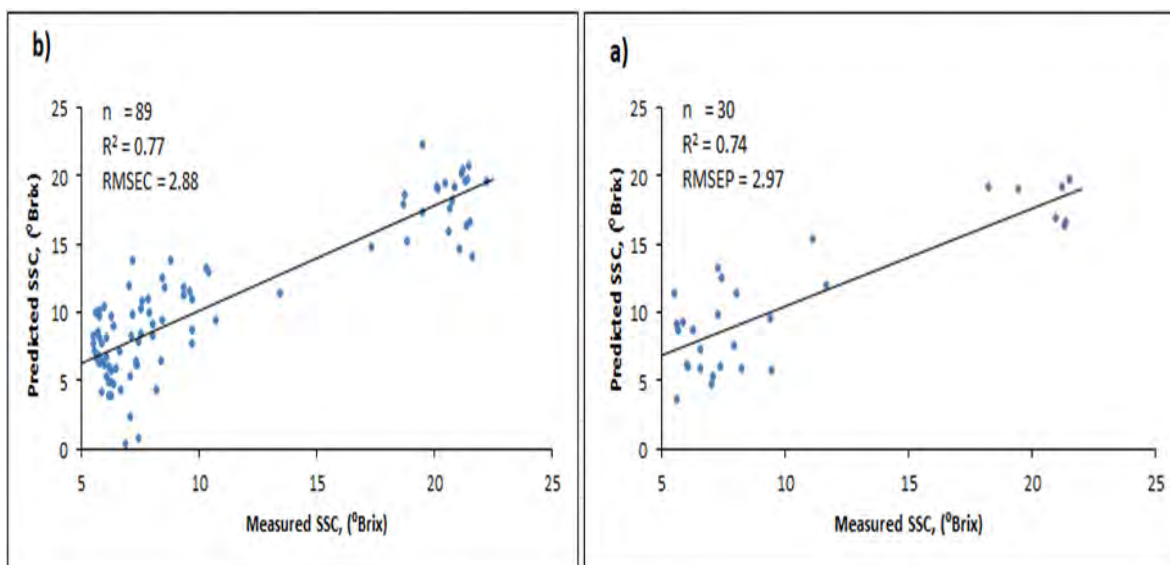


Figure 3. Prediction (a) and Calibration (b) models of SSC for the skin surface

4. CONCLUSION

In conclusion, the SWNIR spectroscopy was found to be promising in predicting SSC from jackfruit skin samples. The PLS model for calibration yielded good R² value of 0.77 with low RMSEC value of 2.88 Brix. For the prediction model, the R² and RMSEP values were 0.74 and 2.97 Brix, respectively. The prediction accuracy can be improved by increasing the jackfruit sample numbers harvested from different varieties. Thus, it can be concluded that the SWNIR spectrometer could be utilized for predicting maturity of jackfruit by scanning the SSC of the fruits from the skin surface.

5. REFERENCES

- Baliga, M. S., A. R. Shivashankara, R. Haniadka, J. Dsouza, and H. P. Bhat, 2011. Phytochemistry, nutritional and pharmacological properties of *Artocarpus heterophyllus* Lam (jackfruit): A review. *Food Research International*, 44(7), 1800-1811.
- Begum, R., M. G. Aziz, M. B. Uddin, and Y. A. Yusof, 2014. Characterization of jackfruit (*Artocarpus heterophyllus*) waste pectin as influenced by various extraction conditions. *Agriculture and Agricultural Science Procedia*, 2, 244-251.
- Department of Agriculture. 2017. Ministry of Agriculture and Agro-Based Industry Malaysia.



CIGR 2018

XIX. World Congress of CIGR



- El-Masry, G., N. Wang, A. El-Sayed, and M. Ngadi. 2007. Hyperspectral imaging for nondestructive determination of some quality attributes for strawberry. *Journal of Food Engineering*, 81(1), 98-107.
- Gomez, A. H., Y. He, and A. G. Pereira. 2006. Non-destructive measurement of acidity, soluble solids and firmness of Satsuma mandarin using Vis/NIR-spectroscopy techniques. *Journal of Food Engineering*, 77(2), 313-319.
- Hsieh, C. and Y. Lee. 2005. Applied visible/near-infrared spectroscopy on detecting the sugar content and hardness of pearl guava. *Applied Engineering in Agriculture*, 21(6), 1039-1046.
- Jie, D., L. Xie, X. Fu, X. Rao, and Y. Ying. 2013. Variable selection for partial least squares analysis of soluble solids content in watermelon using near-infrared diffuse transmission technique. *Journal of Food Engineering*, 118(4), 387-392.
- Leong, C. M., M. A. Noranizan, M. Kharidah, and W. S. Choo, 2016. Physicochemical properties of pectin extracted from jackfruit and chempedak fruit rinds using various acids. *International Food Research Journal*, 23(3). 64-71.
- Liu, Y., X. Sun, and A. Ouyang. 2010. Nondestructive measurement of soluble solid content of navel orange fruit by visible–NIR spectrometric technique with PLSR and PCA-BPNN. *LWT-Food Science and Technology*, 43(4), 602-607.
- Lu, R. 2004. Multispectral imaging for predicting firmness and soluble solids content of apple fruit. *Postharvest Biology and Technology*, 31(2), 147-157.
- Madruga, M. S., F. S. M., de Albuquerque, I. R. A., Silva, D. S., do Amaral, M., Magnani, and V. Q. Neto. 2014. Chemical, morphological and functional properties of Brazilian jackfruit (*Artocarpus heterophyllus* L.) seeds starch. *Food Chemistry*. 143, 440-445.
- McGlone, V. A., R. B. Jordan, and P. J. Martinsen. 2002. Vis/NIR estimation at harvest of pre- and post-storage quality indices for ‘Royal Gala’ apple. *Postharvest Biology and Technology*, 25(2), 135-144.
- McGlone, V. A., and S. Kawano. 1998. Firmness, dry-matter and soluble-solids assessment of postharvest kiwifruit by NIR spectroscopy. *Postharvest Biology and Technology*, 13(2), 131-141.
- Moons, P., A. Dardenne, A. Dubois, and M. Sindic. 1997. Non-destructive visible and NIR spectroscopy measurement for the determination of apple internal quality. *Acta Horticulturae*. 517, 441-448.
- Nawi, N. M., G. Chen, T. Jensen, and S. A. Mehdizadeh, 2013. Prediction and classification of sugar content of sugarcane based on skin scanning using visible and shortwave near infrared. *Biosystems Engineering*, 115(2), 154-161.



CIGR 2018

XIX. World Congress of CIGR



Nicolai, B. M., B. E. Verlinden, M. Desmet, S. Saevens, W. Saeys, K. Theron, and A. Torricelli. 2008. Time-resolved and continuous wave NIR reflectance spectroscopy to predict soluble solids content and firmness of pear. *Postharvest Biology and Technology*, 47(1), 68-74.

Schmilovitch, Z. E., A. Mizrach, A. Hoffman, H. Egozi, and Y. Fuchs. 2000. Determination of mango physiological indices by near-infrared spectrometry. *Postharvest biology and technology*, 19(3), 245-252.

Swami, S. B., N. J. Thakor, P. M. Haldankar, and S. B. Kalse. 2012. Jackfruit and its many functional components as related to human health: a review. *Comprehensive Reviews in Food Science and Food Safety*, 11(6), 565-576.

Van Beers, R., B. Aernouts, R. Watté, A. Schenk, B. Nicolai, and W. Saeys. 2017. Effect of maturation on the bulk optical properties of apple skin and cortex in the 500–1850 nm wavelength range. *Journal of Food Engineering*, 214, 79-89.

Wu, D., L. Feng, C. Zhang, and Y. He. 2008. Early detection of *Botrytis cinerea* on eggplant leaves based on visible and near-infrared spectroscopy. *Transactions of the ASABE*, 51(3), 1133-1139.

Zhang, J. P., P. Q. Liao, H. L. Zhou, R. B. Lin, and X. M. Chen. 2014. Single-crystal X-ray diffraction studies on structural transformations of porous coordination polymers. *Chemical Society Reviews*, 43(16), 5789-5814.



CIGR 2018

XIX. World Congress of CIGR



Assessment of Calibration and Validation of CropSyst model in winter wheat productivity in Mediterranean Environments

Ahmet Cilek^{1*}, Suha Berberoglu¹, Muge Unal Cilek¹, Cenk Donmez¹

¹Cukurova University, Landscape Architecture Department, Adana, 01330, Turkey
acilek@cu.edu.tr

ABSTRACT

This study aims to evaluate CropSyst model for winter wheat without irrigation in a Mediterranean Environment. In this study, we examine from a set of representative sites how soil influences wheat yields simulated with a process-based crop model, and climate variability observed in Cukurova Plain, Turkey. CropSyst, a process-based simulation model, was used to simulate the growth and development of potential for winter wheat. The CropSyst model was calibrated and validated for winter wheat grown in 1999/2000, 2000/2011 and 2011/2002 at previous fields studies of Cukurova Plain. The study area was mapped by soil series, the lowest and most detailed soil classification units. Soil profiles, profile depth, pH values, organic matter, salinity texture, soil volume and total porosity have been studied in detail for the soil series in the study area. During the 1999-2000 winter period, simulated LAI values were calibrated by the model for wheat, and a similar distribution was modelled. It was observed that the times of plant development stages such as bolting, flowering, and physiological maturity were identical to measurement data. Tilling stage was reached 20 days after plantation, bolting stage was reached on day 103, flowering on day 129, and physiological maturity stage was reached on day 158. While there was a 100 kg/ha difference between the measurements and the model results in the 2000-2001 winter period, the calculated results were similar to the measured values between 2000-2002.

Keywords: CropSyst, Crop Modelling, Wheat, Turkey

INTRODUCTION

Soils are losing their fertile characteristics due to intensive production, and productivity is decreasing due to uncontrolled use. Therefore, sustainability in agriculture has gained importance and the conservation of resources has become an important topic. Fertilizers that are used to increase agricultural production and quality make a significant contribution to food safety, increasing living standards, and fighting famine with a 40% yield increase. However, uncontrolled use of fertilizers negatively affects agricultural productivity and natural environment. Therefore, in order to determine the appropriateness of agricultural landscaping, nature conservation strategies have been developed in this study for agricultural areas affecting



CIGR 2018

XIX. World Congress of CIGR



important biotope areas by changing the agricultural product pattern for the Lower Seyhan Plain (LSP), taking into account the present conditions (Cilek and Berberoglu, 2019).

In the world, a significant portion of the freshwater resources (72%) is used in agricultural irrigation (Geerts and Raes, 2009). The rapid increase in world population and the need for more water use across sectors increase the importance of more efficient use of irrigation water. Thus, determining the optimum strategies for management and planning of existing water resources in agriculture is becoming a national and global priority (Smith, 2000).

As work continues to increase agricultural production in the world, measures are being taken to minimize the negative effects of agricultural activities on the environment (Morgan, 2003). With the rapid decline of water resources in recent years, researchers have concentrated on topics such as water sensitivity and water-production functions of plants during different developmental periods. One of the promising approaches is the study of water use analyses based on the efficiency of the consumed water, instead of product yield, by determining the relationship of water potential with soil, plant, and atmosphere (Molden and Sakthivadivel, 1999). Especially in locations and periods where water is scarce, knowing the periods when plants are most affected by water stress has become very important in terms of irrigation management. In such cases, obtaining the highest production per unit water is possible by administrating existing water during critical growth stages (Sezen, 2000).

Product development models for estimating and simulating plant and environment interactions include different geodetic scales for different objectives (Boote et al., 1996) such as evaluation of management strategies (Bergez et al., 2010) and environmental impact assessment (Ewert et al., 2009). They can be used at any scale from global issues such as the impact of climate change to local studies such as land quality and product change. In general, they are designed to model the complex interactions between product management, soil, and atmosphere, and to estimate agricultural yields, taking into account the environmental impacts of crop breeding systems such as N-wash, erosion (Adekalu and Fapohunda, 2006; Barbosa et al., 2007; Bechini et al., 2006; Gary et al., 1998).

2. MATERIALS AND METHODS

2.1 Study Area

The Çukurova Delta, located between the Iskenderun Gulf and the Mersin Gulf in the eastern part of the Mediterranean Region, is one of the most fertile plains in our country. Thanks to alluviums carried by Seyhan and Ceyhan rivers and Berdan Stream, Çukurova Delta has become the biggest delta in Turkey. The Ceyhan and Seyhan rivers, which have a narrow reservoir, both have very high-water flow rates. Due to melting snow and high precipitation in the spring, major

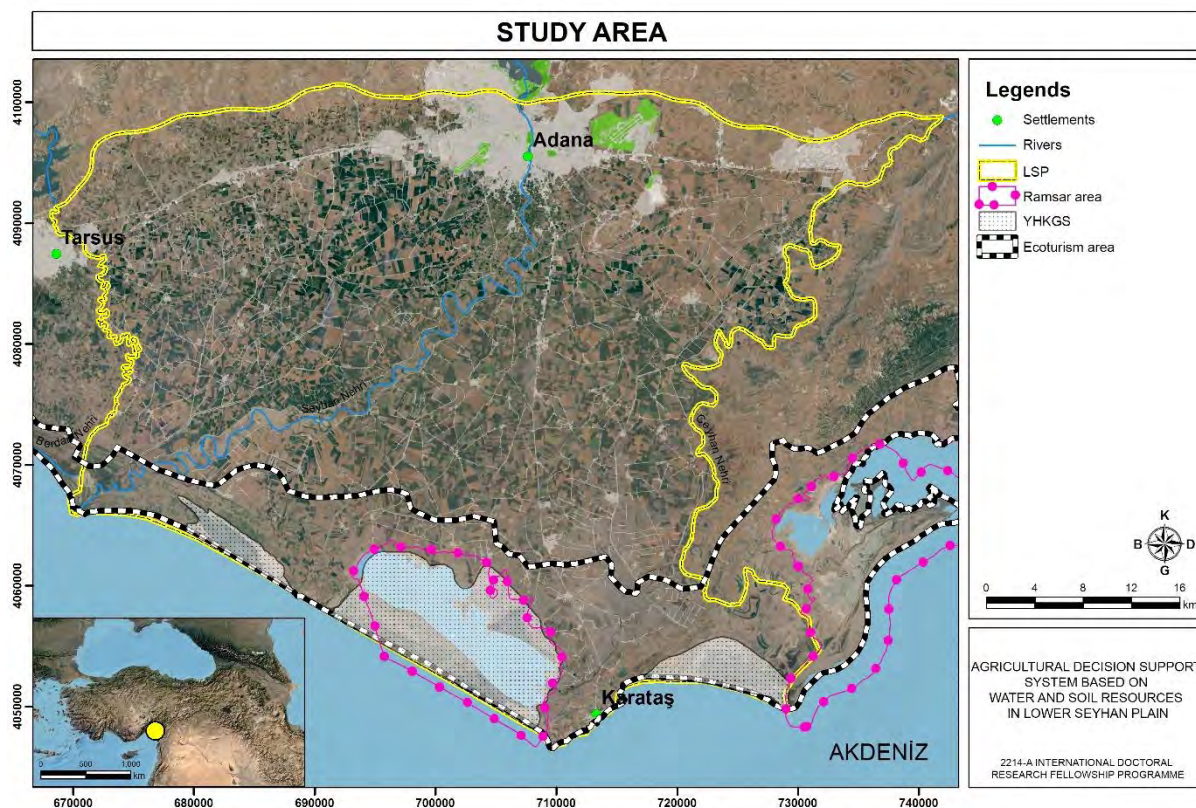


CIGR 2018

XIX. World Congress of CIGR



floods have occurred in the plain in the past, and the beds of the rivers have changed frequently (Figure 1). Thus, many ponds, lagoons, meanders and marsh areas have formed especially to the south of the plain. There are four major lagoons in the area from west to east: Tuzla, Akyatan, Ağyatan, and Yumurtalık lagoons (Cilek and Berberoglu, 2019; Dinçer, 2007)



2.2 Data

The Seyhan and Ceyhan rivers play an important role in the formation of the soil in Çukurova Delta. Vertisol soil (76.5%) and Red Brown Mediterranean soil (10.6%) are widely present in the Çukurova Region. For the Çukurova region, the LSP and Tarsus-Mersin lands were mapped on the basis of soil series, the lowest and most detailed soil classification units. Soil profiles, profile depth, pH values, amount of organic matter, variable cation values, amount of lime, texture, volume and total porosity have been studied in detail for 20 soil series in the study area.

LSP has a Mediterranean climate with an average annual temperature of 18-19 °C. Lowest average monthly temperature is 9-10 °C (January), and the highest is 28 °C (August). The low annual temperature difference in the plain allows agriculture to be carried out throughout the



CIGR 2018

XIX. World Congress of CIGR



year. The average annual precipitation is 721 mm and the dominant wind direction is north/northeast in winter and south/south west in summer (Çelik et al., 2013; TSMS, 2017). Since the amount of evapotranspiration is higher than the amount of precipitation between November and April, irrigation for the plain is also carried out during this period. In this region, which does not receive rainfall in the summer months, the winds sweeping from the southwest carries the sand dunes around the wetlands to inner regions of the plain, and the opposite occurs in winter. The ground water level in the region, which is rich in underground and surface water assets, ranges between 80-120 cm, and an average of 430 million m³ of water is used annually from the wells (**Hata! Başvuru kaynağı bulunamadı.**).

2.3. Method

This study aims to evaluate CropSyst model for winter wheat without irrigation in a Mediterranean Environment. Calibration and validation of the agricultural crop yield estimation model was performed, and the effects of the results on water-soil and environment were determined by running different scenarios (**Hata! Başvuru kaynağı bulunamadı.**). The CropSyst plant development model was developed to serve as an analytical tool to investigate the impacts of climate, soil, and management on productivity and the environment. CropSyst simulates soil-water budget, soil-plant nitrogen budget, plant phenology, canopy and root growth, biomass quantity, yield, residue quantity and decomposition, soil erosion, and saltness. These processes are influenced by plant management practices such as climate, soil characteristics, crop characteristics and planting season, variety selection, irrigation, nitrogen fertilization, soil and irrigation salinity, soil treatment and residue management.

The development of CropSyst began at the beginning of the 1990s. It is based on appropriate observations that require plant development models that are not particularly capable of regular crop alternations for their development. Model developers have collaborated with many researchers to design this fast and low-cost computer software for users in scientific projects (Stöckle et al., 2003)

CropSyst is a multi-year multi-crop simulation model developed to study the effect of cropping systems management on productivity and environment (Stöckle et al., 2010, 2003). This model has been used to model the growth and development of several crops such as wheat, maize, barley, soybean and sorghum in the western USA, southern France, northern and southern Italy, northern Syria, northern Spain and western Australia with generally good results (Stöckle and Nelson, 2000). CropSyst has also been used to investigate potential impacts of climate change on crop production (Donatelli et al., 2003; Tubiello et al., 2000). It was also calibrated and validated for the site under study using 5 years of maize grain yield and phonological data (Abraha, 2003). The model consists of several integrated components and different management options. Details about components and uses can be found in the model user's manual (Stöckle and Nelson, 2000).



CIGR 2018

XIX. World Congress of CIGR



3. RESULTS

The CropSyst crop development model was applied to the Lower Seyhan Plain for the modeling of crop development in agricultural products, crop yield estimation and agricultural pollution in 2010-2016. For the CropSyst model, preliminary field trial data were collected for the calibration of plant phenology of agricultural products and management practices suitable to the study area (Müjdecı et al., 2005). Plant phenological stages for wheat, cotton and corn, leaf area index (LAI), biomass, yield data, irrigation and fertilization practices were used in the calibration. Parameters used in the model, parcel trial data and model results were evaluated for each product. The data used for the wheat product contains the 2000, 2001, and 2002 data of the trial performed on the field by Müjdecı (2004). Müjdecı (2004) used parcels of 8 m in length, with 15 cm between the feet so that there are 450 seeds per square meter. Phenological properties of the wheat product were calibrated by using the development period dates and total temperature values (day-degree) recorded for 2000, 2001, and 2002 (Table 1).

During the 1999-2000 winter period, simulated LAI values were calibrated by the model for wheat, and a similar distribution was modeled. It was observed that the times of plant development stages such as bolting, flowering, and physiological maturity were similar to measurement data. Tillering stage was reached 20 days after plantation, bolting stage was reached on day 103, flowering on day 129, and physiological maturity stage was reached on day 158.

Table 1. Field measurement of wheat

Müjdecı (2004) Field measurement						
Growth period	1999-2000		2000-2001		2001-2002	
	Date	GDD (°C)	Date	GDD (°C)	Date	GDD (°C)
Sowing	10.12.1999	0	27.11.2000	0	17.01.2002	0
Emergence	29.12.1999	248	15.12.2000	273	8.02.2002	239
Tillering	9.02.2000	580	2.01.2001	427	19.02.2002	375
Stem extension	21.03.2000	994	30.01.2001	733	18.03.2002	773
Flag leaf	9.04.2000	1290	10.03.2001	1215	5.04.2002	1007
Spike	17.04.2000	1436	22.03.2001	1421	12.04.2002	1123
Flowering	18.04.2000	1462	4.04.2001	1656	27.04.2002	1374
Phenological maturity	17.05.2000	2009	25.04.2001	2025	18.05.2002	1795



CIGR 2018

XIX. World Congress of CIGR

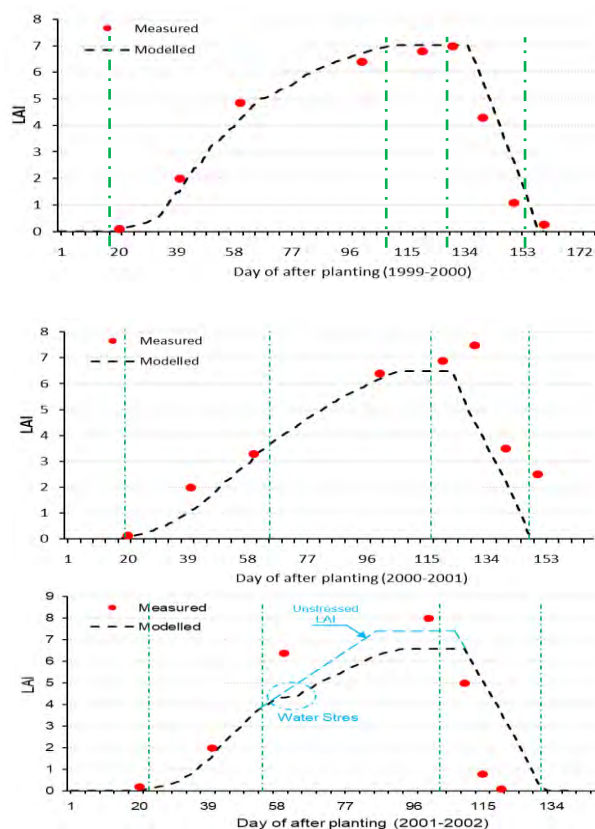


Figure 2. Calibration and validation results of wheat between 1999 to 2002.

Calibrated values were modeled during the specified plantation period in the trial in 2000-2001 for wheat, and LAI distribution was tested. According to the model results, spurt stage was reached on day 19 after plantation, flowering stage was reached on day 116, and physiological maturity was reached on day 147. LAI values measured between days 120 and 130 were obtained. The reason for this was the early flowering in the model. However, a 2-day difference was found in the physiological maturity times. While there was a 100 kg/ha difference between the measurements and the model results in the 2000-2001 winter period, the calculated results were similar to the measured values between 2000-2002 (Table 2).

Table 2. Measurement and modelled yield

Year	Measured yield (kg/ha)	Model yield result (kg/ha)
1999-2000	6490	6479.51
2000-2001	3690	4644.733
2001-2002	6370	6348.838



CIGR 2018

XIX. World Congress of CIGR



4. CONCLUSION

In conclusion, the regions in the study area affected by intensive agricultural activities were identified and modeling, mapping and analyses were carried out in order to create a base data for the sustainability of the environment, and suggestions for agricultural activities that could be applied in these areas were developed. The issues to be considered and planned in the various processes of agricultural use analyses are as follows:

Use of geodetic models as well as declaration-based agricultural data will ensure early and accurate calculation of production reports.

Land use classification, and determination of the purpose of conservation and use for natural and cultural areas

In yield-based systems, the damage to agriculture by non-agricultural land uses can be more accurately calculated, and the long-term damage of non-agricultural use to the economy and ecosystem can be demonstrated in concrete terms. When agricultural areas are considered in the context of ecosystem services, the contribution of economic value to the ecosystem can also be calculated accurately.

5. REFERENCES

- Adekalu, K.O., Fapohunda, H.O., 2006. A numerical model to Predict Crop Yield from Soil-Water Deficit. *Biosyst. Eng.* 94, 359–372. <https://doi.org/10.1016/j.biosystemseng.2006.03.012>
- Barbosa, O., Tratalos, J.A., Armsworth, P.R., Davies, R.G., Fuller, R.A., Johnson, P., Gaston, K.J., 2007. Who benefits from access to green space? A case study from Sheffield, UK. *Landsc. Urban Plan.* 83, 187–195. <https://doi.org/10.1016/j.landurbplan.2007.04.004>
- Bechini, L., Bocchi, S., Maggiore, T., Confalonieri, R., 2006. Parameterization of a crop growth and development simulation model at sub-model components level. An example for winter wheat (*Triticum aestivum* L.). *Environ. Model. Softw.* 21, 1042–1054. <https://doi.org/10.1016/j.envsoft.2005.05.006>
- Bergez, J.E., Colbach, N., Crespo, O., Garcia, F., Jeuffroy, M.H., Justes, E., Loyce, C., Munier-Jolain, N., Sadok, W., 2010. Designing crop management systems by simulation. *Eur. J. Agron.* 32, 3–9. <https://doi.org/10.1016/j.eja.2009.06.001>
- Boote, K.J., Jones, J.W., Pickering, N.B., 1996. Potential uses and limitations of crop models. *Agron. J.* <https://doi.org/10.2134/agronj1996.00021962008800050005x>
- Çelik, M., Kızılelma, Y., Gülersoy, A., Denizdurduran, M., 2013. Investigation Of The



CIGR 2018

XIX. World Congress of CIGR



Emerging Change In Wetlands In South Of Lower Seyhan Plain By Using Different Remote Sensing Technics (1990-2010). Turkish Stud. - Int. Period. Lang. Lit. Hist. Turkish or Turkic 8, 263–284.

Cilek, A., Berberoglu, S., 2019. Biotope conservation in a Mediterranean agricultural land by incorporating crop modelling. Ecol. Modell. 392, 52–66. <https://doi.org/10.1016/j.ecolmodel.2018.11.008>

Dinçer, A., 2007. Relationship Between The Develop Of Water Resources And Lagoons In Lower Seyhan Plain (LSP). Msc thesis, Cukurova University, Environmental Engineering, Adana. 72 p.

Donatelli, M., Bellocchi, G., Fontana, F., 2003. RadEst3.00: Software to estimate daily radiation data from commonly available meteorological variables, in: European Journal of Agronomy. pp. 363–367. [https://doi.org/10.1016/S1161-0301\(02\)00130-2](https://doi.org/10.1016/S1161-0301(02)00130-2)

Ewert, F., van Ittersum, M.K., Bezlepina, I., Therond, O., Andersen, E., Belhouchette, H., Bockstaller, C., Brouwer, F., Heckeley, T., Janssen, S., Knapen, R., Kuiper, M., Louhichi, K., Olsson, J.A., Turpin, N., Wery, J., Wien, J.E., Wolf, J., 2009. A methodology for enhanced flexibility of integrated assessment in agriculture. Environ. Sci. Policy 12, 546–561. <https://doi.org/10.1016/j.envsci.2009.02.005>

Gary, C., Jones, J.W., Tchamitchian, M., 1998. Crop modelling in horticulture: State of the art. Sci. Hortic. (Amsterdam). 74, 3–20. [https://doi.org/10.1016/S0304-4238\(98\)00080-6](https://doi.org/10.1016/S0304-4238(98)00080-6)

Geerts, S., Raes, D., 2009. Deficit irrigation as an on-farm strategy to maximize crop water productivity in dry areas. Agric. Water Manag. <https://doi.org/10.1016/j.agwat.2009.04.009>

Molden, D., Sakthivadivel, R., 1999. Water Accounting to Assess Use and Productivity of Water, International Journal of Water Resources Development. <https://doi.org/10.1080/07900629948934>

Morgan, C.L., 2003. Quantifying soil morphological properties for landscape management applications. Soil Science, University of Wisconsin, Madison.

Müjdeci, M., Sariyev, A., Polat, V., 2005. Mathematical Modelling of Wheat Yield (*Triticum aestivum* L.). J. Agric. Sci. 11, 349–353.

Sezen, S.M., 2000. Determination of Nitrogen-Water-Yield Relationships in Wheat by Cukurova and Harran Ovası Conditions and Testing Ceres-Wheat V.3 Model. PhD thesis, Cukurova University, Department of Agricultural Structures and Irrigation, Adana.

Smith, M., 2000. The application of climatic data for planning and management of sustainable rainfed and irrigated crop production, in: Agricultural and Forest Meteorology. pp. 99–108. [https://doi.org/10.1016/S0168-1923\(00\)00121-0](https://doi.org/10.1016/S0168-1923(00)00121-0)

Stöckle, C.O., Donatelli, M., Nelson, R., 2003. CropSyst, a cropping systems simulation model,

A Cilek, S Berberoglu, M Unal Cilek, C Donmez “ Assessment of Calibration and Validation of CropSyst model in winter wheat productivity in Mediterranean Environments”



CIGR 2018

XIX. World Congress of CIGR



in: European Journal of Agronomy. pp. 289–307. [https://doi.org/10.1016/S1161-0301\(02\)00109-0](https://doi.org/10.1016/S1161-0301(02)00109-0)

Stöckle, C.O., Nelson, R., 2000. Cropsyst User's manual (Version 3.0). Biological Systems Engineering Dept., Washington State University, Pullman, WA.

Stöckle, C.O., Nelson, R.L., Higgins, S., Brunner, J., Grove, G., Boydston, R., Whiting, M., Kruger, C., 2010. Assessment of climate change impact on Eastern Washington agriculture. *Clim. Change* 102, 77–102. <https://doi.org/10.1007/s10584-010-9851-4>

TSMS, 2017. Climate data, 1975–2017. Adana: Regional Directorate of State Meteorological Service, Turkish State Meteorological Service. [WWW Document]. URL <https://www.mgm.gov.tr/>

Tubiello, F.N., Donatelli, M., Rosenzweig, C., Stockle, C.O., 2000. Effects of climate change and elevated CO₂ on cropping systems: Model predictions at two Italian locations. *Eur. J. Agron.* 13, 179–189. [https://doi.org/10.1016/S1161-0301\(00\)00073-3](https://doi.org/10.1016/S1161-0301(00)00073-3)



A ROS-Enabled Out-Door Robotic Perception System

V. Moisiadis¹; I. Menexes¹; G. Vasileiadis¹; A. Balafoutis¹; D. Bochtis¹

¹Centre for Research and Technology - Hellas, Institute for Bio-economy and Agri-technology,
57001 Themi, Thessaloniki, Greece

Corresponding Author: D. Bochtis, Institute for Bio-economy and Agri-technology, Centre for
Research and Technology – Hellas, 57001 Themi, Thessaloniki, Greece,
d.bochtis@certh.gr

ABSTRACT

In tandem with cost deduction and production efficiency, Unmanned Ground Vehicles (UGVs) are documented to be a radical advancement in outdoor procedures related with precision agriculture. In this work, a series of implemented low level algorithms were developed in Robot Operating System (ROS) to schedule and operate high level activities, such as the implementation of path and position finding, image and pattern recognition and goal assignment. With the use of a depth RGB (RGB-D) camera and a laser scan sensor, an algorithm for the detection and registration of tree-entities in orchards was developed. The algorithm takes advantage of image recognition software which identifies regions of interest within the visible camera range along with their relative coordinates. These regions are registered into a database and they represent the current image of the field. The developed algorithm combines the procedure above with the mapping procedure and adaptive sampling for the localization of the UGV and the mapping of the surrounding environment. Moreover, the algorithm facilitates the UGV's movement with the implementation of a pseudo-random movement using a mathematical formula moving the UGV to the direction with the largest angle increment, while at the same time avoiding both static and dynamic obstacles.

As a next step, an algorithm for precision scanning was developed. The resulting database indicates the exact position of the trees in relation to the UGV. Thus, all subsequent actions will occur considering the current image of the field enabling precise execution of procedures. Additionally, it is possible to assign extended information for each individual registration indicating current tree-state and actions that should subsequently take place. Moreover, the overall UGV's navigation to the outdoor environment is governed by the ability to avoid dynamic obstacles. Should an obstacle appear, the UGV re-calculates its optimized path to the assigned goal and avoids the obstacle. Finally, the user can supervise all stages of the automated navigation with the option to interact with the system to prevent any unscheduled activities.

The system integrating this series of algorithms has shown high simulation efficiency with the UGV completing all assigned tasks on time. Moreover, for the board governed task (field scouting) the UGV was successfully achieve all the recurrent assignments maintaining the time



CIGR 2018

XIX. World Congress of CIGR



and costs intervals. Additionally, in the precise governed scenarios, the UGV navigated accurately to each individual registered tree-entity and optimized its path to the nearest available position in relation to their actual relative coordinates.

Keywords: Out-door environment perception, autonomous navigation, orchard mapping algorithm, Greece

1. INTRODUCTION

Using Unmanned Ground Vehicles (UGV) for agricultural purposes would be a revolution, as a series of field activities, such as tillage, sowing, transplanting, weeding, spraying and harvesting could be assigned to them leading to reduced person power requirement, better quality of work and eventually lower cost of production. However, agricultural environment can be hostile for autonomous vehicles, due to various obstacles spread within the range of the vehicle's movement, including permanent and moving subjects. Therefore, such vehicles should be able to detect obstacle autonomously fast and accurately to ensure safety and high efficiency. To achieve this goal, different technologies for exact navigation have been proposed, such as vision and laser scanning. A survey about vision technologies for UGV navigation was prepared by Desouza (DeSouza et al., 2002), where they primarily differentiated autonomous obstacle detection and navigation technology between indoor and outdoor environment, while they also classified them based on the topography into structured and unstructured environment. It is important to point out that UGVs' autonomous movement within indoor and structured environments has been successful, as the system under evaluation from the UGV is simple and unexpected obstacles are rare. On the other hand, outdoor UGV navigation is a lot challenging due to unexpected scenes and terrains that require more powerful perception capability.

The main sensors for outdoor navigation are laser range finder and camera. Laser scanners can provide refined and easy-to-use information about the surrounding area, but they have one degree of freedom, large size and high energy consumption, while cameras are capable of handling large amount of data, consume low energy, have small size and provide high resolution imagery (Cong et al., 2010). Therefore, the combination of these two sensor types could provide high quality data that could be translated into navigation information through integrated algorithms.

A very common control system for UGV navigation is Robot Operating System (ROS). ROS is a graph-based middleware which explores the potentials of each individual robot with the advantage of third-party hardware and software (Quigley et al., 2009; Wei et al., 2016). The use of ROS as a robust robotic system to embed and evaluate high level activities in precision agriculture, concatenates both state of the art robotic technologies and agricultural processes and provides a profound advantage across the economic and environmental constituents (Jensen et



CIGR 2018

XIX. World Congress of CIGR



al., 2014). Therefore, many researchers have used ROS for autonomous vehicle navigation control with a lot of advantages in comparison to other systems (Das et al., 2015; Gopi et al., 2017; Pierzchała et al., 2018). ROS's modular architecture grants remarkable system flexibility which provides convenient ways to integrate a variety of components. In particular, ROS brings networking solutions to problems regarding the communication across ROS nodes, located in numerous networked computers and devices, allowing them to intercommunicate without restrictions to structure. Providing plethora of libraries and drivers, low level hardware interconnection and cooperation are handled with no difficulties. Additionally, ROS offers means of message recording and playback, saving great amount of time during data analysing and debugging which, in conjunction with the great documentation provided through its formal Wiki, makes it a greatly useful tool for developing robotic related systems (Jensen et al., 2014).



2. MATERIALS AND METHODS

2.1 Mapping Performance

A fully functional substitute to real world robots is the integrated simulation environments. With a use of simulated environments, it is possible to develop and test algorithms without unnecessary operational costs as the project is in a preparatory stage. To that end, Gazebo simulation environment (Koenig et al., no date) was used for the UGV's integration as well as for the surrounding outdoor environment. The UGV simulated in Gazebo was a Husky robot (Clearpath Robotics Inc., Kitchener, ON, Canada) (Figure 14).



Figure 14 UGV's gazebo simulation

The initialization of the overall process took place at the stage of simultaneous localization and mapping (SLAM) using a customized algorithm for the outdoor environments. The Gmapping algorithm along with the incorporation of Rao-Blackwellized Particle Filter and adaptive sampling (Grisetti et al., 2005) was used to facilitate the UGV's localization processes related to the demands of outdoor environments. To leverage the procedure above, the navigation of the UGV's initiative undertaking was determined by two essential operations. The first was the traditional teleoperation of the UGV which is waif to the operator's supervision.

The second, was an algorithm that automates the autonomous navigation in outdoor environments. This algorithm received real-time data from the embedded sensors and calculated the path with the largest incremented path by incorporating the following parameters: (i) laser beam range as the actual distance between the UGV's position and every obstacle is included within the range of 180o; (ii) the minimum; (iii) maximum and (iv) increment angle from the ROS laser scan message (Foote Tully, no date). For each received data, the linear and angular UGV's speed was determined by the parameters above (Moisiadis et al., 2017).



2.2 Object Identification

Sequentially with the mapping procedure, an algorithm for object identification and registration was initialized. Associating the embedded sensors for IMU measurements (accelerometer, gyroscope, encoders) and the KINECT RGB-D sensor (Microsoft, Syracuse, NY, USA), combined with the find_object ROS package, provided the capability to identify entities in the surrounding environment, which in the case of orchards are the individual trees. Find_object package identified regions of interest within the entities and publishes their coordinates, relative to the UGV's position, over the ROS server. Each point of interest was generated by the difference in RGB values of the pixels within the visible frame and compared with stored illustrations of tree-entities (Lowe, 1999; Labbe, 2011) (Figure 15).

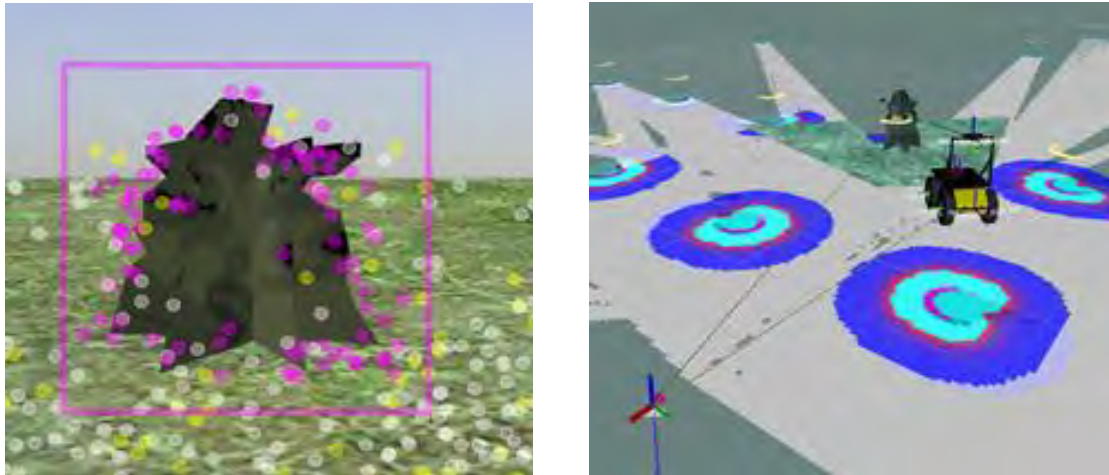


Figure 15 Mapping procedure and object identification

This research work was based on the algorithm above, developing a distance estimation between the UGV's initial point and the estimated position of each identified entity, registering and constantly publishing this relative position using the X-Y and Z-axes as reference through the Transform Library (Foote, 2013) along with a unique sequence number (Figure 16).

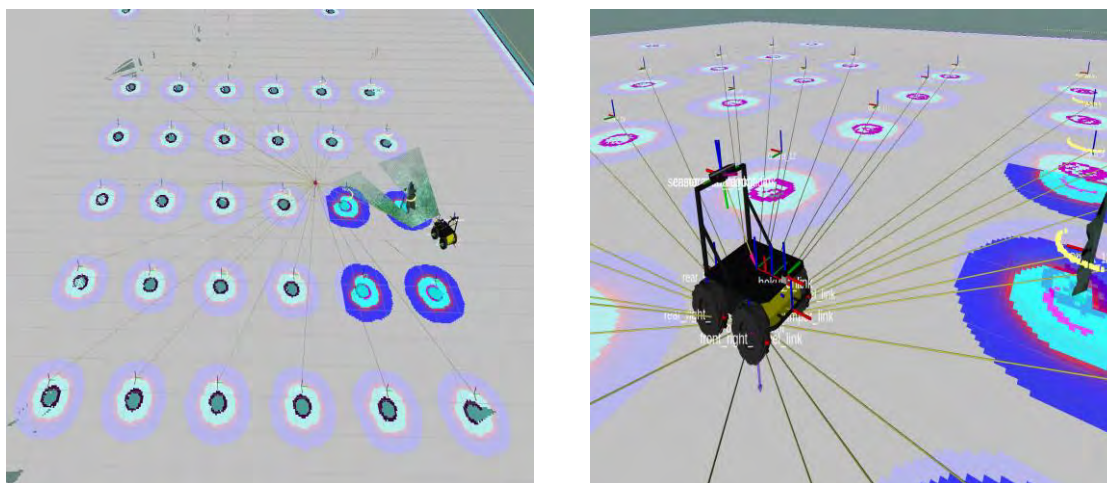


Figure 16 Illustration with the registered tree-entities

2.3 Autonomous Navigation

The aforementioned database was populated with data-entries which carry the information of the identified tree-entities' relative location, inside the field. This data made the UGV capable of receiving precise goals and task assignments that refer to each one of the database's entries. Then, based on the above database, an algorithm for precise navigation was developed by making use of the collected data. The algorithm was initialized by post-processing and structuring the gathered raw data, generating an image which depicted the current state of the orchard. Thus, the system had the ability to optimize all of the individual assignments that could occur. As a next step, the algorithm navigated the UGV to the top left corner of the field. Finally, the algorithm initialized a scouting procedure to the registered entities, by incorporating Navigation Stack (Quigley et al., 2009) and the optimization of path finding implementing the A-star algorithm (Lu, no date). For each individual field an optimized path (tramline) had been calculated. With the use of Carrot Planner (Marder-Eppstein et al., no date) as local planner, the optimized approach of the tree-entities has been denoted. Combining the above with a dynamic map creation, the UGV was able to avoid both static and dynamic obstacles (Figure 17). This way, we could facilitate frequent and time-consuming assignments, such as field scouting (using multispectral or hyperspectral cameras) to reduce typical agronomist visits in the field, or even agricultural applications like fertilization, spraying, etc. in case this navigation system is applied to larger UGVs with higher payload and power to cover such applications.

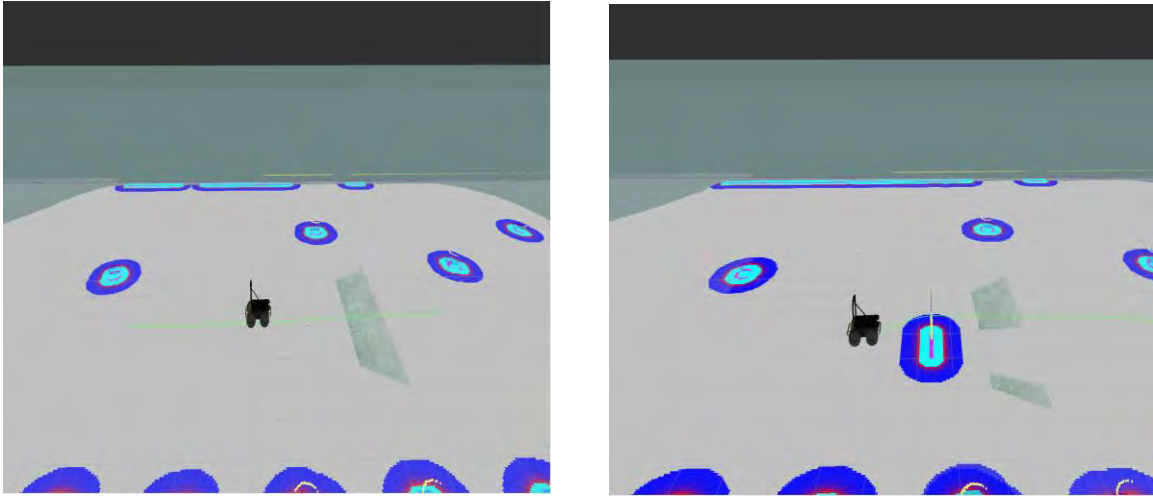


Figure 17 Dynamic obstacle avoidance

3. IMPLEMENTATION IN VARIOUS TYPES OF FIELDS

The methods described above were developed considering the various field types that the algorithm might have to successfully cope with. Thus, due to the lack of ideally structured fields, the necessity for an approach where the algorithm can perform efficiently and with high accuracy in different outdoor environments was rendered inevitable. Such flexibility is achieved through the stored tree-entities data processing, during which the algorithm evaluates the current field's layout. Upon the completion of the evaluation procedure, a value defining the average offset, as distance between trees, is passed as parameter to the tree-entities quantization process. The former, aims at clarifying the actual structured frame, in which the tree-entities are contained and finalizes its operation by creating an updated version of the existing map-image, the use of which is of great importance for the UGV to understand the exact field's layout.

The developed algorithm behaves properly in numerous intergraded field structures by optimizing its path for each individual scenario (Figure 18). Moreover, the tested field not only varies in number of columns but also in number of rows due to the lack of tree-entities within the field. The key performance indicator used to assess the algorithm's overall performance was the successful completion of the identification procedure of each tree-entity. All the testing implementation took place taking into account this assumption.

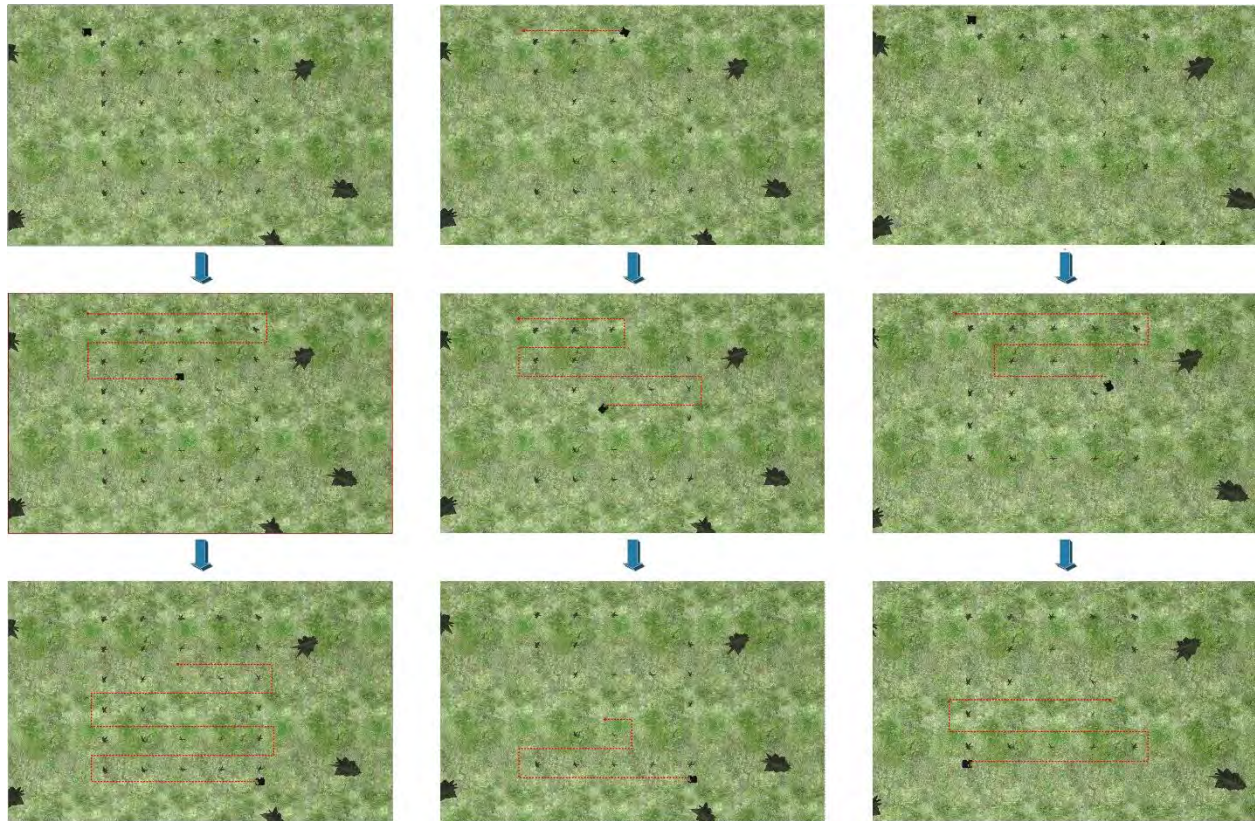


Figure 18 Implementation in various types of fields

4. RESULTS AND CONCLUSIONS

As described in Section 2.1, the navigation for the UGV took place with two methods, with the access of the automated algorithm and with teleoperation. It was observed that the automated algorithm fell short in comparison to teleoperation, as the percentage of identified tree-entities was significantly lower (Table 13). As the field tree density was increasing, the identification from the algorithm was reducing with relatively high pace. In particular, doubling tree density from 25% to 50% and from 50% to 100% showed a decrease of identified tree-entities of 23,6% and 28,6% respectively. This means that the automated algorithm was unable to cope with this process due to its fundamental disadvantage that the navigation of the UGV was based on the principle of following the path with the largest increment. Moreover, as the UGV's path was narrowed around the field's boundaries, the inner part of the field was not included, and a series of tree-entities was left unidentified. The use of laser scanner as a primary sensor resulted that the Gmapping algorithm was left unaffected by the aberration above. This was a result of the wide range of laser scan sensor, combined with the object identification procedure and its crucial



CIGR 2018

XIX. World Congress of CIGR



dependence from a low range sensor (i.e. KINECT RGB) for object identification. The essential purpose of this algorithm in its initial implementation (Moisiadis et al., 2017), was to cover bordered indoor environments. Therefore, the navigation of the UGV was constricted around the field. Consequently, in this outdoor application, the UGV attempted to reach the boundaries and follow them until the whole field was mapped even if the tree-entities in the inner part were not included in the identification process. This was the reason that the increased density was translated into lower identification percentage.

Table 13 Identified tree-entities

Field Density (%)	Identified tree-entities with Automated Algorithm (%)	Identified tree-entities with Teleoperation (%)
100	30	100
50	42	100
25	55	100

Moreover, the algorithm for precision agriculture operations (Section 2.3) optimized the UGV's path within the orchard's tramlines repeatedly. Consistency of the algorithm performance was high for all the implemented field structures. When a dynamic obstacle interfered to the UGV's optimized path, the UGV avoided it and the generated path recovered to the appropriate tramline, based on the condition that the centreline of the path is equidistant to the adjacent colorized contours (Figure 19).

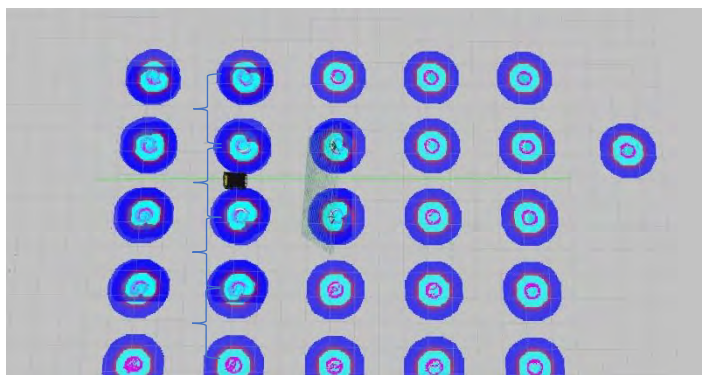


Figure 19 Optimized tram-line follower

Therefore, as a conclusion it could be said that the combination of the developed algorithms allowed the UGV to move autonomously within an orchard of individual tree-entities with limited problems, providing the ability to run different agricultural practices during a growing season, even if the field conditions are differentiated within time. In order to optimize the object identification process (increased tree-entities identification), a first step would be the adaptation of the algorithm that navigates the UGV to outdoor environments by implementing pattern recognition algorithms and correlating them with the 2D snapshot of the field.

V. Moisiadis, I. Menexes; G. Vasileiadis; A. Balafoutis; D. Bochtis. "A ROS-Enabled Out-Door Robotic Perception System



CIGR 2018

XIX. World Congress of CIGR



5. ACKNOWLEDGMENTS

The work was supported by the project "Research Synergy to address major challenges in the nexus: energy-environment-agricultural production (Food, Water, Materials)" - NEXUS, funded by the Greek Secretariat for Research and Technology (GSRT) – Pr. No. MIS 5002496.

6. REFERENCES

- Cong, Y. et al. (2010) 'V-disparity Based UGV Obstacle Detection in Rough Outdoor Terrain', *Acta Automatica Sinica*. China Science Publishing & Media Ltd., 36(5), pp. 667–673. doi: 10.3724/SP.J.1004.2010.00667.
- Das, J. et al. (2015) 'Devices, systems, and methods for automated monitoring enabling precision agriculture', in *2015 IEEE International Conference on Automation Science and Engineering (CASE)*. IEEE, pp. 462–469. doi: 10.1109/CoASE.2015.7294123.
- DeSouza, G. N. and Kak, A. C. (2002) 'Vision for mobile robot navigation: A survey', *IEEE Transactions on Pattern Analysis and Machine Intelligence*. Institute of Electrical and Electronics Engineers ({IEEE}), 24(2), pp. 237–267. doi: 10.1109/34.982903.
- Foote, T. (2013) 'Tf: The transform library', in *IEEE Conference on Technologies for Practical Robot Applications, TePRA*. IEEE. doi: 10.1109/TePRA.2013.6556373.
- Foote Tully (no date) *sensor_msgs: sensor_msgs::msg::_LaserScan::LaserScan Class Reference*. Available at: http://docs.ros.org/diamondback/api/sensor_msgs/html/classsensor_msgs_1_1msg_1_1_LaserScan_1_1LaserScan.html (Accessed: 26 April 2018).
- Gopi, S., Muir, A. and Bhavani, R. R. (2017) 'Naturalistic gestures based Human Robot Interaction on a UGV for outdoor use', in *2017 1st International Conference on Electronics, Materials Engineering and Nano-Technology, IEMENTech 2017*. IEEE. doi: 10.1109/IEMENTECH.2017.8077017.
- Grisetti, G., Stachniss, C. and Burgard, W. (2005) 'Improving grid-based SLAM with Rao-Blackwellized particle filters by adaptive proposals and selective resampling', in *Proceedings - IEEE International Conference on Robotics and Automation*. IEEE, pp. 2432–2437. doi: 10.1109/ROBOT.2005.1570477.
- Jensen, K. et al. (2014) 'Towards an Open Software Platform for Field Robots in Precision Agriculture', *Robotics*. {MDPI} {AG}, 3(2), pp. 207–234. doi: 10.3390/robotics3020207.
- Koenig, N. and Howard, A. (no date) 'Design and use paradigms for gazebo, an open-source multi-robot simulator', in *2004 IEEE/RSJ International Conference on Intelligent Robots and*



CIGR 2018

XIX. World Congress of CIGR



Systems (IROS) (IEEE Cat. No.04CH37566). IEEE, pp. 2149–2154. doi: 10.1109/IROS.2004.1389727.

Labbe, M. (2011) ‘Find Object’. IEEE. doi: 10.1109/robot.2009.5152831.

Lowe, D. G. (1999) ‘Object recognition from local scale-invariant features’, in *Proceedings of the Seventh IEEE International Conference on Computer Vision*. IEEE, pp. 1150–1157 vol.2. doi: 10.1109/ICCV.1999.790410.

Lu, D. (no date) *global_planner - ROS Wiki*. Available at: http://wiki.ros.org/global_planner (Accessed: 21 April 2018).

Marder-Eppstein, E. and Chitta, S. (no date) *carrot_planner - ROS Wiki*. Available at: http://wiki.ros.org/carrot_planner#preview (Accessed: 21 April 2018).

Moisiadis, V. et al. (2017) ‘Intelligent autonomous vehicles in industrial environments’, in *6th ICMEN International Conferences*. Thessaloniki.

Pierzchała, M., Giguère, P. and Astrup, R. (2018) ‘Mapping forests using an unmanned ground vehicle with 3D LiDAR and graph-SLAM’, *Computers and Electronics in Agriculture*. Elsevier {BV}, 145, pp. 217–225. doi: 10.1016/j.compag.2017.12.034.

Quigley, M. et al. (2009) ‘ROS: an open-source Robot Operating System’, in *ICRA Workshop on Open Source Software*, p. 5. doi: <http://www.willowgarage.com/papers/ros-open-source-robot-operating-system>.

Wei, H. et al. (2016) ‘RT-ROS: A real-time ROS architecture on multi-core processors’, *Future Generation Computer Systems*. Elsevier {BV}, 56, pp. 171–178. doi: 10.1016/j.future.2015.05.008.



CIGR 2018

XIX. World Congress of CIGR



Proximate Sensing and Application for Variable Rate Nitrogen Application on Corn Field.

Ufuk Türker¹ İbrahim Güçdemir², Ergin DURSUN¹, Uğur YEGÜL¹

¹Ankara University, Faculty of Agriculture Farm Machinery and Technologies Engineering
Department-06130, Ankara, Turkey,

² Soil and Fertilizer Research Enstitute
uturker@agri.ankara.edu.tr

ABSTRACT

In this study, a multispectral proximate sensor was mounted to a tractor to determine corn crop N status as it varies across the field by measuring the reflectance from crop canopies in a approximately 40 ha corn field in Çukurova region. To determine N efficiency, six different level of N application plots were established in 500 m long and 18 row wide test plots in the field. Each plot has been scanned by sensor and harvested separately with a combine harvester that implemented with yield mapping system. Economic optimum N level was found to be approximately 310 kg/ha for this field after economic analyses. But it has been proved that the field has three different production level according to the previous soil and yield maps. In order to match to this conditions, a proximate sensor was connected to a modified variable rate row fertilizer spreader. This modified unit was then used to apply variable rate N according to actual demand as on-line, in real time mode. In the first year of the study, 20% of N has been saved without any yield loss. This application enabled farmer to have more uniform growth and yield in his field in the first year.

Keywords: Precision Agriculture, Proximate sensing for nitrogen, N-sensor, Variable rate nitrogen fertilizer application, Site specific fertilizer management, Nitrogen management.

INTRODUCTION

Fertilizer application in conventional agriculture is applied uniformly across a field regardless the variability. In this production system, all variability about geographical terrains, physical and chemical properties (soil and plant characteristics, topography, etc.) do not take into consideration by growers and this means using less or more fertilizer than their actual needed. Variable rate fertilizer technology as an important part of precision agriculture which is based on



CIGR 2018

XIX. World Congress of CIGR



differences in soil and crop nutrients and apply fertilizer in various rate to optimize productivity and maximize the return in each part of a field (Ebelhar et al., 2005). Therefore to achieve maximum net return, it is essential to apply nitrogen at optimum level corresponding to site specific soil and crop condition. Variably apply of nitrogen result in an increase nitrogen use efficiency, net return, yield quality and quantity while preventing over application of nitrogen (Ferguson et al., 2005; Goovaerts, 1998; Grisso et al., 2011; Holland et al., 2010).

Sensor-based system can apply the variable rate of inputs without using prior map or data collection involved. In this system, desired measurement made by real time sensors from soil or crop properties can be processed immediately to control variable rate applicators. The obtained data can be geo-referenced and recorded using in future site specific practices as well as to provide real time application records for the growers (Koch et al., 2004). One of the examples of using the sensor based nitrogen application are reported in cereal grain production by Raun et al., 2002. In this research, an optical sensor was used to measure the spectral reflectance to estimate the plant nitrogen uptake and eventual yield and modulate the addition of nitrogen fertilizer during early stage of growth. The initial index for in-season estimates of grain yield was computed using NDVI and the number of days from planting to sensing. The results demonstrated the capability of using this system to use at spatial scales of 1 m² (Lan et al., 2009). Developing in-season nitrogen recommendation model is the objective of an investigation carried out by Holland (Holland et al., 2010) using canopy sensors and remote sensing data. They have a model which was developed based on the general shape of an N fertilizer response function and the relationship between N rate and in-season crop vegetation index data used in corn production. The results of a three year investigation emphasizes on model capability to make in-season nitrogen recommendation without need to estimate of potential yield because only sufficiency index and growth stage data were required (Raun et al., 2002).

The goal of this study was to optimize the applied amount of fertilizer to the local requirement of the corn crop, so to benefit both economically and environmentally through implementation and use of a proximate sensing technique for variable rate nitrogen application. Corn yield response to variable rates and uniform applications was investigated and extracted results were evaluated economically.

2. MATERIAL AND METHODS

2.1 Experimental Field

The study site was 38 ha of commercial farms with irrigated corn located at the Yolgecen town (36° 57' 49 N, 035° 08' 08 E), Adana province, Turkey. The study area contains alluvial origin soils derived from sedimentary deposits of Seyhan river flooding at different times located in Seyhan Delta.



2.2 System Description

The unit consists of diode-array spectrometers, fiber optics and a microprocessor in a box mounted on top of a tractors roof (the blue unit in Figure 2). One spectrometer registers light reflectance on four spots around the vehicle through fiber optics (two on each side, directed obliquely outwards (64° from nadir)). The second spectrometer senses irradiance from the sky hemisphere and registers ambient light in order to compensate for varying light conditions. One scan per second (the scanned area is about 50 m^2) is normally collected and recorded in a user terminal mounted inside the vehicle. These estimations are based on two preset quotients ("S1" and "S2"). It is not publicly known how S1 and S2 are determined, but they can be regarded as vegetation indices analogue to e.g. NDVI, RVI and others. S1 is mainly correlated to the chlorophyll content of the crop whereas S2 is correlated to the biomass (Hydro Agri, 2000). Before scanning the sensor is calibrated. A maximum and minimum N application rate is set. So S1 determines the N-demand except in areas with a poorly developed vegetation, below the biomass cutoff (Figure 1), where the N-demand is determined by the S2 value, resulting in a decreasing N-application. This means that the N-requirement is determined relative to the calibration value.

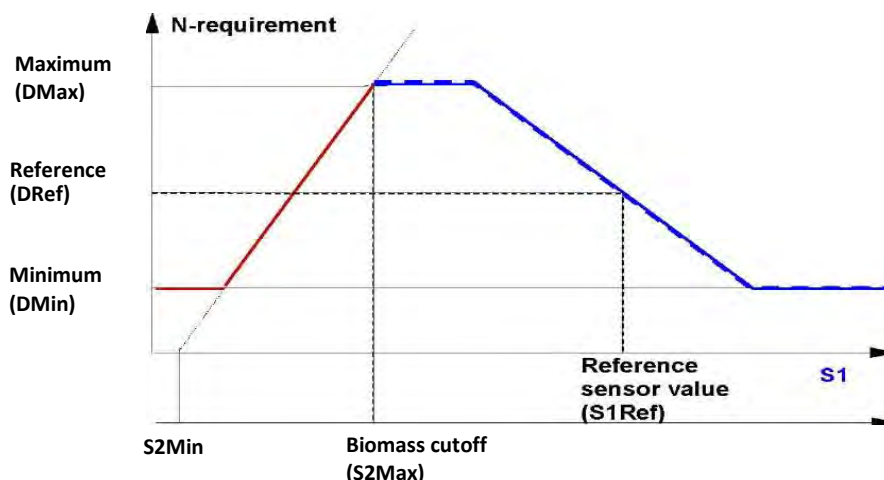


Fig. 1. Before scanning the sensor is calibrated in the field whereas Dref is specified by the user. The figure shows the relationship between S1, S2 and N-demand. When the S1-value reaches a certain low level (the biomass cutoff), the N-requirement is determined by S2.

”



CIGR 2018

XIX. World Congress of CIGR



2.2.1 Setting up the system to tractor and fertilizer machine

N-Sensor was mounted on the tractor at the height of 2.8 meters and sensing differences in light reflectance from selected bandwidth, converting obtained values which correlated with the crop biomass or crop chlorophyll density into an optimum application rate enabling the variable rate application equipment to apply the required rate for that specific part of the field (Figure 2). Although the sensor-based system was operated as a stand-alone system without the input of a GPS signal, however in order to assess the information need to produce application map and data evaluation EGNOS (European) compatible GPS was used. Positioning system consisted of a satellite computer, the reference station, the global positioning device (GPS), radio antenna and software. The system was controlled by a terminal that has been installed in the cabin. All measured crop data combinations with positioning data record in a PCMCIA card at 1 Hz intervals. Control system used to adjust the level of application and send as signals to the spreader was comprised of satellite computer and control terminal and board computer.

2.2.2 Field Calibrations

Field agronomic calibration of N sensor was carried out at V6 stage of vegetation in average rate as representing the whole field. 50 meters of selected row were scanned. After this calibration, considering the percentage of light reflections and biomass indices, the pre-determined the optimum rate was entered into the system. Variable rate nitrogen application was performed in May in the first year. Descriptive statistics relate to result of soil analysis are summarized in Table 1. All analysis related to the availability of nutrients, sufficiency levels and their coefficient of variation in the study area were analyzed according to McBratney 1986 (McBratney et al., 1986).

”



CIGR 2018

XIX. World Congress of CIGR



Table 1. Descriptive statistics of soil nutrients.

Plant Nutrients	Mean	Min	Max	Std	CV (%)	Variability level	Critical value range
Total Nitrogen (%)	0,1	0,03	0,15	0,025	23,1	Medium	< 1
Phosphorus (P ₂ O ₅) (kg/da)	2,9	0,4	29	1,88	65,6	High	< 6
Potassium (K ₂ O) (kg/da)	72,9	11	134	27,5	37,7	High	< 30
Lime (%)	26,2	23	29	1,17	4,5	Low	1-15
Iron (Fe) (ppm)	14,3	4,85	35,9	6,13	42,8	High	< 4,5
Boron (B) (ppm)	1,3	0,38	2,35	0,43	33,9	High	< 0,2
Zink (Zn) (ppm)	0,5	0,07	6	0,96	175	High	< 0,7
Manganese (Mn) (ppm)	4,7	0,49	10,75	2,34	50	High	< 1



Figure 2. N sensor and terminals used in sensor – based application

3. RESULT AND DISCUSSION

To avoid excessive use of fertilizers in low yielding areas and under fertilizing high yielding areas, combining yield mapping and soil testing could reduce the amount of unnecessary fertilizers (O'Halloran et al., 1985; Wittry et al., 2004). With the aim of identifying the potential of yielding in the studied area, the area was harvested with combine implemented with yield mapping system. Yield map related the first year given in Figure 3. Spatial variation in yield can be understood with an investigation of map and table related to yield (Figure 3).



CIGR 2018

XIX. World Congress of CIGR

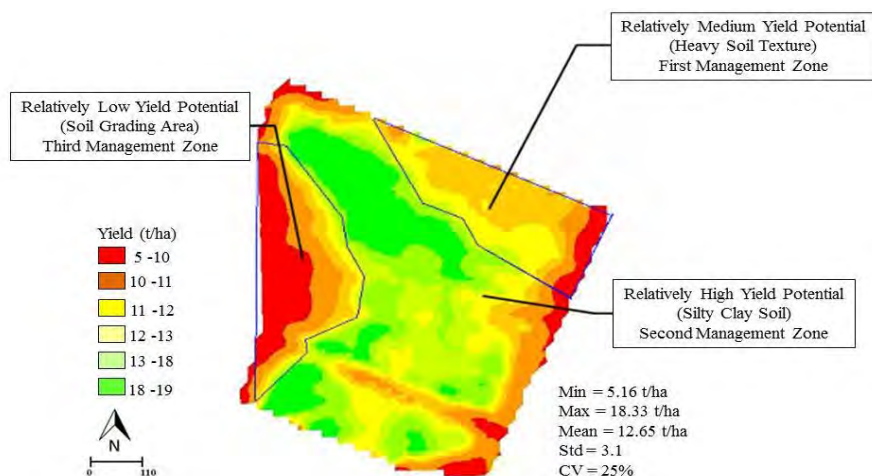


Figure 3. Yield map of the study area and zones with different yield potential.

Nitrogen rate based on the sensor, farmers rate, %25 less than farmers rate and %25 more than farmers rate where chose as four nitrogen rate were all repeated in related blocks. Plant biomass and consequently the nitrogen status determined by sensor were mapped in all blocks (Figure 4).

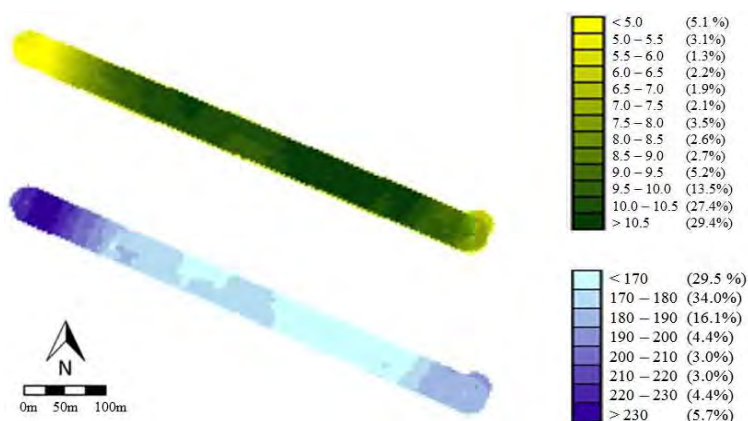


Figure 4. Biomass distribution map (above) and corresponding variable rate nitrogen application map(kg/ha)

The results of two year sensor-based nitrogen application shows the average value of 180 kgN/ha (390 kg Urea/ha) and 201 kgN/ha (437 kg Urea/ha) during first and second year application respectively (Table 1). Considering the amount of 230 kgN/ha (500 kg Urea/ha) as used by farmers, 22% and 15% savings in nitrogen fertilizer were recorded in first and second year application respectively.



CIGR 2018

XIX. World Congress of CIGR



Table 1. Descriptive statistics of variable rate nitrogen fertilizer applications

App.	Variation	Min	Max	Mean	Sd	CV%
First	Average rate of N in variable rate application (kgN/ha)	117	246	179,82	15.75	8.7
	Yield (ton/ha)	5,0	18,0	12,05	2,26	19
Second	Average rate of N in variable rate application (kgN/ha)	142	260	201	15.7	7.8
	Yield (ton/ha)	5,0	16,65	12,4	2,24	18

In order to study the effect of nitrogen rate on yield, the fertilizer applications were repeated 9 times in 4 topics as an application that consists of 36 plots. The results indicate different values for each individual year that mean value gained from sensor-based application was determined more than what was gained from the farmer's application. The differences between the average yields obtained from different applications have been tested by variance analysis. The result of the analysis was shown no differences between the yield mean values obtained in the first year ($P=0.21$). So it can be said that different nitrogen application caused no significant differences in terms of yield. The same analysis was done with second year values and differences between mean yield values were determined as significant ($P=0.039$). So it can be said that using different treatment in nitrogen application led to significant differences in terms of yield values. Duncan grouping for mean yield ($P=0.05$) clearly identified different groups between both sensor-based and farmer's applications and other two applications.

4. CONCLUSIONS

Farmer applications and variable rate applications were compared in terms of fertilizer input and yield. Accordingly, it has increased the efficiency with real time applications made with nitrogen sensor. Farmer practices and other conventional applications were remained and lag behind variable rate applications. Economic optimum N level was found to be approximately 310 kg/ha for this field after economic analyses. But it has been proved that the field has three different production level according to the previous soil and yield maps. To match the conditions, a proximate sensor connected to a modified variable rate row fertilizer spreader. This modified unit was then used to apply variable rate N according to actual demand as on-line, in real time mode. In the first year of the study, 20% of N has been saved without any yield loss. As a result of this study, the effects on the environment were examined and it was determined that the variable rate applications decreased nitric acid and etc. harmful substances discharged from the drainage water.

”



CIGR 2018

XIX. World Congress of CIGR



5. REFERENCES

- Ebelhar, S. A., Varsa, E. C., Robertson, G. K., Wyciskalla, T. D., Hart, C. D., & Hamson, J. (2003). The Use of Variable Rate Technology (VRT) and Yield Mapping for Optimizing Fertilizer Recommendations for Corn and Soybeans. *Illinois Fertilizer Conference Proceeding January 27-29*.
- Ferguson, R. B., Hergert, G. W., Schepers, J. S., Gotway, C. A., Cahoon, J. E., & Peterson, T. A. (2002). Site-specific nitrogen management of irrigated maize. *Soil Science Society of America Journal*, 66(2), 544-553.
- Goovaerts, P. (1998). Geostatistical tools for characterizing the spatial variability of microbiological and physico-chemical soil properties. *Biology and Fertility of Soils*, 27(4), 315-334.
- Grisso, R. B., Alley, M., Thomason, W., holshouser, D. & Roberson, G. T. (2011). Precision Farming Tools: Variable-Rate Application. *Virginia Cooperative Extension*.
- Holland, K. H., & Schepers, J. S. (2010). Derivation of a variable rate nitrogen application model for in-season fertilization of corn. *Agronomy Journal*, 102(5), 1415-1424.
- Hydro Agri. 2000. Precise: a sixth sense for agriculture. Hydro Agri, Upton, UK.
- Koch, B., Khosla, R., Frasier, W. M., Westfall, D. G., & Inman, D. (2004). Economic feasibility of variable-rate nitrogen application utilizing site-specific management zones. *Agronomy Journal*, 96(6), 1572-1580.
- Lan, Y., Zhang, S., Li, W., Hoffmann, W. C., & Ma, C. (2009). Variable rate fertilization for maize and its effects based on the site-specific soil fertility and yield. *Agricultural Engineering International: CIGR Journal*.
- McBratney, A. B., & Webster, R. (1986). Choosing Functions for Semivariograms of Soil Properties and Fitting them to Sampling Estimates. *Journal of Soil Science*, 37, 617 – 639.
- O'Halloran, I. P., Kachanoski, R. G., & Stewart, J. W. B. (1985). Spatial variability of soil phosphorus as influenced by soil texture and management. *Canadian journal of soil science*, 65(3), 475-487.
- Raun, W. R., Solie, J. B., Johnson, G. V., Stone, M. L., Mullen, R. W., Freeman, K. W., ... & Lukina, E. V. (2002). Improving nitrogen use efficiency in cereal grain production with optical sensing and variable rate application. *Agronomy Journal*, 94(4), 815-820.
- Wittry, D. J., & Mallarino, A. P. (2004). Comparison of uniform-and variable-rate phosphorus fertilization for corn–soybean rotations. *Agronomy Journal*, 96(1), 26-33.

”



The Accuracy in Seed Spacing of a Seeder with Variable Ratio

¹Erdem Aykas, ¹Pınar Ercan Yıldız

Department of Agricultural Engineering and Technology, Faculty of Agriculture,
Ege University, Izmir, Turkey

ABSTRACT

The purpose of this research is to design a new single grain seeder that can seed with variable ratio. In this study servo motor, software, geographic position system, variable ratio application, soil and crop efficiency maps, geographic information system and etc. are used. In the design vertical disc of seeder of single grain seeder gets rotation movement from servo motor that is assembled on machine in spite of existent tractors wheel. Thus machine's seeder disc in case of necessity could be rotated independent of tractors going speed. In the design, the servo motors get the comments from the software. Also there is a GPS on the machine to determinate the position of machine in a field. The software gets the GPS datas in the design. Thus according to a yield map, the machine can seed with variable ratio with software. The distance between thrown grain are measured; nominal planting distance and the deviation of these are established, acceptable grain distance % rates are determined with the aim of establishing the row grain distribution uniformity trials on sticky belt. Thus the seeder machine performance of grain distribution uniformity is exposed.

Consequently, prototype is manufactured by using the precision agriculture technology with designing proper variable rate seed on the project. For that purpose, seeder system is rotated with servo motor which is placed on the machine instead of wheel, according to speed and position of tractor seeder system axle rotation speed could be changed, therefore pneumatic grain machine with variable ratio seeder is designed.

Keywords: seeder with variable ratio, seeder system, servo motor, software

INTRODUCTION

With the development of technology, developments in agricultural machinery as well as in all fields are increasing rapidly. In precision agriculture it is important to provide good quality, efficient, rich product and also to reduce environmental pollution, the costs of seeds, fertilizers, spraying and etc. It is essential in terms of precision agriculture to implement the process according to the property of the soil in order to be laid most efficiently from the soil. With this study, in order to utilize the existing agricultural lands in the most efficient way, the seeder with variable ratio production is carried out for getting different seed spacing according to the field yield map.

In this study software is used for command the servomotor, and in order that take control of the seeder system. The determinations of servo motors rotation ratio according to seed spacing and vacuum plates' (disk's) hole number are done and also these determinations and calculations are adapted on software. The settings are made by software. It is easy to setup the distance of seed spacing on software device. In laboratory experiments the different velocities and different seed



CIGR 2018

XIX. World Congress of CIGR



spacing are experience. The velocity values are 1m/s and 1.5m/s. The seed spacings are changes seed to seed. For sunflower seed spacings are 20cm, 28cm, 36 cm. For corn seed spacings are 15cm, 20cm, 25cm. For cotton seed spacings are 10cm, 15cm and 20cm. In experiments the velocity varyaty and seed spacing varied are determinated.

The tests are made with rising velocities 1m/s to 1,5m/s with decreasing velocities 1,5m/s to 1m/s, with no slope, 5° right side slope, 10° right side slope on sticky belt. In the tests the seed spacings are also rising and decreasing. Here only the some of the laboratory experiments and its results are shown.

MATERIAL

The new single grain seeder that can seed with variable ratio is manufactured (Figure 1). The software is prepared by expert firm (Figure 3). Sunflower seed, corn seed and cotton seed are used in labrotory tests. Servo motor which rotates the seeder system is on the seeder machine (Figure 2). The tests are made on a sticky belt test setup which is in Ege University Agriculture Machines Depertman's laboratory (Figure 4).



Figure 1. The seeder with variable ratio



Figure 2. Servo motor



Figure 3. Software device



Figure 4. Sticky belt system



CIGR 2018

XIX. World Congress of CIGR



The seed spacing are measured with meter and computer setting system for cotton seed, sunflower seed and corn seed.

METHOD

The test results are concluded according to seed spacing definition and Performance criteria based on main seed distribution for precision seeding.

The following equation is used to determine the seed distribution for the precision seeders.

$$Z = \frac{\pi \cdot D}{i \cdot k}$$

Z: rated sowing distance (cm)

D: wheel diameter of seeder (cm)

i: transmission rate ($i = nd/nw$)

nd: disk number of revolution (rpm)

nw: wheel number of revolutions (rpm)

k: number of disk holes

The seed spacing are measured on the sticky belt, between 0,5-1,5 Z values are acceptable values; smaller than 0,5 Z values are multiples, bigger than 1,5 Z values are misses. The obtained test values are evaluated according to Table 1.

Definition of the seed spacing distribution indexes

Table1. Seed spacing definition

Seed Spacing	Definition
$< 0.5 Z_s$	Multiple index (I_{mult})
$(0.5-1.5) Z_s$	Quality of feed index (I_{qr})
$> 1.5 Z_s$	Miss index (I_{miss})

Table2. Performance criteria based on main seed distribution for precision seeding.

Quality of feed index (I_{qr} , %)	Multiple index (I_{mult} , %)	Total Miss index (I_{miss} , %)	Classification
> 98.76	< 0.62	< 0.62	Very good
$> 90.6 - \leq 98.76$	$\geq 0.62 - < 2.92$	$\geq 0.62 - < 2.92$	Good
$\geq 90.50 - \leq 94.60$	$\geq 2.92 - \leq 4.75$	$\geq 2.92 - \leq 4.75$	Moderate
< 90.50	> 4.75	> 4.75	Insufficient



CIGR 2018

XIX. World Congress of CIGR



RESULTS

The test results for sunflower seeds, corn seeds and cotton seeds which are tested on sticky belt set up, are shown at the Figure 5 to Figure 28.

Sunflower Results:

The results of constant speed is shown at Figure 5, declining speed (1,5m/s to 1m/s ,decreasing velocities) for sunflower seed, are shown at Figure 6, increased speed (1m/s to 1,5 m/s, rising velocities) is shown at Figure 7 . (These test are made without slope).

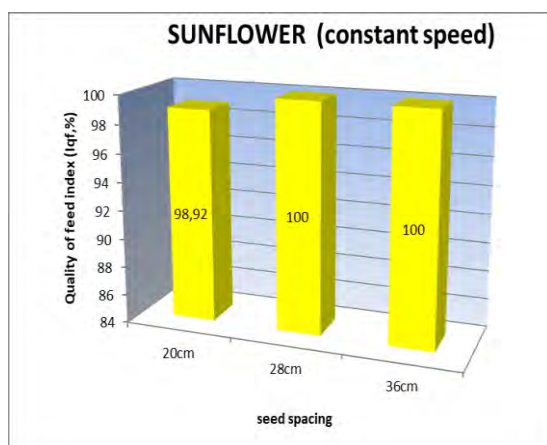


Figure 5. 1,5m/s constant speed

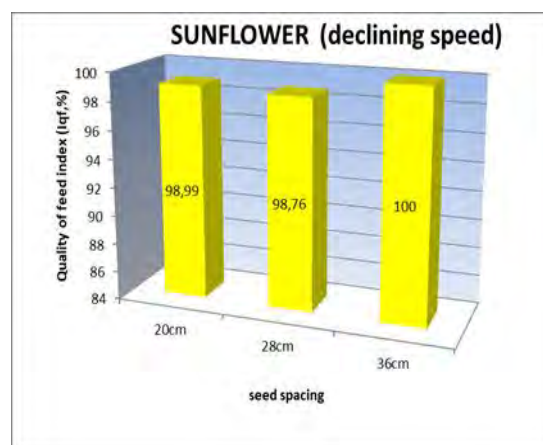


Figure 6. 1,5m/s to 1m/s declining speed

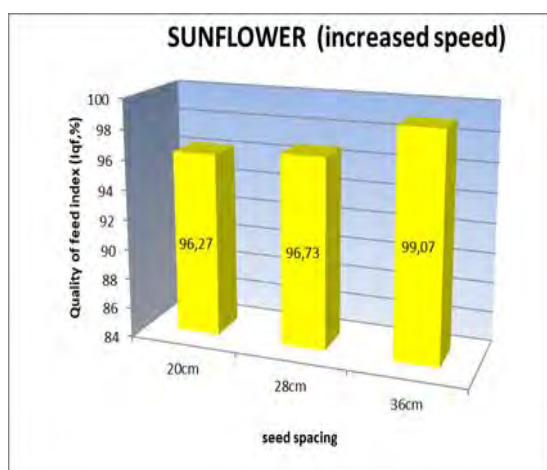


Figure 7. 1m/s to 1,5 m/s increased speed

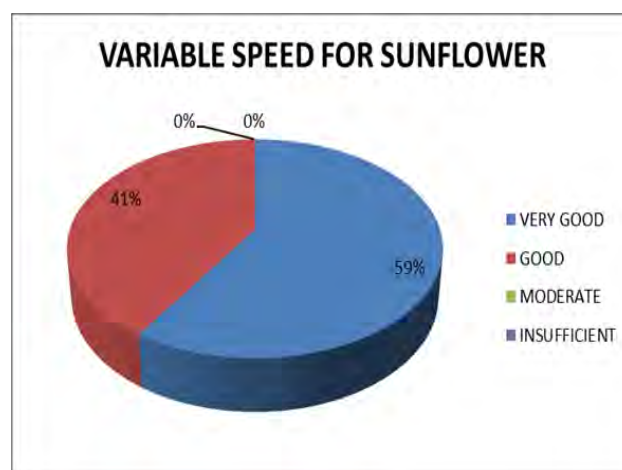


Figure 8. The Avarage Results of Variable Speed for Sunflower



CIGR 2018

XIX. World Congress of CIGR



These tests results cover also with 5°right side slope and 10° right side slope which are not shown here. The average of test results (without slope, 5° right side slope, 10°right side slope) for sunflower when the speed is constant, rising and decreasing is shown at Figure 8. The result evaluation is made according to Table 2.

The results of seed spacing for sunflower seed, seed spacings are changing from 20cm to 28 cm, from 28cm to 20 cm in constant speed (1,5m/s), are shown at Figure 15. The results of seed spacing, seed spacings are changing from 20cm to 36 cm, from 36cm to 20 cm in constant speed (1,5m/s), are shown Figure 16. The results of seed spacing, seed spacings are changing from 28cm to 36 cm, from 36cm to 28 cm in constant speed (1,5m/s), are shown at Figure17.

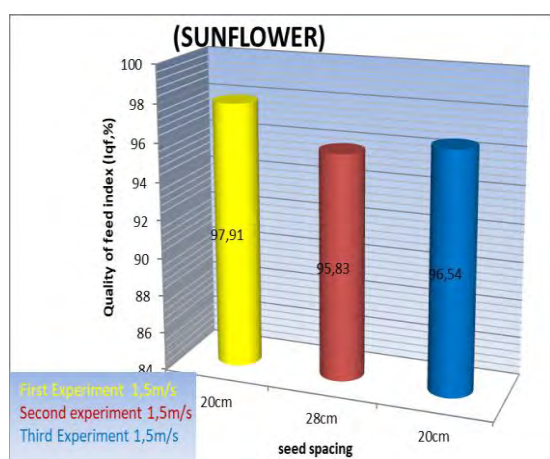


Figure 9. Seed Spacing 20cm-28cm-20cm

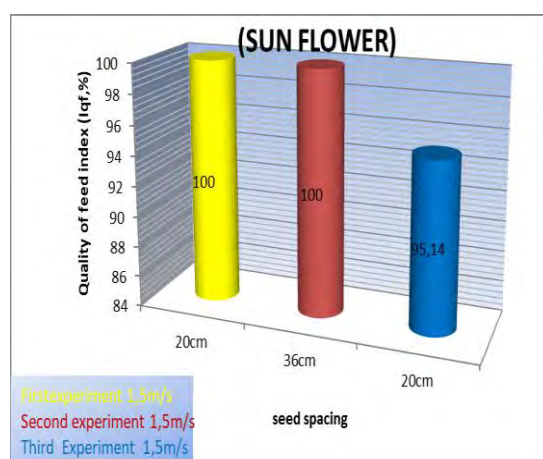


Figure 10. Seed Spacing 20cm-36cm-20cm

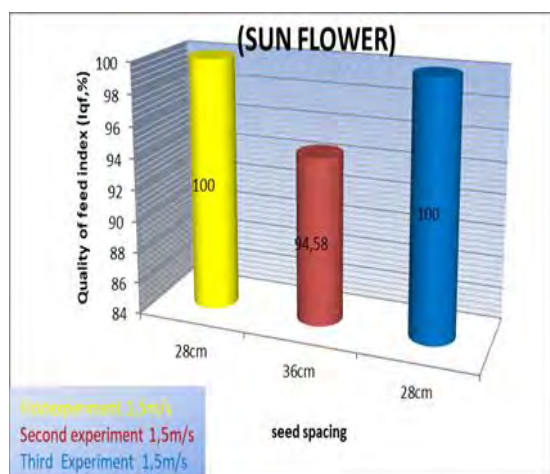


Figure 11. Seed Spacing 28cm-36cm-28cm

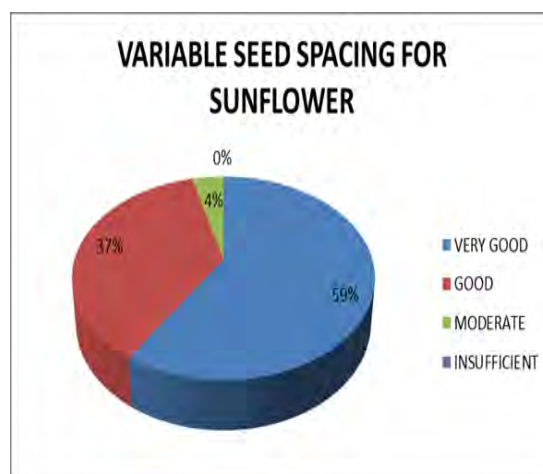


Figure 12. The Average Results of Variable



Seed Spacing for Sunflower

These tests cover also with 5°right side slope and 10° right slope for sunflower seed which are not shown here. The average of test results (without slope, 5° right side slope, 10°right side slope) for sunflower when the seed spacing rising, decreasing and again rising is shown at Figure 12. The result evaluation is made according to Table 2.

Corn Results:

The results of constant speed is shown in Figure 13, decreasing velocities(declining speed 1,5m/s to 1m/s) , for corn seed, are shown in Figure 14, rising velocities (increased speed 1m/s to 1,5 m/s) is shown in Figure 15 . These are made with no slope.

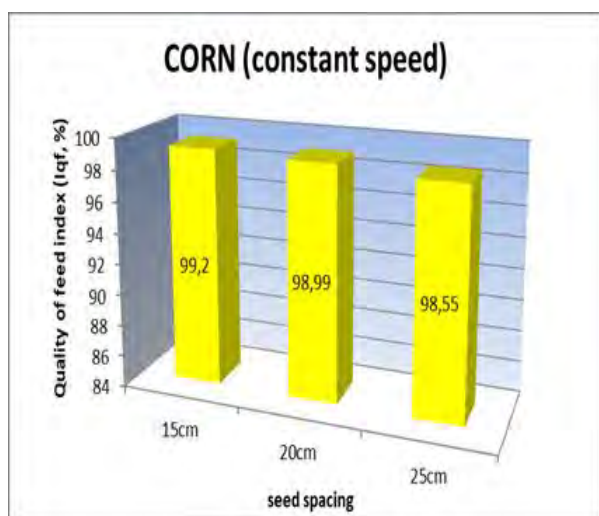


Figure 13. 1,5m/s constant speed

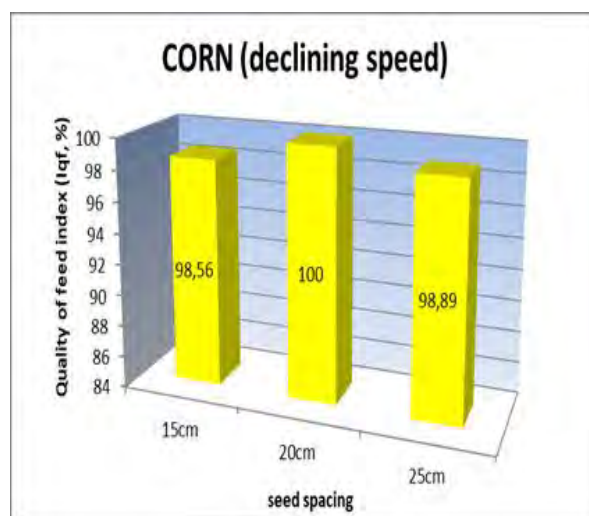


Figure 14. 1,5m/s to 1m/s declining speed



CIGR 2018

XIX. World Congress of CIGR

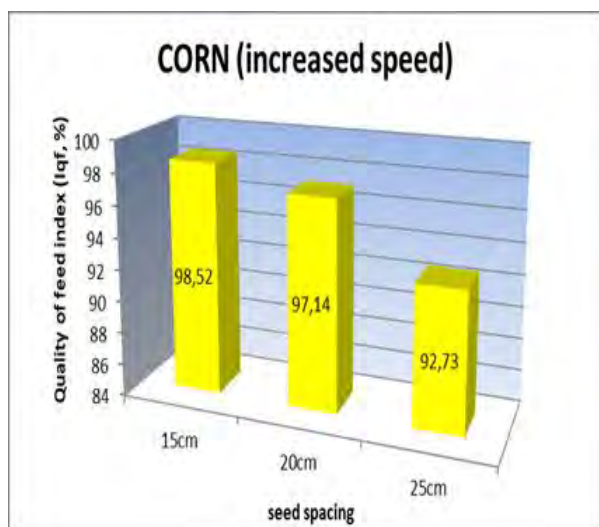


Figure 15. 1m/s to 1,5 m/s increased speed

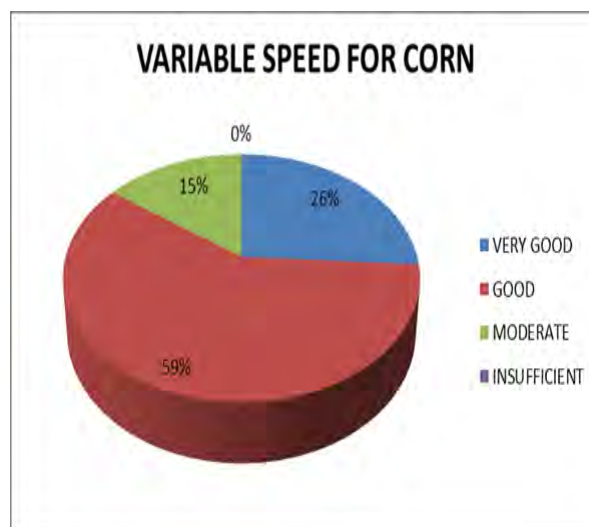
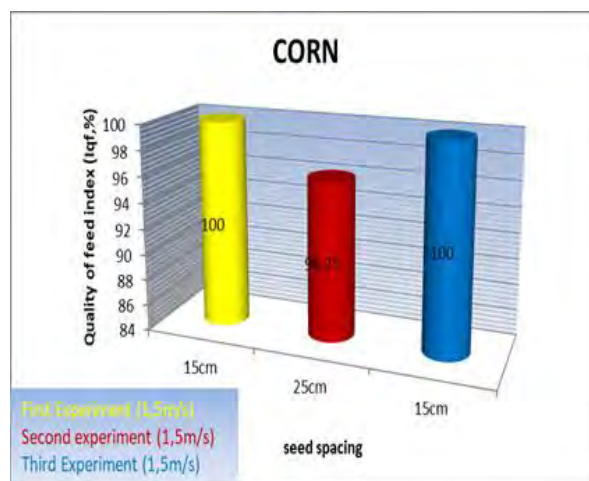
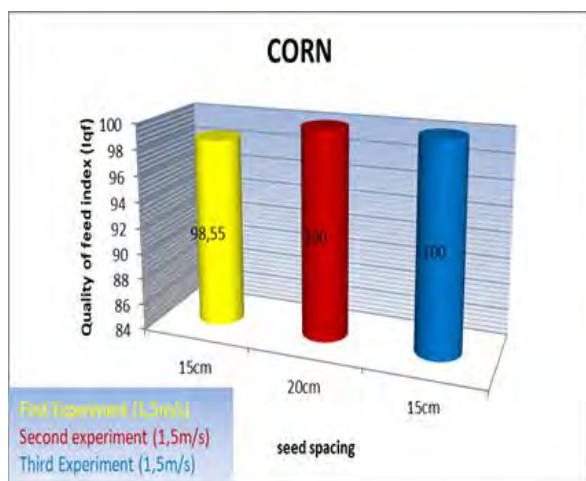


Figure 16 The Avarage Variable Speed for Corn

These tests cover also 5°right side slope and 10° right slope for corn seed which are not shown here. The avarage of test results (without slope, 5° right side slope, 10°right side slope) for corn when the speed is constant, rising, decreasing is shown Figure 5. The result evaluation is made according toTable 2.





CIGR 2018

XIX. World Congress of CIGR



Figure 17. Seed Spacing 15cm- 20cm-15cm

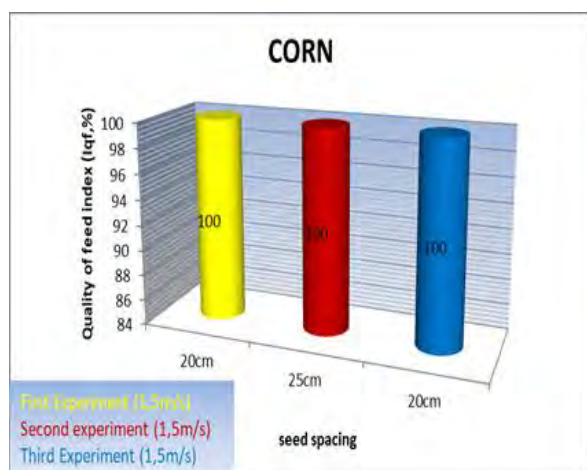


Figure 19. Seed Spacing 20cm-25cm-20cm

Figure 18. Seed Spacing 15cm-25cm-15cm

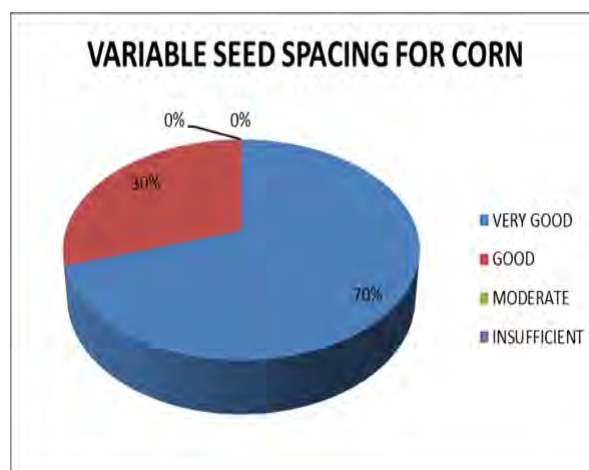


Figure 20. The Average Variable Seed Spacing Results for Corn Seed

The results of seed spacing for corn seed, seed spacings are changing from 15cm to 20cm, from 20cm to 15 cm in constant speed (1,5m/s), are shown Figure 17. The results of seed spacing, seed spacings are changing from 15cm to 25 cm, from 20cm to 15 cm in constant speed (1,5m/s), are shown Figure 18. The results of seed spacing, seed spacings are changing from 20cm to 25 cm, from 25cm to 20 cm in constant speed (1,5m/s), are shown Figure 19.

These tests cover also 5°right side slope and 10° right slope for corn seed which are not shown here. The average of test results results (without slope, 5° right side slope, 10°right side slope) for corn when the seed spacing rising, decreasing and again rising is shown Figure 20. The result evaluation is made according to Table 2.

Cotton Results:

For cotton seed ,the results of constant speed are shown in Figure 21, decreasing velocities (declining speed 1,5m/s to 1m/s) are shown in Figure 22, rising velocities (increased speed 1m/s to 1,5 m/s are shown in Figure 23 . (These test are made with no slope)



CIGR 2018

XIX. World Congress of CIGR

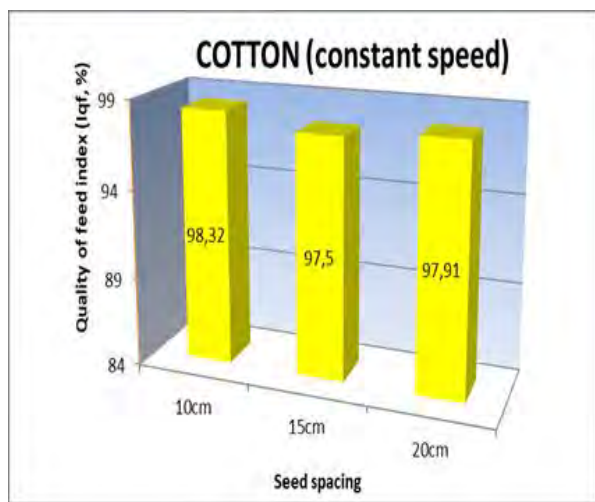


Figure 21. 1,5m/s constant speed

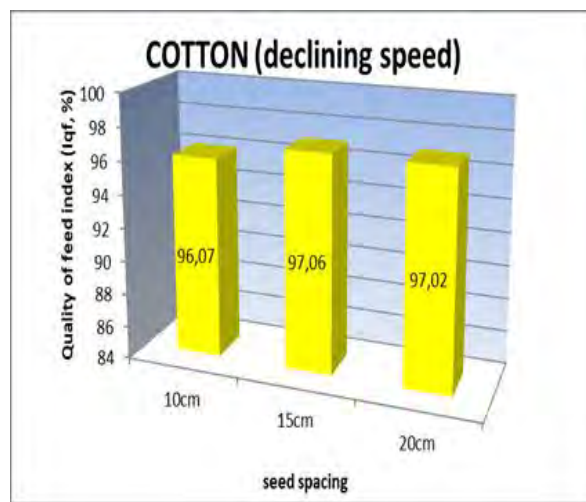


Figure 22. 1,5m/s to 1m/s declining speed

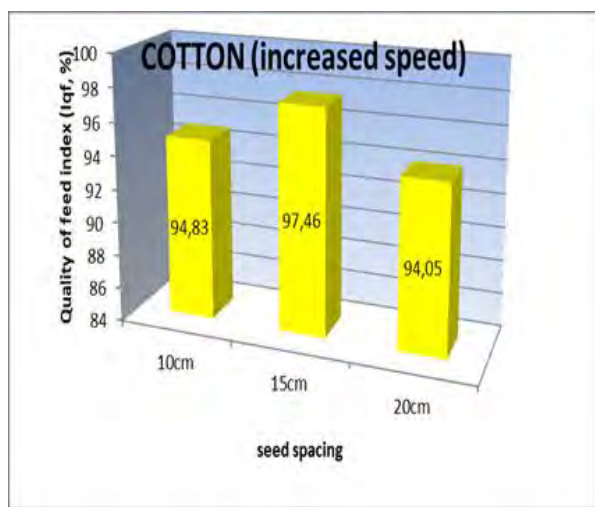


Figure 23. 1m/s to 1,5 m/s increased speed

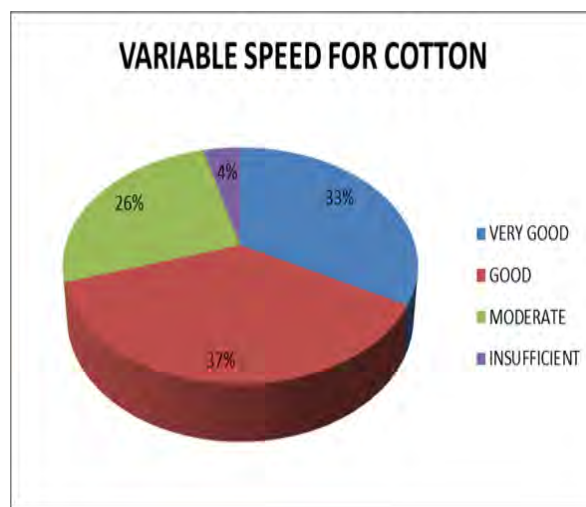


Figure 24. Variable Speed for Cotton

These test results cover also 5°right side slope and 10° right slope for cotton seed which are not shown here. The avarage of test results results (without slope, 5° right side slope, 10°right side slope) for cotton when the speed is constant, rising and decreasing is shown Figure 24. The result evaluation is made according to Table 2.

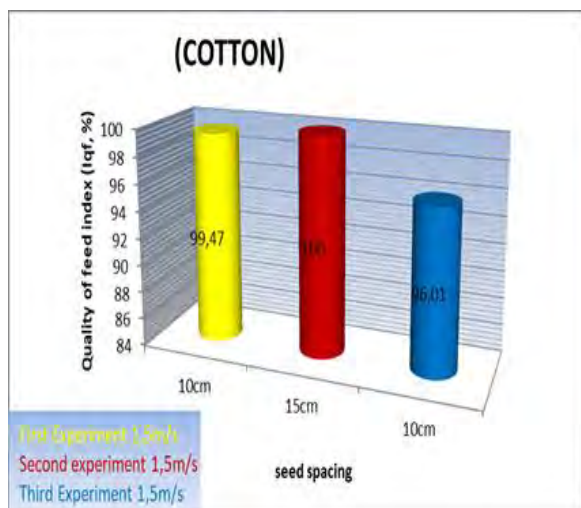


Figure 25. Seed Spacing 10cm-15cm-10cm

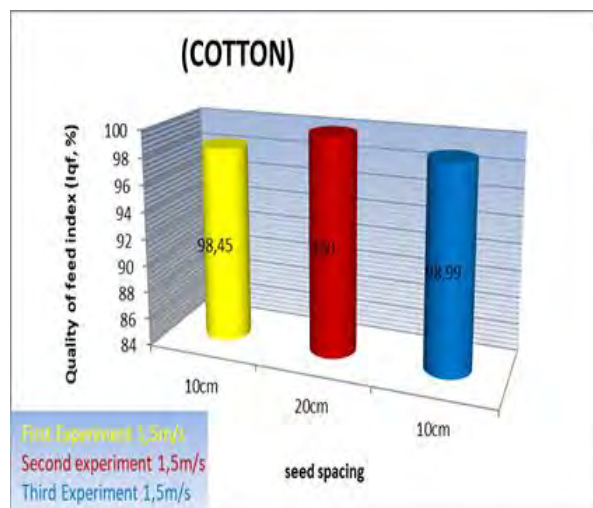


Figure 26. Seed Spacing 10cm-20cm-10cm

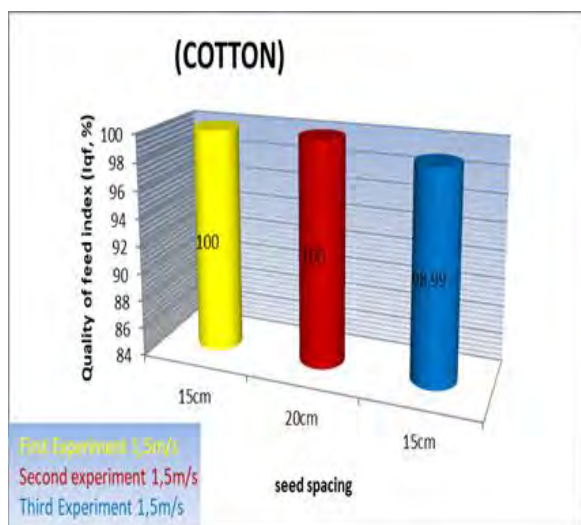


Figure 27. Seed Spacing 15cm-20cm-15cm

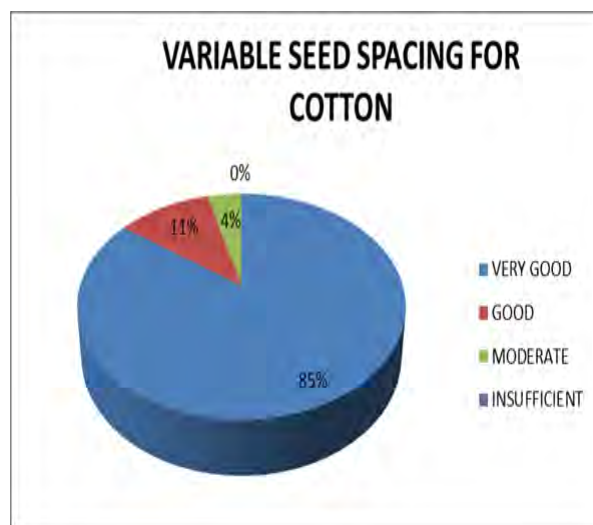


Figure 28. The Average Variable Seed Spacing for Cotton

For cotton seed the results of seed spacing; the test that seed spacings are changing from 10cm to 15cm, from 15cm to 10 cm in constant speed (1,5m/s), are shown Figure 25. The results of seed spacing, seed spacings are changing from 10cm to 20 cm, from 20cm to 10 cm in constant speed (1,5m/s), are shown Figure 26. The results of seed spacing, seed spacings are changing from 15cm to 20 cm, from 20cm to 15 cm in constant speed (1,5m/s), are shown Figure 27. (without slope).

These test results cover also 5° right side slope and 10° right slope for cotton seed which are not shown here. The average of test results results (without slope, 5° right side slope, 10° right side



CIGR 2018

XIX. World Congress of CIGR



slope) for cotton when the seed spacing rising, decreasing and again rising is shown Figure 28. The result evaluation is made according to Table 2. As it's shown in the figures the test results are mostly very good and good. Successful results were obtained with this seeder with variable ratio.

CONCLUSION

Yield can be increased by the use of single grain seeder with variable ratio. In the study, the use of pneumatic single grain seeder with variable ratio cultivation is used with the intention of using less grain to get yield increased and dissemination of this method instead of the constant ratio cultivation system. With this machine it is easy to set the seed spacing by software device. According to laboratory test results, this new seeder with variable ratio is good at sowing.

REFERENCES

- Aykas.E., H.Yalçın., A.Yazgı. 2013 Balta Tipi Gömücü Ayağa Sahip Tek Dane Ekim Makinalarının Farklı Bölgelerde Mısır Ekiminde Ekim Performanslarının Karşılaştırılması Tarım Makinaları Bilimi Dergisi (Journal of Agricultural Machinery Science) Cilt .9 Sayı. 1 .s.567-72
- Duncan, W.G., A Theory to Explain the Relationship Between Corn Population and Grain Yield, Crop Science, Vol. 24, November-december 1984.
- Emekli, N.Y., Topakçı, M. (2009) Hassas Uygulamalı Tarım Teknolojilerinin Sulama Alanında Kullanımı, GOÜ, Ziraat Fakültesi Dergisi, 26 (2): 9-17.
- Elms, M. K., GREEN, C. J., UPCHURCH, D. R. (1998), Cotton yield variability and correlations between yield, previous yield, and soil properties. Eds: Dugger, P.;Richter, D. Proceedings Beltwide Cotton Conferences, San Diego, California, USA, 5-9 January 1998. Volume 1. 1998 pp. 630-636.
- Hacıseferoğulları, H. (2005) Vakumlu Tip Pnömatik Hassas Ekim Makinası İle Şeker Pancarı Ekiminde Sıra Üzeri Bitki Dağılım Düzgünlüğü Ve Tarla Çıkış Oranları Üzerine Ekim Mesafelerinin Ve İlerleme Hızlarının Etkisi, SÜ Ziraat Fakültesi Dergisi, 19 (35): 30-40.
- Önal, İ., 1975. Bir Pnömatik Hassas Ekim Makinası İle Şeker Pancarı Tohumunun Ekim Olanakları Üzerinde Bir Araştırma. Şeker Dergisi, Sayı:96, 14-24, Ankara.
- Önal, İ., 1987. Vakum Prensibiyle Çalışan Bir Pnömatik Hassas Ekici Düzenin Ayçiçeği, Mısır ve Pamuk Tohumu Ekim Başarısı. Ege Ün.Zir.Fak. Dergisi, Cilt:24, Sayı:2, 105-117.
- Önal, İ. (2011) Ekim, Bakım, Gübreleme Makinaları, Ege Üniversitesi Yayınları, Ziraat Fakültesi Yayın No: 490, 611s.



CIGR 2018

XIX. World Congress of CIGR



Reyns, P., Missotten, B., Ramon, H., Baerdemaeker, J.D., 2002. A Review of Combine Sensors for Precision Farming. *Precision Agriculture*, 3(2), 169-182.

Shanahan, J.F., Doerge, T.A., Johnson, J.J, Vigil, M.F. (2004) Feasibility of Site-Specific Management of Corn Hybrids and Plant Densities in the Great Plains, *Precision Agriculture*, 5, 207–225.

Tekin, A.B. (2005) Değişken Düzeyli Uygulamaya Yönelik Mineral Gübre Dağıtma Makina Tasarımı Üzerine Bir Araştırma, Ege Üni., Fen Bilimleri Ens., Tarım Makineleri ABD., Doktora Tezi.

Yalçın.H., E.Aykas., Yazgı.A.2013Yerli Yapım Baltalı Tip Tek Dane Ekim Makinalarının Laboratuvar ve Tarla Koşullarında Ayçiçeği Ekim Performansının Belirlenmesi. *Tarım Makinaları Bilimi Dergisi (Journal of Agricultural Machinery Science)* Cilt .9 Sayı. 3 .s.247-256s.231-238



Precise Point Positioning for a Robot Tractor using LEX Signal Transmission from Quasi-Zenith Satellite System

Hao Wang¹, Noboru Noguchi²

¹ Graduate School of Agriculture, Hokkaido University.

² Research Faculty of Agriculture, Hokkaido University, Kita 9 Nishi 9, Sapporo, Hokkaido, 065-8589, Japan.
noguchi@cen.agr.hokudai.ac.jp

ABSTRACT

This paper addresses problems of automatic guidance of the robot tractor for precision farming. Robust and precise kinematic positioning is fundamental to the robot tractor that utilizes Global Navigation Satellite System (GNSS) as the main positioning method. However, this is somewhat problematic in Australia, where the farms usually locate in remote and sparsely populated areas in which reference stations are sparse and mobile network is difficult to access reliably. Therefore, classical solutions of real-time kinematic GPS (RTK-GPS) can hardly be adopted in these cases. On the contrary, the precise point positioning (PPP) technique is a viable approach to tackle this problem. PPP positioning with ambiguity resolution (PPP-AR) gets the ambiguity resolution within 30 minutes and achieves centimeter level horizontal positioning accuracy for dynamic receivers. This paper describes a robot tractor system developed for the Australian sugar industry to plow, fertilize, or spray crops automatically. It utilizes real-time correction messages from the L-band Experiment (LEX) signal transmitted by the Japanese Quasi-Zenith Satellite System (QZSS). This research is a true display of the labor-saving possibilities of precise agriculture that the robot tractor is able to follow the planned route with a lateral deviation less than 5cm (RMS).

Keywords: Autonomous vehicle, QZSS, GPS, PPP, PPP-AR, precise agriculture

INTRODUCTION

An autonomous agricultural vehicle is mainly used for agriculture operations, such as leveling, plowing, sowing, spraying, harvesting, transporting, and so on. It is considered to be one of the most efficient ways of improving productivity and quality of farming. Considerable researches have been reported on the application of Global Positioning System (GPS) with an inertial measurement unit (IMU) for agricultural robots and precision farming (Backman et al., 2012; M. Kise et al., 2001; Reid et al., 2000; Zhang et al., 2008). The integration of two sensors can improve positioning accuracy and robustness compared to either of the subsystem. Modern positioning methods, including the real-time kinematic GPS (RTK-GPS) technique, multiple reference stations RTK (MRS-RTK), and the virtual reference station RTK (VRS-RTK) method



can deliver centimeter-level positioning results (Castleden et al., 2004; Fotopoulos and Cannon, 2001; Lachapelle et al., 2000; O'connor et al., 1996). However, MRS-RTK and VRS-RTK require a communication link and dense reference stations network to transfer the correction data to the rover. This is somewhat problematic in remote and sparsely populated areas where reference stations are sparse and mobile network is difficult to access reliably.

The precise point positioning (PPP) method is anticipated as an alternative to RTK-GPS as it, instead of using ground stations as reference points, requires only single GNSS receiver and a coarse network of reference stations distributed sparsely in the coverage area of the satellites (Castleden et al., 2004; Choy et al., 2015; Kouba and Héroux, 2001; Zumberge et al., 1997). However, PPP requires precise information of satellite orbits and clocks, and it is critical for real-time applications to transmit correction data to PPP users. There are several major requirements when the PPP is used for the agricultural vehicles. The first is accuracy in dynamic conditions, which is about ± 5 cm required by precise farming work (Mi. Kise et al., 2001). Especially for inter-row farming work, repeatable straight line accuracy is essential to ensure that the vehicle remains in the intended stubble inter-row. The second requirement is robustness. With the presence of tall trees and mountains around the farm, blocked signal from satellites and multi-paths may degrade the positioning accuracy. In addition, the conventional PPP method is restricted by ambiguity resolution and convergence time.

This research aims to develop an autonomous tractor for precise farming. The robustness of the navigation system becomes more challengable in tropical areas because of the increased level of ionospheric activities. A Quasi-Zenith Satellite System (QZSS) based PPP method with ambiguity resolution (PPP-AR) is adopted in this research to provide centimeter-level accuracy positioning information for the robot tractor. The accuracy of the positioning information and the performance of the robot tractor system are evaluated at a Homebush cane farm in north Queensland, Australia.

2. OVERVIEW OF QZSS AND AUGMENTATION SERVICE

The QZSS, developed by Japan Aerospace Exploration Agency (JAXA), is able to broadcast navigation signals that are compatible and interoperable with other GNSSs. Figure 1 shows the configuration of QZSS. It consists of a satellite system corresponding to the space segment, a ground system corresponding to the control segment and the rover corresponding to the user segment. The satellite system is a constellation of the first Quasi-Zenith Satellite (QZS1 nicknamed 'MICHIBIKI') launched in September 2010, and another two quasi-zenith orbits (QZO) satellites and one geostationary orbit (GEO) satellite (Japan Aerospace Exploration Agency, 2016). In order to complement to the GPS, Quasi-Zenith Satellites (QZSSs) transmit four positioning signals of the same frequency as GPS including L1 and L2 signals. It offers an increased number of available satellites in East Asia and Oceania region. In addition, it is easy to create an idealistic geometry deployment with small GDOP, because at least one QZO satellite maintains a high elevation angle. QZSSs also broadcast augmentation information to realize centimeter-class positioning quality through the L6 signal to provide high positioning accuracy for the coverage area. The QZS1 is mainly used for confirming the potential of the system for



navigation application, as well as identifying possible challenges in its utilization. The L6 signal of QZS1 is also called L-band Experiment (LEX) signal (Collier et al., 2015). The augmentation data are generated by using part of continuously operating monitoring stations throughout Japan and other areas within the coverage. From April 2018, a combination of QZSS satellites broadcast navigation and augmentation signals over the coverage area 24 hours a day, seven days a week. Experiments in this paper are conducted under the cooperation of Japan government and related companies such as Mitsubishi Electric Corporation and Hitachi Zosen Corporation.

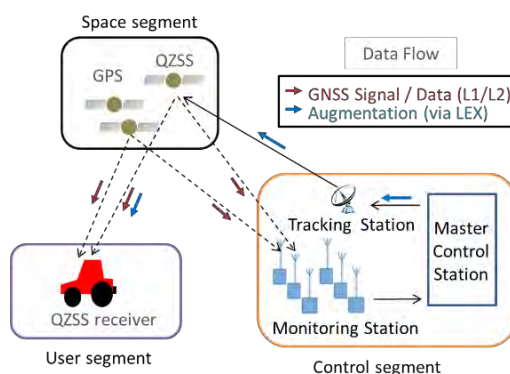


Figure 1. The overall architecture of the QZSS based positioning system.

3. CONFIGURATION OF THE ROBOTIC SYSTEM

The user segment of the satellite-based automation system includes a robot tractor and navigation sensors. The experimental tractor used to evaluate the navigation method is a half-crawler tractor, EG105C (YANMAR Co., Ltd., Japan). As shown in Figure 2, authors modified the commercial tractor using a QZSS based positioning system and an inertial measurement unit (IMU) as navigation sensors (Wang and Noguchi, 2016). The augmentation data providing the corrections of GNSS satellites clocks and ephemeris errors can be broadcasted via the LEX signal of QZS1. In this study, the function of Hitachi Zosen's multi-GNSS analytic software, RTNet, is used to obtain the precise point positioning with ambiguity resolution (PPP-AR) (Hitachi Zosen Corporation, 2015). Classical PPP methods use correction messages from International GNSS Service (IGS) and Multi GNSS Monitoring Network operated by JAXA (Choy et al., 2014). The augmentation information does not include the corrections of ionospheric delay parameters and tropospheric delay parameters. Therefore, it takes long convergence time to estimate the interference of ionosphere and troposphere. On the contrary, RTNet uses correction information from regional electronic datum points to achieve centimeter-level accuracy within 30 minutes, which is much faster than the PPP method (Choy et al., 2017). Since the LEX messages cannot be processed by current commercial GNSS receivers, a specific QZSS receiver (T03 in Figure 2) is used to decode the signals and get the PPP-AR solutions. The VRS-RTK results are recorded simultaneously to evaluate the accuracy of the PPP-AR results.

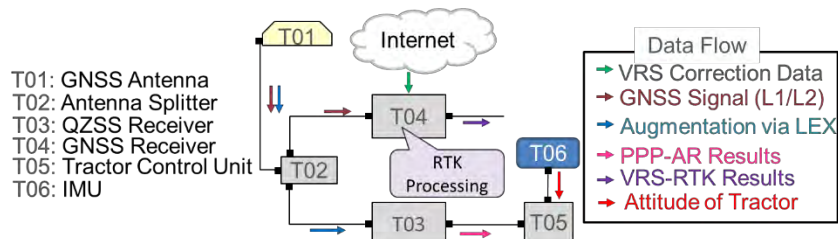


Figure 2. Scheme of the positioning system.

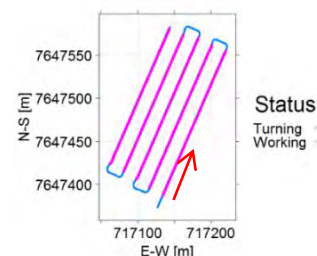
Autonomous operations of the robot tractor include following the predetermined path and controlling the hitch function, power-take-off and engine speed set and others based on a pre-designed navigation map. To follow the straight guidance path, a proportional integral controller is applied to control the robot tractor (Wang and Noguchi, 2016). The accuracy of the robot tractor is evaluated by the value of the lateral error, the perpendicular distance from the center of gravity of the tractor to the navigation path.

4. EXPERIMENTS AND DISCUSSION

The robot tractor performed farming work at a Homebush cane farm at Mackay in north Queensland where is a typical example of tropical areas with an increased level of ionospheric activity. Fluctuations of the radio wave in the ionosphere and troposphere in this area affect the connection between rover and satellites and reduce the positioning accuracy in the calculated distance between the user and the positioning satellites. Therefore, Mackay as a typical example of tropical areas is suitable to evaluate the robustness and the accuracy of the navigation system. The trajectory of the robot tractor in one test is shown in blue line in Google Earth (Figure 3 (a)) and the Universal Transverse Mercator (UTM) coordinate system (Figure 3 (b)), separately. There are 5 paths from the right to the left of the figure, and the path space is set to 20 m. The working order of the paths is sequent, from Path 1 (near the arrow in Figure 3) to Path 5 with four times turns. The turning method is the U-turning with 2 m go forward straightly before the start of turning procedure (Torisu et al., 1996). The speed of the robot tractor during work is 6.6 km/h.



(a) Trajectory showed in Google Earth



(b) Trajectory showed in UTM coordinate system.

Figure 3. The trajectory of the robot tractor after one trail.

4.1 Accuracy of PPP-AR in the Dynamic Condition



To evaluate the accuracy of the LEX signal based PPP-AR, the VRS-RTK fix solutions are recorded simultaneously during the movement of the tractor. The difference between the two results is termed as the error/offset of PPP-AR. During the test, offsets of the QZSS are calculated in the UTM coordinate shown in Figure 4. The shade represents the density of points in the heat map. The offset in East-West direction ranges from -3.2 cm to 2.6 cm. The offset in North-South direction ranges from -4.3 cm to 3.1 cm. The horizontal deviation is within 4.3 cm. The circular error probable (CEP) is 1.1 cm, 50% rounds land within 1.1 cm of the mean impact (Blischke and Halpin, 1966). The center of the estimated circle is (-0.6, -0.9). Therefore, it can be concluded that the PPP-AR results correspond to the VRS-RTK, because the CEP error is about 1.1 cm, and the maximum error is less than 4.3 cm. It means that the LEX signal from QZSS provides robust and accurate augment information for navigation.

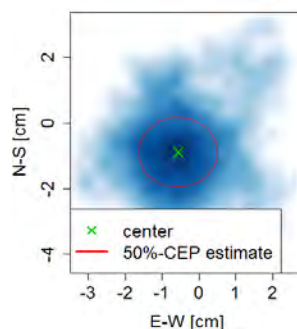


Figure 4. Offsets between QZSS and RTK-GPS coordinates.

4.2 Accuracy of the Robot System

To fully verify that augmentation signals transmitted from the QZSS can be used in precision farming in Australia, experimental farming activities, including leveling, tillage, boom spraying, and fertilizer spreading were conducted all day long. In each experiment, the robot tractor should follow the same navigation map. As mentioned in Section 2, QZS1 was the only satellite broadcasting the augmentation signal. The elevation of QZS1 viewed from Mackay is shown in Figure 5. It illustrates that the elevation is about 20 deg. around 14:00 in Australian Eastern Standard Time (UTC+10) when the signal of the LEX signal is the weakest period during a day. The fertilizer spreading experiment was conducted around 14:56 on December 9, 2016. The lateral error of each path during the experiment is listed in Table 14. It shows that the maximum RMS of the lateral deviation value is 5.4 cm; the minimum value is 3.2 cm. The average of the deviation in all paths is about 4.6 cm.



CIGR 2018

XIX. World Congress of CIGR

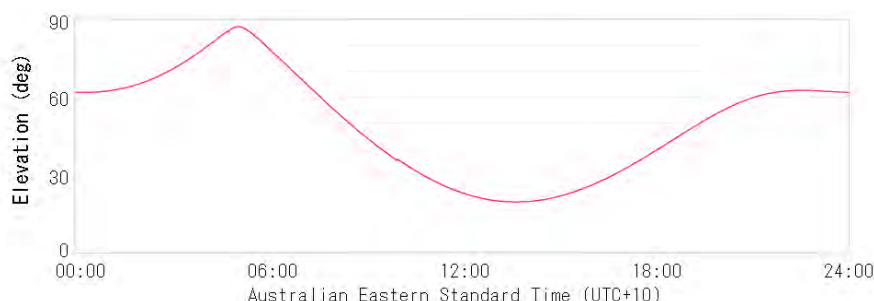


Figure 5. Estimated visibility of QZS1 from the view of Mackay, Queensland, Australia. Date: December 9, 2016

Table 14. The lateral error (RMS) in fertilizer spreading test

Path order	1	2	3	4	5	Average
Lateral error [cm]	3.2	5.3	4.7	4.3	5.4	4.6

The lateral error of all the 5 paths of fertilizer spreading experiment is shown in Figure 6. The blank areas indicate the turning period from one working path to the next. The maximum lateral error was about 0.3 m after the first turning. The large deviation and posture at the start of one path are mainly caused by the turning algorithm in limited headland space (Wang and Noguchi, 2016). From the figure, it can be seen that lateral errors are varying around zero. The lateral errors are large after turning, but they can converge soon within 5 seconds. From these results, it can be concluded that the robot tractor can follow the working map within 4.6 cm lateral error at the speed of 6.6 km/h.

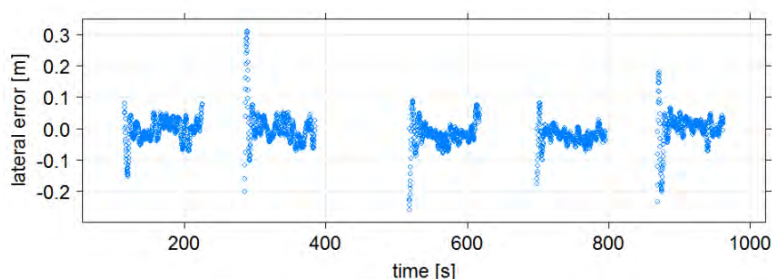


Figure 6. The lateral error of fertilizer spreading test

5. REFERENCES

Backman, J., Oksanen, T., Visala, A., 2012. Navigation system for agricultural machines: Nonlinear Model Predictive path tracking. *Comput. Electron. Agric.* 82, 32–43. <https://doi.org/10.1016/j.compag.2011.12.009>

Blischke, W.R., Halpin, A.H., 1966. Asymptotic Properties of Some Estimators of Quantiles of Circular Error. *J. Am. Stat. Assoc.* 61, 618. <https://doi.org/10.2307/2282775>

<H. Wang, N. Noguchi>. < Precise Point Positioning for a Robot Tractor using LEX Signal Transmission from Quasi-Zenith Satellite System >.



- Castleden, N., Hu, G.R., Featherstone, W.E., Abbey, D. a., Earls, C.J., Weihing, D., Øvstedal, O., 2004. First results from Virtual Reference Station (VRS) and Precise Point Positioning (PPP) GPS research at the Western Australian Centre for Geodesy. *J. Glob. Position. Syst.* 3, 79–84. <https://doi.org/10.5081/jgps.3.1.79>
- Choy, S., Harima, K., Li, Y., Choudhury, M., Rizos, C., Wakabayashi, Y., Kogure, S., 2015. GPS Precise Point Positioning with the Japanese Quasi-Zenith Satellite System LEX Augmentation Corrections. *J. Navig.* 68, 769–783. <https://doi.org/10.1017/s0373463314000915>
- Choy, S., Harima, K., Li, Y., Choudhury, M., Rizos, C., Wakabayashi, Y., Kogure, S., 2014. High accuracy real-time precise point positioning using the Japanese Quasi-Zenith satellite system LEX signal. *CEUR Workshop Proc.* 1307.
- Choy, S., Sunil Bisnath, B., Chris Rizos, B., 2017. Uncovering common misconceptions in GNSS Precise Point Positioning and its future prospect. *GPS Solut.* 21, 13–22. <https://doi.org/10.1007/s10291-016-0545-x>
- Collier, P., Harima, K., Choy, S., Kakimoto, H., Kogure, S., 2015. Utilisation of the Japanese Quasi-Zenith Satellite System (QZSS) Augmentation System for Precision Farming in Australia, IGNSS, Gold Coast, Australia.
- Fotopoulos, G., Cannon, M.E., 2001. An Overview of Multi-Reference Station Methods for Cm-Level Positioning. *GPS Solut.* 4, 1–10.
- Hitachi Zosen Corporation, 2015. Utilizing a Self-steering Robotic Tractor in the Developmental Phases of Rice --Feasibility Study on Using Quasi-Zenith Satellite System for Precision Farming in Australia [WWW Document]. Hitachi Zosen Corp. URL <http://www.hitachizosen.co.jp/english/release/2015/01/001512.html> (accessed 1.5.17).
- Japan Aerospace Exploration Agency, 2016. Interface Specification for QZSS.
- Kise, M., Noguchi, N., Ishii, K., Terao, H., 2001. Field Mobile Robot Navigated by RTK-GPS and FOG (Part 1): Estimation of Absolute Heading Angle by Sensor-fusion with RTK-GPS and FOG. *J. Japanese Soc. Agric. Mach.* 63, 74–76.
- Kise, Mi., Noguchi, N., Ishii, K., Terao, H., 2001. Field Mobile Robot Navigated by RTK-GPS and FOG (Part 2): Autonomous operation by applying navigation map. *J. Japanese Soc. Agric. Mach.* 63, 80–85.
- Kouba, J., Héroux, P., 2001. Precise Point Positioning Using IGS Orbit and Clock Products. *GPS Solut.* 5, 12–28. <https://doi.org/10.1007/PL00012883>
- Lachapelle, G., Alves, P., Fortes, L.P., Cannon, M.E., 2000. DGPS RTK Positioning Using a Reference Network, in: *Proceedings of the 13th International Technical Meeting of the Satellite Division of The Institute of Navigation (ION GPS 2000)*. pp. 1165–1171.
- O ’connor, M.L., Elkaim, G.H., Parkinson, B.W., 1996. Carrier-Phase DGPS Control of Farm and Vehicles for Closed-Loop Construction. *Navig. J. Inst. Nauigation* 43.



CIGR 2018

XIX. World Congress of CIGR



Reid, J.F., Zhang, Q., Noguchi, N., Dickson, M., 2000. Agricultural automatic guidance research in North America. *Comput. Electron. Agric.* 25, 155–167. [https://doi.org/10.1016/S0168-1699\(99\)00061-7](https://doi.org/10.1016/S0168-1699(99)00061-7)

Torisu, R., Nakatsubo, T., Imea, J., 1996. Minimum time control problem of tractor lateral motion, 1: Formulation and field experiment for minimum time control of tractor lane change maneuver. *J. Japanese Soc. Agric. Mach.* 58, 5–12.

Wang, H., Noguchi, N., 2016. Autonomous Maneuvers of a Robotic Tractor for Farming, in: 2016 IEEE/SICE International Symposium on System Integration (SII). IEEE, pp. 592–597.

Zhang, Y., Gao, F., Tian, L., 2008. INS/GPS integrated navigation for wheeled agricultural robot based on sigma-point kalman filter. 2008 Asia Simul. Conf. - 7th Int. Conf. Syst. Simul. Sci. Comput. ICSC 2008 1425–1431. <https://doi.org/10.1109/ASC-ICSC.2008.4675598>

Zumberge, J.F., Heflin, M.B., Jefferson, D.C., Watkins, M.M., Webb, F.H., 1997. Precise point positioning for the efficient and robust analysis of GPS data from large networks. *J. Geophys. Res. Solid Earth* 102, 5005–5017. <https://doi.org/10.1029/96JB03860>



CIGR 2018

XIX. World Congress of CIGR



Aerial Machine Vision, Geographical Information System and Hue for Pattern Classification in Agriculture

Marcel Pinton de Camargo^{1*}, Tamara Maria Gomes², Giovana Tommaso³

^{1*} Department of Biosystems Engineering, “Luiz de Queiroz” College of Agriculture, University of São Paulo, Av. Pádua Dias, 11, Piracicaba – SP 13418-900, Brazil.

marcel.camargo@usp.br, pacoca0880air@gmail.com

² Department of Biosystems Engineering, College of Animal Science and Food Engineering, University of São Paulo, Brazil.

³ Department of Food Engineering, College of Animal Science and Food Engineering, University of São Paulo, Brazil.

ABSTRACT

In this research we aim to achieve cybernetic cohesion information flow in precision agriculture, integrating machine learning methods, computer vision, geographical information system and UAV-photogrammetry in an irrigated area with slaughterhouse wastewater, under five treatments (W100 - irrigation with superficial water and 100% of nitrogen mineral fertilization, E0, E33, E66 and E100 - irrigation with treated effluent from slaughterhouse and addition of 0, 33, 66 and 100% of nitrogen mineral fertilization, respectively) and four replications on grassland (*Cynodon dactylon* (L.) Pers.). Several images (between one hundred and two hundred) with red, green, blue (RGB) color model were captured using a quadcopter flying at 20 meter altitude and obtaining spatial resolution of 1 centimeter on a surface of approximately 0.5 ha. The images were orthorectified together with nine ground control points done by differential global positioning system (GPS), both processed in the Agisoft PhotoScan software. Fifteen photogrammetric projects were done over time with 30-day revisit, the root mean squared error (RMSE) was used as accuracy measurement, and reached values lower than 5 centimeters for x, y and z axis. The orthoimage obtained with unmanned aerial vehicle (UAV) photogrammetry was changed from RGB to hue, saturation, value (HSV) color model, and the hue color space was chosen due to independence of illumination, beyond it has a good description of exposure of soil and vegetation, but it is dependent of light source temperature, so difficult to establish a static threshold, so we selected an unsupervised classification method, K-Means, to classify the unknown patterns along the area. Polygons were drawn delimiting the area represented by each portion and a supervised classification method based on entropy was used, the decision tree, to explore and find patterns that recognize each treatment. These steps are also displayed in forms of georeferenced thematic maps and were executed in the open source softwares Python, QGIS and Weka. The rules defined on the hue color space reached an accuracy of 100% on the training set, and provided a better understanding about the distribution of soil and vegetation on the parcels. This methodology shows a great potential for analysis of spectral data in precision agriculture.

Keywords: Precision agriculture; UAV-photogrammetry; QGIS; Python; Agricultural reuse, Brazil.



INTRODUCTION

The integration between the computational intelligence and geographic information system reaches a degree of cybernetic cohesion in information flow worthy of third revolution in the area of computing and geographic quantification (Openshaw, 1992). The alliance of these areas has been successfully used recently to identify fire susceptibility in forests (Bui et al., 2017), locate suitable areas for water catchment in rivers (Al-Abadi et al., 2017), suggest favorable areas to rice cultivation (Maddahi et al., 2017), to map the risk of erosion in soils (Ai et al., 2013).

Emergent option in the area of remote sensing for the management of farms, are the remotely piloted aircraft with vertical take-off and landing, that counts on technological advances in the control and planning of autonomous flights (Duan et al., 2017). The advantage of the information obtained by this aerial platform lies in the readiness of the image in raster data structure, where the pixels are the smallest informative elements and together of their neighbors form the grid matrix, with more than one attribute analyzed from the grid matrix with tessellated structure. This form of data organization facilitates the process of automation and implementation of computational algorithms (Burrough et al., 2015). In the geographical information system, the improvement in the accuracy of the latitude, longitude and height attributes is achieved with the use of modernized GPS that have the codes of the spectral signals L5 (1176.45 MHz), L2C (1227.60MHz) and L1C (1575.42MHz), broadly used in civil applications ([Grewal et al., 2013](#)).

Light is considered an electromagnetic radiation, produced by electrically charged particles, described in terms of wavelengths (Foley and Matlin, 2010), and comprises the visible region (400 to 700 nanometers) in electromagnetic spectrum. The RGB color space is extensively used by many schools around the world for machine vision systems, although its components are strongly correlated with lighting conditions, and therefore sensitive to these changes, especially in outdoor fields where conditions vary rapidly (Meng et al., 2015). Finally, the relationships between bands are unsuccessful attempts to eliminate the adverse effect of lighting (Liu and Moore, 1990).

An "intuitive" development of color spaces, designed in the way human perception is the HSV (Hue, Saturation, Value). In the transformation of the RGB-HSV color spaces, the data leave the Maxwell triangle and pass to the Cartesian coordinates (Meng et al., 2015). In this new arrangement there is the decoupling of luminance (V) and chromaticity (H + S). Hue provides the numerical description of the spectral range or dominant wavelength in a primary color mixture, so the problem of light dependence is avoided (Liu and Moore, 1990). However, changes in the temperature of the light source imply variations in the perceived hue of objects, so in open fields, it is little adherent to fix a threshold for segmentation or extraction of information in images (Ruiz-Ruiz et al., 2009).

The impasse of variable illumination condition for image acquisition in outdoor fields, is solved by using an automatic grouping method for machine learning, the K-means. This is a compact, powerful, unsupervised clustering algorithm for partitioning data sets into separate, predetermined groups. In histograms characterized by flat spaces with one dimension, the euclidean distance (sum of the quadratic errors), is the score function that must be minimized, the algorithm becomes a Hill-Climbing method, where at each iteration the solution is



improved and the sum of squared errors converge to a local minimum (Zaki and Meira, 2014). In practice the user predetermines the number of groups that the samples will be partitioned, the algorithm is executed multiple times and the best solution is chosen, assuming that it is a global minimum. In precision agriculture the use of k-means on the channel hue, with four and two clusters, results in the separation between soil and vegetation (Ruiz-Ruiz et al., 2009).

One need for precision agriculture is to identify heterogeneous areas to assert the concept of applications at variable rates. Another method of learning machine specialized in this topic are the decision trees. These are constructed recursively from top to bottom, using divide and conquer algorithm, consisting of internal nodes representing the decisions corresponding to the division points, and the leaves representing the partitions in the data spaces in which the majority classes are designated. A tree can be read as a set of decision rules, the set of rules can be interpreted as a set of alternatives or disjunctions, and cover the whole space, therefore can be transformed into a rules induction system (Zaki and Meira, 2014).

2. OBJECTIVES

Achieve cybernetic cohesion information flow by integration of unmanned aerial vehicle photogrammetry, computer vision techniques, machine learning algorithms, precision agriculture differential global positioning system, that are able to extract nuances of a crop in an area of agricultural reuse.

To integrate the open source softwares Quantum GIS, Python and Weka.

3. MATERIAL AND METHODS

3.1 Cybernetic Coesion Information Flow

In order to know the cybernetic coesion information flow from a cultivated field with an experimental crop about 200 images were used acquired via a digital format red, green, blue (RGB) camera coupled to an aerial platform. The exact location of each attribute was obtained with the use of control points, positioned with georeferencing of precision.

The images and control points were orthorectified by Agisoft PhotoScan Professional software. The main products were the RGB raster map and the terrain digital elevation model. With this methodology we explored the first product, the following steps were directed to compact, reduce and extract important information about the object of study.

A world-wide-used data analysis platform is the open-source software Python 2.7, in this release the OpenCV, Matplotlib and Numpy libraries are well implemented and are responsible for the computational vision, figure plots and scientific computing packages.

In the QGIS software the parcels were manually delimited in the raster map under visual examination of the RGB color channels. Then the raster map was led to the Python software where undergone a non-linear transformation from the RGB color space to the HSV (hue, saturation, value) color space. The hue channel was chosen because has information capable of discriminate soil and vegetation. The histogram of this channel was calculated and in order to reduce the information, the K-means algorithm with 6 clusters was applied. The hue channel was taken back to QGIS software where was responsible to quantify the pixels in each cluster.



The information was exported in .csv format and ready to go to the Weka software, another open-source software, which has many algorithms for data mining. In WEKA 3.8 the decision tree was performed and the reports on classifier evaluation, confusion matrix and rules were automatically issued (Figure 1).

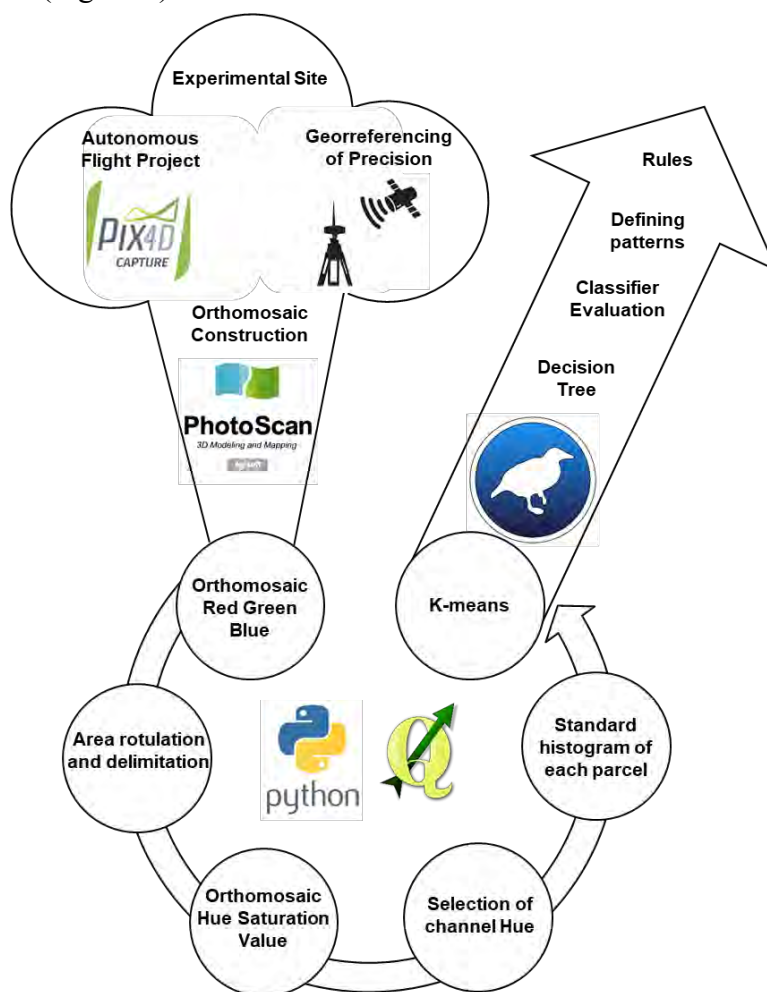


Figure 1 - Cybernetic Cohesion Information Flow. Source: own author.

3.2 Experimental Site

The scientific experiment was located at the College of Animal Science and Food Engineering, University of São Paulo, Pirassununga/SP, Southeast Brazil. The experimental design was in random blocks, with four replications and five treatments as follows: (i) W100 - water irrigation with 100% of nitrogen mineral fertilization; E0, E33, E66 and E100 - irrigation with treated effluent from slaughterhouse and addition of 0, 33; 66 and 100% nitrogen mineral fertilization, respectively. Being the nitrogen fertilization (NF) 300 kg ha⁻¹ year⁻¹ of nitrogen, in the form of urea. The crop cultivated is coastcross-grassland (*Cynodon dactylon*(L.)Pers.) planted in march 2012, the reactor UASB (upflow anaerobic sludge blanket) started the effluent treatment of



wastewater slaughterhouse in April 2017, the sprinkler irrigation system was installed in October 2016 with irrigation interval of two days and the crop cuts occurred when reaching the height of 0.25 m.

3.3 Autonomous Flight Project

Phantom 4's remotely piloted aircraft from Chinese company DJI has four rotors responsible for vertical takeoff and landing. Digital camera in RGB format with 12.4 megapixels resolution (3000 x 4000), 20 mm focal length and 94 ° viewing angle. It already has a gimbal accessory, which compensates for unwanted movements in the z, x, y (yaw, roll, pitch) axes and adjustable range from 0 to 90 ° in the latter. Payload of 1380 grams, including the battery with real duration of approximately 20 minutes. The flight paths were carried out autonomously, doubly repeated and preprogrammed in the software Pixel4DCapture. Ideally each flight path occurred at 20 meters high, with 96 images collected in the time of 11 minutes, frontal and lateral overlaps of 75 and 76%, pixel of size 0.88 centimeters, camera positioned at 90° in relation to the direction of displacement, balance of black and white automatic and with the option of acquiring images when stopping the aircraft on the waypoints.

Table 1 - Aspects of project during the autonomous flight.

Aerial evaluations	Dates (day/month/year)	Number of images	Spatial resolution (cm/pixel)	Fly height (m)	Time (hours:min) (start - end)
Time 8	02/02/2018	156	0.92	24.6	11:47 – 12:17

Table 2 – Accuracy on geographical positions evaluated by root mean squared error (RMSE).

Aerial Evaluations	RMSExy (cm)	RMSEz (cm)	RMSEtotal (cm)	RMSEpixel
Time 8	9.26	15.19	17.79	3.036

3.4 Orthomosaic Construction

The Universal Transverse Mercator (UTM) coordinate system (Zone 23S, WGS84, EPSG:32723) West-East and South-North of the analyzed area were (246800, 246916) and (7570585, 7570700), respectively. The orthomosaic of dimensions 116 x 115 m (13340 m²) and spatial resolution set to 1 cm per pixel was produced by overlap of RGB images, therefore the orthomosaic contained 116000 x 115000 pixels, the mosaicing was executed in the comercial low-cost software Agisoft PhotoScan Professional photogrammetric mapping, for this procedure a high performance machine was necessary, we used an Intel Core i7-6700HQ CPU, with a 2.60 GHz processor, 32GB of RAM memory and video card NVIDIA GeForce GTX 1070.

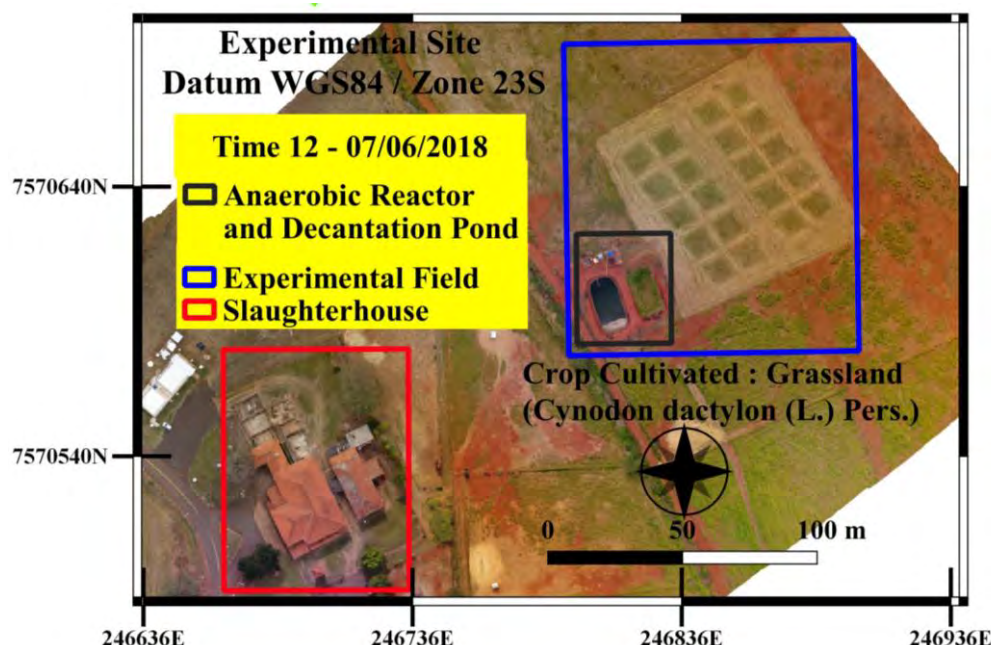


Figure 2 - Aerial overview of the experimental site located in College of Animal Science and Food Engineering, University of São Paulo.

4. RESULTS AND DISCUSSION

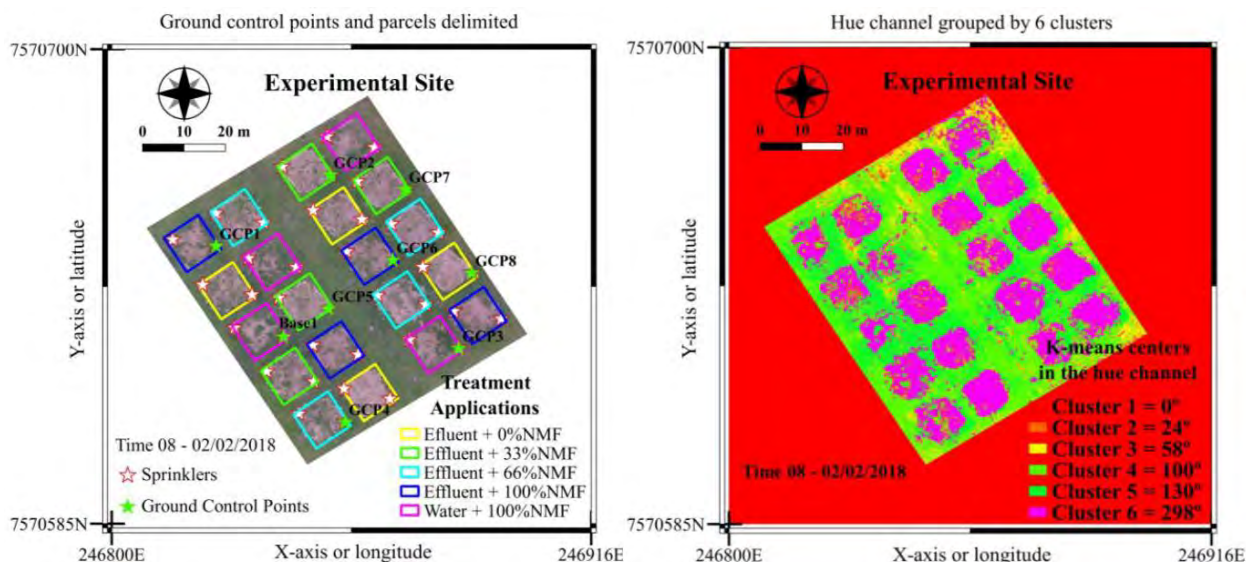


Figure 3 – a) Georeferenced thematic map of the eighth aerial evaluation in RGB channels, with the delimited parcels, sprinklers of irrigation system and ground control points. b) Georeferenced thematic map of the eighth aerial evaluation about the hue channel grouped by 6 k-means. The first step was to match several images in the software AgisoftPhotoScan Professional to construct the RGB orthomosaic and then led it to QGIS software, where there was the



construction of the georeferenced thematic map displaying the RGB channel and the characteristics of the experimental field (figure 3-a). Then in Python software occurred the non-linear transformation from RGB to HSV color space and the hue channel was selected. Still in Python software the k-means algorithm with 6 clusters was applied and the histogram was calculated (figure 4). The hue channel image grouped by k-means with 6 clusters algorithm was led to QGIS software through the “georeferencer” tool, and in this platform there was the construction of another georeferenced thematic map (figure 3-b). The hue channel is very useful for agriculture in outdoor fields because avoid the effect of illumination and contains the information about the soil and vegetation, so it’s possible to reach their separation utilizing machine learning techniques (Figure 5-a and 5-b).

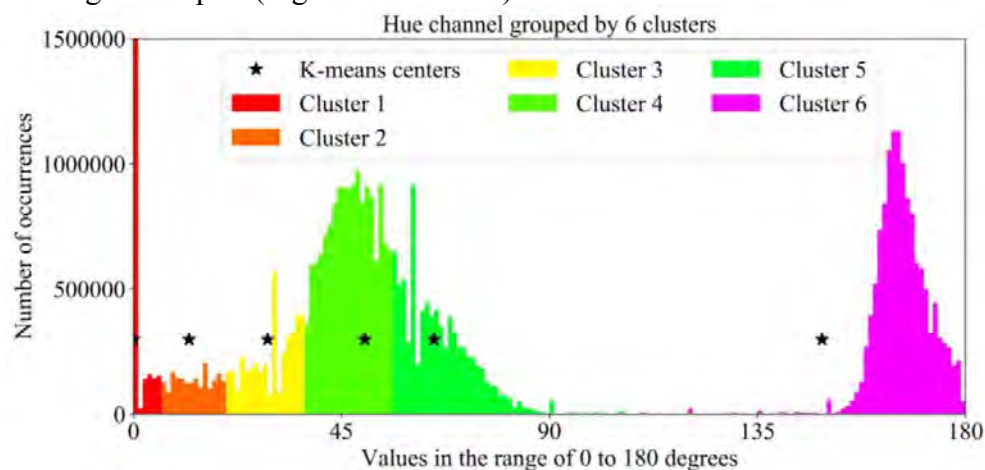


Figure 4 – Histogram of the hue channel grouped by 6 clusters k-means, showing the centers of each cluster and the classified groups.

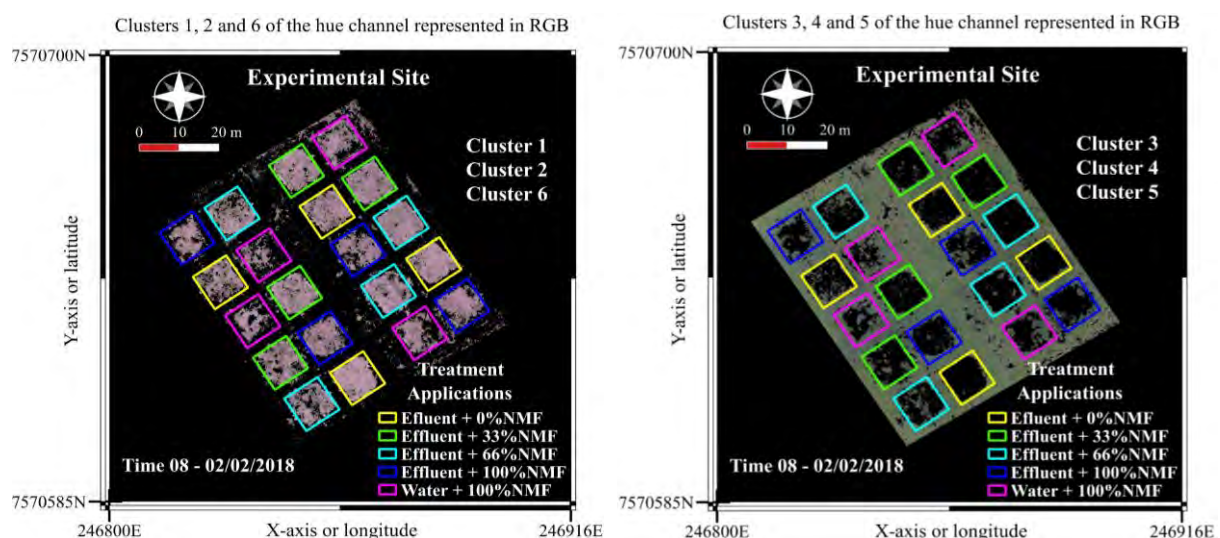


Figure 5 – a) Georeferenced thematic map illustrate the formation of soil group by the clusters 1, 2 and 6. b) Georeferenced thematic map showing the vegetation group by the clusters 3, 4 and 5.



By human visual comparison and inspired by set theory, we assigned that Cluster 1 \subset Soil, Cluster 2 \subset Soil, Cluster 6 \subset Soil, Cluster 3 \subset Vegetation, Cluster 4 \subset Vegetation, Cluster 5 \subset Vegetation. The amount of clustered pixels in each parcel was quantified in QGIS software utilizing the “zonal histogram” algorithm, available in the toolbox of the raster analysis, and generate a table that was exported in .csv format and directly led to the Weka software. Then the decision tree J48 algorithm was applied and two decision tree were generated the first was setted with a minimum of 2 instances per leaf and the second with 1 instance per leaf. The reports about the performance of the algorithm are stated in the Table 3 and Figure 6.

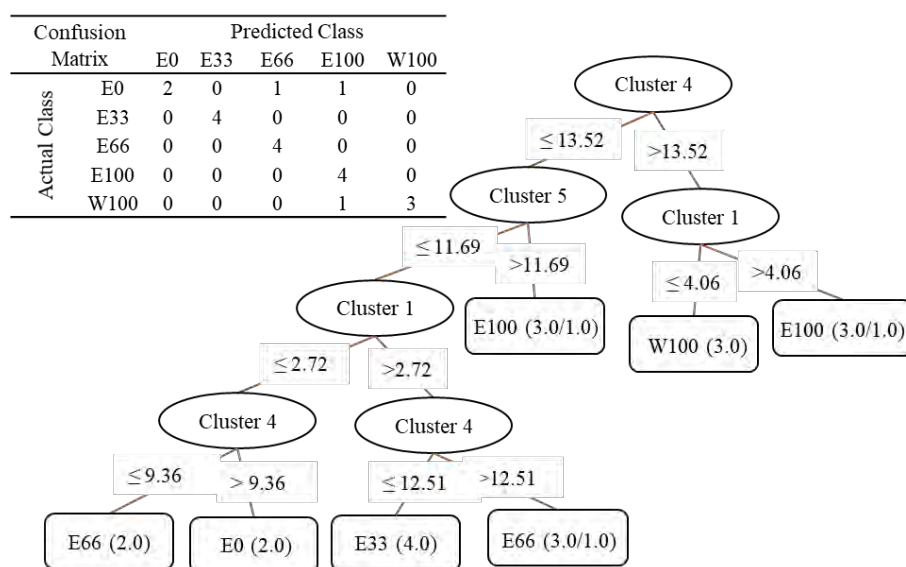


Figure 6 – Decision tree that explored the paths that recognized the wastewater treatments in the eighth aerial evaluation and confusion matrix evaluating the classifier. W100 - water irrigation with 100% of nitrogen mineral fertilization; E0, E33, E66 and E100 - irrigation with treated effluent from slaughterhouse and addition of 0, 33; 66 and 100% nitrogen mineral fertilization.

By decision tree analyse, we examined the rule that led to the water treatment (W100), so if Cluster 4 > 13.52 and Cluster 1 ≤ 4.06 then W100. Previously was induced the knowledge that cluster 4 is a subset of vegetation and cluster 1 is a subset of soil. So by an induction process we infer that in this evaluation time there was more vegetation and less soil in these parcels of the water treatment (W100) than in another treatments.

Table 3 - Decision tree outputs about the size and complexity of the system.

Aerial Evaluation	Color Space	First Decision Tree Accuracy	Leaves	Nodes	Second Decision Tree Accuracy	Leaves	Nodes
Time 08	Hue	85%	7	13	100%	10	19

5. CONCLUSION

The cybernetic cohesion information flow was achieved with success because no discontinuance in the information extraction process in an agricultural crop was found.



CIGR 2018

XIX. World Congress of CIGR



We have succeeded in integrating the platforms Quantum GIS, Python and Weka. Their power to analyze the RGB spectral information was evident.

6. ACKNOWLEDGMENTS

This study was financed in part by the Coordenação de Aperfeiçoamento de Pessoal de Nível Superior - Brasil (CAPES) - Finance Code 001

7. REFERENCES

- AL-ABADI, A. M. et al. A GIS-Based Integrated Fuzzy Logic and Analytic Hierarchy Process Model for Assessing Water-Harvesting Zones in Northeastern Maysan Governorate, Iraq. *Arabian Journal for Science and Engineering*, v. 42, n. 6, p. 2487-2499, Jun 2017.
- BUI, D. T. et al. A hybrid artificial intelligence approach using GIS-based neural-fuzzy inference system and particle swarm optimization for forest fire susceptibility modeling at a tropical area.
- BURROUGH P. A., MCDONNELL R. A., LLOYD C. D. *Principles of Geographical Information Systems*. (3rd edition), 352 p. Oxford University Press, 2015.
- DUAN, T. et al. Dynamic monitoring of NDVI in wheat agronomy and breeding trials using an unmanned aerial vehicle. *Field Crops Research*, v. 210, p. 71-80, Aug 2017
- FOLEY, H. J., MATLIN, M. W. *Sensation and perception* (5th ed.). Boston: Allyn & Bacon, 2010
- GREWAL, M.; ANDREWS, A.P.; BARTONE, C.G. *Global navigation satellite systems, inertial navigation, and integration* (3rd edition), John Wiley & Sons, Inc., Hoboken, New Jersey, 2013
- LIU, J. G.; MOORE, J. M. Hue image RGB color composition - a simple technique to suppress shadow and enhance spectral signature. *International Journal of Remote Sensing*, v. 11, n. 8, p. 1521-1530, Aug 1990.
- MADDAHI, Z. et al. Land Suitability Analysis for Rice Cultivation Using a GIS-based Fuzzy Multi-criteria Decision Making Approach: Central Part of Amol District, Iran. *Soil and Water Research*, v. 12, n. 1, p. 29-38, 2017.
- MENG, Q. K. et al. Development of agricultural implement system based on machine vision and fuzzy control. *Computers and Electronics in Agriculture*, v. 112, p. 128-138, 2015.
- OPENSHAW, S. Some suggestions concerning the development of artificial-intelligence tools for spatial modeling and analysis in GIS. *Annals of Regional Science*, v. 26, n. 1, p. 35-51, Apr 1992
- Agricultural and Forest Meteorology*, v. 233, p. 32-44, Feb 2017.
- RUIZ-RUIZ, G.; GOMEZ-GIL, J.; NAVAS-GRACIA, L. M. Testing different color spaces based on hue for the environmentally adaptive segmentation algorithm (EASA). *Computers and Electronics in Agriculture*, v. 68, n. 1, p. 88-96, Aug 2009.
- ZAKI M.J.; MEIRA W. Jr. *Data mining and analysis fundamental concepts and algorithms*. New York:Cambridge University Press; 2014.



CIGR 2018

XIX. World Congress of CIGR



Optimization of Drying Process of Coconut Meat (*Cocos Nucifera* L.) with Aid of Image Analysis

C. Mizera^{1,*}, D. Herak², P. Hrabě³, M. Kavalek⁴

^{1,2}Czech University of Life Sciences Prague, Faculty of Engineering, Department of Mechanical Engineering, Kamýcká 129, 165 21 Praha 6 Suchbát, Czech Republic

³Czech University of Life Sciences Prague, Faculty of Engineering, Department of Material Science and Manufacturing Technology, Kamýcká 129, 165 21 Praha 6 Suchbát, Czech Republic

⁴Farmet a.s., Division Oil & Feed Tech, Jirinkova 276, 552 03 Ceska Skalice, Czech Republic
mizera@tf.czu.cz

ABSTRACT

The aim of this study was focused on the optimization of drying process of Coconut (*Cocos nucifera*) meat (copra) with regard to energy consumption and final product quality. Copra, originally from Indonesia, were used in this experiment. With aid of image analysis using HD camera the quality of final dried product was described and compared with quality standards. Acquired pictures were analysed by the digital image analyses using ImageJ software that utilises java based image processing. The default threshold method based on IsoData algorithm was used in this experiment. Copra in three variants of particle size (2.99 ± 0.96 , 9.33 ± 1.54 mm and 16.89 ± 2.96 mm) were dried at different air temperatures (40, 60, 80, 100, 120 °C). Experimental drying curves at different temperatures, drying rate and particle size were determined and energy consumption were measured. The measured values of weight loss for different drying temperatures were analysed with computer program Mathcad 14, uses Levenberg-Marquardt algorithm for data fitting. The determined models of drying curves were statistically verified by using ANOVA. Based on the determined data optimal conditions of copra drying process were determined. It was found, that the drying temperature can be within the range 40 – 60 °C. For higher temperatures, the colour of the copra is changing, which is undesirable for food use. The coefficients of determined model were statistically significant with suggest that the determined model could be used as a background for further research focused on copra utilization with respect on final product quality.

Keywords: Farmer 20, oil recovery efficiency, pressing energy, Czech Republic

INTRODUCTION

Coconut is a fruit of coconut tree (*Cocos nucifera*, L.), a hollow, unproductive fruit of a perennial coconut. It is considered a tree of life because the tree and the fruits themselves have many uses. Coconuts are widely cultivated in the seaside regions of Asia (Philippines, India, Indonesia, Malaysia, etc.). Tree is used as building material; fibers are used in composites, while



coconut is the source of vegetable oil and other food products. It is used for consumption in various types of products - coconut milk, coconut flour, coconut juice and dried coconut. Gently chopped and dried coconut with a moisture content of about 3 % d.b. (Niamnuy and Devahastin 2005), is used to decorate ice creams, cakes and donuts and as the main flavour in chocolate bars. Food processing is an integral part of the removal of moisture from solids, including coconuts. Drying occurs at least once during preparation for the final product. Moisture reduction can be achieved by flowing air, vacuum and dryer. The dried coconut is dried to a final moisture content of about 3 %. Many studies have dealt with kinetics of thin layer drying for the drying of fruit and vegetables and their by-products from industrial processes - mint leaves (Doymaz, 2006), olive cake (Akgun and Doymaz, 2005), strawberries (Doymaz, 2008), slices of organic apple (Sacilik and Elicin, 2006), green beans (Doymaz, 2005), corn (Doymaz and Pala, 2003), carrot (Doymaz, 2004), young coconut (Madamba, 2003) and extraction of olive oil (Celma et al., 2007). As the key factor affecting the kinetics of drying fruits and vegetables, the drying temperature closely participated in the drying constants of the drying models. As a result, several studies have found different drying rate constants, each for a specific temperature (Doymaz, 2005, Doymaz, 2008, Doymaz and Pala, 2003 Doymaz, 2004), while others attempted to combine drying rate constants with drying temperature (Sacilik and Elicin, 2006, Madamba, 2003, Celma et al., 2007). Hot air is used in many industrial drying applications due to several advantages including rapid and even drying (Minguez-Mosquera et al., 1994, Ayensu 1997). Some the coir pith producers in Sri Lanka also use hot air to dry coir pith by the flash drying. However, it is difficult to control the process and also to obtain the required quality parameters. This may be due in particular to the lack of reliable information on the appropriate drying temperature and drying kinetics of coconut meat. By drying of coconut meat is also important change in colour. Colour change causes deterioration in quality and lower economic profit. Mathematical modelling and simulation of the drying curve allow for better control over drying and thus obtaining a high quality product (Meisami-asl et al., 2009). The principle of modelling is based on a set of mathematical equations that can describe drying curve (Garavand et al., 2011).

The aim of this study is to find the most suitable drying temperature, with respect to the change of colour, and the mathematical description of the drying curves of coconut meat.

MATERIALS AND METHODS

Sample

Commercially available old coconuts, the fruits of the coconut tree (*Cocos nucifera*), were used for this experiment. All coconuts were initially centre-drilled to allow removal of coconut water. The coconut nuts were split into halves to remove the coconut meat. Fresh coconut meat was grated to a size of 1-2 mm. The moisture content $M_c = 43.9 \pm 1.9$ % (w.b.) of fresh coconut meat was determined using the standard oven method, ASAE method (ASAE S410.1 DEC97, ASAE, 1998). The procedure was that the initial mass of the sample before and after oven drying was weighed. For measuring of mass of each sample m_s (g) an electronic balance (Kern 440–35, Kern & Sohn GmbH, Balingen, Germany) was used. The test was repeated three times and result averaged. Freshly grated coconut meat was used for drying procedure to determine the colour change.



Drying experiments

Drying of samples were carried out in the drying moisture balance (Radwag, MA 50.R, Poland). Moisture balance is equipped with IR emitter heating module 400 W and was set to a standard drying profile (Fig. 1). To explore the effect of drying temperature on drying rate of meat, drying experiments were carried out at temperatures of 40, 60, 70, 80, 100 and 120 ± 1 °C. Fresh grated coconut meat of weight $m_0 = 10 \pm 1$ g was inserted into the moisture balance and gradually dried. The weight loss changes per minute were recorded in the memory.

Mathematical modelling of drying curves

The measured values of weight loss for different drying temperatures were analysed with computer program Mathcad 14 (MathCAD 14, PTC Software, Needham, MA, USA), (Pritchard, 1998) uses Levenberg-Marquardt algorithm for data fitting (Marquardt 1963). The determined models of drying curves were statistically verified by using ANOVA.

Image analysis

After drying coconut samples were visually recorded using a Canon HD camera (EOS M10, Canon, Tokyo, Japan). Acquired pictures were analysed by the digital image analyses using ImageJ software that utilises java based image processing. The default threshold method based on IsoData algorithm was used in this experiment. Using Image J software colour RGB histogram were determined for each picture. The total pixel Count was calculated and displayed, as well as the Mean, standard deviation (StdDev), minimum (Min), maximum (Max) and modal (Mode) grey value. The peaks and their position were compared with undried processed sample.

RESULTS AND DISCUSSION

The initial moisture content of freshly grated coconut meat was observed to be $M_c = 43.9 \pm 1.9$ % (w.b.). Fig. 2 shows the moisture ratio as a function of drying time of coconut meat at the air temperature range of 40 – 120 °C. Drying continued until the final moisture content was ca. 3 % (w.b.). Drying time was estimated at 18, 24, 30, 39, 66 and 174 min at 120, 100, 80, 70, 60 and 40 °C, respectively. The results indicate that increasing drying air temperature can extensively enhance drying process.



CIGR 2018

XIX. World Congress of CIGR

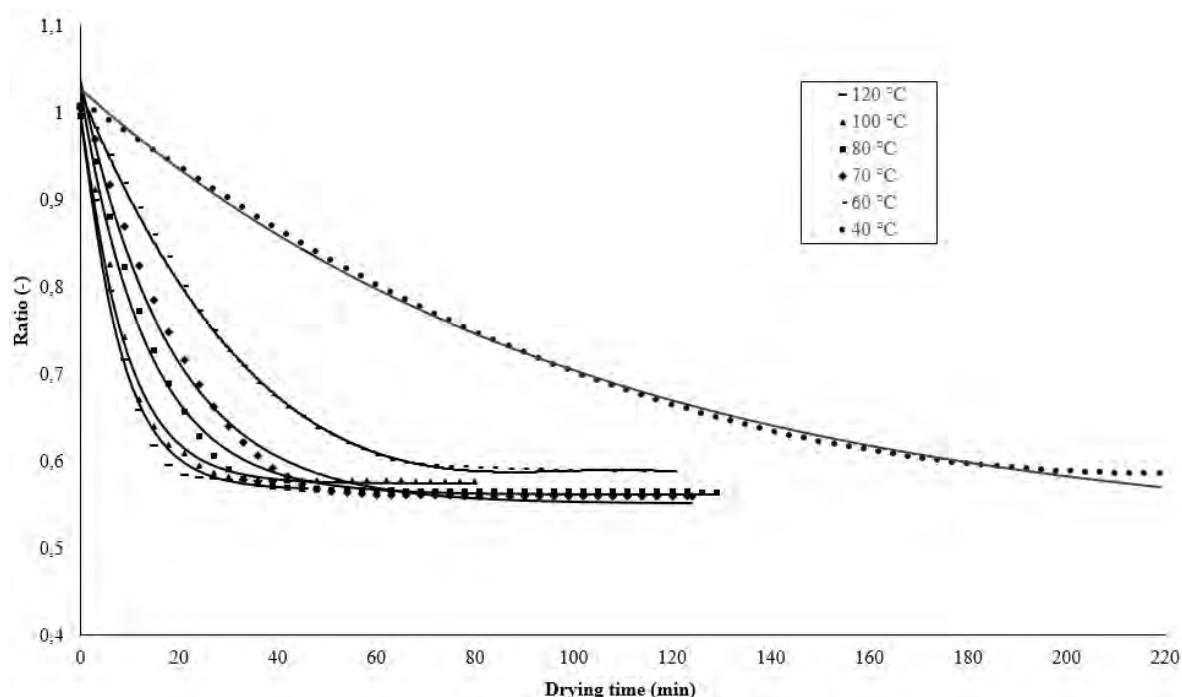


Figure 1. Measured values of moisture ratio and fitted models of drying curves in the air temperature range of 40 – 120 °C

The drying curves of the coconut meat at 6 drying temperatures are presented in Fig. 1. Measured and calculated values for different drying curves were fitted by exponential curve using Marguardt Levenberg algorithm and it is described by Eq. 1.

$$\delta(d, t) = d_0 + d_1(e^{d_2 t}) + d_3(e^{d_4 t}) \quad (1)$$

where: d_0, d_1, d_2, d_3, d_4 – coefficients of exponential curve, -; t – drying time, -.

The values of coefficients d_0, d_1, d_2, d_3, d_4 from Eq. 1 are presented in Table 1.

Table 1. Estimated values of coefficients for Eq. 1

Temperature of drying °C	d_0 (-)	d_1 (-)	d_2 (min ⁻¹)	d_3 (-)	d_4 (min ⁻¹)
40	0.509	0.176	-0.009	0.343	-0.009
60	0.585	0.197	-0.071	0.197	-0.071
70	0.551	0.202	-0.055	0.287	-0.055
80	0.562	0.210	-0.074	0.256	-0.074
100	0.574	0.323	-0.114	0.124	-0.114



CIGR 2018

XIX. World Congress of CIGR



120

0.567

0.228

-0.128

0.228

-0.128

From statistical analysis ANOVA (Table 2) follows, that measured amounts of drying curves at different temperatures and results from the general exponential model (Eq. 1) were statistically significant at significance level 0.05, that is, the values of F_{crit} (critical value comparing a pair of models) were higher than the F_{rat} values (value of the F – test) for all the measured Ensete fibres and values of P_{value} (significance level at which it can be rejected the hypothesis of equality of models) (Table 2) were higher than 0.05 which is also confirmed by very high coefficients of determination R^2 .

Table 2. Statistical analysis of general models

Drying temperature	F_{rat}	F_{crit}	P_{value}	R^2
(°C)	(-)	(-)	(-)	(-)
40	$1.012 \cdot 10^{-13}$	3.906	1	0.998
60	$1.274 \cdot 10^{-13}$	3.960	1	0.999
70	$4.838 \cdot 10^{-13}$	3.955	1	0.991
80	$1.021 \cdot 10^{-13}$	3.952	1	0.989
100	$2.918 \cdot 10^{-13}$	4.027	1	0.992
120	$1.048 \cdot 10^{-13}$	4.149	1	0.991

Modeling of drying curves of coconut meat was studied by the authors Fernando (2016) and Meisami-asl (2009). Both studies approach to modeling curves in different ways. After the drying was complete, the coconut samples were analyzed by imaging. Coconut samples after drying for different drying air temperatures are shown in Figure 2. From Figure 2 it is clear that the drying temperature affects the color change of the coconut meat.

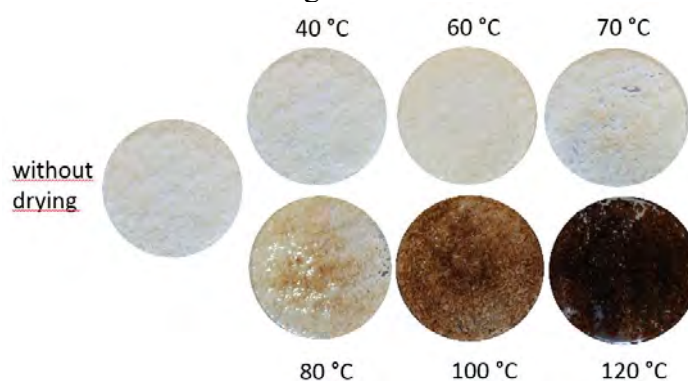


Figure 2. Samples of coconut meat after drying in the air temperature range of 40 – 120 °C

The individual images were converted to a grey scale. The thresholding method for grey-level histogram (Fig. 3) was used. Figure 3 shows the frequencies for different drying temperatures. It can be seen from the figure 3 that a significant change in the distribution curve occurs at a drying temperature 80 °C.

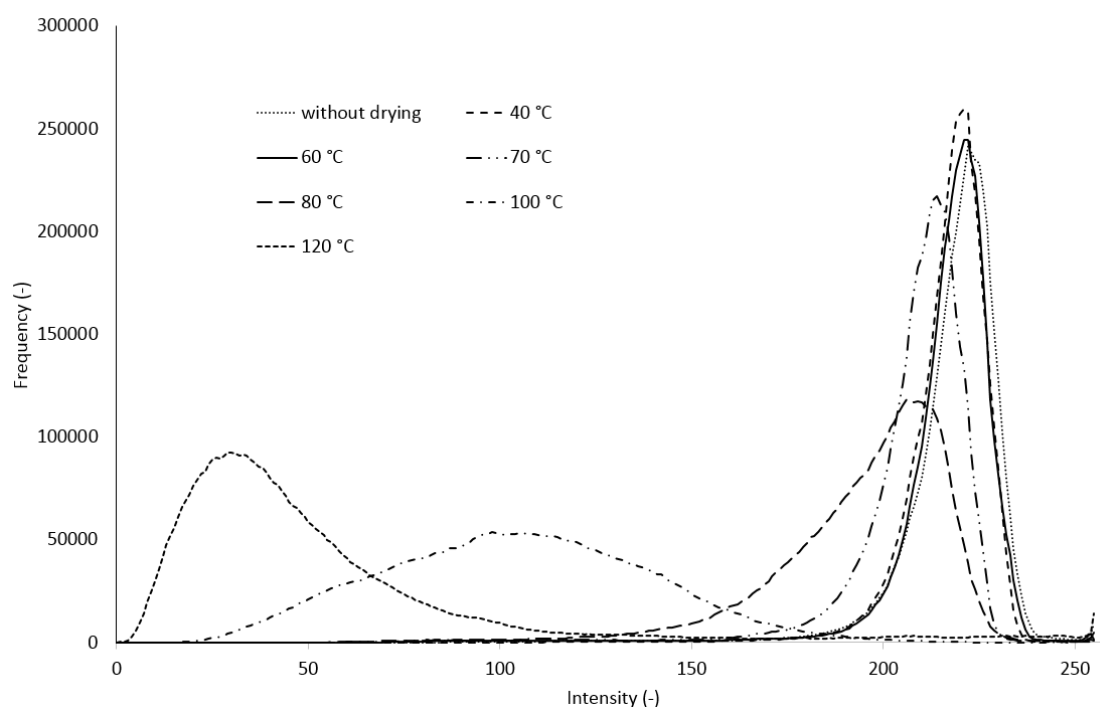


Figure 3. Samples of coconut meat after drying in the air temperature range of 40 – 120 °C

Authors Guarte (1996) have found that coconut colour changes occur at temperatures above 80 °C. The browning of copra at higher temperatures is due to the Maillard reaction. Even in the light brown colour there is no loss of quality, so it is possible to dry the copra up to 80 °C (Roberto, 1996).

4. CONCLUSION

This study was focussed on the drying process of Coconut meat (*Cocos nucifera*). Dependency between weight loss and drying time was observed and transformed into general mathematical model describing hot air drying of Coconut meat. Mathematical model in this study could be used for the development of further models which will describe drying process of Coconut meat and it can help to design of technology for drying of Coconut meat. Drying temperature of 80 °C is found to be optimum to produce high quality copra at the least drying time.

ACKNOWLEDGEMENT. This paper has been supported by Internal Grant Agency of Faculty of Engineering – Czech University of Life Sciences Prague – IGA 2018: 31130/1312/3110.



5. REFERENCES

- Akgun, N. A. and Doymaz, I. 2005. Modelling of olive cake thin-layer drying process. *Journal Food Engineering* 68(4): 455-461.
- Ayensu, A. 1997. Dehydration of food crops using solar dryer with convective heat flow. *Solar Energy* 59(4-6): 121-126.
- ASAE S410.1 DEC97. 1998. Moisture measurement of peanut. In: ASAE standards, 45th edition. 560-561.
- Celma, A. R., Rojas, S., Lopez, F., Montero, I. and Miranda, T. 2007. Thin-layer drying behaviour of sludge of olive oil extraction. *Journal Food Engineering* 80(4): 1261-1271.
- Crowe, T. W., Johnson, L. A. and Wang, T. 2001. Characterization of extruded-expelled soybean flours. *Journal of the American Oil Chemists' Society* 78(8): 775-779.
- Doymaz, I. and Pala, M. 2003. The thin-layer drying characteristics of corn. *Journal Food Engineering* 60(2): 125-130.
- Doymaz, I. 2004. Convective air drying characteristics of thin layer carrot. *Journal Food Engineering* 61(3): 359-364.
- Doymaz, I. 2005. Drying behavior of green beans. *Journal Food Engineering* 69(2): 161-165.
- Doymaz, I. 2006. Thin-layer drying behavior of mint leaves. *Journal Food Engineering* 74(3): 370-375.
- Doymaz, I. 2008. Convective drying kinetics of strawberry. *Chemical Engineering and Processing* 47(5): 914-919.
- Evon, P., Vandenbossche, V., Pontalier, P. Y. and Rigal, L. 2009. Aqueous extraction of residual oil from sunflower press cake using a twin-screw extruder: Feasibility study. *Industrial Crops and Products* 29(2-3): 455-465.
- Evon, P., Amalia Kartikac, I., Cerny, M. and Rigala, L. 2013. Extraction of oil from jatropha seeds using a twin-screw extruder: Feasibility study. *Industrial Crops and Products* 47: 33-42.
- Fernando, J. A. K. M. and Amarasinghe, A. D. U. S. 2016 Drying kinetics and mathematical modeling of hot air drying of coconut coir pith. *SpringerPlus* 5:807.
- Garavand, A. T., Shahin, R. and Keyhani, A. 2011. Mathematical modeling of thin layer drying kinetics of tomato influence of air dryer conditions. *International Transaction Journal of Engineering, Management, & Applied Sciences & Technologies* 2(2): 147-160.
- Guarte, R. C. G., Mühlbauer, W. and Kellert, M. C. 1996 Drying characteristics of copra and quality of copra and coconut oil. *Postharvest Biology and Technology* 9: 361-372.
- Herak, D., Sleger, V., Mizera, C. and Sedlacek, A. 2015. Mechanical behaviour of bulk rapeseeds under quasi dynamic compression loading. *Engineering for Rural Development* 14: 28-32.



- Isobe, S., Zuber, F., Uemura, K. and Noguchi, A. 1992. A new twin-screw press design for oil extraction of dehulled sunflower seeds. *Journal of the American Oil Chemists' Society* 69: 884-889.
- Kabutey, A., Herak, D., Choteborsky, R., Dajbych, O., Sigalingging, R. and Akangbe, O. L. 2017. Compression behaviour of bulk rapeseed: Effects of heat treatment, force, and speed. *International Journal of Food Properties* 20: 654-662.
- Karaj, S. and Müller, J. 2011. Optimizing mechanical oil extraction of *Jatropha curcas* L. seeds with respect to press capacity, oil recovery and energy efficiency. *Industrial Crops and Products* 34(1): 101-1016.
- Madamba, P. S. 2003. Thin layer drying models for osmotically pre-dried young coconut. *Drying Technology* 21(9): 1759-1780.
- Madhiyanon, T., Phila, A. and Soponronnarit, S. 2009. Models of fluidized bed drying for thin-layer chopped coconut. *Applied Thermal Engineering* 29(14-15): 2849-2854.
- Marquardt, D. W. 1963. An Algorithm for Least-Squares Estimation of Nonlinear Parameters. *Journal of the Society for Industrial and Applied Mathematics* 11(2): 431-441.
- Meisami-asl E., Rafiee S., Keyhani A. and Tabatabaefar A 2009. Mathematical modeling of moisture content of apple slices (var. Golab) during drying. *Pakistan Journal of Nutrition* 8(6): 804-809.
- Minguez-Mosquera, M. I., Jaren-Galan, M. and Garrido-Fernandez, J. 1994. Influence on industrial drying process on pepper fruits (*Capsicum annum* cv. Bola) for paprika on the carotenoid content. *Journal of Agricultural and Food Chemistry* 42(5): 1190-1193.
- Niamnuy, C. and Devahastin, S. 2005. Drying kinetics and quality of coconut dried in a fluidized bed dryer. *Journal Food Engineering* 66(2): 267-271.
- Pritchard, P. J. 1998. *Mathcad: A tool for engineering problem solving*. McGraw-Hill Science Engineering, New York, 336 pp.
- Sacilik, K. and Elicin, A., K. 2006. The thin layer drying characteristics of organic apple slices. *Journal Food Engineering* 73(3): 281-289.
- Singh, J. and Bargale, P. 1990. Mechanical expression of oil from linseed (*Linum usitatissimum* L). *Journal of Oilseeds Research* 7(1): 106-110.
- Singh, K. K., Wiesenborn, D. P., Tostenson, K. and Kangas, N. 2002. Influence of moisture content and cooking on screw pressing of crambe seed. *Journal of the American Oil Chemists' Society* 79(2): 165-170.
- Uitterhaegen, E., Nguyen, Q. H., Sampaio, K. A., Stevens, C. V., Merah, O., Talou, T., Rigal, L. and Evon, P. 2015. Extraction of Coriander Oil Using Twin-Screw Extrusion: Feasibility Study and Potential Press Cake Applications. *Journal of the American Oil Chemists' Society* 92(8): 1219-1233.



CIGR 2018

XIX. World Congress of CIGR



Uitterhaegen, E. and Evon, P. 2017. Twin-screw extrusion technology for vegetable oil extraction: A review. *Journal of Food Engineering* 212: 190-200.

Zheng, Y., Wiesenborn, D. P., Tostenson, K. and Kangas, N. 2003. Screw pressing of whole and dehulled flaxseed for organic oil. *Journal of the American Oil Chemists' Society* 80(10): 1039-1045.

Zheng, Y., Wiesenborn, D.P., Tostenson, K. and Kangas, N. 2005. Energy analysis in the screw pressing of whole and dehulled flaxseed. *Journal of Food Engineering* 66(2): 193-202.



CIGR 2018

XIX. World Congress of CIGR



A New Approach to Calculation of Parcel Index for Abdurrahmanlar District

Kenan Büyüктаş¹, Ahmet Tezcan^{1*}, Şerife Tülin Akkaya Aslan², Ismail Sarı³

¹ Department of Agricultural Structures and Irrigation, Akdeniz University, 07058, Antalya, Turkey

² Department of Biosystem Engineering, Uludag University, Bursa, Turkey

³ Department of Computer Technology, Pamukkale University, Denizli, Turkey
atezcan@akdeniz.edu.tr

ABSTRACT

One of the most important steps in the land consolidation process the parceling process should be done so that the owners will be satisfied. Therefore, in order to a fair distribution a new place having the same value with the old places should be given to the landowners. For this purpose, the parcel index value is determined for each parcel in the land consolidation projects and the parcels are evaluated on this value. In the present condition, the parcel index is determined by taking 70% of soil index and adding the efficiency score of 10 points and the location score among 0-30 points in the land consolidation projects. In this system which is regulated for narrow purposes and mainly developed for the purpose of land consolidation and distribution, the deficient parts of the parcel index calculations are being discussed and tried to be developed even today. In this study, the effect on the number of parcel by determining of the parcel index as detailed method in land consolidation of Abdurrahmanlar district was determined. For this purpose, 14 different questions were asked to determine the value of parcels in terms of socio-economic, cultural and physical aspects of the each of plots located in Abdurrahmanlar district and other criteria scores were determined as a result of these questions. Then, 50% of the soil score and 50% of the other criteria score were added and the parcel index classified for each parcel was determined. Using the parcel index obtained, the parcel value numbers of each parcel were determined and the results were compared with the parcel value numbers obtained by the present method. Thus, a new method which is calculates detailed and multi-criteria in parcel index calculations which must be fair and precise in redistribution was proposed in the land consolidation studies which is required state support in projects and the large investments.

Keywords Abdurrahmanlar, land consolidation, parcel index, regional criteria.

INTRODUCTION

Land consolidation (LC) for agricultural purposes is an activity or an instrument that is implemented in order to consolidate fragmented agricultural holdings or, in other words, to unite the scattered parcels of the distinct farms. Land consolidation is carried out by means of projects in clearly bordered parts of the rural area. For each project a project management will be appointed. Land consolidation may also include the improvement of the road system and of the water management system, as well as of the landscape and the conditions of nature in such a



project area (Sonnenberg, 2002). It is a useful way of improving land effectiveness, changing landscape patterns, facilitating environmental management, and implementing developmental policies (Bonfanti et al., 1997; Cay et al., 2010; Pasakarnis and Maliene, 2010; Cay and Iscan, 2011; Huang et al., 2011). The procedure of land consolidation is a set of activities of technical, administrative and legal nature, aimed at designing a new layout of plots in the area advantageous from the point of view of agricultural activity. The effects of land consolidation works most often have an economic dimension (Lerman, 2002), but they are seen also in the context of improving the quality of landscape (Gu et al., 2008), protection of the environment (Crecente et al., 2002) and the improvement of the functioning conditions of the local community.

In Turkey, land consolidation works are made by two different regulations today. One is principles set out in the Technical Instruction of Land and Classification Standards and Land Consolidation Technical Instructions prepared by the General Directorate of Agricultural Reform according to Article 17 of Law No. 5403, while another one is agricultural reform in the irrigation areas of Law No. 3083. However, six different regulations have been used from 1961 till today. In studies requiring large investments such as land consolidation, no standard equality has been developed. In this case, it is necessary to develop a standard equation that is compatible with all projects, taking into account the physical, geographical and socio-economic characteristics of the region. Because correcting inaccuracies in land consolidation processes requires large government investments. The most serious errors in land consolidation processes are performed in the land redistribution process because the existing method is superficial.

The most accurate and fair land distribution can be achieved by detailed calculating the parcel value numbers. It is important to determine the parcel value numbers correctly. The parcel index should be calculated in detail in order to calculate the parcel value numbers correctly. Thus, it can be achieved much more fair re-distribution (Tezcan et al., 2018).

Parcel index are calculated with three superficial parameters in Turkey. These are soil index, productivity and location score. These parameters are not enough to determine the real value of a parcel. For this reason, current parcel index equation needs to be revised and should be more detailed.

In this study, to ensure the land distribution which are the most appropriate and fair, it is aimed to compare the parcel value numbers determined by the current method with parcel value numbers determined by the new method which is more detailed.

2. MATERIAL AND METHOD

2.1. Material

Abdurrahmanlar district was chosen as study area from the land consolidation area in Aksu in Antalya province. Study area is located to the 26 km east of Antalya city center (Fig 1). The altitude of district is 11.81 m.



The agricultural area is 6698.10 da while the total area of the district is 11228.67 da. There are 377 parcels in Abdurrahmanlar district and average parcel size is 17.77 da (DSI, 2016). Typical Mediterranean climate is seen in the study area. The summers are warm and dry, the winters are warm and rainy (Tezcan et al., 2018). The most valuable soils of the study area are the soils located in the south part of the area. This can be seen from the soil survey map of the Abdurrahmanlar district (Fig. 2).



Figure 1. Study area

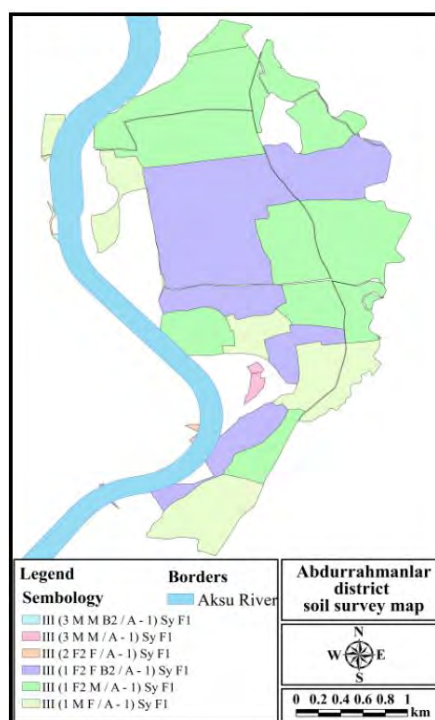


Figure 2. Soil survey map belongs to study area

Cadastral situations, current map, parcel information, land registry records showing landowners, property and parcel information, information on land owners, parcel number, parcel area and share information and parcel index of each parcel in the study area are taken from the General Directorate of State Hydraulic Works (SHW) 13th Regional Directorate.

2.2. Method

The parcel index in land consolidation studies in Turkey was calculated using three parameters according to principles set out in the Technical Instruction of Land and Classification Standards and Land Consolidation Technical Instructions prepared by the General Directorate of Agricultural Reform according to Article 17 of Law No. 5403. These parameters are soil index, productivity and location score (Equation 1). However, these parameters are superficial and not enough to determine the real value of a parcel. Much more parameters should be used to determine the real value of a parcel. For this reason, equation 2 that can perform much more detailed calculations has been developed in this study.



$$\text{Parcel Index} = \text{Soil index} * (\%70) + \text{Productivity (10 p)} + \text{Location score (0-20 p)} \quad \text{Eq. 1}$$

$$\text{Parcel Index} = \text{Soil index} * (\%50) + \text{Land Quality Index} * (\%50) \quad \text{Eq. 2}$$

There are two parameters in equation 2. Soil index (S.I.) is the same parameters as in the equation 1, only its ratio has been changed. Land quality index (L.Q.I.) is the new parameter which is added by us to calculate the parcel index. L.Q.I. contains 14 different questions determined according to geographical, physical and social-economic structure of the study area. These questions were created basically by inspiration of USDA, 2011. Then, they were revised with the preliminary study by asking to farmers in the study area, engineers who are working in the project and academic expert about land consolidation. The questions used in the L.Q.I. are “parcel area”, “share situation”, “lands adjacent to agricultural areas”, “land use status”, “fixed facility (greenhouse, garden, etc.) situation within parcel”, “zoning situation of agricultural area”, “distance to the district center”, “distance to the highway”, “the existence of agricultural drainage system”, “distance to the natural resources such as river, lake, etc.”, “the existence of electricity on parcel”, “closeness to forest and its facade of parcel”, “the existence of historical area on parcel”, “status of receiving the state support of the parcel”.

In the redistribution stage, landowners want their land equal to the amount of their old land after land consolidation. This is the most crucial and critical process. Because mistakes made in this stage may lead to the failure of the consolidation. In this process, redistribution of lands does according to parcel value numbers. Parcel value number should be calculated more detailed not to make a mistake. In this study, parcel value numbers were calculated according to Equation 3.

$$\text{Parcel Value Number} = (\text{Parcel Index} / 100) * \text{Parcel Area (m}^2\text{)} \quad \text{Eq. 3}$$

3. RESULT AND DISCUSSION

The parcel index values determined by the current method are mapped for the study area (Fig 3). This map is the map used by government institution made the land consolidation. In addition, parcel index of each parcel are also calculated and mapped in detail with the new equation (Fig 4). The parcel indexes determined by the new method are calculated according to 14 different criteria in detail.

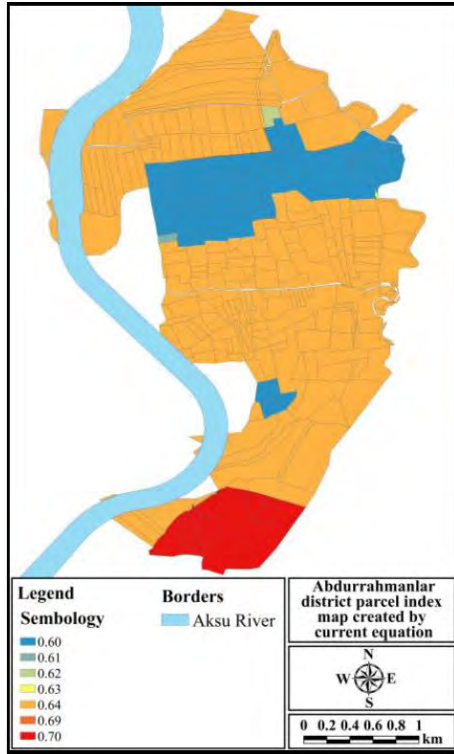


Figure 3. Parcel index map produced by current equation

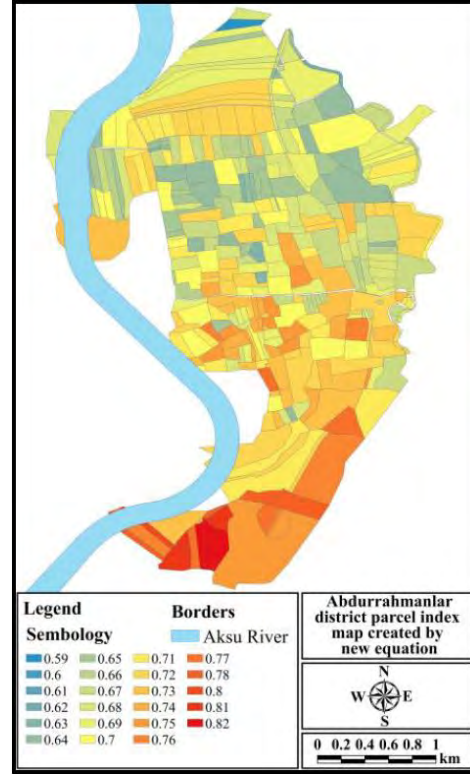


Figure 4. Parcel index map produced by new equation

The study area was represented by 23 different index which distributions close to each other (Fig 4). In the Abdurrahmanlar district, 13.0% of the parcels were 0.72 points, 12.2% were 0.68 points, 10.6% were 0.67 points, 10.3% were 0.69 points and 8.5% were 0.70 points. Besides this, other parcels are scattered at rates close to other points. Compared to the current equation, parcel indexes do not seem to concentrate on a few points, and they appear to be scattered at rates close to a number of points. This shows how detailed the process made is. While 77.5% of the parcel index calculated by the current equation is 0.64 points, the index value with the highest percentage in the new equation is 13.0% to 0.72 points. In addition, the parcel index ratio having 0.64 points in the new equation is 5.6%. As can be clearly seen from here, the parcel index values calculated by the current equation give superficial results. It is also a matter of debate how accurately the value of the relevant parcel is calculated. This shows that the parcel index values calculated by the new equation gives more accurate results than the parcel index values calculated by the current equation. Parcel value number maps created by the current and new equations belong to each parcels of Abdurrahmanlar district are given in Figure 5 and 6.



Figure 5. Parcel value number map produced by current equation

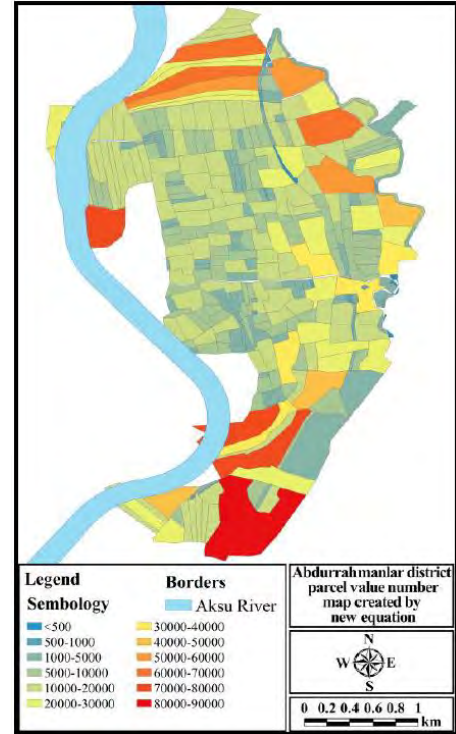


Figure 6. Parcel value number map produced by new equation

Figure 5 and Figure 6 show the maps of parcel value numbers generated by two different equations according to size groups. When the figures are examined, it is seen that the parcel value numbers are in general similarity in both equations. In order to give a more detailed interpretation, Figure 7 which shows changing of parcel value numbers entering in groups of the same size in the equations used in the study were given.

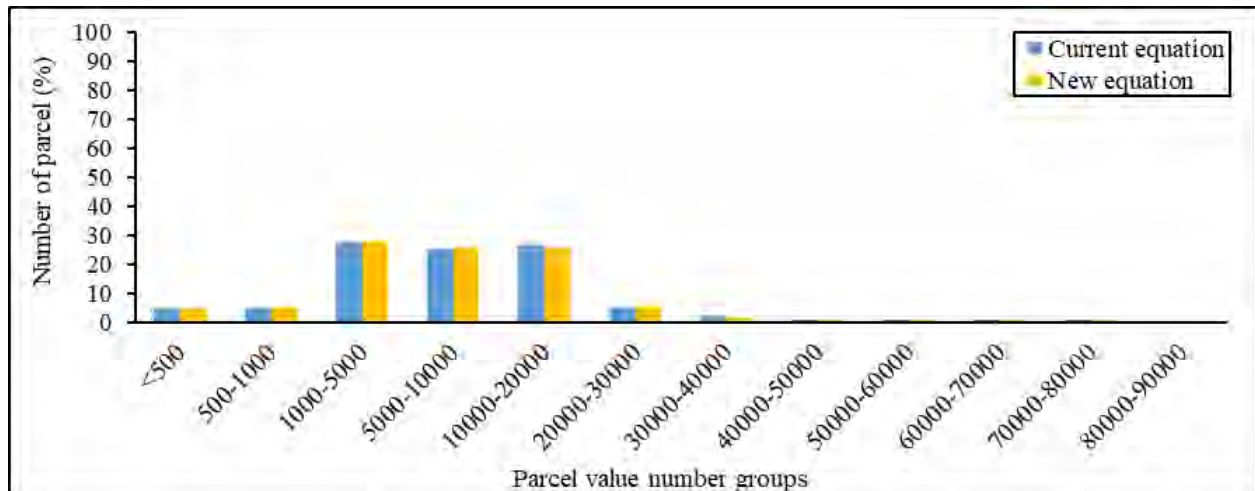




Figure 7. Change of parcel value numbers according to equations

The number of parcels with parcel number less than 500 and among 500-1000, 1000-5000, 5000-10000, 20000-30000 increased compared to the current equation. However, the number of parcels with a parcel value of 30000-40000 decreased in the new equation compared to current equation. In addition, the number of parcels with parcel value number between 10000 and 20000 also decreased in new equation compared to the current equation. The number of parcels with the parcel value number of 40000-50000, 60000-70000 and 80000-90000 are the same in both equations.

Gündoğdu et al., (2003) have tried to determine the parcel value numbers using the possibilities and capabilities of the geographical information system and to try it on a sample project. With the method they used, the parcel value numbers of the parcels in the field of land consolidation were able to determine very precisely and were able to determine the real values of the parcels of the participants. In this study, parcel value numbers were determined in a very detailed way using geographical information systems and similar results were obtained. Yomralioglu, (1993) identified 40 factors affecting land parcel value in the land redistribution process. In order to determine the land value in rural land consolidation, the topography, parcel shape, current available area, location and size of parcel, parcel surroundings, wind condition, soil quality and depth, taxes paid, current selling price of parcel, distance from important point in terms of location such as city center, ring road, railroad, water transportation way, recreation areas, existence of irrigation water source, existence of drainage system are the important factors that can be used to determine the parcel value in the same way. In this study, 14 different criteria were used to determine parcel value and similar results were obtained with the Yomralioglu, (1993). Tomić et al., (2016) conducted a study to determine land values in land consolidation work in Croatia. In the study, they investigated the priority areas for the implementation of land consolidation as a prerequisite for the development of rural areas and agricultural land. They reported that in the determination of the values of the priority areas, the criteria such as the share of the agricultural land in the land consolidation area, average agricultural parcel size, parcel shapes, fragmentation index of agricultural holdings, the share of agricultural lands belong to state (treasury land), regional development index, number of agricultural holdings within the land consolidation area etc. have to be used. In this study, 14 different criteria were used to determine parcel value and similar results were obtained.

4. CONCLUSION

In the study conducted, soil index was kept constant both in current and new equations which are used to determine parcel indexes. For this reason, the difference between the equations is due to the other parameters used in the calculation. In the current equation, the location score and the efficiency score are not in detail and they are superficial. However, since the land quality index parameters are detailed, the parcel indices were calculated in a detailed and more accurate way.



CIGR 2018

XIX. World Congress of CIGR



As a result, it was clearly understood that the new method is needed to use to determine the parcel indices in land consolidation studies. The results such as new method increases the initiative of the rating commission and makes their works easier, it is not standard for all regions and it can be modified according to region and project, it calculated parcel values in more detail according to international criteria taking into consideration the geographical, physical, cultural and socio-economic structure of the region where the land consolidation is made according to many parameters can be listed as the method used in the study and the innovations that the findings will bring to the land consolidation studies.

5. ACKNOWLEDGEMENT

This study was supported by The Scientific Research Projects Coordination Unit of Akdeniz University with the project number FBA-2017- 2279. The authors thank to the General Directorate of State Hydraulic Works 13th Regional Directorate because of their support to this study. The authors also would like to special thanks to Ag. Eng. Hikmet Avcı for his contributions.

6. REFERENCES

- Bonfanti, P., Fregonese, A., Sigura, M. 1997. Landscape analysis in areas affected by land consolidation. *Landscape Urban Plan.* 37 (1-2): 91–98.
- Cay, T. and Iscan, F., 2011. Fuzzy expert system for land reallocation in land consolidation. *Expert Syst. Appl.* 38 (9): 11055-11071.
- Cay, T., Ayten, T. and Iscan, F. 2010. Effects of different land reallocation models on the success of land consolidation projects: social and economic approaches. *Land Use Policy* 27 (2): 262–269.
- Crecente, R., Alvarez, C., Fra, U. 2002. Economic, social and environmental impact of land consolidation in Galicia. *Land Use Policy* 19 (2): 135–147.
- DSI, 2016. Antalya Aksu flood protection project, land consolidation and IFDS project social structure survey report of Abdurrahmanlar District. T.C. Ministry of Forestry and Water Management General Directorate of State Hydraulic Works. SHW 13th Regional Directorate. pp. 43.
- Gu, X.K., Dai, B., Chen, B.M. 2008. Landscape effects of land consolidation projects in Central China – A case study of Tianmen City, Hubei Province. *Chinese Geograph. Sci.* 18 (1): 41–46.
- Gündoğdu, K.S., Akkaya Aslan, T.Ş., Arici, İ., 2003. Determination of parcel value numbers in land consolidation using geographical information system U.Ü. *Journal of Agricultural Faculty.* 17(1):137–148
- Huang, Q.H., Li, M.C., Chen, Z. and Li, F. 2011. Land consolidation: an approach for sustainable development in rural China. *AMBIO* 40 (1), 93–95.
- Lerman, Z. 2002. Productivity and efficiency of individual farms in Poland: a case for land



CIGR 2018

XIX. World Congress of CIGR



consolidation. In: Annual Meeting of the American Agricultural Economics Association, Long Beach, CA, July 28–31, 2001.

Pasakarnis, G. and Maliene, V., 2010. Towards sustainable rural development in Central and Eastern Europe: applying land consolidation. *Land Use Policy* 27(2): 545-549.

Sonnenberg, J. 2002. Fundamentals of Land Consolidation as an Instrument to Abolish Fragmentation of Agricultural Holdings, FIG XXII International Congress, April 19-26 2002. Washington, D.C. USA.

Tezcan A., Büyüктаş K. and Akkaya Aslan Ş.T. 2018. Determination of Parcel Value Number with Detailed Method in the Land Consolidation. *Asian Research Journal of Agriculture*. 9(4): 1-10.

Tomić, H., Roic, M., Mastelić Ivić, S., Mičević, B., Jurakić, G., 2016. Use of Multi-Criteria Analysis for the Ranking of Land Consolidation Areas, in: Symposium on Land Consolidation and Readjustment for Sustainable Development. 9-11 November 2016. Apeldoorn, Netherlands, pp. 1-12.

USDA, 2011. National Agricultural Land Evaluation and Site Assessment (Lesa) Handbook, United States Department of Agriculture Natural Resources Conservation Service.

Yomralioglu, T., 1993. A nominal asset value-based approach for land readjustment and its implementation using GIS. University of Newcastle upon Tyne.



Changes in Low-flow Frequency under Global Warming in Tanada Catchments

Shinichi Takeshita¹, Tshiswaise Rudzani¹, Hiroyuki Seo¹

¹Faculty of Agriculture, University of Miyazaki, Gakuen kibanadai-nishi, Miyazaki 889-2192,
Japan
rtakeshita@cc.miyazaki-u.ac.jp

ABSTRACT

In Japan, terraced paddy fields (known as Tanada in Japanese) span an area of over 20,000 ha. Because most terraced paddy fields are located on mountain slopes, irrigation water is withdrawn from mountain streams with small catchments. As a possible outcome of global climate change, reductions in precipitation could directly decrease surface water streamflow and exacerbate the irrigation water demand by terraced paddy fields. This paper presents the results of an investigation of the impact of these effects on Sakamoto Tanada in southeastern Japan. The investigation examined the effects of precipitation and streamflow changes, especially the low-flow frequency, under global warming. Streamflow was simulated using the hydrological model TOPMODEL using large ensemble climate simulations. Before the numerical simulation, the adequacy of TOPMODEL was verified using observational data. The Database for Policy Decision-Making for Future Climate Change (d4PDF) dataset was used as global warming simulation data, which is intended for use in impact assessment studies and adaption planning for global warming, has many ensembles of 20-km regional climate model simulations over Japan. The results of the 3000 members of past climate simulations and 5400 members of global warming climate simulations were compared, and the change in low-flow frequency was analyzed. Although the probability density distribution of average precipitation and streamflow in the irrigation period during May to September did not change in the simulation of warmer climate, the distribution spread on both sides, indicative of the increased occurrence frequency of droughts. Finally, the return period of a low-flow frequency of less than 2.5 mm/day changed under global warming from 10.0 years to 5.5 years. Overall, these results indicate that the risk of drought in terraced paddy fields in Japan will increase under global warming.

Keywords: Terraced paddy field, Hydrological simulation, Return period, Drought, Irrigation period, Japan

INTRODUCTION

Scientific research indicates that the Earth's climate is changing due to increased atmospheric greenhouse gas concentrations. Driven by increases in global average temperatures, climate change is expected to strongly affect the hydrological cycle worldwide in the coming decades (IPCC, 2014). Hence, a number of studies have projected that climate change is likely to have

Shinichi Takeshita, Tshiswaise Rudzani, Hiroyuki Seo "Changes in low-flow frequency under global warming in tanada catchments"



significant impacts on precipitation patterns, including increased occurrence of extreme events such as flooding and drought (e.g., Tachikawa *et al.*, 2010; Reshmidevi *et al.*, 2018). For instance, Takeshita *et al.* (2010) reported that the total amount of precipitation and number of rainy days over the past 30 years in Miyazaki Prefecture, Japan, has significantly decreased, especially in spring. Variations in precipitation patterns have been recognized to be largely linked with changes in stream flows, especially in forested mountainous catchments (e.g., Shinohara *et al.*, 2009). This has been reported by studies in Japan, which have confirmed that the total precipitation is expected to change significantly, resulting in significant changes to water resources (e.g., Takara *et al.*, 2009; Kim *et al.*, 2010). Recent studies of water resource changes have performed experiments using predicted hydrological data from large ensembles from the database for Policy Decision making for Future climate change (d4PDF), which considers reported climate change uncertainties (Mizuta *et al.*, 2016). Changes in water resources have large impacts on agricultural irrigation water use (Kudo *et al.*, 2012; Kudo *et al.*, 2017). Most studies have analyzed large river basins with reservoirs or diversion weirs. However, large areas of farm land use irrigation canals without water storage facilities. For example, there are over 20,000 ha of terraced paddy fields in Japan, most of which are located on mountain slopes and are irrigated with water from mountain streams with small catchments (Nakajima, 1999).

In this study, to assess impacts of climate change on irrigation water resource on mountainous terraced paddy fields, changes in stream water during the irrigation period were analyzed. The changes in stream water were investigated, especially the low-flow frequency, which were described by climate change prediction data based on ensemble data from d4PDF experiments (Mizuta *et al.*, 2016).

2. METHODOLOGY

Mizoguthi catchment, Japan, was used as the study area, and the discharge was calculated using the TOPMODEL hydrological model (Beven and Kirkby, 1979). Climate change prediction data were used as the input data for the calculations. Observational data were used to verify the accuracy of the runoff calculations. The parameters of TOPMODEL were adjusted so that discharge could be reproduced under the current climate conditions as well as possible. The climate change impact assessment used the discharge calculated from the historical experimental dataset and 4-K-warmer climate simulation experimental dataset from d4PDF. In particular, we focused on the duration curve properties, and analyzed low flows during the irrigation period.

2.1 Study areas and observational data

The mountainous Mizoguthi Catchment (0.396 km²) is located in the Sakatani River Basin in southern Miyazaki Prefecture, Kyushu Island, Japan, which is characterized by natural forest land over mountainous topography. The elevation of the study area ranges from 330 to 960 m a.s.l. The average temperature and total annual precipitation in this area are about 16.7°C and 2,478 mm, respectively. There is almost no snow cover. This study focused on the streamflow of the Mizoguthi Catchment (Fig. 1), which is used in Sakamoto terraced paddy fields (*tanada*) for irrigation.

Shinichi Takeshita, Tshiswaise Rudzani, Hiroyuki Seo “Changes in low-flow frequency under global warming in tanada catchments”



The discharge measurements were conducted in 2011 at the irrigation diversion weir. The rain gage and meteorological observation station were located in the Sakamoto terraced paddy field, about 800 m southwest of the diversion weir, and data from 2011 were used. Evapotranspiration was estimated using the Penman–Monteith method from the average temperature, solar radiation, relative humidity, and wind speed.

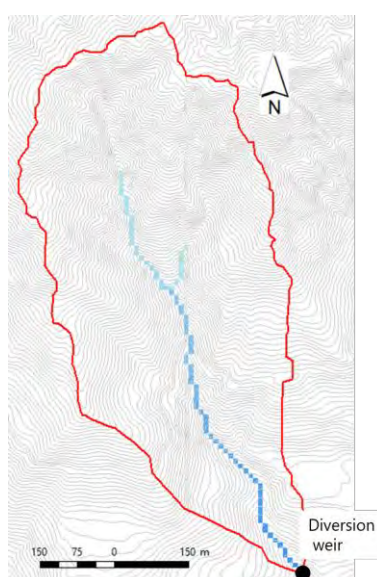


Figure 1. Overview of the Mizoguthi catchment

2.2 Hydrological model

The stream flow was simulated using the hydrological runoff model TOPMODEL, developed by Beven and Kirkby (1979). TOPMODEL is a semi-distributed, mass conservative model that relies on a simple representation of basin characteristics and runoff mechanisms (Beven, 1997), as compared to other fully distributed models that are more complex and require higher-quality data. The topographic index of Mizoguthi Catchment was calculated using a 5-m mesh digital elevation model. This topographic index was used for the discharge calculations.

TOPMODEL contains seven types of parameters. These parameters were optimized using observational data, such as precipitation, evapotranspiration, and discharge, collected during 2011–2012. The parameter optimization method was performed using the evolution strategy algorithm, which is a type of genetic algorithm (Fujihara *et al.*, 2003; Salimans *et al.*, 2017).

The two objective functions were used to decide the goodness-of-fit of the parameters, including the root-mean-squared error (RMSE) and coefficient of determination (R^2). The parameter set was determined using these objective functions, where the weights of the RMSE and R^2 were the same. The optimized parameter set from 100 trials was based on different initial values determined.



The observed data for the period 2015–2016 (two years) were used for the model validation. The results indicated that the calculated discharge using TOPMODEL with the aforementioned parameter set was appropriate. The RMSE and R^2 were 7.03 and 0.71, respectively, indicating good performance of the model in simulating the stream flow of Mizoguthi catchment. These results support the application of TOPMODEL to the external independent dataset.

2.3 Climate simulation

The climate simulation data (i.e., precipitation) were input into the hydrologic model to simulate the stream flow to assess the climate change impact on stream flow in the Mizoguthi Catchment. The General Circulation Model outputs used in this study were archived in the d4PDF (Mizuta *et al.*, 2016).

The d4PDF is a large ensemble of climate forcing simulations with the atmospheric general circulation model (AGCM) MRI-AGCM3.2 (horizontal resolution: ~60 km) and is dynamically downscaled around Japan using a 20-km-resolution regional climate model (RCM) developed by the Meteorological Research Institute, Japan (MRI). The d4PDF ensembles comprise historical and future AGCM simulations. The historical ensembles for the 60-year period of 1951–2010 were simulated with 50 RCM members. The future ensembles for the period of 2051–2110 (60 years) were simulated with 15 members of +4 K global warming taken from six surface sea temperature (SST) patterns and using the 2090 conditions of the RCP8.5 scenario (van Vuuren *et al.*, 2011). Therefore, the historical ensembles included 3000 years (50 members \times 60 years), and the future (4-K-warmer) ensembles contained 5400 years (6 SST patterns \times 15 members \times 60 years).

Precipitation (mm/day) and latent heat flux (W/m^2) data based on the historical and 4-K-warmer ensembles were used for the study. Before using the d4PDF dataset (i.e., precipitation) to simulate the hydrological impact on the Mizoguthi Catchment, it was compared to AMeDAS observation data to clarify the performance of the AGCM and to check for bias error. Historical precipitation data (1979–2017) were obtained from the Fukase AMeDAS observation station located near the catchment. The comparison of the annual mean precipitation from the d4PDF dataset and AMeDAS observations revealed that the shapes of the probability density distribution were generally similar. However, precipitation from the d4PDF dataset was underestimated by around 19.5%. The highest underestimations were observed in June and September, possibly due to the occurrence of the rainy season and typhoon rainfalls, respectively. Therefore, the d4PDF dataset showed a high degree of consistency for periods with less precipitation, but some inconsistencies during periods with high precipitation. The analysis of climate change impact on stream flow was based on the simulated stream flow dataset. The simulated stream flow dataset was computed by inputting the climate change dataset (d4PDF) into TOPMODEL. Therefore, the historical and 4-K-warmer climate stream flow datasets contained 3000-year and 5400-year experiments, respectively.



3. RESULTS AND DISCUSSION

3.1 Changes in precipitation

Figure 2 shows a comparison of the probability density distribution of irrigation period precipitation from the historical and 4-K-warmer ensembles. The average precipitation did not change under the 4-K-warmer climate conditions, and the distribution of the precipitation was more dispersed under the 4-K-warmer conditions.

3.2 Changes in discharge

Figure 3 shows a comparison of the probability density distribution of historical and 4-K-warmer irrigation period streamflow. The average streamflow did not change under the 4-K-warmer climate conditions. Moreover, the frequency of low streamflow decreased slightly under the 4-K-warmer climate conditions, contradicting the expected unchanged frequency of low precipitation. This confirmed the similarity between the changes in precipitation and streamflow.

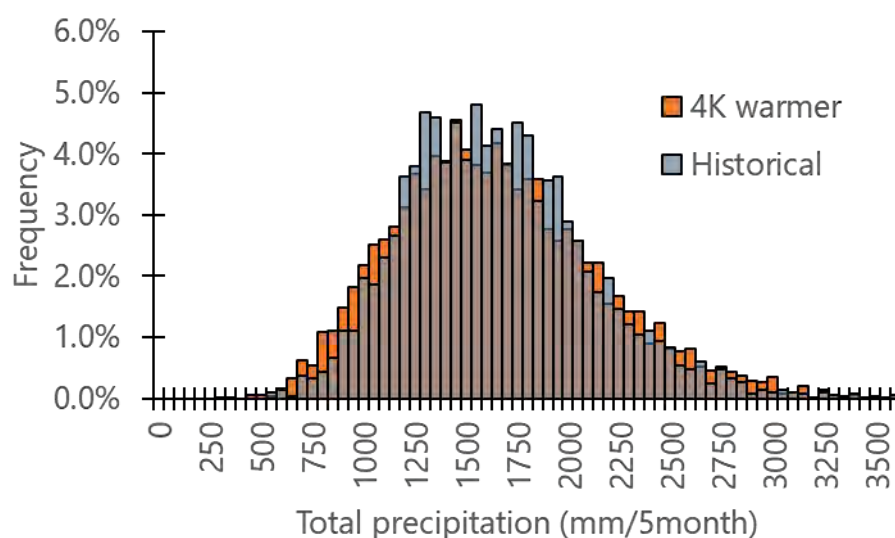


Figure 2. Probability density distribution of irrigation period precipitation.

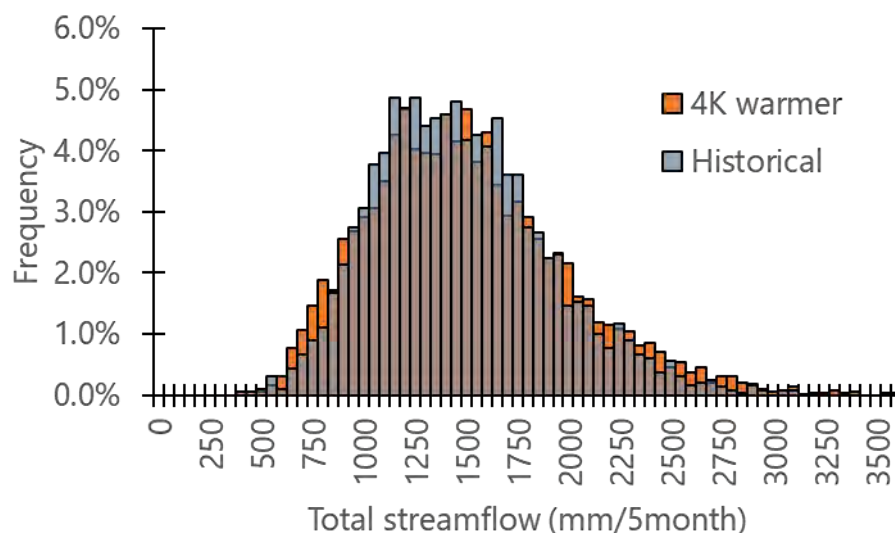


Figure 3. Probability density distribution of irrigation period streamflow.

3.3 Low-flow frequency

Statistical frequency analysis of the changes in streamflow was performed through the implementation of flow duration curves. The curves showed a decreased in the minimum streamflow under the 4-K-warmer climate conditions. Meanwhile, the results of the predicted impacts of climate change on water resources by Asadieh and Krakaur (2017) were in agreement with those of this study, in that the lowest discharge was expected to decrease under global warming. This was also in agreement with the conclusions of Matthew and Nigel (2014), who noted that changes in precipitation in summer have many impacts on low flows. Such conditions might worsen drought hazards.

Table 1 shows a comparison of the average (Q_{50}), low (Q_{95}), and high (Q_{10}) streamflow under the historical and 4-K-warmer climate conditions to further analyze the flow duration curves. The IQRs increased for the Q_{50} , Q_{95} , and Q_{10} streamflow under 4-K-warmer climate conditions.

Table 1. Comparison of historical and 4 K warmer climate flow duration properties

	Q_{10}		Q_{50}		Q_{95}	
	Historical	4K warmer	Historical	4K warmer	Historical	4K warmer
Lower whisker	3.80	4.02	1.70	1.94	0.83	0.75
Lower quartile	9.63	9.94	3.88	3.91	1.68	1.63
Median	11.67	12.16	4.47	4.59	1.98	1.95
Upper quartile	14.14	14.73	5.11	5.29	2.31	2.32
Upper whisker	29.91	33.80	9.03	9.60	4.02	4.61
IQR	4.51	4.79	1.23	1.38	0.63	0.69



Similar trends were observed for the median Q_{10} and Q_{50} streamflow, whereas the Q_{95} discharge showed a projected decrease under the 4-K-warmer climate conditions. This decrease in Q_{95} and its lower whisker suggest that the catchment is likely to become drought prone under 4-K-warmer climate conditions. Meanwhile, the noticeable increase in Q_{10} and its upper whisker might have contrasting negative impacts, such as flooding, on the catchment under 4-K-warmer climate conditions.

Finally, the analysis of low streamflow (Q_{95}) was performed because extreme low streamflow conditions can have negative impacts on agriculture systems, such as terraced paddy fields. Figure 4 shows a slight decrease in the low streamflow on return periods under the 4-K-warmer climate conditions. The 10-year return period of low streamflow slightly decreased under 4-K-warmer climate conditions, where the return period of 2.5 mm/day decreased from 10 to 5.5 years. These results might not present major challenges to water resources in the catchment under 4-K-warmer climate conditions.

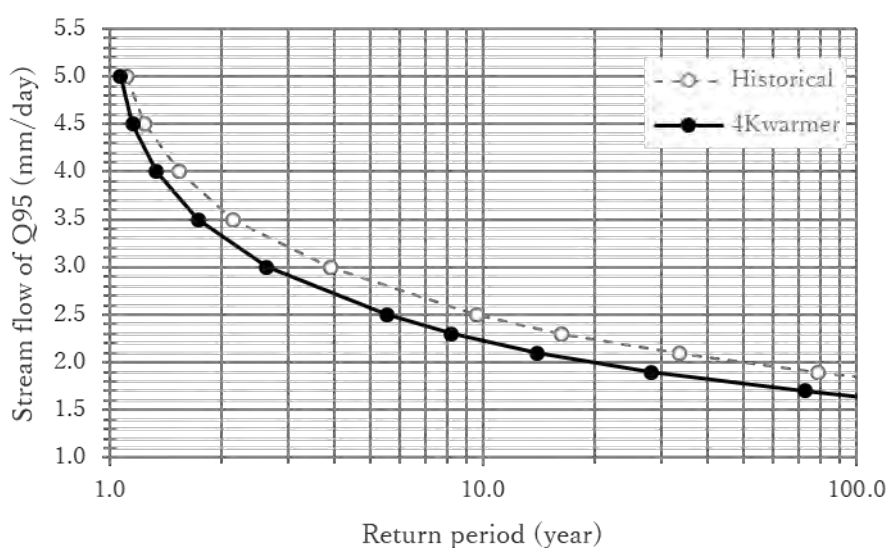


Figure 4. The return period of Q_{95} streamflow under historical and 4-K warmer climates

4. CONCLUSIONS

This study offers a comprehensive analysis of climate change impacts on precipitation and streamflow, especially the low-flow frequency in the Mizoguthi Catchment in Japan using a large ensemble of d4PDF historical and 4-K-warmer climate simulations and the TOPMODEL hydrological model. The d4PDF dataset was compared with AMeDAS observation data to assess its performance and check for bias error before use in the hydrological impact simulation. The d4PDF data showed general consistency with the AMeDAS data, supporting their use in this study.



CIGR 2018

XIX. World Congress of CIGR



Although the probability density distribution of mean total precipitation and streamflow in the irrigation period during May to September did not change in the simulation of warmer climate, the distribution spread on both sides. Based on probability density distributions, under the 4-K-warmer climate conditions, the showed that the frequencies of low irrigation period streamflow decreased slightly. The results of the flow duration curve analysis indicated that the catchment could experience a decrease in low and lowest discharges under climate change. These results suggest that the Mizoguthi Catchment will likely be prone to drought under global warming.

Finally, the return period results showed impacts of drought due to the expected decrease in low streamflow. To assess the impacts of climate change on streamflow in mountainous areas more comprehensively, it is crucial to consider the uncertainty about the hydrological modeling and simulation. These results can be used to adopt appropriate adaptive strategies to mitigate the negative impacts of drought on Mizoguthi Catchment.

This research was supported by the “Integrated Research Program for Advancing Climate Models (TOUGOU program)” from the Ministry of Education, Culture, Sports, Science and Technology, Japan.

X. REFERENCES

- Asadieh, B. and Krakauer, N.Y. (2017): Global change in streamflow extremes under climate change over the 21st century, *Hydrol. Earth Syst. Sci.*, 21, pp.5863-5874.
- Beven, K.J. (1997): *Distributed hydrological model-ing: applications of the TOPMODEL concept*, John Wiley and Sons Ltd., Chichester, U.K.
- Beven, K.J. and Kirkby, M.J. (1979): A physically based variable contributing area model of basin hy-drology, *Hydrol. Sci. Bull.*, 24, pp.43-69.
- Fujihara, Y., Tanakamaru, H., Hata, T., and Tada, A. (2003): Calibration of rainfall-runoff models using the evolution strategy, *Trans. of JSIDRE*, 227, pp.119-129 (in Japanese with English abstract).
- IPCC (2014): *Climate change 2014 synthesis report. Contribution of working groups I, II and III to the Fifth Assessment Report of the Intergovernmental Panel on Climate Change*, 151p.
- Kim, S., Tachikawa, Y., Nakakita, E., and Takara, R. (2010): Climate change impact on water resources management in the Tone river basin, Japan, *Annu. Disas. Prev. Res. Inst., Kyoto Univ.*, 52B, pp.587-606.
- Kudo, R., Yoshida, T., and Masumoto, T. (2017): Na-tionwide assessment of the impact of climate change on agricultural water resources in Japan using multi-ple emission scenarios in CMIP5, *Hydrol. Res. Lett.*, 11(1), pp.31-36.
- Matthew, B.C. and Nigel, W.A. (2014): Assessing the impacts of climate change on river flows in England using the UKCP09 climate change projections. *J. Hydrol.*, 519, pp.1723-1738.
-
- Shinichi Takeshita, Tshiswaise Rudzani, Hiroyuki Seo “Changes in low-flow frequency under global warming in tanada catchments”



CIGR 2018

XIX. World Congress of CIGR



Mizuta, R., Murata, A., Ishii, M., Shiogama, H., Hibino, K., Mori, N., Arakawa, O., Imada, Y., Yoshida, K., Aoyagi, T., Kawase, H., Mori, M., Okada, Y., Shimura, T., Nagatomo, T., Ikeda, M., Endo, H., Nosaka, M., Arai, M., Takagashi, C., Tanaka, K., Takemi, T., Tachikawa, Y., Temur, K., Kamae, Y., Watanabe, M., Sakai, H., Kitoh, A., Takayabu, I., Nakakita, E., and Kimoto, M. (2016): Over 5000 years of ensemble future climate simulations by 60 km global and 20 km regional atmospheric models, Bull. Am. Meteorol. Soc., DOI:10.1175/BAMS-D-16-0099.1

Nakajima, M. (1999): TANADA Japanese rice ter-races, KOKON, pp.21-30.

Okada, Y., Hiramatsu, K., Shikasho, S., and Mori, M. (2005): Rainfall runoff modeling in a small mountainous basin using TOPMODEL, Sci. Bull. Fac. Agr., Kyushu Univ., 60(2), pp.151-1632 (in Japanese with English abstract).

Reshmidevi, T.V., Nagesh Kumar, D., Mehrotra, R., and Sharma, A. (2018): Estimation of the climate change impact on a catchment water balance using an ensemble of GCMs, J. Hydrol., 556, pp.1192-1204.

Salimans, T., Ho, J., Chen, X., and Sutskever, I. (2017): Evolution strategies as a scalable, Alternative to Reinforcement Learning, arXiv: 1703.03864v2 [stat.ML].

Shinohara, Y., Kumagai, T., Otsuki, K., Kume, A., and Wada, N. (2009): Impact of climate change on run-off from a mid-latitude mountainous catchment in central Japan, Hydrol. Process, 23, pp.1418-1429.

Tachikawa, Y., Takino, S., Yorozu, K., Kim, S., and Shiiba, M. (2010): Estimation of climate change impact on flood discharge at Japanese river basins, Disaster Prev. Res. Annu., 53B, pp.23-36 (in Japanese with English abstract).

Takara, K., Kim, S., Tachikawa, Y., and Nakakita, E. (2009): Assessing climate change impact on water resources in the Tobe river basin, Japan, using super-high-resolution atmospheric model output, J. Disaster Res., 4(1), pp.12-23 (in Japanese with English abstract).

Takeshita, S., Hosokawa, Y., and Inagaki, H. (2010): Precipitation characteristics of spatial and temporal variability in Miyazaki prefecture, J. Rainwater Catchment Sys., JRCSA, 15(2), pp.67-72 (in Japanese with English abstract).

Van Vuuren, D.P., Edmonds, J., Kainuma, M., Riahi, K., Thomson, A., Hibbard, K., Hurtt, G.C., Kram, T., Krey, V., Nakicenovic, N., Smith, S.J., and Rose, S.K. (2011): The representative concentration pathways: an overview, Clim. Change, 109, pp.5-31.



CIGR 2018

XIX. World Congress of CIGR



A Deep Neural Network Model for Runoff Analysis

Tomoki Izumi¹, Ayane Kan², Noriyuki Kobayashi³

¹ Graduate School of Agriculture, Ehime University, 3-5-7 Tarumi, Matsuyama, Japan 790-8566,
t_izumi@agr.ehime-u.ac.jp

² Faculty of Agriculture, Ehime University, 3-5-7 Tarumi, Matsuyama, Japan 790-8566

³ Graduate School of Agriculture, Ehime University, 3-5-7 Tarumi, Matsuyama, Japan 790-8566

ABSTRACT

A deep neural network (DNN) to represent the nonlinear relation between rainfall and river discharge is developed. DNN is composed of one input layer, five middle layers and one output layer, and predicts a dairy river discharge from input data of a day unit. Generally, a time series of rainfall data is used as input in runoff analysis. In this study, however, the soil water index (SWI) is used instead of rainfall data to reflect a time history of rainfall in the output of dairy river discharge more accurately. SWI represents a condition of soil water content and is calculated from rainfall data by use of the tank model consisting of three tanks. In order to avoid the problem of “gradient vanishing” resulting from multilayering, ReLU (Rectified Linear Unit) function is employed as the activation function instead of the sigmoid function that is usually used in conventional neural networks. DNN model developed is applied to runoff analysis in Shigenobu River basin, Ehime Prefecture, Japan. Compared with conventional models, effectiveness of the model is assessed through investigation of calibration and verification errors in terms of three statistical performance indices. From the results, it is found that the error in DNN model is the smallest and that DNN model is the most accurate in all models. It is also found that training period considered in this study does not influence on calibration and verification results.

Keywords: Runoff analysis, neural network, deep learning.

1. INTRODUCTION

Runoff analysis is an important technique for prediction of drought and flood. Runoff models such as conceptual or physical models are used in runoff analysis. However, it is difficult to express the relation between rainfall and discharge due to its high nonlinearity.

Application of artificial neural network (ANN) to runoff analysis is effective for the expression of nonlinearity. Hsu et al. (1995) applied a hierarchical neural network (HNN) model to runoff analysis and demonstrated its effectiveness through comparing with the linear ARMAX



(autoregressive moving average with exogenous inputs) time series approach or the conceptual SAC-SMA (Sacramento soil moisture accounting) model. Minns and Hall (1996) implemented runoff analysis using HNNs in a hypothetical catchment and evaluated the performance of ANNs. Dawson and Wilby (1998) developed an HNN model and applied it to flow forecasting in two rivers. Sajikumar and Thandaveswara (1999) developed a monthly rainfall-runoff model using an HNN and investigated its performance through comparing with functional series models. Abe et al. (2000) developed an HNN model and applied to long-term (10 years) daily runoff analysis. Kiyama et al. (2003) developed an HNN model to predict flood discharge and discussed its predictability or applicability.

Previous works showed applicability or effectiveness of HNN models for runoff analysis. On the other hand, it is indicated that the problems of "vanishing gradient" and "overfitting" occur in conventional HNNs when the number of layers and computational nodes (neurons) increases for the purpose of obtaining more accurate expression of the relation between rainfall and discharge. Recently, deep learning methods are proposed to overcome those problems (LeCun et al., 2015; Schmidhuber, 2015). Izumi et al. (2016) and Izumi and Kobayashi (2017) developed deep neural network (DNN) models for runoff analysis. Their models consist of one input layer, two or three middle layers, and one output layer. In order to avoid the vanishing gradient, the layer-wise pre-training by the auto-encoder is employed (Bengio, 2006). For the problem of overfitting, the number of training run is limited based on the early-stopping technique (Kamishima et al., 2015). The model effectiveness is shown by comparing the DNN and HNN model output in terms of the reproducibility and predictability for observed data. However, DNN model with pre-training by the auto-encoder is time-consuming. Also, river discharge or water level are generally predicted from rainfall in runoff analysis. However it is considered that using data which reflect time histories of rainfall as input leads to increase the model accuracy. The soil water index (SWI) developed by Okada et al. (2001) is suitable for input data because it represents amount of soil water reflecting antecedent rainfall.

In this study, DNN model without pre-training is thus developed, learning from time-series of SWI. Effectiveness of the model is assessed through the comparison of conventional models.

2. DNN MODEL

2.1 Network Structure

DNN model developed in this study consists of one input layer, five middle layers, and one output layer shown in Fig. 1. In order to avoid the gradient vanishing, ReLU (Rectified Linear Unit) function is used as the activation function instead of sigmoid function which is widely used in conventional HNNs. The output in j -th layer is described as follows:



$$f(u_j) = \begin{cases} u_j & (u_j > 0) \\ 0 & (u_j \leq 0) \end{cases} \quad (1)$$

with

$$u_j = \sum_{i=1}^n w_{ij} x_i - \theta_j \quad (2)$$

where, $f(u_j)$ is output value in j -th layer, x_i is input in j -th layer, w_{ij} is weight coefficient, θ is threshold value, n is the number of node in i -th layer. The training procedure is used the error backpropagation algorithm (Rumelhart et al., 1986). In the algorithm, the weight coefficients and threshold values are adjusted based on errors between resultant outputs from the network and expected outputs (teacher signals).

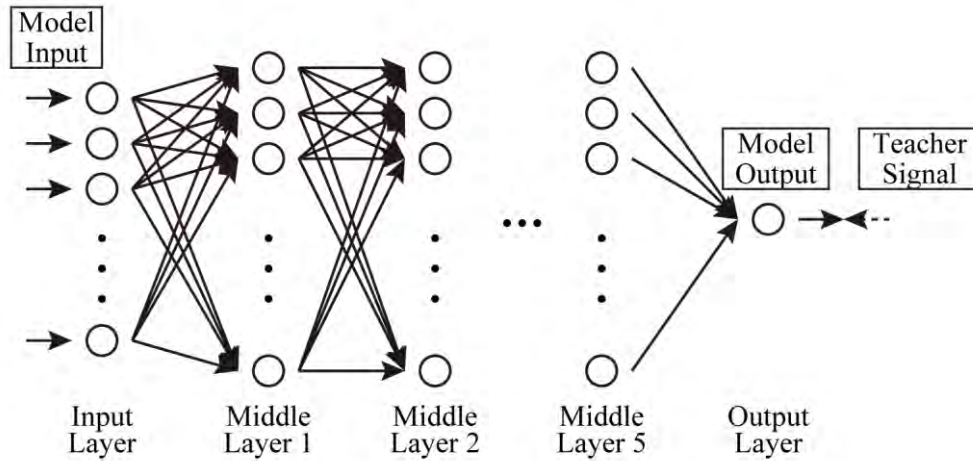


Figure 1. DNN model.

2.2 Input Data

Time-series of SWI is used as input data in this study. SWI is now used as a criterion to issue weather warning by Japan Meteorological Agency and is calculated from rainfall data by means of the tank model consisting of three tanks (Ishihara and Kobatake, 1979; shown in Fig. 2) as follows:

$$SWI(t) = S_1(t) + S_2(t) + S_3(t) \quad (3)$$

where S_1 , S_2 , and S_3 are the storage depth in each tank. S_1 , S_2 , and S_3 are calculated as follows:

$$\frac{dS_1(t)}{dt} = R(t) - q_1(t) - \beta_1 S_1(t) \quad (4)$$



$$\frac{dS_2(t)}{dt} = \beta_1 S_1(t) - q_2(t) - \beta_2 S_2(t) \quad (5)$$

$$\frac{dS_3(t)}{dt} = \beta_2 S_2(t) - q_3(t) - \beta_3 S_3(t) \quad (6)$$

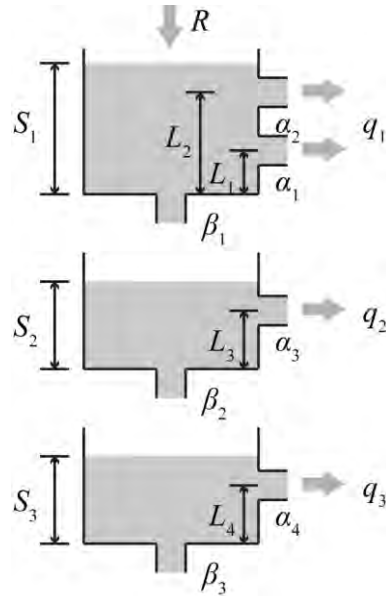


Figure 2. Tank model.



with

$$q_1(t) = \begin{cases} \alpha_1(S_1(t) - L_1) + \alpha_2(S_1(t) - L_2), & L_2 < S_1(t) \\ \alpha_1(S_1(t) - L_1), & L_1 < S_1(t) < L_2 \\ 0, & S_1(t) < L_1 \end{cases} \quad (7)$$

$$q_2(t) = \begin{cases} \alpha_2(S_2(t) - L_3), & L_3 < S_2(t) \\ 0, & S_2(t) < L_3 \end{cases} \quad (8)$$

$$q_3(t) = \begin{cases} \alpha_3(S_3(t) - L_4), & L_4 < S_3(t) \\ 0, & S_3(t) < L_4 \end{cases} \quad (9)$$

Table 1. Parameters used in tank model.

	1st tank	2nd tank	3rd tank
Height of side outlet (mm)	$L_1=15, L_2=60$	$L_3=15$	$L_4=15$
Discharge Coefficient (1/hour)	$\alpha_1=0.1, \alpha_2=0.15$	$\alpha_3=0.05$	$\alpha_4=0.01$
Percolation Coefficient (1/hour)	$\beta_1=0.12$	$\beta_2=0.05$	$\beta_3=0.01$

where t is time, R is rainfall, q_1, q_2, q_3 are the discharge from side outlet in each tank, L_1, L_2, L_3, L_4 are the height of each side outlet, $\alpha_1, \alpha_2, \alpha_3, \alpha_4$ are the discharge coefficients in each side outlet, $\beta_1, \beta_2, \beta_3$ are the percolation coefficients in each percolation outlet. Although model parameters are generally depend on soil texture, those for granite proposed by Ishihara and Kobatake (1979) are employed to calculate SWI (shown in Table 1).

3. MODEL ASSESSMENT

3.1 Study Area

DNN model is applied to runoff analysis in Shigenobu River basin, Ehime prefecture, Japan as shown in Fig. 3. Shigenobu River is 36 km length and flows into Seto Inland Sea. The basin area is 445 km² and 70% of the basin is covered by forest. The alluvial fan, Dogo Plain, is formed in the downstream basin. The average annual rainfall in the plain is approximately 1,300 mm/year, which is less than that of Japan (1,700 mm/year).

The discharge and rainfall data are obtained from Water Information System and database of Japan Meteorological Agency, respectively. Also, the discharge and rainfall are observed at the observatory of Deai (N33° 48' 21'', E132° 43' 31'') and Matsuyama (N33° 50' 36'', E132° 46' 36''), respectively. The observed data of discharge and rainfall are used for teacher signal and calculating SWI.

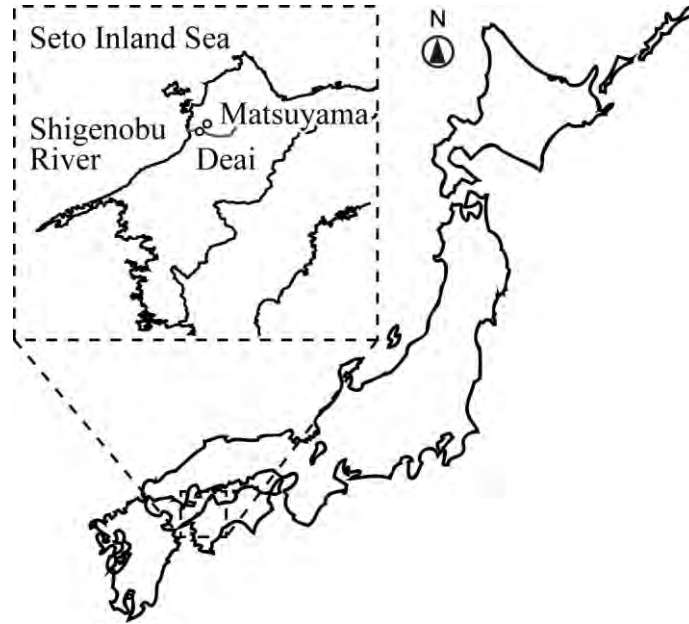


Figure 3. Study area (Shigenobu River basin).

3.2 Conditions of Runoff Analysis

In this study, DNN model reproduces or predicts daily discharge from daily SWI. Generally, daily discharge depends on rainfall before several days. Thus, rainfall before 10 days are used based on the hyeto and hydro graph at the observatory of Deai and Matsuyama. That is, daily SWI is calculated from rainfall data using the tank model, and daily SWI before 10 days are used for input of DNN model. This means that the number of computational nodes in input layer is set as 10. While the number of computational nodes in five middle layers can be arbitrary determined, in order to minimize the error between model output and teacher signal, those are determined as 17 nodes in all middle layers by trial and error method.

In order to assess effectiveness of the DNN model, the calibration and verification results are compared with conventional models: (1) DNN model with pre-training (CM 1), (2) HNN model (CM 2), (3) ARMAX (CM 3). CM1 consists of one input layer, three middle layers, and one output layer. The number of computational nodes in three middle layers are 7, 5 and 3 for the respective layers. The number of computational nodes in the input and output layer are set as 10 and 1, respectively, as same as this DNN model. In order to avoid the problem of gradient vanishing, pre-training by the auto-encoder is employed. CM 2 consists of one input layer, one middle layer, and one output layer. The number of computational nodes in the input, middle and output layer are set as 10, 5 and 1, respectively. CM 3 is described based on Hsu et al. (1995) as follows:

$$z(t) = -\sum_{i=1}^{n_a} a_i z(t-1) + \sum_{j=1}^{n_b} b_j x(t-j) + \sum_{k=1}^{n_c} c_k e(t-k) + e(t) \quad (10)$$



CIGR 2018

XIX. World Congress of CIGR



where $z(t)$ is the discharge, $x(t)$ is the rainfall, $e(t)$ is the model error, n_a , n_b and n_c are the number of past outputs, inputs and error terms, respectively, and are set as 10 to be the same conditions with other models.

Two cases of calibration (training) periods are considered in this study, and are set from 1961 to 2010 (Case 1) and from 1986 to 2010 (Case 2). The number of datasets in Case 1 and 2 are thus 18,253 and 9,122 for the respective training periods. The verification (prediction) period is set from 2011 to 2013 for both two training periods. The number of training is set as two hundred thousand. In CM 2, the number of pre-training is set as 3,000. The learning rate is set to be constant values of 0.001, 0.40 and 0.55 in this DNN model, CM 1 and CM 2, respectively.

4. RESULTS AND DISCUSSION

4.1 Statistical Performance Indices

In this study, the model effectiveness is assessed by three statistical indices: the root mean square error ($RMSE$), the correlation coefficient (R), and the coefficient of efficiency (E) proposed by Nash and Sutcliffe (1970). These equations are calculated as follows:

$$RMSE = \frac{\sqrt{\sum_t (Q^{com}(t) - Q^{obs}(t))^2}}{\sum_t Q^{obs}(t)} \quad (11)$$

$$R = \frac{\sum_t (Q^{obs}(t) - Q_m^{obs})(Q^{com}(t) - Q_m^{com})}{\sqrt{\sum_t (Q^{obs}(t) - Q_m^{obs})^2 \sum_t (Q^{com}(t) - Q_m^{com})^2}} \quad (12)$$

$$E = \frac{\sum_t (Q^{obs}(t) - Q_m^{obs})^2 - \sum_t (Q^{com}(t) - Q_m^{com})^2}{\sum_t (Q^{obs}(t) - Q_m^{obs})^2} \quad (13)$$

where $Q^{obs}(t)$ is the observed discharge at time t , $Q^{com}(t)$ the reproduced or predicted discharge at time t , N the total number of discharge data, Q_m^{obs} the mean observed discharge, Q_m^{com} the mean reproduced or predicted discharge.

4.2 Calibration Results

As calibration results, the mean values of the statistical indices for the models are summarized in Table 2. The minimum and maximum values of $RMSE$ are 14.9 m³/s in DNN model (Case 1) and 29.3 m³/s in CM 3 (Case 2). The minimum and maximum values of R are 84% in DNN model



(Case 2) and 210% in CM 1 (Case 1). The maximum and minimum values of E 0.856 in DNN model (Case 1) and 0.435 in CM 3 (Case 2).

4.3 Verification Results

As verification results, the mean values of the statistical indices for the models are summarized in Table 3. In verification, the number of training in DNN model, CM 1 and CM 2 are 143, 369 and 200, respectively, in Case 1, and 136, 115 and 39, respectively, in Case 2. In those number of training, prediction errors become the minimum. The minimum and maximum values of $RMSE$ are 22.0 m³/s in DNN model (Case 2) and 32.3 m³/s in CM 3 (Case 1). The minimum and maximum values of R are 90% in DNN model (Case 1) and 358% in CM 1 (Case 2). The maximum and minimum values of E 0.695 in DNN model (Case 2) and 0.408 in CM 3 (Case 1).

4.4 Discussion

From the calibration results, it is found that $RMSE$ -value and R -value are the smallest in DNN model, and E -value is the nearest to one in DNN model. This means that the error in DNN model is the smallest and that DNN model is the most accurate in all models which are applied. It is also found that training period does not influence on calibration results though it is expected that long training period increase model accuracy.

From the verification results, it is found that $RMSE$ -value and R -value are the smallest in DNN model, and E -value is the nearest to one in DNN model. This means that the error in DNN model is the smallest and that DNN model is the most accurate in all models which are applied. It is also found that training period does not influence on verification results though it is expected that long training period increase model accuracy.

TABLE 1: Statistical performance indices in calibration results

Model (Computational nodes)	Indices	Case 1	Case 2
DNN model (10-17-17-17-17-17-1)	$RMSE$ (m ³ /s)	14.9	16.3
	R (%)	109	84
	E (–)	0.856	0.824
CM 1 (10-7-5-3-1)	$RMSE$ (m ³ /s)	21.9	19.0
	R (%)	210	187
	E (–)	0.686	0.762
CM 2 (10-5-1)	$RMSE$ (m ³ /s)	20.4	17.8
	R (%)	180	171
	E (–)	0.728	0.792



CIGR 2018

XIX. World Congress of CIGR



CM 3	<i>RMSE</i> (m ³ /s)	20.5	29.3
(10-1)	<i>R</i> (%)	129	130
	<i>E</i> (–)	0.450	0.435

TABLE 2: Statistical performance indices in verification results

Model (Computational nodes)	Indices	Case 1	Case 2
DNN model (10-17-17-17-17-17-1)	<i>RMSE</i> (m ³ /s)	24.7	22.0
	<i>R</i> (%)	90	93
	<i>E</i> (–)	0.615	0.695
CM 1 (10-7-5-3-1)	<i>RMSE</i> (m ³ /s)	26.1	23.0
	<i>R</i> (%)	159	358
	<i>E</i> (–)	0.571	0.667
CM 2 (10-5-1)	<i>RMSE</i> (m ³ /s)	26.7	24.8
	<i>R</i> (%)	152	333
	<i>E</i> (–)	0.551	0.612
CM 3 (10-1)	<i>RMSE</i> (m ³ /s)	32.3	32.1
	<i>R</i> (%)	107	109
	<i>E</i> (–)	0.408	0.415

5. CONCLUSION

A DNN model without pre-training for runoff analysis is developed. Compared with the application results of conventional models, effectiveness of DNN model is assessed. For calibration and verification results, three statistical performance indices are shown. From the results, it is found that the error in DNN model is the smallest and that DNN model is the most accurate in all models. It is also found that training period considered in this study does not influence on calibration and verification results.

6. ACKNOWLEDGMENTS

This study is supported by JSPS 16H04997.

7. REFERENCES

- Abe, K., H. Kikuchi, K. Furukawa and Y. Shiotsuki. 2000. Study on a system of runoff (daily) analysis using neural network. *Journal of Japan Society Civil Engineering*, 656, II-52, 1-13 (In Japanese with English abstract).
- Bengio, Y., P. Lamblin, D. Popovici and H. Larochelle. 2006. Greedy layer-wise training of deep networks. In *Proc. Advances in Neural Information Processing Systems*, 19, 153-160.
- Izumi, T., A. Kan and N. Kobayashi. “A Deep Neural Network Model for Runoff Analysis”.



CIGR 2018

XIX. World Congress of CIGR



- Dawson C.W., and R. Wilby. 1998. An artificial neural network approach to rainfall-runoff modelling. *Hydrological Sciences*, 43(1), 47-66.
- Hsu, K., H.V. Gupta, and S. Sorooshian. 1995. Artificial neural network modeling of the rainfall-runoff process. *Water Resources Research*, 31(10), 2517-2530.
- Ishihara, Y. and S. Kobatake. 1979. Runoff model for flood forecasting. *Bull. Disaster Prevention Res. Inst., Kyoto Univ.*, 29, 27-43.
- Izumi, T., M. Miyoshi and N. Kobayashi. 2016. Runoff analysis using a deep neural network. In *Proc. 12th International Conference on Hydrosience & Engineering*, 173-176.
- Izumi, T. and N. Kobayashi. 2017. Runoff analysis model with a deep learning. In *Proc. 37th IAHR World Congress*, 3939-3945.
- Kamishima, T., H. Asho, M. Yasuda, S. Maeda, D. Okanohara, T. Okatani, Y. Kubo and D. Bollegala. 2015. *Deep Learning*. Kindaigaku-sha, 267pp.
- Kiyama, T., H. Toyama, K. Sasahara, S. Mama, M. Seki and H. Takemura. 2003. Basic study of the use of a neural network to predict flooding on the Abukuma River. *Advances in River Engineering*, 9, 173-178 (In Japanese with English abstract).
- LeCun, Y., Y. Bengio and G. Hinton. 2015. Deep Learning. *Nature*, 521, 436-444.
- Minns, A.W. and M.J. Hall. 1996. Artificial neural networks as rainfall-runoff models. *Hydrological Sciences*, 41(3), 399-417.
- Nash, J.E. and J.V. Sutcliffe. 1970. River flow forecasting through conceptual models part I — A discussion of principles. *Journal of Hydrology*, 10(3), 282-290.
- Okada, K., Y. Makihara, A. Jinbo, K. Ngata, M. Kunitugi and K. Saito. 2001. Soil water index. *Tenki*, 48(5), 349-356 (In Japanese).
- Rumelhart, D.E., G.E. Hinton and R.J. Williams. 1986. Learning representations by back-propagating errors. *Nature*, 323, 533-536.
- Sajikumar, N. and B.S. Thandaveswara. 1999. A non-linear rainfall-runoff model using an artificial neural network. *Journal of Hydrology*, 216, 32-55.
- Schmidhuber, J. 2015. Deep learning in neural networks: An overview. *Neural Networks*, 61, 85-117.



Physical Requirements for Vineyard Monitoring Robots

V. Saiz-Rubio^{1a}, M.P. Diago², F. Rovira-Más¹, A. Cuenca¹, S. Gutiérrez², J. Tardáguila²

¹ Agricultural Robotics Laboratory, Universitat Politècnica de Valencia, Valencia, Spain

² Televitis, Universidad de La Rioja, Logroño, Spain

vesairu@upv.es

ABSTRACT

The global market for service robots is steadily growing, and its growth is expected to sky-rise in the next two decades. Among them, agricultural robots in particular are getting much attention for the actual benefits of automating repetitive tasks in harsh, low-populated environments. However, endowing agricultural equipment with autonomous navigation involves overcoming a series of reliability and safeguarding challenges of difficult solution. To face them, the VineScout project, an EU-funded initiative that features an industry-academia consortium of five partners, has committed to design a market-ready monitoring robot for the wine industry by 2020. The new robot follows a user-centered design according to the instructions given by the project end-user. The VineScout concept departs from a Technology Readiness Level (TRL) of 6/7, and is expected to reach the commercial stage at TRL 9. The vineyard robot weighs 100 kg, and has been conceived to be cost-efficient and energy-saving, with only electric drives, lithium batteries, and solar panels. This paper describes the advances carried out during the first year of the project, where a compact design has been proposed to protect internal electronics, and a 4-wheel independent suspension system with customized springs assures the necessary agility to monitor vineyards at a rate of one hectare per hour. Preliminary rolling and vehicle dynamics results obtained after testing the prototype in the university experimental vineyard demonstrate that the robot is ready for the intense data acquisition season of the summer of 2018 in a Portuguese commercial vineyard.

Keywords: Autonomous navigation, agricultural robots, vineyard monitoring, proximal sensing, robot architecture, precision agriculture

INTRODUCTION

There exist information on economic data that prove that robotics is clearly a growing economy, where the growth of service robots is expected to sky-rise in the next decade. Autonomous vacuum cleaners have already seen several generations over the last ten years, and their sales have been growing since the first machine was manufactured. Its success roots in the competitive price, which is quite comparable to regular high-performance vacuum cleaners, and the fact that it offers a technology that easily merges with daily life. Of course, the hazard posed by a small robot like this is low, but taking an autonomous machine to the outdoors where the environment is harsh, unpredictable, and typically of large dimensions, is something radically different. Nonetheless, expectations are high, and there already exist solutions for open spaces. Naturally,



these are limited, totally controlled spaces such as private courtyards, but they imply a step ahead in automation and artificial intelligence. According to the *Global Agricultural Robots Market Professional Survey Report 2017*, the major field robotics players in the global agriculture market are Harvest Automation Inc. (USA), Clearpath Robotics (Canada), PrecisionHawk Inc. (USA), Naïo Technologies (France), SenseFly SA (Switzerland), and Shibuya Seiki (Japan). Under the generic category of “Agricultural Robots”, the following possibilities are typically included: unmanned aerial vehicles (UAV), driverless tractors, milking robots, automated harvesting machines, and unmanned ground vehicles (UGV). Following *Research Nester report* (www.researchnester.com), automated solutions can be classified on the basis of end-user applications as field farming, dairy management, indoor farming, horticulture, and other applications. For VineScout project, only field farming is to be considered, although certain operations in horticulture could benefit from the technology developed in the VineScout project. The VineScout monitoring robot is being designed to provide the water status of vines in real time. This will allow end-users to track this key parameter as often as it deem appropriate for the management of their vineyards.

This paper describes the advances carried out during the first year of the project, where a compact design has been proposed to protect internal electronics, and a 4-wheel independent suspension system with customized springs assures the necessary agility to monitor vineyards at a target rate of one hectare per hour.

2. PROPOSED SOLUTION

VineScout project, an EU-funded initiative that features an industry-academia consortium of five partners, has committed to design a market-ready monitoring robot for the wine industry by 2020. Regarding the optimization of its mechanical design and external appearance, the robot needs to adapt to the harsh working conditions in the field. Traction abilities and power sufficiency are crucial features. The design of figure 1a was VineScout first version that has been modified to a more compact design (figure 1b) in its new second version. This last version and its compact design has favored to ease autonomous driving, and to protect internal electronics.

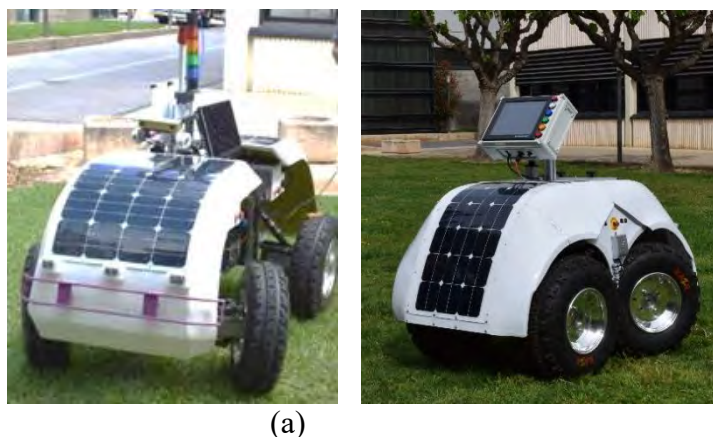


Figure 1. External design for VineScout robot first version (a), and compact design for the second version (b).



Regarding the suspension system, the springs were also modified and have been calculated for a better shock absorbance, with a constant K equal to $1 \text{ kg} \cdot \text{mm}$ for a more stable performance. The specifications of the springs are 170 mm long, 50 mm of the spiral external diameter, 5.5 mm spiral internal diameter (thickness) and 12 coils.

The propelling system consists of a four independent electrical motors each one powering one of the four wheels of the robot. A fifth electrical motor is linked to a pinion-rack (figure 2) that executes the steering commands through the front wheels. A linear potentiometer was connected to the steering mechanism (tie rod) to estimate the actual angle turned by the front wheels (Ackerman angle) in real time. After carrying out some preliminary tests to validate the geometry, the robot's steering dimensions for the last prototype are:

Steering rods: 190 mm.

The useful rack length: 160 mm.

Distance between holes in the rack (supports of the steering rods): 233 mm.

Self-lubricated guiding, providing softness and durability

Tough end-of-stroke plaques

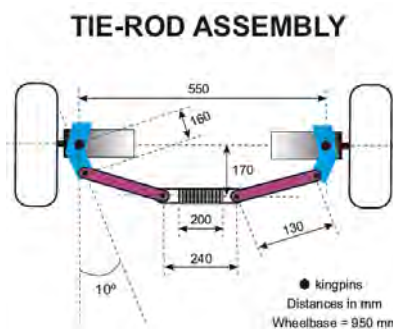


Figure 2. Pinion-rack system

The behavior achieved can be compared to the effect of a MacPherson strut suspension (Gillespie, 1992), but with no viscous damper and a severe inclination angle for the coil spring.

The steering structure in the robot was designed based on the steering system described in Rovira-Mas, Millot & Saiz-Rubio (2015), and Saiz-Rubio, Rovira-Mas, & Millot (2017) to assure agility at the headland turn.

The navigation systems is divided into two exclusive modes: in-row guidance and headland turning. The former relies on a stereoscopic camera assisted by a non-rotational LIDAR (Pepperl+Fuchs, Mannheim, Germany) and short-range sonars facing sideways (Maxbotix, Brainerd, Minnesota, USA). The latter uses the LIDAR rangefinder and lateral sonars in addition to occasional dead-reckoning when negotiating the 180-degree turn. Safeguarding is achieved contactless with the LIDAR rangefinder, and in case of failure a mechanical feeler and a network of 3 emergency stops strategically spaced, one being in the control console.

The robot is also equipped with a non-invasive thermal radiometer Apogee SI-121 (Apogee Instruments, Inc, North Logan, Utah, USA). The sensor has a field of view of 36° that, at 1 m, is able to measure an area of 0.332 m^2 . This target area is a circle from which 98 percent of the radiation is captured by the detector. Therefore, the thermal radiometer is pointed directly to the



grapevine canopy to make temperature readings from the leaves. It has been widely acknowledged that grapevine water status is notably related to canopy temperature, since during leaf transpiration, there is an inverse correlation between water loss through stomata and leaf temperature. For this reason, adding a thermal sensor to the robot makes it capable of infer the vineyard water status, a key trait in grapevines.

3. RESULTS

Preliminary rolling and vehicle dynamics results obtained after testing the second prototype in the campus experimental vineyard demonstrate that the robot is ready for the intense data acquisition season in the summer of 2018 in a commercial vineyard. However, to demonstrate the usefulness of this unmanned ground vehicle, UGV, it was tested in Portuguese commercial vineyards. The field trials took place in Quinta do Ataíde, Portugal (Coordinates: 41.24484041 North, 7.114694504 West) on 29-30 August 2017. The robot went through the vineyard rows autonomously driven, except for the headland turns, which were done manually with a joystick linked to the robot. The infrared radiometer was located on the robot's pole, facing to one side of the vineyard canopy. The sensor took data while the robot was moving forward through the field at approximately 1 km/h. Once the robot scanned around great part of the field, temperature data were retrieved. The temperature map registered during the experimental session is shown in figure 3.

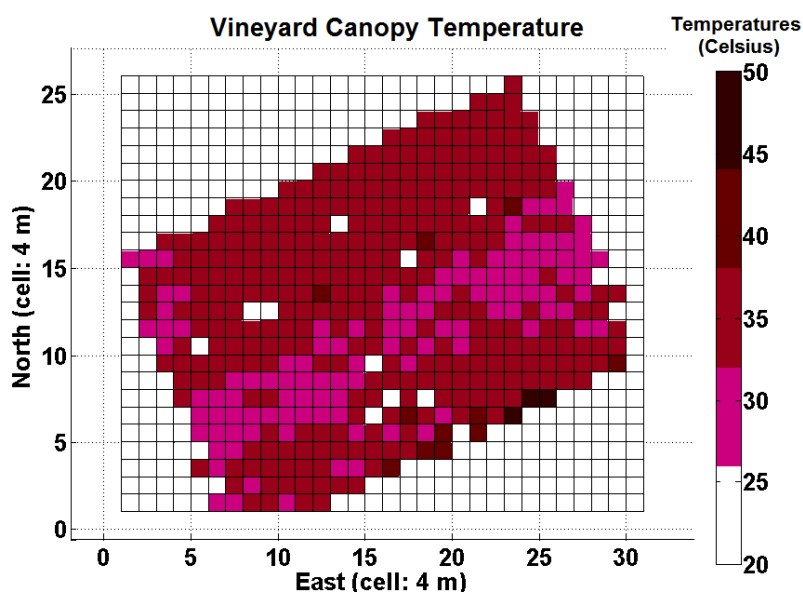


Figure 3. Temperature map of a vineyard field in Quinta do Ataíde, Portugal, built with data retrieved from VineScout robot and the Apogee sensor.

4. CONCLUSIONS



CIGR 2018

XIX. World Congress of CIGR



The VineScout robot, an Unmanned Ground Vehicle (UGV), has been built for scouting vineyard fields and retrieving key agronomical data. The first prototype was autonomously driven within the rows, and manually operated to change rows. These preliminary tests showed good behavior for difficult terrains in self-guided mode. To demonstrate that the robot can deliver field data and be functional, an infrared radiometer was placed on the robot to take temperature information from the canopy and display it in maps.

The second VineScout prototype was improved respect the first version in terms of steering and suspension systems, autonomous navigation, and safety. This version will be fully tested in summer 2018.

Future steps will be adjusting parameters in the autonomous driving when turning in the headlands. Also, a longer separation between wheels axes will be considered for a future prototype to ease the robot's behavior when encountering big stones in the terrain.

5. REFERENCES

Gillespie, T. (1992). *Fundamentals of vehicles dynamics*. Warrendale, PA.: Society of Automotive Engineers, Inc.

Rovira-Mas, F., Millot, C., & Saiz-Rubio, V. (s.f.). *Navigation strategies for a vineyard robot*. ASABE Paper No. 152189750. St. Joseph, Mich.: ASABE.

Saiz-Rubio, V., Rovira-Mas, F., & Millot, C. (2017). Performance Improvement of a Vineyard Robot through its Mechanical Design ASABE Paper No.1701120. St. Joseph, MI.: ASABE.

6. ACKNOWLEDGEMENTS

This research article is part of a project that has received funding from the European Union's Horizon 2020 research and innovation programme under grant agreement N°737669. The opinions expressed reflect only the authors' view. Neither the European Commission, nor the funding agency, nor its services are responsible for any use that may be made of the information this publication contains.



Database of Traction Indicators of Domestic and Foreign Tractors for OECD and ISO Systems.

Izmailov A. Yu.¹, Moskovskiy M.N.¹, , Lavrov A.V.¹, Shevtsov V.G.¹

¹Federal Scientific Budget State Institution Federal State Agricultural Center VIM, Moscow, Russia.

Keywords: rolling resistance coefficient, agricultural tractor, database, traction tests, matching technique, ground.

INTRODUCTION

Now days there are more 100 models of imported tractors [1] in the Russian market it is necessary to consider their characteristics, which on the one hand would be obtained in comparable conditions, and at the same time, made it possible to evaluate the effectiveness of using these models in specific national conditions. At first, it should include traction indicators of agricultural tractors to these characteristics. It is necessary to analyze two tractor test systems, which can be called the European one, based on ISO standards, and the second, which has found international recognition, on the basis of «OECD STANDARD CODES FOR THE OFFICIAL TESTING OF AGRICULTURAL AND FORESTRY TRACTOR» CODE 2 [2].

The aim does not contradict the current practice, a similar task, without correlation with traction classes, was solved in Research Institute "RosNIITM" [3, 4, 5]. However, in our formulation, it is necessary to more strictly assess the discrepancies between GOST (ISO) and the OECD Tractor Code 2.

The database of agricultural tractors traction indicators is developed to harmonization the ISO and OECD standards, as well as for predicting the performance indicators MTU (machine tractors unit) with foreign tractors in the Russian economic conditions. For rational aggregation of foreign tractors with an evaluation of traction properties on the concrete, we provides the design characteristics related to the stubble in our database.



CIGR 2018

XIX. World Congress of CIGR



For Russian tractors, which have protocol dates of traction indicators on the stubble, it was calculated characteristics on concrete, which allows comparison with foreign models on the Russian market [6, 7].

MATERIALS AND METHODS

We are considered the results of traction tests recorded in the test reports of the OECD and ISO as source information. The order of research of the traction indicators determination according to the OECD standard [8, 9].

The peculiarity of Russia is the simultaneous application in relation to the testing of tractors in Interstate standards adopted in the different countries (the Republic of Azerbaijan; Republic of Armenia; Republic of Belarus; Georgia; The Republic of Kazakhstan; Republic of Kyrgyzstan; The Republic of Moldova; Russian Federation; The Republic of Tajikistan; Turkmenistan; The Republic of Uzbekistan; Ukraine) harmonized with ISO-789 standards and State Standards (GOST):

- GOST 7057-2001 «Agricultural tractors. Test methods». Instead, GOST 7057-81. Date of introduction - 01/01/2003;
- GOST 30745-2001 (ISO 789-9-90) «Agricultural tractors. Definition of traction indicators». Introduction date - 01.01.2003;
- GOST 30747-2001 (ISO 789-1-90) «Agricultural tractors. Definition of indicators testing through a power take-off shaft» Introduction date - 01.01.2003;

The general methodology of harmonization includes the following stages:

- analysis of available protocol materials based on the results of traction tests according to OECD and ISO standards;
- design algorithm to bring the results of determining the maximum power on the coupling device according to the OECD standard to the indicators of the traction-power classification of the type of tractors in Russia;
- design database of traction indicators of Russian and foreign agricultural tractors defined by the International (ISO) and OECD.



RESULTS OF RESEARCHES

Algorithm of determination of the maximum power on the drawbar device to the indicators of the traction-power classification of the tractors type in Russia, taking into account the background during the tests and the type of engine-transmission unit

Design the algorithm of the traction indicators of a wheeled tractor measured on concrete according to the OECD standard, we applied the index «b», and the index «c» to the traction indicators on the stubble. Consider algorithm based on the analysis of forces and power flows in Fig. 1.

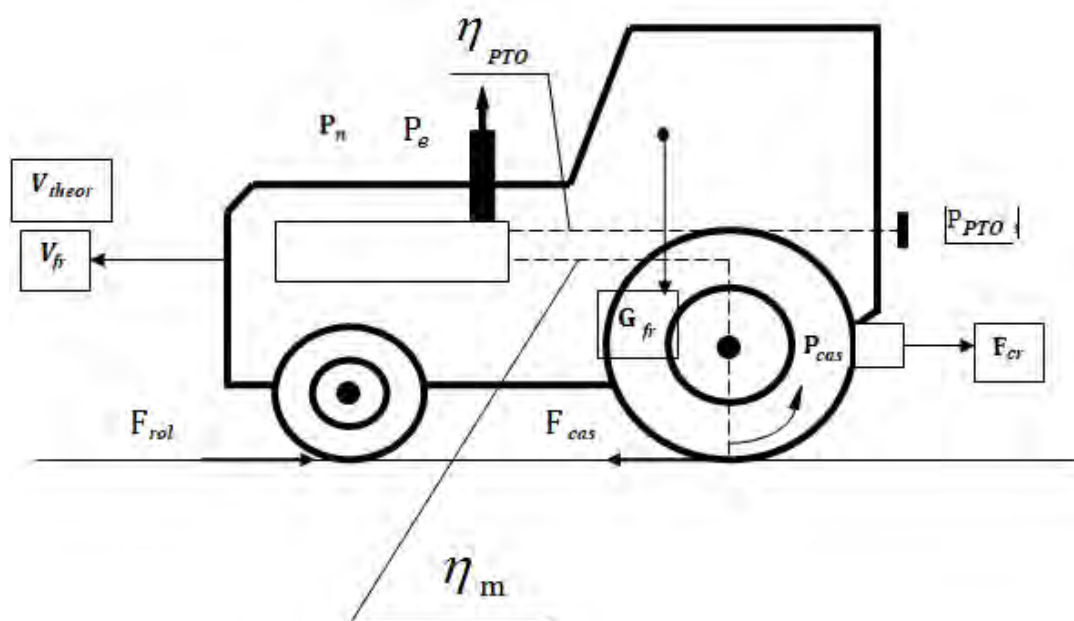


Figure 1 - Scheme of forces and power flows acting on the tractor with traction tests

Measuring indicators according to the OECD standard are given in the test protocol at maximum pulling power:

- V_{tr}^c traction on the hook;
- v_{tr} working speed;



CIGR 2018

XIX. World Congress of CIGR



- theoretical speed;

- G_{tr}^c tractor drawbar weight;

- δ skidding $\left(\eta_{\delta}^c = \frac{100 - \delta}{100}\right)$;

- P_p nominal engine power.

($P_e = 0,9$; P_p – operational engine power. $P_e = \frac{P_{PTO}}{\eta_{PTO}}$).

Required to determine for the conditions on the stubble:

$$F_{kp}^c, V_{tr}^c, P_{kp}^c, \eta_{tr}^c \text{ при } \delta^c = 15\% \left(\eta_{\delta}^c = 0,85\right),$$

and equal theoretical speeds:

$$V_{theor.}^c = \frac{V_{tr}^c}{\eta_{\delta}^c} = \frac{V_{tr}^s}{\eta_{\delta}^s} \text{ или } \frac{V_{tr}^c}{1 - \delta^c} = \frac{V_{tr}^s}{1 - \delta^s}, \text{ where}$$

1) Determination of speed on the stubble.

$$V_{tr}^s = \frac{V_{tr}^c}{\eta_{\delta}^c} \cdot \eta_{\delta}^s = \frac{V_{tr}^c}{(1 - \delta^c)} \cdot (1 - \delta^s) = 0,85 \frac{V_{tr}^c}{1 - \delta^s} \quad (1)$$

2) Definition of tractive force on stubble.

From the equation of traction power on the stubble:

$$F_{cr}^s \cdot V_{tr}^s = N_{cas} \cdot \eta_{\delta}^s - F_{rol}^s \cdot V_{tr}^s,$$

get traction:

$$F_{cr}^s = \frac{N_{cas} \cdot \eta_{\delta}^s - F_{rol}^s \cdot V_{tr}^s}{V_{tr}^s}, \quad (2)$$

From the equation of traction power on asphalt concrete



CIGR 2018

XIX. World Congress of CIGR



$$N_{\text{cas}} = \frac{F_{\text{cr}}^c \cdot V_{\text{fr}}^c + F_{\text{rol}}^c \cdot V_{\text{fr}}^c}{\eta_{\delta}^c} \quad (3)$$

Substituting (3) and (1) in (2), we get:

$$F_{\text{cr}}^s = \frac{\left(\frac{F_{\text{cr}}^c \cdot V_{\text{fr}}^c + F_{\text{rol}}^c \cdot V_{\text{fr}}^c}{\eta_{\delta}^c} \right) \cdot \eta_{\delta}^s - F_{\text{rol}}^s \cdot \frac{V_{\text{tr}}^c}{\eta_{\delta}^c} \cdot \eta_{\delta}^s}{\frac{V_{\text{fr}}^c}{\eta_{\delta}^c} \cdot \eta_{\delta}^s}$$

or

$$F_{\text{cr}}^s = F_{\text{cr}}^c + F_{\text{rol}}^c - F_{\text{fr}}^s; \quad \text{or} \quad F_{\text{rol}}^c = G_{\text{fr}} \cdot f_c; \quad F_{\text{rol}}^s = G_{\text{fr}} \cdot f_s.$$

$$F_{\text{cr}}^s = F_{\text{cr}}^c - G_{\text{fr}} (f_s - f_c), \quad (4)$$

где: f_c ; f_s - accordingly, the rolling resistance coefficient of the tractor on asphalt concrete and stubble.

Rolling resistance coefficients

Type of covering	Wheel tractor	Caterpillar tractor
Concrete	0,018	0,035...0,045
Stubble	0,10...0,12	0,07...0,08

For wheel tractor: при $f_c=0,11$ $f_s=0,018$ $F_{\text{cr}}^s = F_{\text{cr}}^c - 0,092 G_{\text{tr}}$.

For caterpillar tractor: при $f_c=0,075$ $f_s=0,04$ $F_{\text{cr}}^s = F_{\text{cr}}^c - 0,035 G_{\text{tr}}$.

3) Determination of traction power on the stubble.

$$P_{\text{cr}}^s = F_{\text{cr}}^s \cdot V_{\text{tr}}^s = \left[F_{\text{cr}}^c - G_{\text{t}} (f_s - f_c) \right] \cdot \frac{V_{\text{tr}}^c}{\eta_{\delta}^c} \cdot \eta_{\delta}^s.$$

for $\delta^s=15\%$; $\eta_{\delta}^s=0,85$.



CIGR 2018

XIX. World Congress of CIGR



$$P_{cr}^c = 0,85 \cdot \left[F_{cr}^{\delta} - G_t (f_s - f_c) \right] \cdot \frac{V_{tr}^c}{\eta_{\delta}^c}.$$

4) Determination of conditional traction efficiency on the stubble. $\eta_{tr}^c = \frac{P_{cr}^c}{P_e} = \frac{P_{cr}^c}{P_p \cdot 0,9}.$

Database of russian and foreign agricultural tractors defined by Interstate (ISO) and OECD standards

As a result of data processing of test protocols on the concrete and the stubble, and calculations carried out according to the method of harmonization of traction indicators of OECD and ISO test standards. It was designed the database «Traction indicators of russian and foreign tractors by Interstate (ISO) and OECD standards at maximum engine power» [10]. It contains 5 information blocks and a control block which allow to apply a number of information requests (by operating weight, maximum traction power, etc.).

It was designed the following database structure in connection with the tasks (Figure 2).

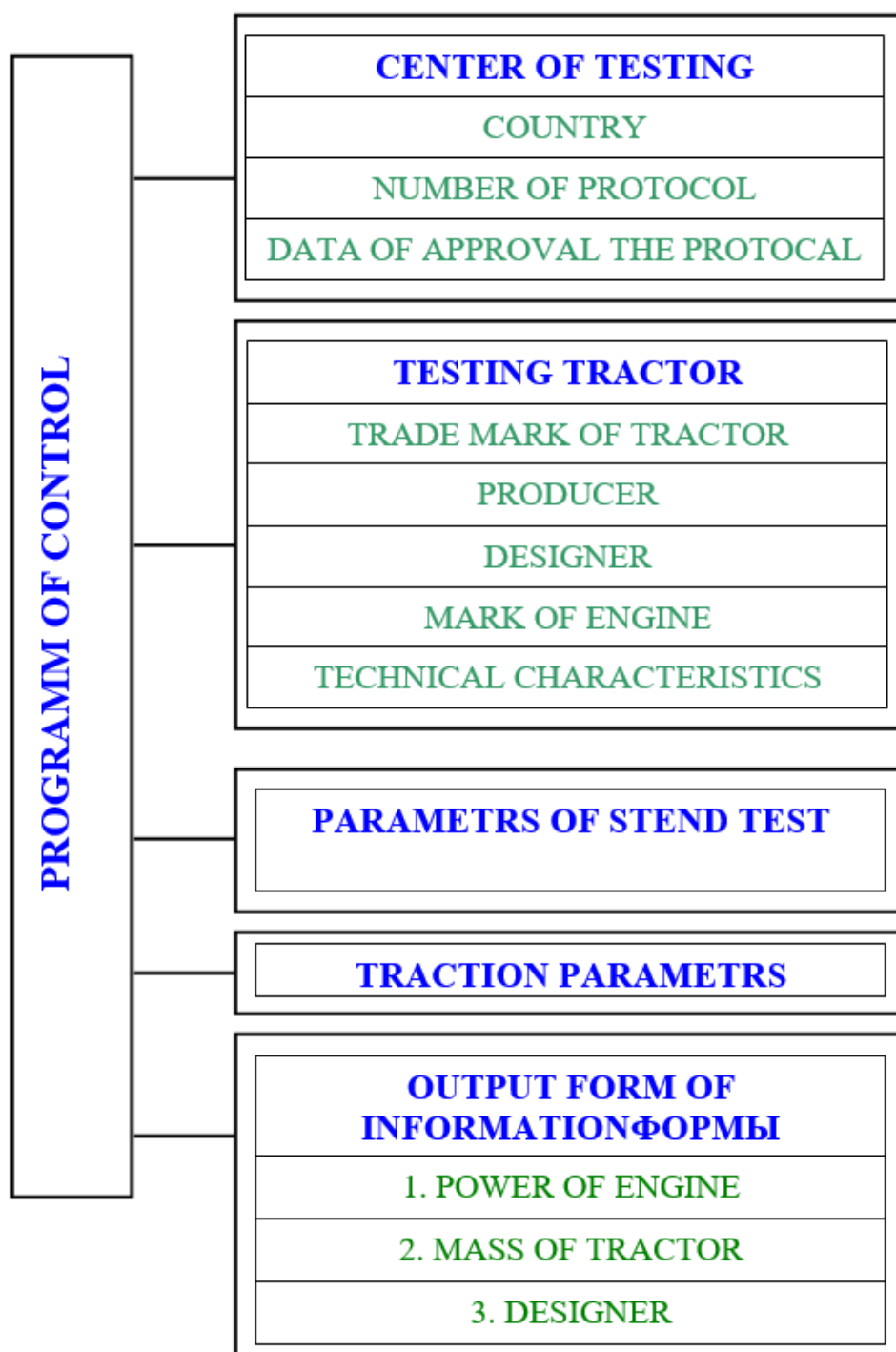


Figure 2 - Block structure of the database of traction indicators of russian and foreign agricultural tractors, defined by the Interstate (ISO) and OECD standards for the maximum operating power of the engine



CIGR 2018

XIX. World Congress of CIGR



The database contains information about results of official agricultural tractors tests according to OECD standards in Germany (11 models), France (8 models), Italy (8 models), and also Austria, India, and the Republic of Korea (only 37 models), each on 2 covering: concrete and stubble, as well as the classification of tractors for pulling force.

The block management program allows to calculate the required traction indicators, as well as to make a request to the database in the form of a comparative table with traction indicators on agricultural stubble and concrete.

An example of the calculation of traction indicators of the Massey Fergusson agricultural tractor on the stubble is shown in Table 2.

Table 2 - The results of traction tests according to the OECD standard and the results of theoretical calculations of the traction parameters for coordination with the ISO standard

Number of indicator	Indicators	Trade tractor mark			
		Massey Fergusson			
		Stubble (ISO)	Concrete Code2 (OECD)	Stubble (ISO)	Concrete Code2 (OECD)
		Number of protocol			
1	2	3	4	5	6
1	Country		Protocol		France
2	Test centre		Protocol		CEMAGREF, Antony
3	Number of protocol	Evaluating	Protocol	DESIGN	16551
4	Data of approval protocol		Protocol		16.11.2010
5	Production firm		1.1		AGCO S.A.
6	Designed firm		1.1		
7	Type of tractor		1.1		4WD
8	Type of engine				SISU/AGCO POWER Inc. 66.633CTA-4V/Diesel
9	Power at PTO at nominal engine speed, kW		3.1.2		80,4
10	Rated engine speed		3.1.2		2200
11	The volume of developments, m h				
12	Maximum power at PTO, kW, P_{BOM}^{max}		3.1.1		94,0

Izmailov A. Yu., Moskovskiy M.N., , Lavrov A.V., Shevtsov V.G. "Database of Traction Indicators of Domestic and Foreign Tractors for OECD and ISO Systems"



CIGR 2018

XIX. World Congress of CIGR



13	Rotational speed, min ⁻¹	Engine crankshaft, $n_{\text{ДВОМ}}$		3.1.1		2000
14		PTO, $\eta_{\text{ВОМ}}$		3.1.1		983
15	Transmission efficiency from engine to PTO accepted				0,93	0,93
16	Maximum engine operating power, kW $P_{\text{еэ}}^{\text{max}}$				101,1	101,1
17	Transmission type			1.3		Hidrostatic variable cylinder in the both ways with two mechanical ranges
18	Tractor operating weight, kg, mte			2.3	7235	7235
19	Tire model	- front wheels		2.6		GOODYEAR TM 818
20		-the rear wheels		2.6		GOODYEAR TM 818
21	Tire size	- front wheels				540/65R28
22		-the rear wheels				650/65R38
23	Tire pressure, MPa	- front wheels		2.6		0,16
24		-the rear wheels		2.6		0,16
25	Transfer number			3.3.1		T5
26	Maximum traction power, kW $P_{\text{кр}}^{\text{max}}$			3.3.1	53,97	78,6
27	Traction effort, kN			3.3.1	23,55	30,2
28	Speed km / h			3.3.1	8,25	9,37
29	Engine crankshaft speed, min ⁻¹ , $n_{\text{ДЛЯГ}}$			3.3.1	2000	2000
30	Skidding, %, δ			3.3.1	15	3,5
31	Specific fuel consumption, g / kW · h, q			3.3.1	439,8	302
32	Transmission efficiency (grade for concrete), η_{TP}				0,840	0,840
33	Conditional Traction Efficiency, $\eta_{\text{ТУ}}$				0,534	0,777
34	Traction class				2	
35	ISO Rear Mounted Category			1.6		CAT 3
36	Maximum lifting force of the rear hinged system, kN			3.2.2		60,8

Based on the results of the research, proposals were submitted to the OECD Committee for the harmonization of ISO and OECD Standards in relation to the determination of tractive indicators for agricultural tractors according to agreed methods.

4. CONCLUSION

Izmailov A. Yu., Moskovskiy M.N., , Lavrov A.V., Shevtsov V.G. "Database of Traction Indicators of Domestic and Foreign Tractors for OECD and ISO Systems"



CIGR 2018

XIX. World Congress of CIGR



1. Methodology for harmonizing traction indicators of domestic and foreign tractors has been developed, which for the first time provides an agreed assessment of their characteristics according to the CODE 2 OECD standard on concrete and according to the International Standard GOST 30745-2001 (ISO 789-9-90) on stubble with classification according to traction classes in accordance with GOST 27021.
2. Database of the results of traction calculations carried out according to ISO and OECD standards, obtained by theoretical and experimental methods, was developed.
3. The classification of foreign tractors according to traction classes allows us to recommend the use of sets of machines for the rational use of foreign tractors in accordance with the traction classes listed in the System of Machines and Technologies.
4. In the future, it is planned to prepare proposals on the basis of the developed database on harmonization of the OECD and Russian Federation standards for determining traction indicators of agricultural tractors.

REFERENCES

- Kryazhkov V.M., Shevtsov V.G., Gurylev G.S., Lavrov A.V. Market analysis of agricultural tractors in Russia in 2008-2013 // Agricultural machines and technologies. - 2014. - № 5. - p. 12-16.
- CODE 2. OECD STANDARD CODE FOR THE OFFICIAL TESTING OF AGRICULTURAL AND FORESTRY TRACTOR PERFORMANCE.
- Polyakov O.Ya., Shilin V.E., Denyak S.M. Traction performance tractors firm "MASSEY FERGUSON" Series 8200 // Collection of works KubNIITM, Novokubansk, 2003.
- Tabashnikov, A.T., Polyakov, O.A. / Indicators of tractors of foreign firms according to tests conducted in 2000–2006. in accordance with the methodology of the OECD standard, Code 1 and 2 / Informational and analytical review // Novokubansk: FGNU "RosNIITM", 2006. - 69 p.
- Polyakov O.A., Tarnievsky V.E., Shilin V.S., Dyanyak S.M. Methods for determining the performance properties of tractors according to the traction tests carried out according to the OECD standard // Collected Works KubNITiM, Novokubansk, 2000.
- Kryazhkov V.M., Godzhaev Z.A., Shevtsov V.G., Gurylev V.G., Lavrov A.V. Park of tractors: state and directions of development // Rural mechanization. - 2015. - №9. - pp. 3-5.
- The Development of the Russian Agricultural Tractor Market from 2008 to 2014. Shevtsov V., Lavrov A., Godzhaev Z., Kryazhkov V., Gurulev G. SAE Technical Papers. 2016. doi: 10.4271 / 2016-01-8128.
-
- Izmailov A. Yu., Moskovskiy M.N., , Lavrov A.V., Shevtsov V.G. "Database of Traction Indicators of Domestic and Foreign Tractors for OECD and ISO Systems"



CIGR 2018

XIX. World Congress of CIGR



Luis Márques, Dr. Ing. Agrónomo. TRACTORES AGRIOLAS: TECNOLOGIA Y UTILIZACIÓN. Impreso en España, Depósito Legal: M-2075-2012.

NEBRASKA OECD TRACTOR TEST 1997-SUMMARY 778 VERSATILE 305 DIESEL 16 SPEED.

Database "Traction indicators of domestic and foreign tractors, defined by the International (ISO) and OECD standards at the maximum operating engine power" [Text] // VG. Shevtsov, O.S. Marchenko, A.V. Lavrov, A.A. Soloveitchik, A.Kh. Tekushev, V.V. Fedyunin, E.P. Seleznev / Database Registration Certificate No. 2014620063, the date of registration is 09/01/2014.



Effect of Top Cutting Height of Cotton Stalk On Cotton Yield

F. Göksel Pekitkan ¹,

Reşat Esgici ²

Abdullah Sessiz ^{1*}

¹ Dicle University, Faculty of Agriculture, Department of Agricultural Machinery and Technologies Engineering, Diyarbakir, Turkey

² Dicle University, Bismil Vocational High School, Diyarbakir, Turkey

* Corresponding author e-mail: asessiz@dicle.edu.tr

ABSTRACT

The objective of this study was to determine the effect of top cutting height of cotton stalk on cotton (*Gossypium hirsutum* L.) yield and cutting properties such as cutting force and cutting strength. The cutting tests materials were obtained from experimental field from the different top cut heights of cotton stalk. Cutting test was made by Instrument test machine in laboratory. The results of an analysis of variance showed that the effect of top cutting height of cotton stalk was found to be significant on cotton yield and cutting properties of cotton stalk. The differences between cutting top heights and other applications (control and pix application) were found to be significant according to yield. On the other hand, maximum cotton yield were obtained at pix chemical application as 6.440 kg ha⁻¹ and the lowest yield were obtained at 20 cm cutting top height as 5.316 kg ha⁻¹.

Keywords: Cotton, yield, cutting force, shearing force, stalk topping.

INTRODUCTION

Cotton (*Gossypium hirsutum* L.) is known as white gold and it is one of the most important commercial crops in Worldwide. One of the important producing countries is Turkey. Turkey is Europe's largest textile manufacturer and it is the seventh largest producer of cotton in the world. So, cotton and cotton based industry is importance for Turkey and the world. In Turkey, cotton is cultivated primarily in the Aegean Region, Çukurova Basin and Southeast Anatolia Region. Southeast Anatolia Region is known as GAP. With GAP (Southeastern Anatolian Project) irrigation project in Turkey, the irrigated farmland and in terms of total production, planting area and cotton yield in Southeast Anatolia region (Diyarbakır, Şanlıurfa, Mardin and Batman Provinces) has increased rapidly since 2000 year. That is, cotton production area was shift from Aegean and Çukurova region to Southeastern Anatolia region. Nowadays, more than half of the national cotton production is produces from Southeastern Anatolia region. This situation has led to the considerable development of industries based on cotton in the region (Sessiz and Esgici 2015). This production ratio in region is important for region's development, human resources development and rural development. Therefore, cotton has a strategic importance for the region's, Turkey's economy and even the development of world textile industry. However, from sowing to ginning stages, many cultural operations are made. During this stages, production costs and time consumption is very high. So, for the sustainability of the cotton production, we have to increase the ratio of cotton production and cotton yield, reduce of production costs, improve profits, reducing of cotton losses and protection of fiber quality. However, the farmers in region still use human labour for many of the operations like top cutting height and picking for these operations. In addition to conventional operations, cotton topping is another cultural



practice that should be done during the vegetation period (Aydin and Arslan 2018). Almost all cotton top cutting height is made by hand. Therefore, the production cost is very high depending on cultural application during the production season. Production costs can be decreased and profits can be increased by mechanization. Therefore mechanization in cotton cultivation will play a key role in keeping the cost under control. Additionally, there will be productivity increase driven by high density planting. Especially, the cotton production costs are considerably high in harvesting and cutting of plant topping section. It has been reported by cotton producers that the top cutting of cotton the stalks operation is directly related to increase the yield, quality of cotton lint and reduces bollworm infestations without negatively affecting cotton yields. The similar results were reported by Obasi and Msaakpa (2005), Yang et al. (2008), Renou et al. (2011) and Aydin and Arslan (2018). According to these researchers, the cutting of top section of cotton plants increases the yield and quality of cotton and improves the earliness, limiting the vegetative growth of the plant and improving the development of generative organs of the cotton plants. At present, chemical topping technology is being used instead of mechanical application and worker in some cotton production country. Chemical topping inhibits the growth of stem tops by means of plant growth regulators instead of the manual removal of stem tops. Chemical topping reduces labor costs and improves labor productivity relative to hand topping, and is the inevitable trend of a fully mechanized cotton planting system. Manual topping only removes the top of main stem, while chemical topping inhibits the growth of the top of the main stem, and the growth and development of the lateral branches and leaves are also subject to a certain degree of inhibition. Therefore, it is necessary to further study the mechanisms of cotton chemical capping and its influence on the agronomic traits of cotton in order to master the appropriate spraying time and dosage, thereby speeding up the development of chemical topping specifications (Feng et al. 2017). However, we are well known that there are many negative effect of chemistry on human, animal and nature environment. Therefore, we need to use of mechanical equipment instead of chemicals.

Cotton Farmers in region are interested to mechanize cotton shoots for topping but have limited information and knowledge about mechanization process. To design a new stalk cutter or chopper, the first step is to measure cutting force of cotton stalk depending on cross-section area (cutting height). Cutting forces required to cut plant materials play a significant role in determine the power requirements of the process under given conditions and designing energy efficient equipment (Persson 1987, Srivastava et al. 2006, Ghahraei et al. 2011, Kusinska and Starek 2012, Mathanker et al. 2015).

The objectives of this study was (1) to determine cutting force and cutting strength depend on cross-section area of cotton stalk (topping height) and (2) to determine the relationship between top cutting height and cotton yield. Therefore, cutting tests were carried out at 5 cm intervals four different hight from the top of the plant toward to the bottom.

MATERIALS AND METHODS

This study was carried out in two stages, field experiments and laboratory experiments. In the first stage of the experiment, the relationship between top cutting height of cotton stalk and cotton lint yield were determined. In the second phase of the experiment, the effect of plant top cutting height (cross-section area) on stalk cutting force and cutting strength were determined.

Field Studies

The field experiment was conducted at a commercial farm in 2017 during the growing season at the Bismil district, Diyarbakır province (latitude 37°53'N and longitude 40°16'E, 680 m altitude), Southeast part of Turkey. In this study, the BA-440 cotton variety was planted on 12 April in 2017 by four-row a pneumatic planter under irrigated conditions. A randomized complete block design with three replications was used in this study. Experimental area consisted of 18 plots with each measuring 12 m x 6 m with an inter row spacing of 0.7 m distance.

Top cutting operations of cotton plant were made in twelve plots in order to determine the effect of top cutting height on yield. Cutting operations and other applications were conducted during the vegetation period. The top cutting operations were done for each height (0-5, 5-10, 10-15, 15-20 cm) in three plots of all plants before opening the cotton bolls, also for compare the applications, any application was not made in three plots for control, on the other hand, pix chemical application were made in three plots.

From soil tillage until cotton harvesting, the same cultural applications such as practices of irrigation, fertilization, pesticide were conducted for all plots during the growing season.

The cotton in all experiment plots were harvested by hand in order determines the relationship between top cutting height and cotton lint yield. Top cutting operations were conducted in twelve plots.

Laboratory Study

As you know, the cross-sectional area of the cotton stalks reduced gradually from the bottom to the top of the stalk. The top cutting operations were done from 4 different heights (at 5 cm intervals from top to down) of plant before opening the cotton bolls. The cotton stalk specimens for cutting tests were obtained from whole cotton plants randomly selected three different locations at the experimental field, uprooted from soil surface and then transported to the laboratory. Then, the leaves were removed from the plants in the laboratory. Prior to the tests, the samples were taken from the top of cotton plants toward the plant bottom (Fig. 1) into four different groups according to top cutting heights, namely at 0-5 cm, 5-10 cm, 10-15 cm and 15-20 cm. During the cutting operations, the average plant height was measured as 96 cm.

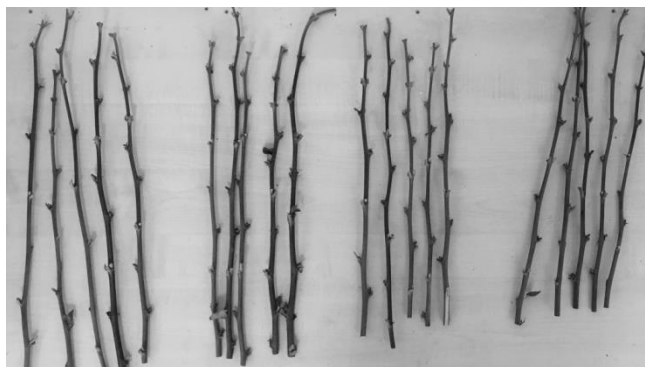


Figure 1. The test samples of cotton stalk.

According to stalk height, the plant stalk diameters before cutting were measured with a digital caliper with five replications at about the cutting point near the node section of an each test specimen. The average diameters were measured between internodes as 3.80, 4.40, 5.00 and 5.50 mm depending on along stalks. The ranges of diameter of the stalk were converted to cross-section area in mm^2 (11.33, 15.20, 19.62 and 23.750 mm^2 , respectively). Testing was completed as rapidly as possible in order to reduce the effects of drying. The moisture content of each sample was determined using an oven-drying method according to ASABE standard method (ASABE Standards 2008) at 105°C for 24 h before the cutting tests. The average moisture content was determined as 48.40% during the cutting tests.

In order to provide some cutting data required for the development of a chopping machine and tapper, A Material Testing Machine (Lloyd LRX Plus) was used to measure the cutting force of cotton stalks from different plant heights (Fig. 2) with two mouth smooth surface knife. The knife was held as fixed to testing machine (Fig. 2). The cutting tests was carried out under compression mode at a constant loading speed of 5 mm s^{-1} . A computer data acquisition system recorded all the force-displacement curves during the cutting process by testing machine. A typical force-deformation is given in Fig. 3. As you seen in Fig. 3, the first peak corresponds to the yield point (offset yield) at which stalk damage was initiated. The second peak (upper yield) corresponds to maximum force (Fig. 3). The measured maximum force values were considered for all tests.

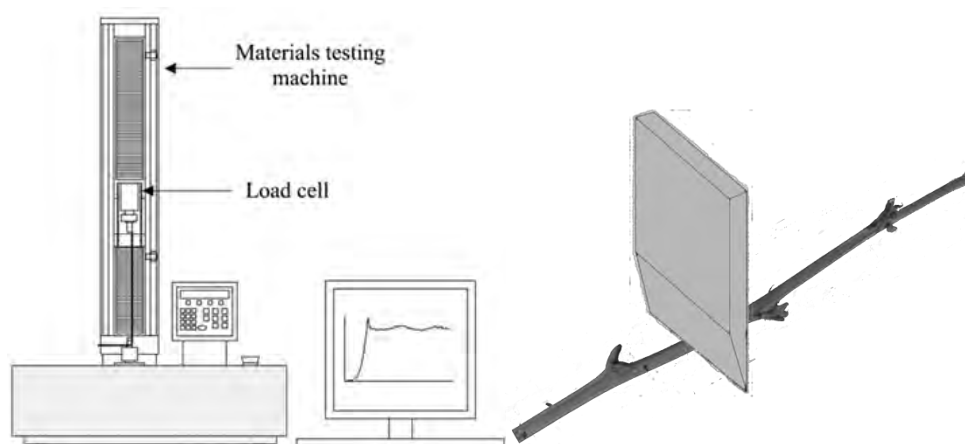


Figure 2. The Lloyd LRX Plus Materials Testing Machine and cutting blade.

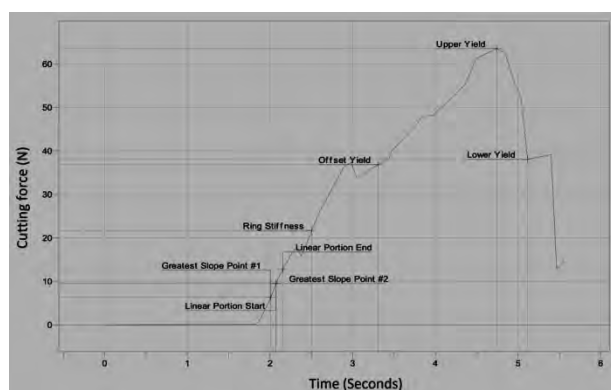


Figure 3. Typical force-deformation curve for cutting of cotton stalk.



The cutting strength, obtained from the cutting force findings, was determined by the following equation (Mohsenin 1986, Sessiz et al. 2013, Esgici et al. 2017):

$$\sigma_s = \frac{F_{\max}}{A} \quad (1)$$

Where: σ_s is the maximum cutting strength in (N mm⁻²), F_{\max} is the maximum cutting force in (N) and A is the cross-sectional area in (mm²).

In the second phase of the study, the cotton yield was measured in the harvesting season. Cotton yield data randomly were measured separately at 5, 10, 15 and 20 cm cutting heights from the top of the cotton plant in each experimental plot. In addition, yield has been measured in the control plots and Pix chemical applications plots. The measurements of yields were made in two middle rows and 5 m in-row spacing in each plot (7 m²). The cotton fiber was harvested by hand. Then, it is weighed by an electronic balance and converted to kg ha⁻¹. The obtained yield values were compared each other statistically.

Data were analyzed by ANOVA (MSTATC software). One factor randomized complete block design with 5 replications was performed to detect significant differences in the observations. Independent variables were top cutting height of cotton plant. Dependent variables were maximum cutting force, cutting strength and yield. Means were compared at a 1% level of significance using Duncan's multiple range tests to identify the specific differences among treatments means.

RESULTS AND DISCUSSION

The averages values of cutting force and cutting strength from measured and calculated data are presented in Table 1 and Fig. 4. The results of variance analysis showed that the effect of cross-section area (stalk diameter or top heights) has found to be statistically significant on cutting force. The significant differences were found between all cross-sectional areas at 1% probability level. The cutting force increased with an increase cross-sectional area (from bottom to top). Cutting forces varied from 44.50 and 91.66 N. The maximum cutting force was obtained at 23.75 mm² cross-sectional area as 91.66 N, while the minimum value of cutting force was obtained at 11.33 mm² cross-sectional area as 44.50 N (Table 1). However, the effect of cross-section area on cutting strength was not significantly ($p>0.05$). The cutting strength was found slightly to decrease with increase stalk diameter. The values cutting strength varied between 3.85 - 4.17 N mm⁻². This situation can be explained with the increased cross-sectional area decrease cutting strength per unit cross-section area. The effect of stem diameter on the maximum cutting force and cutting energy is consistent with Chen et al. (2004), who reported that both the cutting energy and maximum cutting force are directly proportional to the cross-sectional area of hemp stalk. Similar results were reported by Sessiz et al. (2013) for olive sucker, by Ozdemir et al. (2015) for grape sucker, by Sessiz et al. (2015) for cane of some different grape variety. These results also are in agreement with Aydin and Arslan (2018) who determined shearing force and energy for shoot of cotton plant at different height of plant.

Table 1. The average cutting force and cutting strength.

Cross-section area (mm ²)	Cutting force (N)	Cutting strength (Nmm ⁻²)
11.33	44.50d*	3.93
15.20	63.33c	4.17
19.62	75.66b	3.85
23.75	91.66a	3.86
Mean	68.80	3.95
LSD	4.95	Ns
**CV (%)	5.85	5.85

* the same letter in each column are not significantly different by Duncan's multiple range test at the 1% level.

**CV: coefficient of variation.

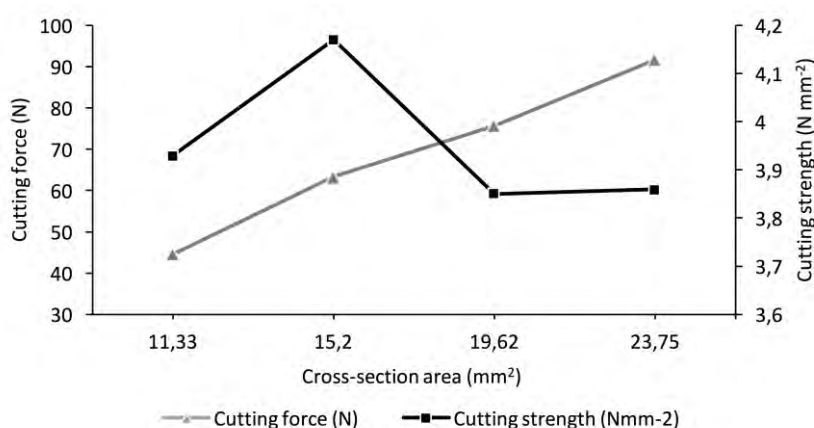


Figure 4. The average cutting force and cutting strength values depend on cross-section area.

The mean cotton yield values according to top cutting heights and other applications are given in Table 2 and Fig 5. The effect of top cutting height and other applications (pix chemical application and control) were found significant on the cotton yield ($p < 0.01$). The significant differences were found to be between 15 cm, 20 cm top cutting height ($p < 0.01$), pix chemical application and control plot. While the highest yield were observed at pix treatment methods as 6.440 kg ha^{-1} , followed by 5 cm, 10 cm, control, 15 and 20 cm, the lowest value were found at 20 cm cutting height from the top of cotton plant as 5.316 kg ha^{-1} . On the other hand, the difference between 5 top cutting heights and 10 cm top cutting height was no significant. According to these results, the yield values decreased with the cutting height increased from plant top (Table 2 and Fig 5) and when we consider the best result is obtained in the pix method, we can say that there is no need for top cutting of cotton plant. If it is taken into account that the use of chemicals is detrimental, it is more beneficial to cut height of the plant top at 5 cm or 10 cm by mechanical application. Even when we take into consideration the control values, there is no need to do anything process. Because there is no statistical difference between the highest value and the control value according to yield. When the cotton yield values in Table 2 and the cutting force values in Table 1 are examined together, the highest yield value and the lowest cutting force value were obtained at 5 cm top cutting height after control method. The lowest yield value and the maximum cutting force values were obtained at 20 cm top cutting height of cotton stalk. The diameter at this height is the highest. The cutting force value is therefore higher than others and energy requirement is high naturally at this diameter.

The relationships between cutting properties and cotton yield depend on top cutting height is very important and valuable a result for decide a new design a top cutting equipment of cotton stalk.

Table 2. The relationship between top cutting heights and cotton yield.

Top cutting height of cotton stalk (cm) and other applications	Cotton fiber yield (kg ha ⁻¹)
5	6.311a
10	6.286a
15	5.818ab
20	5.316b
Pix chemical application	6.440a
Control (no treatment)	6.158a
Mean	6.055
LSD	73.67
**CV(%)	6.76

* the same letter in each column are not significantly different by Duncan's multiple range test at the 1% level.

**CV: coefficient of variation.

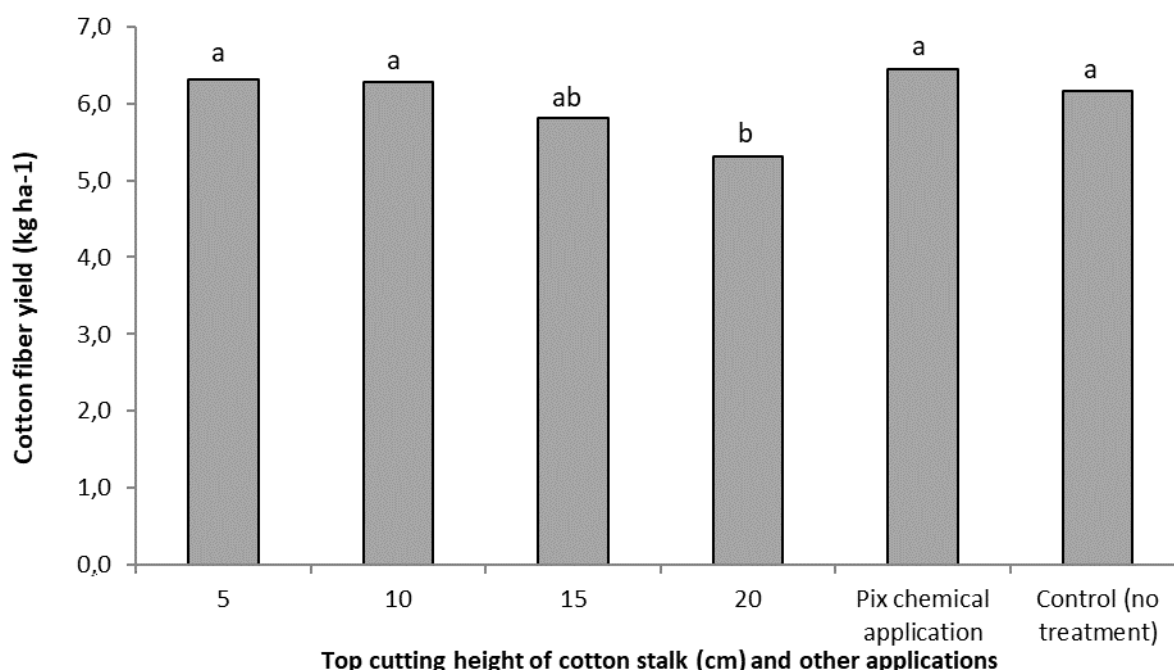


Figure 5. The relationship between top cutting heights and cotton yield.

CONCLUSIONS

Cutting tests show that top cutting heights are significant factor in cutting force, while cutting strength is not. Cutting force is highest directly affected by cross-sectional area and the cutting force increased with an increase cross-sectional area. The maximum cutting force was obtained at 23.75 mm² cross-sectional area as 91.66 N, while the minimum value of cutting force was obtained at 11.33 mm² cross-sectional area as 44.50 N. However, the effect of cross-section area was not found significant on cutting strength ($p > 0.05$). The strength slightly decreased with increase stem diameter. The cutting strength was changed between 3.85 - 4.17 N mm⁻².

F. Göksel Pekitkan, Reşat Esgici, Abdullah Sessiz. "Effect of Top Cutting Height of Cotton Stalk On Cotton Yield"

The highest cotton yield were observed at pix treatment methods as 6.440 kg ha⁻¹, followed by 5 cm, 10 cm, control, 15 cm and 20 cm. The lowest value was found at 20 cm top cutting height of cotton stalk as 5.316 kg ha⁻¹.

The highest yield value and the lowest cutting force value were obtained at 5 cm top cutting height after control method. The lowest yield value and the maximum cutting force values were obtained at 20 cm top cutting height of cotton stalk. The diameter at this height is the highest. The cutting force value is therefore higher than others and energy requirement is high naturally at this diameter. The relation between the cutting properties and the yield values obtained depending on cutting height was found to be important. These results can be considered valuable for design of new machine of top cutting of cotton stalk.

ACKNOWLEDGMENTS

This study was carried out with the test machine that the buy a project supported by the Scientific Research Funding (DUBAP-08-ZF-59) of Dicle University. The authors would like to thank Dicle University for providing the Material Test Machine and financial support.

REFERENCES

- ASABE Standards 2008. S358.2. *Moisture Measurement – Forages*. American Society of Agricultural and Biological Engineers, St. Joseph, MI.
- Aydin, İ. & Arslan, S. 2018. Mechanical properties of cotton shoots for topping. *Industrial Crops & Products* 112 (2018) p. 396–401
- Chen, Y., Gratton, J.L. & Liu, J. 2004. Power requirements of hemp cutting and conditioning. *Biosystems Engineering* 87(4), p. 417–424.
- Esgici, R., Özdemir, G., Pekitkan, F.G., Elicin, A.K., Öztürk, F. & Sessiz, A. 2017. Some enginnering properties of the Şire grape (*Vitis Vinifera* L.). *Scientific Papers. Series B, Horticulture*. Vol. LXI.
- Feng L., Dai, J., Tian, L., Zhang H., Li, J. & Dong, H. 2017. Review of the technology for high-yielding and efficient cotton cultivation in the northwest inland cotton-growing region of China. *Field Crops Research* 208 (2017) p. 18–26
- Ghahraei, O., Ahmad, D., Khalina, A., Suryanto, H. & Othman, J. 2011. Cutting tests of kenaf stems. *Transactions of the ASABE*, 54(1), p. 51-56.
- Kusinska, E. & Starek, A. 2012. Effect of knife wedge angle on the force and work of cutting peppers. Teka. *Commission of Motorization and Energetics In Agriculture – 2012*, 12(1), p. 127–130.
- Mathanker, S.K., Grift, T.E. & Hansen, A.C. 2015. Effect of blade oblique angle and cutting speed on cutting energy for energycane stems. *Biosystems Engineering* 133(2015), 64-70.



- Mohsenin, N.N. 1986. Physical properties of plant and animals materials. 2nd edition. New York, NY: Gordon and Breach Science Publishers.
- Obasi, M.O. & Msaakpa, T.S. 2005. Influence of topping, side branch pruning and hill spacing on growth and development of cotton (*Gossypium barbadense* L.) in the Southern Guinea Savanna Location of Nigeria. *J. Agric. Rural Dev. Trop. Subtrop.* 106(2), p. 155–165.
- Ozdemir, G., Sessiz, A., Esgici, R. & Elicin, A. K. 2015. Cutting properties of wine grape cultivars. *Scientific Papers. Series B, Horticulture.* Vol. LIX.
- Persson, S. 1987. Mechanics of cutting plant material. ASAE Publications, St Joseph, MI, USA.
- Renou, A., Téréta, I. & Togola, M. 2011. Manual topping decreases bollworm infestations in cotton cultivation in Mali. *Crop Prot.* 30(10), p. 1370–1375.
- Sessiz, A., Elicin, A.K., Esgici, R., Özdemir, G. & Nozdrovicky, L. 2013. Cutting Properties of Olive Sucker. *Acta Technologica Agriculturae. The Scientific Journal for Agricultural Engineering*, The Journal of Slovak University of Agriculture in Nitra. 16(3), p. 80–84.
- Sessiz, A. & Esgici, R. 2015. Effects of cotton picker ages on cotton losses and quality. *Scientific Papers. Series A. Agronomy* Vol. LVIII, p. 417-420.
- Sessiz, A., Esgici, R., Özdemir, G., Elicin, A.K. & Pekitkan, F.G. 2015. Cutting properties of different grape varieties. *Agriculture & Forestry* 61(1), p. 211-216. DOI: 10.17707 / AgricultForest. 61.1.27 Podgorica
- Srivastava, A.K., Goering, C.E. & Rohrbach, R.P. 2006. Engineering principles of agricultural machines. *ASAE Textbook Number 6. Pamela De Vore-Hansen*, Editor, Books&Journals. 601 p.
- Yang, Y., Ouyang, Z., Yang, Y. & Liu, X. 2008. Simulation of the effect of pruning and topping on cotton growth using Cotton2K model. *Field Crops Res.* 106, p. 126–137.



Foreign Body Detection Approaches In Food And Beverage Products

Mohammad Reza Zarezadeh*, Mohammad Aboonajmi

Department of Agro-technology, Abouraihan Campus, University of Tehran, Tehran, Iran

Email address: mr.zarezadeh@ut.ac.ir

ABSTRACT

The presence of foreign bodies (FBs) in food and drinking products are major concern to the producer. They often include pests, metal, glass and plastic pieces. However they may be a healthy eating and drinking but are not main product such existing a bean in canned tomato paste. To prevent any potential harm to consumers and maintain their confidence it is necessary for the food industry that all foreign bodies are detected and removed from food products before they reach the consumers. In this paper we evaluate and discuss about using different approaches for detection of foreign bodies. There are many non-destructive method to detect them ranging from simple to complex which the most important of them are include optical, microwave reflectance, nuclear magnetic resonance imaging, electrical impedance, ultrasound, X-rays etc. The objective of this article was summarizing the mentioned approaches to food quality assurance with respect to foreign body detection.

Keywords: Foreign Body, Detection, Food Safety, Non-destructive, Iran

1. INTRODUCTION

Quality and food safety are among important elements to be considered in the food production industry. Responsible food manufacturers will gain public confidence in their products by incorporating the food safety assurance programs and hygienic practices in their operations. Food contamination must be avoided because it has an impact on a large scale. High standards and regulations are gazetted by the World Health Organization (WHO) in order to prevent any disease that may occur due to food contamination. Cholera, typhoid, diarrhea, and hepatitis B are such diseases caused by food contamination. The food industry has used a variety of tools and sensors as a proactive measure to ensure that the produced food is totally safe to eat. The sensors are used in two parts; first, chemical inspection such as to detect bacteria and viruses (Shukla et al. 2012). The second part is physical inspection which is to detect the impurities in food and identify the dented cans or change in food texture (Mohd Khairi et al. 2016).

Foreign bodies (FBs) in food and beverage are defined as objects that may be exist in food, and are not intended to be present in them. Included within this very broad definition are packaging materials, by-products of food materials that have been inadequately removed such as bone in meat, leaves, stalks and other extraneous vegetable matter (known as EVM) in fruit and the introduction of materials inadvertently through the food chain, such as string and metal or insects.



Figure. 1. Foreign object in foods

The food Industry has recognized that the most effective method of controlling foreign bodies is through the implementation of a Hazard Analysis and Critical Control Point (HACCP) system. The scope of its use has been subsequently extended by many food operations to include physical and chemical food safety hazards. HACCP has gained international acceptance with the guidance developed by the Codex Alimentarius Commission in common usage. Codex defines, in its Food Hygiene Basic Texts, seven HACCP principles as stated below (Edwards, 2004):

- Principle 1: Conduct a hazard analysis
- Principle 2: Determine the critical control points (CCPs)
- Principle 3: Establish critical limits
- Principle 4: Establish a system to monitor control of the CCP
- Principle 5: Establish the corrective actions to be taken when monitoring indicates that a particular CCP is not under control
- Principle 6: Establish procedures for verification to confirm that the HACCP system is working effectively
- Principle 7: Establish documentation concerning all procedures and records appropriate to these principles and their application.

However, despite the best efforts of food and beverage manufacturers, sometimes foreign objects accidentally appear in final products. Generally major foreign objects observed in packed food and beverages, are include: pests, glass, metals (Djekic et al., 2017), plastic particles, wood, rock, bone, etc. FBs are so common that in sensitive industries such pharmacy can be observed (fig. 2). However they may be a healthy eating or drinking but are not main product such existing a bean in canned tomato paste. These foreign bodies can be result of variety reasons, such as due to employee carelessness, equipment failure, pests and even accidental input. Fortunately for food producers, there are a wide range of foreign body detection methods

available to help processors and packagers find unwelcomed substances. Food and beverage processors and packers rely on several technologies to detect foreign bodies in food which include: metal detection, X-ray detection, visible/infrared (IR)/ hyper-spectral imaging systems (camera/laser-based), mechanical detection, electrical impedance tomography, ultrasonic approach and etc. Each of these methods and technologies come with their own strengths and weaknesses.



Figure. 2. Foreign object in acetaminophen pills

2. MATERIALS AND METHODS

Following some of important mentioned approaches are given:

2.1. First approach, metal detection

Metal detectors for food provide effective protection against ferrous and non-ferrous metals (aluminum, stainless steel, etc.). They can be established in each point of the production process. It can be used for wide range of applications, e.g. for the inspection of bread and bakery products, fruits, soda and all kinds of juices, vegetables, meat and sausage product, dairy products, spices, sugar, etc. In food and beverage products, metal existence can cause concern and even injury to consumers, and compensation may run into much of cost, but the effect of bad publicity arising from such an incident could damage a brand's reputation beyond repair, causing a loss of sales that could be worth millions.

Types of metal detection systems

The basic principle of metal detection is based on the transmitting and receiving electrical impulses, much like radio waves. All metals have characteristics that will cause an alteration in a transmitted signal, because of their conductivity and magnetic properties. What metal detectors do in food processing lines is to compare the signal received with the expected signal and identify the presence of a contaminant if a variation is observed. There are three types of detection system in use today, one of which comprises over 90 % of those in current use. The systems are: pulse technology, ferrous in foil detection, and the balanced three coil system.

2.1.1. Pulse technology

Pulse technology is limited to finding relatively large pieces of metal in raw materials, such as nails or cans in sacks of potatoes. Usually a transmitter is placed on one side of a conveyor and a receiver on the other side. The transmitter sends a pulse signal and the receiver will detect a spike from that signal. Normally that spike will grow and decay in a quick and regular pattern.

When metal is present it will cause the decay of the spike to become elongated; it is this change in the pattern of the decay that indicates the presence of metal contamination.

2.1.2. Ferrous in foil detectors

Ferrous in foil detectors also have limited applications and are specifically aimed at detecting ferrous metal contamination within products packed in foil trays, such as pies, quiches and casseroles. Ferrous in foil detection is used in cases where there is so much metal passing through the detection system that other types of detection will not give a sensitive enough result or where the change in signal caused by the packaging would swamp any signal change caused by contaminants. This system uses magnetism for detection and is, therefore, only capable of detecting metals with a ferrous content. It comprises upper and lower discrete permanent magnets, between which there is a strong magnetic field, and coils mounted across the centre of the two magnets. Any piece of ferrous metal passing through the magnetic field will be magnetized; as it passes through or under the coils the magnetism will generate a small current within the coils. The coils are connected to amplifiers which produce an output signal to a control device that in turn operates a reject system. Sensitivity, which determines how small a piece of metal might be detected, is relative to the height of the aperture between the magnets. A 100 mm high aperture can generally find a 1.0 mm piece of ferrous metal, so a maximum effective aperture height is generally thought to be 200mm. Metal detection 49 Ferrous in foil detection systems were particularly popular and relevant when processing machinery contained a high proportion of mild steel. Now that most processing plant is made with 300 grade stainless steel, which has virtually no magnetic potential, the system is becoming less relevant to the industry.

2.1.3. Balanced three coil detectors

The balanced three coil detection system is the most common type found today. This system accounts for between 90 and 95 % of all systems in use at the present time because its primary characteristic is a high level of sensitivity. It works by comparing the signal variance received by two receiver coils, placed either side of a transmitter coil, along the length of the conveyor. As Fig. 3 shows, the receiver coils are wound in opposite directions so that the values of the signals received from the transmitter coil should balance each other out. Subtracting the value of the signal received at one coil from that at the other should result in a total value of zero.

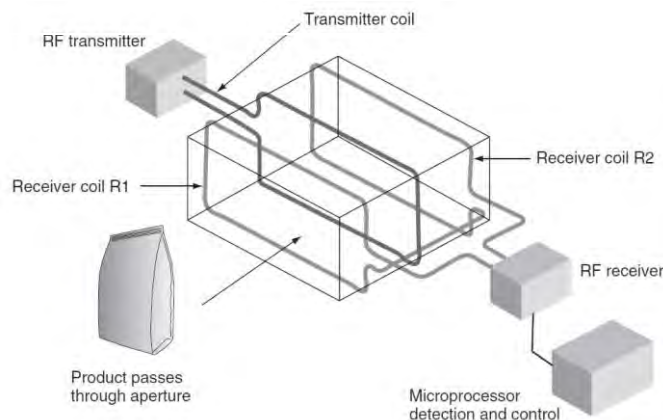


Figure. 3. Outline construction details of a balanced three-coil detection system

2.2. Second approach, X-ray detection:

The ability of X-rays to examine the internal structure of food materials and packages and to detect embedded foreign bodies is very attractive. Indeed, there is no practical alternative, in many cases. X-ray inspection provides non-contact sensing, which is inherently hygienic and does not damage even the most delicate and fragile macro-structures. At the low X-ray doses involved, there is insignificant damage to molecular and other sub-cellular structures. There is a popular misconception that X-rays make materials radioactive (Batchelor. et al. 2004). X-ray systems can detect various contaminants such as metals, non-ferrous metals, stones, glass, PVC plastic, bones, concrete, ceramic, Teflon plastic, sugar or flavor clumps and any missing products. X-rays are easy to operate and requires minimal training. High-end machines are even easier to operate with touch screen interfaces. Just like ultrasound systems, they can maintain high production rate with less false rejects. (Šuška, 2017). Nielsen et al. (2013) detected organic foreign bodies (paper and insects) in two food products using X-ray dark-field imaging with a grating interferometer. They found detection ability ability to detect the foreign body is quantified using a measure of the contrast-to-noise ratio.

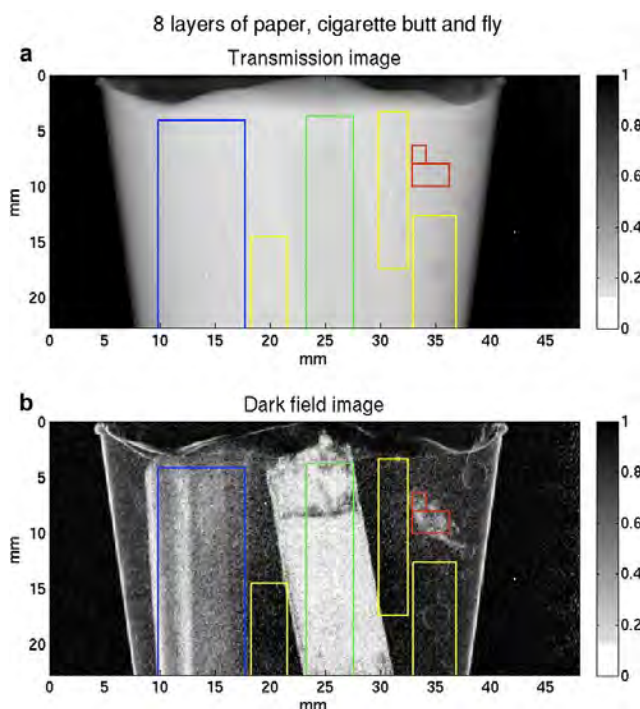


Figure. 4. Sour cream: X-ray images of sour cream with three FBs; 8 layers of paper (left), a cigarette butt (middle) and a fly (right). a) Transmission radiogram. b) Dark-field radiogram.

2.3. Third approach, Electrical impedance:

The field of impedance measurements sits between conventional metal detection systems and those using microwave-based approaches. Conventional metal detection systems generally rely on differences in electromagnetic fields and this overlaps with impedance measurements. In terms of microwave-based approaches there is a continuum from the frequencies used in

impedance spectroscopy, which are generally referred to as radio frequencies, up to those that are classified as microwave. However, compared with conventional metal detection systems an approach based upon measuring changes in the electrical properties of the food opens the possibility for detecting a much broader range of potential materials such as glass, plastic and wood as well as both ferrous and non-ferrous materials, all by a single instrument. Impedance-based systems have for a number of years been used in the food industry for a variety of purposes; measuring changes in the dielectric properties of food is a potentially promising route as the basis of a foreign body detection system. The determination of moisture levels in various foodstuffs such as grain (Nelson et al., 2001) has been conducted for a number of years based upon measurements of dielectric properties. A development of the impedance measurement described above has been made by Kaiku Limited which has modified its existing in-line chemical analysis system for use as a foreign body detector for pipeline applications. The system is currently undergoing performance evaluation. Kaiku's technology consists of a non-electrically conducting pipe that has a pair of electrodes on the outside of it forming a flow cell. Figure 5 depicts the flow cell and shows the electrodes as a pair of plates that are separated by a small gap. One of the key elements of the system is that the electrodes are located on the outside of the pipe and so do not suffer any of the problems associated with sensor fouling or cleaning issues (Dowdeswell, 2004).

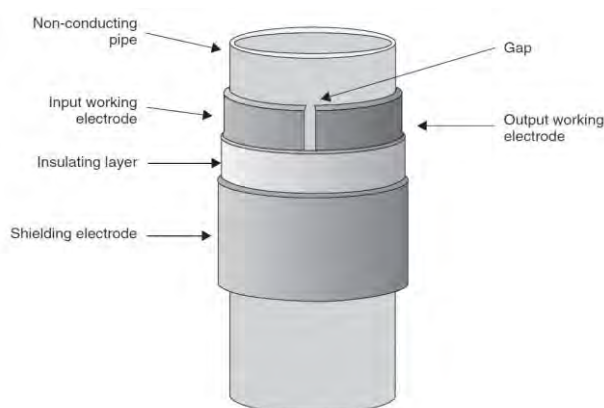


Figure. 5. Internal representation of Kaiku sensor

The challenge for any impedance-based foreign body detection system, or in fact for any method of detection, is to apply a measurement technique to a continuously changing baseline product where you are required to identify the occurrence of a rare event. Due to the wide range of material types and size that constitute foreign bodies, there is a considerable challenge in defining the change in measurement in the signal that can be defined as a positive 'hit'. However, this approach still offers the potential for the detection of those materials such as glass, plastic and bone that are considered difficult to find by other measurement techniques while metallic material is still detected.

2.4. Fourth approach, ultrasound:

A salient feature of ultrasonic imaging is that a quantitative characterization of materials is realizable as the result of the complicated manner in which the ultrasound signal interacts with the material. A number of ultrasound propagation parameters can be used to characterize a



medium such as food. These parameters include attenuation/absorption, backscatter, velocity and nonlinearity (Shung et al., 1992). There are several works that investigated ultrasound application in food quality evaluation (Fathizadeh and Aboonajmi (2017), Ouacha et al. (2015), Luis Elvira et al. (2014), Meftah and Mohd Azimin (2012), Basir and Zhao (2004), Haeggstrom and Luukkala (2001), etc. However another advantage of ultrasonic-based systems is that they are more adaptable to various test environments and conditions than systems based on other techniques. Ultrasound sensors can be made as small as a catheter tip of 1.2mm diameter, on which a circumferential array of 64 elements can be formed and placed in the coronary arteries or veins of the heart to image blood flow. (Crowe et al, 2000)

Haeggstrom and Luukkala (2001) detected and identified some FBs in packaged cheeses using a piezoelectric transducer. Experiments were conducted in a water tank using the pulse/echo mode. FBs included stones and spheres of bone, wood, glass, plastic and steel. These materials were implanted in the cheese samples. To control the facing of FBs to the transducer, half of the FB samples were made of a spherical shape. Using an A-mode analysis, FBs implanted at 75 mm deep in the cheese were detected. A 50mm detection depth enabled the inspection of a standard package with 400 g mass. An effective, reliable, fast and low cost FB detection system, including the method and equipment, should be designed based on product and packaging specifications. The earliest available FB detection systems seem to be those for soft bottled beverages using air coupled transducers with moderate inspection speed. Typical inspection speeds were around 0.8 m/s with 3mm pixel using thru-transmission mode for honeycomb plates. (Strycek et al., 2000 & Cotter et al., 2000). Mohd Khairi (et al. 2016) used two dimensional (2D) of finite element method in order to detect the foreign body in food container using an ultrasonic measurement system. They applied Comsol acoustic module to detect the foreign body in the dairy product where various conditions such as frequency, foreign body material and thickness of container wall were simulated. They used high frequency (300 kHz) due to detecting much smaller foreign bodies (they used two most visited FB: steel and glass). They reported that the total acoustic pressure is reduced significantly from 0.420 Pa to 0.350 Pa when the size of steel was increased from 5 mm to 10 mm. A similar correlation was also obtained for glass material where 0.354 Pa was reduced to 0.278 when the size of glass was increased to 10 mm. they also used low frequency (45 kHz) results showed that a higher frequency presents a more significant difference in total acoustic pressure compared to lower frequency. Also demonstrated that the finite element method can assist the designing and development of an ultrasonic measurement system in the food industry field

3. CONCLUSIONS

There are many non-destructive method to detect FBs ranging from simple to complex which the most important of them are include optical, microwave reflectance, nuclear magnetic resonance imaging, electrical impedance, ultrasound, X-rays etc. Each one has strengths and weaknesses. According to our condition and food texture, we can select the best approach.

REFERENCE

- B. G. Batchelor. E. R. Davies. M. Graves. (2004). Detecting foreign bodies in food. Woodhead Publishing Limited, chapter 13, Using X-rays to detect foreign bodies. pp 226-260
- Zarezadeh M. R., Aboonajmi M. "Foreign Body Detection Approaches In Food And Beverage Products"



- Cotter d j, michael s t e, michael s j e, kass d, stanton m e, kosenko i v and hotchkiss f h c (2000). Squirter, roller probe, and air-coupled ultrasonic transducer techniques for low frequency inspection of advanced composites materials. 15th WCNDT, Roma.
- Crowe J. R. (2000). Blood speed imaging with an intraluminal array. IEEE Transactions on ultrasonics, ferroelectric, and frequency control, 47(3), pp 672–81.
- E. Ouacha, B. Faiz, A. Moudden, I. Aboudaoud, H. Banouni, M. Boutaib (2015). Non-destructive detection of air traces in the UHT milk packet by using ultrasonic waves. Physics Procedia 70 pp. 406–410.
- Edward Haeggstrom and Mauri Luukkala (2001). Ultrasound detection and identification of foreign bodies in food products. Food Control 12. pp 37-45
- Fathizadeh, Zahed and Aboonajmi, Mohammad (2017). Nondestructive air-coupled ultrasound measurement in the food industries. Proceedings of the 4th Iranian International NDT Conference Feb 26-27.
- Ilija Djekic, Danijela Jankovic, Andreja Rajkovic, (2017). Analysis of foreign bodies present in European food using data from Rapid Alert System for Food and Feed (RASFF). Food Control.
- J. P. Craig, (2004). Detecting foreign bodies in food. Woodhead Publishing Limited, chapte4, Metal detection. pp 47-63
- Luis Elvira, Carmen M. Durán, José Urréjola, Francisco R. Montero de Espinosa. (2014). Detection of microbial contamination in fruit juices using noninvasive ultrasound" Food Control 40, pp 145-150.
- Meftah, H. and Mohd Azimin, E. (2012). Detection of foreign bodies in canned foods using ultrasonic testing. International Food Research Journal 19(2) pp. 543-546
- Mikkel Schou Nielsen, Torsten Lauridsen, Lars Bager Christensen, Robert Feidenhans. (2013). X-ray dark-field imaging for detection of foreign bodies in food. Food Control.
- Miroslav Šuška, (2017). <http://qualifoodacademy.com>. Accessed 10.10.17
- Mohd Taufiq Mohd Khairi, Sallehuddin Ibrahim, Mohd Amri Md Yunus, Mahdi Faramarzi, Muhammad Abdul Illah Abd Rahman, Muhammad Sani Gaya. (2016). Finite element simulation for detecting the foreign body based on ultrasonic sensor. Journal of Food Process Engineering.
- Nelson S. O., .trabelsi s and kraszewski A W (2001). RF sensing of grain and seed moisture content, IEEE Sensors Journal. 1(2), pp 119–26.
- O. A. Basir and B. Zhao (2004). Detecting foreign bodies in food. Chapter 12 Ultrasound. pp 204-223
- R. Dowdeswell, (2004). Detecting foreign bodies in food. Woodhead Publishing Limited, chapter 11: Electrical impedance. Pp.193-203.
- Shiva Kant Shukla, Pablo Resa, Carlos Sierra & José Urréjola. (2012). A new ultrasonic signal amplification method for detection of bacteria. Measurement Science and Technology, Volume 23, (10).
- Shung K. K., smith M. B. and Tsui B. M. W. (1992). Principles of Medical Imaging. San Diego, Academic Press, pp 85–91.
- Strycek j o, loertscher h p and starman s (2000). High speed large area scanning using air-coupled ultrasound. 15th WCNDT, Roma.



New trends in numerical modeling and control of photovoltaic pumping systems

Dan Craciunescu¹, Cengiz Akdeniz², Laurentiu Fara^{1,3*}, Paul Sterian³

¹Faculty of Applied Sciences, Polytechnic University of Bucharest, Splaiul Independentei 313, Bucharest, Romania

²Department of Agricultural Machinery, Faculty of Agriculture, Ege University, Izmir, Turkey

³Academy of Romanian Scientists, , Splaiul Independentei 54, Bucharest, Romania

ABSTRACT

The authors studied a photovoltaic (PV) pumping system for irrigation. A mathematical model of the photovoltaic pumping system that deals all its components is discussed, considering the determination of the characteristic equations. These have been used together with the proposed SISIFO simulation software to achieve the performances of the mechanical and electrical components of the considered PV pumping system. The performances of the complex photovoltaic pumping system, namely monthly energy yield, monthly pumping yield, and monthly total performances (energy and flow rate) were introduced. Two case studies were conducted for two sites, namely Alexandria (Southern Romania) and Antalya (Southern Turkey) regarding irrigation potential, taking into account the main meteorological parameters (solar irradiance and ambient temperature), related to each site. This approach allowed the implementation of the proposed simulation model, thus achieving a complete characterization of the analyzed photovoltaic pumping system. The use of the Maximum Power Point Tracking (MPPT) method and the MATLAB / Simulink software has led to an operational optimization of the photovoltaic pumping system, with major implications for the development of these PV pumping systems on large-scale.

Keywords: Photovoltaic pumping system, irrigation, performances, meteorological parameters, maximum power point tracking, control, monitoring, simulation tools

1. INTRODUCTION

Solar energy is the most important renewable energy source and could represent, 13-15% of the total energy mix in the year 2035 [1, 2], due to the progress of photovoltaic technologies and the diminution of non-renewable sources. It is envisaged that solar energy-based projects offer a wide range of possibilities for both stand-alone and complex applications [3, 4].

The evolution of photovoltaic panels has made possible the development of water pumps powered by solar energy, allowing irrigation of the soil without the need to connect to the electrical grid. The use of PV pumping systems for irrigation in different rural areas is also

* corresponding author : lfara@renerg.pub.ro



a more efficient method of storing the potential energy of water [5, 6, 7]. The concept of the pumping system is presented in Figure 1.

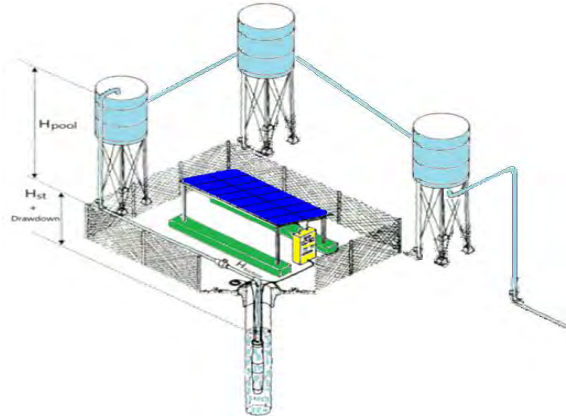


Figure 1. The concept of the PV pumping system for irrigation application [7]

It should be noted that solar pumps offer the possibility of delivering water for both irrigation and local drinking water supply. These pumps usually have DC motors that can use the current produced by the photovoltaic panels or the current in the storage batteries [8].

It is possible also to equip solar pumps with AC motors but this involves the use of complex control systems based on inverters, converters, etc [9].

Modeling and simulation of complex PV pumping has been studied until now by various authors.

J. Muñoz et al [10] implemented the SISIFO simulator that allows forecasting pumped water flow, depending on the characteristics and performance of the PV generator used.

A Taufik, et al [11] has developed a simple and efficient photovoltaic pumping system by using two MPPT algorithms and control methods; the results of the simulations showed the performance parameters of the PV pumping system, respectively the total energy daily produced and the pumped water flow per day.

M. Kumar [12] has developed a photovoltaic pumping system using the MPPT method and a boost converter, which has enabled the optimized operation of a PMDC (Permanent Magnetic Direct Current) motor.

Z Glasnovic and J Margeta [13] studied an integrated PV pumping system, analyzing the influences of the local climate, the soil used, the harvests obtained and the irrigation method considered; on this basis it was proposed a hybrid optimized model for irrigation which has been tested satisfactorily.

M. S. Shebani and T. Iqbal [14] studied the modeling of a photovoltaic pumping system using Homer software; the performance of the system was evaluated using the MPPT technique, resulting an improvement in the efficiency of the PV pump.

M. EL-Shimy [15] studied the optimization of a stand-alone photovoltaic pumping system for irrigation from the point of view of the impact of the tilt angle of PV array. The results indicated the capability and accuracy of the method used to size PV stand-alone pumping systems.



Considering the present state of art in the field of irrigation photovoltaic pumps, the authors have proposed in this paper the following objectives: 1) performing numerical modeling for evaluation of the main parameters of a PV pumping system, 2) analyses of the influence of the main meteorological parameters, respectively solar irradiance and temperature for performance evaluation of the PV pumping system operation in two specific case studies, namely Alexandria (South of Romania) and Antalya (South of Turkey), and 3) optimization of the PV pumping system based on an advanced MPPT algorithm.

2. Background: mathematical model and simulation tool

2.1. Mathematical model of the pumping PV system

The mathematical model of the photovoltaic pumping system considers the characterization of its components [16]. A correlation between the electrical parameters (specific parameters of the PV panels, motor and inverter, the supplied energy by the structure, as well as respectively the PV system power) and the non-electric ones (flow rate and pumping height) taking into account the main meteorological parameters (solar irradiance and temperature) is established. On this basis, it is possible to correctly estimate the irrigable potential of the PV pumping system. The equations defining the studied PV pumping system are presented below.

2.1.1. PV generator

The output maximum DC power, P_{DC} , is obtained using the relationship:

$$P_{DC} = P_{max} \cdot \frac{G}{G'} \cdot \frac{\eta}{\eta'} \quad (1)$$

where P_{max} is the maximum power under Standard Test Conditions (STC, defined by normal solar irradiance of $G' = 1000 \text{ W/m}^2$ and solar cell temperature of $T'_C = 25^\circ\text{C}$, and AM1.5 spectrum), $\eta = \eta(G, T_C)$ is the conversion efficiency as a function of the incident solar irradiance, G , and cell temperature, T_C , and η' is the conversion efficiency under STC, $\eta' = P_{max}/A \cdot G'$, where A is the active area of the PV generator.

The calculation of the conversion efficiency, η is based on a “Only temperature effect” model, namely

$$\frac{\eta}{\eta'} = 1 + \gamma (T_C - T'_C) \quad (2)$$

where γ is the coefficient of variation of power with temperature, in $[\text{C}^{-1}]$, and T_C is calculated from the ambient temperature, T_A , using the equation with the Nominal Operation Cell Temperature, (T_{NOCT}), obtained from the manufacturer datasheet:

$$T_C = \left(T_A + 0,9 \frac{T_{NOCT} - 20}{800} G \right) = T_A + k \cdot G \quad (3)$$



where T_A and T_{NOCT} are given in °C, G is given in $W \cdot m^{-2}$, and k is a thermal resistance called Ross coefficient, which is given in $^{\circ}C \cdot m^2/W$. The 0.9 factor is an experimental correction factor.

2.1.2. Inverter

The inverter conversion efficiency ($\eta_{inverter}$) could be calculated knowing its nominal power (P_{inv}), its maximum output power (P_{AC}) and three experimental parameters (k_0 , k_1 and k_2), associated to the inverter losses, as follows:

$$\eta_{inverter} = \frac{P_{AC}}{P_{DC}} = \frac{p_{ac}}{p_{ac} + (k_0 + k_1 p_{ac} + k_2 p_{ac}^2)} \quad (4)$$

where $p_{ac} = P_{AC}/P_{inv}$, P_{AC} is the AC output power of the inverter, which can be determined from P_{DC} (power at the inverter input) and parameters k_0 , k_1 and k_2 , which must be fitted, either from the conversion efficiency curve provided by the manufacturer, or from experimental measurements [17, 18].

2.1.3. Current Transformer

The ratio low voltage/medium voltage transformer (LV/MV) is characterized by its nominal power, copper and iron losses. The conversion efficiency of this transformer, $\eta_{transformer}$, is calculated as a ratio between the output power P_{out} and the input power P_{AC} :

$$\eta_{transformer} = \frac{P_{out}}{P_{AC}} = \frac{P_{out}}{P_{out} + P_{Core} + P_{Cu}} \quad (5)$$

where P_{Core} are the core losses, and P_{Cu} the copper losses.

2.1.4. Pumping

The calculation of the pumping parameters, respectively the motor efficiency (η_{motor}), the pumping height (H) and the pumping flow rate (Q), takes into account the input power of the motor P_{in} , the available electric power $P_{AC/DC}$, and the power developed at the shaft of the motor (P_{shaft}).

So, the motor efficiency could be calculated with the equation:

$$\eta_{motor} = \frac{P_{shaft}}{P_{in}} = \frac{p_{shaft}}{p_{shaft} + (k_{m0} + k_{m1} p_{shaft} + k_{m2} p_{shaft}^2)} \quad (6)$$

where $p_{shaft} = P_{shaft}/P_{shaft,nom}$, and k_{m0} , k_{m1} and k_{m2} are the losses coefficients.

The pumping height $H(Q)$ and shaft power $P_{shaft}(Q)$ depending on flow rate (Q) could be fitted with second order polynomials, as follows:

$$H(Q) = k_{B0} + k_{B1}Q + k_{B2}Q^2 \quad (7)$$

$$P_{shaft}(Q) = k_{p0} + k_{p1}Q + k_{p2}Q^2 \quad (8)$$



where H is the pump height, and k_{B0} , k_{B1} , and k_{B2} are the second degree polynomial coefficients that represent the best fit for H , while k_{P0} , k_{P1} , and k_{P2} are the coefficients for P_{shaft} .

The pumping height is computed using the static height (k_{S0}) and friction losses (k_{S2}) of the system; it is also a second order polynomial:

$$H_s(Q) = k_{S0} + k_{S2}Q^2 \quad (9)$$

Equations (6), (7), (8) and (9) characterize system operation at nominal frequency. Since the system can operate at different frequencies, as the pump's operating point depends on the available PV generator power, it is necessary to obtain different PV pump curves, according to frequency, in order to determine the optimum operating points. To achieve this goal, the affinity laws for the optimum operation of PV pumping are considered, namely:

$$\frac{Q_1}{Q_2} = \frac{\omega_1}{\omega_2} \quad (10)$$

$$\frac{H_1}{H_2} = \left(\frac{\omega_1}{\omega_2}\right)^2 \quad (11)$$

$$\frac{P_{shaft1}}{P_{shaft2}} = \left(\frac{\omega_1}{\omega_2}\right)^3 \quad (12)$$

where ω_1 and ω_2 represent instantaneous frequencies for two different points on the same affinity curve. The essential objective of the photovoltaic pumping modeling is to establish the relationship between flow rate (Q) and motor shaft power (P_{shaft}); under the terms of (12) affinity law; this relationship has the expression:

$$Q(P_{shaft}) = k_{Q0} + k_{Q1}P_{shaft} + k_{Q2}P_{shaft}^2 + k_{Q3}P_{shaft}^3 \quad (13)$$

where k_{Q0} , k_{Q1} , k_{Q2} and k_{Q3} are the third degree polynomial coefficients.

2.2. Simulation tool

The authors proposed the use of the SISIFO [18] programming environment in order to numerically model the photovoltaic pumping system studied.

The software allows analysis of the electrical parameters and non-electric ones for the photovoltaic pumping system using the equations of the mathematical model regarding the main components, respectively the PV generator, the inverter, the current transformer and the motor pump. The analysis of the complex PV pumping system with the SISIFO platform allows two approaches:

1) the technical approach of the main pumping parameters, flow rate and pumping height according to the electrical characteristics of the pump motor (efficiency of the shaft motor); the results of the simulations are consistent with the mathematical model of the pumping system based on polynomial approximation and affinity laws.



2) the performance of the complex PV pumping system approach; there are obtained the monthly/annual supplied energy, the pumping efficiency, the pumping flow rate depending on the influence of the main meteorological parameters, respectively solar irradiance and the monthly/annual minimum/maximum temperature. The monthly and annual average values for the power produced by the PV generator, as well as monthly/annual pumping flow rate are evaluated.

Meteorological data are automatically obtained from its own database (PVGIS) for the two cases studies.

The pumping system is implemented for the following locations, namely: Alexandria (Southern Romania) and Anatolia (Southern Turkey), with input data the PV generator power of 40 kWp and the maximum height of 250 m considered for the pump.

The operational optimization of the pumping system is analyzed using the MPPT technique in order to increase the irrigation capacity of the system.

3. Simulation results and discussions

3.1. Establishing the performances of the mechanical components for the photovoltaic pumping system

The analyzed pumping system was based on the Caprari online catalog [19]. In Table 1, respectively in Table 2 are shown the pump and motor input data, based on the models E6P35 / 15A and MAC630A-8V.

Using the input data of the two essential components of the PV pumping system for irrigation and using the equations (9)-(13) of the mathematical model discussed in Chapter 2, the authors established: 1) the operating characteristics of the photovoltaic pump (the pumping height and the power to the shaft depending on the rate flow), see Figure 2 and 2) the pump motor operation characteristics (efficiency of the pump motor depending on the power), see Figure 3.

Table 1 Input data for PV pump [19]

Pump Curve		Shaft power curve	
Q [m ³ /h]	H [m]	Q [m ³ /h]	P _{shaft} [kW]
0.00	207.75	17.68	16.23
21.33	189.44	23.13	18.09
24.97	184.06	26.76	18.99
28.57	177.30	30.40	19.72
32.21	168.33	34.03	20.21
35.85	156.58	37.67	20.46
39.48	142.05	41.30	20.41
43.12	124.74	44.93	20.05
52.20	65.80	52.20	18.30

Table 2 Input data for motor

Pump Curve	Shaft power curve
P _{shaft} [kW]	Efficiency [%]
0	0.00
5.45	77.80
10.97	83.80
14.24	84.20
16.55	84.20
21.86	83.08
22.22	83.53
22.87	83.00
23.13	82.00

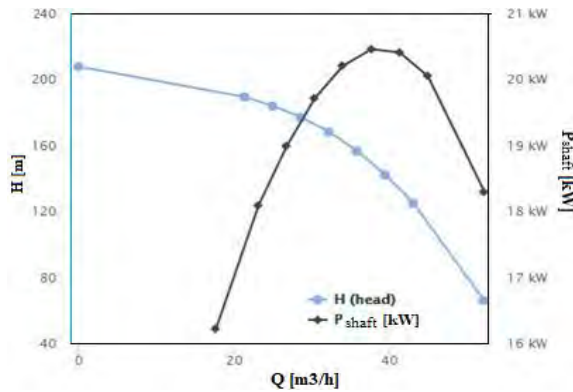


Figure 2: PV pump characteristics

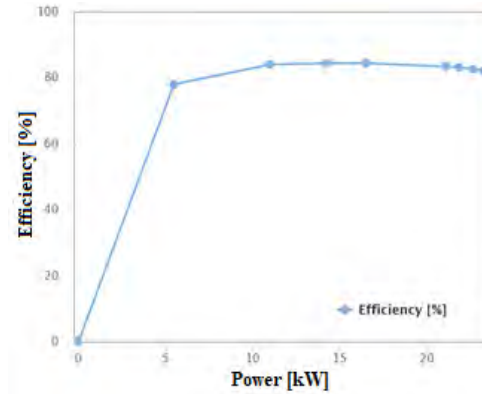
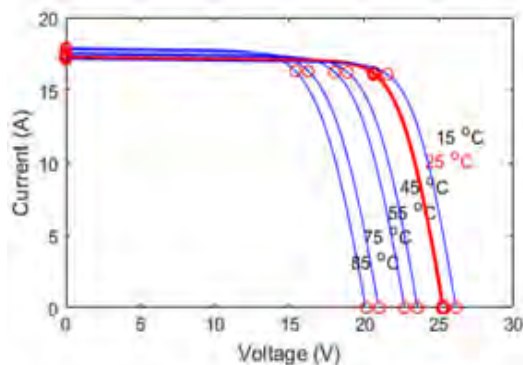


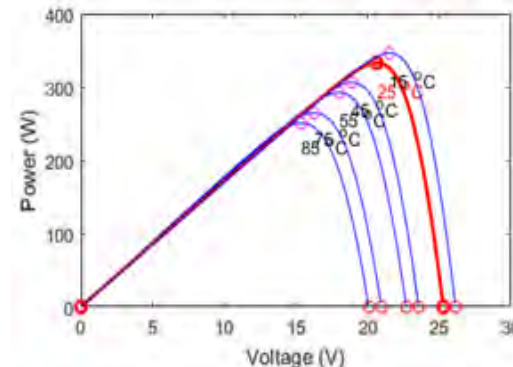
Figure 3: Pump motor characteristic

3.2. Establishing the performances of the electrical components for the photovoltaic pumping system

The characteristics and performance of the PV generator were determined from the point of view of two main meteorological parameters: 1) solar irradiance (in the range 100 -1000 W/m²) (see Figures 4a and 4b). and 2) temperature (in the range between 15-85 °C) (see Figures 5a and 5b). The obtained results are in good agreement with literature [20, 21].

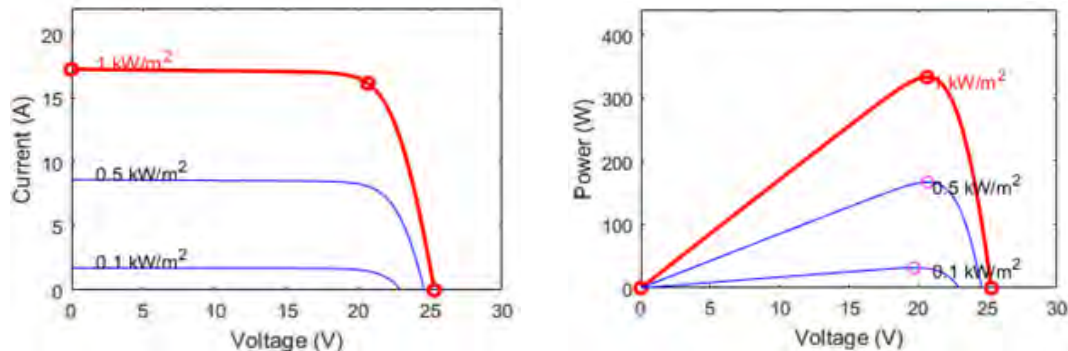


a) I-V characteristics for PV generator
for different values of temperature



b) P-V characteristics for PV generator
for different values of temperature

Figure 4. I-V (current – voltage) and P-V (power – voltage) characteristics for the analyzed PV generator for different values of temperatures



a) I-V characteristics for PV generator for different values of solar irradiance
b) P-V characteristics for PV generator for different values of solar irradiance
Figure 5. I - V (current – voltage) and P-V (power – voltage) characteristics for the analyzed PV generator for different values of solar irradiance

The performance of the inverter of the PV pumping system is obtained using the input data from the catalog (nominal power, output power, and inverter losses) and the equation (4) of the mathematical model discussed. As it was expected the inverter efficiency for the operation range (see Figure 6) is very high, in good agreement with literature [22].

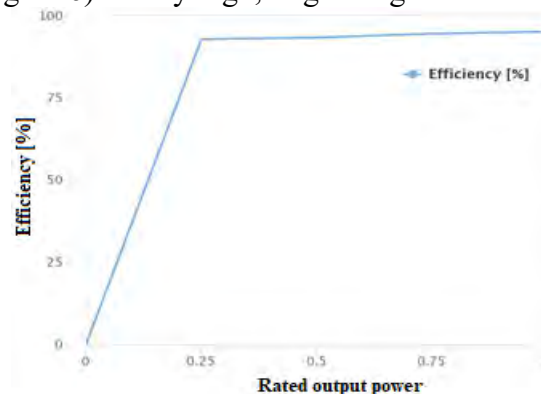


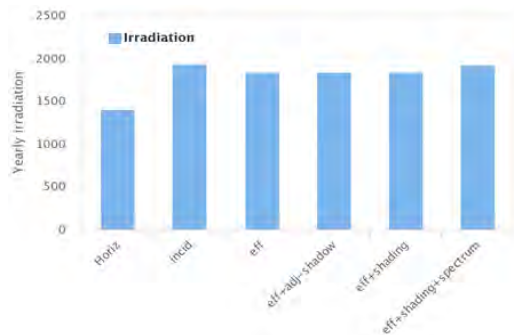
Figure 6: The inverter efficiency depending of the rated output power

3.3. Meteorological characteristics of the site considered

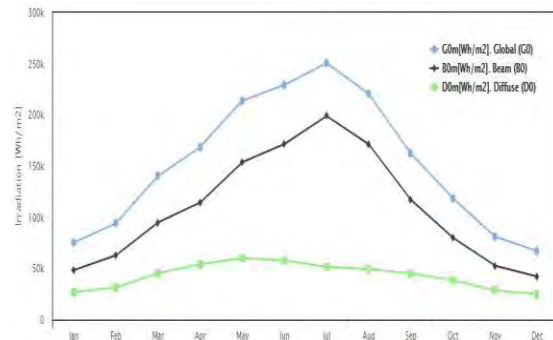
The photovoltaic pumping system for irrigation considered is studied for the Alexandria site (South of Romania) in meteorological conditions that are favorable for exploiting solar potential and in a region with high irrigation potential. The main meteorological parameters, namely the solar irradiance and the ambient temperature, are extracted from the SISIFO - PVGIS platform database. This simulation platform takes into account the real operating conditions of photovoltaic panels, including both the influence of dust and shading, separately and by mixing of these factors. Figure 7a shows the annual solar irradiance for different actual operating conditions of photovoltaic panels in the analyzed site. Figure 7b represents the fitted monthly solar irradiance for Alexandria (south of



Romania) over a year under real operating conditions (dust, shadow and mix of these factors).



a)



b)

Figure 7. a) Annual solar irradiance taking into account different actual operating conditions of PV panels and b) Monthly solar irradiance for Alexandria (South of Romania) - the analysed site

Figure 8 shows the minimum and maximum monthly temperature values over a year. The results obtained in Figures 8 and 9 based on the characteristics of the solar irradiance and ambient temperature for the analyzed site are used to determine the performances of the irrigation pumping photovoltaic system.

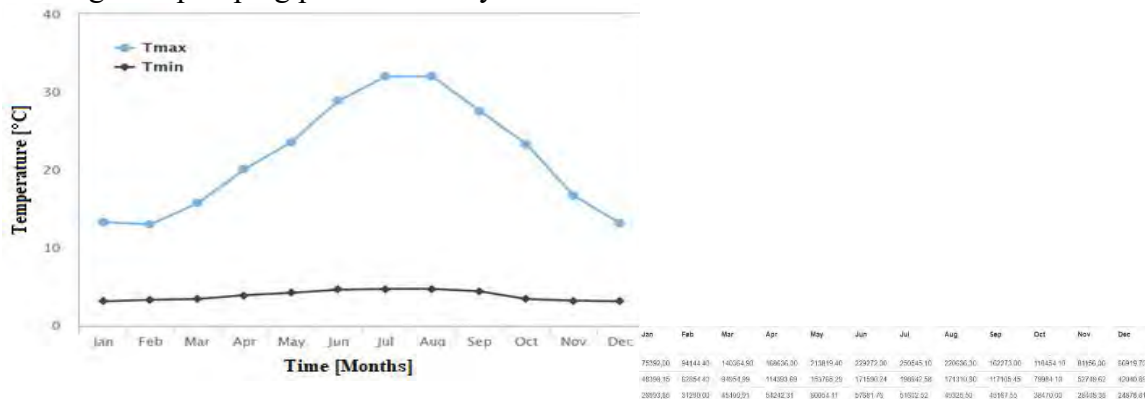


Figure 8 Minimum and maximum monthly ambient temperature

3.4. Performance of the photovoltaic pumping system

Using the input data from the § 3.1, 3.2 and 3.3 and the SISIFO simulation platform we could obtain the main performances of the analysed photovoltaic pumping system.

So, in Figure 9 is plotted the monthly energy yield of the photovoltaic pumping system over a period of a year, respectively the DC energy yield, AC energy yield and hydraulic energy. We could see that the significative period for irrigation is the interval March – October what is confirmed by the values obtained for the energy yield. The maximum value of the DC energy yield of 8 kWh/kWp, respectively AC energy yield of 7 kWh/kWp



for the PV pumping system is obtained in July. The maximum value of the hydraulic energy yield is roughly 4.2 kWh/kWp.



Figure 9 Monthly energy yield of the PV pumping system irrigation (Alexandria, Romania)

Another important performance of the PV pumping system is the monthly pumping yield presented in the Figure 10. The maximum value of this performance is 12.5 m³/kWp and is obtained in July.



Figure 10 Monthly pumping yield of the PV pumping system (Alexandria Romania)

The total performances of the PV pumping system analysed are plotted in Figure 11. They are : the monthly flow rate, the monthly DC energy at the input of the pump motor, the monthly mechanical energy of the pump motor and the monthly hydraulic energy, all of them divided by the electrical energy produced by the PV generator. The maximum values of these quantities are obtained in July. All these performances define the best operation period of the PV pumping system, namely from March to October.



Based on this simulations it is possible to obtain a clear characterization of the system from the point of view of the electrical and hydraulic performances. This approach could be useful to forecast both the sizing, and operation of a such PV pumping system for different meteorological conditions.

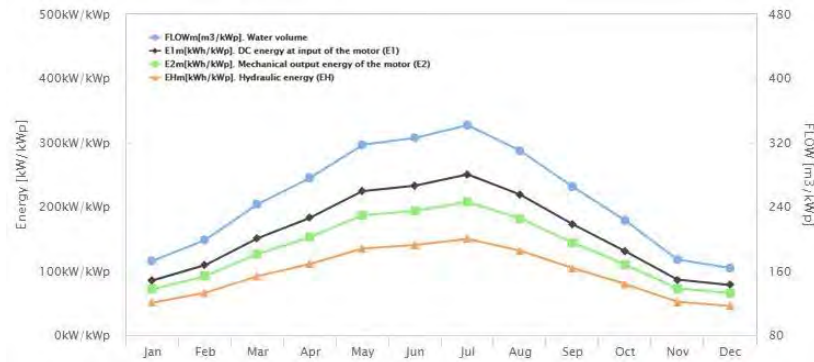


Figure 11 The total performances of the PV pumping system for Alexandria, Romania

3.5. Comparison of two case studies for PV pumping system: Turkey and Romania

We have analyzed two case studies for the PV pumping system based on two sites, namely:

- Alexandria, South of Romania
- Antalya, South of Turkey

For comparison we have considered by simulation the main performances of the PV pumping system, namely:

- 1) Monthly energy yield for Antalya (see Figure 12) and Alexandria (see Figure 9)
- 2) Monthly pumping yield for Antalya (see Figure 13) and Alexandria (see Figure 10)
- 3) The total performances of the PV pumping system for Antalya (see Figure 14) and Alexandria (see Figure 15).

The results indicate a higher irrigation potential for Antalya in comparison with that for Alexandria; so, the maximum value of flow rate, indicated by the Figures 14 and 15, is 450 m³/kWp for Antalya, respectively 340 m³/kWp for Alexandria. This difference is due to the solar higher irradiance potential measured (for Antalya) by the SISIFO - PVGIS platform tools.

All other performances have the same trend, showing a significant increase for Antalya in comparison with that for Alexandria.

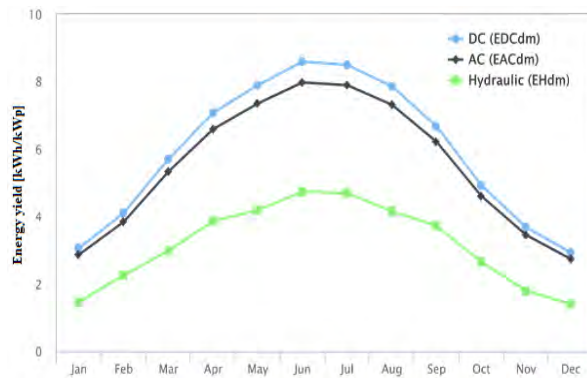


Figure 12 Monthly energy yield of the PV pumping system (Antalya, Turkey)

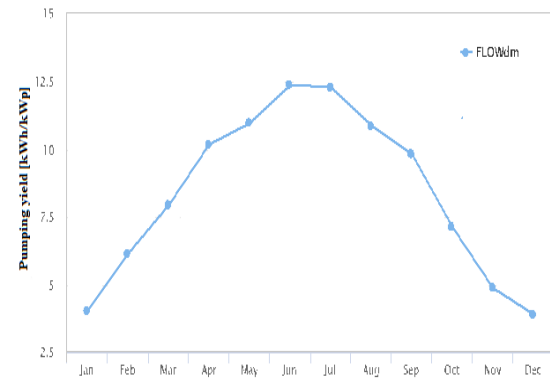


Figure 13 Monthly pumping yield of the PV pumping system (Antalya, Turkey)

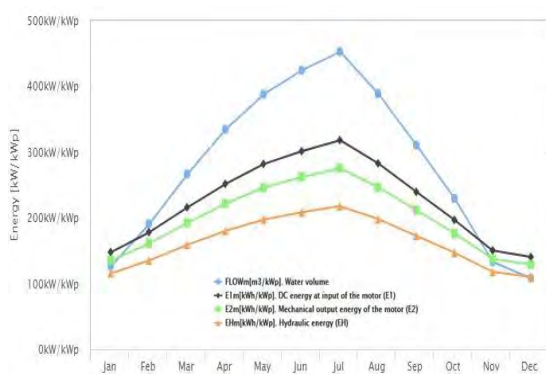


Figure 14 The total performances of the PV pumping system for Antalya, Turkey

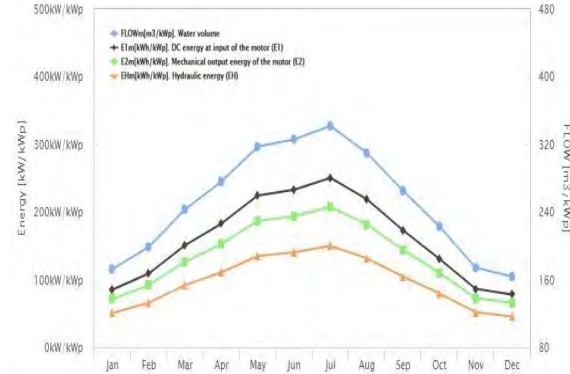


Figure 15 The total performances of the PV pumping system for Alexandria, Romania

4. Optimization of the PV pumping system.

In order to analyse an optimized operation of the PV pumping system the authors proposed an original approach based on MPPT algorithm and frequency converter (Pulse Width Modulation-PWM); it was developed and implemented in MATLAB/Simulink software. An operation and control block diagram based on these concepts is presented in Figure 16. All the components of the PV pumping system, respectively PV generator, pump motor, MPPT controller and PWM were represented using the electronic layouts, too; they included all sub-systems belonging to each block component.

This approach achieved a performant control and monitoring of the parameters for the PV generator and pump motor. This analyses could be implemented for real applications using suitable sensors and Arduino platform, what would allow a further improvement of the operation for the PV pumping system.

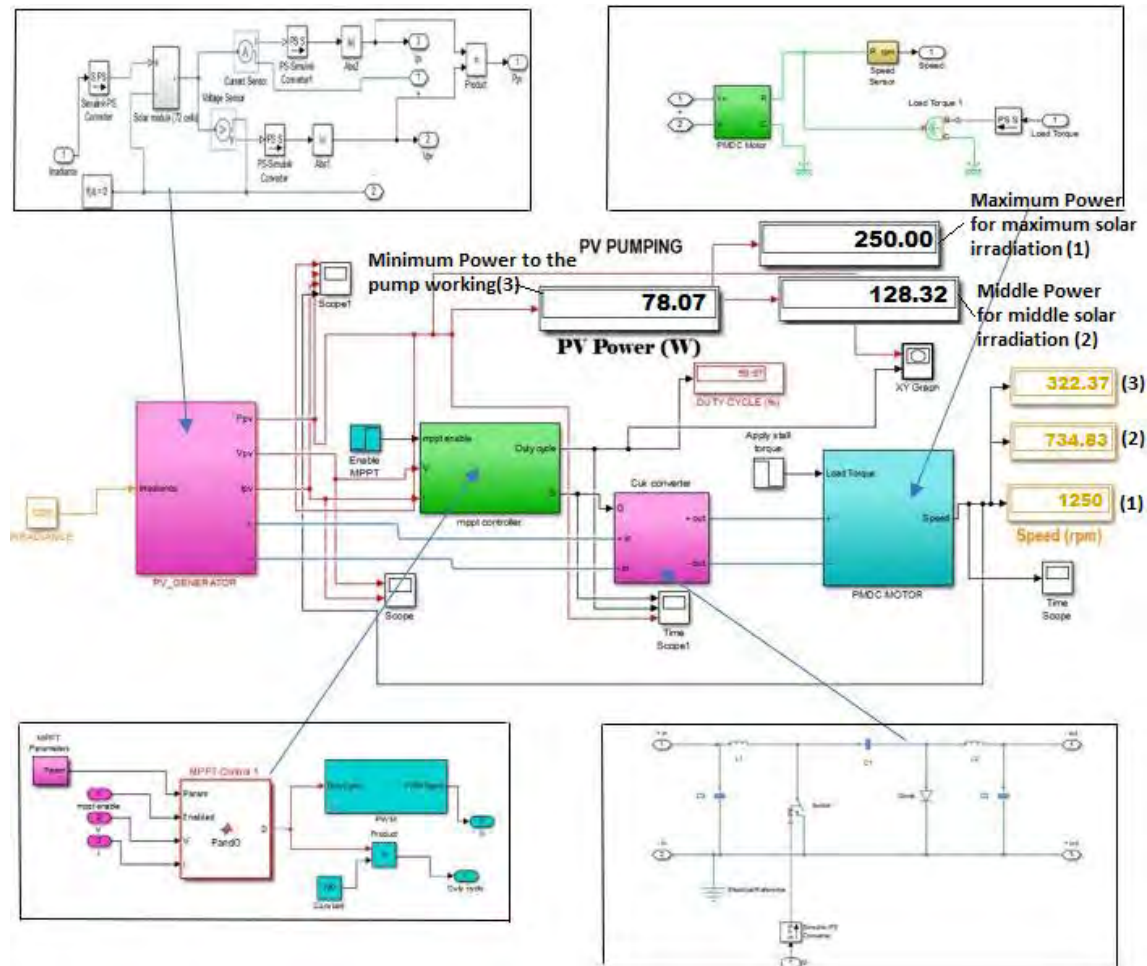


Figure 16 Operation and control block diagram based on MPPT and PWM.

Using the operation and control block diagram based on MPPT controller and PWM frequency converter, as well as MATLAB/Simulink software the authors obtained the behavior of the PV pumping system for two cases, namely:

- without MPPT controller (according to Figure 17)
- with MPPT controller (according to Figure 18)

In the Figures 17 and 18 are presented the output power of the PV generator, respectively of the pump motor for these two cases. It is remarked that:

- The fluctuations of the output power of the PV generator are important in the case when the MPPT controller is not used and are significantly reduced when the MPPT controller is used.
- The output power of the pump motor is much influenced by the fluctuations of the output power of the PV generator and could determine non-functionality of the system in the case without MPPT. It is significantly increased in the case when the MPPT controller is used.



This analyses shows the importance of utilization of the MPPT controller and PWM frequency converter for the PV pumping. These devices ensure the stability of the photovoltaic pumping system throughout its operation duration.

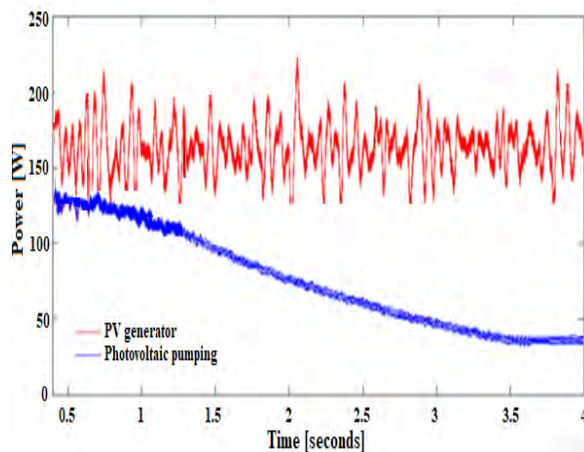


Figure 17 The performances of the PV pumping system in the case without MPPT

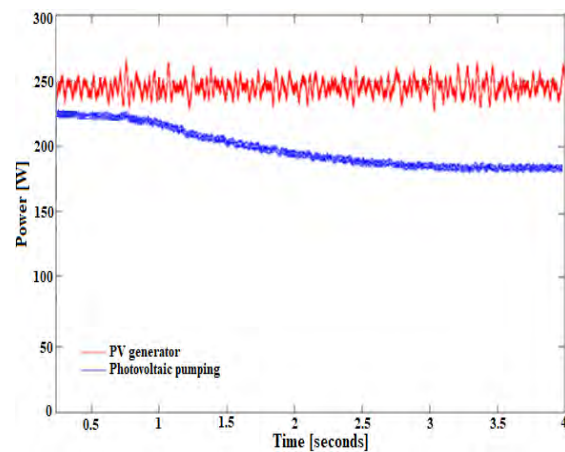


Figure 18 The performances of the PV pumping system in the case with MPPT

5. Conclusions

The novelty of this contribution consisted in: 1) a unified approach of all the components of the PV pumping system using the SISIFO simulation software, and 2) an optimized functionality and operation of the system using a performed controller based on MPPT algorithm. It was also conceived an original block diagram of the PV pumping system developed in the MATLAB/Simulink

The main conclusions obtained by the authors in this study can be synthesized as follows:

- Analysis of the complex PV pumping system was developed based on a specific simulation software and a mathematical model that allowed the establishing of specific equations for all system components.
- The numerical modeling has led to a complete characterization of the investigated photovoltaic structure through clear defined performance indicators, which highlight its irrigation potential. The results obtained by simulations are consistent with different models developed in specialized literature [1,7,8,9,10].
- Two case studies have been proposed for the implementation of the complex pumping system at Alexandria (Southern Romania) and Antalya (Southern Turkey), which have been assessed through the essential meteorological parameters (solar irradiance and ambient temperature), which dictated the irrigation potential for each case.
- In order to improve the performance and operational stability of the photovoltaic pumping system, the authors developed and implemented an original block diagram in the MATLAB / Simulink environment using a MPPT controller and a PWM



frequency converter. On this basis, a significant increasing is achieved both in the use of the photovoltaic generator, and the pump motor.

- The authors approach can contribute to the introduction of this type of photovoltaic pumping structure for complex applications requiring monitoring and efficient control of the functioning of such installations in disadvantaged areas, both from the point of view of pluviometric regime, and from that of a poor electrical grid.

Acknowledgment

The authors are grateful for the financial support of Ministry of Research and Innovation, Romanian Executive Agency for Higher Education, Research, Development and Innovation Funding (UEFISCDI), no. 34/2016 contract, SOLHET project “High-performance tandem hetero-junction solar cells for specific applications”.

References

- [1] J. Muñoz, J. Carrillo, F. Martínez-Moreno, L. Carrasco and L. Narvarte, "Modeling and simulation of large PV pumping systems," in Proceedings of the 31th European Photovoltaic Solar Energy Conference and Exhibition, Hamburg, 2015.
- [2] K. Mohanlal, J. C. Joshi, “Performance Analysis of a Directly Coupled Photovoltaic Water-Pumping System” IEEE transactions on energy conversion, vol. 19, no. 3, september 2004.
- [3] A. Taufik, A Master Thesis on Design and Simulation Of PV Water Pumping System” Presented on 2005. California Polytechnic State University ,San Luis Obispo.
- [4] F. Martínez-Moreno, E. Lorenzo, J. Muñoz, and R. Moretón. “On the Testing of Large PV Arrays.” Progress in Photovoltaics: Research and Applications 20, no. 1 (2012): 100–105, 2012.
- [5] M. Jantsch, H. Schmidt, J. Schmid. Results of the concerted action on power conditioning and control. 11 th European Photovoltaic Solar Energy Conference: 1589-1592, 1992.
- [6] S. J. Chapman, Electric Machinery Fundamentals. 5th edition, McGraw-Hill, 2011.
- [7] B. W. W. Lawrance and D. Langridge, “Simulation and performance of a photovoltaic pumping system,” in Proc. IEEE Int. Conf. Power Electronics and Drive Systems, 1995, vol. 1, pp. 513–518.
- [8] A. Hadj Arab, M. Benghanem, and F. Chenlo, “Motor-pump system modelization,” Renewable Energy, vol. 31, pp. 905–913, 2006.
- [9] T. S. Surendra and S. V. V. Subbaraman, “Solar PV water pumping comes of age in India,” in Proc. IEEE Photovoltaic Specialists Conf., 2002, pp. 1485–1488.
- [10] J. Muñoz, J.M. Carrillo, F. Martínez-Moreno, L.M. Carrasco, L. Narvarte, European Photovoltaic Solar Energy Conference and Exhibition, 3882–87, 2013
- [11] A. Taufik, A. Makbul, Mohammad Taufik, Modeling and Simulation of Photovoltaic Water Pumping System, Third Asia International Conference on Modelling & Simulation, 2009.



-
- [12] K. Mahesh, Modeling and Simulation of Solar Photovoltaic dc water pumping system Using MPPT, International Research Journal of Engineering and Technology (IRJET), Volume: 04 Issue: 05 | May -2017
- [13] Z. Glasnovic J. Margeta, A model for optimal sizing of photovoltaic irrigation water pumping systems, Solar Energy 81 (2007) 904–916, 2012
- [14] M. S Muamer. and T. Iqbal, Dynamic Modeling, Control, and Analysis of a Solar Water Pumping System for Libya, Hindawi Journal of Renewable Energy Volume 2017, Article ID 8504283, 13 pages <https://doi.org/10.1155/2017/8504283>, 2014
- [15] M. EL-Shimy Sizing optimisation of stand-alone photovoltaic generators for irrigation water pumping systems, International Journal of Sustainable Energy, 32:5, 333-350, DOI: 10.1080/14786451.2012.697463, 2013
- [16] Suehrcke, H., J. Appelbaum, and B. Breshef. Modelling a Permanent Magnet DC Motor/centrifugal Pump Assembly in a Photovoltaic Energy System. Solar Energy. Vol. 59, no. 1–3,: 37–42. doi:10.1016/S0038-092X(96)00117-X, 1997
- [17] Brandemuehl MJ, Beckman WA. Economic evaluation and optimization of solar heating systems. Solar Energy 1979;23:1–10, SolarJack Solar Pumping Products. Manufacturer_s Catalog, 2002.
- [18] A. Diaconu, D. Craciunescu L. Fara, P. Sterian, C. Oprea and S. Fara “Estimation of electricity production for a photovoltaic park using specialized advanced software”, Proceedings of the ISES EuroSun 2016 Conference ISBN: 978-3-9814659-6-9 pp. 1180-1182, 2017
- [19] The current version of SISIFO is accessible through the following website: <http://sisifo.adminia.es/>
- [20] L. Fara and D. Craciunescu “Output Analysis of Stand-Alone PV Systems: Modeling, Simulation and Control”, Sustainable Solutions for Energy and Environment, EENVIRO 2016, 26-28 October 2016, Bucharest, Romania, Energy Procedia 112 1-2 DOI: 10.1016/j.egypro.2017.03.1125 pp 595 – 605, 2017
- [21] L. Fara, D. Craciunescu and A. Diaconu “Results in performance improvement and operational optimization of photovoltaic components and systems”, Annals of the Academy of Romanian Scientists Series on Physics and Chemistry Sciences, ISSN 2537-4761 Volume 2 pp 7-30, Number 1/2017, 2017
- [22] A. Diaconu, L. Fara, P. Sterian, D. Craciunescu and S. Fara “Results in Sizing and Simulation of PV Applications Based on Different Solar Cell Technologies”, Journal of Power and Energy Engineering, 2017 Online: 2327-5901, ISSN Print: 2327-588X, DOI: 10.4236/jpee.2017.5100, 5, pp. 63-74, 2017.



SPONSORS & SUPPORTERS



AGROTEK SPRAYING MACHINES



www.agrotek.com.tr/en

ALPLER AGRICULTURAL MACHINERY



www.alpler.com.tr/defaultEN.aspx

ALPLER AGRICULTURAL MACHINERY is the largest agricultural machinery producer in Turkey, and is one of the few leading companies in the world in the agricultural equipment sector. The company is operating in its modern facilities, established on a total area of 120.000 square meters located in Organized Industrial Zone of Aydin. ALPLER AGRICULTURAL MACHINERY is marching into the future with reliance on the synergy created by its more than 400 creative, productive and well experienced employees, working with the ambition and enthusiasm to manufacture better and higher quality products day by day.

As a result of many years of experience, ALPLER AGRICULTURAL MACHINERY has the widest manufacturing and after-sales service program in Turkey. The company has adopted a customer oriented administration and Total Quality policy, and provides it equipment to the farmers in Turkey, throughout its more than 300 dealers all around the country. Today ALPLER exports its products to 70 different countries in 5 different continents all around the World.

Since 1926 ALPLER AGRICULTURAL MACHINERY has remained a private enterprise, and today the company is in its third generation of ownership by the Özalp family. Great importance is attached to integration with worldwide advanced production technologies and research to satisfy market needs. Much of the fabrication work involves the use of robot welders and CNC machining, enabling a high degree of quality assurance to be maintained during production. Additionally ALPLER AGRICULTURAL MACHINERY conducts its operations in compliance with the technical requirements of the European Union, and has been operating under the ISO 9001 quality system since 2004.

In its sector, ALPLER AGRICULTURAL MACHINERY is the only plant which operates IN-HOUSE production conditions in Turkey with custom design equipment for different needs of individual soil conditions for domestic and foreign fields.

Because of its high performance, long life and low operating cost products ALPLER AGRICULTURAL MACHINERY will continue to be the choice of professional farmers worldwide.

Aiming to serve you the best for many years..



ALTINTAR



www.altintar.com.tr

Altintar was established in 1988 in Antalya for the purposes of marketing products for plant nutrition. With foliar fertilizers, drip fertilizers and plant growth regulators, Altintar has a wide range of products. During the initial days of when drip fertilization applications first started in Turkey, Altintar put a great deal of effort to informing and educating the farmers about the correct methods of using and the spreading of the use of drip fertilizer systems. Altintar always gives importance to quality and service. In 1995, the company started importing some of the best products from some of foremost companies known all around the world.

ANTALYA METROPOLITAN MUNICIPALITY



www.antalya.bel.tr/?l=en

ANTALYA CHAMBER OF COMMERCE AND INDUSTRY



english.atso.org.tr

Antalya Chamber of Commerce and Industry (ACCI), which is among the oldest Chambers of Commerce and Industry in Turkey, was established under the name of “Commission of Agriculture and Commerce” on April 3, 1882.

ACCI has 29.927 active members as of April 2018. ACCI has agencies in Serik, Kemer, Korkuteli, Elmalı, Gazipaşa, and Akseki districts of Antalya.

There are 49 professional committees in ACCI, members of which are elected every four years. Also, the Chamber has an Assembly of 111 members, who are elected by the professional committees, an Executive Board comprising 11 members, and 119 chamber staff.

ANTALYA COMMODITY EXCHANGE



www.antalyaborsa.org.tr/en

Antalya Commodity Exchange was established in 23.06.1920, started activities on 07.02.1920 as Antalya Commodity and Grain Exchange.

Our Exchange is the third oldest in our country, most developed of the lakes region.

Our Exchange adapted to the Law No: 655 in 1924, Law No: 4355 in 1944, Law No: 5590 in 1950 and earned the title of Antalya

Commodity Exchange and adapted to the Law No: 2567 in 1981.

Our Exchange had 45 members in founded, the number of members continuously increased.

ANTALYA GOVERNORSHIP



www.antalya.gov.tr

BAYER



www.bayer.com

Bayer is a global enterprise with core competencies in the Life Science fields of health care and agriculture. Its products and services are designed to benefit people and improve their quality of life. At the same time, the Group aims to create value through innovation, growth and high earning power. Bayer is committed to the principles of sustainable development and to its social and ethical responsibilities as a corporate citizen. In fiscal 2017, the Group employed around 99,800 people and had sales of EUR 35.0 billion. Capital expenditures amounted to EUR 2.4 billion, R&D expenses to EUR 4.5 billion. For more information, go to www.bayer.com.



TURKISH POULTRY MEAT PRODUCERS AND BREEDERS ASSOCIATION (BESD-BİR)



www.besd-bir.org/en

BESD-BİR is an association founded by the Turkish poultry meat producers, broiler hatcheries and breeder (parent stock) companies. 28 member companies represent the 95% of the Turkish poultry meat production. The main objectives of BESD-BİR are; to maintain the coordination between government and industry, to create the policies for the development of the poultry industry for the benefit of the country, to produce the statistics, to promote the high quality and safety production, to create the demand to poultry products and spend efforts to increase the consumption of healthy and nutritious poultry products all over the country, to organize the conferences, seminars and symposiums, collaborate with the other associations and to represent Turkish poultry meat sector internationally on this regards.

DOĞA TARIM (AGRICULTURE)



www.dogatarim.com

Çevreye ve insana saygıyı ön planda tutarak Türk Tarımına yenilikler kazandırmak amacı ile kurulan Doğa Tarım, en kaliteli ürün ve hizmetleri müşterilerimize sunarak, dürüst ve yenilikçi firma imajı ile 25 yıldır Türk Tarımına hizmet etmektedir.



GROW FIDE (SEEDLINGS)



www.growfide.com/eng/index.html

Grow Fide Üretim ve Ticaret A.Ş. was founded in 2001 in Antalya with participation of Turkish partners and Grow Group B.V., a company of Dutch origin which is one of the World's leading vegetable plant growers.

Grow Fide produces healthy and highly productive vegetable and flower seedlings that the growers need to produce high quality products. The Company is the pioneering establishment in Turkey in the field of grafted seedlings and is known by its highest technology and quality in the sector. It is not only the first company producing grafted eggplant and watermelon seedlings in Turkey, but it also trains Turkish farmers about growing these seedlings and benefiting from this technology.

Though Grow Fide is a relatively new company, it has shown a rapid development and has been able to expand its production fields to a total of 100.000 (of which 10.000 are used as special grafting laboratory) square meters from 13.000 in 2001.

Grow Fide, which has reached an annual capacity of about 100 million seedlings, produces all kinds of grafted and non-grafted vegetable seedlings as well as seasonal flower seedlings. The Company, with its products grown with state-of-the-art technology, has in a short time become a world-wide known producer of grafted seedlings. Along with its domestic sales, the Company also makes exports to some European and Middle East countries.



KONYA COMMODITY EXCHANGE



www.ktb.org.tr/?cat=61

Konya Commodity Exchange established in 1907 and it is one of the biggest Exchange around Turkey, Konya Commodity Exchange has eight branch office and one center in Konya.

Konya Commodity Exchange maintain different committees that are specialized on specific products and issues. The committee members are big traders or producers of the mentioned goods whom are selected. Special Committees are Cereal, Pulse, Feeders, Live Stocks Traders, Butchers, Leather, Wheat Flour, Dairy Products, Vegetable Oil, Fleece producers and traders Committees.

Konya Commodity Exchange is one of the most valuable exchange of Turkey. All mentioned goods are processing but KEC specialized especially on Cereals. Because Konya has the biggest plantation for cereals and Pulse. In Konya 12 % of Wheat production and 14 % of Barley production held.

Daily Prices are determined according to the transactions on Our Exchange Hall. Goods bring into Exchange and sold by auction. On the Crop season nearly 4000-5000 MT of Goods to be sold.

Exchange can determine prices of 130 different product per hour. In our Board those goods are effected transaction.

Cereals (Wheat, Barley, Oat, Rye, Maize)

Pulse (Pea, Lentil, Bean, Soybean, Broad Bean) Spices
(cumin etc.)

Cereal Products (Wheat Flour, Pounded Wheat..etc) Textile
raw materials (mohair, wool,...etc)

Live Stocks (cattle, sheep) Raw

Leather (animal leathers)

Oil Seeds (sunflower, flax, hemp)

Vegetable Oil (vegetable butter) Pyrene
(Apricot, almond pyrene etc)

To arrange and register the trade of commodities and to establish and announce daily prices,

To create general rules and decisions, with the acceptance of TOBB, about obligation of delivery, taking delivery and payment, arbitration procedures in conflicts.

To follow and communicate with domestic and foreign exchange s and markets.

To construct laboratory and technical offices to establish types and qualities of materials that are traded in the exchange,

To arrange and announce the custom and practices of exchange and make duties given by other regulations and ministry of industry and trade.



THE TURKISH ASSOCIATION OF AGRICULTURAL MACHINERY & EQUIPMENT MANUFACTURERS (TARMAKBİR)



www.tarmakbir.org/en/about-us.html

TARMAKBİR, The Turkish Association of Agricultural Machinery & Equipment Manufacturers, is an initiative of Turkish private sector and founded in 1978. Being the representative of the Turkish agricultural machinery industry, currently it has around 250 members those are senior manufacturers of tractors and agricultural equipments.

TARMAKBİR is one of the oldest member associations in "Mechanical Industry Sector Platform of TURKEY" and has been entitled to use the word "Turkish" at the beginning of its title by a former decision of the Turkish Council of Ministers. Being in a continuous interaction with governmental bodies and national & international organizations, TARMABİR serves as a common platform for the industry and supports its members through regulations, technical and scientific improvements, commercial issues, environmental issues and data providing.

TURKISH AIRLINES / OFFICIAL AIRLINE OF CIGR 2018



www.turkishairlines.com

TURKISH FEED MANUFACTURERS' ASSOCIATION



www.yem.org.tr

Turkish Feed Manufacturers' Association (TÜRKiYEMBİR) established in 1974 by 7 feed manufacturers following the entry into force of Turkish Feed Law.

It is a unique NGO of feed manufacturers in Turkey and acts for sustainable development of Turkish compound feed sector, it aims to increase the sector competitiveness around the world and provide opportunities to citizens for their healthy and affordable protein consumption.

Currently Turkiyem-Bir has got 160 members which constitute 80% of the Turkey's compound feed production



TÜRKAY AGRICULTURAL MACHINERY / MINOS AGRI



www.minosagri.com

Our company, activating in agricultural mechanization field which has great importance for improvement of agriculture in our country since 1959, manufactures Rotary Tillers, Seed Drills, Inter Row Rotary Cultivator, Fertilizer Spreaders, Mulchers, ReaperBinder, Maize Chopper, Rotary Mowers, Rotary Windrowers, Tedder, Balers, Subsoilers, Cultivators, Chisel, Disc Tiller used in agricultural works such as handling, fertilizing and harvesting starting from preparation of soil at the pre-sowing period until plantation, in compliance with stage of the art technology.

Considering the agricultural needs of our country, Minos Agricultural Machinery has put the Mixer-Feeders into service with the quality, privilege, guarantee and assurance of Minos, which are designed to have strong and reliable structures, be easy to use and eco-friendly machines.

Our company following the global technological advancements is always beside farmers and at the service of state agriculture with quality machinery conforming to standards and on-site applications.

ÜNLÜ



www.unluziraat.com.tr/about-150.html

Our company was founded in Manisa – Turkey in 1971. We have been operating in 17.000 m² closed, totally 30.000 m² factory area with our trained and qualified staff. The company own quality controlsystem certificate of ISO 9001:2015 and by controlling the production in every stage it's provide of the product. Our all products is getting controlled of quality and qualification by related departments of universities and the exported items getting contolled in the testing department and get confirmation from them. All of the raw materials, that we use while manufacturing our products, are supplied from the recognized companies of Turkey. All of them are certified and have high quality.

In all regions of Turkey, and in overseas there's many our dealers so they serving and solving our clients problems with portable services.

YANMAR



www.yanmar.com

Since YANMAR's founding more than 100 years ago, our company has been driven by a pioneering spirit for world-leading technology. Today, this continues to be a core focus, allowing us to utilize and transform all kinds of energy resources into power that can be harnessed for highly efficient human convenience.

Using our advancing technology, YANMAR continuously strives to exceed customer expectations, deliver exceptional lifetime value by integrating our products, services and knowledge into superior quality, comprehensive solutions.

Sustainable prosperity for all and, A Sustainable natural environment.

YSL AGRICULTURE



www.ysltarim.com.tr

FOCUSED TO HAVE OUR PRODUCERS BENEFIT MORE

As YSL Agriculture Foreign Trade, our researches which started about how to obtain healthier and more economical products with better quality have made us an important and pioneering stakeholder in the field of plant nutrition in our country.

Bunu sağlayabilmek için de girdileri düşürmek ve harcadığımız her kuruşun hakkını almak mecburiyetindeyiz. Bu anlayışla, gerek yurtdışında ki lisansör firmaları aracılığı ile gerekse bünyesinde yer alan kimyagerlerinin çok uzun yıllara dayanan araştırma ve geliştirme faaliyetleri sonucu ortaya koydukları ürünleri üreticimizin kullanımına sunarak, üreticimizin artık daha karlı bir şekilde faaliyet göstermesine odaklanmıştır."

As a producer we know very well that growing agricultural products intense as of labor and costly business line at the same time. When we think of today's competitive environment, as a breeder we have to obtain more healthy and quality products from the unit area in order to be able to receive the salvation of our labor after the harvest. In order to be able to achieve this, we have to reduce input. With this understanding, we have focused on to have our producers operate more profitably by providing them the products of licensors abroad or products produced with the research and development activities of chemists who are in the field.

EXPORTING ABROAD

YSL Agriculture Foreign Trade is proud to add value to the thousands of farmers who prefer our products in our country and to the producers in different regions of the world using our exported products. We took to offer quality, economical, humanitarian and nature-friendly products to our producers and the producers located in different geographical areas in the World as a mission in the field of Plant Nutrition. Our vision is to develop new formulations as a result of continuous research and development activities, and to continue to be the pioneer of the industry by providing superior products developed within the country or abroad to the service of producers.

As YSL Agriculture Foreign Trade Corporation; we use our products which we have produced with many years of experience in our own land in the province of Kayseri (Yeşilhisar). We also provide service to our farmers to whom we reach by our distributors.

